LBL-13500
UC-13 c.2

RECEIVED
LAWRENCE
BERKELEY LABORATORY

OCT 30 1986

LIBRARY AND
DOCUMENTS SECTION

Annual Report
FY 1981

Energy & Environment Division

TWO-WEEK LOAN COPY

This is a Library Circulating Copy which may be borrowed for two weeks.

September 1982

Lawrence Berkeley Laboratory
University of California, Berkeley

Prepared for the U.S. Department of Energy under Contract DE-AC03-76SF00098

LBL-13500 c.2

DISCLAIMER

This document was prepared as an account of work sponsored by the United States Government. While this document is believed to contain correct information, neither the United States Government nor any agency thereof, nor the Regents of the University of California, nor any of their employees, makes any warranty, express or implied, or assumes any legal responsibility for the accuracy, completeness, or usefulness of any information, apparatus, product, or process disclosed, or represents that its use would not infringe privately owned rights. Reference herein to any specific commercial product, process, or service by its trade name, trademark, manufacturer, or otherwise, does not necessarily constitute or imply its endorsement, recommendation, or favoring by the United States Government or any agency thereof, or the Regents of the University of California. The views and opinions of authors expressed herein do not necessarily state or reflect those of the United States Government or any agency thereof or the Regents of the University of California.

LBL-13500

ENERGY & ENVIRONMENT DIVISION ANNUAL REPORT FY 1981

Elton J. Cairns
Head, Energy & Environment Division
and
Associate Director, LBL

Report Coordinator
Maya Osowitt

Energy and Environment Division
Lawrence Berkeley Laboratory
University of California
Berkeley, California 94720

Prepared for the U.S. Department of Energy under Contract No. DE-AC03-76SF00098

FOREWORD

The mission of the Energy & Environment Division is to research the complex energy issues that confront our nation. The research base is broad and is organized into five major programs: Chemical Process Research and Development, Solar Energy, Energy Efficient Buildings, Environmental Research, and Energy Analysis. The goal of these programs is to make key contributions to the solution of the critical problem of providing environmentally acceptable energy options for the future. Although researchers in each program use special expertise to conduct their studies, they are increasingly joining forces with the staff of other programs in the Division to investigate particular aspects of related problems. For example, the Windows and Daylighting Group in the Energy Efficient Buildings Program and the Passive Analysis and Design Group in the Solar Energy Program are jointly studying the effects of natural lighting on building energy efficiencies.

The Chemical Process R&D Program is investigating four major research areas: (1) bioconversion of cellulose to liquid fuel, (2) production of synthetic fuels from fossil fuels, (3) electrochemical energy storage, and (4) environmental protection from the hazards of synthetic-fuel production. The strong commonality of these research areas is the application of the principles of transport of mass and energy, chemical kinetics, thermodynamics, physical chemistry, and organic chemistry to develop approaches for solution of various aspects of energy-related problems.

The objective of the Solar Energy Program is to advance the development and application of solar energy as a supplement to traditional, nonrenewable energy resources, thus decreasing the rate at which these resources are depleted. The Solar Program consists of a number of applied and basic research projects, including (1) active solar cooling of buildings, (2) passive solar heating and cooling, (3) the conversion of solar energy to electricity, e.g., by means of the Small Particle Heat Exchange Receiver (SPHER), and (4) the photochemical conversion of sunlight to energy.

The efficient use of energy in buildings is the emphasis of the Energy Efficient Buildings Program (EEB), which comprises the following related groups: (1) Building Envelopes, (2) Efficient Windows and Daylighting, (3) Efficient Artificial Lighting, (4) Ventilation and Indoor Air Quality, (5) Building Energy Simulation using the DOE-2 computer model, and (6) Building Energy Data Compilation and Analysis.

The objective of the Environmental Research Program is to study the hazardous effects of energy generation and use. The program is divided into seven major research areas that encompass transport and transformation, impacts, characterization, and abatement. These major areas are (1) Atmospheric Aerosol Research, (2) Laser Spectroscopy, (3) Combustion Research, (4) Oil Shale Research, (5) Lake Ecotoxicology and Acid Rain, (6) Instrumentation Survey, and (7) Trace Element Analysis.

The Energy Analysis Program assesses economic and public policy and their relevance to the critical issues affecting national and regional energy supply and demand. The Program is organized into four study areas: (1) building energy use, (2) energy and peak demand forecasts, (3) international energy demand, and (4) energy supply. All of the research emphasizes the importance of energy policy relevance, quantitative analysis (often based on computer models), development of analysis tools, the potential for keeping the public informed, and the interdisciplinary nature of the research.

The Energy & Environment Division has close ties with several departments at the University of California, Berkeley, in particular the Mechanical Engineering and Chemical Engineering departments and the multidisciplinary Energy Resources Group.

LAWRENCE BERKELEY LABORATORY
UNIVERSITY OF CALIFORNIA
ENERGY & ENVIRONMENT DIVISION

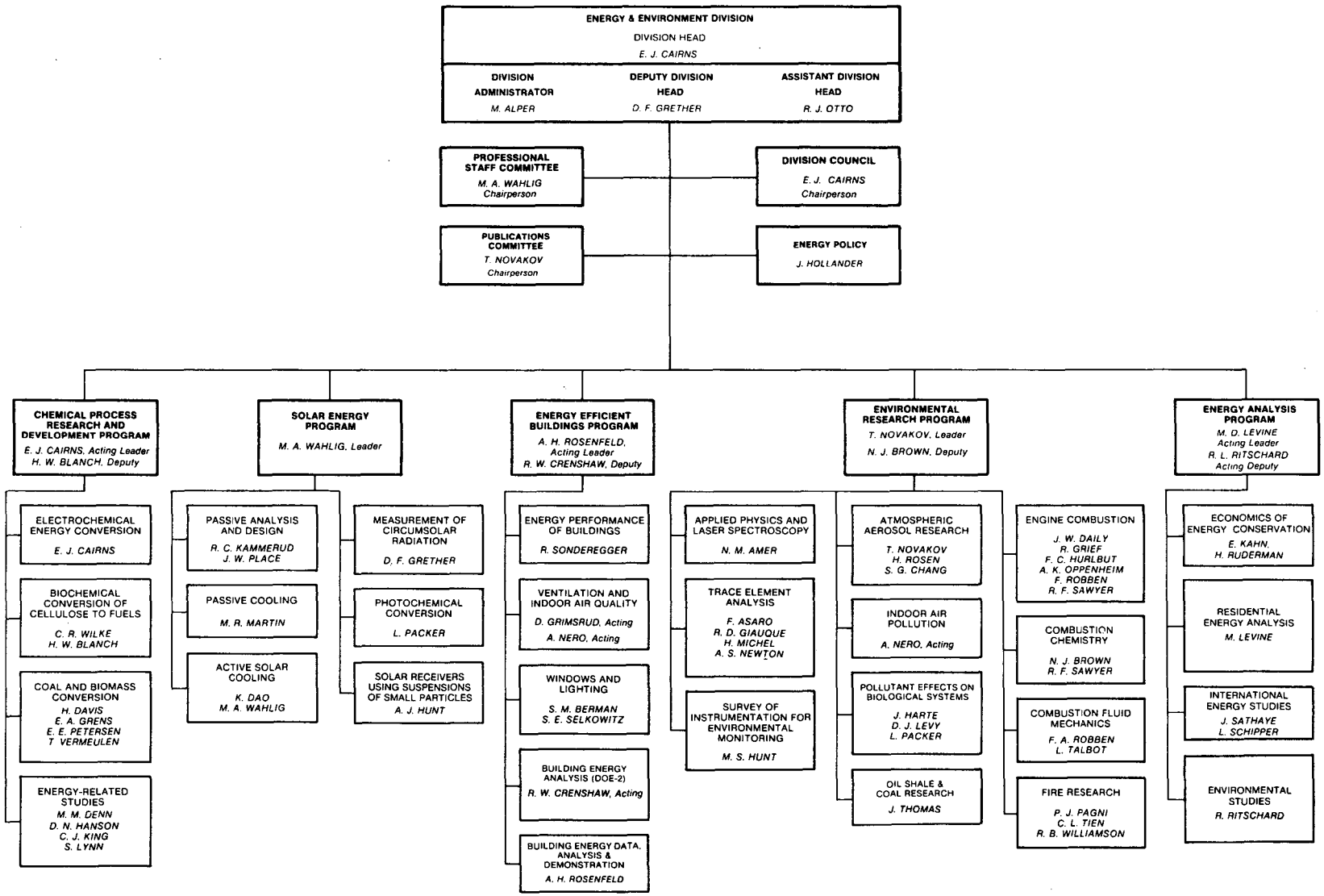

MAY 1982

CONTENTS

CHEMICAL PROCESS RESEARCH AND DEVELOPMENT PROGRAM

Introduction 1-1

Chemical Liquefaction of Biomass

Operation of the Continuous Bench-Scale Unit for Direct Liquefaction of Biomass
C. Figueroa and H.G. Davis 1-2

Characterization of Products from Direct Biomass Liquefaction
L.L. Schaleger, D. Kloden, and H.G. Davis 1-7

Chemistry and Mechanism of Wood Liquefaction
H.G. Davis, L.L. Schaleger, and N. Yaghoubzadeh 1-11

Fuels from Biomass by Biochemical Processes

Ethanol Production and Recovery from Biomass Sugars
H.W. Blanch, C.R. Wilke, B.L. Maiorella, and T.K. Murphy 1-14

Production of Sugars from Cellulose
C.R. Wilke, H.W. Blanch, G.B. Dove, N.A. Hendy, A. Mancuso, S.T. Orichowskyj, J.M. Perez, A.F. Sciamanna, and D.F. Wiley 1-19

Oil Shale and Petroleum-Related Research

Molecular Substituent Parameters Applied to the Speciation of Inorganic Arsenic and Organoarsenic Compounds in Shale Oil and Oil Shale Kerogen by HPLC-GFAA
R.H. Fish, F.E. Brinckman, and C.S. Weiss 1-23

Speciation of Vanadyl Porphyrins and Non-Porphyrin Compounds in Heavy Crude Oils by HPLC-GFAA and the Competitive Equilibria Between Vanadyl Porphyrins and Multidentate Ligands
R.H. Fish, J.J. Komlenic, and T. Vermeulen 1-27

Reactions of Inorganic and Organoarsenic Compounds with Substituted Catechols
R.H. Fish and R.S. Tannous 1-29

Homogeneous Catalytic Hydrogenations of Model Synthetic Fuel Compounds
R.H. Fish, G.A. Cremer, T. Vermeulen, and A. Thormodsen 1-31

Coal-Related Research

Processing of Condensate Waters from Coal Conversion
C.J. King, D.H. Mohr, P.D. MacKenzie, J.D. MacGlashan, C.L. Munson, and R.E. Thompson 1-34

A Kinetic Study of Reactions Involving Ferrous Nitrosyl Complexes
D. Littlejohn, S. Lynn, and S.G. Chang 1-38

The Thermodynamics and Kinetics of the Coordination of NO to Fe(II)NTA in Aqueous Solutions
N.-H. Lin, D. Littlejohn, S. Lynn, and S.G. Chang 1-40

Kinetics of Reactions in a Wet Flue Gas Simultaneous Desulfurization and Denitrification System
S.G. Chang, S. Lynn, D. Littlejohn, and N.-H. Lin 1-43

Electrochemical Energy Storage Research

Applied Battery and Electrochemical Research Program
E.J. Cairns and F.R. McLarnon 1-48

Battery Electrode Studies
E.J. Cairns, F.R. McLarnon, M. Katz, K. Miller, and J. Nichols 1-50

SOLAR ENERGY PROGRAM

Introduction 2-1

Passive Research and Development
R.C. Kammerud, J.W. Place, M.R. Martin, P.H. Berdahl, D. Elmer, B. Andersson, F.S. Bauman, W.L. Carroll, A.J. Gadgil, A. Mertol, S.U. Choi, M.B. Curtis, E. Ceballos, M. Tavana, T.L. Webster, M.W. Nansteel, C.C. Conner, P. Coutier, M. Fontoynont, E.F. Altmayer, G. Schiller, V. Horan, H. Michaels, and N.A. Friedman 2-2

Active Solar Cooling
M.A. Wahlig, K. Dao, M.L. Warren, J.E. Rasson, R.A. Armer, H. Angerman, and A. Heitz 2-8

Appropriate Energy Technology
F.B. Lucarelli, J.D. Kessel, H.R. Clark, J.M. Kay, and J. Linse 2-15

Energy Conversion by the Retinal Protein, Bacteriorhodopsin
L. Packer, A.T. Quintanilha, R.J. Mehlhorn, I. Fry, J. Herz, E. Lam, S. Tristam-Nagle 2-16

Measurement and Analysis of Circumsolar Radiation
D.F. Grether, D.B. Evans, A.J. Hunt, S.G. Kanzler, M. Harms, and M.A. Wahlig 2-20

Support for SOLERAS Solar Cooling Engineering Field Tests
M.A. Wahlig and F.H. Salter 2-23

LBL Building 71 Solar Cooling Project
F.H. Salter 2-25

Development of a 30-kW High Temperature Solar Receiver Using Small Particles as the Heat Exchanger
A.J. Hunt, M. Deiringer, D.B. Evans, L. Hansen, P.G. Hull, and D. Paydarfar 2-26

Diffractive Solar Collection Systems
D.B. Evans and A.J. Hunt 2-29

ENERGY EFFICIENT BUILDINGS PROGRAM

Introduction 3-1

Energy Performance of Buildings (EPB)
J.W. Adams, R.C. Diamond, D.J. Dickerhoff, J.B. Dickinson, J.Y. Garnier, D.T. Grimsrud, R.D. Lipschutz, M.P. Modera, M.H. Sherman, B.V. Smith, and R.C. Sonderegger 3-3

Building Ventilation and Indoor Air Quality Research

Combustion-Generated Pollutants

The Effects of Ventilation on Residential Air Pollution Due to Emissions from a Gas-Fired Range
G.W. Traynor, M.G. Apte, J.F. Dillworth, and C.D. Hollowell 3-12

Pollutant Emission Rates from Indoor Combustion Appliances and Sidestream Cigarette Smoke
J.R. Girman, J.R. Allen, M.G. Apte, C.D. Hollowell, V.M. Martin, and G.W. Traynor ...3-15

Organic Contaminants/Passive Monitors

Organic Contaminants
R.R. Miksch, C.D. Hollowell, and H.E. Schmidt 3-18

A New Passive Monitor for Determining Formaldehyde in Indoor Air
K.L. Geisling, J.R. Girman, R.R. Miksch, S.M. Rappaport, and M.K. Tashima 3-21

Radon and Its Daughters

Distribution of Indoor Radon Concentrations and Source Magnitudes: Measurements and Policy Implications
A.V. Nero Jr., M.L. Boegel, S.M. Doyle, B.A. Moed, and W.W. Nazaroff 3-24

Instrumentation for a Radon Research House
W.W. Nazaroff, A.V. Nero Jr., K.L. Revzan, and A.W. Robb 3-27

Field Monitoring of Indoor Air Quality

Indoor Air Quality in New Energy-Efficient Houses and Retrofitted Houses
C.D. Hollowell, J.V. Berk, S.R. Brown, J.F. Dillworth, J.F. Koonce Jr., J.H. Pepper, and R.A. Young 3-30

Low-Infiltration Housing in Rochester, New York: A Study of Air-Exchange Rates and Indoor Air Quality
F.J. Offermann, J.F. Dillworth, D.T. Grimsrud, C.D. Hollowell, J.F. Koonce Jr., W.W. Nazaroff, J.H. Pepper, A.W. Robb, G.D. Roseme, and R.A. Young 3-34

Mechanical Ventilation Systems Using Air-to-Air Heat Exchangers

Performance Measurements for Residential Air-to-Air Heat Exchangers
W.J. Fisk, K.M. Archer, R. Bitton, P. Boonchanta, B. El-Adawy, R. Haynes, C.D. Hollowell, and G. D. Roseme 3-37

Energy Efficient Windows and Daylighting
S.E. Selkowitz, S.M. Berman, R.L. Johnson, J.D. Kessel, J.H. Klems, C.M. Lampert, and M.D. Rubin 3-40

Lighting Systems Research
R.R. Verderber, S.M. Berman, R.D. Clear, and F.M. Rubinstein 3-49

Building Energy Simulation Group
J.J. Hirsch, W.F. Buhl, R.B. Curtis, A.E. Erdem, K.H. Olson, and F.C. Winkelmann 3-54

Buildings Energy Data Group
A.H. Rosenfeld, J.P. Harris, B.L. Gardiner, C.A. Goldman, A.K. Meier, B.C. O'Regan, J.C. Ribot, H.D. Ross, B.D. Wagner, T.J. Usibelli, and L.W. Wall 3-64

ENVIRONMENTAL RESEARCH PROGRAM

Introduction 4-1

Atmospheric Aerosol Research

SO_2 Oxidation of Soot Particles Exposed to Water
W.H. Benner, E. Ljungstrom, and T. Novakov 4-2

Aqueous Reactions of Nitrite with Bisulfite Ions in Sulfate Aerosol Formation
S.B. Oblath, S.G. Chang, S.S. Markowitz, and T. Novakov 4-5

Carbon Particles in the Arctic
H.J. Rosen and T. Novakov 4-7

Application of Thermal Analysis and Photoelectron Spectroscopy for the Characterization of Particulate Matter
R.L. Dod and T. Novakov 4-10

Theoretical Studies of the Thermal Decomposition of Carbonaceous Aerosol Particulates
A.D.A. Hansen and T. Novakov 4-13

Application of Selective Solvent Extraction to Carbonaceous Aerosols
L.A. Gundel and T. Novakov 4-16

The Relation Between Concentrations of Polynuclear Aromatic Hydrocarbons and Black Carbon
L.A. Gundel, H.J. Rosen, and T. Novakov 4-20

Determination of Low-Z Elements Simultaneously by Charged Particle Activation Analysis
M. McKinney, S.S. Markowitz, and T. Novakov 4-22

Applied Physics and Laser Spectroscopy Research
N.M. Amer, M.S. Cooper, R.W. Gerlach, R.P. Hall, W.B. Jackson, R.L. Johnson, S.E. Kohn, S.J. Kulik, M.A. Olmstead, A. Skumanich, D.R. Wake, and Z.A. Yasa 4-24

Laser Photoacoustic and Photothermal Measurements and Characterization 4-24

Amorphous Photovoltaic Semiconductors 4-29

Liquid Crystal Research 4-33

Novel Laser Systems 4-35

Oil Shale Research

A Mathematical Model for Leaching of Organic Carbon from In-Situ Retorted Oil Shale
W.G. Hall, R.E. Selleck, and J.F. Thomas 4-37

Development of Low-Cost Grouts from Spent Oil Shale
P. Persoff 4-40

Analytical Methods for Quantitating Performance of Oil Shale Wastewater Treatment
C.G. Daughton, B.M. Jones, R.H. Sakaji, and J.F. Thomas 4-45

Microbial Aspects of Oil Shale Wastewater Treatment
B.M. Jones, R.H. Sakaji, J.F. Thomas, and C.G. Daughton 4-51

Processes for the Physico-Chemical Treatment of Oil Shale Wastewaters
R.H. Sakaji, B.M. Jones, J.F. Thomas, and C.G. Daughton 4-57

Combustion Research

Collision Dynamics Studies of Selected Hydrogen/Oxygen Reactions
N.J. Brown, J.A. Miller, and O. Rashed 4-63

Combustion Instabilities Leading to Flashback
L. Vaneveld, K. Hom, and A.K. Oppenheim 4-66

Ignition Studies
A.K. Oppenheim, F.C. Hurlbut, F. Robben, R.B. Peterson,
P.A. Coico, and H.E. Stewart 4-70

Optical Measurement of Combustion Products by Tunable Atomic Line
Molecular Spectroscopy
E. Cuellar and N.J. Brown 4-73

Combustion in a Turbulent Boundary Layer
T.T. Ng, R.K. Cheng, F. Robben, and L. Talbot 4-77

Velocity Statistics in Premixed Turbulent Flames
R.K. Cheng, T.T. Ng, F. Robben, and L. Talbot 4-80

Lean Engine Combustion Studies
R.F. Sawyer, A.K. Oppenheim, J.W. Daily, R. Greif, K. Hom, H.E. Stewart,
J.B. Woodard, and D. Hirvo 4-82

A Staged Fluidized-Bed Combustor for the Study of Pollutant Formation and Destruction
R.F. Sawyer, J.F. LaFond, and J.R. Hart 4-84

Chlorine and Bromine Inhibition of a Polyethylene Opposed-Flow Diffusion Flame
W.J. Pitz and R.F. Sawyer 4-85

Spouted-Bed Combustion
R.F. Sawyer, K. Ohtake, and J.R. Hart 4-86

Characteristics of Fly Ash from Laboratory Combustion of Pulverized Coal
G.M. Parsons, P. Sherman, R. Greif, and F. Robben 4-87

Two-Point Rayleigh Scattering Measurements in a V-Shaped Turbulent Flame
M. Namazian, L. Talbot, and F. Robben 4-90

Numerical Modeling of Turbulent Combustion
A.J. Chorin, A.F. Ghoniem and A.K. Oppenheim 4-93

The Formation and Reduction of Nitrogen Oxide in the Combustion of Condensed Fuels
D. Lucas and N.J. Brown 4-98

Tests and Criteria for Fire Protection of Cable Penetrations
R.B. Williamson and F.L. Fisher 4-101

Lake Ecotoxicology Research

Optimum Microcosm Design for Ecotoxicology
J. Harte, D.J. Levy, G.P. Lockett, J.M. Oldfather, J.T. Rees, E.I. Saegebarth,
and R.A. Schneider 4-104

Acid Precipitation: Microcosm Applications and Field Studies
J. Harte, G.P. Lockett, R.A. Schneider, and K. Tonnessen 4-107

Trace Element Analysis

The Survey of Instrumentation for Environmental Monitoring
M.S. Quinby-Hunt, C.W. Case, R.D. McLaughlin, G.A. Morton, D. Murphy,
A.V. Nero, Jr., and A.T. Quintanilha 4-111

Iridium Anomaly Approximately Synchronous with Terminal Eocene Extinctions
W. Alvarez, F. Asaro, H.V. Michel, and L.W. Alvarez 4-113

Precise Characterization of New World Obsidian Sources and the Cost-Effective Determination of Provenience of Selected Artifacts
F.H. Stross, F. Asaro, and H.V. Michel 4-116

Organic Compounds in Coal Slurry Pipeline Water
A.S. Newton, H.M. Villarreal, W.E. Walker, and J.P. Fox 4-119

The Development and Application of X-Ray Fluorescence Analytical Techniques
R.D. Giauque and L.E. Sindelar 4-121

Asymmetry of the Mitochondrial Membrane
R.J. Mehlhorn and L. Packer 4-122

ENERGY ANALYSIS RESEARCH PROGRAM

Introduction 5-1

Energy Supply Studies

Coastal Zone Assessment Program
R.L. Ritschard 5-2

Estuarine Impacts of Fossil-Fuel-Based Technologies: A Case Study
R.L. Ritschard, V.J. Berg, and M.A. Henriquez 5-5

Environmental Impacts of Marine Biomass
R.L. Ritschard, V.J. Berg, and S. Killeen 5-8

Effectiveness and Implications of Technical Innovations to Reduce Water Use
J. A. Sathaye, R.L. Ritschard, M.M. El-Gassier, and S.C. Rainey 5-11

Groundwater Impacts of Enhanced Oil Recovery
J.A. Sathaye 5-14

Growth and Energy Development in the Rural West
R.G. Sextro and J.M. Bernier 5-17

California Energy Systems Assessment Models
J. A. Sathaye, H. Ruderman, P.T. Chan, and H. Schmidt 5-20

Mineral Requirements for Energy Scenarios
J.A. Sathaye and H. Ruderman 5-22

Energy Demand Studies

Residential End-Use Demand Modeling: Improvements to the ORNL Model
J.E. McMahon 5-25

Analysis of Appliance Efficiency Standards
J.E. McMahon, M.D. Levine, and H.J. Herring 5-27

Residential Hourly and Peak-Demand Model
G. Verzhbinsky and M.D. Levine 5-29

Analysis of Energy Conservation Measures in Residential Buildings
J.G. Ingersoll, J. Huang, J.J. Mass, and M.D. Levine 5-32

Assessment of Energy Conservation Rating Systems
P.G. Cleary, J.G. Ingersoll, J.J. Mass, and M. D. Levine 5-35

Determinants of Residential Energy Use
P.P. Craig, J.C. Cramer, T.M. Dietz, B. Hackett, D.J. Kowalczyk, M.D. Levine, and E.L. Vine 5-38

Analysis of Energy Conservation Measures in Commercial Buildings
I. Turiel, D.A. Boschen, M.D. Levine, J.R. Smith, and M. Zentner 5-41

Energy Conservation in Kenya: Progress, Potentials, Problems
L.J. Schipper, J.M. Hollander, M.V. Milukas, J. Alcamo, S.P. Meyers, and S. Noll 5-45

Indicators of Residential Energy Use and Conservation
L.J. Schipper, S.P. Myers, and A.N. Ketoff 5-49

APPENDIX: ENERGY & ENVIRONMENT DIVISION PERSONNEL

Division Office Staff A-1

Chemical Process Research and Development Program Staff A-1

Solar Energy Program Staff A-2

Energy Efficient Buildings Program Staff A-2

Environmental Research Program Staff A-3

Energy Analysis Research Program Staff A-4

CHEMICAL PROCESS RESEARCH AND DEVELOPMENT PROGRAM

INTRODUCTION

The Chemical Process Research and Development Program has four main areas of application of chemistry and chemical engineering to problems related to production of unconventional fuels, their environmental impact, and energy storage. These areas are:

a. Production of synthetic fuels, predominantly by coal liquefaction

b. Processing of effluent gas and liquid streams, resulting from such synthetic fuels production, to provide acceptable waste or recycle streams

c. Production of liquid fuels from biomass

d. Electrochemical energy storage.

Uniting all these projects is a common thread of transport process principles, chemical kinetics, thermodynamics, separation processes, and organic and physical chemistry.

The first of these areas is focused on the liquefaction of coal. The objective is to selectively hydrogenate and thus achieve a substantial conversion of coal to liquid at moderate temperatures. Homogeneous metal-organic catalysts have interesting selectivities with respect to their ability to promote different types of hydrogenation and cracking involved in liquefaction. These are examined using model organic compounds in place of coal, initially, so that mechanisms and rates can be determined. Another aspect of this work involves examining metal impurities in fossil fuels, especially crude petroleum and shale oil. These impurities have been shown to be metal-organics. Their isolation and identification is thus of great practical interest in devising means to separate them from the fossel fuels. One approach taken to separate these impurities will be the use of metal-organic complexing.

The second area involves research related to the development of novel and improved methods for processing synfuel condensate waters to make them suitable for recycle, thereby minimizing process water requirements. The main emphasis is on physiochemical methods, particularly solvent extraction and stripping, for the removal of organics from these waters. Identification of the contaminating organics is a difficult but necessary step to permit development of appropriate solvents for their removal. In addition, exploratory studies have successfully examined simultaneous solvent extraction in removal of ammonia and acid gases by stripping.

The conversion of biomass to liquid fuels has been an area of considerable research and development within the Chemical Process Program over the past several years. Two main approaches have been taken. The first involves the liquefaction of biomass and peat. A bench-scale continuous liquefaction unit has been developed to evaluate the process steps and to determine the relevant engineering parameters and optimal conditions for reduction of the biomass with synthesis gas or H_2-CO mixtures. Low-severity liquefaction has been examined for dewatering wet substrates, such as peat. Catalytic hydrogenation has been used to increase the value of the product oils. The second biomass liquefaction approach is the biological conversion of wood and agricultural residues to ethanol. An enzymatic hydrolysis of these cellulosic materials has been developed to yield monomeric hexose and pentose sugars. These can be subsequently fermented to produce ethanol. Various high-rate fermentation processes have been developed, and novel processes for ethanol recovery which are less energy intensive than conventional processes are being examined.

The electrochemical energy storage program provides research to develop advanced battery systems for electric vehicle and stationary energy storage applications. General problem areas include identification of new electrochemical couples for advanced batteries, determination of technical feasibility of the new couples, improvements in battery components and materials, establishment of engineering principles applicable to electrochemical energy storage and conversion, and the assessment of fuel cell technology for transportation applications. Major emphasis is given to applied research which will lead to superior performance and lower life-cycle costs.

CHEMICAL LIQUEFACTION OF BIOMASS

Operation of the Continuous Bench-Scale Unit for Direct Liquefaction of Biomass*

C. Figueroa and H. G. Davis

There are several cogent reasons why a successful biomass liquefaction process is needed. Long-range reasons stem from the fact that biomass is the ultimate organic feedstock after most fossil fuels have been exhausted. There are also more immediate reasons.

In many parts of the world, various forms of biomass (wood or plants) can be grown on marginal land or are available as waste materials. Although some of these materials can be used directly as fuel, others are not suitable because of their high water content or low bulk density, or for other reasons. Solids are often difficult or inconvenient to feed into a reactor, whether it is a gasifier, boiler, chemical unit, or carburetor. Solids are also costly to store and transport. Liquefaction offers a chance to dewater and concentrate the diluted calories of biomass into a dense material which can be pumped as a liquid. This primary crude liquid is then available as a boiler fuel, feed to a gasifier, or feed to a refinery producing automotive fuels, solvents, and chemical feedstocks. In every case, the biomass oil replaces petroleum or natural gas, thereby reducing our dependence on imports.

So far, emphasis has been almost entirely on methods of producing the crude liquid economically. Emphasis in the United States has been on producing crude biomass oil from a single feedstock, Douglas fir wood; liquefaction of Douglas fir is the subject of this report. Extension of the findings to other woods and other forms of biomass, agricultural wastes, and energy plants should, however, be a relatively easy task.

As of the beginning of FY 1981, there was only one operational unit for direct liquefaction, the Albany process development unit (PDU) operated for DOE by the Rust Engineering Division of Wheelabrator-Frye. Rebuilding and improving the LBL bench-scale continuous liquefaction unit (CLU) were completed early in the second quarter of FY 1981. As of this writing, the CLU appears to be the only continuous direct liquefaction unit operating on biomass because the PDU was placed on stand-by condition in April 1981 after production of a sizable amount of oil by both the PERC (oil-slurry/recycle) process and the LBL (water-slurry/single-pass) process. While the CLU to date has operated only with water slurries of partially prehydrolyzed Douglas fir, there is no apparent reason why it cannot operate with water slurries of other biomass materials or of peat (low-rank fossil fuel).

During FY 1981, Rust Engineering Co. made two lengthy runs using the PERC process. The final run, TR-12, was particularly satisfying operationally, with excellent material balances and overall oil yields of about 53 weight percent from wood. Two somewhat less satisfactory runs, TR-10 and TR-11, were made with the LBL process. It was shown that both water and oil slurries can be preheated to reaction temperature in a direct-fired tubular preheater under turbulent conditions. This was a highly significant finding with regard to future commercialization.

Unfortunately, successful operation of the PERC process was reached at a very low feed concentration of wood flour, about 7.5 percent by weight in a slurry of recycle oil, recycle water, and catalyst (Na_2CO_3) solution. The oil recycle ratio was approximately 19 to 1, and there was also a large recycle of water. Thus, development of a single-pass process, such as the LBL water-slurry process, remains an important objective. The results obtained with the CLU during the summer of 1981 are described in this report. In two following reports, we discuss the chemistry of the reaction and the characterization of the products.

ACCOMPLISHMENTS IN FY 1981

In FY 1981, the LBL experimental program involved the rebuilding, operation, and maintenance of the continuous liquefaction unit. To support this program, we made an intensive effort to characterize both the oil and the water-soluble products of liquefaction. This study provided a much-improved knowledge of the chemical properties of the products. Most importantly, it resulted in advanced analytical techniques which enable us to

*This work was supported by the Assistant Secretary for Conservation and Solar Energy, Office of Solar Applications for Industry, Biomass Energy Systems Division of the U.S. Department of Energy under Contract No. DE-AC03-76SF00098 and was funded through Battelle Pacific Northwest Laboratory, Lead Laboratory for the U.S. Department of Energy, Biomass Energy Systems Division, Thermochemical Conversion Program under Contract No. DE-AC06-76LO 1830.

follow quantitatively the effects of process changes on product quality. Batch liquefaction experiments were conducted in stirred autoclaves to screen ideas, to test thoughts on mechanism, and to determine the effect of process water recycle. Efforts to study the prehydrolysis step were initiated. The phenomenon of "solvolysis" (dissolution of wood by appropriate solvents) was further studied. The results obtained at the Albany PDU were followed and analyzed for ideas about the chemistry of the liquefaction process.

Operation of the CLU

In the initial efforts to operate the CLU, a tubular reactor was employed (Fig. 1). Because of the small size of the equipment (the reactor was made of 1/4-in. I.D. tubing) and the flow regime, believed to be laminar, there was a serious problem of plugging. Runs were of short duration. Data from the runs that lasted long enough to be granted a run number are given in Table 1. The product collection system and reactor controls worked reasonably well. Problems of plugging by the heavy oil product downstream of the reactor were solved, but it was finally concluded that the scale was too small for a tubular reactor to work reliably. Because the operation at Albany had shown that a tubular heater does work at a scale where turbulent flow conditions can be maintained, it seemed inadvisable to spend further time trying to make the tubular reactor work at bench scale. It was therefore replaced with a one-liter autoclave, installed on-line as a stirred back-mixed reactor (Fig. 2). The feed, product-recovery, and pressure-letdown systems remain essentially as they were. The runs since the changeover have been much more successful. Data are given in Table 2. Some characteristics of oil products are given in the reports which follow.

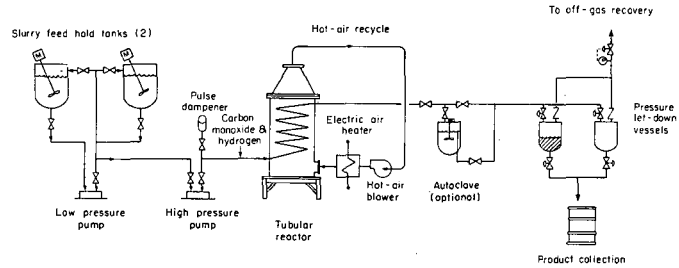

Figure 1. Biomass liquefaction process evaluation unit, LBL Process.

(XBL 7910-4293)

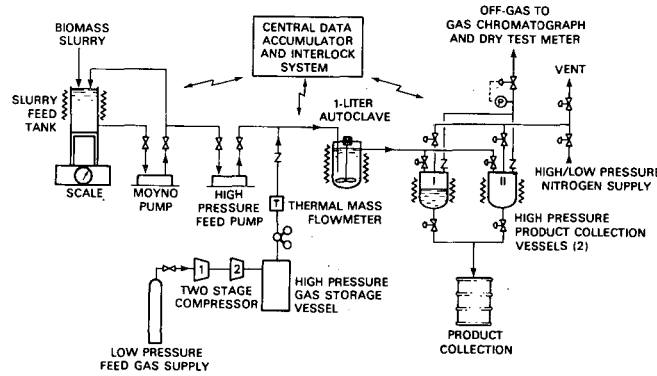

Figure 2. Biomass continuous liquefaction unit.

(XBL 817-1023)

Before discussing the detailed results, however, we need to make some qualitative observations. There is clearly phase separation in the reactor. The ratio of water to crude, heavy wood-

Table 1. CLU: Summary of runs with tubular reactor.

Run No.	Date	Total duration, (hr)	Temperature, (°C)	PSIG	Reaction time,[a] (min)	Reason for termination	Comments
A	6/28/80	0.5	340	3000	18	Gas leak	After second attempt, 7/80, decision made to rebuild.
B	3/13/81	1.0	345	3000	18	Reactor plug	Yield of recovered oil 26 wt %.
C	5/6/81	2.0	350	3000	9	Reactor plug	
D	5/15/81	1.0	350	3000	12	Reactor plug	
1	5/22/81	0.5	350	3000	7	Reactor plug	Down-flow reactor plug in exit lines.

[a]Reaction time estimated as (reactor volume)/(3 x slurry feed rate). In Runs B through 1, evidence of intermittent plugging: pressure drop swung, at roughly 1-minute intervals, from a low range of 30 to 100 psi to a high range of 80 to 300 psi.

Table 2. CLU: Summary of runs with back-mixed reactor.

Run No.	Date	Total duration, (hr)	Temperature (°C)	PSIG	Reaction time,[a] (min)	Slurry feed rate, (kg/hr)	Gas feed (l/min)	Mass recovery, (wt %)	Recovered oil yield, (wt %)	Reason for termination	Comments
2	6/28/81	1.5	350	3000	13	1.8	1.8	-	-	Plug	Plugging generally in exit lines where heavy oil congealed on cooling. Better control of line temperatures helped in later runs.
3	7/1/81	1	350	3000	13	1.8	1.8	-	-	Plug	
4	7/7/81	2	350	3000	17	1.4	1.6	80	24	Plug	
5	7/16/81	15	345	3000	18	1.3	1.6	92	20	Plug	
6	8/4/81	5	354	3000	29	0.8	1.6	100	15	Gas leak	Water completely vaporized; see text.
7	8/24/81	10	350	3000	15	1.6	2.2	91	31	Off-gas line plugged	
8	9/2/81	24	330	3000	26	0.9	1.6	100	32	Voluntary	
9	9/25/81	4	350	3400	23	1.0	1.0	-	-	Check valves not operating	Feed gas switched from H_2:CO = 1 to 100% CO for runs 9 on.
10	9/29/81	10	350	3400	21	1.1	1.0	95	27	Feed line plugged	Outlet gas composition: H_2, 35%; CO, 10% CO_2, 55%.

[a]Average residence time in CSTR assuming one-liter autoclave contains 350 g water + oil at reaction conditions.

Feed Slurry: Prepared 11/80 at Albany PDU; about 20% solids + wood-derived organics; pH (runs 2-8) 7-8; pH (runs 9-10) 8-9.

oil product is 10 to 1 or higher. To avoid a build-up of oil in the reactor and a resulting long residence time, violent agitation is necessary. The object is to maintain an oil-in-water emulsion with the oil droplets small enough and well enough dispersed to enable a uniform mixture of oil and water to be withdrawn.

It is also necessary that the exit port of the reactor enable the water phase and oil droplets to exit at rates proportional to the average oil concentration in the reactor. Failure to achieve these goals results in build-up of oil in the reactor. Although not necessarily harmful to the quality of the oil, this makes it difficult to calculate the oil residence time. It may also lead to coking.

Several observations made us realize we were not achieving a uniform oil and water dispersion in the early runs. Most important, very little product oil was obtained in samples collected at less than five hours after start, although reactor turnover times are estimated to be less than one-half hour. Also, at run termination, the oil/water ratio in the reactor was greater than 1 to 10. A similar phenomenon was noted in LBL-mode run Tr-10 at Albany, in which the reactor was the PDU 120-gallon autoclave. Several changes in the stirring were made without solving the problem. Visual observation of stirring water-heavy oil and water-sand mixtures led to the conclusion that a single propeller, pitched to throw oil upward, gave us as good or better stirring than any other turbine impeller or propeller type or combinations we examined. Starting with run CL-8, such a propeller has been used at maximum speed. The results indicate at least a reduction in oil build-up in the reactor.

Results of Tubular Reactor Runs

Some data for the runs made with the tubular reactor in place are given in Table 1. These experiments were primarily useful in teaching us how to run a small-scale reactor. The conclusions can be summarized as follows:

- Wood oil products similar to those made in the PDU (run TR-7) or in autoclaves can be made at 350°C outlet; minimum residence times should be greater than about 10 minutes.
- A downflow tubular reactor is less likely to plug rapidly than an upflow reactor.
- Any downstream line that is below about 70°C is also likely to plug with liquid product. Product cooling should be gradual; air cooling is safer than use of a water condenser.

Results of Back-Mixed Reactor Runs

Runs CL-2 through CL-10 were carried out in the back-mixed continuous reactor. The first really successful run was CL-5 (July 16, 1981), and the first runs with improved agitation were CL-9 (September 24, 1981) and CL-10 (September 29, 1981). The results of individual runs were sufficiently instructive to indicate that we should discuss them separately or in groups.

CL-2 to CL-4

In these runs, we mainly learned how to cope with the new mechanical and other operating problems of the revised reactor system. "Plugs" developed in feed lines from over-preheating, in take-off lines from congealed liquid product, or in valves from overheating. Once identified, these problems were controllable. Mass recoveries were poor because run times were short. However, oil samples were obtained, and it was possible to make comparisons with oil products made in the PDU or in the tubular-reactor runs.

CL-5

The overall run time was about 16 hours. Good samples were obtained, and the overall material balance was fair, about 92 percent. It was found that overly rapid release of pressure from the product recovery vessels leads to a loss of oil product by a foaming mechanism. Hence, in CL-5 a disproportionate amount of oil was contained in the 8 percent overall loss, and the actual oil yield was higher than the 20 percent shown in Table 2. A series of improvements in the letdown procedure corrected the loss problem, especially from run 8 on.

CL-6

Although CL-6 was a short run, aborted because of a system gas leak, there were interesting results. The aqueous effluent was found to be very low in titratable anion and, therefore, in sodium salts in general. This suggested that little or no water had exited from the reactor as liquid; on the contrary, it had left almost totally as vapor, leaving the sodium salts behind. Calculation showed (Table 3) that at reaction conditions of 3000 psig, 354°C, 0.8-kg/hr slurry feed, and 1.6-l/min synthesis gas, total vaporization of water could indeed be expected. Further, the small amount of oil product obtained had the lowest molecular weight and was the most fluid of any wood oil we have seen. Presumably, we were only recovering the vaporized lighter ends. Most oil remained in the reactor and coked.

CL-7

This was a good run at 350°C with synthesis gas and a moderate gas-to-slurry input ratio (1.72 Mol per 100 g wood or wood hydrolysate).

CL-8

This was the best run to date. It showed us that, at the reaction times available in the CLU (the liquid space-time was 60 minutes and the residence time about 30 minutes), the 330°C product is heavy and viscous and probably underreacted. If these are undesirable qualities, the range of temperatures which should be studied is fairly narrow, about 340-360°C. Because of the vaporization problem pointed out above, it is best to use 100 percent CO rather than synthesis gas to raise the total pressure somewhat for temperatures above about 340°C. These two steps reduce the ratio of fixed gas flow at reaction conditions to water flow and, therefore, the percentage of water which exits the reactor as vapor.

CL-9,-10

A single upward thrust propeller was used for stirring in these runs, and the feed gas was 100 percent CO. Shortly after the start of CL-9, the check valves on the gas produce line were found to be stuck in the open position. The run was stopped, double check valves in series were

Table 3. Vaporization of water from slurry reactor at 3000 psia.

Temperature, (°C)	Vapor pressure (psia)	Mols H_2O vaporized per Mol fixed gas[a]	Water, (6 Mol/hr fixed gas, 1 kg/hr water feed)		
			Vaporized	Unvaporized	
			Grams	Grams	cm^3
320	1540	1.1 - 1.8	157	843	1190
330	1860	1.6 - 2.7	232	768	1200
340	2120	2.4 - 4.3	362	638	1050
350	2410	4.1 - 8.1	650	350	615
360	2708	9.3 - 20.8	1000	0	0
370	3050		1000	0	0

[a]Based for approximate calculation: Partial pressure fixed gas - 3000 - V.P. (H_2O);
Low value Mol (H_2O)/Mol (fixed gas) = V.P. (H_2O)/partial pressure (fixed gas.
High value = Low value · Density (real water vapor)/density (H_2O, perfect gas).

installed, and run CL-10 was started. With 100 percent CO as the gas feed, it was immediately apparent that the water-gas shift was occurring to a considerable extent. Also, substantial amounts of formate ion were formed in the aqueous layer. Shortly after start-up, the molar gas composition lined out, at 10 percent CO, 35 percent H_2, and 55 percent CO_2. The pressure ratio $H_2 \cdot CO_2/(H_2O \cdot CO)$ is estimated to be about 1, compared to an equilibrium constant at 350°C of 20, so that water-gas shift equilibrium is approached but not reached. Some additional carbon dioxide, calculated for run 10 to be about 2/3 Mol/hour, is dissolved in the liquid phases. This is significant in the material balance but not in the shift reaction pressure ratio.

CONCLUSIONS

- Operation of the CLU was achieved in a back-mix mode. Plugging problems were determined to be insurmountable in the tubular reactor under laminar flow conditions.
- Operation below about 340° led to a heavy viscous oil product. The degree of shift reaction was shown to be a function of the amount of alkaline catalyst (Na_2CO_3) present in the feed slurry. Whether this was significant for reduction of wood-oil oxygen by CO remained an open question (see following reports).
- At temperatures near 360°C, operation is made difficult by the high percentage of slurry water vaporized in the reactor at 3000 psig.
- The CLU is available for experimentation with water slurries of other forms of biomass.

PLANNED ACTIVITIES FOR FY 1982

A partial factorial-designed set of experiments has been set up for operation in FY 1982. With reduced funding, it may not be possible to complete this set, and we plan to proceed along a path of selected experiments within the general pattern. Important variables include:

1. Composition of process gas. If, in the LBL process, little or no CO is used as reducing agent, perhaps an alternate reducing gas (H_2) or an inert gas (CO_2 or N_2) can be used, or no gas, other than steam, may be needed. Since much CO is reacted by the water-gas shift, its replacement as process gas has great economic advantages.

2. Slurry pH (or sodium carbonate content). In FY 1981, although we showed that increased sodium carbonate led to increased shift reaction, we could detect little or no effect on the liquefaction reaction or product. Lower carbonate content, which also has an economic advantage, will be tested.

3. Slurry concentration. In experiments to date, we have used slurry from a large batch prepared at the Albany PDU, with about 19 percent total wood solids. More concentrated slurries, up to 30 percent or more solids, will be prepared in a 10-gallon autoclave installed in FY 1981 for this purpose. Again, the advantage of higher concentrations is economic.

4. Other variables already under study. Reactor temperature, total pressure, residence time, and process gas/wood ratio will be further studied. An important experiment will incorporate finely divided hydrogenation catalyst with H_2 as process gas. Use of a two-stage back-mixed reactor, or a back-mixed reactor followed by a tubular reactor, is an interesting possibility. However, this probably will be eliminated for budgetory reasons.

5. Alternate feedstocks. At least one or two runs with a slurried alternate biomass form are planned. Available biomass forms include rice straw, rye-grass straw, sugar-beet residues, and Jerusalem artichokes.

Characterization of Products from Direct Biomass Liquefaction*

L. L. Schaleger, D. Kloden, and H. G. Davis

By the end of FY 1980, it was clear that oil made by the direct liquefaction of Douglas fir wood chips was very different from petroleum and from the coal liquefaction product. Although very low in the elements nitrogen and sulfur, wood oil contains much oxygen, 8 to 20 percent by weight, and little or no hydrocarbon. It was known that a high percentage of the oil is aromatic and phenolic and that there are ketones and ethers present. Many individual compounds had been identified, but most of the work was highly qualitative. This group's objectives in FY 1981 included developing quantitative methods of separating the product oil into fractions by polarity, determining molecular weight distributions, and identifying key components at least semi-quantitatively. The primary purpose of this effort was to develop methods of following the effects of liquefaction-process variables on product characteristics. The methods should, of course, also permit a better understanding of the product and of the problems of further refining and end use.

Some of the product was known to be water-soluble and to exit the process dissolved in effluent water. It was also known that this was more significant in the water slurry, or LBL, process than in the oil slurry, or PERC, process. Again, however, little that was truly quantitative was known, and it appeared to be important that the water-soluble products be identified for possible recovery or disposal.

ACCOMPLISHMENTS IN FY 1981

Characterization of Products from CLU and PDU Runs

We have used several characterization techniques, besides the usual elemental analysis, to characterize the oil product of liquefaction. These include:

- GC-MS to identify key compounds and also compound types.
- Liquid column chromatography by the SESC[1] technique to separate the crude oil product into fractions according to polarity.
- Gel-permeation chromatography, using HPLC instrumentation, to estimate molecular-weight distribution of whole crude oil and of SESC fractions.
- A specific column chromatographic technique devised[2] to separate biomass oil products by acidity and molecular weight into several phenolic and non-phenolic fractions.

Through the GC-MS technique, we have made credible identifications of all major and many minor gas chromatographic peaks in whole oil samples. This covers compounds boiling up to about 300-350°C, perhaps 30 to 40 percent of the whole oil. Details of the procedure and identification are currently being prepared and will be presented in a later report.

The SESC technique, originally developed for coal-derived liquids by Farcasiu[1] and others at Mobil, has been especially useful in determining differences among various wood oil samples. The method we have adopted employs a specially prepared silica gel column. An oil sample (~ 2g), suspended with silica gel in hexane and/or benzene, is added to the top of the column. Sequential washings with nine solvents remove portions of the oil according to increasing polarity. After evaporation of solvent, the recovered fractions are weighed, and a reasonably good material balance can be obtained. Generally, the recovery is 85 percent by weight plus, and recoveries of less than about 80 percent indicate the presence of fractions of extremely high polarity and/or of molecular weight above about 1500-2000. Some properties of typical eluted fractions are shown in Table 1.

Table 2 shows data collected for a number of oil samples made in the CLU or PDU. Also included are average molecular weight results obtained by the gel-permeation technique (HPSEC). Considerable information, such as the following, can be determined from this table:

- The two runs with the lowest proportion of F1-F5 are CL-8 and TR-10, which also had the

Table 1. Molecular weights of CLU-6 SESC fractions by HPSEC.[a]

	F1, 2	F3	F4	F5	F6	F7-8	
						LMW	HMW
$(\bar{M}_n)^b$	143	172	173	210	350	181	687
$(\bar{M}_w)^c$	158	210	211	286	604	195	892
$(P.D.)^d$	1.10	1.22	1.22	1.36	1.73	1.08	1.30

[a]Each number represents the average of 2-4 determinations made at two different wavelengths, 254 and 280 nm, and on different days.
[b]Number average molecular weight.
[c]Weight average molecular weight.
[d]Polydispersity (= $\bar{M}_w/\bar{M}_n$).

*This work was supported by the Assistant Secretary for Conservation and Solar Energy, Office of Solar Applications for Industry, Biomass Energy Systems Division of the U.S. Department of Energy under Contract No. DE-AC03-76SF00098 and was funded through Battelle Pacific Northwest Laboratory, Lead Laboratory for the U.S. Department of Energy, Biomass Energy Systems Division, Thermochemical Conversion Program under Contract No. DE-AC06-76LO 1830.

lowest total recovery and probably the highest molecular weight (CL-8 not completed at this writing). The highest severity LBL run, CL-6, has the highest proportion of F1-F5, 100 percent recovery, and the lowest average molecular weight. As discussed above, we believe this sample was vaporized from the reactor, leaving heavy ends (F6-F9 and residue) behind.

- Oils from CLU runs made at 350°C begin to approximate the better quality PDU oils, TR-7 and TR-12. Differences in the F1 to F5 distribution can be attributed to the much higher residence times in the PDU, especially in PERC mode runs such as TR-12 (oil recycle ratio about 19 to 1).

- Unless we approach liquefaction as a simple dewatering operation leading to a heavy bitumen and a decantable water phase, the temperature range for study should be 340°C and up, or we will make large amounts of very polar, high-molecular-weight material.

The HPSEC or gel-permeation molecular weight procedure has been useful in following the SESC fractions and in comparing the average molecular weights and polydispersities of oils made in various ways. Typical results are shown in Tables 1 and 2. The technique used gives a broad distribution rather than individual peaks. However, particular samples may show bimodal distributions. This is true of samples from PDU run TR-8, where the residual start-up anthracene oil gives a definite early peak. The SESC fractions F6 and F7-8 show a high degree of polydispersity (Table 1). In F6, a shoulder on the chromatogram cannot be resolved, but F7-8, at least for the product of CL-6, is definitely bimodal. Typical HPSEC curves are shown in Figures 1, 2, and 3. Complete descriptions of the HPSEC and SESC procedures are given in the LBL Quarterly Reports.[3,4]

Table 2. SESC fractionation of biomass oils.

	Sample							
	CL4-3[a]	CL5-3[a]	CL-6[a]	CL7-3[a]	CL8-4[b]	TR7[b]	TR10[b]	TR12[b]
Reactor temperature (°C)	345	350	354	350	330	~330	~330	>350
Fraction								
F1	-	-	-	-	-	-	-	-
F2	3%	1	6	1	1	1	1	6
F3	2	5	9	2	2	16	6	12
F4	13	21	28	19	5	39	17	21
F5	47	46	41	50	37	19	35	34
F6	13	10	3	15	26	14	19	14
F7	-	-	-	2	2	1	-	-
F8	11	16	13	5	10	6	6	2
F9	-	-	-	-	-	3	4	-
% F1 - F5	65	73	84	72	45	75	59	73
% TOTAL	89	99	100	94	83	99	88	89
$\bar{M}_n$	271	213	176	242	-	215	286	240
$\bar{M}_w$	483	319	232	384	-	306	467	370

[a]Methanol-chloroform extract.

[b]Raw oil. Note: Oil samples are generally about 98-99% soluble in the methanol-chloroform mixture.

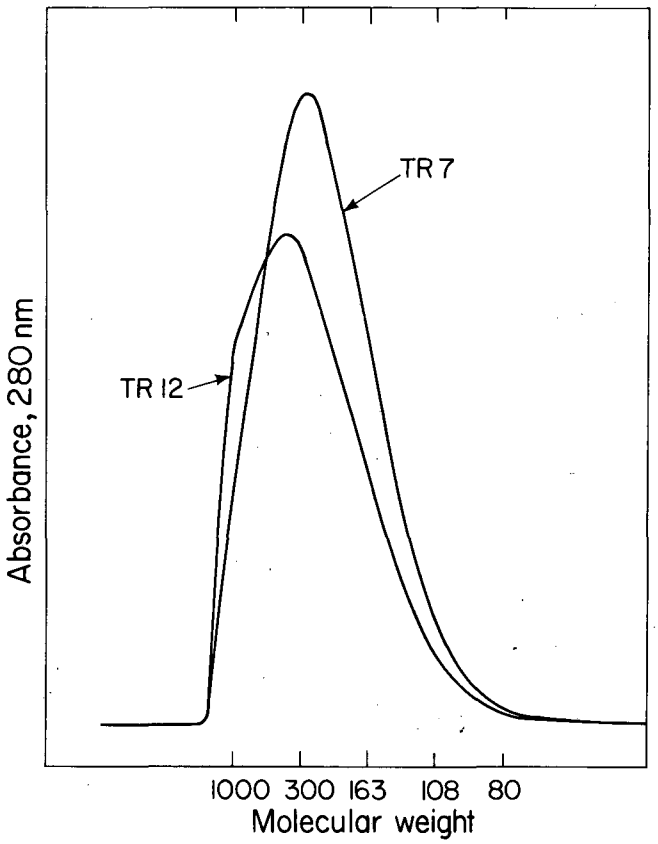

Figure 1. HPSEC of biomass oil, exclusion limit 1000.

(XBL 8110-1422)

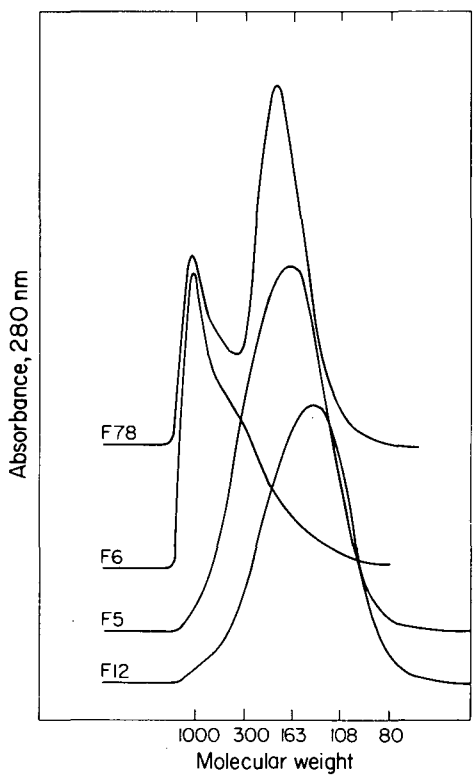

Figure 2. HPSEC of CL6 SESC fractions, exclusion limit 1600.

(XBL 8110-1421)

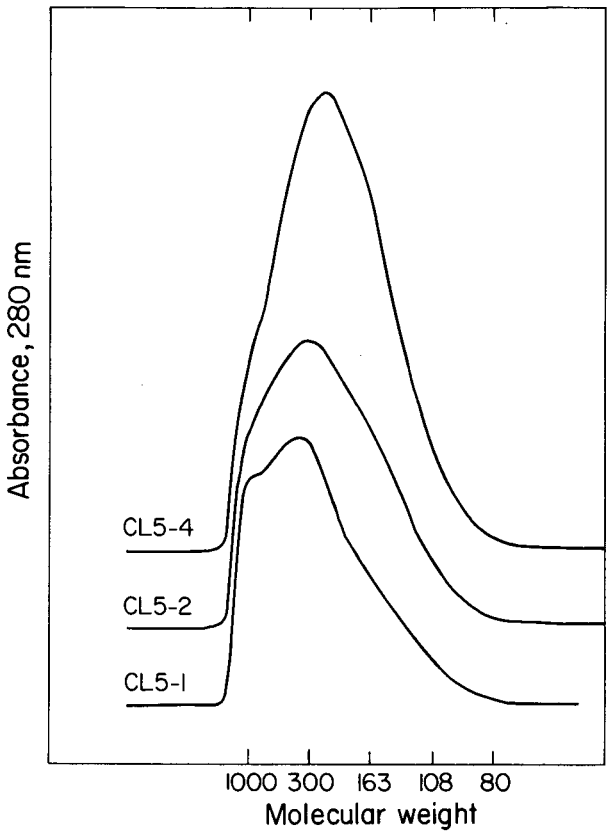

Figure 3. HPSEC of CL5 oils, exclusion limit 1600. (XBL 8110-1420)

Characterization of Water-Soluble Products

Whether liquefaction is run in the LBL mode (water-slurry feed) or in the PERC mode (wet oil slurry plus aqueous catalyst), there is a large amount of aqueous effluent. In the LBL mode, a prehydrolysis step results in the solubilization of approximately 30 percent of the input solids. Thus, a substantial part of the overall liquefaction process must take place within the aqueous phase. In fact, the aqueous streams of both the PERC and LBL modes contain fairly large amounts of organics which pose a difficult recovery or a serious disposal problem. For these reasons, we have undertaken an investigation of several aspects of the chemistry of the aqueous phase, including a study of the stoichiometry of prehydrolysis, a detailed examination of the acid-base chemistry of aqueous process effluent, and a preliminary study to speciate and quantify major constituents of the water phase.

Prehydrolysis. Douglas fir wood has cellulose, hemicellulose, and lignin contents of about 41, 26, and 28 percent, respectively. The remaining 5 percent includes uronic acid moieties, extractives, acetyl groups, and ash. Acid hydrolysis of wood chips of 1 1/4 inch nominal length at about pH 2.0 and 180°C for 45 minutes results mainly in the hydrolysis of the hemicellulose fraction. Hydrolysis accompanied by vigorous agitation also causes near total breakdown of the fibrous character of the lignocellulosic residue. The resulting solids consist of small particles, half of which are less than 5 mm in diameter, and friable, partially hydrolyzed chips. These larger pieces are readily comminuted by passage through a disc refiner or colloid mill to give a slurry with a consistency similar to that of a milk shake. Slurries containing 20-30 percent total solids show little tendency to settle; they can be pumped into and through a liquefaction reactor.

Hemicellulose is almost completely hydrolyzed under these conditions, but cellulose is only slightly hydrolyzed. The aqueous phase contains reducing sugars; formic, acetic, and levulinic acids, plus traces of other acids; sugar degradation products such as furfural; and other organics.

Batch autoclave runs were made with the aqueous liquor and the washed solids from prehydrolysis treated separately with CO. Water-soluble products and oil were made from both substrates. However, the greater part of the oil is formed from the solids and the greater part of the water-solubles from the aqueous portion. Under the batch conditions, roughly 20 percent of the water-soluble organics wound up as oil and about 45 percent as carboxylic acids, the remainder being other water soluble organics and a small amount of CO_2. About 60 percent of the carboxylic acid product was already present in the prehydrolysate. The general conclusion is that 80 percent of the total oil product comes from the solids and 20 percent from aqueous liquid, with about 70 percent of the water-solubles arising from aqueous liquid and 30 percent from the solids.

Acid-Base Titrations. In the Albany PDU operation, the aqueous effluent exits as two streams: an aqueous condensate, recovered by cooling vapors obtained after the main pressure letdown valve, and a liquid aqueous effluent collected with the wood-oil product. The condensate contains water-soluble, volatile, light organics, both acidic and nonacidic. The liquid effluent contains similar materials that are, on average, less volatile and of higher molecular weight. Since the liquid aqueous effluent is recycled with the oil product in the PERC runs, samples of the PDU stream are likely to be quite high in organics. Since these are largely sodium salts of acetic and other acids, the specific gravity is high. Rust Engineering personnel report a range of about 1.15 to 1.25.

A number of aqueous effluents have been titrated with aqueous sodium hydroxide to determine free acid and with hydrochloric acid to determine carboxylates. The general conclusion is that the acid plus anion content is substantial, about 0.2 to 0.5 gram equivalent per kilogram for single-pass total aqueous effluent. Also, the yield of acid plus anion is a significant part of the total material balance, 4 to 10 percent or more of the dry wood feed.

Samples of the two effluent streams from PDU run TR-12 (PERC mode)[5] were titrated to pH around 8-9 with 1N NaOH, then back-titrated with 1N HCL to determine total acid plus anion. As the overhead condensate contained no anion, the acid and base titers were nearly identical. As the liquid aqueous effluent was recovered with pH > 7, it contained very little free acid. Figure 4 shows the results of potentiometric titrations of the anions

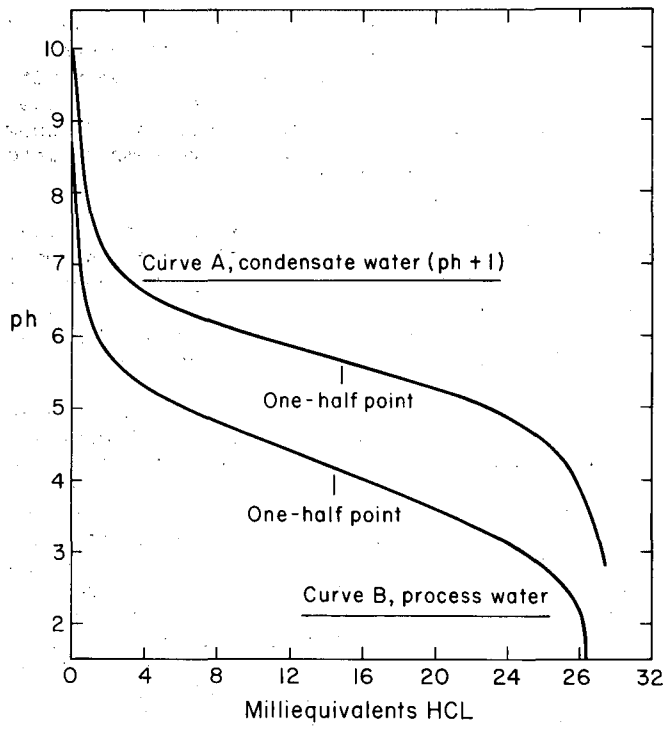

Figure 4. Results of potentiometric titrations of anions with HCl.

(XBL 815-810)

with HCl.

Because the recycle ratio was high and most of the acids were retained in the slightly alkaline bottom water, the anion concentration increased to a high level. Total organic carbon was determined as 14.3 percent, and the sodium carboxylate content was about 35 percent. Nonacid organics, extracted with chloroform and recovered by evaporation, were 1.3 percent, but much of this fraction was lost by failure to extract or by volatilization during evaporation. From the organic carbon and the elemental analysis of the acidic components, we estimate the total neutrals content at about 3 percent by weight.

The curves for HCl titrations of both bottom and condensate waters are shown in Figure 4. Because the concentration of acids in the condensate was low, we titrated a large sample; the amount of titrant was multiplied by 5 before plotting. Both curves in Figure 4 have been corrected for the excess 1N HCl required to reach the low values of pH near the end point. The half-titration point of the upper curve (condensate water) is at about pH 4.65, roughly equal to the pK_a of acetic acid, 4.75. As expected, the small amounts of organic acid that rise with product vapor are simple, volatile carboxylic acids.

The lower curve has a half-titration point at about 4.15 and a very broad, straight region between about 4.9 and 3.5. This type of curve is typical of all those we have obtained with total or bottom water products from the CLU, the PDU, or both laboratory samples. It indicates that a significant proportion of the acids present is much stronger than acetic acid, succinic acid, or their homologues. Such acids could be alpha-substituted acids (e.g., glycolic acid, pK_a = 3.8, citric, first ionization 3.1, etc.). A significant part of the strong acid component has now been shown to be formic (pK_a = 3.75), including a high percentage of the total in the TR-12 recycle water. As of this writing, we are looking for an improved, quantitative analytical procedure. However, single-pass water effluents from CLU runs appear to be 0.03 to 0.2 in formate ion. Table 3 shows elemental analyses of some materials recovered from aqueous effluents. The water-soluble materials, whether acidic or neutral, have oxygen contents comparable to that of the original wood.

Also shown in Table 3 are total organic carbon analyses and acid plus anion contents determined on several product waters. A very rough estimate of the non-acidic content of the waters can be made from the total organic carbon, the estimated percent acid plus anion, and information about the equivalent weight and carbon analysis of the acid/anion fraction. This is generally more than we have been able to recover by extraction and evaporation. However, this was not surprising because many of the compounds are highly hydrophilic, highly volatile, or both.

The equivalent weight of product carboxylic acids has been estimated in several ways:

1. A sodium carboxylate solution (e.g., the bottom water from PDU run TR-12) is titrated to determine the equivalents present and then evaporated and weighed. Waters from several runs gave values from ~79 to ~85. The highly concentrated TR-12 water was run twice, giving 78 and 85, with probable errors tending to raise the result rather than lower it.

2. The dried sodium carboxylate from TR-12 water was analyzed for sodium. If one assumes one Na per carboxyl, the calculated

Table 3. Liquefaction of Douglas fir wood: analyses of soluble organics in aqueous streams.

SAMPLE	Total Organic Carbon, wt %	Acids + Anions[a] wt%	Acids + Anions[a] wt% carbon	Estimated neutrals[c] wt %
Batch, 0 min, 330°C	4.70	4.6	2.2	5.0
Batch, 60 min, 330°C	2.92	3.3	1.3	2.6
Batch, 0 min, 360°C	2.72	2.7	1.3	2.8
Batch, 0 min, 340°C water recycled	-	5.6	2.6	-
Continuous, 20 min 350°C, laboratory	1.60	1.54	0.74	1.7
Water from wood used in continuous slurry run	3.57	1.29	0.62	6.0
PDU-TR-10 Bottom water, LBL run no recycle	1.96	2.80[b]	1.34[b]	1.2
PDU-TR-12 Bottom water, PERC run, recycle	14.3	27.0[b]	12.7	3.2
PDU-TR-12 Condensed overhead water	3.56	0.43	0.21	6.7

[a]From titration with equivalent wt = 80, % C in acids = 48, in neutrals = 50.

[b]Sample 7 - Extracted acids (1.9% of sample) had C - 53.5, H - 6.8, O - 39.7%
Sample 8 - Total acid from sodium salt had C - 47.2, H - 6.9, O - 45.9%
Sample 7 - Extracted neutrals (0.8% of sample) had C - 56.6, H - 6.65, O - 36.7%

equivalent weight is 79. Extracted acids from run TR-10 were titrated with NaOH solution. The result obtained, 93, is expected to be high because of loss of volatiles in evaporation and light or dicarboxylic acids in the extraction. A value of 80 should be reliable to perhaps ± 5 for the overall aqueous carboxylic acid product.

Major Components of the Aqueous Phase. Analysis by capillary GC-MS of ether, methylene chloride, or chloroform extracts of aqueous process waters reveals the presence of many of the same neutrals and phenols found in product oil. This is not surprising because these oxygenated species all exhibit partial water solubility. However, a large part of the water-soluble organic fraction consists of carboxylic acids, a large number of which have been identified as their methyl esters by GC-MS. A list of some of the major acids that we have thus far been able to identify is given in Table 4.

Table 4. Some acidic components of the water soluble product.[a]

Monocarboxylic acids	Dicarboxylic acids	Oxo- or hydroxy-acids
Acetic	Succinic	Levulinic
Propionic	Glutaric	2,3-Dihydroxybenzoic
Butyric	Methylsuccinic	4-Oxohexanoic
Isobutyric	Adipic	Glycolic
Palmitic	2-Methylglutaric	

[a]Identifications were made by capillary GC-MS of the methyl esters.

PLANNED ACTIVITIES FOR FY 1982

In FY 1982, we plan to apply the techniques learned in FY 1981 to the products now coming from the regular CLU runs. We anticipate some improvement in analyses for specific acids such as formic and acetic, probably using HPLC techniques. We also expect to improve both the SESC and the HPSEC techniques.

REFERENCES

1. Farcasiu, M. (1977), Fuel 56, pp. 9-14.

2. Davis, H., et al. (1980), Catalytic Biomass Liquefaction Quarterly Report to U.S. Department of Energy, Nov. 1980, Lawrence Berkeley Laboratory Report LBID-314.

3. Davis, H., et al. (1981), Research and Development Activities on Direct Liquefaction Technology, Quarterly Report July-September 1981, Lawrence Berkeley Laboratory Report LBID-458.

4. Davis, H., et al. (1981) Research and Development Activities on Direct Liquefaction Technology, Quarterly Report April-June 1981, Lawrence Berkeley Laboratory Report LBID-426.

5. Rust Engineering Co. (July 1981), Technical Progress Report, Test Run Number 12.

Chemistry and Mechanism of Wood Liquefaction*

H. G. Davis, L. L. Schaleger, and N. Yaghoubzadeh

Two procedures for direct liquefaction of wood have been tested on a process development unit at DOE's Albany, Oregon, Process Development Unit (PDU). Extremely smooth operation at a production rate of about 50 gallons wood-oil product per day was achieved in February-March 1981 by the oil recycle or PERC process.[1] Successful operation, however, required an extremely dilute slurry and, therefore, a very high recycle ratio of about 19 parts of recycle to 1 part of net make. The feed slurry also contained two or three parts of water per part of wood-flour feed. Substantial quantities of oil product were also made by the single-pass water slurry, or LBL process. The PDU was not well-adapted to the water-slurry process, and there were operating problems involving phase separation, plugging, and coking. Also, there were indications that the chemistry might be different in the two processes.

During 1981, the bench-scale continuous liquefaction unit (CLU) at LBL became operative;[2] and successful runs, which throw light on these questions, have been made. Also, several batch autoclave tests bearing on the chemistry were made.

The objective of this report is to clarify the stoichiometry of liquefaction, especially as it differs between PERC and LBL processes, and to discuss the role of reducing gases (CO, H_2, or both) in the LBL process.

Since the PDU was shut down and placed in stand-by condition in April 1981, the CLU is currently the only operational continuous unit used

*This work was supported by the Assistant Secretary for Conservation and Renewable Energy, Biomass Energy Technology Division of the U.S. Department of Energy under Contract No. DE-AC03-76SF00098 and funded through Battelle Pacific Northwest Laboratory, Lead Laboratory for the U.S. Department of Energy, Biomass Energy Technology Division, Thermochemical Conversion Program under Contract No. DE-AC06-76LO 1830.

for biomass liquefaction.

ACCOMPLISHMENTS DURING FY 1981

Stoichiometry of PERC and LBL Runs

The excellent material balances achieved by Rust Engineering Company in PDU run TR-12 enable us to make a much more satisfactory estimate of the stoichiometry of the PERC process than was previously possible.[3,4] Carbon monoxide appears to react definitely as a reducing agent removing oxygen from intermediate products. As is well-known, it also reacts with water in the water-gas shift reaction to form CO_2 and H_2. At the highest temperatures used in TR-12, the TR-12 stoichiometry may be compared with an approximate stoichiometry for LBL process CLU run CL-11 (Table 1). Not shown in Table 1 is the amount of CO reacted to form H_2 and CO_2 by the shift reaction, about twice as much as was used in reducing wood oil or about 1.1 to 1.2 M/100 lb wood.

In the LBL process, three major differences appear:

1. The yield of water-soluble product is much higher and therefore the oil yields are lower;
2. There does not seem to be much, if any, utilization of CO (except by shift reaction); and
3. It is difficult to get to as low an oxygen content as in the PERC process.

All of the above might be expected when we compare a single-pass process, having residence times of the order of 15 to 30 minutes, with a recycle process, with average residence times for oil of the order of 300 minutes. Nevertheless, items (1) and (3), especially (1), are serious problems.

Item (2), except as it may be a cause of the high residual oxygen content, is a net gain. If no CO is used, it should be possible to replace CO with H_2 or even an inert gas. Indeed, runs in early FY 1982 indicate that H_2 can replace CO in the LBL process, with no apparent difference in results. Since there is now no shift reaction, there is virtually no H_2 utilization and, therefore, only minor process-gas cost.

A comment must be made on the 43-percent-by-weight oil yield shown by the LBL process. Actual recoveries in the CLU also have not been above 35 percent thus far and have been quite variable, down from 35 percent. Because of the water dilution, there are probably losses in both the primary recovery and the final oil/water separation. The laboratory procedure for the latter involves a solvent work-up ending in vaporization of solvent and final traces of water. Some volatile product is lost, perhaps 3 percent or more of the weight of the feed wood. The viscous product oil foams during the pressure letdown required for primary recovery, and some may be lost, although efforts to strip oil from effluent gas have been unsuccessful. Because the oil certainly coats all available surfaces, small amounts may be lost through vent lines. Finally, coke formation, which has varied somewhat randomly from 0.3 to 10 percent by weight and therefore seems to be a function of operating problems rather than basic process chemistry, results in a loss of oil. It seems unlikely that the true total water-insoluble product, at 17 per-

Table 1. Stoichiometry comparison of PDU run TR-12 and LBL Process run CL-11 (Input and Yield in lbs).

PDU run TR-12				LBL Process run CL-11			
Input		Yield		Input		Yield	
Wood	100	Oil	52	Wood	100	Oil	42.8 (+ char)
C	51.0	C	41.0 78.8%	C	51.0	C	32.5 75.9%
H	5.8	H	4.3 8.2%	H	5.8	H	3.0 7.0%
O	43.0	O	6.4 12.3%	O	43.0	O	7.3 17.1%
CO	16.8 (0.60M)	CO_2	48.4 (0.47M)	CO	±0.0	CO_2	24.0 (0.55M)
C	7.2	C	13.2			C	6.5
O	9.6	O	35.2			O	17.5
		Water solubles	8			Water solubles	24.0
		C	4.0			C	12.0
		H	0.6			H	1.8
		O	3.4			O	10.2
		H_2O	8.4 (0.47M)			H_2O	9.0 (0.5M)
		H	0.9			H	1.0
		O	7.5			O	8.0
Total input		Total yield		Total input		Total yield	
C	58.2	C	58.2	C	51.0	C	51.0
H	5.8	H	5.8	H	5.8	H	5.8
O	52.6	O	52.5	O	43.0	O	43.0
	116.6		116.5		99.8		99.8

cent oxygen, is much under 40 percent by weight.

Mechanism of CO Reaction

Paradoxically, while seemingly showing that CO is not used up as a wood-oil oxygen reducing agent, we have shown that the putative intermediate for this reduction, formate ion, is indeed formed and decomposed readily at operating conditions. Qualitative tests have indicated significant formate ion is present in all our slurry feeds and effluent waters. It must be concluded that formate is involved in the shift reaction but that its presence, formation, and decomposition do not guarantee that CO will reduce wood-oil oxygen.

- A one-molar aqueous solution of sodium formate was held at 350°C for 30 minutes under pressure of CO and steam (CO cold pressure 800 psig). The water-gas shift was catalyzed so that the final gas analysis was 43 percent H_2, 30 percent CO_2, and 29 percent CO; there was a net conversion of 30 percent of the formate to bicarbonate.

- After similar treatment of 0.2M sodium carbonate solution, the product mixture was found to be 75 percent formate and 25 percent bicarbonate. Again, the gas analysis was much changed from the initial 100 percent CO to 39 percent H_2, 33 percent CO_2, and 28 percent CO, showing that the water-gas shift had been catalyzed.

- Two slurry liquefaction runs were made under much less severe conditions: 50 percent H_2, 50 percent CO, 340°C, zero reaction time. In one, 10 percent sodium formate by weight of the slurry was added. Analysis of products showed that a fraction, probably about one-third, of the formate reacted. The final gas analyses were 46.8 percent H_2, 12.5 percent CO_2, and 40.7 percent CO in the runs without formate, and 51.2 percent H_2, 20.1 percent CO_2, and 28.7 percent CO in the runs with formate. The lower percentage of carbon monoxide in the second case shows increased catalysis of the shift reaction.

The rapid interconversion of bicarbonate and formate under reaction conditions permits interpretation of the differences between runs CL-7 and CL-10, both at 350°C. Between runs 7 and 10, additional sodium carbonate, about 0.08M/kg water phase, was added to the slurry, and the reaction gas was changed from 50 percent CO and 50 percent H_2 to 100 percent CO. Outlet gas analyses in runs 7 and 10 were 54 and 35 percent H_2, 31 and 55 percent CO_2, and 16 and 10 percent CO, respectively.

Clearly, the shift reaction was strongly catalyzed during run 10, and the excess carbonate was largely converted to formate ion.

PLANNED ACTIVITIES FOR FY 1982

The FY 1981 experience has already led to using H_2 as a replacement for CO in the LBL process. Further experiments are planned at a variety of slurry pH's and concentrations and over a range of temperatures and residence times. Elimination of all reducing gas will be tested.

When hydrogen is used, the presence of a standard hydrogenation catalyst may be desirable. Experiments are planned with small amounts of very finely divided catalyst, e.g., molybdenum, nickel, iron, and chromium.

An improved formic acid analytical technique is being developed. This should permit quantitative comparison of the dependence of formate ion on the conditions of operation and thus throw further light on its production mechanism.

REFERENCES

1. Rust Engineering Co. (1981), Technical Progress Report, Test Run Number 12, July 1981.

2. Davis, H. et al. (1981), Research and Development Activities on Direct Liquefaction Technology--Quarterly Report, July-September 1981, Lawrence Berkeley Laboratory Report LBID-458.

3. Davis, H.G., Kloden, D.J., and Schaleger, L.L., (1981) Chemistry and Stoichiometry of Wood Liquefaction, 3rd Symposium on Biotechnology in Energy Production and Conservation, Gatlinburg, Tenn., May 13-15, 1981, paper 13, Biotechnology and Bioengineering Symposium Series, Lawrence Berkeley Laboratory Report LBL-12202.

4. Davis, H.G. (1980), Stoichiometry of Wood Liquefaction, Lawrence Berkeley Laboratory Report LBL-11776.

FUELS FROM BIOMASS BY BIOCHEMICAL PROCESSES

Ethanol Production and Recovery from Biomass Sugars*

H. W. Blanch, C. R. Wilke, B. L. Maiorella, and T. K. Murphy

RECYCLE OF BY-PRODUCTS AND INHIBITION STUDIES

Inhibition by secondary fermentation products may limit the ultimate productivity of new glucose to ethanol fermentation processes. New processes under development will selectively remove ethanol from the fermenting broth to eliminate ethanol inhibition effects. High productivities have been projected, but these projections neglect the possibility that these processes may concentrate minor secondary products to the point where they become toxic to the yeast.

Using a laboratory vacuum fermentation, Cysewski found that the buildup of some nonvolatile inhibitor(s) limited the ultimate productivity of the fermentation.[1] In the vacu-ferm process, the fermentation is conducted at reduced pressure, approximately 50 mm Hg. Ethanol is boiled off at/or 35°C as it is produced, maintaining the beer ethanol concentration at below 3.5 weight percent. Ethanol end-product inhibition is alleviated, and the specific ethanol productivity (g ethanol/g cells-hr) is increased. A concentrated glucose feed can be fully converted to ethanol. The product leaves as a concentrated vapor stream, thus reducing distillation costs. Cells grow during fermentation but cannot escape the fermentor in the vapor product stream. Therefore, the yeast density increases, further increasing the fermentor productivity.

Figure 1 shows the results of a continuous vacuum fermentation of a 334 g/l glucose feed solution. Cell density and fermentor productivity increase for the first 40 hours of operation, with a maximum ethanol productivity of 44 g/l-hr, ten times the average for a conventional batch fermentation. After 48 hours, however, the density of viable cells and, hence, the productivity sharply declined. The sharp decline in viable cells after two days is indicative of the buildup of some nonvolatile components to a level toxic to the yeast.

To assess the potential effects of major by-products on new fermentation processes, by-product production rates, and inhibition levels in continuous fermentation with Saccharomyces cerevisiae have

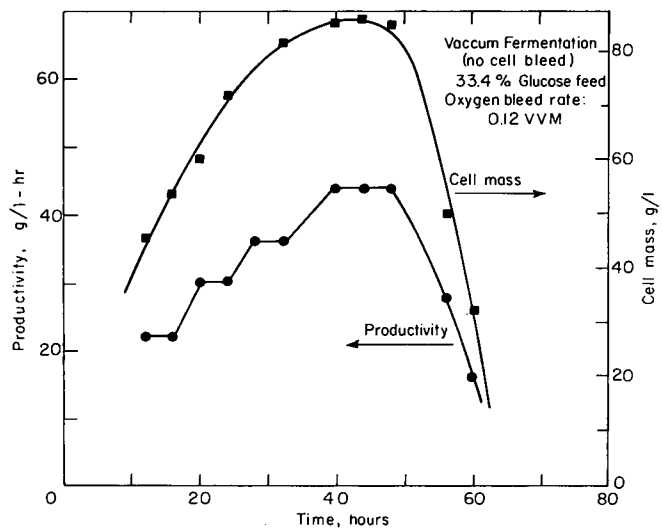

Figure 1. Continuous vacuum fermentation (after Cysewski[1]).

(XBL 761-6164)

been determined for acetaldehyde; glycerol; formic, lactic, and acetic acids; 1-propanol; 2-methyl-1-butanol; and 2,3-butanediol.

The observed inhibition effects are well illustrated in the case of acetic acid, which inhibits in the range from 0.5 to 9 g/l, (Fig. 2).[2] Acetate is soluble in the lipids of the cell membrane.[3] Samson[4] has shown that acetic acid (or sodium acetate) inhibits by chemically interfering with membrane transport of phosphate. Phosphate transport through the cell membrane is an activated transport process requiring the expenditure of ATP. Acetic acid interference results in an increase in the ATP requirement for this maintenance function. Typical of this type of inhibition, cell production (μ) decreases while specific ethanol production (ν) increases to make available sufficient ATP for cell maintenance. Chemical interference effects typically can occur at very low inhibitor concentrations; and, where membrane disruption is involved, as in acetic acid attack, cell morphology is altered, with cells becoming irregular and elongated (Fig. 3). At sufficiently high inhibitor concentrations, cell growth is totally limited, and the culture dies. Production rates and inhibitory concentrations of the major fermentation by-products are summarized in Tables 1 and 2.

*This work was supported by the Director for Energy Research, Office of Basic Energy Sciences, U.S. Department of Energy under Contract No. DE-AC03-76SF00098.

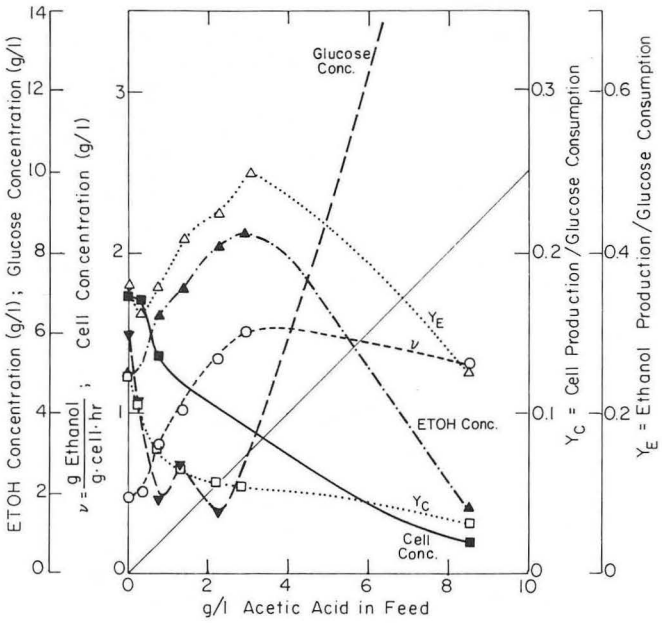

Figure 2. Acetic acid inhibition of ethanol fermentation.

(XBL 812-5294)

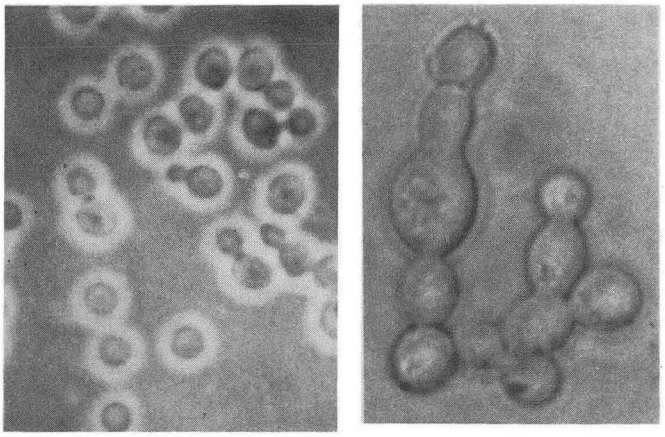

Figure 3. Yeast morphology with acetic acid fermentation. (a) Normal (b) acetic acid.

(XBB 814-3225A)

Table 1. Products of the alcoholic fermentation of glucose by Saccharomyces cerevisiae.

Product	mM Product/100 mM Glucose
FROM SYNTHETIC MEDIA:	
Ethanol	177.0
Carbon Dioxide	180.8
2,3-Butanediol	0.48
Acetoin	--
Glycerol	6.60
Acetic Acid	0.69
Butyric Acid	0.32
Formic Acid	0.42
Lactic Acid	0.38
Succinic Acid	0.26
Acetaldehyde	5.0
ADDITIONAL FROM MOLASSES MEDIA:	
Fused Oil: 1-Propanol	0.34
2-Methyl-1-Butanol	~0.11

Table 2. By-product inhibition summary.

By-product	Concentration at high inhibition[a] (g/l)	Inhibition mechanism
Ethanol	70	Direct inhibition of the ethanol production pathway
Formic acid	2.7	Chemical interference with cell maintenance functions
Acetic acid	7.5	Chemical interference with cell maintenance functions
Lactic acid	38	Chemical interference with cell maintenance functions
1-Propanol	12	Chemical interference with cell maintenance functions
2-Methyl-1-butanol	3.5	Chemical interference with cell maintenance functions
2,3-Butanediol	90	Chemical interference with cell maintenance functions
Acetaldehyde	5.0	(Largely reconsumed)
Glycerol	450	Osmotic pressure effects
Glucose	380	Osmotic pressure effects

[a]80% reduction in cell mass.

On the basis of these results, operating parameters for a scheme for continuous fermentation can be developed. A small "bleed" of fermentor liquid is removed to carry away nonvolatile inhibitors. When the ratio of the bleed to feed rates is sufficiently large, long-term, stable, high-productivity fermentation can be maintained (Fig. 4).

ALTERNATIVE ETHANOL RECOVERY PROCESSES

Introduction

The goal of the work on alternative ethanol recovery processes is to develop methods of ethanol recovery that are energetically and economically preferable to distillation. The main rationale for seeking alternatives to distillation as a product recovery method lies in the hope of reducing the considerable energy cost of distillation in the case of ethanol-water. As shown in Table 3, the energy required to produce 95 weight percent ethanol by distillation is over forty times the reversible thermodynamic work required to completely separate a 5 weight percent ethanol solution into pure ethanol and water. This is due to the nature of the ethanol-water vapor-liquid equilibrium, particularly to the existence of the ethanol-water azeotrope. Operation at reduced pressure can reduce the energy requirement by altering the vapor-liquid equilibrium favorably, but the savings in energy is offset somewhat by considerable capital expense for compressors and other equipment. It should be noted that the energy cost of distillation increases greatly as the feed concentration of ethanol decreases. Therefore, the development of an economical ethanol recovery method for dilute feeds may enable consideration of some ethanol production schemes that have been considered unfeasible because their products could not be purified economically by distillation.

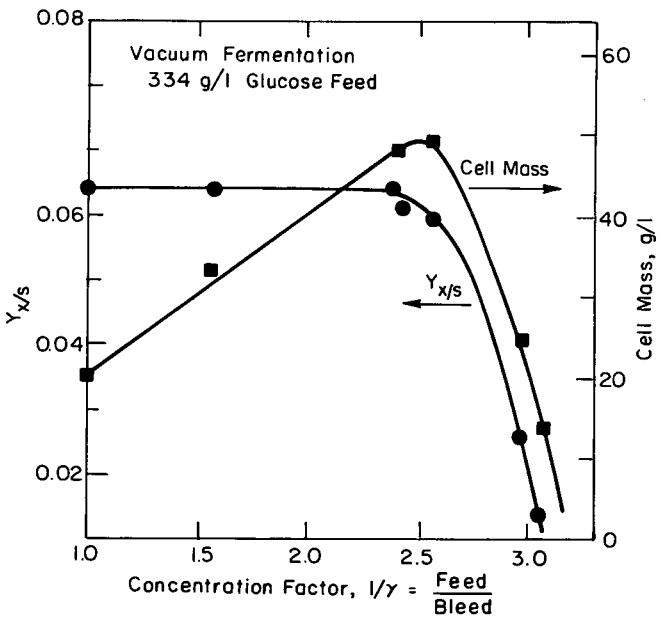

Figure. 4. Vacuum fermentation, 334 g/l glucose feed (after Cysewski[1]).

(XBL 761-6167A)

Table 3. Energy requirements for ethanol recovery.

	Energy required (kJ/l)
Theoretical minimum (Complete separation of $X_\varepsilon = 0.02$)	147
Distillation, conventional (to azeotrope only)	6216
Distillation, vacuum (to azeotrope, calculated)	3568
Extraction (potential, calculated)	1700

This work has focused primarily on solvent extraction as an alternative recovery method. Analysis of conceptual designs indicates that this process has the potential for recovering ethanol using less energy than distillation, especially for dilute ethanol feed conditions.

Several properties can be identified as desirable for a good extraction solvent for ethanol. The solvent should have a high distribution coefficient, D_E, defined as the ratio of the molarity of ethanol in the solvent to the molarity of ethanol in the aqueous phase with which it is in equilibrium. If D_E is too low, the required solvent flows will be too large to handle in a practical process. The separation factor, S, which is the ratio of D_E to D_W (the distribution coefficient for water), should also be high. If not, little separation of ethanol from water is achieved. In water recycle systems, low toxicity is an additional solvent requirement. Others, depending on the process used, may include low water solubility, low volatility, and ease of emulsion breakup.

In comparing the properties of available solvents with these desirable properties, it is useful to first examine the distribution coefficient and separation factor data. Table 4 presents a summary of data for ethanol in various classes of solvents. These data include some references in the literature[5,6] as well as those obtained using gas chroma-

Table 4. Properties of extraction solvents for ethanol at 25°C ([EtOH] = 1 - 2M).

	$D_E = \frac{\text{EtOH organic}}{\text{EtOH aqueous}}$	$S = D_E/D_W$
Alkanes	0.005 - 0.008	up to 300
Aromatics	0.02 - 0.1	90 - 120
Esters and ketones	0.1 - 0.3	10 - 20
Alkyl phosphates	up to 0.7	1 - 20
Chlorinated hydrocarbons	0.1 - 0.15	75 - 170
Higher alcohols	0.2 - 0.8	10 - 40

tographic analysis of batch equilibrations in this work. It can be seen that, in general, the higher the separation factor, the lower its distribution coefficient. The separation factors in Table 4 are low. To produce azeotropic ethanol from 1M solution requires that S be greater than 350. There are several approaches to improving the separation factor. One method employs a mixed solvent system to achieve better overall solvent properties than would be realized by using any single solvent. The use of TOPO, trioctyl phosphate oxide, in nonpolar diluents is an example of this approach.

A second approach tested uses organic salts to salt ethanol into the solvent. Notable among these salts are those involving the large tetralkyl ammonium ions. It was reasoned that, by using salts of these ions, which would have very little water solubility but be soluble instead in an organic phase, an improved extraction solvent for ethanol might be devised. Table 5 shows some results of initial tests of this concept. While the effects in the cases of the ester solvents are small due to the small concentrations employed, at higher concentrations in triethyl benzene, tetrabutyl ammonium benzoate clearly salts ethanol into the organic phase. The extra ethanol brought in is slightly more than 0.5 moles of ethanol per mole of salt. In the case of tetrabutyl ammonium iodide, however, salting out of ethanol is indicated, pointing to the importance of an anion in this interaction. This is confirmed by the work of Arnett et al.,[7] who found, in a study of the hydration of ions in non-aqueous media, that the influence of the tetralkyl ammonium cation is small compared to the anion effect. The salting out by iodide is in keeping with other evidence that, compared to electrophilic sites, water is better able to compete with ethanol for nucleophilic sites in an organic medium.

Another method involves altering the aqueous phase to increase the activity of ethanol and decrease the activity of water. This can be achieved simply by adding salt. The salting-out effect has been known for nearly a century and has been extensively studied by Furter and others,[8] especially with regard to vapor-liquid equilibria. It should be noted that the beneficial effects of salting out apply to distillation as well as to extraction for ethanol recovery.

This leads to the concept of a salt-containing fermentation, because no salt is inexpensive enough to use without recovery or recycle. The specific salt used in this type of fermentation is important. Results to date show that potassium chloride can be used at higher concentration levels (greater than 1M) than other salts before causing complete inhibition of fermentation. This is reasonable, considering the high potassium content of the yeast intracellular material (0.3M). However, even potassium chloride produces problems when used in a conventional yeast fermentation.

Table 5. Salting ethanol into organic solvents.

Solvent	Salt	$[EtOH]_{aq}$,M	D_E
Dibutyl phthalate	None	1.0	0.123
Dibutyl phthalate	TBA benzoate, 0.04M	1.0	0.116
Triethyl citrate	None	1.5	0.072
Triethyl citrate	TBA benzoate, 0.03M	1.5	0.091
Triethyl benzene	None	1.0	0.097
Triethyl benzene	TBA iodide, sat.	1.0	0.088
Triethyl benzene	TBA benzoate, 0.18M	1.0	0.171

TBA ≡ tetrabutyl ammonium

The results of two sets of experiments involving continuous culture studies of the effect of potassium chloride on the fermentation of glucose by S. cerevisiae are shown in Table 6. The first set compares the fermentation of 20 g/l glucose solution with that of a continuous fermentation of a 19.6 g/l glucose solution containing 75 g/l KCl. There is incomplete sugar utilization in the latter case at a dilution rate of 0.11 hr^{-1}, while, in the absence of salt, the fermentation is essentially complete at the dilution rate of 0.15 hr^{-1}. This is due to the slower growth of the yeast in the presence of 1.0M KCl, reflected in the decreased cell mass. The ethanol yield is also decreased by almost 12 percent.

The second set of experiments shows the effect of adding ethanol to the feed in each of the above-described fermentations. In the case of the fermentation without salt, adding 2.5 percent ethanol to the feed at a low dilution rate does not affect sugar utilization or cell yield. When ethanol is added to the salt fermentation, however, even at a dilution rate slightly less than one in which nearly complete sugar utilization was seen without ethanol, sugar utilization drops to less than 85 percent. More significant, however, is the decrease in ethanol yield that is observed with ethanol addition to the feed. While this does occur without salt in the feed, in the salt-containing-feed case, the ethanol yield is reduced by more than 50 percent. It seems likely that the sugar is metabolized to glycerol and other products, as reported by Watson[9] for the case of a fermentation containing NaCl. As a result, an ethanol fermentation using potassium chloride does not appear feasible with this organism. Other, salt-tolerant, ethanol-producing organisms may give better results. Because the ease of separation of ethanol increases with salt concentration, it would be desirable to select an organism that could tolerate as high a concentration of salt as possible. In the case of 1M KCl studied, the distribution coefficient K_D for ethanol between the aqueous beer and selected organic solvents was increased by a factor of 1.5.

If water recycle or extractive fermentation is to be carried out, then obviously the toxicity of the solvent is an important consideration. A number of batch experiments to test solvent toxicity have been conducted using solvent at either saturation or one-tenth of saturation concentrations. For any particular solvent, growth and ethanol production were inhibited to the same extent. Unfortunately, solvents with better distribution coefficients and separation factors are also the most toxic. This leads to consideration of some process alternatives, which will be briefly discussed. It may be possible to remove the solvent selectively, as would be done with other inhibitors, if a toxic solvent is employed. Figure 5

Table 6. Continuous fermentation with S. cerevisiae--effects of KCl and EtOH.

KCl Conc. (M)	D (hr^{-1})	Feed EtOH (g/l)	Feed glucose (g/l)	Residual glucose (g/l)	Product EtOH (g/l)	Product cell mass (g/l)	(g/g-hr)	Y_{xs} (g/g)	$Y_{E/g}$ (g/g)
0	0.15	0	20.0	0.15	8.5	1.73	0.75	0.09	0.43
0	0.06	0	20.0	0.10	8.3	1.84	0.27	0.09	0.42
1	0.11	0	19.6	6.10	5.0	0.55	1.02	0.04	0.37
1	0.06	0	19.6	0.38	7.4	0.75	0.56	0.04	0.38
0	0.24	24.7	19.1	7.91	28.5	1.04	0.87	0.09	0.34
0	0.06	24.7	19.1	0.09	30.8	1.86	0.20	0.10	0.32
1	0.06	27.6	19.0	2.9	30.5	0.57	0.26	0.04	0.18

shows a process that could be used to employ a solvent with a low distribution coefficient. The removal of ethanol from the solvent in a bed of absorbant would obviate the need to supply sensible heat to a large recirculating, low-volatility, solvent stream. Alternatively, a low-boiling solvent could be considered, expanding the possibilities for solvent selection. A different approach to the solvent toxicity problem is illustrated in Figure 6. In this scheme, the fermenter beer is steam-stripped of ethanol, as in a conventional beer still; and ethanol is then selectively absorbed by the solvent. The steam is recycled back to the beer still but can first be rectified as needed to remove the solvent to the required level of concentration. For a low-volatility solvent, this rectification need not consume much energy.

PLANNED ACTIVITIES FOR FY 1982

The study of solvent mixtures, including those involving organic salts, will continue with experimental investigations. In addition, calculations based on a molecular thermodynamic model of liquids will be used to correlate and predict ethanol distribution data.

A separate analysis of the energy requirements and relative economics of the process alternatives is being developed. It will allow an optimization of the ethanol extraction process with regard to process type and solvent.

Experimental investigation of the adsorption of ethanol has begun, using ion exchange resins of various forms and molecular sieves as candidate adsorbers. This work will continue, and the options for low-energy regeneration of such systems will be studied.

REFERENCES

1. Cysewski, G.R., and Wilke, C.R. (1977), "Rapid Ethanol Fermentations Using Vacuum and Cell Recycles," Biotechnol. Bioeng. 19, 1124.

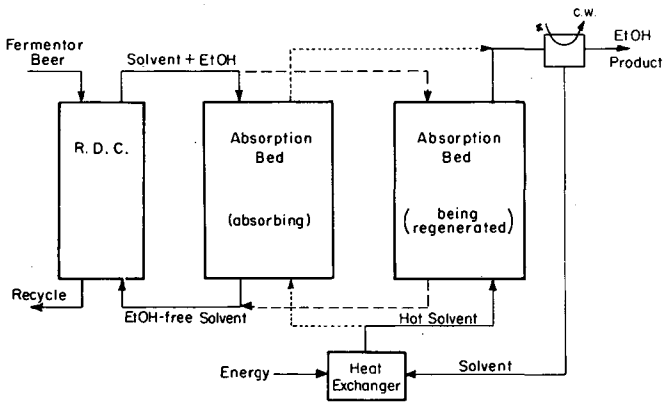

Figure. 5. Extractive fermentation for ethanol production, Process B: low volatility, nontoxic solvent with low distribution coefficient.
(XBL 815-5821)

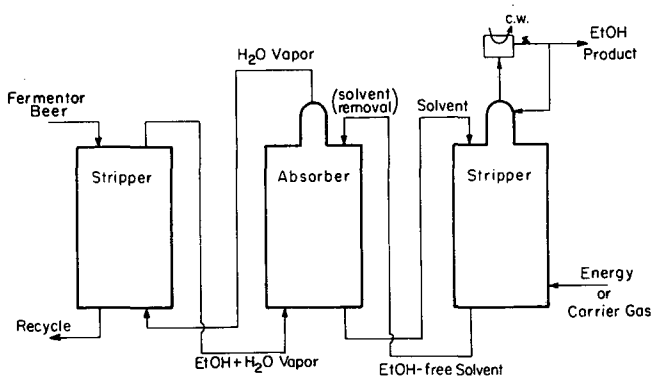

Figure. 6 Ethanol fermentation for ethanol production, Process C: low volatility, toxic solvent or emulsion-forming solvent.
(XBL 815-5820)

2. Maiorella, B., Blanch, H., and Wilke, C.R. (1981), "By-Product Inhibition Effects on Ethanolic Fermentation by Saccharomyces cerevisiae." Submitted to Biotechnol. Bioeng.

3. Conway, E.J., and Downey, N. (1950), "An Outer Metabolic Region of the Yeast Cell," Biochem. J. 47, 347.

4. Samson, F.E. (1955), "Effects of Acetate and Other Short-Chain Fatty Acids on Yeast Metabolism," Archs. Biochem. Biophys. 54, 406.

5. Roddy, J.W. (1981), "Distribution of Ethanol-Water Mixtures to Organic Liquids," Ind. Eng. Chem. Process Des. Dev. 20, 104.

6. Korenman, I.M., and Chernorukova, Z.G. (1974), "Distribution of Normal Alcohols between Organic Solvents and Water," J. Appl. Chem. USSR 47, 11, Pt. 2, p. 2595.

7. Arnett, E.M., Chawla, B., and Hornung, N.J. (1977), "The Hydration of Anions in Nonaqueous Media," J. Solution Chem. 6, 12, p. 781.

8. Furter, W.F., Ed. (1979) Thermodynamics of Electrolytes in Mixed Solvents--II. Advances in Chemistry Series 177. American Chemical Society.

9. Watson, T.G. (1979), "Effects of Sodium Chloride on Steady-State Growth and Metabolism of Saccharomyces Cerevisae," J. Gen. Microbiology 64, 91.

Production of Sugars from Cellulose*

C. R. Wilke, H. W. Blanch, G. B. Dove, N. A. Hendy, A. Mancuso, S. T. Orichowskyj, J. M. Perez, A. F. Sciamanna, and D. F. Wiley

ENZYME PURIFICATION AND KINETICS

A kinetic model was developed for predicting the time course of enzymatic hydrolysis of rice straw with the cellulase complex derived from Trichoderma reesei, Rut-C30. This model incorporates the effects of substrate multiplicity, inhibition by the products of hydrolysis, and patterns of adsorption of enzyme components on cellulosic materials, using a shrinking sphere to model the sites available for adsorption.

The multiplicity of substrate reactivity is represented by a substrate consisting of amorphous and crystalline fractions, whose hydrolysis proceeds at differing rates but with each proportional to filter paper activity. The rate of hydrolysis of amorphous cellulose is found from initial rates and that of crystalline cellulose from hydrolysis rates at higher over-all conversions, where conversion of the amorphous fraction is complete. Inhibition is treated as consisting of mixed inhibition of β-glucosidase activity by glucose and of competitive inhibition of the activity of the cellobiohydrolase-endoglucanase complex by cellobiose. Since the reaction is heterogeneous and the concentration of enzyme is high, Michaelis-Menten kinetics do not apply, and adsorption of cellulase on cellulose is modeled by a Langmuir isotherm to obtain an effective enzyme concentration, as shown in Figure 1.

Results of this model are compared with experiment in Figures 2 and 3. This model was also applied to prediction of hydrolysis of corn stover.

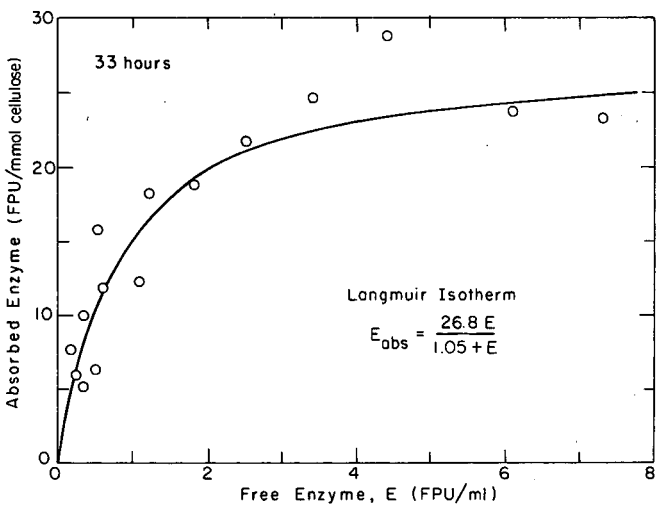

Figure 1. Adsorption isotherm for cellulase on cellulose.

(XBL 8112-12706)

Fractionation of the components of cellulase will extend this model to include the effects of relative concentrations of endoglucanase, cellobiohydrolase, glucohydrolase, and β-glucosidase, which constitute the complete system of enzymes responsible for saccharification. In this way, the optimum composition of enzyme solution may be found and parameters in the model estimated from the separate enzyme activities.

Enzymatic hydrolysis of corn stover with cellulase was evaluated for pretreated acid and for steam-explosive, decompression-pretreated material, producing 50 and 80 percent conversions to glucose, respectively. An algorithm was developed to evalu-

*This work was funded by the Solar Energy Research Institute, Golden, Colorado, under Contract No. DR-0-9058-1 through the U.S. Department of Energy under Contract No. DE-AC03-76SF00098.

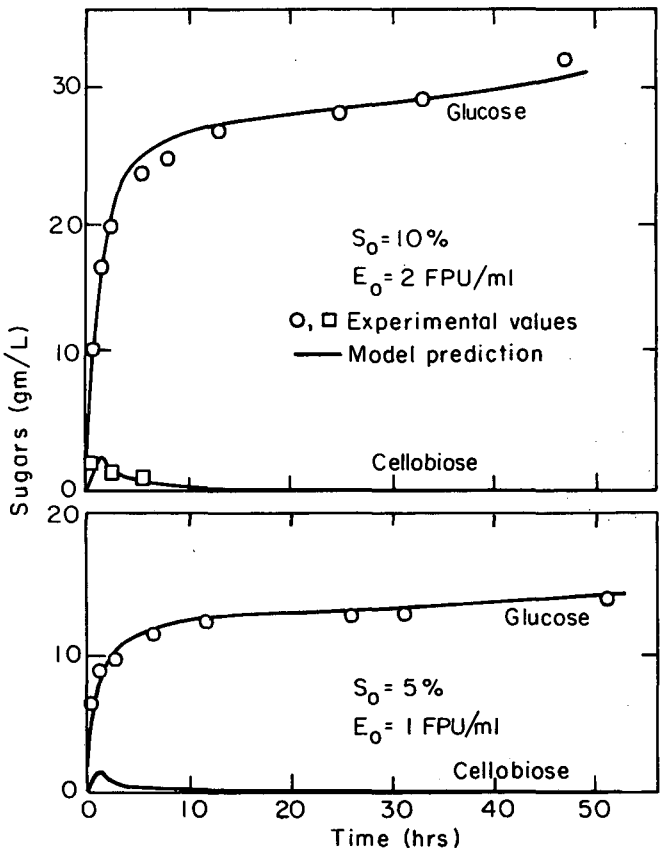

Figure 2. Model performance for low substrate concentrations.

(XBL 8110-11979)

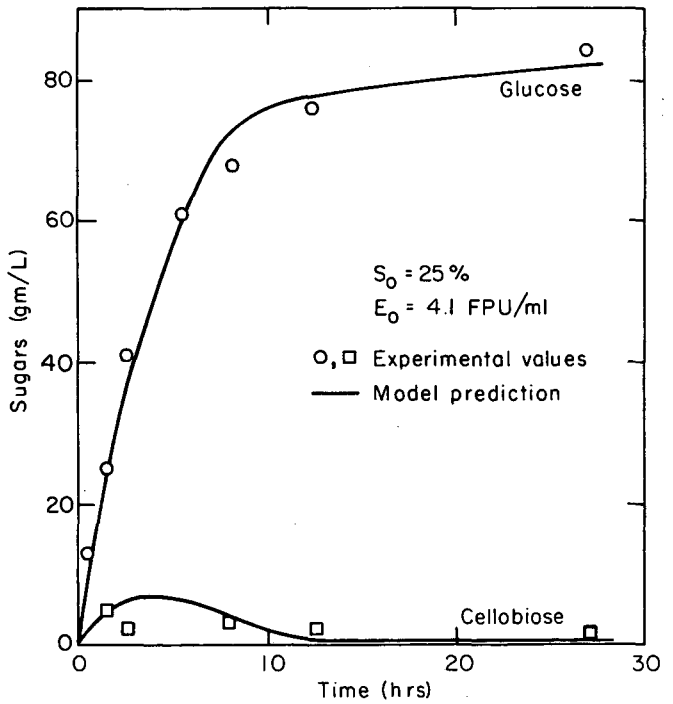

Figure 3. Model performance for high substrate concentration.

(XBL 8112-12719)

ate process design alternatives and experimental conditions. Results of this selection of alternatives predict costs of 12 to 22 cents per pound of glucose produced and 10 to 15 cents per pound for these two pretreatments, for substrate costs of 0 to 30 dollars per ton. Major costs are those of substrate and enzyme production.

PRODUCTION OF CELLULASE BY TRICHODERMA REESEI

Batch and continuous cultivation studies have been conducted using the hyperproducing Trichoderma reesei mutants QM9414 and Rut-C30. In batch production, temperature and pH profiling of the QM9414 strain has proved to be beneficial in raising the cellulase productivity. Although this technique does not greatly increase the final cellulase activity obtained, shorter fermentation times result in higher productivity.

Temperature-pH profiling during batch growth of the Rut-C30 strain was not found to increase the concentration of cellulase and actually caused a slight decrease in productivity. Maximum cellulase production is obtained by maintaining the pH and temperature at constant levels of 5.0 and 28°C, respectively. In this manner, Rut-C30 produces approximately twice the cellulase activity of QM9414.

In batch studies of Rut-C30, it has been found that the expensive medium constituent, proteose peptone, can be replaced with relatively inexpensive corn steep liquor (CSL). With an equal concentration of CSL and Solka Floc (2 percent in most trials), production of cellulase activity not only equaled that obtained when peptone was used, but increased approximately 20 percent. Further trials will continue to determine the optimum concentration of CSL, with respect to Solka Floc concentration, and to what extent the other constituents of the medium may be deleted when CSL is included.

Consistent with the gains made with pH profiling of QM9414 in batch production, two-stage continuous cellulase production with this strain occurred at different optimal conditions in each stage. The first stage operated at pH 3.75-4.25 and the second stage at pH 5.0.

However, in two-stage continuous production, Rut-C30 produces maximum cellulase when both stages are maintained at pH 5.0 and 28°C. Over a range of dilution rates, maximum productivity was obtained with the first stage operating at 0.046 h^{-1} and the second stage at 0.028 h^{-1}. The dilution rate is especially critical in the second stage, with any increase in dilution rate giving a sharp drop in productivity, as shown in Table 1.

Future work will include cell recycle to raise the cell mass in the second stage. This should provide higher dilution rates and thus give a higher productivity.

ENZYME RECOVERY

The economics of enzymatic hydrolysis of cellulose to a sugar solution are greatly affected by

Table 1. Enzyme productivity of Rut-C30 in two-stage continuous fermentation over a range of dilution rates, in international units/liter-hour.

First stage		Second stage	
Dilution rate (hr^{-1})	Productivity (IU/l-hr)	Dilution rate (hr^{-1})	Productivity (IU/l-hr)
0.038	95	0.023	81
0.040	88	0.024	82
0.046	97	0.028	92
0.050	90	0.030	81
0.053	64	0.032	67

the recovery of enzyme. After the hydrolysis step has been completed, a considerable amount of enzyme remains adsorbed onto the residual solids. The product solution also contains a significant amount of enzyme that should be recovered for re-use. Various methods of recovering the Rut-C30 enzyme are presently under investigation.

The recovery of enzyme can be enhanced by modifying its adsorption onto the solids. This can be achieved by altering the substrate, the enzyme, or the bulk solution. The addition of various nitrogenous salts can maximize the fraction of enzyme that remains in solution. Urea was found to be the most efficient, retaining 65 percent of the available enzyme in solution. The feasibility of a process, in which urea would be added in solid form to the hydrolysis stage and then recovered as part of the bottoms leaving the ethanol distillation column, has been investigated. The optimum concentration of urea in the hydrolysis stage would be approximately 1.0M. The sugar/urea solution from hydrolysis would then have to be concentrated by a factor of 5 to 7 to yield a concentrated ethanol product from the fermentation stage. This would result in a urea concentration well above the limit of 1.0M, and S. cerevisiae would no longer be able to function in a stable manner. No economical means of removing urea prior to fermentation has been found.

In an alternative method, which has also been investigated, the hydrolyzed solids would be with a concentrated urea solution to remove adsorbed enzyme. After being washed with urea, the solids would be filtered and burned for power generation. The filtrate would enter an ultrafiltration unit where the enzyme would be concentrated and returned to the hydrolysis stage. The urea solution would be recycled for the washing of solids. This has been compared to the current process in which fresh solids are contacted counter-currently with the hydrolysis product solution. It was found that the savings over the counter-current process are exceeded by the expense of additional equipment and urea.

A modification of the process employing the concentrated urea wash would recover the enzyme from the wash by precipitation with acetone as an alternative to ultrafiltration. It was found that the acetone precipitation is less economical than ultrafiltration.

These studies of enzyme recovery employing urea lead to the conclusion that the most economical method of removing enzyme from solution would be the present process of counter-current contacting. Use of a concentrated urea wash would be three to four times more expensive when ultrafiltration is employed, while precipitation with acetone would be six to eight times more expensive than counter-current contacting.

In the present scheme of counter-current contacting, the cellulosic solids are milled and pretreated with sulfuric acid to break down the lignocellulosic material. The solids are then contacted counter-currently with a hydrolysis product solution containing sugar and enzyme. The recovery of enzyme is governed by the ability of the solids to adsorb as much of the enzyme as possible. Pretreatment plays an important role in affecting this ability as well as in the extent of hydrolysis. Present work is concerned with the possibility of using steam explosion for pretreatment as an alternative to pretreating with sulfuric acid. Results of a preliminary enzymatic hydrolysis of a sample of steam-exploded wood showed better than 90 percent carbohydrate conversion. Adsorption studies with steam-exploded corn stover are presently under way in an effort to optimize the conditions of enzyme recovery with respect to temperature and solids concentration.

XYLOSE FERMENTATION

The hemicellulose fraction of cellulosic biomass is predominately composed of the five-carbon sugar xylose. Xylose represents approximately one-fourth of the total carbohydrate content of biomass.[1] Although many yeasts are capable of producing high yields of ethanol from glucose, they are not able to ferment xylose.[2] Two species of bacteria, Bacillus macerans and Clostridium thermohydrosulfuricum, which have the metabolic capability to produce ethanol from xylose, have been examined for their possible use in an economical industrial-scale process to convert biomass to ethanol.

Bacillus Macerans

To investigate the economic feasibility of producing ethanol from xylose with Bacillus macerans, the bacterium was grown in continuous culture on medium containing one percent xylose. At a dilution rate of 0.06 hr^{-1}, a yield of 0.2 g ethanol/g xylose was obtained. By-products of the fermentation were predominately carbon dioxide and acetic acid. Dilution rates higher than 0.06 hr^{-1} resulted in incomplete carbon utilization. During continuous culture studies, it was observed that small perturbations of the system, e.g., a small change in dilution rate or residual xylose concentration, caused a cessation of growth and almost complete washout of the cells. The apparent unstable behavior of cultures of Bacillus macerans is believed to be the result of poor regulation within the cells during xylose metabolism.

Because of the fairly low growth rate and the instability during continuous operation, experimen-

tal work with Bacillus macerans has been terminated.

Clostridium Thermohydrosulfuricum

C. thermohydrosulfuricum is an extreme thermophile that grows only under strict anaerobic conditions. The high optimal growth temperature, 65°C, is advantageous because it facilitates subsequent product-purification steps. In addition, contaminants in an industrial-scale fermentation with this bacterium are unlikely because very few organisms grow at 65°C.

C. thermohydrosulfuricum strain 39E has been shown to produce 0.39 g of ethanol per gram of xylose fermented in the absence of substrate and end-product inhibitions.[3] The theoretical maximum yield is 0.51 g ethanol/g xylose.

The organism appears to have complex nutritional requirements because growth does not occur in mediums deficient in amino acids and vitamins.

The objectives of the work being done with this organism are:

1. To produce ethanol at a high yield from xylose.
2. To develop a strain that will be able to ferment high concentrations of xylose to produce high ethanol-content beer, thereby reducing subsequent separations costs.

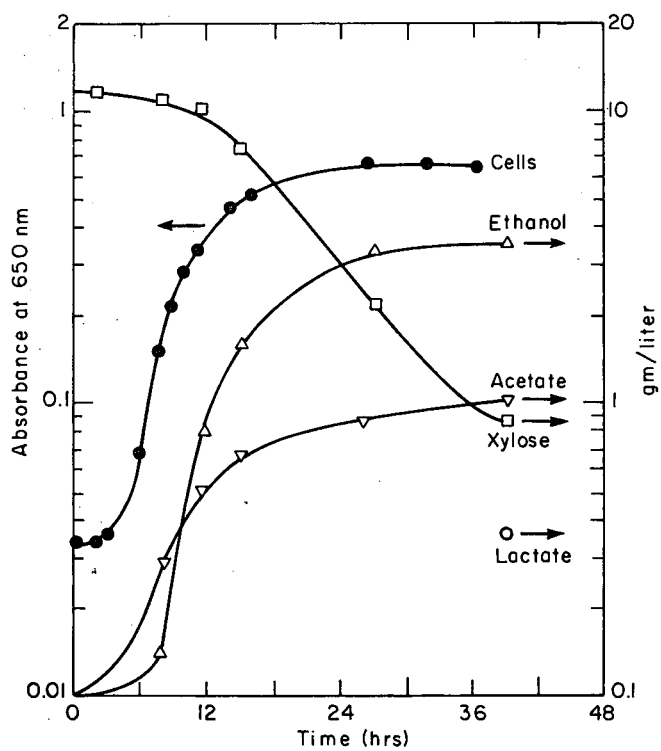

Figure 4. Batch growth C. thermohydrosulfuricum, strain 39E, on xylose and yeast extract at 65°C with pH 7.2 decreasing to 6.5 at 40 hours.
(XBL 8111-12841)

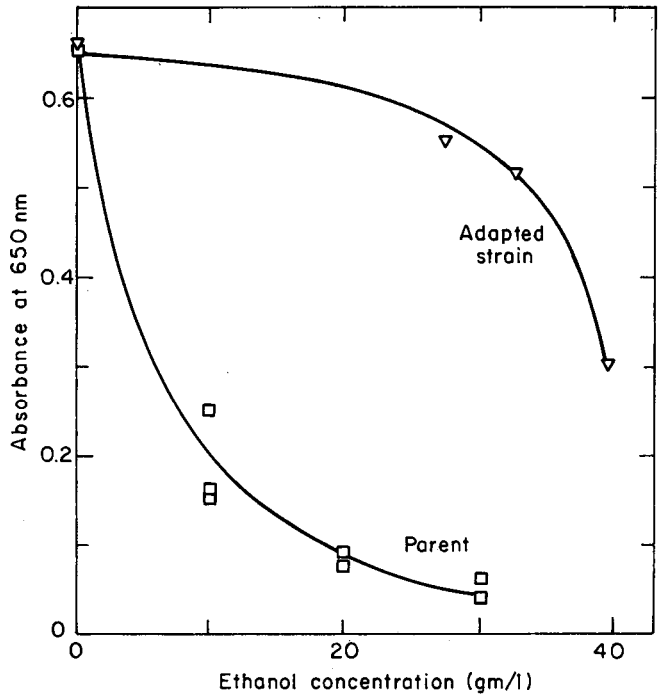

Figure 5. Effect of ethanol on the growth of C. thermohydrosulfuricum, parent and adapted strains. Cultures were grown on 10 g/l xylose, 2 g/l yeast extract, and 0.4 g/l cysteine hydrochloride which was used as a reducing agent.
(XBL 8111-12840)

3. To find an economical source of amino acids and vitamins that will support growth and maintain the high ethanol yield.

The results of a typical batch fermentation are shown in Figure 4. The minimum specific growth rate and the maximum specific productivity of ethanol were 0.40 and 0.34 hr^{-1}, respectively. Because of end-product inhibition by ethanol, the yield was only 0.32 g ethanol/g xylose. By-products of the fermentation were acetate and lactate.

To overcome the problem of ethanol inhibition, cultures were transferred serially into a medium containing increasing concentrations of ethanol. The ethanol concentration was increased by 2 g/l between transfers, and the highest concentration in which growth was observed was 40 g/l. Figure 5 compares the effects of ethanol on the growth of the parent and adapted strains. As can be seen, the adapted strain is much more capable of tolerating high ethanol concentrations than the parent strain.

The yield of ethanol from xylose by the adapted organism is presently being determined. It is hoped that the organism will be able to produce a fairly high concentration of ethanol (30 g/l) at a high yield (0.40 g ethanol/g xylose).

Future work will include a mutation and selection program aimed at eliminating the production of acetate and lactate to help improve the ethanol yield. In addition, batch experiments will be per-

formed in medium supplemented with economic sources of amino acids and vitamins, such as corn steep liquor, a by-product in corn milling.

REFERENCES

1. Wilke, C.R., et al. (1981), "Raw Materials Evaluation and Process Development Studies for Conversion of Biomass to Sugars and Ethanol," Biotechnol. Bioeng. 23, pp. 163-183.

2. Slininger, et al. (1981), "Conversion of Xylose by the Yeast Pachysalen tannaphilus," Report prepared for Northern Regional Research Center, Agricultural Research, Science and Education Administration, U.S. Department of Agriculture, Peoria, Illinois.

3. Ng, T.K., ben-Bassat, A., and Zeikus, J.G. (1981), "Ethanol Production by Thermophilic Bacterium: Fermentation of Cellulosic Substrates by Concultures of Clostridium Thermocellum and Clostridium Thermohydrosulfuricum." Appl. Environ. Microbiol. 41, No. 16, pp. 1337-1343.

OIL SHALE AND PETROLEUM-RELATED RESEARCH

Molecular Substituent Parameters Applied to the Specification of Inorganic Arsenic and Organoarsenic Compounds in Shale Oil and Oil Shale Kerogen by HPLC-GFAA*

R. H. Fish, F. E. Brinckman†, and C. S. Weiss†‡

The molecular characterization, or chemical speciation, of metal and metalloid species at trace levels has provided valuable information in the areas of the aquatic chemistry of trace metals, the microbial transformations of trace metals, the biochemistry of trace metals, and the chemistry of controlled release biocides containing metals. This information is not obtainable by total trace-metal analysis.

A widely used method for trace-metal speciation is the chromatographic separation of the metal-containing compound, with element-selective detection in either on-line or off-line modes. This technique is capable of characterizing trace-metal species in the presence of numerous other interfering compounds that may prohibit the use of many, if not all, direct spectroscopic identification techniques. Thus, chromatographic separations with element-selective detection have been and will be used extensively to characterizei trace-metal-containing compounds in the variety of complex matrices generated from energy-related processes. In general, both gas and liquid chromatographic systems are used. Element-selective detectors are preferably used on-line, thereby minimizing sample handling, analysis time, and the time needed to optimize the chromatographic system. The element-selective detectors include emission and atomic absorption spectroscopy, and electrochemical and radioactivity detectors. The technique relies upon the elution of the trace-metal-containing compound with a retention time different from all other compounds containing the trace metal under investigation, as determined by an authentic standard.

Gas chromatographic retention has been related to volatility, and that relationship has provided a useful index of retention, the Kovats Index.[1] In speciation studies involving liquid chromatographic separations, it would be useful to have a rational system based on thermodynamic properties, with due consideration of kinetic rates on the chromatographic time scale, in order to

a. Predict the retention of a sought-after compound,

b. Predict the possible structure(s) of unknown compounds from the experimentally determined retention times,

c. Predict the possible co-elution of interfering compounds, and

d. Optimize chromatographic systems for the desired separation.

The relationship between structural substituent parameters and chromatographic retention has

*The work at LBL was supported by the Assistant Secretary for Fossil Energy and the Assistant Secretary for Oil, Gas and Shale Technology, and the Bartlesville Energy Technology Center of the U.S. Department of Energy under Contract No. DE-AC03-76SF00098.

†National Bureau of Standards.

‡NRC-NBS Postdoctoral Research Associate 1980-1982.

provided a starting point for such a system and has been applied to the separation of many organic compounds.

The electronic structural substituent parameter, σ, is based on the ionization of a derivable compound with respect to its parent compound. The determination of σ is based on Equation 1.

$$p\sigma = \log K_x - \log K_H \quad , \qquad (1)$$

where K_x is equal to the ionization constant of the derivative compound, and K_H is the ionization constant of the parent compound. The constant was first introduced by Hammett[2] in 1935, based on benzoic acid as the parent compound, with meta and para derivatives. In 1953, Jaffe et. al[3] published values for aromatic phosphonic acids. In 1956, Mastryukova and Kabachnik[4] published σ^{ϕ} values for the aqueous ionization of a large variety of substituted phosphorous acids.

The first application of thermodynamic principles to the chromatographic retention of organometal molecules involved the separation of di- and triorganotins by ion-exchange chromatography with atomic absorption detection. Jewett and Brinckmann[5] demonstrated a linear relationship between the logarithm of the chromatographic capacity factor k' and the σ^{ϕ} molecular substituent parameter, with a correlation coefficient of 0.992, based on 23 individual k' values for five trialkyltin compounds, separated in water as the R_3Sn^+ cations.

ACCOMPLISHMENTS DURING FY 1981

Chromatographic Retention and Molecular Substituent Parameter Relationships

The calculation of the $\Sigma\sigma^{\phi}$ values for the arsenic compounds chromatographed is simply the linear sum of the σ^{ϕ} parameters of the individual molecular substituents which replace the ionic oxygen substitutents in the parent compounds. The method for calculating the $\Sigma\sigma^{\phi}$ values is presented in Table 1; the parent compound is taken as the trisubstituted form of arsenic whose $\Sigma\sigma^{\phi}$ value is designated as 0, where A = B = C = O^-. The ionic form of the derivative compound is very important because simple monoprotonation of the compound contributes -0.39 σ^{ϕ} unit to the total $\Sigma\sigma^{\phi}$ value of the derivative. In most cases, the ionic form of the derivative was determined by considering the pK_a of the compound with respect to the pH of the eluting solvent. For dimethylarsinic acid and the diphenylarsinic acid, the neutral forms were considered in an attempt to obtain the best fit of the data. Considering the pK_a's of these compounds, to ascribe these as neutral forms is not entirely satisfactory; however, there might be some nonadditive electronic effects due to the presence of two organic substituents on the central arsenic atom.

The separation of the arsenicals, using the HPLC-GFAA system, is shown in Figure 1. The nonresponse of the UV absorbence detector is to be noted with the exception of the chromophore 4-aminophenylarsonic acid. The histogrammic output of the GFAA signal results from the discrete sampling of the HPLC effluent limited by the drying, charring, atomization, and cooling cycle of the graphite furnace at approximately 45-second intervals.[6]

Table 1. The calculation of the $\Sigma\sigma^{\phi}$ for organoarsenic acids.

Parent Compound 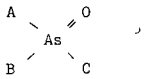 $\Sigma\sigma^{\phi} = 0$

Substituent	(Ref. 1)
$-O^-$	0.00
-OH	-0.39
-Ph	-0.48
$-CH_3$	-0.96

Molecular Ion	Substituents A	B	C	$A + B + C = \Sigma\sigma^{\phi}$
$HAsO_4^{2-}$	O^-	O^-	OH	0 + 0 + (-0.39) = -0.39
$H_2AsO_4^-$	OH	OH	O^-	(-0.39) + (-0.39) + 0 = -0.78
$Ph\text{-}AsO_3H^-$	Ph	OH	O^-	(-0.48) + (-0.39) + 0 = -0.87
$CH_3AsO_3H^-$	CH_3	OH	O^-	(-0.96) + (-0.39) + 0 = -1.35
$(CH_3)_2AsO_2^-$	CH_3	CH_3	O^-	(-0.96) + (-0.96) + 0 = -1.92
$(CH_3)_2AsO_2H^o$	CH_3	CH_3	OH	(-0.96) + (-0.96) + (-0.39) = 2.00

The relationship between the natural logarithm of the chromatographic capacity factor for the arsenic compounds and the calculated $\Sigma\sigma^{\phi}$ values for these compounds is presented in Figure 2. The relationship is linear, with a correlation coeffi-

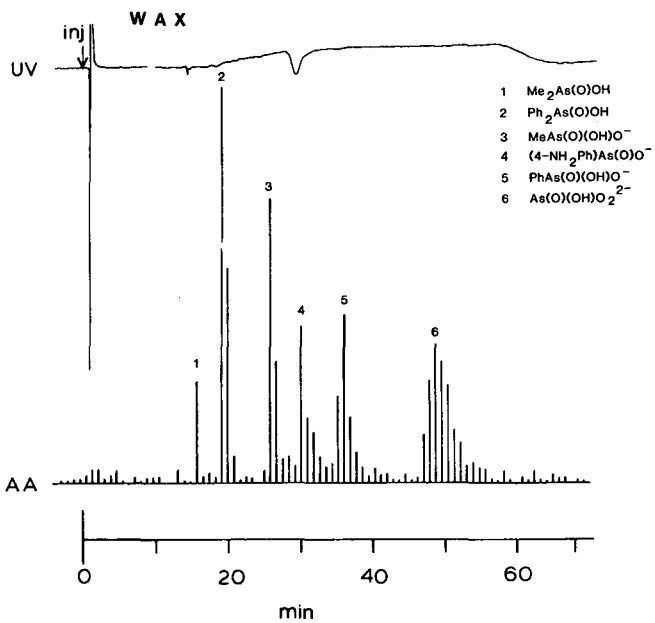

Figure 1. UV and arsenic-specific AA chromatograms for an aqueous solution containing five organoarsenic acids and arsenate (as numbered) are compared. Complete separations of this and similar mixtures of other arsenicals were effected in comparable analysis times.

(XBL 8112-13100)

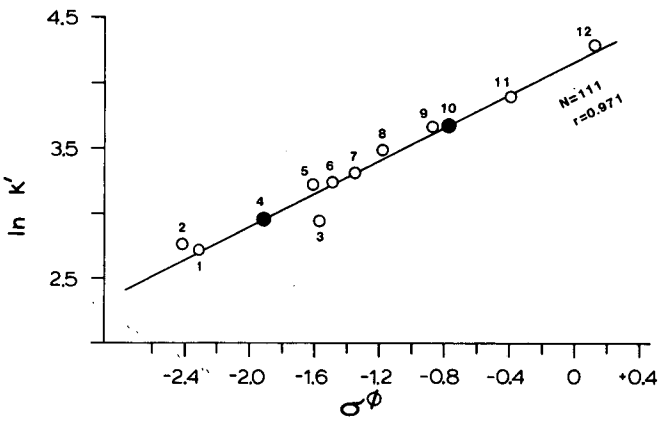

Figure 2. The linear regression between ln k' and $\Sigma\sigma\phi$ obtained on a weak anion exchange column (WAX) is shown for the following arsenicals:

1. $Me_2As(O)OH$
2. $Pe_2As(O)O^-$
3. $Ph_2As(O)OH$
4. $Me_2As(O)O^-$,
5. $BuAs(O)(OH)O^-$
6. $EtAs(O)(OH)O^-$
7. $MeAs(O)(OH)O^-$
8. $(4\text{-}NH_2Ph)As(O)(OH)O^-$
9. $PhAs(O)(OH)O^-$
10. $AsO(OH)_2O^-$
11. $As(O)(OH)O_2^{2-}$
12. $(4\text{-}NO_2Ph)As(O)O_2^{2-}$

The black circles indicate estimated ln k' for alternate choices of protonated or deprotonated arsenic species not acceptable in the fit shown.

(XBL 8112-13103)

cient of 0.971 based on 111 data points. Similar linear relationships also were obtained using different nonlinear convex and concave HPLC elution gradients. This linear relationship provides a method for predicting the retention time of a sought-after compound based on the calculated $\Sigma\sigma\phi$ value and for optimizing the desired separation by changing the chromatographic system to achieve the needed change in retention time for the difference in $\Sigma\sigma\phi$ values of the compounds to be separated.

Application to Oil Shale Kerogen and Shale Oil. Elemental analysis of sedimentary deposits has shown the enrichment of a number of elements, including As, in the carbonaceous deposits of coal, black shale, petroleum, and asphalt over average crystal abundances.[7] In general, both coal and oil shale contain higher concentrations of these elements than petroleum. The increased used of coal and oil shale as alternatives to petroleum will cause the redistribution of arsenic contained in these matrices, depending upon the form of arsenic originally present, the type of process used to convert these materials to conventional liquid fuels, and their final use.

The association of arsenic with sulfide deposits in coal, particularly pyrite, has been reported,[8] although no analogous conclusions have been given for arsenic in oil shale. The accumulation of arsenic by modern-day algae may indicate the manner of enrichment of arsenic in oil shale (the fossilized remnants of ancient algal mats) by initial bioaccumulation and the subsequent metamorphosis of arsenic.[9]

The partitioning of arsenic during simulated in-situ oil shale retorting has shown that a significant quantity of arsenic is distributed to the product oil and the retort waters.[10] The application of the weak anion exchange separation of arsenic-containing compounds to a number of retort waters generated during oil shale retorting has been performed[8] and is illustrated in Figure 3a. The chromatogram reveals the presence of arsenate, phenylarsonic acid and a neutral arsenic-containing compound.

The origin of these organoarsenic compounds is not clear. It is possible that they are synthesized during the retorting process by the reac-

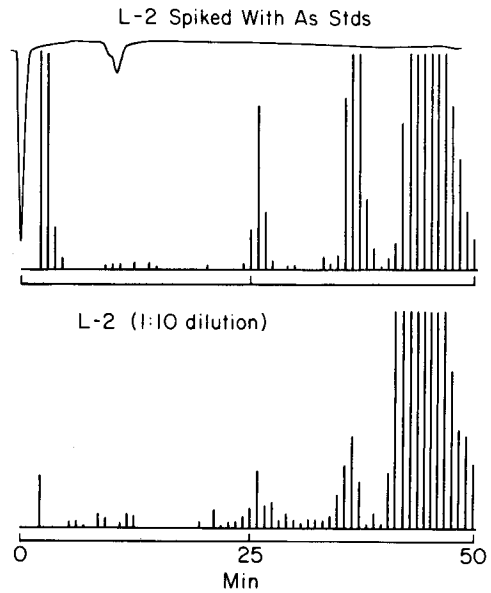

Figure 3a. The separation of arsenicals in a process water generated by a simulated in-situ retorting process (Lawrence Livermore National Laboratory L-2).

(XBL 8112-13101)

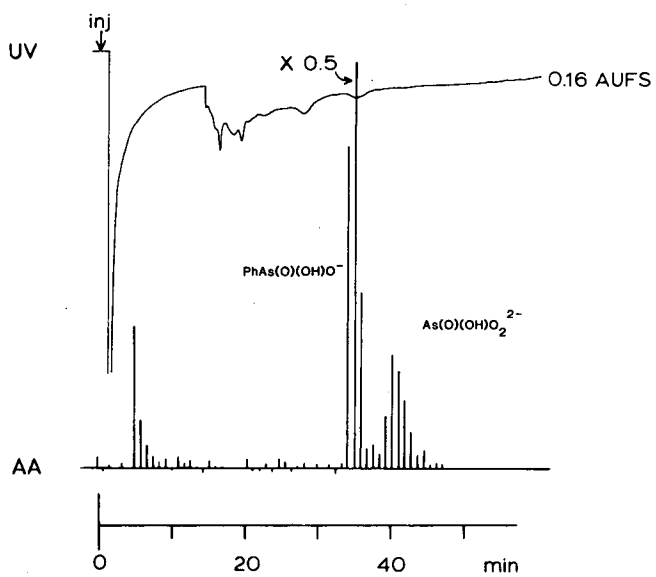

Figure 3b. The separation of arsenicals in a methanolic extract of ground oil shale (National Bureau of Standards).

(XBL 8112-13102)

tion of alkyl halides with arsenate, according to the Meyer reaction.[11] It is also conceivable that these organoarsenicals were initially present in the oil shale, being liberated during the retorting and partitioned into the retort waters. To investigate this possibility, ground oil was extracted with methanol, using a Soxlet apparatus. Figure 3b shows the separation of arsenic-containing compounds in this methanol extract, indicating the presence of a neutral arsenic-containing compound, phenylarsonic acid, and arsenate. At the present time, the identification of phenylarsonic acid is only tentative because of interference from a less ionic form of arsenate found in methanolic solutions, as previously reported.[6] This less ionic form of arsenate is probably the dimethyl ester of arsenate, which has a $\Sigma\sigma\Phi$ value of -0.24. It is therefore predicted to elute from the column with a retention time similar to phenylarsonic acid. A recent report on the hydrolysis of arsenate triesters indicates that the first and second hydrolysis steps are very rapid when conducted at pH $\sim$ 12.[12] In the present work, the hydrolysis rate does not appear to be as rapid on the chromatographic time scale, possibly due to the lower pH (7.1 to 8.1) of the eluting solvent, the ammonium carbonate buffer, and the presence of the column substrate. Preliminary hydrolysis experiments of the methanol oil shale extract indicate the presence of phenylarsonic acid, but more extensive kinetic experiments and the use of an alternate measurement method are now necessary to confirm and quantitate phenylarsonic acid.[13]

PLANNED ACTIVITIES FOR FY 1982

The correlation of the linear sum of the appropriate structural substituent parameter with the logarithm of the chromatographic capacity factor for organoarsenicals ($\sigma\Phi$) has been found to be linear. This enables prediction of: the retention time of a sought-after compound, the possible structure(s) of unknown compounds from experimentally determined retention times, and the possible co-elution of interfering compounds. In addition, this relationship can be used to optimize diverse chromatographic systems, including ion exchange and solvophobic mechanisms, for a desired separation. The analysis of a methanol oil shale extract has demonstrated the utility of structural substituent parameters as a diagnostic tool in the liquid chromatographic speciation of trace metals and metalloids in complex matrices commonly associated with energy-related processes.

REFERENCES

1. Baker, J.K. (1979), "Estimation of High Pressure Liquid Chromatographic Retention Indices," Anal. Chem. 51, pp. 1693-1697.

2. Hammett, L.P. (1935), "Some Relations between Reaction Rates and Equilibrium Constants," Chem. Rev. 17, p. 125.

3. Mastrykova, T.A. and Kabachnik, M.I. (1969), "The Application of the Hammett Equation with the Constants in the Chemistry of Organophosphorous Compounds," Russian Chem. Rev. 38, 10, pp. 795-811.

4. Hansch, C., and Leo, A. (1979), Substituent Constant for Correlation Analysis in Chemistry and Biology, John Wiley and Sons, New York, p. 339.

5. Jewett, K.L., and Brinckman, F.E. (1981), "Speciation of Trace Di- and Triorganotins in Water by Ion-Exchange HPLC-GFAA" J. Chromatogr. Sci. 19, in press.

6. Parks, E.J., Brinckman, F.E., and Blair, W.R. (1979), "Application of a Graphite Furnace Atomic Absorption Detector Automatically Coupled to a High Performance Liquid Chromatograph for Speciation of Metal-Containing Macromolecules," J. Chromatogr. 185, pp. 563-572.

7. Karuskopf, K.B. (1955), "Sedimentary Deposits of Rare Metals," Econ. Geol. 50th Anniversary Volume, pp. 411-470.

8. Finkleman, R.B. (1980), Modes of Occurrence of Trace Elements in Coal, Ph.D. Dissertation, University of Maryland.

9. Fish, R.H., Brinckman, F.E., and Jewett, K.L. (1982), "Fingerprinting Inorganic Arsenic and Organoarsenic Compounds in In Situ Oil Shale Retort and Process Waters Using a Liquid Chromatograph Coupled with an Atomic Absorption Spectrometer as a Detector," Environ. Sci. Technol. 16, p. 174; Lawrence Berkeley Laboratory Report LBL-11476.

10. Fox, J.P. Mason, K.K., and Duvall, J.J. (1979), "Partitioning of Major, Minor, and Trace Elements during Simulated In Situ Oil Shale Retorting in a Controlled-State Retort," in Twelfth Oil Shale Symposium Proceedings, Gary, J.H., Ed., Colorado School of Mines Press, Golden, Colo., pp. 58-71.

11. Meyer, G. (1883), Ueber Einige Anomale Reaktionen. Ber. 16, 1439.

12. Baer, C.D., Edwards, J.O., and Riger, P.M. (1981), "Kinetics of the Hydrolysis of Arsenate (V) Triesters," Inorg. Chem. 20, pp. 905-907.

12. In a recent experiment (LBL), we have identified phenylarsonic acid unequivocally by derivatization followed by capillary column gas chromatography-mass spectrometry analysis.

Speciation of Vanadyl Porphyrins and Non-Porphyrin Compounds in Heavy Crude Oils by HPLC-GFAA and the Competitive Equilibria Between Vanadyl Porphyrins and Multidentate Ligands*

R. H. Fish, J. J. Komlenic, and T. Vermeulen

The identification of vanadyl porphyrin and non-porphyrin compounds in heavy crude oils is mandatory if methods for vanadium removal are to be implemented. The use of high-performance liquid chromatography for the separation of the above-mentioned compounds and graphite furnace atomic absorption for detection (HPLC-GFAA) of vanadium (318.4 nm) compounds will be discussed.

The removal, with multidentate ligands, of VO^{2+} ion from etioporphyrin represents a novel approach for the possible future utilization of polymeric multidentate ligands for removal and recovery of vanadium from heavy crude oils.

ACCOMPLISHMENTS DURING FY 1981

Speciation Studies of Vanadium Compounds in Heavy Crude Oils

We have initiated speciation studies on heavy crude oils (Cerro Negro, Wilmington, and Prudhoe Bay) by the HPLC-GFAA combination and have demonstrated the usefulness of this technique to identify known vanadyl complexes and as a tool to fingerprint the oils.

Figure 1 demonstrates the potential nature of the HPLC-GFAA combination with known compounds (visible detector at 400 nm, GFAA detector at 318.4 nm for vanadium) using a solvent system of 30 percent chloroform in hexane to 70 percent chloroform in hexane for 20 minutes and held at 70 percent chloroform to 30 percent hexane for 10 minutes (flow rate 2.0 ml/min).

Figure 2 demonstrates the fingerprint of a pyridine extract of Cerro Negro heavy crude oil (Venezuelan) at 400 nm (visible detector) which was extracted to isolate the vanadyl porphyrins.[1] The separation was not maximum, however, fully demonstrating the complexity of vanadyl porphyrins in heavy crude oils. Both Wilmington and Prudhoe Bay oils had their own fingerprints, with Wilmington's similar to Cerro Negro and Prudhoe Bay's different from the other two. We are presently trying to maximize our separations by changing the visible wavelength detector to define various porphyrin substitutions.

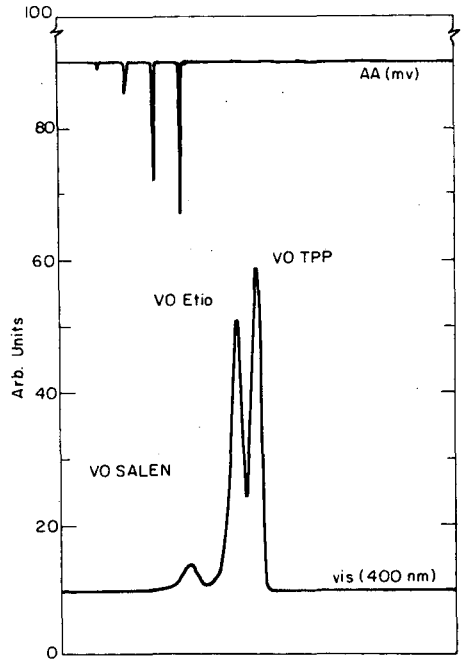

Figure 1. Potential nature of HPLC-GFAA combination with known compounds.

Mixture:	VO SALEN	Column Conditions:
in	VO TPP	30-70% $CHCl_3$ in hexane over 20 min.
$CHCl_3$	VO Etio	70% $CHCl_3$ in hexane 10 min.
Flow rate:	2.0 ml/min.	

(XBL 8112-13181)

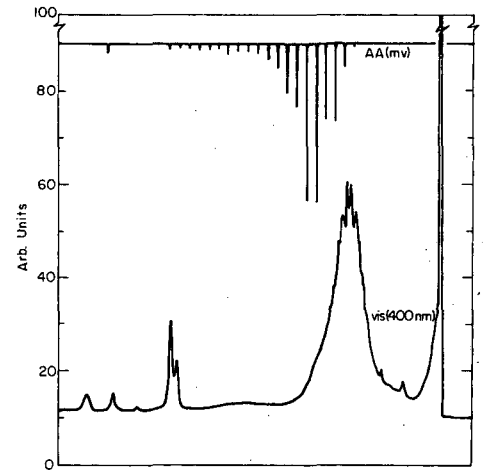

Figure 2. Fingerprint of a pyridine extract of Cerro Negro heavy crude oil. Column conditions: 0-100% CH_2Cl_2 in hexane over 30 min., 100% Ch_2Cl_2 in hexane 15 min.; flow rate: 2.0 ml/min.

(XBL 8112-13182)

*This work was supported by the Assistant Secretary for Fossil Energy, the Assistant Secretary for Oil, Gas, and Shale Technology, and the Bartlesville Energy Technology Center of the U.S. Department of Energy under Contract No. DE-AC03-76SF00098.

Competition Experiments Between Vanadyl Etioporphyrin and Multidentate Ligands

We have initiated our competition experiments by analyzing the equilibrium mixtures using HPLC-GFAA as well as multicomponent UV-VIS analysis with a microprocessor.

Figure 3 shows a competition experiment with the following equilibrium:

$$\text{EtioVo} + \text{TPPH}_2 \rightleftharpoons \text{TPPVO} + \text{EtioH}_2 \qquad (1)$$

as analyzed by HPLC-GFAA. Using this technique we can make an instantaneous analysis of vanadyl porphyrins and free bases, i.e., EtioH_2 or EtioVo.

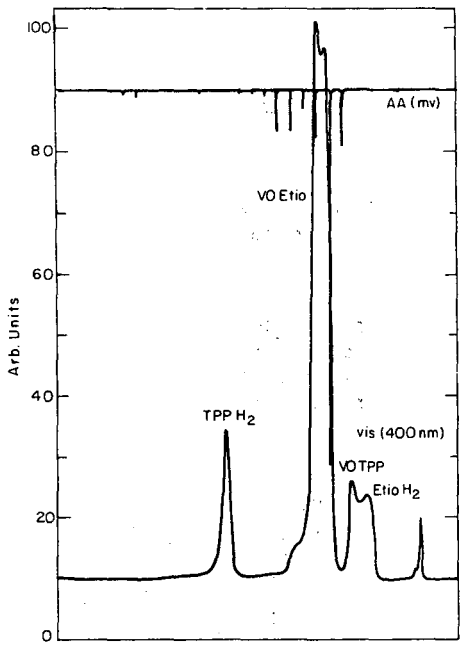

Figure 3. Competition experiment with equilibrium: EtioVo + $\text{TPPH}_2 \rightleftharpoons$ TPPVO + EtioH_2. Mixture: VOTPP, TPPH_2, VOEtio, EtioH_2; column conditions: 40-50% CH_2Cl_3 in hexane over 30 min.; flow rate: 2.0 ml/min.

(XBL 8112-13183)

By multicomponent analysis of this equilibrium with both a Cary 219-Apple II and H.P. 8550 UV-VIS instrument, we infer a definite shift to the right, i.e., TPPVO is favored. We are evaluating both methods for future competition experiments.

PLANNED ACTIVITIES FOR FY 1982

It is hoped that the HPLC-GFAA combination will help facilitate both the speciation and identification work. The vanadium chemistry is focusing on new multidentate ligands, and we have synthesized a number of new ligands and their vanadyl complexes, for example, compounds 2 and 3.

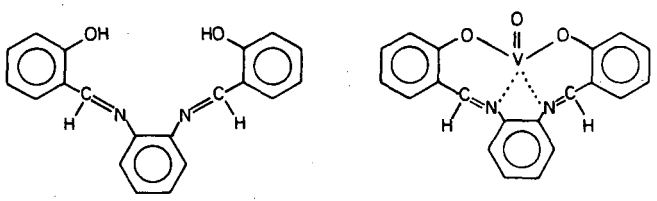

Compound 2 is presently being tested in competition experiments.

REFERENCE

1. Baker, E.W. (1969), in Organic Geochemistry, Eglington and Murphy, Eds., Springer-Berlin, Chap. 19, p. 464.

Reactions of Inorganic and Organoarsenic Compounds with Substituted Catechols*

R. H. Fish and R. J. Tannous†

Heavy crude oils will have a significant role in meeting future energy needs for the United States. These energy sources, however, are not without their economic and environmental problems. For example, heavy crude oils are extremely high in transition metal content,[1] e.g., V, Cr, Fe, Ni, etc.; and shale oils are high in arsenic.[2] These metals can affect subsequent catalytic hydroprocessing and can plug catalyst pores, as well as react chemically with active sites or support material.[3]

Thus, it is extremely important to remove and recover these metals to alleviate not only economic refining problems, but also some of the environmental problems, related to the health of workers and the contamination of air and water resources, caused by these crude and shale oils. For these reasons, we have embarked on a comprehensive program to study innovative ways to remove and recover transition metals and arsenic compounds from heavy crude oils and shale oils.

ACCOMPLISHMENTS DURING FY 1981

The initial stages have been directed toward obtaining: (a) total metal content analysis of various heavy crude oils, shale oils, and coal liquids; (b) speciation or molecular characterization studies of these materials by high performance liquid chromatography in combination with graphite furnace atomic absorption detection[4]; and (c) coordination chemistry of arsenic with multidentate ligands capable of being placed in a polymeric backbone for future percolation column studies.[5]

For over forty years,[6,7] it has been known that catechol derivatives can coordinate a wide variety of metals including arsenic. Thus, we thought that catechols with functional groups, which would permit future attachment to a polymeric support for use in a percolation-type column, would be important ligands to react with the arsenic compounds we identified previously.[4] Recent studies by LBL scientists have confirmed the utility of catechol derivatives in sequestering metals such as iron.[8-10]

The following multidentate ligands, 1-6, were reacted with methyl and phenylarsonic acid, while compound 7 was reacted with arsenate (Chart 1).

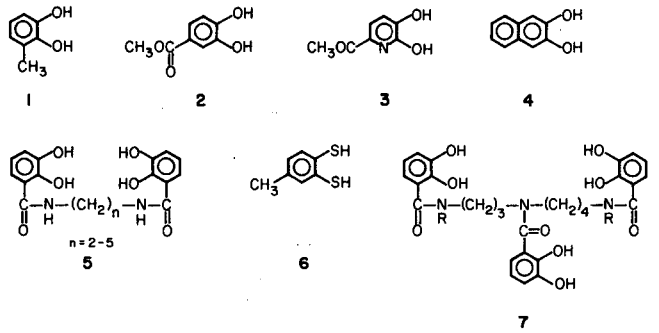

Chart 1. Multidentate ligands used in synthesis reactions with arsonic acids and arsenate.
(XBL 818-10974)

The reaction of compounds 1-6 provided the five-coordinate organoarsenic compounds (Eq. 1), several of which were a mixture of cis and trans isomers as determined by ^{1}H nuclear magnetic resonance spectroscopy.

Synthesis of Five-Coordinate Organoarsenic Catecholates

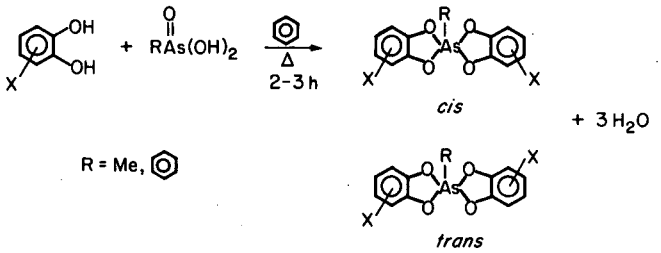

X	R	% cis	% trans
3-CH_3	CH_3	~50	~50
"	Ph	~10	~90(?)
3,3'-C(=O)N(H)$(CH_2)_2$N(H)C(=O)	CH_3	100	
"	Ph	100	
4-$CH_3OC(=O)$-	CH_3		100(?)
"	Ph	5	95(?)

Arsenate, AsO_4^{3-}, reacted with 3,4 LICAM to give an encapsulated arsenic atom (Eq. 2). This octahedrally coordinated arsenic anion is optically active (d,l enantiomers), and represents the first such metal compound of this new class of ligands to be isolated and characterized.

These compounds (Eqs. 1 and 2) were characterized by nuclear magnetic resonance spectroscopy, mass spectrometry, infrared spectroscopy, and elemental analyses. Figures 1 and 2 provide the high field nmr spectrum and electron impact mass spectrum, respectively, of the phenylarsonic acid-3-

*This work was supported by the Assistant Secretary for Fossil Energy, the Assistant Secretary, Oil, Gas, and Shale Technology, and the Bartlesville Energy Technology Center of the U.S. Department of Energy under Contract No. DE-AC03-76SF00098.
†UCB-LBL Undergraduate Special Research Topic Student, 1981-82.

Six-Coordinate Arsenic Tricatecholate Anion

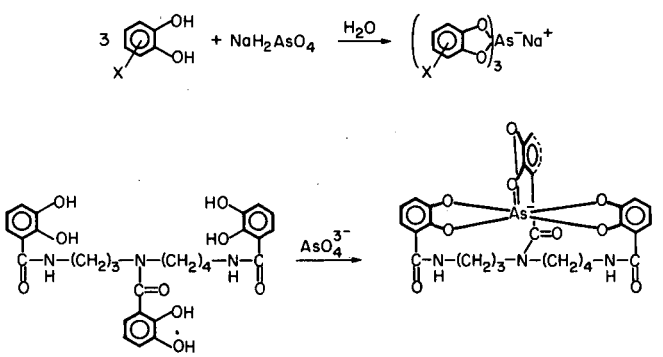

methylcatechol derivative and clearly demonstrate the use of these techniques in the structural elucidation of these compounds.

PLANNED ACTIVITIES FOR FY 1982

We hope to synthesize polymeric derivatives of the substituted catechols and verify, in column experiments with the speciated inorganic and organoarsenic compounds, that these polymeric catechols are potentially capable of removing these arsenic compounds from complex matrices, such as shale oil and retort waters.

REFERENCES

1. Yen, T.F. (1975), Role of Trace Metals in Petroleum, Ann Arbor Science Publishers, Ann Arbor, Mich., Chap. 1, p. 1.

2. Yen, T.F., and Chillingarianm, G.V., Eds. (1976), Development of Petroleum Science, Vol. 5, "Oil Shale," Elsevier Scientific Publishing Co., Amsterdam.

3. Silbernagel, B.G., and Riley, K.L. (1980), Catalyst Deaction, B. Delmon and G.F. Froment, Eds., Elsevier Scientific Publishing Co., Amsterdam, p. 313.

4. Fish, R.H., Brinckman, F.E., and Jewett, K.L. (1982), "Fingerprinting Inorganic Arsenic and Organoarsenic Compounds in In-Situ Oil Shale Retorted Process Waters Using a Liquid Chromatograph Couple with an Atomic Absorption Spectrometer as a Detector," Environ. Sci. Technol. 16, p. 274; Lawrence Berkeley Laboratory Report LBL-11476.

5. Fish, R.H., and Weitl, F.L. (1981), "Arsenic Coordination Chemistry: Reactions Substituted Catechols that are Potential Ligands for Removal of Arsenic Compounds from Shale Oil," in Abstracts, Tenth International Conference on Organometallic Chemistry, Toronto, Canada, August 9-14, 1981, Abstract 1D12, p. 62; Lawrence Berkeley Laboratory Report LBL-12249.

6. Schmidt, H. (1933), U.S. Patent 1,889,383.

7. I.G. Farben Industries A-G, (1931), United Kingdom Patent 376,346.

8. Weitl, F.L., Harris, W.R., and Raymond, K.N. (1979), "Sulfonated Catecholamide Analogues of Enterobactin as Iron Sequestering Agents," J. Med. Chem. 22, p. 1281.

9. Weitl, F.L., et al. (1978), "Specific Sequestering Agents for the Actinides. 1. N, N', N", N'''-Tetra (2,3-Dihydroxybenzoyl) Tetraazacyclotetra- and -Hexadecanes," J. Amer. Chem. Soc. 100, p. 1170.

10. Weitl, F.L., and Raymond, K.N. (1979), "Ferric Ion Sequestering Agents. 1. Hexadentate O-Bonding N, N', N"-Tris (2,3-Dihydroxybenzoyl) Derivatives of 1,5,9 - Triazacyclotridecane and 1,3,5 - Triaminomethylbenzene," J. Amer. Chem. Soc. 101, p. 2728.

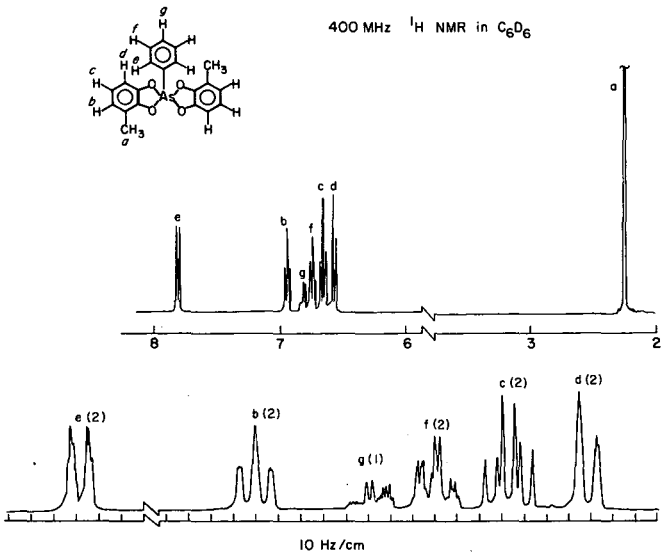

Figure 1. 400 MHz ^1H nmr spectrum of the phenylarsonic acid-3-methylcathecholate derivative.
(XBL 818-10971)

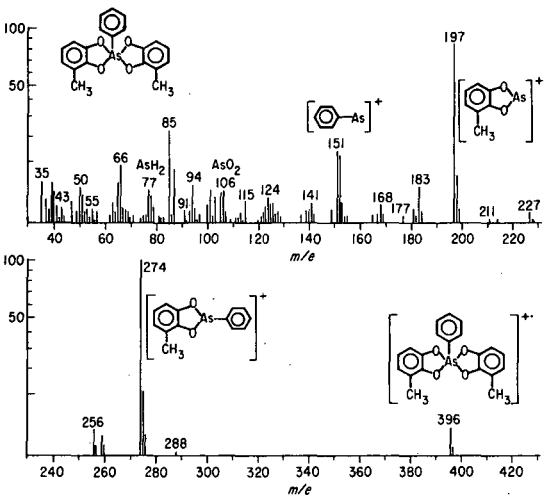

Figure 2. EIMS of phenylarsonic acid-3-methylcatecholate derivative.
(XBL 818-10977)

Homogeneous Catalytic Hydrogenations of Model Synthetic Fuel Compounds*

R. H. Fish, G. A. Cremer, T. Vermeulen, and A. Thormodsen

Pettit and his co-workers recently demonstrated the use of carbon monoxide and water as a reducing agent for the hydroformylation of olefins and the use of carbon monoxide, water, and hydrogen in the reduction of nitroarenes.[1-3] In Pettit's studies, the compounds responsible for these catalytic reactions were transition metal carbonyl hydrides that had been generated catalytically under the reaction conditions (Eq. 1).

$$M_x(CO)_y + OH^- \rightarrow \bar{M}_x(CO)_{y-1}COOH \xrightarrow[+H_2O]{-CO_2} H_2M_x(CO)_{y-1} \quad (1)$$

These results prompted us to study the utilization of these reagents for the reduction of polynuclear aromatic and polynuclear heteroaromatic nitrogen compounds. The importance of studying these types of polynuclear compounds and reducing agents stems from the need to learn more about the basic aspects of coal liquefaction and the hydroprocessing of coal liquids and shale oils.[4] Additionally, it is well known that homogeneous catalytic reductions proceed at lower temperatures and pressures and give higher regioselectivities when compared to their heterogeneous counterparts.[5,6]

ACCOMPLISHMENTS DURING FY 1981

Utilization of Carbon Monoxide and Water or Carbon Monoxide and Hydrogen as a Reducing Agent for Model Fuel Compounds

We wish to demonstrate the potential of carbon monoxide and water or carbon monoxide and hydrogen as reducing agents for polynuclear aromatic and polynuclear heteroaromatic nitrogen compounds (Chart 1), using transition metal carbonyl compounds as homogeneous catalysts. Table 1 provides the results for the reaction of a wide variety of transition metal carbonyl compounds in the reduction of anthracene to 9,10-dihydroanthracene under water-gas shift (wgs) conditions (CO, H_2O, base). Clearly, only manganese, cobalt, and iron carbonyls (substituted phosphine analogs) reduce to any extent, while the carbonyls of Ru, Rh, W, Os, Re, and Mo all produced hydrogen and carbon dioxide but no 9,10-dihydroanthracene.

These results can be rationalized partially by the fact that the latter transition metal carbonyl hydrides are unstable under the reaction conditions

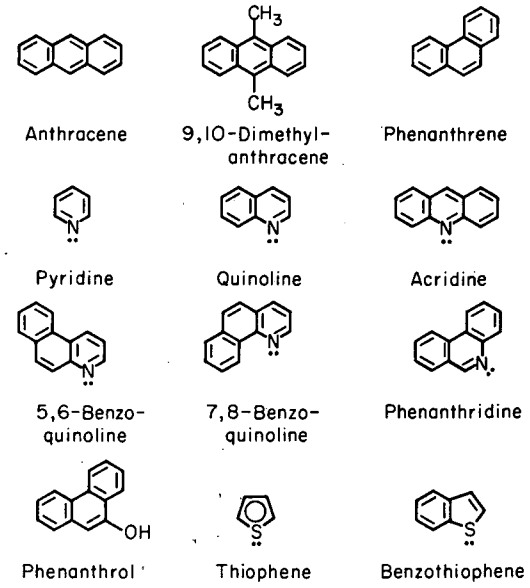

Chart 1. Polynuclear aromatic and polynuclear meteroaromatic nitrogen compounds reacted under water-gas shift or synthesis-gas conditions. (XBL 8110-11796A)

Table 1. Reduction of anthracene, under water-gas shift conditions, with transition metal carbonyls as catalysts.[a]

Catalysts	Temp (°C)	% Product 9,10-dihydroanthracene[b,c]
$Fe(CO)_4Bu_3P$	200	8
$Mn_2(CO)_8(Bu_3P)_2$	200	13
$Mn_2(CO)_8(Bu_3P)_2$	180	8
$Co_2(CO)_6(\phi_3P)_2$	160	3
$W(CO)_6$	200	- d
$Re_2(CO)_{10}$	200	- d
$Os_3(CO)_{12}$	200	- d
$RuCl_2(CO)_2(\phi_3P)_2$	180	- d
$Rh_6(CO)_{16}$	180	- d
$Mo(CO)_5Bu_3P$	180	- d

[a]Solvent THF (12 ml), 0.2 m KOH (3ml), P_{CO} 350 psi, 5 hr, 1 mmole of 1, 10:1 substrate to catalyst ratio in a 45 ml Parr mini-reactor.
[b]The product percentage was found by area ratios of starting material and product using a HP 5880A capillary gas chromatograph with digital integration [12 m x 0.1 mm OV 101 at 60° (10°/min)] and flame ionization detection.
[c]The product was isolated by column chromatography on Florisil (benzene) and identified by GC-EIMS and by nuclear magnetic resonance spectroscopy (250 MHz, ^1H).
[d]A mass spectral analysis of the gases identified both H_2 and CO_2.

*This work was supported by the Director, Office of Energy Research, Office of Basic Energy Science, Chemical Sciences Division, and the Assistant Secretary for Fossil Energy, Office of Coal Research, Liquefaction Division, of the U.S. Department of Energy through the Pittsburgh Energy Technology Center under Contract No. DE-AC03-76SF00098.

and undergo reductive elimination of hydrogen, rather than hydrogen transfer to the polynuclear aromatic substrate, i.e., $k_2 > k_1$ (Eq. 2).

$$M_x(CO)_{y-1} + ArH_2 \underset{k_1}{\overset{+Ar}{\leftarrow}} H_2M_x(CO)_{y-1} \underset{k_2}{\overset{-H_2}{\rightarrow}} M_x(CO)_{y-1} \quad (2)$$

In view of these discoveries, we decided to learn more about the parameters of this reaction, using $Mn_2(CO)_8(Bu_3P)_2$ as the catalyst. The reaction of carbon monoxide and deuterium oxide (D_2O) with anthracene provided only 9,10-dideuteroanthracene,[7] and this result strongly indicates that the hydrogen comes exclusively from water. In addition, the presence of added deuterium gas (D_2) provided no deuterium incorporation, thereby eliminating a mechanism which includes oxidative addition of H_2 to any coordinatively unsaturated manganese species that might be formed[3] and supports the facile reaction (Eq. 1) of hydroxide ion on coordinated CO as the major reaction pathways to the carbonyl hydrides. Several control experiments verified that the reduction product, 9,10-dihydroanthracene, did not undergo exchange of hydrogen for deuterium under the reaction conditions (Table 1).

In an experiment to elucidate the stereochemistry of the anthracene reaction, we reacted an analog, 9,10-dimethylanthracene, with $Mn_2(CO)_8(Bu_3O)_2$ under water-gas shift conditions (180°, 5 hrs, 350 psi CO, 0.2 M KOH in THF, sub/cat = 20), to provide a 30 percent yield of cis and trans-9,10-dihydro-9,10-dimethylanthracene and in a ratio of 53%:4% (Ref. 8). The mechanistic implication of this result strongly suggests a free-radical process for this reaction. A similar result was recently reported by Halpern et al.[9] for the reaction of 9,10-methylanthracene and $Mn_2(CO)_{10}$ and by Taylor and Orchin[10] with $Co_2(CO)_8$ under syn gas conditions (CO_2, H_2 1:1, 200°). We also found that, in the absence of aqueous base and in the presence of hydrogen, i.e., synthesis-gas condition (CO/H_2 = 1), better yields of reduced polynuclear aromatic products could be obtained.

From the results, it is evident that bent polynuclear aromatic compounds are extremely unreactive under either wgs or syn-gas conditions, when compared to anthracene, a linear polynuclear aromatic compound.[11]

It is important that polynuclear heteroaromatic compounds, specifically with nitrogen as the heteroatom, be studied because they are highly prevalent in all coal and oil shale products.[12] We found an increase in reactivity for the polynuclear heterocyclic nitrogen compounds, under either wgs or syn-gas conditions, compared to their carbon analogs, e.g., acridine was more reactive than anthracene. Table 2 summarizes our results with a variety of polynuclear heteroaromatic nitrogen compounds.

PLANNED ACTIVITIES FOR FY 1982

Relevant conclusions from these studies suggest that the homogeneous catalytic hydrogenations of polynuclear heteroaromatic nitrogen compounds, under water-gas shift or synthesis-gas conditions, are more favorable than the polynuclear aromatic compounds. The high regioselectivity, as shown by the ease with which a nitrogen heterocyclic ring gets hydrogenated in preference to a benzene ring, strengthens the above conclusions. This result is consistent with the lowered aromaticity of the nitrogen heterocyclic ring versus their carbon analogs, which provides a lower activation energy for hydrogenation.[13]

The overall observed relative reactivities under either water-gas shift or syn-gas conditions is:

acridine >> anthracene > quinoline > phenanthridine

5,6-benzoquinoline > 7,8-benzoquinoline

≈ pyrene > > > phenanthrene

This order, while qualitative, is still significant because these polynuclear compounds are present in coal, coal liquids, and shale oil. This is the first logical explanation for compound reactivity under catalytic hydrogenation conditions in these complex matrices.

Finally, the fact that Fe, Mn, and Co carbonyls give reduced products, while other transition carbonyls are unreactive, implies important mechanistic differences. In addition to the instability factor for several of the transition carbonyl hydrides in our studies, we found a pronounced carbon monoxide inhibition on the catalytic hydrogenation reactions, especially with the ruthenium carbonyls and report these results in future papers.[14] We are continuing to pursue this important area of fossil energy research.[15]

REFERENCES

1. Kang, H.C., et al. (1977), "Reductions with Carbon Monoxide and Water in Place of Hydrogen. 1. Hydroformylation Reaction and Water Gas Shift Reaction," J. Amer. Chem. Soc. 99, p. 8923 and references therein.

2. Cann, K., et al. (1978), "Catalytic Reductions Using Carbon Monoxide and Water in Place of Hydrogen. 2. Reduction of Aromatic Nitro Compounds to Amines," J. Amer. Chem. Soc. 100, p. 3969.

3. Cole, T., et al. (1980), "Homogeneous Catalysts for Utilization of Synthesis Gas as a Reducing Agent," J. Amer. Chem. Soc. 102, 6182.

4. Whitehurst, D.D., Ed. (1980), Coal Liquefaction Fundamentals, ACS Syn. Series 139, Amer. Chem. Soc., Washington D.C.

5. James, B.J. (1973), Homogeneous Hydrogenations, John Wiley and Son, New York.

6. Parshall, G.W. (1980), "Organometallic Chemistry in Homogeneous Catalysis," Science 2098, 1221.

Table 2. Reduction of polynuclear heteroaromatic nitrogen compounds under water-gas shift[a] (WGS) and syn-gas (SG) conditions[b] with transition metal carbonyls as catalysts.

Substrate	Catalyst	Sub/Cat	Temp.(°C)	Time(hr)	Conditions	Products (%)[d]
Acridine	$Fe(CO)_5$ [c]	10	180	2	WGS	9,10-dihydro-acridine (100)
Acridine	$Mn_2(CO)_8(Bu_3P)_2$	10	200	2	WGS	(38) "
Acridine	$Mn_2(CO)_8(Bu_3P)_2$	20	200	2	SG	(100) "
Acridine	$Co_2(CO)_6(\phi_3P)_2$	20	200	2	SG	(100) "
5,6-benzo-quinoline	$Mn_2(CO)_8(Bu_3P)_2$	20	200	2	SG	1,2,3,4 tetrahydro-5,6-benzo-quinoline (7)
5,6-benzo-quinoline	$Mn_2(CO)_8(Bu_3P)_2$	20	200	5	WSG	(4) "
5,6-benzo-quinoline	$Fe(CO)_4(Bu_3P)$	10	180	5	WSG	(1) "
5,6-benzo-quinoline	$Co_2(CO)_6(\phi_3P)_2$	20	200	2	SG	(8) "
Quinoline	$Fe(CO)_5$	10	180	2	WGS	1,2,3,4-tetrahydro-quinoline (0)
Quinoline	$Mn_2(CO)_8(Bu_3P)_2$	20	200	5	WGS	(4) "
Quinoline	$Mn_2(CO)_8(Bu_3P)_2$	20	200	5	SG	(33) "
Quinoline	$Co_2(CO)_6(\phi_3P)_2$	20	200	1	SG	(70) "
7,8-benzo-quinoline	$Mn_2(CO)_8(Bu_3P)_2$	20	200	2	SG	1,2,3,4 tetrahydro-7,8-benzo-quinoline (2)
7,8-benzo-quinoline	$Mn_2(CO)_8(Bu_3P)_2$	20	200	2	WGS	No Product
Phenanth-ridine	$Mn_2(CO)_8(Bu_3P)_2$	20	200	2	WGS	9,10-dihydro-phenanthridine (1)
Phenanth-ridine	$Mn_2(CO)_8(Bu_3P)_2$	20	200	2	SG	(11) "
Phenanth-ridine	$Co_2(CO)_6(\phi_3P)_2$	20	200	2	SG	(21) "

[a]Reaction run in THF (12 ml) with 0.2M KOH (3 ml), 350 psi CO.
[b]350 psi H_2 and 350 psi CO in THF (15 ml).
[c]800 psi CO.
[d]Determined by capillary GC using a digital integrator (HP 5880A). Isolated by column chromatography (Florisil) and identified by GC-MS and nmr spectroscopy (250 mHz, ^1H).

7. GC-EI mass spectral analysis showed m/e 182 (100%) consistent with two deuteriums being incorporated into compound 1 (m/e 178).

8. The cis and trans isomers of 9,10-dihydro-9,10-dimethylanthracene could be cleanly separated on a 12 x 0.1 mm i.d., fused silica capillary column (OV 101) using a HP 5880A instrument with flame ionization detection (temperature programming 60°-200°, 20°/min).

9. Sweany, R., Buttler, S.C., and Halpern, J. (1981), "The Hydrogenation of 9,10-Dimethylanthracene by Hydridopentacarbonyl Management (I.). Evidence for a Free Mechanism," J. Org. Chem. 213, p. 487.

10. Taylor, P.D. and Orchin, M.J. (1972), "Hydrogenation of 9,10-Dimethylanthracene with Cobalthydride Carbonyl," J. Org. Chem. 37, p. 3913.

11. Friedman, S., et al. (1959), "Selective Hydrogenation of Polynuclear Aromatic Hydrocarbons," J. Org. Chem. 24, p. 1287.

12. Larsen, J.W., Ed. (1978), Organic Chemistry of Coal, ACS Symposium Series 71, Am. Chem. Soc., Washington, D.C.

13. Dewar, M.J.S. (1969), The Molecular Theory of Organic Chemistry, McGraw-Hill, New York.

14. Preliminary accounts of this work were presented at the 182nd National ACS Meeting, Aug. 23-28, 1981, New York, N.Y., Abstract IONR 49 and the Pacific Conference on Chemistry and Spectroscopy, Anaheim, CA, Oct. 12-21, 1981, Abstract 188 (LBL-12518 and LBL-12888).

15. Fish, R.H. and Cremer, G.A. (1981), J. Amer. Chem. Soc., submitted for publication (LBL-13734 and LBL-13735).

COAL-RELATED RESEARCH

Processing of Condensate Waters from Coal Conversion*

C. J. King, D. H. Mohr, P. D. MacKenzie, J. D. MacGlashan, C. L. Munson, and R. E. Thompson

Coal gasification and liquefaction processes produce large volumes of condensate waters, formed as reactor effluents are cooled. These waters typically contain large quantities of ammonia (0.5 to 2.0 percent), neutralized by near-equivalent amounts of CO_2 and H_2S. There are often high concentrations of dissolved organics, reflected by a high chemical oxygen demand (COD). Condensate waters from oil-shale retorting and thermal processing of biomass have similar characteristics.

Conventional biological treatment has been problematic for these waters, with a large degree of dilution often being required to achieve stable operation and with removals of COD often not exceeding 60 to 70 percent. Ammonia stripping, as conventionally practiced or as implemented in the U.S. Steel or Chevron processes for isolation of ammonia as a separate, salable product, requires a large amount of steam, typically in the range of 0.08 to 0.25 kg per kg of condensate water. The principal objective of the present work is, therefore, to develop solely physicochemical processing methods which will allow recycle of the processed water as cooling-tower make-up without an excessive energy requirement for processing. Emphasis is on solvent extraction and stripping, and combinations of those steps.

Our work to date has focused upon four different areas:

1. Analysis of individual components contributing to the chemical oxygen demand (COD) of typical condensate waters;

2. extraction with novel solvents that will allow more complete COD removal and/or lower energy consumption;

3. interpretation of rates of stripping of NH_3, CO_2, and H_2S from samples of real condensate waters; and

4. innovative combinations of extraction and stripping that have potential for substantially reducing the energy consumption for removal and isolation of NH_3.

*This work was supported by the Assistant Secretary for Environment, Office of Environmental Progress, Environmental Technology Division of the U.S. Department of Energy under Contract No. DE-AC03-76SF00098.

Results through 1980 are described in the FY 1979 and FY 1980 annual reports. Phases of the project already completed concern: (a) extractability of phenols with conventional solvents, such as diisopropyl ether (DIPE) and methyl isobutyl ketone (MIBK);[1,2] (b) the effect of pH and temperature upon extractability;[1,2] (c) recovery of residual dissolved solvent through vacuum stripping,[2] and (d) relation of observed stripping rates of NH_3, CO_2, and H_2S to molecular-thermodynamic theory.[3]

ACCOMPLISHMENTS DURING FY 1981

Several samples of condensate water were obtained from the slagging fixed-bed gasifier at the Grand Forks Energy Technology Center (GFETC). This water had not been exposed to air and was sampled and stored under N_2 in the absence of light and in a cold room. Samples were obtained, both unchanged in pH and reduced to pH 2 by the addition of sulfuric acid. Aliquots of these samples were analyzed quantitatively by a gradient-elution high-performance liquid chromatography (HPLC) technique, using a water/methanol gradient with a C-18 μ-Bondapak column. For qualitative identification of individual peaks, both combined gas-chromatography/mass-spectrometry (GC/MS) and co-chromatography tests with known compounds were used.

Analyses of initial results and data reported in the literature strongly suggested that a considerable fraction of the COD is associated with substances that have low volatility and/or are poorly extracted in the standard initial methylene chloride extraction step in GC/MS analysis. For this reason, a new technique of solvent replacement was developed. Isopropanol (HPLC grade) is added to an initially aqueous sample of condensate water, which is then heated to evaporate the mixed isopropanol/water solvent. Repeated addition of isopropanol and evaporation leads to a final sample that is a concentrate of original solutes in isopropanol. This technique was also applied to individual fractions obtained from HPLC fractionation of the condensate water. The procedure is described in more detail elsewhere.[4] There are three principal requirements for the solvent-replacement procedure to work: (1) there must be a large enough concentration of the solute(s) to be identified in the original water, (2) the solute(s) must be soluble in isopropanol, and (3) the solute(s) must be sufficiently less volatile than isopropanol so that it is retained.

By use of the solvent-replacement technique and GC/MS analysis, members of the family of hydantoin compounds were identified in a condensate water for the first time. Most prevalent among these is 5,5-dimethyl hydantoin:

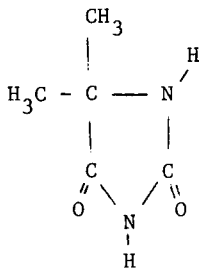

HPLC analyses of three different GFETC condensate-water samples at three different ages are shown in Table 1. In all cases, the pH of the sample was unchanged from the value in the original condensate water, about 8.5. The compounds are divided into three categories: monohydric phenols and their derivatives (nos. 1-7), dihydric phenols (nos. 8-11), and hydantoin compounds (nos. 12-16). There is a substantial difference in relative amounts of hydantoins between samples and, in the case of the third sample, the relative proportion of dihydric phenols.

Preliminary tests have been made to ascertain whether these differences among analyses stem from different water compositions at the time of initial sampling or from different ages of waters. Over an age period of 150 to 515 days, the measured COD of the 6/80 sample did not change significantly within a standard deviation of less than 2 percent. Individual component analyses for monohydric phenols, dihydric phenols, and hydantoins did not change significantly over the same period, except that the concentration of phenol itself may have decreased by up to 10 percent. For the June 10, 1981, sample, the COD and analyses for components in all three classes appeared to be stable over an age period from 40 to 132 days. Over an age range from 40 hours to 33 days, the measured COD and concentrations of Components 1-11 in the Sept. 30, 1981, sample appeared not to change. However, the measured concentrations of 5,5-dimethyl hydantoin increased from 293 ppm at 40 hours age to 407 ppm at 24 days age and to 456 ppm at 38 days age. For all three sampling dates, analyses of samples which had been lowered in pH to 2 or less at the time of sampling gave concentrations of Components 1-11 in good agreement with measurements of samples unchanged in pH, but showed lower concentrations of 5,5-dimethyl hydantoin (653 vs 1755 ppm, 150 vs 294 ppm, and 233 vs 293 ppm for the three samples and ages reported in Table 1). Increasing the pH of one of the acidified waters back to 8.5 caused the level of 5,5-dimethyl hydantoin to increase significantly, and acidifying one of the unchanged-pH waters did not bring about any detectable significant change in the 5,5-dimenthyl hydantoin level over time. Further tests are needed to establish the chemistry of hydantoin compounds and short-term aging effects in these waters more clearly. As is shown in Table 1, the components identified so far account for 71 to 83 percent of the measured COD of GFETC gasifier condensate water.

Table 1. HPLC analyses of GFETC gasifier condensate waters (all concentrations expressed in ppm, w/w).

Date of Sample:	6/80	6/10/81	9/30/81
Sample Age at Analysis:	6 months	6 weeks	40 hours
Components:			
1. Phenol	5028	7405	3528
2. Cresols	3238	4267	2422
3. C_2 Monohydric Phenols	456	473	434
4. o-Methoxy Phenol	259	448	165
5. p-Hydroxy Acetophenone	48	33	3
6. Acetophenone	20	-	-
7. 2-Naphthol	20	-	-
8. Pyrocatechol	973	848	38
9. 4-Methyl Catechol	613	497	21
10. Resorcinol	62	28	2
11. Hydroquinone	33	25	1
12. 5,5-Dimethyl Hydantoin	1755	294	293
13. 5-Methyl, 5-Ethyl Hydantoin	365	-	-
14. 5,5-Diethyl Hydantoin	270	-	-
15. 5-Methyl Hydantoic Acid	99	128	-
16. 5-Methyl Hydantoin	136	41	-
Measured COD:	35,810	46,650	23,510
Fractions of Measured COD Accounted for by:			
Components 1-7	0.621	0.661	0.685
Components 8-11	0.092	0.059	0.005
Components 12-16	0.112	0.014	0.019
All Identified Components	0.825	0.734	0.709

Extraction of Condensate Waters

Components 1-7 in Table 1 are relatively easy to extract and would be removed by common solvents, such as DIPE and MIBK.[1,2] Components 8-11 are more difficult to extract but can be removed by MIBK at sufficiently high solvent/water phase ratios, except at high pH.[1,2] The hydantoin compounds have very low activity coefficients in water, and preliminary tests show that they are not extracted well by common solvents used for extraction of phenols.

Removals of COD by extraction with MIBK and a mixture of 25 percent w/w trioctyl phosphine oxide (TOPO) in MIBK were reported in Table 2 of the FY 1980 Annual Report. Refinements in the technique for measuring COD increase the removals reported in that table by about 2 percent. Measurements of COD removal from the June 10, 1981 GFETC sample at 133 days age by one stage of MIBK extraction, followed by a stage of MIBK extraction at pH 3, show 88.5 percent removal of COD, about 2 percent higher than found for the June 1980 sample at ages of 136 and 498 days. Similar measurements for the Sept. 30, 1981, GFETC sample showed 93 percent removal of COD at a sample age of 40 hours, and 88.6 percent COD removal at 24 days.

In another series of tests with the June 1980 sample at 198 days age, four successive extractions at pH 2 with 25 percent TOPO in MIBK gave cumulative removals of 89.0, 92.2, 93.5, and 94.5 percent, respectively.

These results indicate that it is possible to achieve relatively high removals of COD by solvent-extraction procedures, although acidification is necessary to get the highest removals with

the solvents studied so far. There may also be an effect whereby aging decreases the extractability of COD, as shown by the extraction results for the Sept. 30, 1981, sample at ages of 40 hours and 24 days.

Extraction of Phenols with TOPO

Reexamination of the experimental conditions for the extractions of phenol from synthetic aqueous solutions by 25 percent w/w TOPO in diisobutyl ketone (DIBK), given in Table 3 of the FY 1980 Annual Report, showed that complete phase separation had not been achieved in the cases of higher stoichiometric ratios of TOPO to phenol and higher values of the equilibrium distribution coefficient (K_D). Repetition of these experiments gave values of K_D increasing to 812 at the highest stoichiometric ratio (9.9), at 20-25°C.

Table 2 shows values of K_D measured for extraction of phenol and the various unalkylated di- and tri-hydric phenols from water into 25 percent w/w TOPO in DIBK, with the initial molar ratio of TOPO to the phenolic compounds being 2.50 and the temperature being 30°C in all cases. From the results it is apparent that TOPO is a strong extractant for all the phenols and that it is possible to fractionate effectively among the isomers by TOPO extraction.

The effect of temperature upon K_D was investigated for extraction of phenol and of pyrocatechol from water into 25 percent TOPO in DIBK, with the objective of exploring the possibility of solvent regeneration through back-extraction at higher temperature. Values of K_D ranged from 462 to 148 for phenol and from 250 to 69.4 for pyrocatechol, over a temperature range of 22.5 to 60°C.

Combined Stripping and Extraction for Removal and Isolation of NH_3

At typical pH values of condensate waters (8 to 9.5), NH_3, CO_2, and H_2S are all ionized to a large extent. Since only the un-ionized species is volatile, the ionization suppresses the volatilities of these compounds over aqueous solution and thereby considerably increases the steam requirement for removal of these substances by stripping. If NH_3 and the acid gases are to be isolated from one another, as is needed for sale of an NH_3 product, more complex stripping-process configurations are required, and the steam requirement becomes still greater.

Table 2. Extraction of various phenols from water into 25 percent w/w TOPO in DIBK, and into pure DIBK, at 30°C and an initial molar ratio of TOPO to the phenolic compound of 2.50.

Solute	K_D[a] TOPO/DIBK	K_D[a] DIBK
Phenol	462 [b]	46.2 [b]
Pyrocatechol (1,2-dihydroxybenzene)	203	6.94
Resorcinol (1,2-dihydroxybenzene)	98.3	4.25
Hydroquinone (1,2-dihydroxybenzene)	34.9	2.05
Pyrogallol (1,2,3-trihydroxybenzene)	53.7	0.57
Phloroglucinol (1,2,3-trihydroxybenzene)	20.9	0.30
Hydroxyquinol (1,2,4-trihydroxybenzene)	24.3	0.13

[a]K_D = wt. fraction of solute in solvent phase ÷ wt. fraction of solute in aqueous phase, at high dilution and at equilibrium.

[b]Phenol extraction at 22.5°C.

Following a concept originally proposed by Cahn et al.[5] in the context of liquid-membrane processes, we are exploring selective extraction of ammonia (or acid gases) as a means of lowering (or raising) the pH and thereby making the acid gases (or ammonia) more volatile so that stripping can be carried out with a lesser amount of steam. Stripping and extraction would be carried out simultaneously to derive the synergistic effects of the one separation process upon the other. This approach also isolates the ammonia and acid gases from one another. The loaded extraction solvent then must be regenerated in some manner. One possible means of regeneration would be heating the solvent sufficiently to enable the extracted ammonia (or acid gases) to be stripped or distilled from it without excessive energy consumption. If there can be a substantial temperature difference between the initial extraction-plus-stripping column and the regeneration column, the energy requirements for steam to both columns and heating of the solvent between columns can be less than for stripping alone.

Initial explorations, described in the FY 1980 Annual Report, established that a liquid-ion-exchanger solvent is needed to achieve sufficient extraction of one of the solutes. For several reasons, extraction of ammonia and stripping of acid gases appears to be the more favored combination, requiring a liquid-cation exchanger. We have carried out experiments with two such exchangers, di-2-ethylhexyl phosphoric acid (D2EHPA) and dinonyl naphthalene sulfonic acid (DNNSA). Both have been used commercially in the hydrometallurgical industry.

Because sulfonic acid is the stronger acid, DNNSA gives greater equilibrium distribution coefficients for NH_3. Both extractants exhibit phase settling problems under some conditions, but DNNSA has a somewhat lesser tendency toward poor settling, presumably because of the greater hydrocarbon weighting in the molecule. However, D2EHPA gives values of K_D that should be effective for the process needs and provides satisfactory phase settling if operating conditions are controlled carefully.

In qualitative and semi-quantitative experiments, regeneration of loaded extractant has been attempted through heating and stripping with either steam or nitrogen. At temperatures below 150°C, ammonia is not removed effectively from DNNSA; and at temperatures above 150°C, a solid is formed from DNNSA. Proximate analysis of the solid reveals that it is relatively enriched in oxygen compared to DNNSA; it also contains substantial nitrogen when it is formed from DNNSA laden with NH_3. It thus appears that regeneration of NH_3 from DNNSA will be incomplete, slow, or impossible. Regeneration studies with D2EHPA have not encountered this problem, and we have successfully removed NH_3 com-

pletely, or nearly completely, from D2EHPA by a procedure of nitrogen stripping at a temperature of approximately 200°C and atmospheric pressure.

Finally, we conducted preliminary batch stripping experiments, similar to those performed in earlier work,[3] in the presence and absence of a second phase consisting of 7.4 percent D2DHPA v/v in a C_{12} alkane diluent. In one experiment, a 5:1 volumetric solvent:water ratio was employed, giving an initial stoichiometry of 0.43 moles NH_3 per mole D2EHPA. The aqueous phase initially contained 0.9 percent w/w NH_3, supplied as a nominal $(NH_4)_2CO_3$ reagent. Nitrogen stripping readily removed all the CO_2 from the solution, and about 95 percent of the original NH_3 remained in the solvent phase. The rate of CO_2 removal was not determined quantitatively but appeared to be substantially faster than for stripping in the absence of the solvent.

PLANNED ACTIVITIES FOR FY 1982

We shall continue studies of aging phenomena and hydantoin and dihydric phenol levels in gasification condensate waters. Efforts will continue to identify those substances contributing to the unidentified portion of the COD, including solutes of high molecular weight.

Experimental studies are continuing with MIBK, higher ketones, TOPO, and other candidate solvents to monitor removal of COD and specific compounds in condensate waters. These measurements will be followed by conceptual design calculations to assess the relative attractiveness and effective processing sequences for these and other candidate solvents. Other factors, such as rate of extraction and settling properties, will be evaluated and measured as needed.

Studies of extraction of phenols from synthetic solutions using TOPO/diluent solvents will be directed toward solvent regeneration. Distillation and back-extraction after a temperature change will be among the methods of regeneration considered. Co-extraction of water along with the phenols will also be examined. Similar studies will be made for any other solvents where such data appear to be critical.

In work with combined stripping and extraction using liquid-ion exchangers, we shall carry out quantitative measurements of stripping rates and solvent regenerability and shall also endeavor to elucidate the mechanism of slow settling and to develop effective means for overcoming it. Other effective liquid ion exchangers will also be sought and considered.

REFERENCES

1. Greminger, D.C., and King, C.J. (1979), Extraction of Phenols from Coal Conversion Condensate Waters, Lawrence Berkeley Laboratory Report LBL-9177.

2. Greminger, D.C., et al. (1982), "Solvent Extraction of Phenols from Water," I&EC Process Res. & Devel. 21, p. 51; Lawrence Berkeley Laboratory Report LBL-10480 (1980).

3. Hill, J.D., and King, C.J. (1980), Stripping of Process Condensates from Solid Fuel Conversion, Lawrence Berkeley Laboratory Report LBL-11031.

4. Mohr, D.H., Jr., and King, C.J. (1981), Identification and Removal of the Organic Compounds in Coal-Conversion Condensate Waters, presented at Workshop on Processing of Wastewaters from Synthetic Fuels Processes, U.S. Department of Energy, Germantown, MD, June 24-25, 1981, Lawrence Berkeley Laboratory Report LBL-13584.

5. Cahn, R.P., Li, N.N., and Minday, R.M. (1978), Environ. Sci. Tech. 21, p. 1051.

A Kinetic Study of Reactions Involving Ferrous Nitrosyl Complexes*

D. Littlejohn, S. Lynn, and S. G. Chang

Efficient techniques for removing NO_x and SO_2 from power plant flue gases are needed to meet air quality standards. One promising method for removing NO, which is only weakly soluble in aqueous solutions, is the formation of nitrosyl complexes from chelated metal ions.[1] Some metal chelates react rapidly and reversibly with NO. The nitrosyl complexes can react with the absorbed SO_2 to form a variety of products.[1-8]

Although a number of studies have been made of ferrous nitrosyl complexes,[9-11] little work has been done on the kinetics of the formation of these complexes[12-14]:

$$Fe(II)(L) + NO(aq) \underset{k_{-1}}{\overset{k_1}{\rightleftharpoons}} Fe(II)(L)NO(aq) \quad , \quad (1)$$

where L represents the ligand that is complexed to the ferrous ion. A study indicates that, in one case, the forward rate constant is quite rapid, exceeding 10^8 $M^{-1}sec^{-1}$ for the Fe(II)(EDTA)NO complex. This value was obtained indirectly and can be considered only an estimate.

Since no comprehensive study of the kinetics of ferrous nitrosyl complexes has been done, we have started a systematic study of the kinetics and spectra of these complexes with different ligands. We have investigated the kinetics of the following complexes: $Fe(II)(H_2O)_5NO$, Fe(II)(citrate)NO, $Fe(II)(acac)_2NO$, and Fe(II)(EDTA)NO.

ACCOMPLISHMENTS DURING FY 1981

Spectra

The prepared complexes were transferred under oxygen-free conditions to an evacuated 10-cm cell with Pyrex windows. The spectra of the complexes, obtained with a Cary Model 219 double-beam spectrophotometer, were taken from 800 nm to 300 nm.

Kinetic Studies

The kinetics of the ferrous nitrosyl complexes were investigated with a temperature-jump apparatus similar to that described by Czerlinski and Eigen.[15] A temperature jump of about 8°C was created by discharging a 0.25-mfd capacitor, charged to 20 kV, through a cell with a volume of approximately 1.4 cm^3. The discharge time is dependent on the ionic strength of the solution[16] but is generally less than 10 microseconds.

Results and Discussion

Spectra. The spectra for the complexes studied, shown in Figure 1, were taken at 25°C. The spectra are for $Fe(II)(H_2O)_5NO$ at pH 0.6, Fe(II)(citrate)NO at pH 5.1, $Fe(II)(acac)_2NO$ at pH 7.0, and Fe(II)(EDTA)NO at pH 3.7. The spectra of the complexes without NO are also shown (dashed lines).

Kinetics. All the ferrous nitrosyl complexes investigated in this study displayed a single exponential relaxation in response to the jump in temperature. Consequently, the rate constants can be determined from the equation

$$1/\tau = k_{-1} + k_1([Fe(II)(L)] + [NO]) \quad , \quad (2)$$

where τ is the relaxation time obtained from photographs of the oscilloscope traces and [Fe(II)(L)]

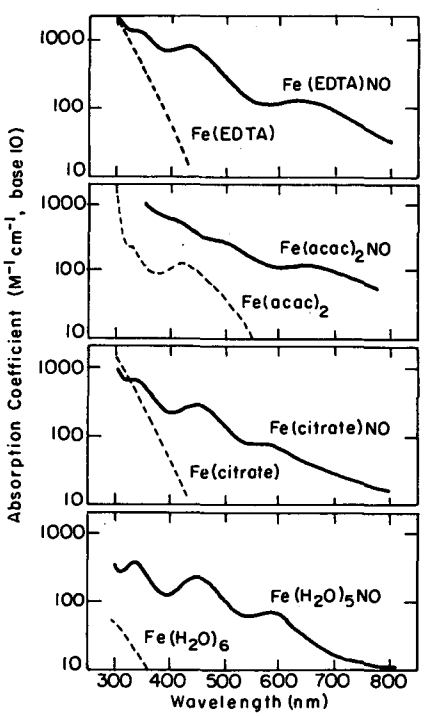

Figure 1. Absorption spectra of ferrous ion complexes from 800 nm to 300 nm for $Fe(II)(H_2O)_5NO$, Fe(II)(citrate)(NO), $Fe(II)(acac)_2NO$, and Fe(II)(EDTA)NO. The dashed lines represent the absorption spectra of the complexes without NO. (XBL 818-6223)

*This work was supported by the Morgantown Energy Technology Center under Contract No. 81MC14002 through the Assistant Secretary for Fossil Energy of the U.S. Department of Energy under Contract No. DE-AC03-76SF00098.

is the concentration of the ferrous ion complex that is not bound to nitric oxide.

The nitric oxide concentration in solution was determined from the nitric oxide pressure over the solution and the Henry's constant for nitric oxide. The Henry's law coefficient of 1.9×10^{-3} M atm^{-1} given by Armor[17] was used, with correction made for ionic strength and temperature.

The data were analyzed by assuming a value for K_{eq} where

$$K_{eq} = k_1/k_{-1} \quad , \tag{3}$$

and calculating the concentration of Fe(II)(L) that should be present. Values for the rate constants k_1 and k_{-1} are obtained from a least-squares fit to the reciprocal relaxation times and the calculated values of ([Fe(II)(L)] + [NO]). From these values of k_1 and k_{-1}, a value for K_{eq} is calculated. If the calculated value of K_{eq} differs significantly from the value assumed, the calculations are reiterated until convergence is obtained.

Fe(II)$(H_2O)_5$NO. A plot of $1/\tau$ vs ([Fe(II)$(H_2O)_5$] + [NO]) is shown in Figure 2. The points are the average of the values of $1/\tau$ obtained from each run, and the line is a least-squares fit to all values of $1/\tau$ obtained. The values corresponding to the line are: $k_1 = 7.1 \pm 1.0 \times 10^5$ M^{-1} sec^{-1}, $k_{-1} = 1.5 \pm 0.6 \times 10^3$ sec^{-1}, and $K_{eq} = 470 \pm 200$ M^{-1}. These values are in good agreement with those given by Kustin et al.[12] and Hikita et al.[13]

Fe(II)(citrate)NO. A plot of $1/\tau$ vs ([Fe(II)(citrate)] + [NO]) is also shown in Figure 2. It was found that values of [Fe(II)(citrate)] greater than approximately 3.5×10^{-3} M gave erratic and inconsistent relaxations, possibly due to interaction between complex molecules or formation of different types of complexes at high concentrations. The least squares fit to the values of $1/\tau$ obtained gave the following values for the rate and equilibrium constants: $k_1 = 4.4 \pm 0.8 \times 10^5$ $M^{-1}sec^{-1}$, $k_{-1} = 660 \pm 240$ sec^{-1}, and $K_{eq} = 670 \pm 200$ M^{-1}.

Fe(II)$(acac)_2$NO. The relaxation times of Fe(II)$(acac)_2$NO were much longer than those of the other complexes studied. A plot of $1/\tau$ vs ([Fe(II)$(acac)_2$] + [NO]) is shown in Figure 3. A least-squares fit to the data provided the following results: $k_1 = 400 \pm 300$ $M^{-1}sec^{-1}$, $k_{-1} = 24 \pm 2$ sec^{-1}, and $K_{eq} = 17 \pm 14$ M^{-1}.

Fe(II)(EDTA)NO. The relaxation times due to the jump in temperature were too fast to be measured with the present system.

An upper limit of 10 microseconds was established for the relaxation time. The limiting factor in the present experimental setup is the length of time it takes to discharge the capacitor through the solution. Teramoto et al.[14] obtained a value of about 1×10^6 M^{-1} for the equilibrium constant for the formation of Fe(II)(EDTA)NO, while the values of ΔH and ΔS for the formation of Fe(II)(EDTA)NO published by Hishinuma et al.[18] yield a value of about 1×10^7 M^{-1} for the equilibrium constant. These results indicate that the equilibrium constant is very high, and essentially all the Fe(II)(EDTA) complex will be bound to nitric oxide. Because the concentration of Fe(II)(EDTA) will be small compared to that of nitric oxide, Equation (2) can be approximated as

$$1/\tau \approx k_{-1} + k_1[NO] \quad . \tag{4}$$

The lowest concentration of nitric oxide used in the experiments with EDTA was 1.6×10^{-3} M. Using the upper limit of as 10 microseconds and Teramoto's value of 1×10^6 M^{-1} for K_{eq}, and $K_{eq} = k_1/k_{-1}$, one obtains a value of about 6×10^7 $M^{-1}sec^{-1}$ for the lower limit of k_1 and a value of

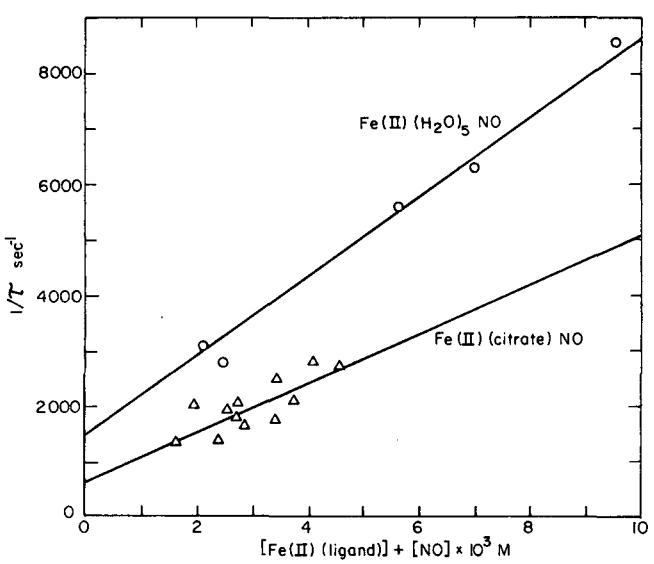

Figure 2. A plot of [Fe(II)(ligand)] + [NO] vs reciprocal relaxation time for Fe(II)(citrate)NO and Fe(II)$(H_2O)_5$NO.

(XBL 817-6133)

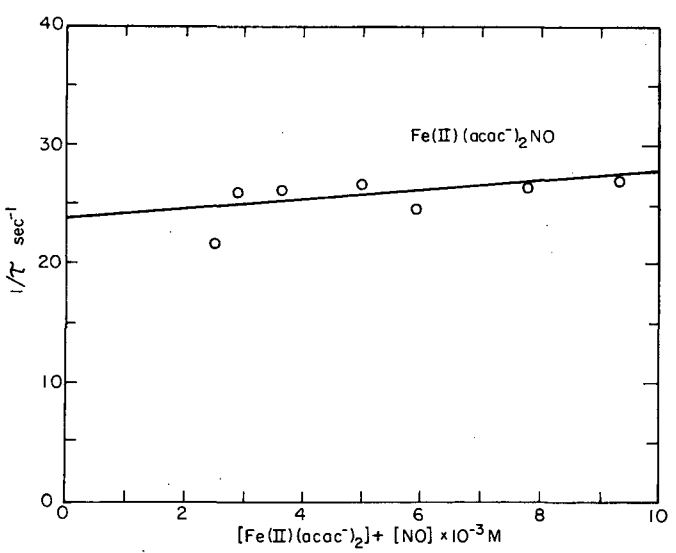

Figure 3. A plot of [Fe(II)$(acac)_2$] + [NO] vs reciprocal relaxation time for Fe(II)$(acac)_2$NO.

(XBL 817-6132)

about 60 sec^{-1} for the lower limit for k_{-1}. The lower limit for k_1 is in good agreement with the value of $k_1 = 1.7 \times 10^8$ $M^{-1}sec^{-1}$ obtained by indirect means by Teramoto et al.[14]

PLANNED ACTIVITIES FOR FY 1982

Values for the rate and equilibrium constants for the formation of $Fe(II)(H_2O)_5NO$ determined in this study are in good agreement with those determined by other groups.[12]

While Fe(II)(EDTA)NO may be of value in wet flue gas denitrification systems, other compounds may be of equal or greater value. A study[19] indicates the Fe(II)(NTA)NO also binds NO rapidly and efficiently. NTA has the advantage of being less expensive than EDTA. Another important consideration is the ability of the nitrosyl complexes to regenerate the metal chelates in a scrubber system by reacting with absorbed SO_2.

Further studies are planned on ferrous nitrosyl complexes with other ligands. In addition, the temperature-jump system has been modified to operate at temperatures other than room temperature. This will enable us to obtain thermodynamic data on the ferrous nitrosyl complexes.

REFERENCES

1. Yaverbaum, L.H. (1979), Nitrogen Oxides Control and Removal, Recent Developments, Noyes Data Corporation, Park Ridge, N.J.

2. Oblath, S.B., et al. (1981), "Kinetics of the Formation of Hydroxylamine Disulfonate by Reaction of Nitrite with Sulfites," J. Phys. Chem. 85, p. 1017.

3. Chang, S.G., Toossi, R., and Novakov, T. (1981), "The Importance of Soot Particles and Nitrous Acid in Oxidizing SO_2 in Atmospheric Aqueous Droplets," Atmospheric Environ. 15, p. 1287.

4. Gomiscek, S., et al. (1981), "Kinetics of the Reaction Between Hydroxylamine and Sodium Bisulfite," J. Phys. Chem. 85, p. 2567.

5. Oblath, S.B., et al. (1981), "Kinetics of the Initial Reaction of Nitrite Ion in Bisulfite Solutions," accepted for publication in J. Phys. Chem.

6. Oblath, S.B., et al. (1981), "Reaction of Nitrite Ion with Hydroxylamine-N-Sulfonate in Aqueous Solutions," submitted to J. Inorg. Chem.

7. Chang, S.G. (1980), Reaction of Sulfite and Nitrite Ions in Aqueous Solutions, paper presented at the Technical Advisory Committee, DOE/Advanced Environmental Control Technology Program, Morgantown, West Virginia, November 6-7, 1980, Lawrence Berkeley Laboratory Report LBL-11800.

8. Chang, S.G. (1981), "Kinetics of Reactions in a Wet Flue Gas Simultaneous Desulfurization and Denitrification System," paper presented at the Symposium on Advances in Flue Gas Desulfurization, American Chemical Society Meeting, Atlanta, Georgia, March 30, 1981, Lawrence Berkeley Laboratory Report LBL-13063.

9. Connelly, N.G. (1972), "Recent Developments in Transition Metal Nitrosyl Chemistry," Inorg. Chim. Acta Rev., p. 47.

10. Caulton, K.G. (1975), "Synthetic Methods in Transition Metal Nitrosyl Chemistry," Coord. Chem. Rev. 14, p. 317.

11. McCleverty, J.A. (1979), "Reactions of Nitric Oxide Coordinated to Transition Metals," Chem. Rev. 79, p. 53.

12. Kustin, K., Taub, I.A. and Weinstock, E. (1966), "A Kinetic Study of the Formation of the Ferrous-Nitric Oxide Complex," Inorg. Chem. 5, p. 1079.

13. Hikita, H., et al. (1977), "Kinetics of Absorption of Nitric Oxide in Aqueous Acidic Solutions of Ferrous Sulfate," J. Chem. Eng. Jpn. 10, p. 120.

14. Teramoto, M., et al. (1978), "Absorption of Dilute Nitric Monoxide in Aqueous Solutions of Fe(II)EDTA and Mixed Solutions of Fe(II)EDTA and NO_2SO_3," J. Chem. Eng. Jpn. 11, p. 450.

15. Czerlinski, G., and Eigen, M. (1959), "Eine Temperatursprung Methode zur Untersuchung chemischer Relaxation," Z. Elektrochem. 63, p. 652.

16. Czerlinski, G. (1962), "Versatile Temperature Jump Apparatus for Following Chemical Relaxations," Rev. Sci. Instrum. 33, p. 1184.

17. Armor, J.N. (1974), "Influence of pH and Ionic Strength Upon Solubility of NO in Aqueous Solution," J. Chem. Eng. Data 19, p. 82.

18. Hishinuma, Y., et al. (1979), "Reversible Binding of NO to Fe(II)edta," Bull. Chem. Soc. Jpn. 52, p. 2863.

19. Lin, N.H., Littlejohn, D., and Chang, S.G. (1981), "The Thermodynamics and Kinetics of Coordination of NO to Fe(II)NTA in Aqueous Solutions," submitted to J. Chem. Eng. Data.

The Thermodynamics and Kinetics of the Coordination of NO to Fe(II)NTA in Aqueous Solutions*

N. -H. Lin, D. Littlejohn, S. Lynn, and S. G. Chang

One approach for simultaneous removal of NO_x and SO_2 from power-plant flue gas is based on absorption of the relatively insoluble NO in aqueous solutions after oxidation of NO by O_3 to NO_2 or by addition of metal chelates in solutions.[1] These metal chelates have the ability to form complexes with NO and thus promote absorption of NO. Once in solution, NO can react with absorbed SO_2 to produce various products, such as N_2, N_2O, NH_2OH, NH_2HSO_3, and NH_4HSO_4.[2-8] A few ferrous and cobalt chelates have been known to bind NO reversibly in aqueous solution and have been proposed as additives in a power-plant flue-gas wet scrubber.[1,9] Identifying an efficient metal chelate for maximum absorption of NO requires knowledge of the thermodynamics and kinetics of the reversible binding of NO to various metal chelates; however, little is known of this. This report discusses the enthalpy, entropy, and equilibrium constants of the coordination of NO to Fe(II)NTA in an aqueous solution. The formation and dissociation rate constants of this reaction have also been measured to determine whether the chemical reaction rate or the mass transfer rate of NO is the rate-limiting step in an absorption tower of a power-plant flue-gas wet scrubber.

ACCOMPLISHMENTS DURING FY 1981

Thermodynamic Studies

Our experimental setup was similar to that of Hishinuma et al.[9] The experiments were carried out by bubbling a mixture of NO and N_2 of known NO concentration through a NaOH solution to absorb NO_2 impurity in the gas. This NO_2-free mixture of NO and N_2 gas was then bubbled through the Fe(II)NTA solution, and the NO concentration in the outlet gas was measured with a Thermoelectron Model 14A chemiluminescent NO_x analyzer.

Kinetic Studies

The spectrum of the Fe(II)(NTA)NO complex was determined with a Cary Model 219 double-beam spectrophotometer. The kinetics of the formation and dissociation of the Fe(II)(NTA)NO complex were investigated using the temperature-jump technique; these experiments were performed in an apparatus similar to that described by Czerlinski and Eigen.[10] A temperature increase of approximately 8°C in less then 10 microseconds was created by discharging a 0.25-microfarad capacitor charged to 20 kV through a cell, with cell volume of 1.4 cm^3.

Results and Discussion

The coordination of NO to NTA can be expressed by the following reaction:

$$nNO + Fe(II)NTA \underset{k_{-1}}{\overset{k_1}{\rightleftharpoons}} Fe(II)(NTA)(NO)_n \quad . \qquad (a)$$

The equilibrium constant of this reaction can be written as

$$K = \frac{k_1}{k_{-1}} = \frac{[Fe(II)(NTA)(NO)_n]}{[NO]^n[Fe(II)NTA]} \qquad (1)$$

$$= \frac{[Fe(II)(NTA)(NO)_n]}{[NO]^n \{[Fe(II)NTA]_0 - [Fe(II)(NTA)(NO)_n]\}} \quad .$$

Equation (1) can be rearranged to become

$$\frac{[Fe(II)NTA]_0}{[Fe(II)(NTA)(NO)_n]} - 1 = \frac{1}{KH^n p_{NO}^n} \quad , \qquad (2)$$

where $[Fe(II)NTA]_0$ is the initial concentration of Fe(II)(NTA), $[Fe(II)(NTA)(NO)_n]$ is the concentration of the NO adduct obtained by graphically integrating the outlet NO concentration, p_{NO} is the partial pressure of NO in the gas, and H is the Henry's constant for solubility of NO in water.

Figure 1 is a log-log plot of

$$\{[Fe(II)(NTA)]_0/[Fe(II)(NTA)(NO)_n]\} - 1$$

versus $1/p_{NO}$ at various temperatures. The slope of these lines is one, indicating that the value of n is one in $Fe(II)(NTA)(NO)_n$. The equilibrium constant at 40, 50, and 60°C was calculated from Equation (2) and is 8.73×10^5, 4.65×10^5, and 2.55×10^5 M^{-1} respectively. The enthalpy and entropy of the formation of Fe(II)(NTA)NO were obtained from a van't Hoff plot (Fig. 2) and are ΔH^o = -11.94 kcal/mole and ΔS^o = -11.08 e.u., respectively.

Figure 3 shows the effect of pH on the molar ratio of absorbed NO to total ferrous ion at 60°C. This ratio was not affected by pH between 9 and 4 and decreased substantially below pH of 4.

*This work was supported by the Morgantown Energy Technology Center under Contract No. 81MC14002 through the Assistant Secretary of Fossil Energy of the U.S. Department of Energy under Contract No. DE-AC03-76SF00098.

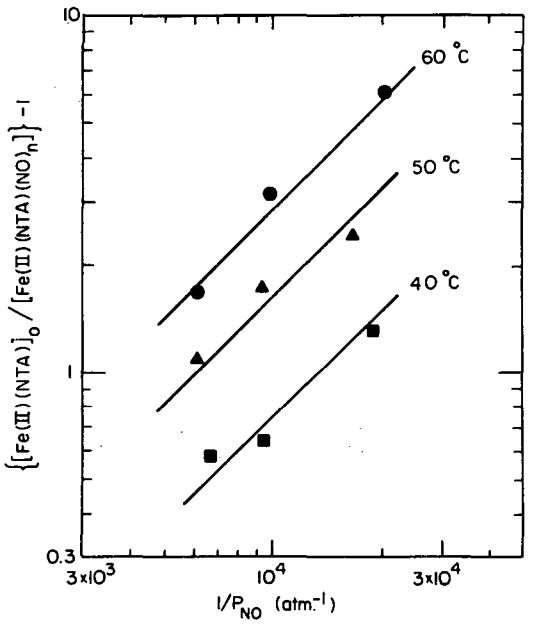

Figure 1. A log-log plot of $[Fe(II)NTA]_0/[Fe(II)(NTA)(NO_n] - 1$ vs $1/p_{NO}$ at 40, 50, and 60°C. $[Fe(II)NTA]_0$ is 0.004 M, and pH of the solution is 5.5.

(XBL 816-5923)

The spectrum of the Fe(II)(NTA)NO complex, recorded from 800-300 nm, shows an increasing absorption toward the blue end of the spectrum, with local absorption maxima at 600 nm, 440 nm, and 340 nm.

The relaxation time obtained from the temperature jump can be related to the forward and reverse rates of the complex formation by the equation[10]

$$1/\tau = k_{-1} + k_1 \{[Fe(II)NTA] + [NO_{aq}]\} \quad . \quad (3)$$

The relaxation time was too rapid to be observed with the present setup. A conservative upper limit of 10 microseconds can be assigned to τ. The major experimental limitation in obtaining a shorter relaxation time is the length of time it takes to discharge the capacitor through the solution and the low signal-to-noise ratio due to the small change in absorption with temperature of the Fe(II)(NTA)NO complex.

An equilibrium constant for Fe(II)(NTA)NO of 2×10^6 M^{-1} at 25°C was obtained by extrapolating the data illustrated in Figure 2. With an upper limit for the relaxation time of 10 microseconds and the lowest NO concentrations of 1.4×10^{-3} $\underline{M}$, lower limits for $k_1 = 7 \times 10^7$ $\underline{M}^{-1}sec^{-1}$ and $k_{-1} = 35$ sec^{-1} at 25°C were obtained. The lower limits obtained for k_1 did not exhibit any pH dependence over the range of pH 5-7. The lower limit of k_1 determined for Fe(II)(NTA)NO is consistent with the value of k_1 obtained by indirect means for a similar complex Fe(EDTA)NO (Ref. 11)--$k_1 = 1 \times 10^8$ $\underline{M}^{-1}$ sec^{-1}--and is much faster than that observed for the $Fe(H_2O)_5NO$ complex[12]-- $k_1 = 6.2 \times 10^5$ $\underline{M}^{-1}sec^{-1}$.

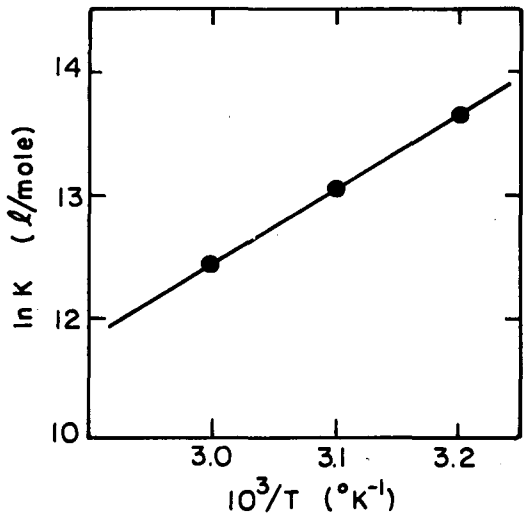

Figure 2. Van't Hoff plot of equilibrium constants for reaction (a).

(XBL 816-5924)

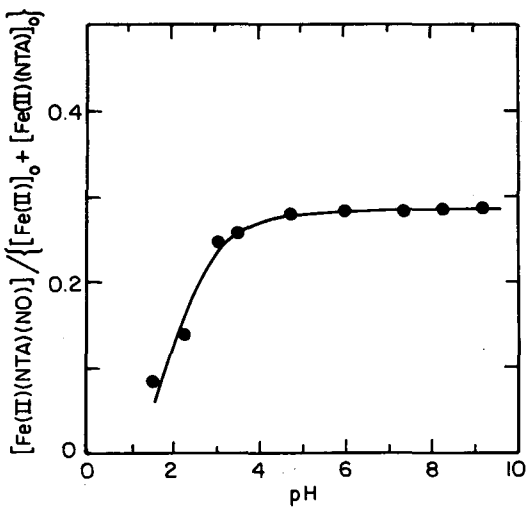

Figure 3. The effect of pH on the molar ratio of the absorbed NO to the total ferrous ion at 60°C. The concentration of the NO inlet is 1200 ppm.

(XBL 816-5925)

PLANNED ACTIVITIES FOR FY 1982

It has been suggested[1] that Fe(II)EDTA can be an effective binding reagent/additive for NO in wet simultaneous flue gas desulfurization and denitrification scrubbers. The equilibrium constant of the reaction of NO with Fe(II)EDTA to form Fe(II)(EDTA)NO (Ref. 9) is about a factor of 2 larger than that with Fe(II)NTA to form Fe(II)(NTA)NO at a typical wet scrubber temperature, T = 50°C. However, NTA is less expensive than EDTA. The rate of binding of NO to form nitrosyl ferrous complexes by both Fe(II)NTA and Fe(II)EDTA is probably within the same order of magnitude and is much faster compared with the mass transfer rate at typical wet scrubber conditions.

Determining the rate of regeneration of these metal chelates by investigating the kinetics of the reaction of Fe(II)(NTA)NO and Fe(II)(EDTA)NO with absorbed SO_2 in aqueous solutions is important for assessing whether NTA or EDTA is an optimum chelating agent.

REFERENCES

1. Yaverbaum, L.H. (1979), Nitrogen Oxides Control and Removal, Recent Developments, Noyes Data Corporation, Park Ridge, N.J.

2. Oblath, S.B., et al. (1981), "Kinetics of the Formation of Hydroxylamine Disulfonate by Reaction of Nitrite with Sulfites," J. Phys. Chem. 85, p. 1017.

3. Chang, S.G., Toossi, R., and Novakov, T. (1981), "The Importance of Soot Particles and Nitrous Acid in Oxidizing SO_2 in Atmospheric Aqueous Droplets," Atmos. Environ. 15, p. 1287.

4. Gomiscek, S., et al. (1981), "Kinetics of the Reaction Between Hydroxylamine and Sodium Bisulfite," J. Phys. Chem. 85, p. 2567.

5. Oblath, S.B., et al. (1981), "Kinetics of the Initial Reaction of Nitrite Ion in Bisulfite Solutions," accepted for publication in J. Phys. Chem.

6. Oblath, S.B., et al. (1981), "Reaction of Nitrite Ion with Hydroxylamine-N-Sulfonate in Aqueous Solution," submitted to J. Inor. Chem.

7. Chang, S.G. (1980), Reactions of Sulfite and Nitrite Ions in Aqueous Solutions, paper presented at the Technical Advisory Committee, DOE/Advanced Environmental Control Technology Program, Morgantown, West Virginia, November 6-7, 1980; Lawrence Berkeley Laboratory Report LBL-11800.

8. Chang, S.G. (1981), "Kinetics of Reactions in a Wet Flue Gas Simultaneous Desulfurization and Denitrification System," paper presented at Symposium on Advances in Flue Gas Desulfurization, American Chemical Society Meeting, Atlanta, Georgia, March 30, 1981; Lawrence Berkeley Laboratory Report LBL-13063.

9. Hishinuma, Y., et al. (1979), "Reversible Binding of NO to Fe(II)edta," Bull. Chem. Soc. Japan 52, p. 2863.

10. Czerlinski, G., and Eigen, M. (1959), "Eine Temperatursprungmethode zur Untersuchung Chemischer Relaxation," Z. Elektrochem. 63 p. 652.

11. Kustin, K., Taub, I.A., and Weinstock, E. (1966), "A Kinetic Study of the Formation of the Ferrous-Nitric Oxide Complex," Inorg. Chem. 6, p. 1079.

12. Pitzer, K.S., and Brewer, L. (1961), Thermodynamics, McGraw-Hill, New York.

Kinetics of Reactions in a Wet Flue Gas Simultaneous Desulfurization and Denitrification System*

S. G. Chang, S. Lynn, D. Littlejohn, and N. -H. Lin

Power-plant flue gas contains several hundred ppm NO_x and hundreds or thousands ppm SO_2. Most NO_x is in the form of NO. Several processes still in the development stage are based on using NO_x as an oxidizing agent for SO_2 in aqueous solution to simultaneously control the emission of both SO_2 and NO_x in the flue gases. These processes can be divided into two different types: one is classified as an oxidation-absorption-reduction technique and the other as an absorption-reduction technique.

Both types of process are being developed mainly in Japan and have not approached the stage of commercial use.[1,2] Part of the reason for this is that, because these processes are recent developments which have not been tested extensively, the chemistry involved in these systems is not yet well understood.

*This work was supported by the Morgantown Energy Technology Center under Contract No. 81MC14002 through the Assistant Secretary of Fossil Energy of the U.S. Department of Energy under Contract No. DE-AC03-76SF00098.

ACCOMPLISHMENTS DURING FY 81

We have reviewed the literature and will discuss the kinetics and mechanisms of reactions involved in both types of process.

Oxidation-Absorption-Reduction Processes

This type of process is based on injecting a gas-phase oxidant, such as O_3 or ClO_2, into the flue gas to selectively oxidize the relatively insoluble NO to the more soluble NO_2. Nitrous and nitric acids are produced in the aqueous phase after NO_2 and/or N_2O_3 are absorbed into solution; and sulfur oxyacids, such as sulfite/bisulfite or pyrosulfite, are formed if SO_2 dissolves in the solution. Interaction among oxides of nitrogen, nitrogen oxyacids, sulfur oxyacids, oxygen, and trace metal ions such as Fe(III) or Mn(II) can take place in a flue gas wet scrubber. Identifying all reactions involved in this complex system is impossible. However, important reactions must be identified and characterized in order to improve the

performance of a scrubber.

Several Japanese processes,[1,2] such as the Ishikawajima, Chiyoda, or Mitsubishi processes in which the NO in the flue gas is oxidized to NO_2 by O_3 and subsequently passed to a NO_2/SO_2 absorber, have shown that a major fraction of the absorbed NO_x is in the form of nitrogen-sulfur complexes, which are the compounds produced in the reaction between nitrite and sulfite ions.

We have reviewed the literature[3] and found that many concurrent and consecutive chemical reactions can occur as a result of the interaction between nitrite and sulfite ions. We will summarize the kinetic results of these reactions and present the results of model calculations that give the concentration profile of species produced in this system as a function of reaction time. The effects of temperature, pH, and concentrations of reactant will be demonstrated.

Review of Previous Kinetic Studies

Nitrous acid and sulfite react to form nitrososulfonic acid, which then continues along one or more of three reaction paths:

1. Further sulfonation to produce hydroxylamine disulfonate and amine trisulfonate. These sulfonates can hydrolyze to form sulfuric acid and reduced nitrogen species. The latter can undergo further reaction with bisulfite and nitrite.

2. Hydrolysis to form sulfuric acid and hyponitrous acid. The latter decomposes to produce nitrous oxide.

3. Reaction with nitrous acid to yield sulfuric acid and nitric oxide. The extent to which these three different paths will contribute to the system depends on the pH, temperature, and concentration of nitrite and sulfite species. It is believed that process 1 favors a neutral or mildly acidic solution; processes 2 and 3 are expected to become increasingly important as the pH of the solution decreases. A summary of reactions that can take place as a result of interaction between sulfite and nitrite ions is shown in the following reaction scheme.

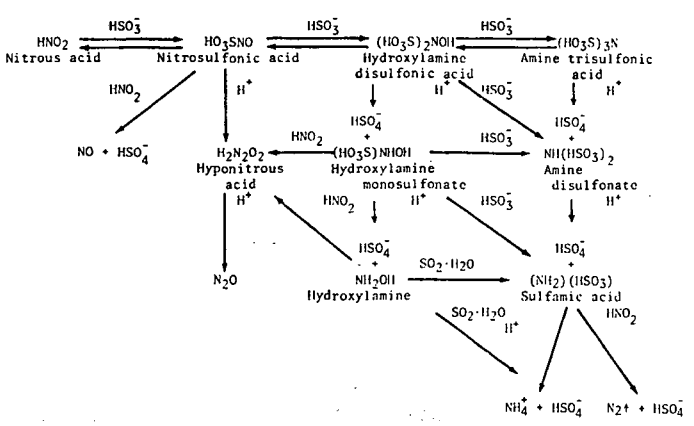

Chemical Kinetics Modeling

The concentration profiles of HADS, HAMS, HA, ATS, ADS, SAM, NH_4^+, N_2, and sulfate as a function of time resulting from the reaction of sulfite and nitrite ions in aqueous solutions was calculated at various conditions (Figs. 1-3). A CHEMK software package developed by Systems Applications, Inc., San Rafael, California, was used for this computation. The following assumptions were made in this calculation:

1. Gas dissolution and liberation rates are much larger than chemical reaction rates.

2. Any reaction involving HNO_3, $NO(\ell)$, $NO_2(\ell)$, $N_2O_3(\ell)$, and $N_2O_4(\ell)$ is neglected.

3. The equilibrium is maintained all the time for reactions 1 through 7. The rate constant of the 14 reactions was adjusted to satisfy the equilibrium condition.

4. Oxidation of NO to NO_2 (both in gas phase and aqueous solution) is discounted.

Figure 1 (at P_{SO_2} = 1000, P_{NO} = 450 and P_{NO_2} = 50 ppm, pH = 5, T = 328°K, and gas-to-liquid ratio, G/l = 75) demonstrates that the removal efficiency of NO is only about 10 percent, although NO_2 can be removed nearly completely because NO alone cannot be converted into nitrous acid. The major product is HADS within the initial 1-1/2 hours; the concentration of HAMS and sulfate increases, and the HADS concentration decreases as the reaction time continues. If the reaction is continued, the final products will be NH_4^+, N_2, and sulfate. Because we disregard the reaction of HAMS and HA with HNO_2 and the hydrolysis of nitrosulfonic acid, no N_2O is formed.

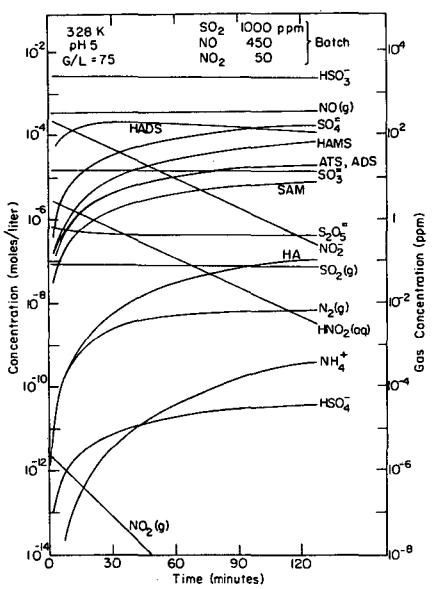

Figure 1. The concentration profile of species as a function of reaction time in a batch reactor (pH = 5 and temp. = 328 K) at the following initial conditions: P_{SO_2} = 1000, P_{NO} = 450, and P_{NO_2} = 50 ppm. The gas-to-liquid ratio, G/L, is 75.
(XBL 8011-6246)

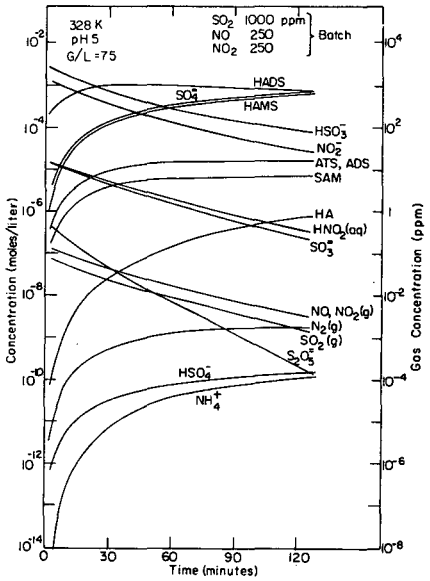

Figure 2. The concentration profile of species as a function of reaction time in a batch reactor (pH = 5 and temp. = 328 K) at the following initial conditions: P_{SO_2} = 1000, and P_{NO} = P_{NO_2} = 250 ppm. The gas-to-liquid ratio, G/L, is 75.

(XBL 8011-6247)

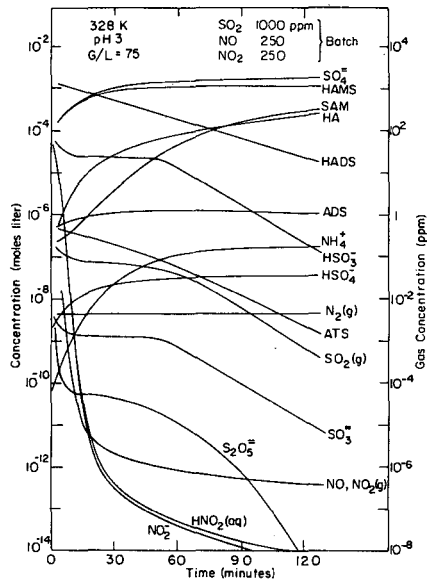

Figure 3. The concentration profile of species as a function of reaction time in a batch reactor (pH = 3 and temp. = 328 K) at the following initial conditions: P_{SO_2} = 1000, P_{NO} = P_{NO_2} = 250 ppm. The gas-to-liquid ratio, G/L, is 75.

(XBL 8011-6245)

The effect of the oxidation of NO to NO_2 on the reaction is illustrated in Figure 2. the result indicates enormous improvement in NO_x removal efficiency. The concentration of HADS, HAMS, ATS, etc., species is larger (compared to Figure 1) because of the larger concentration of nitrite/nitrous acid in the solution. HSO_3^- is also consumed at a larger rate.

The effect of the pH of the solution on the reaction is shown in Figure 3. The reactions speed up at a lower pH (between pH = 5 and 3), and NO_x is reduced at a larger rate. The concentration of HAMS is larger than HADS after about 20 minutes. Similarly, larger concentrations of HA, SAM, N_2, and NH_4^+ are observed at a given time. These are due to the fact that the hydrolysis reaction is acid-catalyzed, and therefore low pH conditions would favor the formation of hydrolysis products.

Absorption-Reduction Processes

This type of process is based on the addition of metal chelates such as Fe(II)EDTA in aqueous solution to promote absorption of NO in solutions.[1,2] These metal chelates can bind NO to form nitrosyl metal chelates that can react with absorbed SO_2 in aqueous solution to produce reduced nitrogen species and sulfate while metal chelates are regenerated.

Identification of an efficient metal chelate for optimum absorption of NO requires knowledge of the thermodynamics and kinetics of the coordination of NO to various metal chelates. Knowledge is also needed on the kinetics and mechanisms of the reaction between nitrosyl metal chelates and absorbed SO_2 in solution to calculate the regeneration rate of metal chelates and to control the products of reaction by adjusting the scrubber operating conditions. Not much of this information is available in the literature, although several ferrous and cobalt chelates have been used as additives for testing in bench-scale wet flue gas simultaneous desulfurization and denitrification scrubbers.

Equilibrium Constants, Enthalpy, and Entropy of the Coordination of NO to Metal Chelates

Complexes of NO have been known for centuries. Many studies have determined the structure of these complexes, yet few have derived their thermodynamic properties and reaction kinetics. Hishinuma et al.[4] and our group[5] have recently determined the equilibrium constants, enthalpy, and entropy for the coordination of NO to Fe(II)EDTA and Fe(II)NTA. Both groups performed their experiments by bubbling a mixture of NO and N_2 of known NO concentration through a metal chelate solution and then measuring the NO concentration in the outlet gas with a NO_x analyzer. NO absorption was carried out until the NO concentration in the outlet gas became equal to that in the inlet gas, i.e., until equilibrium was reached. The experiments were performed at several temperatures to evaluate enthalpy and entropy of the reaction. The results of this study are shown in Table 1.

We recently determined the equilibrium constant for the coordination of NO to $Fe(II)(H_2O)_5$, Fe(II)(citrate), and $Fe(II)(acac)_2$ using a temperature-jump apparatus.[6] The source of the temperature jump is a high-voltage d.c. power supply connected to a capacitor through a solenoid switch. After the capacitor is charged, the switch is disconnected. By closing a variable spark gap, the energy stored in the capacitor can be discharged through a cell containing the reaction under study. A temperature jump of 8°C occurs within several microseconds. The temperature jump

Table 1. Kinetic and thermodynamic data for reversible NO coordination to ferrous chelates.

Ferrous Chelates	k_1 ($\underline{M}^{-1}sec^{-1}$)	k_{-1} (sec^{-1})	K ($\underline{M}^{-1}$ at 298°K)	ΔH (kcal/mole)	ΔS (e.u.)
$Fe(II)(H_2O)_5(NO)$	$(7.1\pm1.0)\times10^5$	$(1.5\pm0.6)\times10^3$	$(4.7\pm2.0)\times10^2$		
Fe(II)(citrate)(NO)	$(4.4\pm0.8)\times10^5$	$(6.6\pm2.4)\times10^2$	$(6.7\pm2.0)\times10^2$		
$Fe(II)(acac)_2(NO)$	$(4.0\pm3.0)\times10^2$	24 ± 2	17 ± 14		
Fe(II)(NTA)(NO)	$\geq7\times10^7$	≥35	2.14×10^6	-11.94	-11.0
Fe(II)(EDTA)(NO)	$\geq6\times10^7$	≥60	1.15×10^7	-15.8	-20.7

induces a change in the concentration of reactants and products as the reaction shifts to a new equilibrium. The shift is monitored by a photomultiplier that responds to changes in absorption of a nitrosyl ferrous chelate. The results are displayed on an oscilloscope, which is triggered by the closing of the spark gap.

The coordination of NO to metal chelates can be written as

$$M(chelates)+NO \underset{k_{-1}}{\overset{k_1}{\rightleftharpoons}} M(chelates)(NO) \quad . \qquad (1)$$

The reciprocal of the relaxation time equals the forward rate constant times the sum of the final equilibrium concentrations of M(chelates) and NO plus the backward rate constant. When the reciprocal of the relaxation time is plotted against the final concentrations of M(chelate) + NO, the slope of the curve gives the forward rate constant (k_1) and the point of interception gives the backward rate (k_{-1}). The results are summarized in Table 1.

By comparing the equilibrium constants of reactions listed in Table 1, it is obvious that Fe(II)(EDTA) and Fe(II)(NTA) have much larger absorption capacities for NO than $Fe(II)(H_2O)_5$, Fe(II)(citrate), and $Fe(II)(acac)_2$.

Formation and Dissociation Rate Constants of Nitrosyl Metal Chelates

The absorption rates of NO in an aqueous solution of Fe(II)EDTA were measured by Teramoto et al.[7] and Sada et al.,[8] using a stirred vessel with a free flat gas-liquid interface. The forward rate constants of the complexing reaction were derived on the basis of the theory of gas absorption. The results are given in Table 1.

With a temperature-jump technique, we have directly measured the formation and dissociation rate constants[6] of $Fe(II)(H_2O)_5NO$, Fe(II)(citrate)NO, $Fe(II)(acac)_2NO$, Fe(II)(EDTA)NO, and Fe(II)(NTA)NO (Table 1). Values for the rate and equilibrium constants for the formation of $Fe(II)(H_2O)_5NO$ determined in this study agree well with those determined by Kustin et al.[9] The forward and reverse rate constants for the formation of Fe(II)(citrate)NO are somewhat smaller than the values for the $Fe(II)(H_2O)_5NO$ complex, and the equilibrium constant is larger. The kinetics for the formation and dissociation of the $Fe(II)(acac)_2NO$ complex are much slower than for any other complex studied.

For both Fe(II)(EDTA)NO and Fe(II)(NTA)NO, the relaxation times due to the temperature jump were too fast to be measured. However, an upper limit of 10 sec was established for the relaxation times for both complexes. Using this value with the equilibrium constants determined for Fe(II)(EDTA)NO and Fe(II)(NTA)NO by Hishinuma et al.[4] and our group, respectively,[5] we calculated the lower limits of forward and reverse rate constants (Table 1).

Kinetics of Reactions of NO and SO_2 in Aqueous Solutions Containing Metal Chelates

Under O_2-free conditions, NO and SO_2 can react with metal chelates such as Fe(II)EDTA in aqueous solution to form Fe(II)(EDTA)NO and $Fe(II)(EDTA)(SO_3^{=})$ respectively. However, when both NO and SO_2 are bubbled into an aqueous solution containing Fe(II)EDTA, species such as N_2O, sulfamate, disulfamate, dithionate, and sulfate are produced.[10] The kinetics and mechanisms of reactions involved in this NO-SO_2-metal chelates-$\ell\cdot H_2O$ system have not been characterized yet. Teramoto et al.[7] have recently proposed the following reactions that could take place in this system:

$$Fe(II)EDTA + NO \rightleftharpoons Fe(II)(EDTA)(NO)$$

$$Fe(II)EDTA + SO_3^{2-} \rightleftharpoons Fe(II)(EDTA)\ (SO_3^{2-})$$

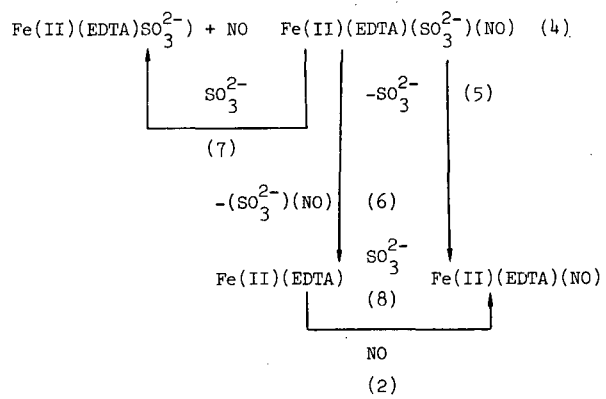

They suggested that reactions 5-7 are slow compared to reaction 8, and the activation energies of reactions 5 and 8 are larger than those of reactions 2 and 4. From the absorption rate study using a stirred vessel, they derived the forward rate constant of reaction 4 as 1.4×10^8 M^{-1} at 25°C. The rate constants of other reactions, the rate law, and the products of all reactions involved have not yet been reported.

We are investigating the kinetics of aqueous reactions between Fe(II)(NTA)NO and sodium sulfite under well-controlled conditions. Our preliminary results indicate that the reaction rate is first order with respect to the concentration of Fe(II)(NTA)NO and first order with respect to the concentration of $SO_3^=$. The major nitrogen product is N_2O. The rate constant is about 2.15×10^3 $M^{-2}sec^{-1}$ at 20°C. Work is in progress to determine the temperature and ionic strength dependence of the reaction and to identify all products for mass balance.

We are also studying the kinetics of the reaction between Fe(II)(NTA)($SO_3^=$) and NO.

Conclusion

Considering the current lack of understanding of the chemistry involved and the present elementary stage of development for this type of process, J. Ando[10] suggested that this wet simultaneous SO_2/NO_x removal technique may be economically competitive with the sequential installation of NO_x control by selective catalytic reduction (SCR) followed by SO_2 control by flue-gas desulfurization. Further research to identify a more effective metal chelate and to characterize important reactions involved could make this type of process an effective and economic scrubber for SO_2/NO_x control in a power plant.

PLANNED ACTIVITIES FOR FY 1982

The important reactions involving HNO_3, NO, and NO_2 with SO_2 in aqueous solution will be identified. These reactions will be included in a chemical reaction modeling scheme for an oxidation-absorption-reduction process.

The kinetics and mechanisms of reactions between nitrosyl metal chelate and sulfite ions will be investigated. The products of this reaction will be identified. These studies will make it possible to assess the economic feasibility of an absorption-reduction process.

REFERENCES AND FOOTNOTES

1. Yaverbaum, L.H. (1979), Nitrogen Oxides Control and Removal, Recent Developments, Noyes Data Corporation, Park Ridge, N.J.

2. Martin, A.E., Ed. (1981), Emission Control Technology for Industrial Boilers, Noyes Data Corporation, Park Ridge, N.J.

3. For references to the literature reviewed, see Chang, S.G., et al. (1981), Kinetics of Reactions in a Wet Flue Gas Simultaneous Desulfurization and Denitrification System, Lawrence Berkeley Laboratory Report LBL-13063.

4. Hishinuma, Y., et al. (1979), "Reversible Binding of NO to Fe(II)edta," Bull. Chem. Soc. Japan 52, p. 2863.

5. Lin, N.H., Littlejohn, D., and Chang, S.G. (1981), "The Thermodynamics and Kinetics of the Coordination of NO to Fe(II)NTA in Aqueous Solutions," submitted to J. Chem. Eng. Data.

6. Littlejohn, D., and Chang, S.G. (1982), "A Kinetic Study of Ferrous Nitrosyl Complexes," to be published in J. Phys. Chem., Feb. 1982.

7. Teramoto, M., et al. (1978), "Absorption of Dilute Nitric Monoxide in Aqueous Solutions of Fe(II)EDTA and Mixed Solutions of Fe(II)EDTA and Na_2SO_3," J. Chem. Eng. Japan 11, p. 450.

8. Sada, E., et al. (1980), "Individual and Simultaneous Absorption of Dilute NO and SO_2 in Aqueous Slurries of $MgSO_3$ with Fe^{II}-EDTA," Ind. Eng. Chem., Process Des. Dev. 19, p. 377.

9. Kustin, K., Taub, I.A., and Weinstock, E. (1966), "A Kinetic Study of the Formation of the Ferrous-Nitric Oxide Complex," Inorg. Chem. 5, p. 1079.

10. Cichanowicz, J.E., Ed. (1979), Proceedings: Second NO_x Control Technology Center, Electric Power Research Institute Report EPRI FP-1109-SR, Palo Alto.

ELECTROCHEMICAL ENERGY STORAGE RESEARCH

Applied Battery and Electrochemical Research Program*

E. J. Cairns and F. R. McLarnon

LBL has lead mission responsibility for management of the Applied Battery and Electrochemical Research Program, which provides supporting research for the Department of Energy (DOE) Electrochemical Systems research programs. The general objective of this program is to help provide advanced electrochemical systems that can satisfy stringent performance and economic requirements for electric vehicle and stationary energy storage applications. The specific goal of the program is to identify the most promising electrochemical technologies and transfer them to industry and/or another DOE program for further development and scale-up.

General problem areas addressed by the program include identification of new electrochemical couples for advanced batteries, determination of technical feasibility of new couples, improvements in battery components, and establishment of engineering principles applicable to batteries and electrochemical processes. Major emphasis is given to applied research which will lead to superior performance and lower life-cycle costs. The program is divided into three major areas: Exploratory Battery R&D, Engineering-Science Research, and Materials Research.

The LBL scientists who participate in the program are E.J. Cairns and F.R. McLarnon, Energy and Environment Division, and L.C. DeJonghe, J.W. Evans, R.H. Muller, J. S. Newman, P.N. Ross, and C.W. Tobias of the Materials and Molecular Research Division.

ACCOMPLISHMENTS DURING FY 1981

LBL monitored 35 research subcontracts during FY 1981 and conducted a vigorous in-house research program. The in-house work, "Development of Electrochemical Synthesis and Energy Storage," is summarized in the 1981 Materials and Molecular Research Division Annual Report and on page 1-50 to 1-52 of this report.

*This work was supported by the Assistant Secretary for Conservation and Renewable Energy, Office of Energy Systems Research, Energy Storage Division of the U.S. Department of Energy under Contract No. DE-AC03-76SF00098.

Exploratory Battery R&D

1. Management responsibility for the ambient-temperature $Zn/NaOH/Fe(CN)_6^{3-}$ hybrid redox system was transferred to Sandia National Laboratory for further development and scale-up.

2. The high-temperature $Ca/molten\text{-}salt/FeS_2$ system was shown to have adequate, but not superior, performance, and no further development work is planned at this time.

3. Work continued on the high-temperature, solid-state $Li/LiI \cdot Al_2O_3$ system, the intermediate-temperature $Na/\beta'' - Al_2O_3/S(AlCl_3 - Cl)$ system, and the ambient-temperature $Li/SO_2/C$ system. Reversible chemistry was established for the $Li/SO_2/C$ cell.

4. Exploration of the new intermediate-tempereature $Na/\beta'' - Al_2O_3/NaNO_3$ system was initiated.

Engineering-Science Research

1. Structural, optical, thermodynamic, and electrical studies of battery electrodes in ambient-temperature Zn/NiOOH, Fe/NiOOH, Al/air, and redox systems continued.

2. Investigations of new electrode/electrolyte formulations and novel separators for the Zn/NiOOH battery continued.

3. Studies of transport processes and measurements of transport properties in Zn/halogen flow systems were initiated.

4. Calorimetry provided extremely accurate measurements of thermal-energy generation rates in high-temperature Li/FeS cells.

5. Measurements of composition profiles in Li/FeS and Zn/NiOOH systems lacked sufficient accuracy to warrant continuing efforts.

6. Investigations of new components for photoelectrochemical energy storage cells were initiated. Amorphous boron photoelectrodes, photointercalation compounds, and antimony redox couples were being studied.

Materials Research

1. NASICON ($Na_{1+x}Zr_2Si_xP_{3-x}O_{12}$) ceramic electrolyte was shown to be unstable in molten Na at 300°C, and no further development work for high-temperature applications is planned. Instead, efforts will be focused on materials research and electrochemical compatibility of new compositions.

2. A novel technique to fabricate thin-walled β''-Al_2O_3 tubes by a tape-wrapping process was shown to be feasible and potentially competitive with conventional methods.

3. Electrical properties of fast Li ion-conducting glasses ($\sigma_{300} \approx 10^{-2}$ $ohm^{-1}cm^{-1}$) in the system Li_2O-$(LiCl)_2$-B_2O_3 have been measured and correlated with glass composition and structure.

4. New ceramic systems, including several NASICON-like structures, have been found to display fast-ion conduction.

5. Work on intermediate-temperature $LiNO_3$-KNO_3 molten salt electrolytes, novel all-solid composite microstructure electrodes (e.g., Li alloy dispersed in a metallic matrix), and ternary lithium-metal oxide positive electrodes has continued.

6. It was demonstrated that the polymer film polyethylene-oxide/lithium-trifluoracetate is, in fact, a solid electrolyte that conducts Li ions ($\sigma_{140} \approx 10^{-4}$ $ohm^{-1}cm^{-1}$). Small quantities of water vapor absorbed by the films increase their ionic conductivities by two orders of magnitude to values in agreement with prior measurements.

7. Work on novel Li and Na ion-conducting membranes continued.

PLANNED ACTIVITIES FOR FY 1982

The scope of LBL's management responsibilities will be expanded to the role of Lead Center for the Technology Base Research (TBR) Project. The TBR Project includes four major elements:

1. Electrochemical Systems Research

   a. Exploratory Battery R&D (included in FY 1981 responsibilities)

   b. Metal/Air Systems (managed by Lawrence Livermore National Laboratory).

2. Supporting Research

   a. Engineering-Science Research (included in FY 1981 responsibilities)

   b. Materials Research (included in FY 1981 responsibilities)

   c. Molten Salt Cell Research

   d. Systems Analysis

3. Fuel Cells for Transportation Application (managed by Los Alamos National Laboratory)

4. Electrolytic Processes

New research projects planned for FY 1982 include:

1. Research on rechargeable ambient-temperature lithium cells.

2. Application of transformation toughening to improve the stability of β''-Al_2O_3 ceramic electrolytes.

3. Investigation of transition-metal macrocyclic complexes as catalysts for fuel cell air electrodes.

Battery Electrode Studies*

E. J. Cairns, F. R. McLarnon, M. Katz, K. Miller, and J. Nichols

The purpose of this research is to study the behavior of electrodes used in secondary batteries and to investigate practical means for improving their performance and lifetime. Systems of current interest include ambient-temperature rechargeable cells with zinc electrodes (Zn/NiOOH, Zn/AgO, Zn/Cl_2, Zn/Br_2, Zn/Air, and $Zn/Fe(CN)_6^{=}$), and rechargeable molten salt cells (Li-Al/FeS, Li-Al/FeS_2, Li-Si/FeS, Li-Si/FeS_2, and Na/β''-Al_2O_3/NaCl-$AlCl_3$-SCl_4). The approach used in this investigation is to study the life- and performance-limiting phenomena under realistic cell operating conditions.

ACCOMPLISHMENTS DURING 1981

Investigations have centered on the zinc electrode, which exhibits satisfactory performance in rechargeable alkaline cells (Zn/NiOOH, Zn/AgO) but has an inadequate cycle life. The short lifetime and continual capacity loss of the zinc electrode are closely related to a phenomenon known as shape charge, the redistribution of active material over the face of the electrode as the cell is cycled.

Computer-Control of Electrode Performance Experiments
(by M. Katz, E. Cairns, and F. McLarnon)

A computer-controlled testing system[1] for cycle-life testing of battery electrodes has been implemented. Eight modular-design current controllers were built and tested to verify independent control of up to eight channels from a single power supply. A variety of cycling regimes, including constant-current, constant-potential, constant-power, pulsed-power, etc., have been tested, and extensive data treatment and display capabilities are available.

Experiments have been planned to establish the effect of various charging techniques on the behavior of Zn/NiOOH cells discharged under EPA urban driving profiles, an example of which is shown in Figure 1. Typical test data for a 2.3 A-hr Zn/NiOOH cell cycled under a 10 Hz (9/1 off/on) pulsed charging regime are displayed in Figure 2.

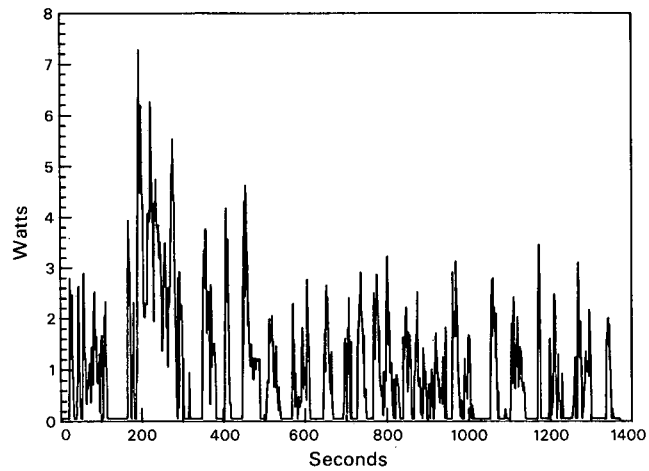

Figure 1. EPA urban driving profile with power requirement scaled to a 2.3 A-hr cell.
(XBL 821-1769)

Zinc Electrode Research
(by J. Nichols, E. Cairns, and F. McLarnon)

Researchers have recognized[2] the need for reduced solubility of the zinc species in alkaline electrolyte to reduce shape change and improve the lifetime of Zn/NiOOH cells. The focus of this project is to identify candidate electrolytes and characterize the effect of lowered zinc solubility on the cycle-life performance of Zn/NiOOH cells.

The tri-electrode cell case[1] was redesigned to reduce machining costs and assure uniform electrode spacing (<2 percent thickness variation across the electrode). Cells were cycled to test Zn electrode fabrication techniques and practical cell cycling regimes. These electrodes were successfully photographed by x-ray transmission at 60 KeV, 200 mAs, and a 100 cm target distance with a 2.5 mm Al filter; Zn geometric distribution was then measured to calculate shape charge rates, ranging from 0.6 to 1.0 percent/cycle, over 87 and 25 cycles, respectively. Five-hour charge rates and three-hour discharge rates were employed; typical charge/discharge curves are shown in Figure 3.

Capacity loss of the zinc electrode is shown to correlate with the loss of ZnO material that occurs each cycle, as shown in Figure 4. It is necessary to overcharge the Zn electrode each cycle to accommodate the inefficiency of the NiOOH electrode, and the repeated overcharging results in a gradual conversion of excess ZnO material to Zn metal.

A literature search has revealed several elec-

*This work was supported by the Assistant Secretary for Conservation and Renewable Energy, Office of Energy Systems Research, Energy Storage Division of the U.S. Department of Energy under Contract No. DE-AC03-76SF00098. This project is part of a larger effort, "Electrochemical Synthesis and Energy Storage," which is reported in the Materials and Molecular Research Division 1981 Report.

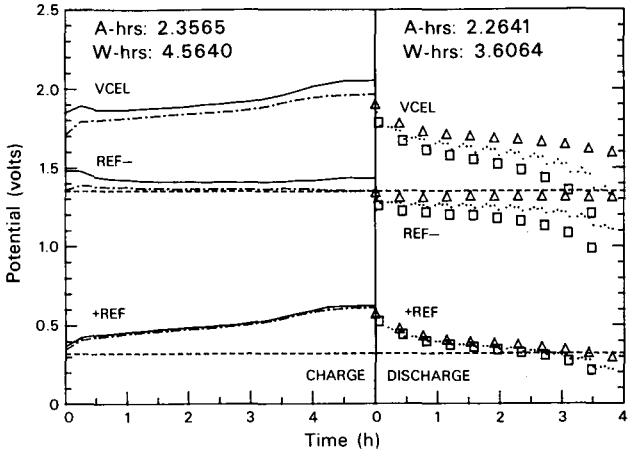

Figure 2. Charge/discharge curves for a 2.3 Ah Zn/NiOOH cell cycled with 10 Hz pulsed-current charging (9/1 off/on) and EPA power-profile discharging (Fig. 1).

CHARGE:

Solid Curves: measurements at current-on time

Dotted-dashed curves: measurements at current-off time

VCEL: NiOOH electrode vs. Zn electrode
REF-: Hg/HgO reference electrode vs. Zn electrode
+REF: NiOOH electrode vs. Hg/HgO reference electrode
Dashed lines: open-circuit values of REF- and +REF.

DISCHARGE:

Triangles: at base load (0.049 W)
Squares: at peak load (7.28 W)
Dots: at intermediate load (2.90 W)
Other notation as in charge portion of this figure.

(XBL 821-1768)

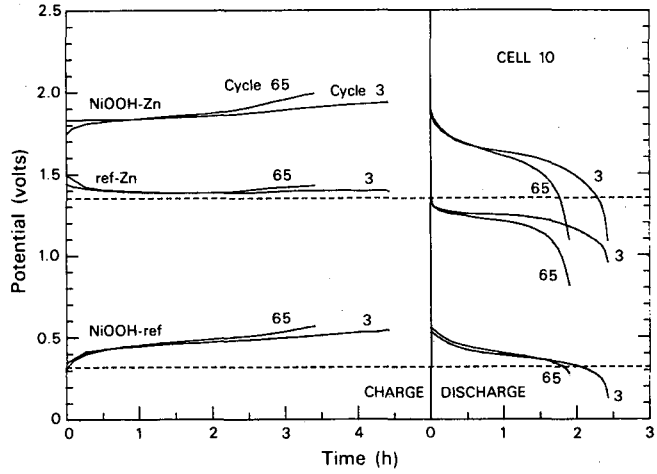

Figure 3. Charge/discharge curves for a 2.3 A-hr Zn/NiOOH cell cycled under constant-current conditions.

(XBL 821-1767)

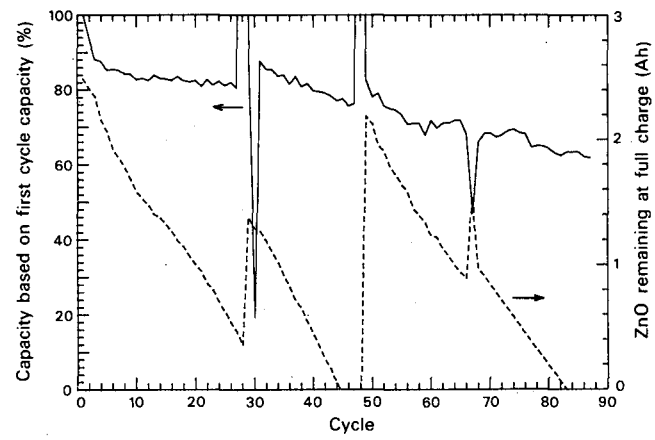

Figure 4. Capacity degradation of a 2.3 A-hr Zn/NiOOH cell during cycling.
_____ Cell capacity (% of cycle 1 capacity)
- - - - - ZnO reserve

(XBL 821-1766)

trolytes with reduced hydroxyl-ion concentration, reduced zinc species solubility, and sufficient conductivity to warrant cycle testing to measure the shape charge rates. SAM, SEM, and Electron Microprobe analysis is underway to elucidate Zn electrode morphology and determine the distribution of various elemental species in the electrode.

Mathematical Modeling of the Zinc Electrode
(by K. Miller, E. Cairns, and F. McLarnon)

It has been found that two factors limiting cycle life of zinc batteries are shape change,[3-5] the redistribution of active material over the face of the electrode, and passivation,[6,7] caused by the formation of an oxide layer on the surface of the electrode. Two one-dimensional models have been proposed to account for these phenomena.[4,5] The purpose of the present study is to develop a two-dimensional mathematical model to account for changes in current density, electrode overpotential, and species concentrations both parallel to and normal to the electrode surface. The aim is to predict the degree of shape change and passivation as the electrode is cycled.

Experiments will be designed to test and verify the modeling results. Preliminary work is under way.

PLANNED ACTIVITIES FOR 1982

Cycle-life testing of Zn/NiOOH cells will be continued, and work on rechargeable molten-salt cells will begin.

REFERENCES

1. Energy and Environment Division Annual Report FY 1980, Lawrence Berkeley Laboratory Report LBL-11990, 1981, p. 3-40.

2. McBreen, J. and Cairns, E.J. (1978), in Advances in Electrochemistry and Electrochemical Engineering, Vol. 11, H. Gerisher and C.W. Tobias, Eds., Interscience Publishers, New York, pp. 273-352.

3. McBreen, J. (1972), "Zinc Electrode Shape Change in Secondary Cells," J. Electrochem. Soc. 119, p. 1620.

4. Choi, K.W., Bennion, D.N. and Newman, J. (1976), "Engineering Analysis of Shape Change in Zinc Secondary Electrodes. I. Theoretical," J. Electrochem. Soc. 123, p. 1616.

5. Choi, K.W., et al. (1976), "Engineering Analysis of Shape Change in Zinc Secondary Electrodes. II. Experimental," J. Electrochem. Soc. 123, p. 1628.

6. Sunu, W.G., and Bennion, D.N. (1980), "Transient and Failure Analyses of the Porous Zinc Electrode. I. Theoretical," J. Electrochem. Soc. 127, p. 2007.

7. Sunu, W.G., and Bennion, D.N. (1980), "Transient and Failure Analyses of the Porous Zinc Electrode. II. Experimental," J. Electrochem. Soc. 127, p. 2017.

SOLAR ENERGY PROGRAM

INTRODUCTION

During FY 1981, the Solar Energy Program at Lawrence Berkeley Laboratory (LBL) has continued to focus on applied research that will extend the technology base for a broad range of solar energy applications and on preliminary development of new approaches to solar energy conversion.

A major effort has been the research on "passive" approaches to solar heating and natural cooling, where careful considerations of architectural design, construction materials, incident solar energy, environmental energy flows, and natural daylighting are used to moderate a building's interior climate and reduce the use of non-renewable energy. Experimental and analytic studies of natural convection heat transfer processes that take place within buildings and between the interior of a building and the environment are used to determine natural ventilation rates, interzone heat transfer, and heat transfer to and from storage masses located within a building. Computer models of convective and other basic heat-transfer processes are being developed, verified, and then incorporated into building energy analysis computer programs that are in the public domain. The resulting computer models are used as a tool to examine the energy consumption impacts of using passive heating and cooling design strategies in residential and commercial buildings. To determine the potential for radiative cooling of buildings in various parts of the country, spectral infrared sky measurements were taken in previous years; the analysis of these data and the study of correlations with other sky parameters continued throughout FY 1981. In addition, a broader based technology assessment of passive cooling resources was initiated, involving other laboratories as well as LBL. Daylighting effects have become an integral part of our building energy studies. Experimental measurements of daylighting levels in scale models of buildings are used to conduct dynamic simulations of the interaction of the daylighting system with the electric lighting and auxiliary heating and cooling equipment in commercial buildings. The result is a true measure of the energy benefits of daylighting designs. A further passive task involved the design of freeze protection techniques for passive thermosiphon solar hot water systems, based on detailed thermal analysis of candidate freeze protection strategies. The analysis was followed by construction of the most promising thermosiphon system and the design and construction of a test facility for experimental verification; testing was initiated near the end of FY 1981.

LBL is also engaged in research activities for the "active" solar cooling of buildings. New advanced thermodynamic cycles being studied have the potential for increasing the efficiency of solar-fired absorption air conditioners by at least a factor of two compared to the current state of the art. An air conditioner based on one of these advanced cycles, the double-effect regenerative absorption cycle, has been designed, and fabrication was nearly completed by the end of FY 1981. The testing of an earlier model, a modified single-effect absorption air conditioner that will constitute the core of the double-effect regenerative machine, was completed in FY 1981. In parallel with the experimental work, a methodology was developed for analysis of the performance and economics of solar cooling systems, to establish realistic cost and performance goals for all solar cooling systems under development in the national DOE program.

Installation of a 25-ton solar absorption air conditioner system in LBL Building 71, as part of the Federal Buildings Demonstration Program, will enable LBL engineers to gain first-hand experience with one of the new solar cooling units developed in the DOE solar R&D program. The design of this system in FY 1981 will be followed by its construction and installation in FY 1982.

In both active and passive solar space conditioning, LBL staff members are providing technical support to DOE/Headquarters and the DOE/San Francisco Operations Office in developing program plans, evaluating reports and proposals, and technical monitoring of R&D activities by other contractors. In a closely related effort, LBL has been providing technical support for the U.S.-Saudi Arabian SOLERAS solar cooling program, which consists of field tests in Phoenix of four of the most advanced solar cooling systems developed to date by the DOE R&D program.

Measurement of solar radiation continued to be an important part of the LBL solar energy program. Special instruments (circumsolar telescopes) previously developed at LBL continued to be used in a systematic program to measure solar and circumsolar radiation (the radiation from near the sun resulting from the scattering of sunlight by small particles in the atmosphere). These measurements provide an important ingredient in predictions of the performance of solar collector systems that use mirrors or lenses to focus and concentrate the sunlight. The measurement program was accompanied by detailed analyses of the data collected over the past few years and by study of correlations between the circumsolar radiation levels and various environmental, seasonal, and location-dependent parameters.

A promising new method for converting and using concentrated solar energy is being pursued at LBL. It involves the use of very small (sub-

micron) particles suspended in a gas stream to absorb the solar energy and transfer the heat to the gas stream. A solar thermal receiver using this technique has been designed, and fabrication was underway at the end of FY 1981. Plans call for the test of this receiver during FY 1982 at one of the country's solar thermal test facilities.

Another project based on the properties of particles of small dimension was initiated at a low level of effort in FY 1981. This project is exploring the use of holographic or diffractive optical elements for solar energy conversion or control (e.g., window) systems.

One of the more basic solar research projects involves biological energy conversion techniques, using one of the simplest biological energy converters known: the pigmented protein bacteriorhodopsin. This research project is attempting to elucidate the molecular details of how this protein uses sunlight to produce an electrical current across bacterial membranes. Such understanding should ultimately lead to the production of novel photoelectric cells and solar batteries.

As part of the DOE Appropriate Energy Technology program, LBL continued to conduct energy and economics analysis to determine the effectiveness of the program. In addition, a technology assessment was carried out for the projects involving the use of wind energy.

Finally, FY 1981 constituted a peak year for the LBL solar energy R&D activities because it is anticipated that the severe DOE cutbacks in the national solar energy program for FY 1982 will adversely affect the LBL solar program. The circumsolar radiation measurement project and the appropriate energy technology project are being cancelled by DOE in FY 1982, and most of the other projects are expected to receive substantial budget reductions.

Passive Research and Development*

R. C. Kammerud, J. W. Place, M. R. Martin, P. H. Berdahl, D. Elmer, B. Andersson, F. S. Bauman, W. L. Carroll, A. J. Gadgil, A. Mertol, S. U. Choi, M. B. Curtis, E. Ceballos, M. Tavana, T. L. Webster, M. W. Nansteel, C. C. Conner, P. Coutier, M. Fontoynont, E. F. Altmayer, G. Schiller, V. Horan, H. Michaels, and N. A. Friedman

The amount of conventional fuel used to heat, cool, and light buildings is determined by (1) the interaction of the building with its environment, (2) the thermal gains associated with the activities occurring within the structure, and (3) the operating characteristics of the equipment used to convert conventional fuels to end-use energy. Traditionally, the building design process has not adequately accounted for the combined influence of these three factors on building energy consumption. By integrating these energy issues into the design process, significant reductions in the fuel used to provide a comfortable environment can be realized. This requires that the designer be sensitized to energy as an element of design; he or she must also have access to information on techniques for properly controlling the interactions of the building with the environment and managing the energy flows within the structure.

Passive heating, cooling, and lighting strategies integrate the energy control and management schemes into the building design, taking into account the design parameters of the building and the environmental conditions to which the structure is exposed. In this context, the passive program at Lawrence Berkeley Laboratory is directed at theoretical and experimental investigations of the thermal performance implications of passive design strategies, with emphasis on passive and hybrid cooling of commercial buildings. The specific objectives of the program are the following:

1. Develop analytic descriptions of the thermal processes which occur within a building or between a building and the environment. These heat transfer algorithms are based on empirical data and/or analysis from first principles.

2. Develop and test advanced passive/radiative cooling system components and evaluate other passive heating and cooling systems.

3. Evaluate the effectiveness of passive systems in reducing energy consumption for space heating, space cooling, domestic hot-water heating, and lighting in the United States and identify effective criteria for passive system design optimization. The strategy used to meet these objectives consists of coordinated experimental and theoretical tasks leading to advanced energy analysis capabilities which can be used in passive system design and evaluation.

To date, the emphasis has been on the development and testing of techniques for predicting (1) the "resource" for passive systems and (2) a building's response to that resource. In this con-

*This research was supported by the Assistant Secretary for Conservation and Renewable Energy, Office of Solar Heat Technologies, Passive and Hybrid Solar Energy Division, of the U.S. Department of Energy under Contract DE-AC03-76SF00098.

text, the term "resource" implies the naturally occurring potentials of the environment to provide heating and lighting (as a result of solar gains) and cooling (via radiation to the sky, conduction to the ground, and ventilation/evaporation with ambient air). These potentials are being investigated in projects in the following areas: convection and natural ventilation, radiative cooling, natural lighting, passive building energy analysis, and passive domestic hot water. Accomplishments and future plans in each of these areas are described below.

ACCOMPLISHMENTS DURING FY 1981

Convection Research

This project consists of both experimental and analytic studies of natural convection heat transfer processes which take place within buildings and between the interior of a building and the environment. The objective of the project is to develop technically sound predictive capabilities for (1) natural ventilation rates, (2) interzone heat transfer, and (3) heat transfer to/from storage masses located within a building. The analytic work attempts to develop and apply detailed numerical models for convection phenomena in order to develop simplified descriptive algorithms to represent the heat transfer process. The experiments provide guidance for the development of the numerical model and produce data for validation of the numerical model and the algorithms.

During FY 1981, the experimental work consisted of measuring the convective heat transfer between two enclosures separated by a doorway. The data were collected in a small-scale experiment for a range of Rayleigh numbers extending from 10^{10} to more than 10^{11}. It was observed that, for the same boundary conditions, the heat transfer rate is relatively insensitive to the horizontal extent of the doorway and is determined largely by the height of the opening relative to the height of the enclosure. Based on these experiments and previously published results, a correlation was developed which led to the identification of an algorithm describing the coupling between enclosures[1]:

$$h = 1.44\left(\frac{H_a}{H}\right)^{0.45}\left(\frac{\Delta T}{H}\right)^{0.25}$$

where h is the interzone heat transfer coefficient ($W/m^2\ {}^oC$), ΔT is the temperature difference between the two endwalls (^oC), H is the height of the enclosure (m), and H_a is the central aperture height (m).

A detailed numerical model which solves the governing Navier-Stokes equations describing laminar convective heat and mass transfer in enclosures was validated using data from earlier LBL experiments.[2] This computer code was then applied to examine the variability of surface convection coefficients in an enclosure as the temperature distributions on the bounding surfaces are altered. This study showed that the coefficients deviate dramatically from the constant or simple temperature-dependent values normally used in the building sciences and that the true variations have a substantial impact on the calculation of energy consumption in buildings.

The numerical model was extended to turbulent flow by addition of a model for turbulent dissipation. This new capability allows examination of wind-driven natural ventilation rates and heat transfer from surfaces under forced or natural ventilation.

Radiative Cooling

Infrared radiative cooling systems are composed of a radiator surface exposed to the sky and a means for transporting heat from the building's interior to the radiator surface. The performance of these systems may be predicted if we know the intensity of infrared radiation produced by the atmosphere as a function of both zenith angle and wavelength.

To obtain data on which estimates of cooling system performance can be based, an experimental program was carried out in 1980 to measure the sky radiance at several U.S. locations. The measurements included the spectral composition of the sky radiance as a function of zenith angle and local climate variables such as drybulb and dewpoint temperatures.[3]

During FY 1981, the spectral radiometer data were analyzed to establish a correlation between the nighttime clear-sky infrared emissivity and the weather variable to which it is most sensitive, dewpoint temperature. The results are shown in Figure 1 in comparison with earlier experimental results; the correlation is based on data obtained from Tucson, Arizona, Gaithersburg, Maryland, and St. Louis, Missouri, comprising 2,945 individual measurements. The apparent discrepancy between the LBL correlation and that of Clark and Allen at low

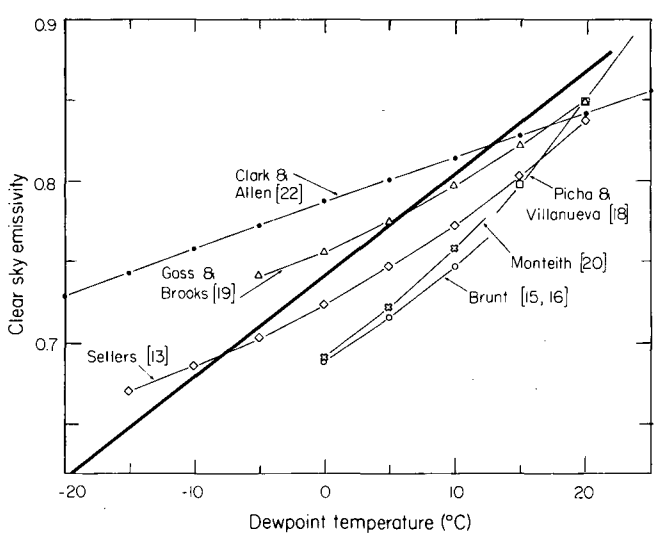

Figure 1. LBL results (heavy line) for clear-sky thermal emissivity compared with the results of previous investigators.

(XBL 813-541)

dewpoint temperatures was resolved by Clark,[4] who noted that their results closely approach the LBL values when accurate on-site temperature measurements are used. Although the sites from which the data were collected do not encompass all the climate types experienced in the United States, the fact that the observed clear-sky data from three diverse locations fall along the same straight line encouraged the belief that this may be a general result for midlatitude climates.

Under conditions of low clouds (below about 2 km), the apparent absolute sky temperature T_{sky} has been given as[5]

$$T_{sky} = (1 - f_w)\, T_{air} + f_w T_c$$

where T_{air} is the ambient air temperature, T_c is the temperature of the cloud base, and f_w represents the fraction of blackbody radiation in the 8- to 14-micron (atmospheric window) region and is equal to 0.3 ± 0.1. Data from the infrared spectral sky radiometers have been used to support this equation. The 11-micron effective sky temperature is used as a best estimate of the cloud base temperature, since the atmosphere is most highly transparent in this part of the spectrum. For the purpose of displaying this data, it is convenient to plot the sky temperature depression ($\delta T_{sky} = T_{air} - T_{sky}$) as a function of the cloud temperature depression ($\delta T_c = T_{air} - T_c$). In terms of these variables, the equation for the sky temperature reads

$$\delta T_{sky} = f_w \delta T_c$$

A plot of δT_{sky} vs. δT_c is shown in Figure 2; agreement is good for a value of $f_w = 0.32$. Based on a typical lapse rate of 5°C/km, the measured points in Figure 2 represent cloud base altitudes of zero to 4 km.

Figures 3 and 4 show the results of spectral infrared sky emissivities for clear sky conditions (558 hourly readings) and all sky conditions (879 hourly readings), respectively. The examples shown here are for Gaithersburg, Maryland, and represent data taken during August 1979 in the 8- to 14-micron waveband. Average hourly sky radiances expressed as emissivities are shown for zenith angles of 0, 20, 40, 60, and 80 degrees. The remaining curve is a weighted average of the angular values which represent the 8- to 14-micron emissivity seen by a horizontally exposed radiator.

For clear skies, the emissivities are nearly independent of time of day, provided the corresponding hourly average dewpoint temperatures

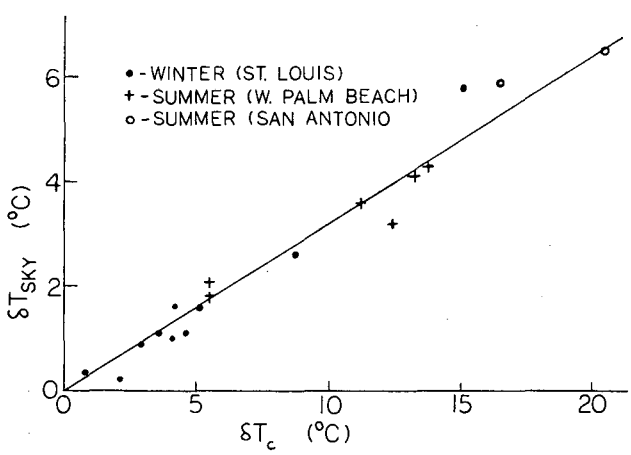

Figure 2. Sky temperature depression vs. cloud temperature depression.

(XBL 827-880)

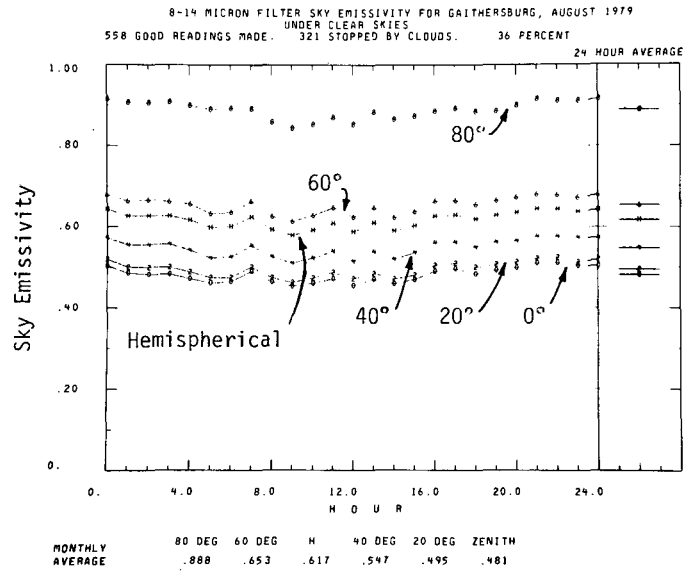

Figure 3. Measured average hourly sky emissivities in the 8- to 14-micron waveband for clear skies, for several zenith angles. The "hemispherical" curve is a weighted average of angular values.

(XBL 823-8209)

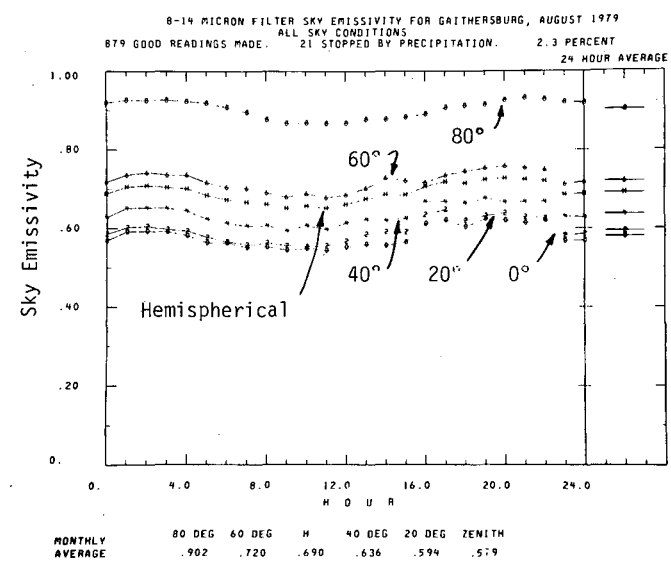

Figure 4. Measured sky emissivities in the 8- to 14-micron waveband. This figure is identical to Figure 3 except that it pertains to all sky conditions, cloudy as well as clear.

(XBL 823-8210)

are also independent of time of day. The clear-sky emissivities show a tendency to be slightly larger at night due to the development of nighttime temperature inversions, which cause the atmosphere to have a higher radiative temperature compared to the air temperature near the ground. The difference between the clear-sky plots and those for all sky conditions is due to clouds. For this particular month, clouds occurred more frequently from 1600 to 2200 hours than during the rest of the day, reducing the radiative cooling potential during this interval. Monthly summaries similar to these examples are being published for all six stations at which infrared sky measurements were taken over a two-year period. This level of detail will be important when designing systems for radiative cooling to be used at a specific location.

Building Energy Analysis

This project consists of the development, experimental verification, and application of computer programs which predict the energy consumption of passively heated and/or cooled buildings. Energy analysis activities are carried out using BLAST[6]; LBL has contributed several passive solar system models to this program in recent years. This program performs thermal load calculations, air handling system simulations, and central energy plant analysis; it is therefore appropriate for application to both residential and commercial buildings.

During FY 1981, BLAST-3.0 development was completed and the program was released into the public domain. Table 1 summarizes the analysis capabilities which relate to passive heating and cooling. BLAST-3.0 simulation results were compared to experimental data collected from a full-scale massive structure located in an environmental chamber at NBS.[7] Owing to its use of a new thermal balance load calculation technique, BLAST gave unusually accurate results in simulating the thermal behavior of the structure. Figure 5 shows a comparison of BLAST predictions with the measured heat fluxes, surface temperatures, and cooling loads; the agreement is shown to be very good.

Applications of BLAST-3.0 to both residential

Table 1. BLAST-3.0 capabilities.

Passive Analysis
Direct Solar Gain
Solar Walls (à la Trombe/Morse Walls)
Sunspaces
Natural Lighting
Direct Ventilation Cooling
Ground Coupling
Roof Ponds/Roof Evaporation
Load Control Analysis
Solar Shading
Solar Control Glazing
Movable Insulation
Thermal Mass
Economizer Systems

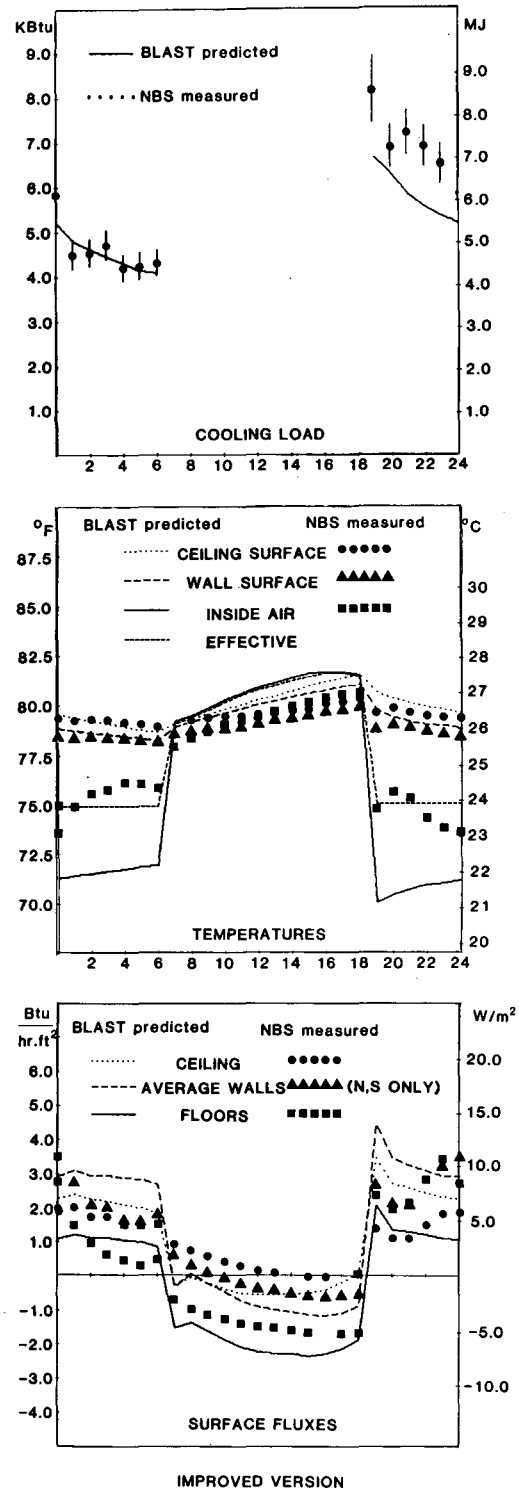

Figure 5. Comparison of BLAST prediction (see text) with NBS measured results: night cooling test, NBS massive structure.

(XBL 824-466)

and commercial buildings have been carried out. In the residential studies, it was shown that the large expanses of south glazing needed for direct-gain heating have a substantial influence on the summertime cooling energy consumption. Considering both heating and cooling, total energy consumption of direct-gain systems using unmanaged south double

glazing is relatively insensitive to the glazed area in most U.S. climates. However, unmanaged east and west glazing is notably detrimental to overall performance owing to its serious impacts on cooling energy consumption. These results imply that a more integrated heating and cooling design approach is mandatory if appreciable energy benefits are to be realized.[8]

An examination of the energy consumption impacts of residential building orientation was completed.[9] It was confirmed that the location of glazing on the east and west facades of a building does not substantially alter heating season performance but can be very deleterious to cooling season energy consumption. In many climates, north orientation of glazing is not substantially inferior to south orientation; in fact, in extreme southern climates, north orientation is preferred, because (1) cooling is the dominant energy consumer and (2) north glazing receives less solar radiation than south glazing, even when the south glazing has a substantial overhang. Figure 6 shows some results from the orientation studies for a moderate U.S. climate (Nashville) and a very warm climate (Miami). In both cases, east and west orientations show the highest combined heating and cooling loads. In Nashville, south orientation shows the lowest combined loads; this advantage is more pronounced farther north. In Miami, because of dominant cooling loads, northern orientations produce the lowest loads.

Ventilative cooling of residential buildings was studied in order to examine the influence of the amount of thermal mass on cooling season performance and to determine the most desirable control strategy in a variety of climate types. It was found that relatively low air volumes (20 air changes per hour) are required to obtain nearly maximum effectiveness; it is interesting to note that this air exchange rate can frequently be accomplished with natural ventilation systems, such as cross ventilation using windows and the prevailing winds. It was also shown that, for some climates, night ventilation is a very effective cooling strategy if substantial amounts of exposed thermal mass are located in the building.[10]

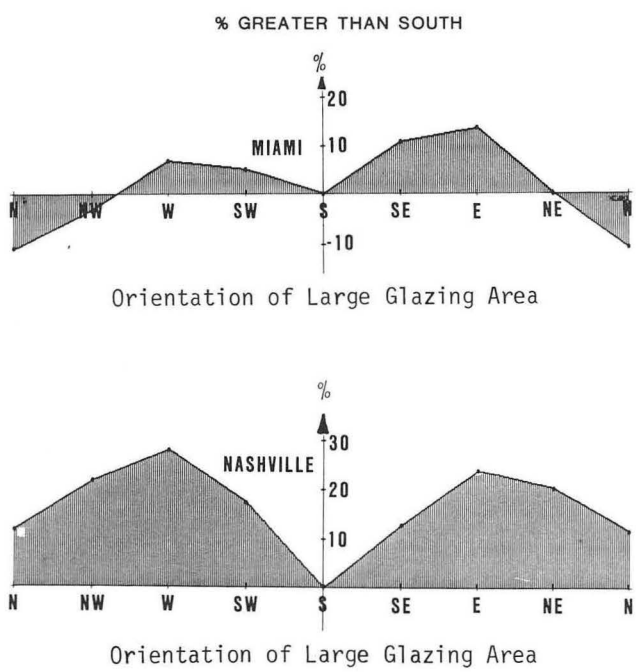

Figure 6. Combined heating and cooling loads in Miami and Nashville.

(XBL 827-879)

Commercial building studies were initiated during FY 1981. A completed study focused on the interaction between the mechanical systems in a commercial building, the environment, and the energy demands of the occupied spaces. This demonstrated that the passive design process for commercial buildings cannot be based on the substantial existing residential experience. In commercial buildings, the thermal load is only loosely coupled to the energy consumption of the mechanical systems; the dominant thermal load does not necessarily correspond to the dominant energy end use. For example, in many buildings the heating load is smaller than the cooling load, but space heating is the dominant consumer of energy at the building boundary. This substantially complicates the selection of appropriate passive heating and/or cooling approaches for commercial buildings and implies that the selection must be based on a comprehensive examination of the anticipated fuel consumption profiles for the building. It is necessary to provide the designer with a new level of technical design information regarding energy use patterns for the commercial sector.

In preparation for comprehensive studies of passive strategies in commercial buildings, a daylighting measurement facility was designed, built, and tested. The facility will be used to gather illumination data from scale models of commercial buildings; the data will be input to BLAST in order to perform total energy analyses of naturally lighted buildings. Future work on this project will provide information regarding the cooling load reductions and/or heating load increases that accompany reduced electric energy consumption for lighting.

Domestic Hot Water

The goal of the hot water project was to develop and test passive solar water heater concepts, with the focus on thermosiphons. For domestic hot water and other low-temperature applications, thermosiphons offer significant advantages over active systems in terms of simplicity, reliability, and cost. Furthermore, the widespread use of thermosiphons in other countries is evidence of the market potential of this concept. The major limitation to the use of conventional thermosiphons in the U.S. is the vulnerability in almost all climates to freezing of the potable water in the low-mass collector. Current methods of freeze-protecting thermosiphons, such as drain-down, tend to compromise the basic attributes of the thermosiphon concept, i.e., simplicity and reliability.

The major thrust of the hot water project has been to carefully quantify the performance of thermosiphons using a non-freezing collection fluid which transfers heat to the potable water through a

heat exchanger. Specific objectives of the project are to

1. Quantify the performance of thermosiphons with heat exchangers relative to systems without heat exchangers.

2. Quantify the performance differences between thermosiphons using horizontal and vertical tanks.

3. Develop and test various heat exchanger concepts and quantify the performance of each to provide the basis for optimizing heat exchanger design.

4. Investigate the significance of reverse flow in these systems and the need for using one-way valves.

5. Develop simplified design tools and application guidelines to foster implementation of these systems.

During FY 1981, a detailed computer program was written for simulating the daytime collection and nighttime reverse-flow losses of a thermosiphon water heater with a simple heat exchanger in the storage tank. Simulations were made with the computer program to determine the performance effects of heat exchanger capacity, tank stratification, tank elevation relative to collector, and system resistance (collector and connecting tube diameter and length).[10]

A simplified computer program was developed to simulate annual performance at hourly time increments using Typical Meteorological Year (TMY) weather tapes. The predictions of the simplified model agree with those of the detailed analysis to within 5 percent. Both the detailed and simplified analyses agree to within 5 percent with the data reported in the literature for non-heat-exchanger configurations.

A detailed analytical model was developed for the simple heat exchanger inside the tank. Performance was found to be sensitive to the tank temperature, collection fluid temperature, and flow rate. The detailed heat exchanger model was used to generate an algorithm which was incorporated into both the detailed and simplified system-simulation computer programs.

A residential-scale thermosiphon test facility was constructed with the following capabilities:

1. Solar collectors powered by electric resistance heaters that are controlled to simulate daily solar radiation cycles.

2. Structure capable of orienting the storage tank vertically or horizontally and at various elevations relative to the collector.

3. Experimental tank capable of accepting various heat exchanger configurations and provision for obtaining detailed tank temperature profiles.

4. Sixty-channel data acquisition system with output to magnetic tape.

A data reduction program was written that can read magnetic data tapes and generate temperature plots and performance reports.

PLANNED ACTIVITIES FOR FY 1982

Convection Research

The emphasis of the convection project during FY 1982 will be on (1) consolidation of existing analysis capabilities by thorough verification of the convection analysis and (2) applications leading to an improved characterization of surface convection coefficients in terms of the boundary conditions on surface temperatures. The zone coupling algorithm developed in FY 1981 will be further tested in order to define its limits of applicability. During the latter portions of the year, studies of wind-driven natural ventilation will be initiated; it is anticipated that this will lead to algorithms describing the ventilation rate as a function of environmental conditions and building design parameters.

Radiative Cooling

The sky radiometer data analysis will be concluded and the results published. A radiative cooling-assembly test facility will be used to examine the cooling performance of assemblies using existing radiator and glazing/wind-screen materials; both blackbody and selective radiator surfaces will be tested. Finally, advanced radiator materials will be tested to determine whether they can produce more cooling power.

Building Energy Analysis

The focus of these activities will be on the application of BLAST to study the energy consumption impacts of the various passive cooling and cooling load control options. These studies will be used to estimate the relative impacts of the individual cooling technologies in various climates across the nation. In conjunction with personnel at the Los Alamos National Laboratory, we will further analyze the thermal performance results in order to estimate the economic impacts of the cooling technologies. In the daylighting area, the illumination measurements and their analysis and the associated thermal analysis will be extended to a variety of design concepts in order to characterize system performance.

Domestic Hot Water

This project will be concluded with the publication of the results of the proof-of-concept experiments.

REFERENCES AND FOOTNOTE

1. Nansteel, M., and Greif, R. (1981), "Natural Convection in Undivided and Partially Divided Rectangular Enclosures," J. Heat Transfer 103,

pp. 623-629, and Lawrence Berkeley Laboratory Report LBL-12525.

2. Bauman, F., et al. (1980), "Buoyancy Driven Convection in Rectangular Enclosures: Experimental Results and Numerical Analysis," presented at ASME Heat Transfer in Passive Solar Systems Conference, 27-30 July 1980, Orlando, Florida, Paper No. 80-HT-66; Lawrence Berkeley Laboratory Report LBL-10257.

3. Martin, M., and Berdahl, P. (1978), "Description of a Spectral Atmospheric Radiation Monitoring Network," in Proceedings, 3rd Conference on Atmospheric Radiation, Davis, California, June 1978.

4. Clark, G. (1981), "Passive/Hybrid Comfort Cooling by Thermal Radiation," in Proceedings, International Passive and Hybrid Cooling Conference, 10-13 November 1981, Miami Beach, Florida.

5. Berdahl, P., and Martin, M., "Thermal Radiance of Skies with Low Clouds," in Proceedings, International Passive and Hybrid Cooling Conference, 10-13 November 1981, Miami Beach, Florida; Lawrence Berkeley Laboratory Report LBL-12533.

6. BLAST (Building Loads Analysis and System Thermodynamics) is trademarked by the Construction Engineering Research Laboratory, U.S. Department of the Army, Champaign, Illinois.

7. Gujral, P., Clark, R., and Burch, D. (1981), "An Evaluation of Thermal Energy Conservation Schemes for an Experimental Masonry Building," U.S. National Bureau of Standards, Building Science Series 137.

8. Place, W., Kammerud, R., and Andersson, B., "The Cooling Implications of Direct-Gain Heating," Lawrence Berkeley Laboratory Report LBL-12355 (in preparation).

9. Andersson, B., et al., "The Importance of Residential Building Orientation," Lawrence Berkeley Laboratory Report LBL-12046 (in preparation).

10. Kammerud, R., et al. (1981), "Ventilation Cooling of Residential Buildings," Lawrence Berkeley Laboratory Report LBL-11386 (in preparation).

11. Mertol, A., et al. (1981), "Detailed Loop Model (DLM) Analysis of Liquid Solar Thermosiphons with Heat Exchangers," Solar Energy 27, 5, pp. 367-386, and Lawrence Berkeley Laboratory Report LBL-10699.

Active Solar Cooling*

M. A. Wahlig, K. Dao, M. L. Warren, J. E. Rasson, R. A. Armer, H. Angerman,† and A. Heitz†

This project has three major tasks: (1) research and development (R&D) of improved absorption cycles for active solar cooling and heating, (2) performance and economic analysis of active solar cooling and heating systems to establish cost/performance goals for the R&D program, and (3) technical support activities for the active solar cooling program.

The objective of the R&D activity is to achieve a significantly higher conversion efficiency than is possible using other approaches for solar cooling and heating of buildings. Because practical temperatures range up to about 350°F for solar collectors used in residential and commercial building applications, absorption-cycle cooling systems have been selected for investigation. Being essentially heat pumps, absorption-cycle chillers can be used for heating as well as cooling if the refrigerant fluid does not freeze in the outdoor coil during heating applications. We restrict our fluid choices to those for which this heating option is available.

The R&D program consists of four phases, each successive phase leading closer to the final machine. The first phase was successfully completed some time ago.[1] By modification of a conventional gas-fired ammonia/water absorption chiller, we demonstrated the capability of our analysis techniques to predict accurately the performance of single-effect, absorption-cycle chillers under operating conditions appropriate for solar-powered cooling.

In the second phase, a completely new solar single-effect chiller[2] was fabricated, using the experience gained during the first phase. Testing of this chiller has just been completed. Evaluation and recommendations concerning this chiller are summarized later in this report.

The third phase investigates the performance improvement obtained by adding a unique second boiling effect to the single-effect chiller tested in the second phase. The basic concept of the resulting double-effect regenerative (or cycle 2R) cycle has been described previously.[3] Fabrication of the major components of the 2R chiller[4] has now

*This work was supported by the Assistant Secretary for Conservation and Renewable Energy, Office of Solar Heat Technologies, Active Heating and Cooling Division of the U.S. Department of Energy under Contract No. DE-AC03-76SF00098.

†Employees of Keller and Gannon, a subsidiary of Lester B. Knight and Associates, Inc.

been completed, and testing is expected to start by mid-FY 1982.

The fourth phase of the R&D activities investigates a new concept in refrigeration absorption cycles, having still higher efficiency and yet requiring less heat exchanger area and thus having a potential for lower cost. The basic concept of this single-effect regenerative cycle (which we call cycle 1R) has also been described previously.[5] The success of the cycle 1R chiller depends on our experience gained from developing the cycle 2R chiller. Locating a refrigerant-absorbent fluid pair with suitable properties at 300°F or higher should further increase the efficiency of the 1R chiller.

The objectives of the performance and economic analysis activities are to establish cost/performance goals for active solar cooling and heating systems and to identify those R&D directions that have the greatest probability of attaining these goals. The desired cost/performance goals are those that will result in significant market penetration of active solar cooling systems, starting in the late 1980's and continuing through the 1990's. A methodology has been developed to derive these goals, and preliminary solar cooling system and subsystem goals have been calculated.

The technical support activities provide assistance in the active solar cooling program area to the DOE San Francisco Operations Office (SAN) Conservation and Solar Division and to the DOE Headquarters (HQ) Active Heating and Cooling Division, Office of Solar Heat Technologies. These activities include program planning, technical monitoring and evaluation of ongoing projects, including site visits and review of progress reports, coordination of review of unsolicited proposals, assistance in the preparation and evaluation of responses to program solicitations, and coordination of related activities by other organizations.

Finally, a related activity, the LBL solar controls program, had as its objective the use of the LBL solar controls test facility to evaluate experimentally the relative performance of different solar heating control strategies for a variety of input meteorological conditions and output load demands, and the carrying out of theoretical studies of collector and load loop performance in support of the experimental work. Work on the LBL controls test facility was concluded early in FY 1981, and the results of theoretical analysis have been presented.

ACCOMPLISHMENTS DURING FY 1981

Absorption Chiller R&D

Testing of the Single-Effect Chiller. The testing of the single-effect ammonia/water chiller has been successfully completed. Most of the performance goals have been achieved as summarized in Table 1.

The chiller has been tested for about 300 hours of run time, from which about 70 performance data sets have been collected. A complete report on the performance of the chiller and its components will be issued shortly.

Table 1. Single-effect chiller test results.

	Realized	Goal
Hot water input temperature, °F	220	216
Condenser/absorber inlet cooling air temperature, °F	95	95
Leaving chilled water temperature, °F	52	45
Capacity, tons	3	3
Coefficient of Performance, COP	0.67	0.70
Condenser/absorber fan power, HP	3/4	3/4
Condenser/absorber fan air flow rate, CFM	6800	6800
Make-up solution pump power, HP	1/2	0

Initial analysis of the data indicated that the absorber was the poorest performer of the chiller components. Its overall heat-transfer coefficient was only 80 Btu/hr-ft^2-°F of tube area as opposed to the expected value of 140. This led to a high absorber temperature and, therefore, a higher chilled water temperature. Other contributions to the high (52°F) chilled water temperature included:

- An unexpected pressure drop of 10 psi across the pipe fittings at the outlet of the generator (manufacturing error);
- A 20-percent lower-than-expected heat transfer coefficient of the condenser; and
- A 35-percent lower-than-expected heat transfer coefficient of the evaporator.

Evaluation of the Single-Effect Chiller. The major results of the single-effect chiller tests are as follows:

1. The concepts of heat recuperation incorporated into the chiller worked as expected, increasing the COP to the 70-percent range.
2. The concept of power recuperation from the weak solution worked reliably: the solution driven pump had no failures during any of the runs.
3. The concept of self-powered operation needed more refinement: the vapor-driven pump did not work well because of vapor absorption in its valve switching lines.
4. Heat transfer coefficients were usually 20 percent lower than design calculation predicted, possibly because of higher fouling factors. Keeping the tubes very clean and rust free might well restore the higher heat-transfer coefficients.

5. The generator outlet pressure can be eliminated by reconnections.

6. The poor heat transfer of the evaporator occurred largely at its outlet, where most of the liquid had been evaporated. By rerouting the last tubings of the evaporator, the poor overall heat-transfer coefficient should be improved.

7. The absorber needs a better design than the conventional finned tubes.

Eliminating the obvious shortcomings, such as rust, dirt, and bad connections, should reduce the chilled water temperature to 48°F. To further lower the chilled water to 45°F, a better absorber design must be used or the hot water input must be raised to 225°F.

Fabrication of the 2R Chiller. The following components of the 2R chiller have now been fabricated:

- Boiler, as shown in Figure 1
- Recuperator
- Generator
- Preheater
- Multistage pump

The installation of the testing facility for the 2R chiller and the fabrication of the remaining chiller components are underway. Testing of this chiller is scheduled to begin in mid-1982.

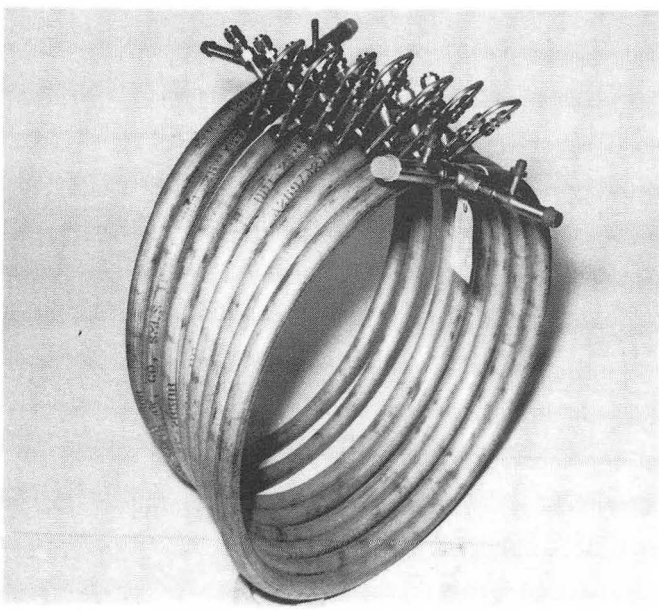

Figure 1. Multi-stage boiler of the 2R chiller. In each turn of the coil, the solution boils at a different pressure. Vapors are taken off at the larger short-tube segments welded to the coil; for further boiling, solutions are expanded to the next pressure stage through the small v-shaped tubings. Hot water from the solar collectors flows inside the inner tube of the coil.

(CBB 818-8154A)

Candidate Fluids for the Cycle 1R Chiller. Under DOE contract and LBL guidance, SRI International conducted a literature search during FY 1981 and followed up with experimental measurements of the properties of absorbent and refrigerant fluids previously identified by LBL to be candidates for high temperature (260 to 360°F) operation of a cycle 1R chiller. These measurements should be completed during the first half of FY 1982.

Performance and Economic Analysis

The principal accomplishments during FY 1981 have been development of preliminary cost/performance goals for active solar cooling/heating systems, preparation of a background report describing a methodology for developing cost/performance goals, work with other contractors performing systems analysis work to define realistic buildings and active solar cooling systems for simulation, completion of the analysis of experimental results from the controls test facility operation and reporting the results, completion of the theoretical analysis of the interaction between the solar heating system and the building response, and reporting the results.

Cost Goal Methodology. A consistent methodology has been developed by which general solar cooling market-capture goals can be and have been translated into specific cost and performance goals for solar cooling systems and subsystems.[6-9] The preliminary results indicate that realistic cost/performance goals can be established for active solar cooling systems. This methodology for establishing cost goals and developing cost and performance improvement pathways to reach those goals is not limited to active solar cooling applications; it could be used equally well for other technologies, such as passive cooling and heating.

A market-penetration scenario was postulated, beginning with commercial introduction of active solar cooling systems in 1986 and attaining a 20-percent annual market share of the entire national cooling capacity by the year 2000. The shape of this postulated market-penetration curve was based upon the actual penetration curve achieved by heat pump sales in the United States during the period 1953 to 1970. This is typical of historic early-market penetrations achieved by major HVAC products. In general, air conditioning demands are expected to grow significantly over the next 20 years, driven by population shifts to the "sun belt" regions of the country. It is estimated that over 90 percent of the new construction in this region will have central air conditioning. Energy conservation and passive cooling measures are expected to reduce significantly the sensible cooling and heating loads. However, the substantial latent (i.e., humidity) cooling loads in all buildings and internal heat gains in commercial buildings will remain and will require the use of mechanical cooling systems.

The annual energy used for cooling of buildings in the year 2000 was estimated by accounting for the expected mix of building types, regional differences in building stock and cooling loads, and residential and commercial building energy

requirements. An estimated annual energy displacement of 0.14 quad of conventional energy sources by solar in the year 2000 (for new residential, new multifamily, retrofit residential, and commercial market sectors) would result from a 20-percent penetration by solar cooling of the annual projected air conditioning market by the year 2000.

Certain cost and economic performance goals must be achieved by the solar industry before market demand will rise to a level that will produce the desired market penetration. Marketing studies[10] indicate that, for heating and air conditioning products, the relationship between market penetration and payback period is as shown in Figure 2. The payback period, the number of years for the undiscounted fuel cost savings to equal the incremental cost to produce those savings, is related to a real return on investment. Postulating market penetration goals per year necessary to achieve a 20-percent annual penetration by the year 2000, the corresponding payback and return on investment goals as a function of year of purchase have been calculated and are shown in Figure 3.

Annual system simulations of the thermal performance of active solar Rankine and absorption cooling/heating systems have been conducted using TRNSYS.[11,12] These calculations have been made for residential solar cooling/heating systems in four cities (Fort Worth, Phoenix, Miami, and Washington, D.C.) and for commercial solar cooling-only systems in three cities (Fort Worth, Phoenix, and Miami) which are representative of the cooling market. Three types of systems were evaluated: residential 3-ton absorption (ARKLA), commercial 25-ton absorption (ARKLA), and commercial 25-ton Rankine (AiResearch).

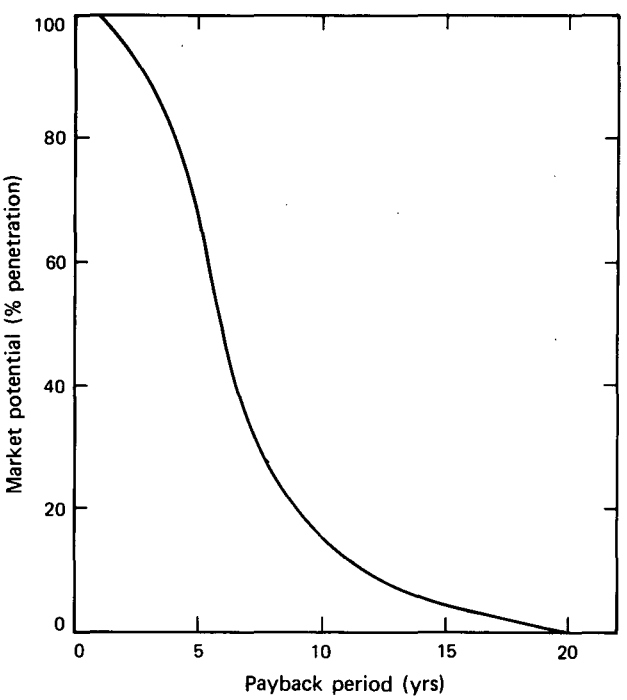

Figure 2. Market potential as a function of payback period. From Garry L. Lilian and Paul E. Johnston, "A Market Assessment for Active Solar Heating and Cooling Products," final report, OR/MS Dialogue, Inc., Cambridge, Mass., September 1980. (XBL 812-368)

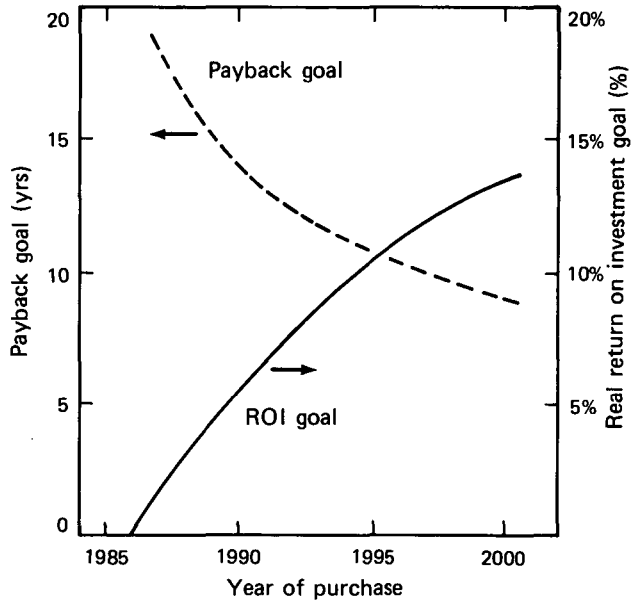

Figure 3. Payback goal and real return on investment (ROI) goal as a function of year of purchase to reach a 20% market penetration in the year 2000. (XBL 812-365)

It is assumed that a solar cooling or cooling/heating system is cost-effective when the incremental solar system cost is equal to or less than the present value of the energy savings. A standard economic analysis is used to calculate the present value of the fuel saved by an active solar system over the life of system (20 years), assuming a given internal real rate of return on the initial investment. The present value is based on the modified uniform present worth, which is a function of the fuel escalation rates and the expected real return on investment. Details of the analysis are presented elsewhere.[6,7,9]

Combining these calculations of the incremental solar-system cost as a function of real return on investment with the real return on investment goals as a function of year (as contained in Fig. 3), incremental system cost goals as a function of year have been generated for residential solar cooling systems and are displayed in Figure 4. Similar analysis has been performed for commercial cooling systems.

System and Subsystem Costs. The total solar-cooling-system cost goals for different locations can, in turn, be subdivided into subsystem cost and performance goals. It is anticipated that the major reductions in subsystem costs will be achieved by technical improvements in subsystem performance, such as increasing chiller efficiency to reduce the size of collector arrays, by volume production economies, and by development of packaged and standardized subsystems to reduce system engineering and installation costs. Preliminary system and subsystem cost estimates for a residential system are shown in Figure 5. These values are based on estimates of current subsystem costs

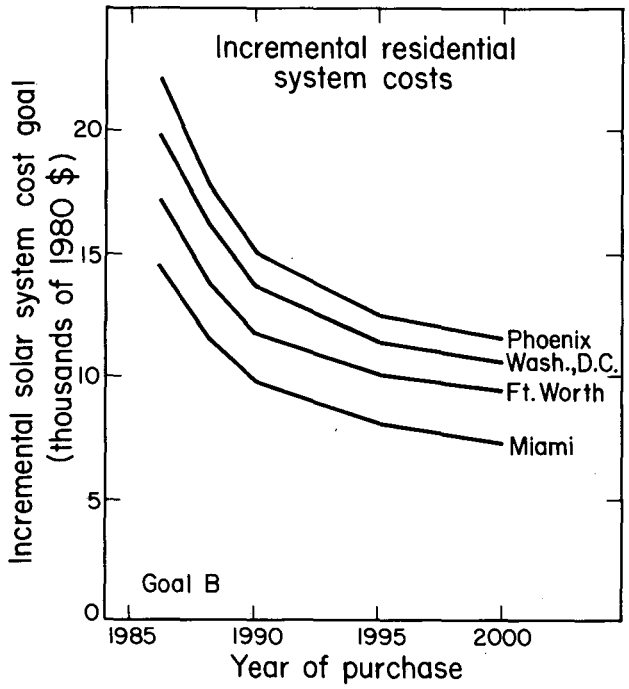

Figure 4. Residential incremental solar system cost goals for representative systems in four cities to achieve goal B, 20% penetration in the year 2000.

(XBL 816-1005)

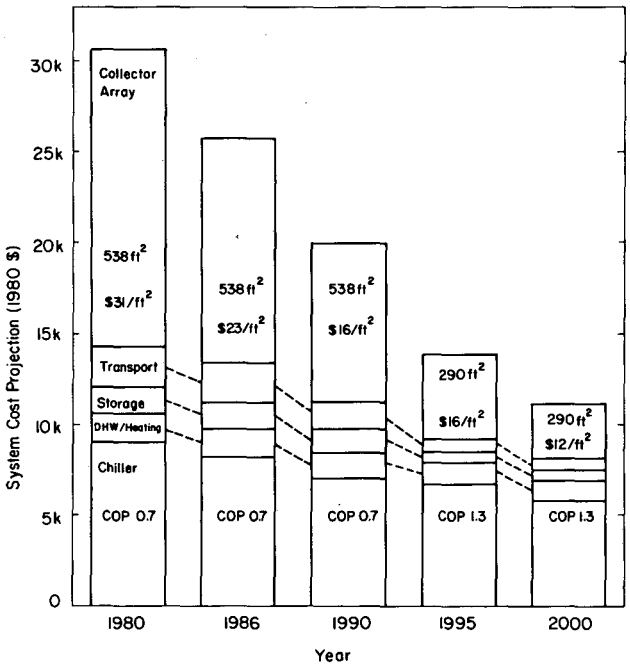

Figure 5. System cost projections for a 3-ton residential absorption cooling, heating, and hot water system showing subsystem costs.

(XBL 814-600)

plus realistic expectations for subsystem cost and performance improvements. Similar analyses have been made for commercial absorption and Rankine systems.

Technical improvements in subsystem performance are anticipated. For the residential 3-ton absorption chiller and for the commercial 25-ton absorption chiller, the current coefficient of performance of about 0.7 should stay relatively constant until the development and introduction of double-effect absorption chillers in these sizes, at which time the COP should increase to about 1.3. For the commercial 25-ton Rankine chiller, the current coefficient of performance of about 0.7 should increase gradually to about 1.5 if the operating temperature is increased to about 500°F.

The collector array is one of the major cost items of any active solar cooling system. The key to cost-effective cooling systems is reducing the collector array costs. For the high-temperature, high-COP future scenario, either evacuated tubes with reflectors or cylindrical trough collectors will likely be used. Collector manufacturing costs of $\$150/m^2$ ($\$14/ft^2$) have been projected[13] for evacuated tube concentrating collectors.

Current chiller technology, with a COP of 0.7 and the distinct advantage of operating at temperatures below 200°F, could be adequate if very low cost, good-performance collectors could be developed. As Figure 5 shows, "very low cost" can be seen to require collector costs of about $\$6/ft^2$. "Good performance" in this context means an efficiency of about 40 to 50 percent at a typical absorption chiller driving temperature of about 185°F. Work underway at Brookhaven National Laboratory[14] is directed toward the development of solar collectors that might possibly meet these types of cost and performance requirements.

Controls Test Facility and Analysis. During FY 1981, work was completed on analyzing and reporting the results of experiments run on the LBL controls test facility.[15-17] The modeling of the thermal behavior of a residential building, a fan coil heat-delivery system, and a bimetal thermostat to simulate the effects of heat input from an active solar space heating system on room air temperature dynamics has been completed.[18]

Technical Support Activities

Overall Solar Cooling Program Planning and Review. The following activities occurred during FY 1981:

- Prepared several revised versions of the Multiyear Program Plan for Rankine and absorption solar cooling systems.
- Prepared documents on the key accomplishments (and their significance) of the active solar cooling R&D program and the controls R&D program, and also on the risk/payoff aspects of the cooling program.
- Participated in major program planning and review meetings for the DOE Active Heating and Cooling Division, in Washington, D.C., and at the Belmont Conference Center.
- Made presentations and joined discussions on the solar absorption and Rankine cooling program at DOE/HQ. Had meetings with DOE/HQ program managers at HQ, at SAN, and at LBL.

- In connection with the Annual Active Solar Heating and Cooling Contractors' Meeting, LBL participated in the planning, reviewed the cooling contractors' papers for the proceedings, made the absorption and Rankine cooling overview presentation,[19] and chaired the cooling session. Similarly, LBL participated in the planning and gave an overview presentation for the May 1981 Solar Cooling Workshop and participated in some of the follow-up debriefings.

Technical Monitoring. The following are some of the major FY 1981 activities by LBL in providing technical monitoring and evaluation of solar cooling projects by outside (non-LBL) contractors:

- Conducted 18 site visits and project reviews covering 11 different DOE contractors; reviewed 25 final reports and phase reports, and 3 follow-on proposals; and assisted DOE/SAN in specifying Statements of Work for several of these contractors.

- Interacted with many of the solar cooling contractors at 13 SAN and LBL meetings with individual contractors. In addition, numerous technical discussions with contractors took place by phone and by mail.

- Prepared and sent to DOE/SAN monthly summary reports on all the DOE solar absorption and Rankine cooling projects.

- Assumed responsibility for technical monitoring of systems analysis projects related to active solar cooling.

Proposals for New Work. During FY 1981, LBL conducted the review of three unsolicited proposals and sent results to DOE/SAN with recommendations for action. LBL also reviewed proposals submitted in response to a solar cooling RFP issued by the American Samoa Energy Office.

Coordination Activities. During FY 1981, LBL staff members in the course of coordinating activities related to the solar absorption and Rankine cooling program:

- Had frequent interactions with the NASA/MSFC (Manned Space Flight Center, Huntsville, Alabama) group responsible for management of the Honeywell solar Rankine cooling project and the Operational Test Sites (OTS), including several meetings at SAN and six joint field visits to OTS by LBL and MSFC staff.

- Held a number of meetings to insure coordination of the DOE solar cooling R&D program and the SOLERAS joint U.S.-Saudi Arabian solar cooling program, which consists of four solar cooling field experiments at sites in Phoenix. The SOLERAS contractors are all also participants in the DOE cooling R&D program.

- Participated as a member of the Heat Pump Integration Task Force, chaired by John Ryan of DOE/HQ, including presentation of an overview paper on the solar cooling program at the initial meeting in June 1981 at McLean, Virginia, and participation in follow-up working group meetings at Chicago in August and at DOE/HQ in September 1981.

- Had cooperative interactions with Gas Research Institute (GRI) staff members involved with gas/solar projects.

- Participated in negotiations to establish a joint U.S.-Greek project in solar heating and cooling, held in Athens during October 1980.

- Had several discussions with members of the DOE/HQ and the SERI International Programs Offices concerning the on-again, off-again joint U.S.-Mexican project on solar refrigeration.

- Participated in reviews of the DOE solar desiccant cooling program at SAN in June and August and in Chicago in September 1981.

- Joined in meetings at SAN and LBL and other locations with staff members of ORNL and other DOE laboratories involved in activities closely related to solar cooling.

- Participated in several meetings per month at SAN to coordinate LBL's technical support with SAN's program management responsibilities for the solar cooling program.

PLANNED ACTIVITIES FOR FY 1982

Absorption Chiller R&D

The major absorption chiller R&D activity in FY 1982 will be debugging and testing the 2R chiller. Because this is the first chiller of its kind ever built, significant operational difficulties may be encountered and would have to be overcome before meaningful performance data can be obtained.

The level of effort spent on the cycle analysis and design of the 1R chiller depends on the progress of the 2R chiller testing. Ideally, work on a first practical design of the 1R chiller should be underway by the end of FY 1982.

Measurements by SRI International of properties of candidate new-fluid pairs for the 1R chiller should be completed during FY 1982.

A complete report on the testing, performance, and evaluation of the single-effect chiller will be published in FY 1982.

Performance and Economic Analysis

Activities during FY 1982 will be directed toward research into intelligent methods of controlling active solar cooling and heating systems and the documentation of the performance of different types of active cooling/heating systems and

the resulting cost/performance goals. Efforts are currently underway to obtain more realistic systems-analysis models of the thermal performance of the cooling systems and better estimates of cost and performance projections. We will continue to work during FY 1982 with other systems analysis contractors to develop realistic models of active solar cooling systems and to develop in-house capabilities for systems simulation and economic analysis for active solar cooling.[20] We will also continue to coordinate the systems-analysis activities of other organizations to determine the research requirements by which a broad spectrum of solar space conditioning systems might attain their respective cost performance goals.

Technical Support Activities

It is anticipated that the technical support activities in FY 1982 will be similar to those carried out in FY 1981. The planning activities will shift from emphasis on solar cooling system integration to a more generic long-term R&D program, consistent with new Administration guidelines. Documentation of cooling program accomplishments and research needs will be prepared because much of the existing cooling program is expected to be phased out.

Site visits to solar cooling contractors and review of progress and phase reports will continue as long as the cooling contracts are active. Unsolicited proposal reviews will continue to be conducted as received.

Finally, the critical coordination activities with other organizations involved in similar programs will continue to be pursued diligently.

REFERENCES

1. Dao, K., Simmons, M., Wolgast, R., and Wahlig, M. (1977), Performance of an Experimental Solar-Driven Absorption Air Conditioner, Lawrence Berkeley Laboratory Report LBL-5911.

2. Dao, K., Wolgast, R., and Wahlig, M. (1979), Development of Solar-Driven Absorption Air Conditioners and Heat Pumps, Lawrence Berkeley Laboratory Report LBL-9630, p. 15.

3. Dao, K. (1978), Conceptual Design of an Advanced Absorption Cycle: The Double-Effect Regenerative Absorption Refrigeration Cycle, Lawrence Berkeley Laboratory Report LBL-8405.

4. Dao, K., Wahlig, M., and Wali, E. (1980), Development of Solar Driven Absorption Air-Conditioners, Lawrence Berkeley Laboratory Report LBL-11175, p. 3-27.

5. Dao, K. (1978), A New Absorption Cycle: The Single-Effect Regenerative Absorption Refrigeration Cycle, Lawrence Berkeley Laboratory Report LBL-6879.

6. Warren, Mashuri L. and Wahlig, Michael (1981), Methodology to Determine Cost and Performance Goals for Active Solar Cooling Systems, Paper 81-WA/Sol-32, Presented at the ASME Winter Meeting, 15-20 November 1981, Washington, D.C., Lawrence Berkeley Laboratory Report LBL-12343.

7. Warren, Mashuri L. and Wahlig, Michael (1981), Cost and Performance Goals for Commercial Active Solar Absorption Cooling Systems, Submitted to the ASME Solar Energy Division, Fourth Annual Technical Conference, Albuquerque, NM, 26-30 April 1982, Lawrence Berkeley Laboratory Report LBL-13050.

8. Warren, Mashuri L. and Wahlig, Michael (1981), Systems Simulation and Economic Analysis for Active Solar Cooling, in Proceedings of the Annual DOE Active Solar Contractors' Review Meeting, CONF-810912, 9-11 September 1981, Lawrence Berkeley Laboratory Report LBL-12752.

9. Warren, Mashuri L. and Wahlig, Michael (1981), Cost and Performance Goal Methodology for Active Solar Cooling Systems, Lawrence Berkeley Laboratory Report LBL-12753.

10. Lilian, Gary L. and Johnston, Paul E. (1980), A Market Assessment for Active Solar Heating and Cooling Products, Category B: A Survey of Decision Makers in the HVAC Market Place, OR/MS Dialogue, Inc., Final Report DOE/CS/30209-T2.

11. Versteegen, P.L., and Morehouse, J.H. (1979), A Thermal and Economic Comparative Analysis of Absorption and Rankine Solar Cooling Systems for Commercial Buildings, Draft Final Report.

12. Hughes, P.J., et al. (1981), Evaluation of Thermal Storage Concepts for Solar Cooling Applications, Science Applications, Inc., Final Report.

13. Chamberlain Manufacturing Corporation (1980), 3x Compound Parabolic Concentrating (CPC) Solar Energy Collector, Final Technical Report DOE/CS/04239-T1.

14. Andrews, John W., and Wilhelm, William G. (1980), Thin-Film Flat-Plate Solar Collectors for Low-Cost Manufacture and Installation, Report BNL-51124.

15. Warren, Mashuri L., Schiller, Steven, and Wahlig, Michael (1981), Controls for Solar Heating and Cooling, in Proceedings of Annual DOE Active Solar Contractors' Review Meeting, CONF-810912, 9-11 September 1981, Lawrence Berkeley Laboratory Report LBL-12751.

16. Schiller, Steven R., Warren, Mashuri L., and Wahlig, Michael (1980), Dynamic Modeling and Experimental Simulation of Active Solar Energy Systems, Presented at the ASME Winter Annual Meeting, 16-21 November 1980, Chicago IL, Paper ASME-80-WA/Sol-14, Lawrence Berkeley Laboratory Report LBL-10825.

17. Schiller, Steven R., Warren, Mashuri L., and Auslander, David (1980), "Comparison of Proportional and On/Off Solar Collector Loop Control Strategies Using a Dynamic Collector Model," Journal of Solar Energy Engineering 102, 4, pp.256-262.

18. Vilmer, Christian, Warren, Mashuri L., and Auslander, David (1980), Interaction of a Solar Space Heating System with the Thermal Behavior of a Building, Presented at the ASME Solar Energy Division, Third Annual Technical Conference, Reno, NV, 27 April - 1 May 1981, Lawrence Berkeley Laboratory Report LBL-11673.

19. Wahlig, Michael, Heitz, A., Angerman, H., Glas, R., and Warren, M. (1981), Overview of Active Solar Absorption/Rankine Cooling Program, Presented at the Annual DOE Active Solar Contractors' Review Meeting, 9-11 September, 1981, Lawrence Berkeley Laboratory Report LBL-13054 Revised.

20. Warren, Mashuri L. (1981), Overview of Systems Analysis, Market Assessment, and Controls Work, Presented at the Annual DOE Active Solar Contractors' Review Meeting, 9-11 September 1981, Lawrence Berkeley Laboratory Report LBL-13052.

Appropriate Energy Technology*

F. B. Lucarelli, J. D. Kessel, H. R. Clark, J. M. Kay, and J. Linse

In 1977, the Energy Research and Development Administration (ERDA), since incorporated into the Department of Energy (DOE), established an appropriate technology small grants program. The purpose of the program is to fund projects that design, manufacture, and/or demonstrate small-scale energy technologies which conserve depletable fossil fuels or use renewable energy resources. DOE makes the grants available annually on a competitive basis to small businesses, individuals, nonprofit organizations, public agencies, and Indian tribes. The maximum grant award is $50,000.

The grants cover a complete spectrum of small-scale energy technologies, including solar active and passive systems, wind machines, biomass conversion systems, energy conservation devices, recycling methods, aquaculture systems, hydroelectric devices, and geothermal heating systems.

ACCOMPLISHMENTS DURING FY 1981

Energy Impact Analysis

Because of the diverse array of technologies and end-use applications of DOE-funded appropriate technology projects, DOE has been unable to assess the program's energy savings potential, an assessment that is necessary to compare the program with other DOE programs. To obtain this information, DOE asked LBL to assess the program's energy savings potential and cost-effectiveness.

We began our analysis in 1979, assessing the energy savings potential of 20 projects from Region IX.[1] We completed the analysis in 1979 and found that most of these projects could save a significant amount of energy either directly, from the original project, or indirectly, from demonstration and commercialization effects. However, the sample was small and specific only to Region IX; therefore, we could not extrapolate our findings to estimate the energy savings potential of the national grants program.

In 1981, we evaluated a sample of 57 projects funded in FY 1979.[2] The 57 projects were selected from eight of the ten Federal regions and cover the full range of technology categories funded: wind, biomass, solar, geothermal, hydro, and conservation.

The analysis was conducted in 4 steps:

1. Evaluation of project energy savings,
2. Assessment of economic feasibility,
3. Estimation of replication potential, and
4. Extrapolation of sample energy savings to estimate program energy savings.

The results of the study include the development of procedures for evaluating energy savings from appropriate technology projects, the calculation for the sample projects of energy savings, and an estimate of program energy savings.

Technology Assessment Study

We also assessed the technical and economic feasibility of small wind-energy systems in the U.S.[3] The projects apply wind systems in the agricultural, residential, and industrial sectors for pumping water, generating electricity, and heating water. Electric projects range in size from 1 to 35 kW. For this study, we assessed each project for technical performance, economic feasibility, and physical infrastructure requirements. The report discusses near-term applications of small wind systems and the physical infrastructure requirements that can make feasible a larger array of small wind-energy applications.

Development of Methods for Evaluating Small Energy Systems

Methods have been developed to evaluate the

*This work was supported by the Assistant Secretary for Conservation and Renewable Energy, Office of State and Local Programs, Small Scale Technology Branch of the U.S. Department of Energy under Contract No. DE-AC03-76SF00098.

energy impacts and cost-effectiveness of small energy systems in the following categories: wind-electric, hydroelectric, geothermal-direct utilization, active and passive solar systems, anaerobic digestion, and conservation-weatherization. A report is being issued discussing these methods of project analysis.[4]

PLANNED ACTIVITIES FOR FY 1982

The Appropriate Energy Technology Program is being phased out by DOE, and LBL will have no further involvement.

REFERENCES

1. Lucarelli, F.B., et al. (1979), The Energy Savings Potential of the Region IX Appropriate Energy Technology Grants Program: An Assessment of Twenty Projects, Lawrence Berkeley Laboratory Report LBL-9715.

2. Lucarelli, F.B., et al. (1981), The DOE Small Grants Program and Its Energy Savings Potential, Lawrence Berkeley Laboratory Report LBL-12253.

3. Kay, J. (1981), A Technical and Economic Assessment of 13 Small Wind Energy Projects, Masters thesis (in progress), University of California, Berkeley, Lawrence Berkeley Laboratory Report, LBL-13676.

4. Lucarelli, F.B. (1981), Assessing the Energy Output and Cost Effectiveness of Renewable Energy Resource Systems, Lawrence Berkeley Laboratory Report LBID-416.

Energy Conversion by the Retinal Protein, Bacteriorhodopsin*

L. Packer, A. T. Quintanilha, R. J. Mehlhorn, I. Fry, J. Herz, E. Lam, and S. Tristam-Nagle

Biological energy-conversion schemes hold considerable promise for harnessing solar energy. Our research is concerned with one of the simplest biological solar-energy converters known: bacteriorhodopsin (bR). This pigmented protein is found in the cell membranes of certain salt-requiring bacteria including Halobacterium halobium. Our research program is attempting to determine the molecular details of how this protein utilizes light from the sun to produce an electrical current across the bacterial membranes. We anticipate that such understanding will ultimately lead to the production of novel photoelectric cells and solar batteries.

Bacteriorhodopsin is the only protein in the purple membrane of Halobacterium halobium. The retinal chromophore is covalently attached to a lysine amino acid side chain of the protein by a protonated Schiff base linkage. In the presence of light, bR functions as a proton (H^+) pump and generates both pH gradients and electrical potentials across the membrane. Following a flash of light, the chromophore undergoes a photocycle in which several intermediates are identified by distinct absorption bands. For the M_{412} intermediate, resonance Raman studies show that the Schiff base is not protonated. This suggests that the chromophore is directly involved in the proton pumping process.

Information on whether other protonatable amino acid residues of the protein participate in the mechanism of H^+ uptake, translocation, and release is very important in correlating the photoreaction cycle with molecular models of photochemical conversion.

The photocycle in bR is initiated after absorption of visible radiation (λ_{max} = 570 nm) by the retinal chromophore in an all-trans configuration. The initial steps of the photocycle involve the isomerization of the chromophore to 13-cis retinal. The deprotonated Schiff base forms with a half-life ($t_{1/2}$) of about 50 μsec. Proton release from the extracellular surface of the protein occurs in this time range. Later, the deprotonated species decays with a $t_{1/2}$ of 3-5 msec, restoring the original all-trans form of the chromophore. During this time, protons are taken up from the cytoplasmic surface of the protein (for a review, see Reference 1). To assess significant structural features of the protein important for the photocycle, we have used chemical modification of amino acid side chains, low temperature, and detergent effects on purple membranes. Reconstituted bR containing synthetic membranes have also been used to derive information on proton pumping activity.

ACCOMPLISHMENTS DURING FY 1981

Chemical Modification Studies

Last year, we reported[2,3] our results with modification of carboxyl and guanidinium groups, suggesting that a charge-transfer complex essential for reprotonation of the Schiff base may exist between these two types of groups. The interaction

*This work was supported by the Office of Energy Research, Office of Basic Energy Science, Division of Biological Energy Research of the U.S. Department of Energy under Contract No. DE-AC03-76SF00098.

between carboxyl groups and at least one amino group of lysine also appeared to be important for H^+ movement. Tyrosines were also found to be involved as H^+ donors for Schiff base reprotonation and for the release of H^+ at the extracellular surface of the purple membrane.

During FY 1981, we have continued and extended studies on modification of tyrosines, lysines, and arginines (Figure 1). The results can be summarized as follows:

a. Tryosine: Tetranitromethane modification of bR shifted the absorption maximum to 530 nm; the reaction was found to be light-dependent at pH 6.0 and to probably involve only one residue.[4] The decay of the M_{412} intermediate was unaffected by nitration, whereas the $t_{1/2}$ of the rise kinetics was accelerated by more than 50 percent. Chymotrypsin digestion showed that most of the 3-nitrotyrosine eluted with the larger of the two protein fragments containing residues 72-248. Circular dichroism (CD) studies showed that the nitrated purple membranes had lost the negative band at 575 nm, characteristic of exciton coupling in native purple membranes. Extensive cross-linking of bR with glutaraldehyde prior to nitration did not prevent the blue-shift of the absorption maximum to 530 nm nor the loss of exciton coupling in the CD spectrum. These studies demonstrate that modification of a tyrosine other than tyrosine 26 (see Reference 5) also leads to a blue shift in the spectral properties of the Schiff-base-linked retinal and that this effect is not due to a disruption of the lattice structure of bR. Tyrosine 185 appears at present to be the most likely candidate. This residue may be sterically restrained because of its location next to proline 186, which may explain the large increase in the amount of 13-cis retinal induced by 3-nitrotyrosine formation of a residue in the large chymotrypsin-cleaved fragment.

b. Lysine: At pH 8.8, with a molar ratio of (the modifier) fluorescamine to bR of 170, about 6 residues of lysine were modified, whereas arginines were not affected at all. Except for the appearance of the fluorescamine peak at 394 nm and some broadening of the chromophore peak at 570 nm, the absorption spectrum of bR was not significantly changed after modification.[6] CD studies indicated a loss of exciton coupling between bR molecules, and rotational diffusion studies suggested a slight increase in the mobility of the chromophore after modification. However, the spectral changes accompanying the light-to-dark adaptation (λ_{max} changes from 570 nm to 560 nm) of purple membranes were not

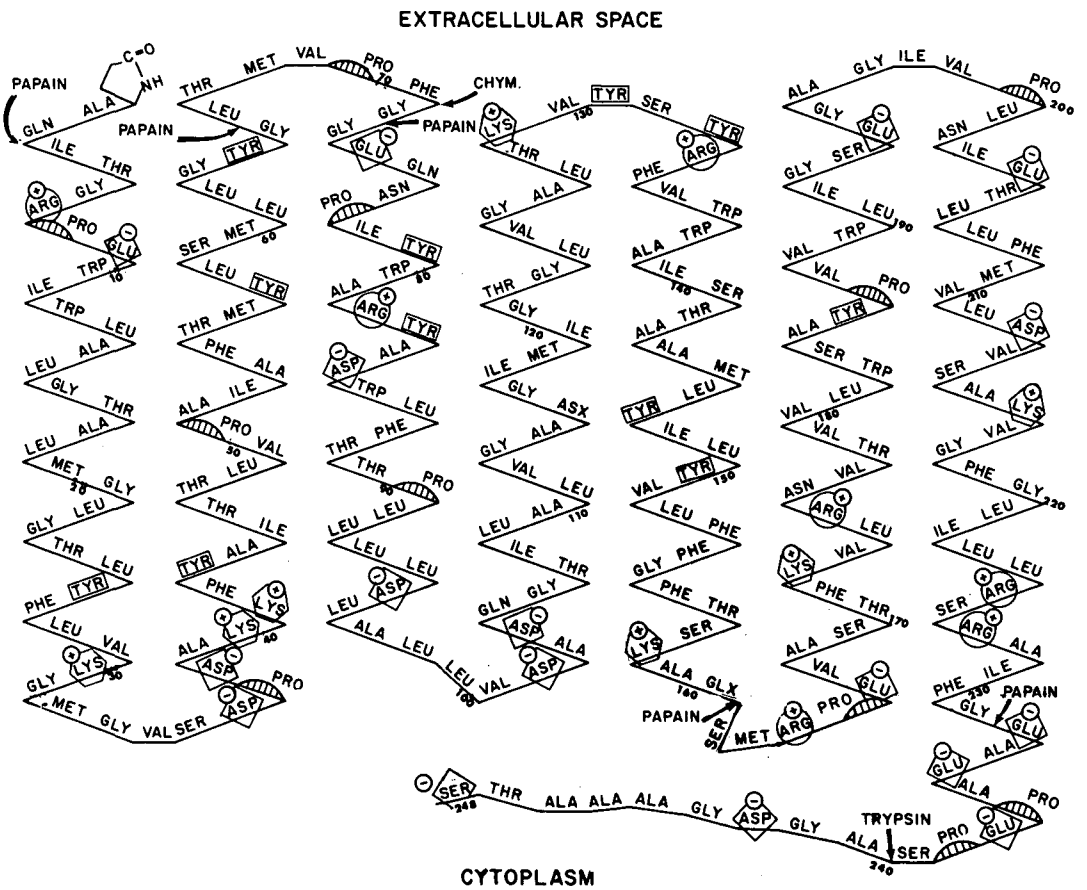

Figure 1. Schematic representation of how the amino acids of bacteriorhodopsin traverse the membrane. Specific amino acids which have been chemically modified are highlighted. The diagram also shows positions where the protein can be cleaned with papain, trpsin or chymotrypsin.

prevented by fluorescamine treatment. Our findings clearly demonstrate that, unlike what has been previously suggested,[7] exciton coupling between neighboring bR molecules in the purple membrane is not required for light-to-dark adaptation.

c. Arginine: At pH 8.2, 2,3-butanedione reacted slowly with all the arginine residues found in bR except two; there was no shift of the 570-nm chromophore λ_{max}. Scatchard and Hill plots of 2,3-butanedione treatment of bR indicated that only 7 arginines were available for modification.[8] A quantitative analysis of the inhibition of photocycling activity revealed that a specific pair of arginines must be modified to cause a marked slowdown (maximal 33-fold) of M_{412} decay and a small (1.7 x) inhibition of the M_{412} rise kinetics. The pH dependence of M_{412} decay and of the H^+ uptake kinetics suggested a direct involvement of arginines in the reprotonation of the Schiff base. We showed that the 2,3-butanedione modification, known to raise the pK of arginine, also leads to a raised pK for M_{412} decay: this is exactly what one would expect if arginine donated its proton to the Schiff base. Alternatively, as found in other enzymes,[9] the role of two specific arginines may be to regulate structural changes during cycling due to their electrostatic binding to negatively charged groups.

Low Temperature Studies

To elucidate the role of tyrosine residues in the blue-shift of λ_{max} and the light-driven proton pumping of bR, the photochemical reactions of tyrosine-iodinated bR (tyr-I-bR) were investigated by low temperature spectroscopy.[10] When bR containing all-trans retinal absorbs light, it goes through several intermediates: bath-, lumi- and meta-trans bR.[11]

After from 4 to 5 of the 11 tyrosine residues of bR were iodinated, the meta-intermediate of the photocycle of tyr-I-bR in 75 percent glycerol solution became so stable that its decay could be observed by a conventional spectrophotometer, even at room temperature. In the dark and at -65°C, it was stable for several hours.

Four different kinds of batho-intermediates were formed by irradiation with green light (500 nm) at -170°C. As in native bR, these batho-intermediates were also formed by irradiation at -60°C. Using the difference spectra between meta-intermediates and tyr-I-bR, the absorption spectra of four kinds of tyr-I-bRs, batho-intermediates, and meta-intermediates were estimated. The absorption maximum of each was at shorter wavelengths than that of its corresponding type in the native bR system.

These results indicate that at least two or more tyrosine residues have some role in the blue shift in λ_{max} for tyr-I-bR and, therefore, that tyrosine residues may be important in determining the color of native bR.

Effects of Non-Ionic Detergents

Treatment of purple membranes with the non-ionic detergents, Triton X-100 and β-octylglucoside, caused a blue shift of the chromophore absorption peak of bR. This effect was maximal at detergent concentrations where the exciton band in the CD spectrum of the chromophore was abolished or drastically reduced. The detergent-induced blue shift was also observed in glutaraldehyde-treated purple membranes, but the detergent effects on the CD spectrum were prevented by the cross-linking treatment.[12]

β-octylglucoside caused a 2- to 3-fold increase in the tryptophan fluorescence of either native or cross-linked purple membranes. Treatment of native or cross-linked purple membranes with either detergent also caused the chromophore to be susceptible to bleaching.

Photocycle kinetics of detergent-solubilized purple membranes showed that the blue-shifted form of the chromophore after solubilization was still converted to a 412-nm absorbing species after a laser flash. With native or cross-linked purple membranes, detergents caused both an acceleration in the rise and a slowing of the decay of the 412-nm intermediate. Both processes became biphasic after detergent treatment at pH 7.0. As the pH is increased from 5.5 to 9.5, the percentage of the slow phase in the decay increased linearly while the $t_{1/2}$ of decay increases logarithmically. With native purple membranes, both rise and decay of the 412-nm intermediate become biphasic as the pH increased beyond 8.5.

Our results suggest that non-ionic detergents

a. Affect retinal-apoprotein interactions, and

b. Cause changes in the protein structure that result in the alteration of pK(s) of amino acid residues which participate in photocycling.

White Membrane Studies

The discovery by Professor Y. Mukohata[13] of Osaka, Japan, of a mutant species of Halobacteria which forms a "white membrane" has enabled us to venture into an exciting and new field of bR studies. The white membrane forms a patch which apparently contains the apoprotein portion of bR but totally lacks retinal; a purple membrane can be formed by the addition of all-trans retinal. In collaboration with Professor Mukohata, we have isolated and purified "white membranes" and have initiated a series of studies on the reconstitution with several retinal analogues. Chemical modification prior to reconstitution is currently being used to identify steric and ionic constraints in the mechanisms of both reconstitution and photocycling.

Discussion

At this stage of the investigation, it seems clear that some tyrosine residues in bR not only may be involved as proton donors and acceptors to

the retinal Schiff base,[2] but also may be responsible for the red shift in the λ_{max} for absorption of retinal, when bound to bacteriorhodopsin. It appears likely that the structural location of tyrosine 26, and possibly 185, in the bR molecule may allow specific interactions with the retinal chromophore that leads to a λ_{max} = 570 nm. Our low-temperature studies confirm the idea that some of the tyrosines in bR are important in determining λ_{max} for this retinoprotein. The fact that iodination of 4 to 5 of the 11 tyrosines produces spectral evidence for four different kinds of batho- and meta-intermediates in the photocycle suggests that a few tyrosines may play a role in the blue shift of λ_{max} in the modified bR.

Whereas exciton coupling was lost after nitration of tyrosine 185 and λ_{max} was shifted to 530 nm, after fluorescamine modification of six lysines in the protein, exciton coupling was also lost, but no change was observed in λ_{max}. Since, in the latter case, the light-to-dark adaptation of bR was unaffected, we conclude that exciton coupling is not a requirement for the mechanism of light or dark adaptation of bR.

Furthermore, a specific pair of arginines may be directly involved in the reprotonation of the Schiff base or in the regulation of structural changes in bR during proton translocation.

Detergents have provided us with a mechanism for affecting retinal-apoprotein interactions without chemically modifying the protein. As in the case of certain modifications, these interactions have resulted in pK shifts of amino acid residues which seem to participate in photocycling.

The foregoing studies have clearly demonstrated the critical role that bacteriopsin and, in particular, certain specific amino acids play in both the spectral and CD characteristics as well as in the complex kinetics of photocycle intermediates and H^+ pumping activity of bR.

PLANNED ACTIVITIES FOR FY 1982

Chemical Modification Studies

White membranes are the material par excellence for chemical modification investigations of the role of the protein structure and different types of retinal analogues in the energy conversion process. We intend to pursue in depth the modification of tyrosine since it appears to be the most probable donor and/or acceptor of protons. Our recent discovery of the nitration of a single tyrosine[4] requires further study; the residue needs to be carefully identified and its effect on the photocycle and electrochemical activities thoroughly investigated.

Site-specific modifications of carboxyl and amino groups will be used to label the protein with nitroxide spin-probes. Since these probes provide us with information on the viscosity and polarity of their micro environment, they will be used to study conformation changes in bR during photocycling, H^+ pumping, and light-to-dark adaption. The steric effects of modification of other groups in the protein will also be investigated by measuring the changes in the local environment of the spin probe(s).

Electrical versus Electroneutral Steps in the Photocycle of Bacteriorhodopsin

The findings that transmembrane and surface electrical potential changes are associated with the photocycle in bR[14,15] raises several fundamental questions: (i) Which steps of the photocycle are related to charge movements in the protein? (ii) Where do these charge displacements occur? (iii) How do they affect the kinetics of the cycle?

To answer these questions, we will make use of several strategies:

a. Chemically modified bR will be used to identify those protein residues which are involved in charge displacements.

b. White membranes and different retinal analogues will be used to study the retinal-apoprotein interactions essential for H^+ pumping and charge displacements.

c. Absorption, resonance-Raman, and low-temperature spectral studies will be used to clarify the effects of the charge displacements on the vibrational modes of the retinal. On a molecular level, this will help to clarify where in the chromophore the electrical fields exert their strong effects.

White Membrane Vesicles Regenerated with All-trans Retinal

These vesicles exhibit full pH gradients when only 10 percent of the bR has been reconstituted, but maximum electrical gradients ($\Delta\psi$) are not observed until 100 percent reconstitution has been achieved. Enzymatic iodination of extracellular tyrosine residues caused an abolition of light-dependent $\Delta\psi$, with a significant increase in the magnitude of the pH gradient. These are very interesting findings which warrant further study.

The effects of other chemical modification protocols will be studied. Among these are treatments of vesicles with permeable and/or side-specific carboxyl, arginine, and lysine specific reagents. We wish to learn about specific structural features of bR that are required for chromophore regeneration and for the generation of Δph and/or $\Delta\psi$. Because of the low time resolution of our measurements (Δs for photocycle and ms for Δph and ($\Delta\psi$), the possible occurrence of rapid but transient signals cannot be tested. We are therefore seeking to develop more permeable ionic spin probes.

REFERENCES

1. Henderson, R. (1977), "The Purple Membrane from Halobacterium halobium," Annual Reviews of Biophysics and Bioengineering 6, pp. 87-109.

2. Packer, L., Quintanilha, A.T., Carmeli, C.,

Sullivan, P.D. Scherrer, P., Tristram, S., Herz, J., Pfeifhofer, A. and Mehlhorn, R.J., (1981), "Molecular Aspects of Light-Induced Uptake and Release of Protons by Purple Membranes," Photochemistry and Photobiology 33, pp. 579-585.

3. Herz, J.M. and Packer, L. (1982), "Structural Involvement of Carboxyl Residues in the Photocycle of Bacteriorhodopsin," Federation of European Biochemical Societies Letters, in press.

4. Katsura, T., Lam, E., Packer, L. and Seltzer, S., "Specific Modification of a Tyrosine Involved in the Interaction Between Bacteriorhodopsin and Retinal," to be submitted for publication.

5. Lemke, H.D. and Oesterheld, D. (1981), "The Role of Tyrosine Residues in the Function of Bacteriorhodopsin. Specific Nitration of Tyrosine 26," European Journal of Biochemistry 115, pp. 595-604.

6. Lam, E. and Packer, L. (1981), "Effect of Fluorescamine Modification of Purple Membranes on Exciton Coupling and Light-to-Dark Adaptation," Biochemical and Biophysical Research Communications 101, pp. 464-471.

7. Casadio, R. and Stoeckenius, W. (1980), "Effect of Protein-Protein Interaction on Light Adaptation of Bacteriorhodopsin," Biochemistry 19, pp. 3374-3381.

8. Tristram-Nagle, S. and Packer, L. (1982), "Effects of Arginine Modification on the Photocycle and Proton Pumping of Bacteriorhodopsin," Biochemistry International, in press.

9. Riordan, J., McElvany, K., and Borders, C. (1977), "Arginyl Residues: Anion Recognition Sites in Enzymes" Science 195, pp. 884-885.

10. Iwasa, T., Takeda, K., Tokunaga, F., Scherrer, P.S. and Packer, L., "The Photoreaction of Tyrosine-Iodinated Bacteriorhodopsin at Low Temperatures," to be submitted for publication.

11. Iwasa, T., Tokunaga, F., and Yoshizawa, T. (1980), "Photointermediates in Bacteriorhodopsin Studied at Low Temperatures," Biophysics of Structure and Mechanism 6, pp. 253-270.

12. Lam, E. and Packer, L. (1982), "Effects of Non-Ionic Detergents on Purple Membranes and the Photocycle of Bacteriorhodopsin," Biochemical and Biophysical Research Communications (in press).

13. Mukohata, Y., Sugiyama, Y., Kaji, Y., Usukura, J. and Yamada, E., "The White Membrane of Crystalline Bacteriorhodopsin in Halobacterium halobium Strain R1mW and its Conversion into Purple Membrane by Exogenous Retinal," Photochemistry and Photobiology 33, pp. 593-600.

14. Carmeli, C., Quintanilha, A., and Packer, L. (1980), "Surface Charge Changes in Purple Membranes and the Photoreaction Cycle of Bacteriorhodopsin," in Proceedings of the National Academy of Sciences (USA), Vol. 77, pp. 4707-4711.

15. Quintanilha, A. (1980), "Control of the Photocycle in Bacteriorhodopsin by Electrochemical Gradients," Federation of European Biochemical Societies Letter 117, pp. 8-12.

Measurement and Analysis of Circumsolar Radiation*

D. F. Grether, D. B. Evans, A. J. Hunt, S. G. Kanzler, M. Harms, and M. A. Wahlig

This project provides measurements and analyses of the solar and circumsolar radiation for application to solar energy systems that employ lenses or mirrors to concentrate the incident sunlight. Circumsolar radiation results from the scattering of direct sunlight through small angles by atmospheric aerosols (dust, water droplets, or ice crystals in thin clouds, etc.). The solar energy system will typically collect all of the direct solar radiation (originating only from the disk of the sun) plus some fraction of the circumsolar radiation. The exact fraction depends upon many factors but primarily upon the angular size (field-of-view) of the receiver. A knowledge of the circumsolar radiation is therefore a factor in predicting or evaluating the performance of concentrating systems.

The project employs unique instrument systems, called "Circumsolar Telescopes," that were designed and fabricated at LBL. Each system has a "scanning telescope" mounted on a precision solar tracker. The telescope is mechanically scanned through an arc of 6°, with the sun at the center of the arc. A digitization of the brightness of the sun or circumsolar radiation is taken every 1.5' of arc, with a complete scan taking one minute of time. One of the auxiliary instruments is a pyrheliometer, having a fixed field of view (typically 5 to 6°) and used to provide an estimate, called the "normal incidence" reading, of the direct solar radiation. The telescope and pyrheliometer have matched, ten-

*This work was supported by the Assistant Secretary for Conservation and Renewable Energy, Office of Solar Electric Technologies, Photovoltaic Energy Systems Division of the U.S. Department of Energy under Contract No. DE-AC03-76SF00098.

position filter wheels: one open or "clear-filter" position, eight interference filters that divide the solar spectrum into eight intervals of roughly equal energy content, and one opaque filter to monitor detector noise. The data are recorded on magnetic tape, with one tape holding one week's data per telescope.

The telescopes have been operated primarily at locations for which the instruments can play a dual role: (1) characterization of a region or climate and (2) provision of site-specific data for proposed or actual concentrating solar energy systems. The data are used at LBL and other DOE-supported institutions, such as Sandia Laboratories and Jet Propulsion Laboratory (JPL) to evaluate the performance of concentrating systems.

A secondary purpose of the project is to relate the data to the atmospheric processes that attenuate the solar radiation available to terrestrial solar energy systems.

ACCOMPLISHMENTS DURING FY 1981

Measurement Program

Altogether, there are four circumsolar telescopes. An instrument at the JPL Parabolic Dish Test Facility at Edwards, California, was operated for the entire year. In addition to providing specific data for the test facility, this telescope also provided climate characterization data for the Mojave desert area. A second telescope, located at the Advanced Components Test Facility at Atlanta, Georgia, was supported through March. The operation of this instrument was terminated in April because of reductions in the project's budget; the telescope was returned to LBL in August. The third telescope was refurbished at LBL during the year, with plans for subsequent relocation of the instrument at Barstow, California, the site of the 10 MWe Central Receiver Pilot Plant that is currently under construction. Sandia National Laboratories, Albuquerque, continued to have the fourth instrument available for measurements in conjuction with tests at the Central Receiver Test Facility.

Systematics of Clear-Filter Data

Sufficient data are now available to investigate systematic behavior of the circumsolar radiation over a multi-year period. For present purposes, a given measurement of the telescope can be considered to consist of the circumsolar ratio, taken as a measure of the level of circumsolar radiation, and the NI reading (for Normal Incidence) of the pyrheliometer. The circumsolar ratio is defined as

$$R = C/(C + S),$$

where

C = circumsolar (from the edge of the sun out to 3°) radiation, and

S = direct solar (coming from the disk of the sun) radiation.

By the design of the telescope,

$$NI \approx C + S \quad .$$

Thus, the circumsolar ratio is approximately the same as the fractional overestimate that a pyrheliometer would make in estimating the direct solar radiation.[1] This overestimate is on the same order as, but somewhat greater than, the error made by a pyrheliometer in estimating the solar radiation available to a solar energy conversion facility that concentrates the incident solar radiation.

It had been observed previously[1] that there is a correlation between NI and R for any given month. Consider the middle of the day, defined as the period from three hours after sunrise to three hours before sunset. During this period the air mass (the amount of atmosphere between the earth and the sun), and thus the attentuation of the direct sunlight by the normal atmospheric constituents, is relatively constant. For very clear skies, NI will be about 1000 watts/m^2. As NI decreases due to increasing amounts of scattering and absorption by atmospheric aerosols or thin clouds, the circumsolar level increases in a systematic way. Any given value of NI is associated with a fairly narrow range of circumsolar ratios. The question addressed this year was whether or not the relationship changes with time and, if so, whether there is a seasonal effect.

The data for a given month were first separated into bins, each 200 watts/m^2 wide in NI. For each bin, the mean value of the circumsolar ratio was calculated. Shown in Figure 1 are the results for two of the NI bins: 700-900 w/m^2, which corresponds to moderately clear skies; and 300-500 w/m^2, which corresponds to hazy skies. In both graphs, the solid curve represents the average annual behavior; the same curve is displayed for each year. For the moderately clear sky case, a definite seasonal pattern is present, with winter peaks in the mean circumsolar ratio of 5 to 10 percent, and summer minima of about 2 to 3 percent. Any algorithm intended to predict the circumsolar ratio based on pyrheliometer readings must clearly take into account the seasonal dependence. On the other hand, the data for hazy skies show large fluctuations about an average circumsolar ratio of approximately 30 percent but no apparent seasonal dependence.

Colored Filter Data

Further progress was made this year in analyzing the colored filter pyrheliometer data for application to wave-length selective systems, such as concentrating photovoltaic devices. The first step in the analysis had been to characterize the transmission function (transmission vs. wave length and time) of each filter over an approximately three-year period of use. The filters are of the interference type (multi-layered dielectrics) and are subject to degradation. The functions were constructed from a combination of: (1) spectrophotometer measurements of the transmis-

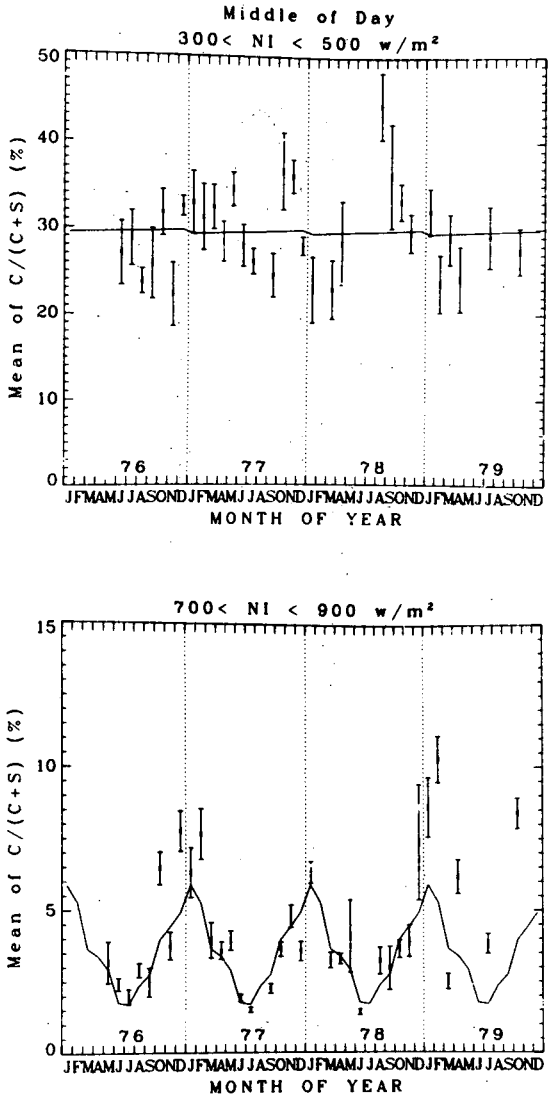

Figure 1. The mean monthly value of the circumsolar ratio, as defined in the text, plotted from May 1976 through December 1979 for Albuquerque. The data are limited by the criterion that the Normal Incidence (NI) value of the pyrheliometer be between certain values as indicated on the graphs. The solid curve represents the average annual behavior of the data points.

(XBL 814-9322)

sion of the filters made at the beginning and end of the measurement period, (2) evidence for the degradation of the filters as obtained from measurements for clear sky conditions, and (3) an atmospheric transmission computer model. Details are given elsewhere.[2,3]

Given a knowledge of the filter transmission functions, the second step was to invert the pyrheliometer readings to obtain the spectral distribution of energy in the sunlight. Because the transmission of any given filter has a complex dependence on wave length, the inversion cannot be carried out exactly, and an estimation method must be used. The method involves calculating an effective transmission over a nominal pass band for each filter.[2] The energy content of the solar spectrum within the nominal pass band is obtained (i.e., the inversion is carried out) by dividing the pyrheliometer reading by the effective transmission. Some monthly average results for two of the filter bands for the Mojave desert area (China Lake and then Barstow) are shown in Figure 2. A given data point is the ratio of the monthly total energy content for the indicated band to the monthly total for the clear ("no") filter case. Thus, the figure shows the relative amount of energy in a given part of the solar spectrum and its dependence on time. For the 0.38-0.46 μm band, there is an obvious seasonal dependence, with winter minima and summer maxima. This behavior is to be expected because, in winter, the atmospheric path is longer and relatively more of the short-wave radiation is absorbed by the atmosphere. For photovoltaic devices the plot for the 0.72-0.85 μm band is of more interest because the peak efficiency of typical (e.g., silicon) solar cells lies in this wavelength region. The data show little if any seasonal dependence (note that the graph has a

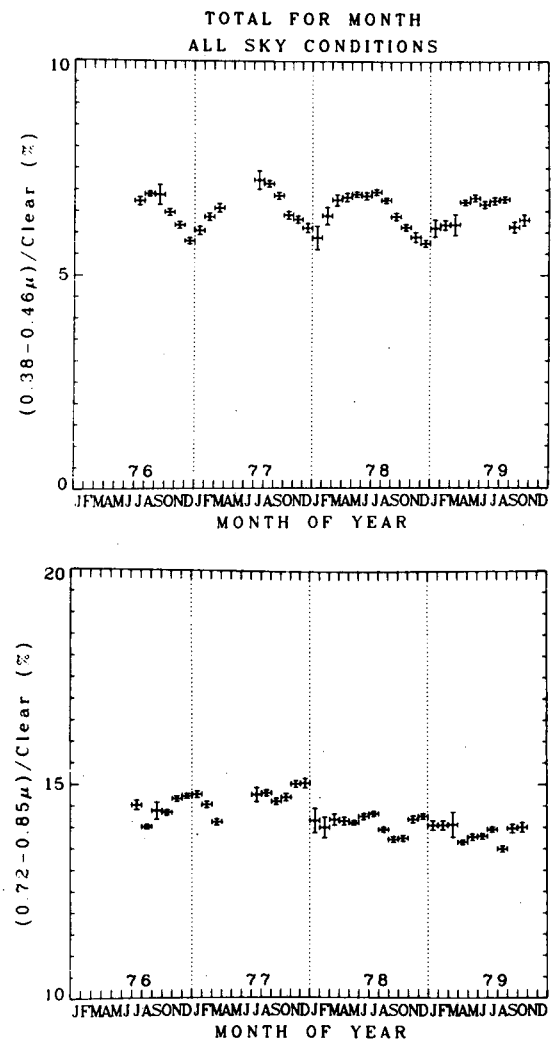

Figure 2. The relative amount of energy in the indicated portions of the solar spectrum for the Mojave Desert area (China Lake and Barstow). The data are from July 1976 through December 1979.

(XBL 814-9321)

suppressed zero). Thus, the preliminary indication is that it may not be necessary to have extensive wave-length-dependent measurements in order to evaluate properly the expected performance of photovoltaic devices if monthly totals, as opposed to hourly values, are being used in the evaluation.

PLANNED ACTIVITIES FOR FY 1982

As a consequence of budget reductions for the DOE Solar Program, this project is unfunded for FY 1982. Plans call for the refurbished telescope (see Measurement Program above) to be moved to Barstow and to be operated as part of the technical evaluation of the performance of the pilot plant.

If a modest level of support is available, work will continue on the analysis of the existing data.

REFERENCES

1. Grether, D., Evans, D., Hunt, A., and Wahlig, M. (1981), "The Effect of Circumsolar Radiation on the Accuracy of Pyrheliometer Measurements of the Direct Solar Radiation," in Proceedings of the Solar Radiation Workshop of the 1981 Annual Meeting of the American Section of the International Solar Energy Society, Philadelphia, PA, May 1981; Lawrence Berkeley Laboratory Report LBL-12707.

2. Evans, D.B., Grether, D.F., Hunt, A.J. and Wahlig, M. (1980), "The Spectral Character of Solar and Circumsolar Radiation," in Proceedings of the Annual Meeting of the American Section of the International Solar Energy Society, Phoenix, Ariz., May 1980; Lawrence Berkeley Laboratory Report LBL-10802.

3. Grether, D.F., Evans, D., Hunt, A., and Wahlig, M. (1980), "Measurement and Analysis of Circumsolar Radiation," in Proceedings of the Annual DOE Insolation Resource Assessment Program Review, Davis, Calif., August 1980; Lawrence Berkeley Laboratory Report LBL-11645.

Support for SOLERAS Solar Cooling Engineering Field Tests*

M. A. Wahlig and F. H. Salter

LBL provides technical consulting and management services to support the Solar Energy Research Institute's overall management of the SOLERAS Solar Cooling Engineering Field Tests. These field tests are part of the Urban Solar Applications Program within the Joint United States--Saudi Arabian Program for Cooperation in the Field of Solar Energy (SOLERAS).

The objective of the Solar Cooling Engineering Field Tests is to bring solar cooling one step closer to commercialization on a competitive basis with conventional cooling systems. To meet this objective, modifications were made to systems developed under the National Solar Cooling Program to advance overall system performances, while at the same time lowering system design, installation, and maintenance costs.

The engineering field test is defined as the fabrication, installation, operation, and evaluation of a complete solar cooling system on an operational building for the purpose of verifying such predicted system parameters as thermal performance, cost effectiveness, reliability, maintainability, and installation ease. The engineering field test is expected to approximate the conditions to which a fully marketable solar cooling system would be subjected.

With the above in mind, two absorption and two Rankine solar cooling systems were installed in Phoenix, Arizona, in the winter/spring of 1981. Phoenix was selected for these installations because its climate is similar to the climate in parts of Saudi Arabia. Three of the four systems have air-cooled chillers to better adapt the system to the limited water availability in Saudi Arabia.

ACCOMPLISHMENTS DURING FY 1981

Installation designs were completed early in FY 1981, and the following systems were installed in Phoenix.

- Carrier Corporation installed a 15-ton water-cooled absorption cycle chiller at BDP-Day and Night Air Conditioning. The building is a high-bay structure of concrete block with a small office area, which is to be cooled, and a large warehouse area. Powered by about 1400 ft^2 of tracking parabolic trough collectors, the absorption unit is designed to deliver 47 kW of cooling to

*This work was supported by the Solar Energy Research Institute, through the U.S. Department of Energy under Contract No. DE-AC03-76SF00098, under an agreement with the United States-Saudi Arabian Joint Commission on Economic Cooperation.

the offices. Storage for the system consists of a large 2500-gallon tank for heat storage and a small thermal ballast tank which helps prevent excessive chiller cycling.

- Carrier Corporation's second project is a 10-ton, air-cooled absorption cycle chiller at Sigler-Faigen. The building is a high-bay, concrete-block building combining office space, showroom space, and a warehouse area. Powered by about 1000 ft^2 of tracking Fresnel-lens collectors, the absorption unit is designed to deliver 36 kW of cooling to a computer room facility. Storage for the system includes a large 4000-gallon cold-storage tank for twenty-four-hour cooling and a small thermal ballast tank.

- Honeywell, Inc. installed a 14-ton air-cooled Rankine cycle unit at an Arizona Public Service building. The building is a single-story brick structure consisting entirely of office and lab space. The system is powered by 2400 ft^2 of evacuated-tube-type collectors and is designed to deliver 46 kW of cooling, about one-half of the entire building load. Gear reduction enables the Rankine turbine to drive a conventional Trane reciprocating compressor. An induction motor with clutches on each end is mounted between the gear box and the compressor to permit the following modes of operation:

  a. Compressor driven by turbine with excess energy converted to electrical power,

  b. Compressor driven by turbine with additional power supplied by the induction motor as needed,

  c. Compressor driven by induction motor,

  d. Induction motor driven by turbine to generate electricity.

  No storage tanks are used with this system because all excess energy is converted to electrical power, utilizing the electrical grid as the storage system.

- United Technologies Research Center installed an 18-ton air-cooled Rankine cycle unit at Hamilton Test Systems. The building is a single-story office structure with extensive external shading provided by overhangs and greenery. Powered by 1300 ft^2 of tracking parabolic-trough collectors, the system is designed to deliver 60 kW of cooling to the building. Storage for the system consists of a 2000-gallon cold tank and a 1500-gallon hot tank. In this system, a small high-speed centrifugal compressor is directly driven by the Rankine turbine.

During FY 1981, LBL's activities in support of these projects was primarily in the following areas:

- Complete critical design reviews,
- Review final construction plans and specifications,
- Factory visits to inspect equipment prior to shipment,
- Frequent site visits to follow and report on construction progress, start-ups, and acceptance tests,
- SOLERAS-DOE design review meeting,
- Dedication of projects.

PLANNED ACTIVITIES FOR FY 1982

LBL's contract expired at the end of FY 1981. However, LBL may be involved in a final series of start-ups and acceptance tests after various improvements are made to the four systems in the spring of 1982.

LBL Building 71 Solar Cooling Project*

F. H. Salter

This active solar cooling project is part of the Department of Energy (DOE) Solar in Federal Buildings Program. The purposes of this program are to demonstrate the Federal Government's confidence in the solar industry and to stimulate growth and technical improvements in solar technology through the installation and demonstration of a variety of commercially applicable solar energy systems in buildings owned or occupied by the Federal Government. The program provides technical and financial assistance through interagency agreements to Federal agencies for design, acquisition, construction, and installation of solar heating and cooling equipment projects.

LBL Plant Engineering Department is responsible for project engineering and contract administration for this project. LBL's duties include: preparing the project proposal, preliminary engineering, conceptional design, design criteria, selection of an outside A/E for final engineering and preparation of plans and specifications, engineering and administrative support for the A/E, periodic review of the final design, administration of the bid process and subcontract negotiations, construction supervision, acceptance testing, and extended field testing of the system. The LBL Active Solar Research Group provides technical assistance and review of the project.

Overall administration of this project is provided by the San Francisco Operations Office of the Department of Energy (DOE/SAN). DOE/SAN has subcontracted technical management of this project to Energy Technology Engineering Center (ETEC). Approval of the final design by DOE/SAN and ETEC is required prior to release of construction funds.

ACCOMPLISHMENTS DURING FY 1981

An intragovernmental order to proceed with the design of the project was received in January 1981. LBL developed preliminary engineering and design criteria for the project. Interactive Resources of Richmond, California, was selected in July 1981 to provide final engineering. The design was about 70 percent complete by the end of FY 1981.

Scope of Project

The Solar Cooling System will provide substitute capacity for the existing Building 71 chilled-water system by installing the new chiller next to and in parallel with the existing electric chillers, which will be retained for backup. The system will consist of roof-mounted collectors, storage tanks, and a nominal 25-ton lithium-bromide chiller package and associated pumps, piping, insulation, valves and fittings, controls, and instrumentation. The chiller package will be supplied by Arkla and will be field-tested in the Solar Cooling System. Because more than 25 tons of cooling are continuously required at Building 71, the solar chiller will operate at full load for an average 6 hours per day.

The following table summarizes design parameters:

Chiller Capacity	22 tons
Chiller COP	0.73
Average Operation	6 hr/day (at 22-ton loading)
Generator Entering Water Temp.	180°F (adjustable 170°F to 200°F)
Leaving Chilled Water Temp.	45°F
Entering Condenser Water Temp.	80°F
Maximum Storage Temp.	250°F
Collector Area	6000 ft^2 (gross area)
Collector Type	evacuated tube collector
Storage Tank	2500 gallons
Thermal Ballast Tank	500 gallons
Expansion Tank	500 gallons

The collector array will utilize stationary mount, concentrating (CPC reflector), and vacuum-tube receiver solar collectors to accomplish the 250°F maximum-design temperature. The collector design will emphasize simplicity and durability to minimize maintenance. This is essential to this project because access to the collectors will be restricted due to roof radiation during operation of the Building 71 accelerator. Because fluid will be contained in continuous copper tubing, glass tube breakage will not disrupt system operation, and tube replacement can be scheduled for periods when the accelerator is not operating. Further reliability will be accomplished by using high quality "Pyrex-type" evacuated tubes that are less prone to breakage. The collectors will have no cover glass, making tube replacement easier.

PLANNED ACTIVITIES FOR FY 82

Final approval of the plans and specifications of the Building 71 Solar Cooling System was given by ETEC and DOE in December 1981.

*This work was supported by the Assistant Secretary for Conservation and Renewable Energy, Office of Solar Heat Technologies, Active Heating and Cooling Division of the U.S. Department of Energy under Contract No. DE-AC03-76SF00098.

Remaining Project Schedule

Advertise for bids
Early February 1982

Construction contract signed by all parties
Early May 1982

Construction complete
September 1982

Acceptance test complete
October 1982

Final construction status report
November 1982

Field Tests

This project has been approved for inclusion in the National Solar Data Network and will have instrumentation installed and data processed by Automation Industries, Inc. - Vitro Laboratories Division.

Development of a 30-kW High Temperature Solar Receiver Using Small Particles as the Heat Exchanger*

A. J. Hunt, M. Deiringer, D. B. Evans, L. Hansen, P. G. Hull, and D. Paydarfar

The solar resource is distinguished from traditional energy sources by two main features. First, sunlight arrives on earth as pure radiant energy, with no conductive or convective heat transfer. Second, sunlight is characteristic of a source with much higher temperature than other present-day energy supplies. Because of these differences, we must independently evaluate the techniques of heat exchange and energy conversion used with solar energy and not simply adopt the technology developed over the last century for using conventional energy sources. The work described here utilizes a novel approach to match the unique characteristics of concentrated sunlight to the requirement of heating a gas.[1,2]

The purpose of this work is to develop a new type of solar thermal receiver that utilizes concentrated sunlight to heat a gas to high temperature to operate a turboelectric generator or to supply industrial process heat. The Small Particle Heat Exchange Receiver (SPHER) uses a very small mass of ultrafine carbon particles suspended in a gas to absorb sunlight and transfer the heat to the gas. The concentrated sunlight, provided by a parabolic dish or system of mirrors, passes through a window into a chamber containing the absorbing suspension. Because the particles are very small, they are not significantly affected by gravitational or inertial forces; they are effectively part of the gas. An extremely small mass of these particles provides a large surface area for solar energy collection and heat exchange. The particles heat until they react chemically with the gas or vaporize. The particles may be used in a once-through fashion because of the very low mass of carbon required.

*This project was supported by the Solar Thermal Test Facilities Users Association, a non-profit corporation which manages high temperature solar thermal testing for the U.S. Department of Energy, under contract DE-AC03-76SF00098.

Major advantages of this receiver are high efficiency, low pressure loss, simplicity, and light weight. Other benefits of this approach are a lower chamber temperature for a given output-gas temperature and freedom from cycling and lifetime problems experienced in other heat exchangers. The SPHER concept is suitable for a wide range of sizes and a variety of applications.

ACCOMPLISHMENTS DURING FY 1981

This year, the project moved from conceptual studies and experimental investigations to a solar proof-of-concept. In an agreement with the Solar Thermal Test Facilities Users Association, we undertook the design and construction of a receiver[3] capable of heating ambient air to approximately 800°C with a power conversion capability of 30 kW. The system consists of two major components, the particle generator and the receiver, and it also includes instrumentation and an air supply system. It is planned to test the receiver in 1982 at the Advanced Components Test Facility (ACTF) on the campus of the Georgia Institute of Technology. The development work performed in FY 1981 on the major components is summarized below.

Particle Generator

The function of the particle generator is to provide a sufficient flow of absorbing particles to insure that more than 90 percent of the radiant energy entering the receiver is absorbed directly in the gas-particle suspension. The particle generator was developed in two stages. A laboratory version of the generator was built to demonstrate that an adequate particle flow could be produced to reach the 30-kW power rating. After the laboratory generator was developed sufficiently to achieve the output required, a new generator suitable for solar testing was designed.

The generator produces particles by pyrolysis of acetylene gas injected with a carrier gas (argon) into a heated tube. A laboratory generator was constructed using a downward flow through a heated quartz tube, as is illustrated in Figure 1. Through a series of experiments and modifications, the output of the generator was increased until a problem was encountered with carbon build-up on the gas injector. The gas injection port was redesigned to provide cooling for the tip, and a further series of experiments resulted in a maximum particle production rate of about 25 mg/sec. This was in excess of the calculated requirement of 16.1 mg/sec for the 30-kW receiver.

After the successful scale-up of the laboratory generator, a new generator was designed that was capable of being transported to a remote site and of being operated on the tower of the solar receiver test facility at Georgia Institute of Technology. This field version of the generator also incorporated design changes to further increase the output and to simplify its operation. A stainless-steel reactor tube was used instead of quartz, and the reaction zone was lengthened to enhance the particle production. The field generator was constructed and underwent preliminary tests at the end of the fiscal year.

The output of the particle generator is monitored by measuring the opacity of the particle suspension with the transmissometer diagramed in Figure 1. It consists of an extinction tube equipped with a series of baffles to isolate the end windows and provide a known extinction path length. A helium-neon laser beam is passed through the tube, and the transmitted light is measured by a detector. To determine the absorption capability of the particles, the particle mass loading must also be determined. This was measured by weighing the particles deposited on a filter from a known volume of gas, as illustrated in Figure 1.

Samples of the particles, taken on Nucleopore filters at all stages of work, were examined with a scanning electron microscope to determine their average size and state of aggregation. The results of an examination of the residual gas using mass spectrometry indicated the residual gas consisted mainly of hydrogen and acetylene.

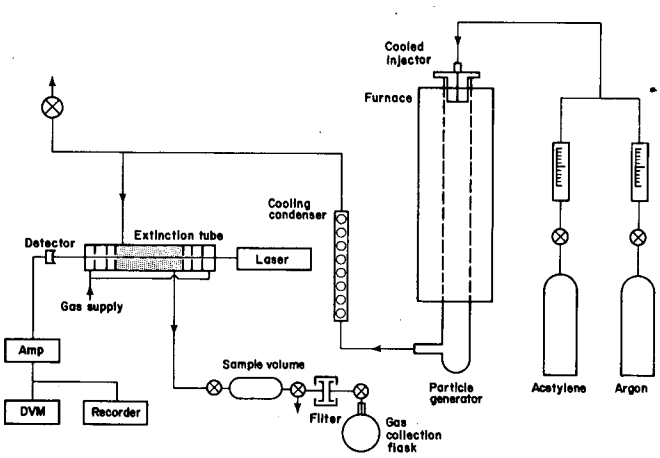

Figure 1. Schematic drawing of the particle generator and measurement apparatus.

(XBL 823-183A)

Receiver Design

The receiver provides containment for the gas-particle mixture while it is being heated. It consists of a window, an open volume in which the sunlight is absorbed, and a gas injection and exhaust system. Because the SPHER is basically different from traditional heat exchangers, a new set of criteria had to be developed to guide its design. The size of the receiver is dictated by the density of the absorbing particle suspension and the allowable flux density on the walls. Considerable effort went into the design to minimize the radiant flux density incident on the receiver walls.

The dimensions of the receiver were dictated by the beam geometry at the ACTF and the desire to maximize the power conversion ability without requiring an excessive scale-up of the particle generator. The completed receiver will be capable of operating at power levels significantly higher than 30 kW by using a particle generator with a larger capacity. The size of the receiver to obtain a specific absorption within its volume is inversely proportional to the rate of particle production. Because there is a capital cost associated with the size of the chamber and an operating cost to supply the absorbing particles, the size of future direct absorption receivers will be determined by minimizing the sum of the capital equipment and operating costs.

The shape of the receiver chamber was determined by positioning the walls at locations to minimize incident flux density. Because the flux density is a function of both the collector field geometry and the absorption occurring in the chamber, a new method to predict the flux was developed based on measurements of the collector system.[4] The measurement was made by placing a small aperture at the planned location of the receiver window. Then the flux density was determined with a scanning calorimeter bar over a plane at a distance behind the aperture that is large compared to the size of the opening. These data provide detailed information about the angular distribution of flux and are used with an analytic method to calculate the flux density on an arbitrary surface. The calculation (implemented on a large-scale computer) also determines the effect of the absorbing suspension. Figure 2 is a map of the flux density in a vertical plane above the focus of the ACTF. Figure 3 is a cross-sectional view of the receiver. The window at the bottom admits the solar flux into the inner region. Comparing Figures 2 and 3 indicates the strong influence of the flux density pattern produced by the concentrator on the shape of the absorption chamber (A in Figure 3).

Figure 3 illustrates the main features of the SPHER design. The gas-particle mixture is routed into the nozzle ring B. A total of 18 nozzles (C) direct the gas flow from the nozzle ring into the chamber to cause a significant swirling motion. This circular motion organizes the flow in the chamber and reduces the possibility of hot spots

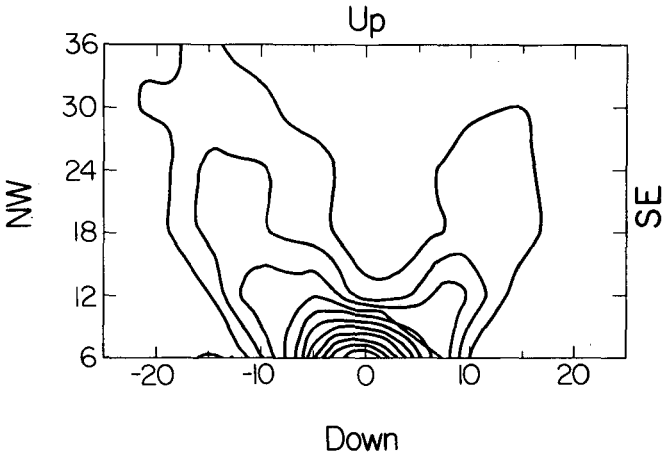

Figure 2. Measured lines of constant flux density inside the SPHER for no absorption. The distances on the axes are measured in inches from the focal point. Flux density contours run from 8 W/cm^2 to 48 W/cm^2 (nearest the focus) in intervals of 4 W/cm^2.

(XBL 823-182)

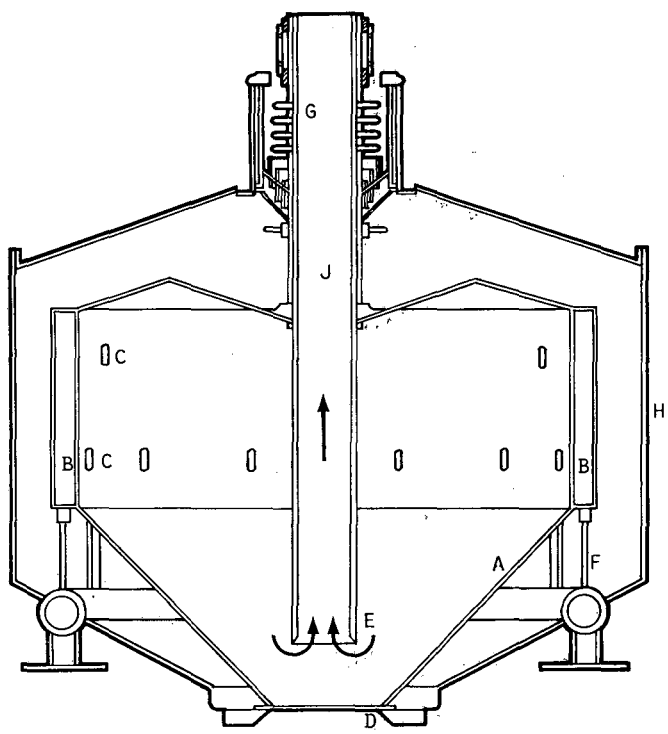

Figure 3. Sectional view of the SPHER absorption chamber: (A) absorption chamber, (B) nozzle ring, (C) gas injectors, (D) window, (E) exhaust tube, (F) spring leg supports, (G) bellows assembly, (H) outer skin, (J) location of radiation shielded thermocouple.

(XBL 823-181A)

originating from axially nonuniform flux distributions. The gas-particle mixture circulates cyclonically to the axis near the window (D), where the exit tube (E) is located. A unique aspect of the design involves the transparent quartz tube that penetrates the high-flux region. The tube acts as an exhaust port and insures that the gas-particle mixture passes through the maximum flux density region before leaving the receiver. The use of a quartz tube provides a refractory exhaust pipe that does not interfere with the flux distribution because it is transparent.

The nozzle ring and absorption chamber are supported by a set of flexible spring legs (F) mounted to a rigid toroidal tube that carries the weight of the receiver. A bellows assembly (G) near the top of the receiver reconciles the thermal expansion of the interior of the chamber with the cool outer skin (H). A thermocouple equipped with multiple heat shields is located in the exhaust tube at location J. The region between the absorption chamber (A) and the outer skin is filled with compressible high-temperature insulation to minimize the heat losses from the absorption chamber.

To minimize costs, no "super" alloys were used in the construction of the receiver or generator. The lining of the receiver is stainless steel, fabricated mostly from sheet metal stock. An air induction system based on the Coanda effect is used to produce the inlet gas flow because of its ease of control and operation.

PLANNED ACTIVITIES FOR FY 1982

The construction of the SPHER will begin in October of 1981. The receiver will be fabricated largely by the sheet metal section of the LBL mechanical shops. The construction will be completed in December and the receiver moved to laboratory facilities at LBL for initial check-out. The air supply and measurement system will be tested, the particle generator connected to the receiver, and the instrumentation completed. A 2.2-kW xenon arc lamp will be used for low-power testing and system check-out. Laboratory flow tests are scheduled for the beginning of December and will continue into 1982. The receiver will be moved to the Georgia Tech facility in the spring or summer of 1982 for solar testing and evaluation.

REFERENCES

1. Hunt, A.J. (1978), "Small Particle Heat Exchangers," Lawrence Berkeley Laboratory Report LBL-7841.

2. Hunt, A.J., (1981), "Development of a Direct Absorption High Temperature Gas Receiver," in Proceedings of the International Solar Energy Society Congress, Brighton, England, August 23-28, 1981, also Lawrence Berkeley Laboratory Report LBL-13234.

3. Hunt, A.J., and Evans, D.B. (1981), "The Design and Construction of a High Temperature Gas Receiver Utilizing Small Particles as the Heat Exchanger," Phase I Report, Solar Thermal Test Facilities Users Association, Lawrence Berkeley Laboratory Report LBL-13755.

4. Evans, D.B., and Hunt, A.J. (1981), "An Empirical Technique for Predicting Solar Flux Distributions," in Proceedings of the Flux Measurement Workshop of the STTF Users Association, Albuquerque, NM, October, 1981, Lawrence Berkeley Laboratory Report LBL-13523.

Diffractive Solar Collection Systems*

D. B. Evans and A. J. Hunt

The purpose of this project is to investigate solar collector systems based on the diffraction of light. Present solar collection systems rely on reflection or refraction of sunlight. The technique proposed here is based on the use of diffractive optics, in particular Holographic Optical Elements (HOE's), to intercept sunlight and diffract it toward an energy conversion or storage device (e.g., photovoltaic cell, solar thermal receiver, or thermal mass).

HOE's can be made by exposing a dye-sensitized emulsion to the interference between two beams of coherent light.[1] The characteristics of the HOE are determined by the position and strength of the optical elements used to form the beams. A simple point focus HOE can be made by interfering a plane-parallel wave front with a coherently related spherical wave front originating from a point source. Diffractive optical elements can be used instead of conventional optics to concentrate, spectrally separate, or redirect sunlight. Because of the unique diffractive properties of HOE's, many effects occur that cannot be achieved with geometrical optical systems. For example, the diffraction characteristics may be used to focus and guide differing wavelengths of light to photocells with matching spectral responses. Theoretical efficiencies for the conversion of light to electricity can exceed 50 percent for an array of photocells with graded band-gap energies. In daylighting applications, holographic coatings may be placed on windows to guide sunlight deep within a room to provide task lighting to areas of the building that would not otherwise receive natural lighting.

Other fascinating possibilities open up when the unique properties of HOE's are applied to solar collection optics. Multiple holographic exposures can be superimposed on an emulsion or arranged side-by-side in narrow strips to successively refocus the moving image of the sun onto a stationary receiver. Using these techniques, sunlight might be focused onto a fixed receiver throughout the day without the need for moving parts. There are, however, potentially significant restrictions on the efficiencies attainable using refocusing techniques.

In addition to being technically feasible, solar HOE's have the potential for low cost, mass production procedures. Once a "master" hologram has been produced with the proper characteristics, it can be duplicated by contact-printing techniques. An even lower cost device may be made by embossing plastic films with metal masters.

*This project was supported by the Director's Discretionary Fund through the U.S. Department of Energy under Contract No. DE-AC03-76SF00098.

ACCOMPLISHMENTS DURING FY 1981

During the past year, the LBL Solar Group has been investigating diffractive collector concepts as part of an overall program to study the optical properties of matter of small dimensions. This diffractive work can be divided into three areas. The first area involves basic studies of the general characteristics of holographic optical elements when considered for solar applications. Topics of interest in this area include the impact of the wavelength-dependent nature of diffractive systems on solar designs and the significance of traditional concepts such as flux concentration when viewed in a diffractive context. The second area of the program has centered around more detailed analytical calculations of the performance of specific concentrating HOE's. An ultimate goal is to develop a set of computer-assisted design tools for solar holographic systems. An interesting by-product of this branch of the research has been the production of computer-generated HOE's using LBL's computer-graphics facilities. The final area of the research has been the development of a complementary experimental program. This experimental effort not only provides validation of our analytical techniques but also has been geared toward developing laboratory techniques for characterizing the true efficiency of HOE's in solar applications.

Analytical Studies

To gain an understanding of perhaps the simplest type of concentrating HOE, analytical studies during FY 1981 began with a detailed analysis of the geometry and spatial distribution of interference fringes for holograms whose image is a coherent point source of light. For this type of HOE, the position of the nth interference fringe is determined by the relation:

$$n = \frac{2}{\lambda}(\rho - z - x \sin\psi),$$

where λ is the wavelength of light, ψ is the angle (assumed to lie in the x-z plane) of the reference beam with respect to a normal to the hologram plane, z is the closest distance from the point source to the hologram plane and ρ is the distance from the point source to a point P(x,y) on the hologram plane. It follows that the fringe spatial frequency in the plane of the hologram is given by

$$f = \frac{2}{\lambda}\left[\left[\frac{x}{\rho} - \sin\psi\right]^2 + \left[\frac{y}{\rho}\right]^2\right]^{1/2}$$

A computer analysis based on the preceding equations was performed to quantify the relationship between various geometrical factors and the

fringe spatial frequency distributions characteristic of sample concentrating HOE's. A result of particular interest from this analysis is the rapid increase in fringe spatial frequency as the reference beam angle, ψ, is increased. It was found that beam angles as small as 3° can be expected to result in fringe spatial frequencies as large as 2000 lines/mm. This result is significant in that it dictates rather stringent resolution requirements for emulsions used to produce off-axis HOE's.

Computer-Generated HOE's

As a next step in the understanding of the basic focusing HOE, the same relations given above were used to make several computer-generated HOE's. For computational purposes, the hologram plane was represented as a finely spaced grid of points. Hologram transmission values for each point on the hologram plane were then calculated and plotted on film, using a high resolution microfilm output device, the Dicomed D48. Figure 1 shows a magnified representation of a typical computer-generated HOE. Based on the fringe spatial frequency analysis, HOE's produced were limited to the on-axis (ψ = 0) type to keep the resulting fringe spatial frequencies within the resolution limits of the graphics device (~200 lines/mm). Despite the limited resolution capabilities of the Dicomed, the computer-generated HOE's exhibited good focusing capabilities, although diffraction efficiency was low.

An interesting feature of the HOE's produced by this technique is what appear to be spurious images on the hologram itself. A closer investigation reveals that this effect is due to quantization errors inherent in the finite mesh technique used to produce the HOE's. An analysis of this effect in terms of its Fourier-transformed image indicates that this "optical noise" is potentially separable. Based on this analysis, we are currently investigating techniques for making high-quality optical copies of these computer-generated HOE's by spatial filtering of the Fourier transform of the image.

Computer Reconstruction of Holographic Images

The techniques used in producing computer-generated HOE's have been extended to provide a simulation of the complete holographic process, including image reconstruction. As described in the previous section, the resultant interference intensity at each point on the holographic plane is represented by a value on a fine mesh grid. Using a suitable model for the hologram of interest, the intensity at each point on the mesh is related to a corresponding value of transmission for the hologram at that point. This resulting transmission is then used to calculate the interference contribution from that point on the hologram to each point on a corresponding grid mesh representing the image plane. The contributions from all points on the hologram are then summed to give the total intensity at each image plane point. Global parameters, such as spot size and efficiency, can easily be calculated by numerical integration of the intensity distribution over an appropriate area of the image plane.

Figure 2 illustrates the results of this technique for the case of an on-axis, point-source HOE. The resultant intensity in the image plane is plotted logarithmically as a function of position along a line through the focus in the HOE's image plane. The fine structure evident in this plot is a result of the finite mesh used on the hologram plane and illustrates the need to use the smallest possible mesh when detailed intensity behavior on the image plane is to be studied. These small-scale perturbations can be neglected when efficiency integrals

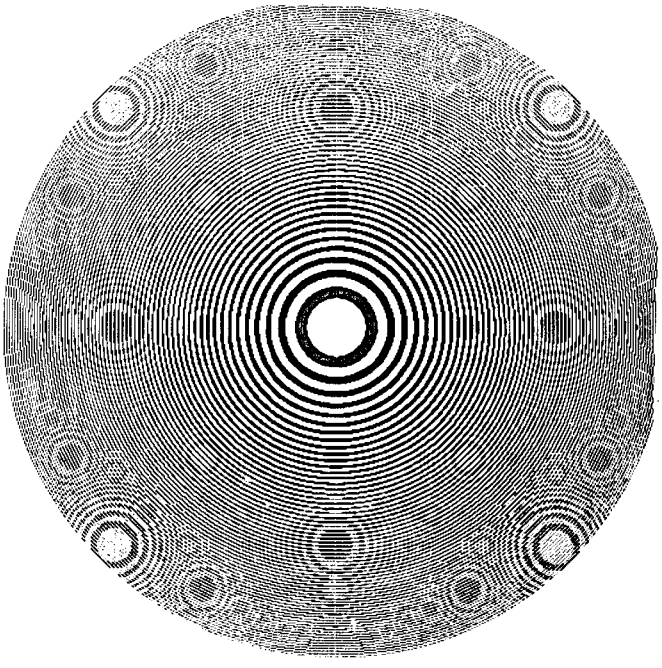

Figure 1. Magnified image of a computer-generated HOE.

(XBL 822-8119)

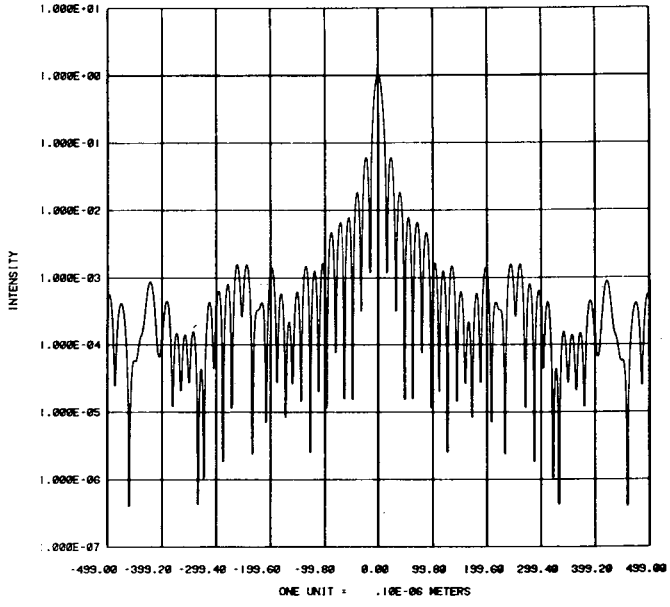

Figure 2. Intensity distribution of a computer-reconstructed image, as described in the text.

(XBL 824-9221)

are being evaluated, as long as their scale is truly small with respect to the given area of integration. This condition may be met by proper selection of the hologram mesh size.

The LBL Experimental Program

In an effort parallel to the theoretical analysis described above, an experimental program has been conducted to more fully understand the practical aspects of the utilization of HOE's for solar applications. One aspect of this experimental program involves the production and characterization of optical HOE's as validation of our analysis techniques. To date, a number of point focus HOE's have been made using high-resolution silver halide emulsions. Some of these HOE's were constructed to match as closely as possible the geometric configurations in our theoretical analyses. The reconstruction intensity distributions of these test HOE's have been measured and will be compared with computer predictions. In addition to the validation effort, efficiency measurements are being made on the test HOE's to gain a practical understanding of the dependence of HOE efficiency on various physical parameters, such as exposure and development conditions.

PLANNED ACTIVITIES FOR FY 1982

The computational techniques currently being used are strictly applicable only to the case of thin holograms and are inconvenient to modify for different construction geometries and/or holographic models. During FY 1982, these calculational techniques will be reorganized into a logically modular structure using an operator representation of the holographic process based on the theories of Nazarthy and Shamir.[2] Using this theoretical structure, each element of the holographic system can be represented as a discrete operator whose detailed specification may be changed as required. Effects due to finite beam size, apertures, and the modulation transfer function of the holographic medium can then be included as additional optical operators. The ability to include these effects is imperative for the study of HOE's illuminated by non-ideal sources such as the sun itself.

The feasibility of extending our analyses to thick or volume holograms will also be addressed. In considering the three-dimensional nature of the volume hologram, a much more complex mathematical theory is required, primarily to account for the depletion of the incident beam as it propagates through a highly efficient diffractive medium. A potential technique involves the Fourier decomposition of a focusing HOE into a series of constant-frequency gratings each of which may be described by a generalized coupled-wave theory.[3-5]

In future years, we plan to extend our experimental program to the characterization of the effects of reconstruction wave length and beam geometry and to a study of the relationship between holographic concentration and field of view in real HOE's. The plan is to develop an operational definition of solar holographic efficiency, while exploring laboratory techniques to measure that efficiency. In pursuing this goal, we plan to use the facilities of local holographics companies while we expand our own laboratory measurement capabilities at LBL.

ACKNOWLEDGEMENT

The authors gratefully acknowledge Dr. Hla Tin of NTS Corporation, the inventor of the Holoconcentrator, for introducing us to the use of holograms for solar concentration.

REFERENCES

1. Collier, R., Burckhardt, C., and Lin, L. (1971), Optical Holography, Academic Press, New York.

2. Nazarthy, M. and Shamir, J. (1981), "Holography described by operator algebra," J. Opt. Soc. Am. 71, pp. 529-541.

3. Moharam, M.G. and Gaylord, T.K. (1981), "Rigorous coupled-wave analysis of planar-grating diffraction," J. Opt. Soc. Am. 71, pp. 811-818.

4. Johnson, K.C. (1981), "General Coupled-Wave Diffraction Theory," Appl. Phys. 25 pp. 169-178.

5. Kogelnik, H. (1969), "Coupled wave theory for thick hologram gratings," Bell Syst. Tech. J. 48, pp. 2909-2947.

ENERGY EFFICIENT BUILDINGS PROGRAM

INTRODUCTION

In 1981, 35 percent of United States resource energy was consumed by the building sector. In contrast, the energy burned as gasoline represents only 14 percent of our energy use. With the scarcity of fuel and the attendant rise in fuel prices, it has been necessary to make radical design changes in automobiles and buildings to enhance their efficiency at the lowest possible cost and without compromising their previous level of service. For new automobiles, Congress mandated a factor-of-two improvement in efficiency. For existing buildings, research has shown that present resource energy use can be similarly reduced by 50 percent through careful retrofitting. In the case of new construction, houses and commercial buildings are already being designed to use only half the energy of their pre-1975 counterparts, but our research findings suggest that, to minimize life-cycle cost, we should--and can--further reduce this figure to 10 percent in the case of residences and to 20 percent in the case of commercial buildings.

The aim of the Energy Efficient Buildings Program is to conduct theoretical and experimental research on various aspects of building technology that will permit such gains in energy efficiency without decreasing occupants' comfort or adversely affecting indoor air quality. To accomplish this goal, we have developed five major research groups whose activities are regularly reported in technical and scientific journals, presented at international conferences, and disseminated in the form of Lawrence Berkeley Laboratory (LBL) reports.

A brief overview of the scope and objectives of each group follows.

ENERGY PERFORMANCE OF BUILDINGS (EPB)

The EPB Group studies the energy flow through all elements of a building. In this framework, the parameters tested are air infiltration rates, thermal characteristics of structural elements, and the behavior of the interface between dissimilar materials. From an analysis of overall performance, we are able to recommend cost-effective solutions for reducing infiltration and thermal losses, either by retrofitting existing buildings or by improving design features for new construction. This research is conducted in the laboratory and in the field; also, EPB maintains a research house in Walnut Creek, Calif., and has recently started infiltration measurements in a Berkeley apartment house and in a high-rise dormitory at the University of California Berkeley campus.

EPB has also developed a public-domain microcomputer program, CIRA (Computerized Instrumented Residential Audit), which is designed to speed and improve the accuracy of residential audits. It automatically provides the homeowner with a tailored list of retrofit options, ordered by return on investment, and a corresponding set of energy labels for the house.

BUILDING VENTILATION AND INDOOR AIR QUALITY

One of the more obvious means of improving the energy efficiency of a building is to reduce air infiltration/ventilation. Lowering this air-exchange rate, however, can seal in indoor-generated pollutants and enable them to build up to potentially harmful levels. In this program, our goal is to furnish a scientific basis for setting energy-efficient ventilation standards and developing system designs that promote energy efficiency while taking into account the comfort, health, and safety of building occupants. Project activities in support of this goal include: (1) development of new methodologies for measuring indoor air-quality parameters; (2) laboratory studies of emissions from building materials, soil, combustion appliances, and household products that may affect indoor air quality; and (3) field monitoring of indoor air quality in different types of buildings (e.g., schools, office buildings, residences) under a variety of ventilation conditions. Integrally related to this work is the investigation of prevention and control strategies for indoor air pollution that do not sacrifice energy efficiency. In this connection, we perform laboratory and field tests of various ventilation systems, including those that incorporate heat recuperation, which can provide the necessary level of ventilation while recovering a substantial portion of the energy that would normally be lost in the exhaust air stream. This recuperated heat can be used to preheat either incoming air or domestic hot water.

Although the group was founded to study the hazards of reduced ventilation, it has become evident that indoor air-quality problems occur more generally in "tightened" buildings and, indeed, that indoor air (which after all is only outdoor air with some additional pollutants) needs as much attention and monitoring as outdoor air. Specifically, we have found that throughout the building stock, there are houses that have unacceptably high levels of radioactive radon gas, formaldehyde, and combustion products. In these cases the problem is to remove the sources of contamination and, only then, to reduce the ventilation.

BUILDING ENERGY SIMULATION GROUP

The Building Energy Simulation Group is responsible for developing, improving, documenting, and validating the computer program, DOE-2, which has been designated the national program for calculating voluntary building-energy-performance standards. DOE-2 can also be used by architects and engineers as a means of designing buildings to improve their energy efficiency and minimize their

life-cycle costs. DOE-2 is systematically updated to incorporate the latest energy-conserving design features (e.g., passive and active solar, thermal storage, natural ventilation, daylighting, and evaporative cooling).

WINDOWS AND DAYLIGHTING

The Windows and Daylighting Group focuses on developing the technical basis for understanding the energy-related performance of windows. If the flow of heat and light through windows and skylights can be properly filtered and controlled, these building elements can not only outperform any insulated wall or roof component, but can also provide net energy benefits to the building. Our investigations are designed to develop the capability of accurately predicting fenestration performance. We develop analytical models and experimental procedures for determining the thermal and solar-optical properties of glazing materials; we also conduct materials-science studies to characterize a new generation of thin-film coatings and other advanced optical technologies that may someday replace conventional glass and plastic glazings. The first generation of windows incorporating transparent heat mirrors (R 4.5 windows) is now reaching the market five years after initial development within our program.

The DOE-2 building-energy analysis model has been modified to enable us to calculate daylighting effects and is being used for extensive parametric studies to determine total building energy use and peak loads as functions of climate, orientation, and window properties. Our daylighting studies now utilize a recently completed 24-foot-diameter sky simulator for testing scale models under carefully controlled conditions. Data from outdoor model tests and daylighting resource studies are still being collected and analyzed. Computational procedures will be validated with our Mobile Window Thermal Test (MoWiTT) facility, now nearing completion. This unique facility combines the accuracy and control of laboratory testing with the realism and complexity of dynamic climatic effects. It should, for the first time, enable controlled measurement of the interaction between fenestration systems and the building HVAC system.

LIGHTING

The research of the Lighting Group is divided into four major categories: technical engineering, building applications, visual impacts, and health impacts.

The Technical Program is concerned primarily with developing new concepts for converting electrical energy into visible light. Areas of interest include mechanisms for reducing the ultra-violet self-absorption in gas-discharge lamps. In addition, the search for high-frequency ranges of optimum excitation of the plasma gas holds the promise of more reliable and inexpensive electronics and more efficient conversion of energy into light.

The Buildings Applications Program concentrates on the effect lighting controls have on energy savings, glare reduction, sun control, visibility, and aesthetics.

The Visual Impacts Program focuses primarily on establishing lighting conditions that enhance productivity in a cost-effective manner. It also seeks to determine any undesirable visual effects, such as excessive fatigue, associated with the use of modern office equipment operating in an advanced lighting environment.

The Health Impacts Program extends artificial lighting research to a wider class of human activities. Here, conditions can be varied, and nonsubjective responses to lighting can be measured by sensitive medical instruments.

Facilities for the Technical Program are located at LBL; the Visual Impacts Program is located at the University of California, Berkeley, School of Optometry; and the Health Impacts Program is located at the Medical Center on the San Francisco Campus of the University of California.

The Lighting Group's successes include advancing the development of high-frequency solid-state "ballasts" (actually high-frequency power supplies) for fluorescent lamps and several energy-efficient light bulbs to replace the familiar incandescent electric lamp. A two-year test of solid-state ballasts in a large office building showed an electricity savings of 40 percent, which, if scaled to the entire country, represents an annual savings of four billion dollars. The energy-efficient light bulbs show savings of up to two-thirds, representing a potential national annual savings of perhaps an additional four billion dollars.

BUILDINGS ENERGY DATA

The Buildings Energy Data (BED) Group compiles and evaluates data on end uses of energy and the costs and performance of energy-efficient technical measures, from both direct field measurements and secondary source. Using these data, we prepare estimates of "least-cost technical potentials" for improving energy efficiency in new and existing homes and commercial buildings, often as a cooperative effort with utilities or state agencies. Individual conservation (or solar) measures can be catalogued in order of increasing unit-cost of conserved energy ($/MBtu or ¢/kWh) with careful attention paid to the interactions among conservation and solar measures that affect certain end uses (notably heating, cooling, and water heating). Using this technique, we create, in effect, a "supply curve of conserved energy," comparable to the supply curves for other market commodities that show the expected levels of production as a function of unit price. The national energy savings that might be achieved as a result of our research are discussed in detail in the BED section of the text.

RELATED BUILDINGS RESEARCH IN OTHER PROGRAMS

Closely related research on energy-efficient

buildings and appliances is carried on in other programs within the Energy and Environment Division and is reported in other chapters of this annual report. Specifically, the Energy Analysis chapter reviews eight studies related to building-energy-performance standards and labels, appliance energy performance, rating systems for auditors and appraisers, and energy and peak-power modeling. The Solar Energy chapter summarizes the research of the Passive Solar Analysis and Design Group.

ENERGY PERFORMANCE OF BUILDINGS (EPB)*

J. W. Adams, R. C. Diamond, D. J. Dickerhoff, J. B. Dickinson, J. Y. Garnier, D. T. Grimsrud, R. D. Lipschutz, M. P. Modera, M. H. Sherman, B. V. Smith, and R. C. Sonderegger

The aim of our group is to provide fundamental data on the energy performance of buildings. Our results will form the basis of design and construction guidelines for new buildings and will also help the formulation of retrofit strategies for existing buildings. Our two primary research areas are air infiltration and wall thermal performance. These studies involve work in the field, in the laboratory, in our research house, and on computer models. A third research area concerns development of an instrumented residential-energy audit that will be field-validated in FY 1982.

Air Infiltration

Air infiltration typically accounts for one-third of the annual space-heating load of residential buildings in the United States. This energy loss can be reduced substantially in new structures by changes in design and construction techniques and, to a lesser degree, in existing structures by careful repair and maintenance. Our work in this area concerns measuring, modeling, and reducing air infiltration. Our objectives are to provide design guidelines for architects and engineers and to develop construction quality standards for optimal air leakage in U.S. buildings. A major achievement of this program has been the development of a new model that identifies a single parameter--the "effective leakage area"--for scaling infiltration rates in different types of buildings. This parameter can serve as a powerful design tool for architects and builders in reducing infiltration in new structures. In addition, we are demonstrating techniques to reduce air leakage in existing structures. In order to quantify the energy-conserving potential of infiltration reduction measures in residential housing, we have participated in three field studies over the past year in widely separated parts of the United States. These studies included fan pressurization, leakage area and tracer gas decay infiltration measurements, "house doctoring" (infiltration reduction), and utility energy-consumption data analysis.

*This work was supported by the Assistant Secretary for Conservation and Renewable Energy, Office of Buildings and Community Systems, Buildings Division of the U.S. Department of Energy under Contact No. DE-AC03-76SF00098.

Walls

Conduction of heat through a building's walls accounts for much of the energy load during the heating season. Although much information is available on the steady-state thermal performance of walls in a laboratory environment, very little information is available concerning actual performance of walls in situ. Existing field measurements do indicate, however, that steady-state wall resistances can show significant degradation when compared with standard calculations. The goal of our walls research is to develop a complete methodology for determining the dynamic performance of walls. The methodology contains two relatively independent constituents: (a) a measurement apparatus capable of both controlling and measuring instantaneous, dynamic heat flows and surface temperatures on both sides of an arbitrary wall and (b) a calculation procedure capable of interpreting heat flows and surface temperatures in terms of physical wall parameters. Once complete, this system for the characterization of the dynamic thermal performance of walls can be used in the field to measure a wide variety of wall constructions and placements to determine their behavior and assess their impact on overall energy consumption.

Computerized, Instrumented Residential Analysis (CIRA)

Government officials, architects, energy auditors, engineers, and contractors all need to know projected energy use in a given house; and sometimes they may need to maximize energy savings in an existing house within the constraints of a budget. Several paper-and-pencil procedures exist to do both of these tasks. Unfortunately, these procedures always require lengthy calculations. Computer programs developed to ease this task often require strict adherence to a particular format or the knowledge of a special language.

Two recent trends appear particularly promising as ways for lessening the burden of calculating energy use in buildings: the introduction of microcomputers and the development of user-friendly programs. Microcomputers have become cheaper than cars, and many different brands are capable of running the same wide selection of programs. User-friendly programs do not require the user to

describe a building in some rigid format or special language. These programs ask questions in plain English and suggest possible answers; the user selects the appropriate answer.

Computerized, Instrumented, Residential Analysis (CIRA), a user-friendly program developed for microcomputers, couples the state of the art in interactive features with the latest developments in simplified computer models of building energy analysis. For the novice, CIRA will provide exhaustive explanations of everything it needs; for the experienced user, the questions and responses are more terse.

ACCOMPLISHMENTS DURING FY 1981

Air Infiltration

MITU. For model validation work, we have been taking measurements in occupied houses over a relatively long period of time. Because these procedures necessarily inconvenience occupants, we sought and found a solution in the MITU--a mobile infiltration test unit that simulates a house and can be moved to different locations to study the effect of different micro-climates on air infiltration rates (see Figure 1). The test unit was designed and built to simultaneously monitor air infiltration, surface pressures, and weather data for extended periods of time.[1] By moving the MITU to different locations, we can study the effect of the leakage area and its distribution on infiltration rates and local terrain and shielding. The data from MITU have been used to test our predictive model of air infiltration discussed below. Comparisons of infiltration predicted by our model and measurements of infiltration in MITU are shown in Figure 2. Surface pressure and infiltration measurements are continuing in different terrain and shielding situations.

Models. Infiltration losses have had no single unified parameter that can be used for modeling, unlike conduction losses where thermal resistance is employed. We have developed a model that uses the effective leakage area for characterizing infiltration losses. Effective leakage area is determined from a fan pressurization test of the structure. In addition to this parameter, the model uses the height of the structure, the inside-outside temperature difference, the terrain class, the shielding class, and wind speed to determine infiltration rates. The model can predict the impact of retrofits or other changes in the building envelope on air infiltration, using measurable performance changes effected in a few parameters. Figures 3 and 4 show comparisons of predictions of the model and measurements of infiltration in houses in Ohio and New York.

AC Pressurization. A technique for examining the low-pressure leakage function of a residence using an oscillating pressure source was extended by developing improved instrumentation and simplifying the analysis procedures. The advantage of this method is the use of the low-pressure range where natural infiltration occurs. However, the method is independent of weather interactions. A second version of this equipment has been built and will soon be field tested.

Field Studies. A major part of the program this year has been our work with several state utilities and local builders in measuring air leakage in houses. These are discussed in more detail below under "Field Measurements and Data Analysis."

Collaborative Activities. Our group was active this year in contributing infiltration-related work to national projects. We have contributed to the work of the ASTM infiltration standards committee that has produced standards E741 Tracer Gas Infiltration Measurements and E779 Air Leakage by Fan Pressurization and to the ASHRAE Technical Committee 4.3 and assisted in writing Chapter 22, "Infiltration and Ventilation," for the ASHRAE 1981 Handbook of Fundamentals.

Construction Quality Standard. A preliminary

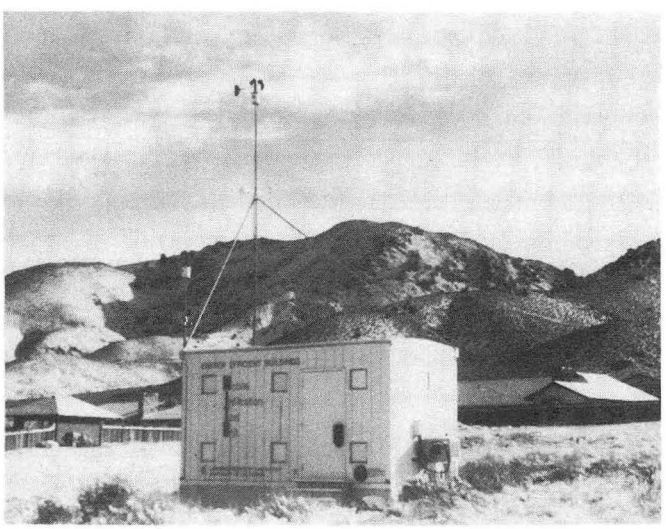

Figure 1. Mobile Infiltration Test Unit in the Reno, Nevada, test site.

(CBB 814-3957)

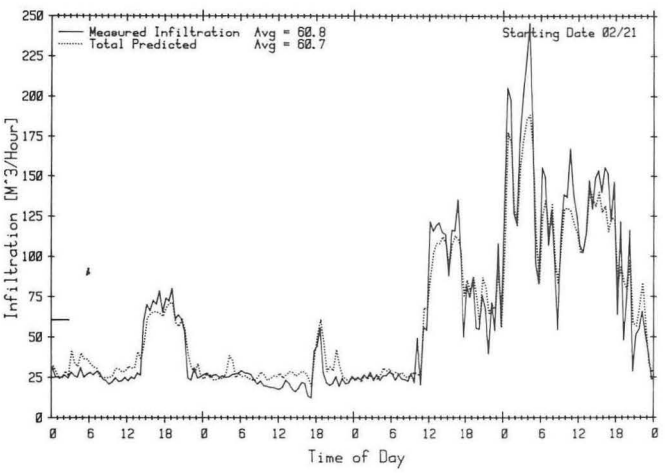

Figure 2. Plot of measured infiltration and infiltration model prediction versus time: four-day test in MITU.

(XBL 814-9394)

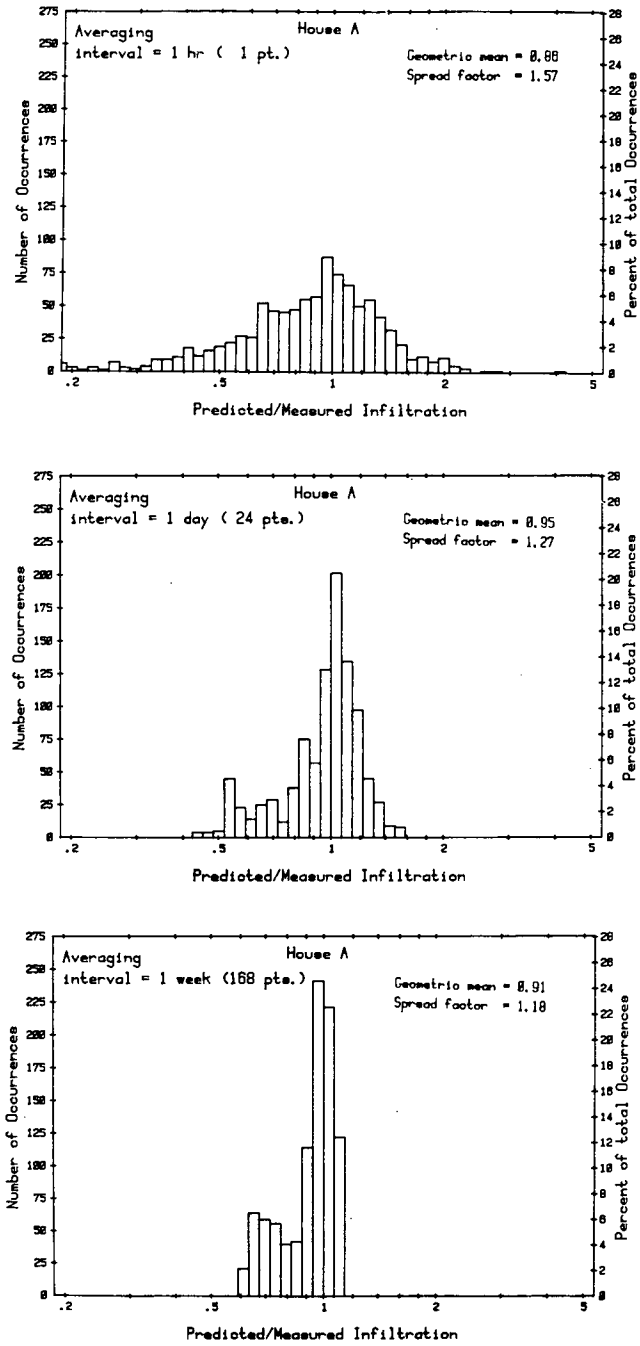

Figure 3. Histogram of predicted versus measured air-infiltration rates for three different averaging intervals for Ohio test house A.

(XBL 8111-12463)

draft of a framework for a construction quality standard for air leakage in residential buildings was prepared and circulated to professional groups for discussion and review. The draft proposes using the newly developed infiltration model to develop a verifiable standard for ventilation in new buildings. Included in the report is a survey of the average infiltration during the heating season for 300 houses throughout North America.

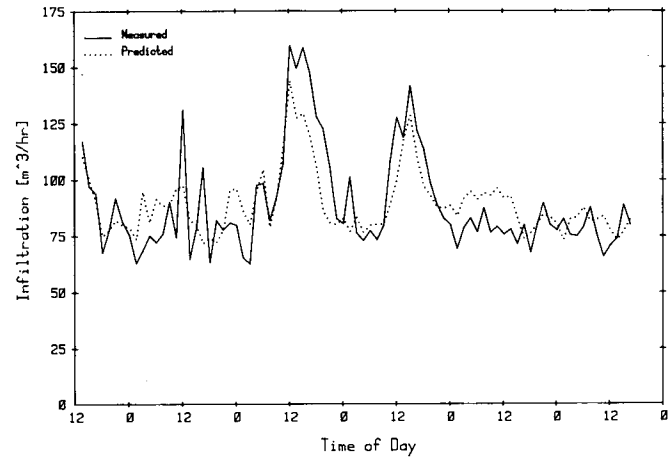

Figure 4. Measured and predicted infiltration versus time in Rochester test house.

(XBL 8112-13046)

Field Measurements and Data Analysis

In cooperation with the Rochester Institute of Technology (RIT) and the Rochester Gas and Electric Company, under a cost-sharing contract from the New York State Energy Research and Development Agency, our group analyzed utility data from three groups of tract houses in Rochester, New York. One group of houses built by Ryan Homes before 1976 was not considered energy-efficient. Houses in the other two groups, built by Ryan and Schantz Homes after 1976, incorporate energy-efficient features. Researchers from RIT measured these houses for leakage area, using an EPB blower door. We analyzed both leakage area measurements and utility data and found a 45 percent reduction in specific leakage area and a 31 percent reduction in energy consumption between the pre- and post-1976 houses.

EPB worked with the Bonneville Power Administration (BPA) on two projects in Midway, Washington, and Eugene, Oregon. Under the terms of the Pacific Northwest Electric Power Planning and Conservation Act of 1980, BPA is required to implement a region-wide program of least-cost conservation measures. The two joint projects are part of BPA's research efforts to determine what conservation measures are most cost-effective and lead to the greatest infiltration reductions. At Midway, we performed house-doctoring infiltration reduction on 12 of 18 houses being monitored for energy consumption. Six of the houses received 22 person-hours of work each, while a second group of six received only 10 person-hours each. Leakage-area measurements were made on the two groups of houses before and after the retrofits. The first group showed a reduction in average leakage area of 27 percent; the reduction in the average of the second group was 20 percent.[2]

The Eugene houses built by Modena Homes, Inc. are Arkansas-style homes with a continuous vapor barrier, high levels of insulation, double-glazed windows, and furnace ducts located in the heated space of the building. We performed both leakage-

area and tracer gas decay infiltration measurements in 12 of these houses, as well as measuring indoor air quality. We found an average specific leakage area for the 12 houses of 2.8 cm^2/m^2 and an average heating season infiltration rate of 0.34 air changes per hour. Infiltration rates measured by tracer gas decay ranged from 0.08 to 0.27 air changes per hour. Theoretical rates were calculated using the infiltration model developed by EPB. The ratio of the average of the geometric means of the measured rates to the theoretical rates was 0.90.[3]

Walls

Before FY 1981, this project focused on the design, construction, and debugging of our prototype apparatus, the envelope thermal test unit (ETTU 1.1). Having completed this task, we began in early FY 1981 to develop a model of dynamic wall performance using laboratory measurements from ETTU 1.1 to help validate the model.

This model[4] characterizes the dynamic thermal performance with a small number (ten or fewer) of physically interpretable parameters, which we call STPs (simplified thermal parameters). The first and most important of the STPs is the steady-state conductance, which is sufficient to describe a massless (i.e., purely resistive) wall. The second STP, the time constant, is required to determine any of the dynamic properties of the wall. These two, steady-state conductance and time constant, are sufficient to describe the dynamics of a homogeneous wall (a wall made of a single layer of material). The remaining simplified thermal parameters are called surface storage factors; they determine the deviation from a homogeneous wall under dynamic conditions. There is one surface storage factor per side for each order of the model; the higher the order of the model, the greater the ability of the model to predict the high frequency behavior of wall, but at the cost of more parameters.

As we made measurements with ETTU 1.1, we gained much experience about the entire measurement procedure. As a consequence, we were able to design and build a field version of the apparatus, ETTU 1.2 (Figure 5), which is smaller, lighter, easier to handle, and more responsive than the prototype version. During the middle of FY 1981, in parallel with the modeling effort,[5] ETTU 1.2 was constructed and debugged.

During the latter part of FY 1981, ETTU 1.2 was calibrated and used on several walls in the laboratory. After the laboratory testing phase was complete, ETTU 1.2 was taken to the field and used repeatedly to measure two stud cavity walls in a ranch style house.[6] To ascertain the effects of field measurements on ETTU, we disassembled ETTU 1.2 and, after checking it over, reassembled and calibrated it.

Computerized Instrumented Residential Analysis (CIRA)

Over the past year, the main thrust of our work was the development of simplified energy-

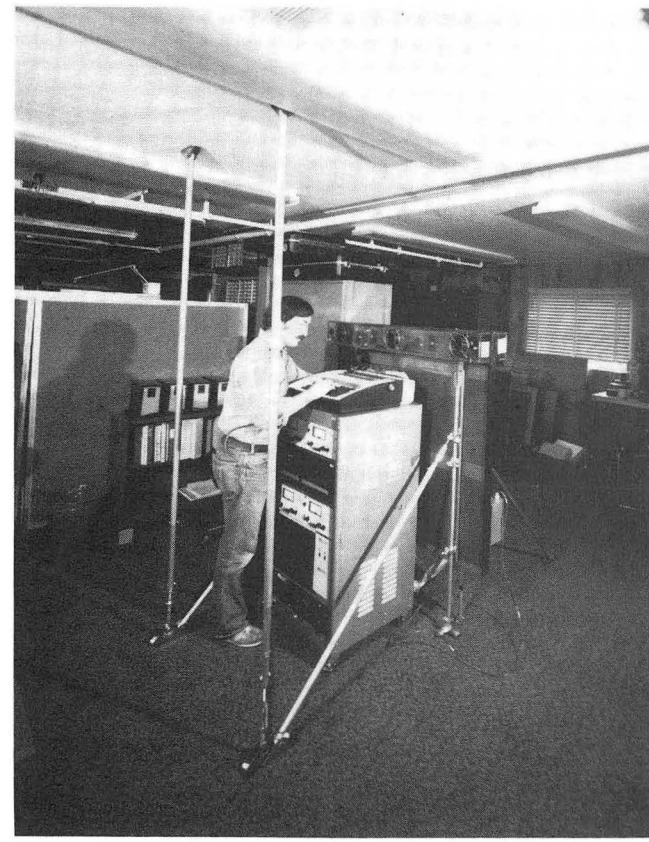

Figure 5. ETTU 1.2 and data-processing equipment in ETTU trailer.

(CBB 816-5845)

calculation algorithms suitable for microcomputer applications. Another area of concern was the development of a truly interactive building-description method for data entry. Both data entry and energy calculations are described below.

Data Entry. In developing CIRA, much effort was devoted to facilitating the tedious process of entering the appropriate building data. Prominent among the features that distinguish CIRA from other computer programs are the following.

Friendliness: The user does not have to learn a special language and does not have to remember any commands. CIRA does the work by asking about wall areas and types, heating system specifications, passive solar features, etc.; the user simply answers the questions displayed on a screen.

Helpfulness: If the CIRA novice does not understand some of the questions, such as

"Terrain Class.....?",

he or she can call for help with a simple keystroke, to which the computer responds with a more detailed explanation of the question, together with examples when appropriate.

Multiple choice: If the user understands the question, such as "Window Glazing.....?", but does

not remember the possible answers, another keystroke displays a list of options in multiple choice style, in this case

S=Single Pane
D=Double Pane
T=Triple Pane

This list will appear automatically whenever more than two invalid answers are given.

Dynamic defaults: Frequently, the user may not know the answer to technical questions, such as the R-value of a wall or the solar-gain factor of a window. What is, for example, the R-value of a 2-ft X 6-ft frame wall whose cavity is insulated with 4 inches of Vermiculite and one inch of exterior insulating sheathing? CIRA provides the answer, in this case R-16.8, at the touch of another special key. We call the values provided by this keystroke dynamic defaults: "defaults," because they step in when the user doesn't know the answer, and "dynamic," because they usually depend on the user's answers to one or more previous questions. Beyond the lay user, the professional can use dynamic defaults to avoid leafing through voluminous handbooks in search of the heat-loss factor for a basement, for example. If asked for help at this point, the computer will describe what method it uses to arrive at a particular default value.

Editing: Often, the user may want to alter previous input, correct mistakes, or re-use a house entered earlier, changing only details such as floor area, the city where it is located, and the window size. By another simple keystroke, the computer enters an editing mode and displays the desired questions and the answers previously given on the screen, along with a request for the new answers. The computer even keeps track of things the user may forget in the process: when changing the city from Denver to San Francisco, for example, the user will be reminded that he or she may also want to change the altitude.

The computer accepts entries on a wide variety of house components and related features:

- Walls, windows, doors
- Roof and subfloor
- Active and passive solar features
- Heating and cooling system
- Information on how the house is oriented and shielded
- Occupant behavior related to energy use
- Prices for the various fuels used.

Some of these entries may require the use of specialized instrumentation, such as: (1) a solar-siting meter to measure the degree of obstruction to solar radiation by trees and adjacent buildings, (2) a combustion-efficiency meter to measure furnace efficiency, (3) a blower door to pressurize the house, and (4) a few smoke sticks to find the air leaks. Most of these instruments can be found in the kit of a "house doctor," who searches a house for hard-to-spot energy leaks and fixes the most conspicuous leaks during a visit. CIRA was designed with the house-doctor approach in mind. The measurements performed by the house doctor feed directly into CIRA which translates them into practical retrofit recommendations. Because of dynamic defaults, however, these measurements and the attendant instruments are not indispensable; CIRA can function as a "stand-alone" diagnostic program. After all questions about the house have been properly answered, the computer will automatically provide monthly and yearly heating and cooling energy consumptions or, on request, recommend several combinations of energy-saving measures suitable for low, medium, and high budgets. Every combination (e.g., storm windows, elimination of air leaks, basement insulation) is chosen to produce the highest energy savings for a given budget. Interest and inflation rates, maintenance costs of the installed measures, and projected period of occupancy are taken into account.

Energy Calculations. To calculate the energy consumed for any given house, CIRA uses heating and cooling algorithms developed at Lawrence Berkeley Laboratory, Princeton University, National Bureau of Standards, Los Alamos National Laboratory, and the University of Wisconsin.[7]

To speed up the energy predictions, some of the calculations, such as air infiltration, total solar radiation distribution and degree-day coefficients, are made in advance for "standard conditions." In an actual application, the precalculated values are corrected to reflect the building and site characteristics under consideration.

Highlights of the heating and cooling algorithms are listed below.

- Variable-base degree-days calculated from monthly temperatures using an empirical correlation formula.
- The concept of an effective outdoor night-and-day temperature that is a function of outdoor temperature, solar and other internal gains, sky radiation losses, thermostat setbacks, and house thermal time constant.
- The calculation of effective conductances for below-ground walls and floors.
- The concept of an effective leakage area and a leakage distribution of the house that, together with terrain information, is used to correct the pre-calculated air infiltration values for standard condition.[8]
- The use of solar apertures and information on overhangs to compute monthly average solar gains. Solar apertures are calculated on the basis of window, wall, and roof types and dimensions.
- The calculation of output capacities and seasonal efficiencies of heating and cooling equipment as functions of indoor and outdoor temperature and of part-load.

In a previous paper,[9] we described some

aspects of a similar calculation procedure. The method described here is a continuation of that work. Algorithms for treating overhangs, radiation loss to the sky, and HVAC equipment efficiencies have been added. Moreover, dynamic degree-days have been improved to become variable-base degree-days correlated to outdoor temperature.

For each month, an energy balance is calculated separately for day and night. First, a heat-transmission coefficient is calculated to determine how much heat the house loses per month and per degree of temperature difference between indoors and outdoors. To this coefficient is added the effect of infiltration, computed on a monthly basis using a method developed at Lawrence Berkeley Laboratory. This method uses information on the leakage area of the house, the type of terrain on which it is located, and the type of shielding surrounding the house, all of which are part of the information requested by CIRA. For terrain and shielding classes, CIRA will display descriptive tables on request. Leakage area is generally measured with a so-called "blower door," a fan-like device that creates an over- or under-pressure in the house and measures the amount of air-flow through the fan necessary to reach several special levels of pressure. Alternatively, the leakage area can be estimated from information on the air tightness of windows, walls, doors, and all other building components. As usual, dynamic defaults are available to provide what the user may not know.

As with most other aspects of heating and cooling energy requirements, air infiltration depends on the local temperatures and wind speeds. The user, however, never need be concerned with such detail. Only the name of the nearest city in CIRA's files is required to obtain information about local weather patterns because the program will prompt for it and display the available options.

Solar gains are computed by taking into account weather-averaged solar radiation in the city chosen by the user; the shading effects of trees, nearby buildings, and overhangs; and the optical characteristics of windows and walls. The shading effects of overhangs and the reflection of glazed surfaces are modeled by using correlation methods developed at Los Alamos National Laboratory. The solar gains, together with other internal gains and radiation losses to the sky, are used to compute an effective outdoor temperature, which is usually higher than the monthly average temperature. The monthly values of effective outdoor temperature, indoor thermostat setting, and heat-transmission coefficient are used to compute monthly heating and cooling loads for day and night. These loads are corrected if night and day thermostat settings are different. Seasonal heating and cooling efficiencies are figured for each month based on: (1) heating and cooling loads, (2) specifications of the heating and cooling equipment, (3) part-load efficiencies, and (4) ambient-dependent output capacities. Finally, heating and cooling loads and efficiencies are combined to arrive at monthly energy consumptions for heating and cooling.

Viewing the Results. After the short time required to digest the input data and to perform the heating and cooling calculations, CIRA displays monthly values and yearly totals (or means, where appropriate) of several quantities, such as:

- Daily and nightly heating and cooling energy consumption
- Daily and nightly heating and cooling loads
- Air infiltration
- Solar gains
- Dollar expenditures for heating and cooling
- Average and effective daily and nightly outdoor temperatures

These results can be displayed either in tabular form or graphically, depending on the user's wishes. By pressing the appropriate key indicated by a menu displayed at the top of the screen, the user may also plot any arithmetic combinations of these figures (e.g., the sum of daily and nightly heating and cooling expenditures). For users with special needs, CIRA can be easily modified to display other types of output, for example, infrared radiation loss to the sky or the percent change in energy consumption for every percent change in infiltration, in solar gains or in similar parameters.

Discussion. This methodology has been applied to the Hastings Ranch house and compared to the predictions obtained with DOE-2.1, the U.S. Department of Energy's building simulation program, for seven U.S. cities representing a wide variety of climatic conditions: Washington, D.C., Albuquerque, Minneapolis, San Francisco, Boise, Seattle, and Portland, Oregon. The results of the comparison for heating loads with a 2.8°C (5°F) thermostat setback are shown in Figure 6 with monthly heating loads predicted by CIRA plotted on the ordinate and those predicted by DOE-2.1 plotted on the abscissa. The scales for both axes are logarithmic due to the large range of loads computed for the different cities: over 10-to-one for cooling and 20-to-one for heating. The solid line indicates the locus of perfect correspondence; the dashed lines indicate ±20 percent discrepancy.

The outliers at the low end of the scale are caused by a peculiarity of CIRA: although DOE-2.1 calculates both heating and cooling loads for every month, CIRA calculates only that load that it estimates is likely to be higher. In a few cases, this criterion of advance choice fails. Of course, CIRA could calculate both heating and cooling loads for each month and then, having compared the two, use the one that is higher. However, this would entail a doubling of the calculation time, presently five seconds for a yearly calculation.

For this figure, the difference between CIRA and DOE-2.1 predictions is 6.5 percent 8.5 percent. Percentages are based on the average DOE-2.1

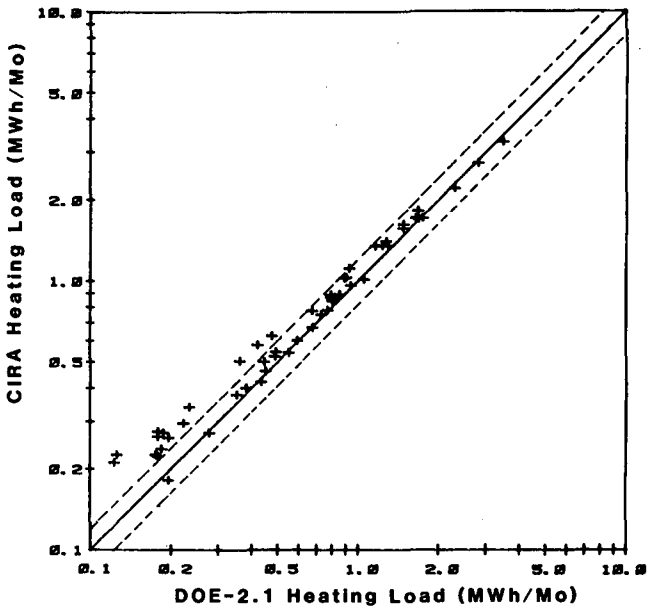

Figure 6. Comparison of predictions of monthly heating loads by CIRA and by DOE-2.1.
(XBL 8112-13049)

predictions. The systematic discrepancies that seem to correlate with the cooling season and thermostat setbacks could be traced to a variety of causes, such as the treatment of thermal mass or solar gains. However, rather than refining the model much further using DOE-2.1 as a reference, future research will concentrate on the comparison of CIRA with actual data.

PLANNED ACTIVITIES FOR FY 1982

Air Infiltration

We plan to continue validation and extension of the LBL residential infiltration model. The primary tool we shall use is the Mobile Infiltration Test Unit (MITU) described above. From field measurements of MITU, we plan to improve our descriptions of shielding and terrain classes and include effects from mechanical ventilation, heating systems, and chimneys or stacks.

Field measurements of residential infiltration using the Averaging Infiltration Monitor (AIM) will be started. Present infiltration measurement techniques generally omit occupant effects in characterizing the infiltration of a house. The AIM measurement, obtained over a two- or three-week period, is an average of total ventilation rates for a house. Therefore, the effects of typical occupant behavior are included in the infiltration value obtained with this unit.

The major new direction of this work will be the investigation of air infiltration and air leakage in multi-family dwellings. We shall develop measurement capabilities (AC pressurization and multi-zone infiltration) to investigate total building infiltration as well as air leakage between contiguous spaces in the building. A future goal of this work is the extension of the LBL infiltration model to multi-zone buildings.

Walls

With completion of the field testing of ETTU 1.2 and the validation of the model of STPs, the effort on the walls project will be somewhat reduced. ETTU 1.2 will be used as a field instrument to measure existing walls of different types and conditions to gain an understanding of the degradation of wall performance with aging.

Although ETTU 1.1 is inappropriate for use as a field device, it will be used as a laboratory apparatus to measure walls having unusual thermal properties. We plan, for example, to measure hollow-core masonry walls and cavity walls with reflective foils that have been carefully constructed in the laboratory to insure that their physical properties are well known.

To support both these efforts, we plan to use numerical modeling techniques to mathematically describe the wall/ETTU systems we will be using.

Computerized Instrumented Residential Analysis

In the year ahead, we plan to add an economic optimization module to CIRA that automatically determines the most cost-effective energy-saving retrofits for a given house. That is, for a given budget, what is the most energy-saving combination of retrofits or what is the highest retrofit budget for which the dollar savings still exceed the expenditures (including maintenance costs)? CIRA will answer both of these questions in a mostly automated process consisting of two stages: the selection of retrofits and their economic optimization.

Retrofit Selection. The retrofit selection will occur as follows: CIRA scans an extensive list on a disk containing several hundred retrofit options and their respective costs per unit, as well as their figures of thermal merit (typically, added thermal resistance, decreased solar gain, decreased leakage area, improved efficiency). CIRA will display only those items appropriate to the structure in question: cellulose insulation for cavity walls, but not for solid masonry walls, and sliding storms for double-hung windows, but not for casement windows.

This reduced selection of retrofits is shown on the screen for each house component (walls, windows, etc.). Costs for do-it-yourself and contractor installation are displayed for each retrofit selected. At this stage, the user may discard any unacceptable item (for example, aluminum insulating blinds in the bedroom).

At the end of this retrofit selection process, the computer determines the best combination of retrofits for the whole house, within the constraint of one or more given budgets. This process involves multiple yearly energy calculations, and may take from a few seconds to a few minutes, depending on the size and complexity of the house,

the climate, and the number of retrofits involved. Dollar and energy savings are shown for each combination of retrofit options, based on the expected period of occupancy for the house under consideration.

Preliminary output for an arbitrary house is shown in Figures 7 and 8. Figure 7 gives the cumulative dollar savings from a series of retrofit measures in their optimum sequence and the cumulative investment in these measures. Three break points are marked: after point A, the next retrofit costs more then it saves; at point B, cumulative savings are equal to cumulative costs (the measures up to this point are listed in Table 1); and at point C, savings are a maximum. Figure 8 shows the percentage of energy savings given by each level of investment for the same measures. The size of the investment and dollar savings depend upon a number of economic variables, such as current and future interest rates. The values can be varied to suit the homeowner's circumstances, such as access to low interest financing. On request the program will display monthly payment schedules for bank loans covering the cost of the retrofits and the tax credits and deductions available.

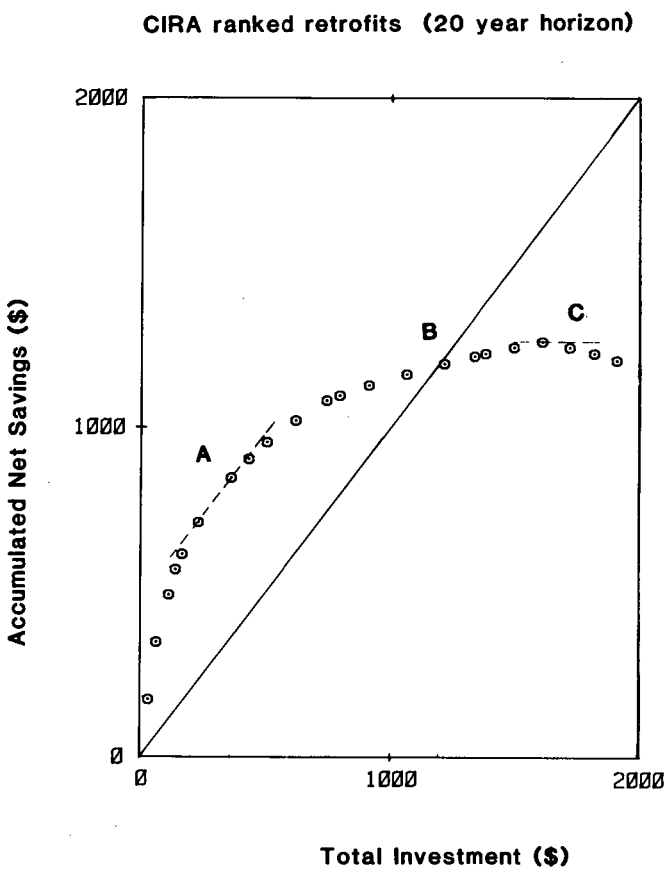

Figure 7. Cumulative savings realized from a series of retrofit measures performed in optimum sequence: (a) marginal savings equal marginal investment, (b) investment equals savings, and (c) savings are at a maximum.

(XBL 8112-13047)

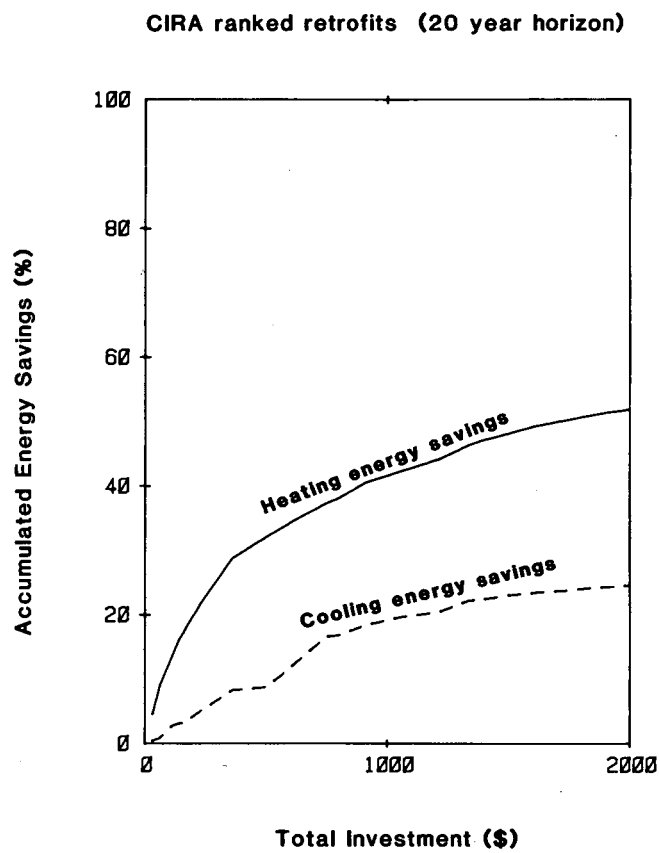

Figure 8. Energy savings versus dollar investment for a series of retrofit measures performed on a residence in optimum sequence.

(XBL 8112-13048)

Table 1. Costs and savings from an optimized series of retrofit measures for an Albuquerque house. Discount rate is 4% real, and horizon 20 years.

	Cost ($)	Net Life Savings ($)
Interior magnetic insulating panel on east-side WINDOWS	32.00	174.08
Interior magnetic insulating panel on back-yard WINDOWS	32.00	174.08
Reduce gas orifice on furnace HVAC-SYS	50.00	144.50
Interior magnetic insulating panel on front WINDOWS	26.80	76.38
Interior magnetic insulating panel on west-side WINDOWS	25.20	46.12
Thermally activated flue damper on Furnace HVAC-SYS	65.00	97.50
Electronically activated flue damper on furnace HVAC-SYS	130.00	135.20
Winter interior glass storm on east-side WINDOWS	71.50	56.49
Winter interior glass storm on back-yard WINDOWS	71.50	51.48
Inside drapes on back-yard WINDOWS	117.00	65.52
Inside reflective drapes on back-yard WINDOWS	123.00	61.50
Winter interior glass storm on front WINDOWS	52.00	15.08
Inside drapes on east-side WINDOWS	117.00	30.42
Triple glaze on back-yard WINDOWS	150.00	34.50

REFERENCES

1. Blomsterberg, A.K., Modera, M.P., and Grimsrud, D.T. (1981), The Mobile Infiltration Test Unit--Its Design and Capabilities: Preliminary Experimental Results, Lawrence Berkeley Laboratory Report LBL-12259.

2. Dickinson, J.B., et al. (1981), Results of the Bonneville Power Administration's Midway Energy Conservation Study. Lawrence Berkeley Laboratory Report LBL-12742.

3. Lipschutz, R.D., et al. (1981), Infiltration and Indoor Air Quality in Energy Efficient Houses in Eugene, Oregon, Lawrence Berkeley Laboratory Report LBL-12924.

4. Sherman, M.H., Sonderegger, R.C., and Adams, J.W. (1981), The Determination of the Dynamic Performance of Walls, Lawrence Berkeley Laboratory Report LBL-13510, to be published in Transactions of American Society of Heating, Refrigeration, and Air Conditioning Engineers, 88-I.

5. Adams, J.W., Sherman, M.H., and Sonderegger, R.C. (1981), Dynamic Measurement of Wall Thermal Performance, Lawrence Berkeley Laboratory Report LBL-13503, to be published in Proceedings of the DOE/ASTM Conference: Thermal Insulations, Material, and Systems for Energy Conservation in the '80s, Clearwater, Fla.

6. Sonderegger, R.C., Sherman, M.H., and Adams, J.W. (1981), The Envelope Thermal Test Unit: Field Measurement of Wall Performance, Lawrence Berkeley Laboratory Report LBL-13436, to be presented at the Third International CIB Symposium on Energy Conservation in the Built Environment, Dublin, Ireland, March 30-April 1, 1982.

7. Sonderegger, R.C., and Garnier, J.-Y. (1981), A Simplified Method for Calculating Heating and Cooling Energy in Residential Buildings, Lawrence Berkeley Laboratory Report LBL-13508, to be presented at the Third International CIB Symposium on Energy Conservation in the Built Environment, Dublin, Ireland, March 30 - April 1, 1982.

8. Sherman, M.H., and Grimsrud, D.T. (1980), Measurement of Infiltration Using Fan Pressurization and Weather Data, presented at the 1st Symposium of the Air Infiltration Centre on Instrumentation and Measurement Techniques, Windsor, U.K., Oct. 6-8, 1980, Lawrence Berkeley Laboratory Report LBL-10852.

9. Sonderegger, R.C., Garnier, J.Y., and Dixon, J.D. (1981), Computerized Instrumented Residential Audit (CIRA), Lawrence Berkeley Laboratory Report Pub-425.

10. Hastings, S.R. (1977), Three Proposed Typical House Designs for Energy Conservation Research, National Bureau of Standards Report NBSIR 77-1309.

BUILDING VENTILATION AND INDOOR AIR QUALITY RESEARCH

COMBUSTION-GENERATED POLLUTANTS

The Effects of Ventilation on Residential Air Pollution Due to Emissions from a Gas-Fired Range*†

G. W. Traynor, M. G. Apte, J. F. Dillworth, and C. D. Hollowell

Laboratory measurements have clearly indicated that, during the operation of combustion appliances, a wide range of pollutants are emitted, such as carbon monoxide (CO), carbon dioxide (CO_2), nitrogen oxides (NO_x = NO + NO_2), sulfur dioxide (SO_2), formaldehyde (HCHO), and respirable particulates.[1-4] Field studies have shown that the use of unvented combustion appliances may cause elevated indoor concentrations of many of these pollutants.[5-7] Obviously, many factors can affect the indoor pollutant concentrations from combustion appliances. One important factor is ventilation achieved by infiltration, a mechanical ventilation device, and/or natural ventilation, i.e., the opening of doors and windows.

ACCOMPLISHMENTS DURING FY 1981

This study investigates the effect of infiltration and two types of mechanical ventilation on indoor CO, CO^2, and NO_x concentrations from a gas-fired range: spot ventilation and whole-house ventilation. A range hood was used to evaluate spot ventilation; and an extensively ducted ventilation system, with three exhaust sites and five inlet sites which incorporated an air-to-air heat exchanger,[8] was used to evaluate whole-house ventilation. Results obtained in these studies are compared to those derived from an indoor air quality model.

All measurements were made at an unoccupied, one-story 107-m^2 (1150-ft^2), experimental research house with a volume of 260 m^3 Figure 1 shows the floor plan of the house, the air sampling sites, the location of the range and range hood, and the location of the exhaust and supply sites for the whole-house ventilation system. The air sampling sites were located 1.5 m above the floor. The range hood was located 0.64 m above the range, and the exhaust and supply sites of the ventilation system were located in the ceiling. The fireplace and all furnace ducts were sealed, and no mixing

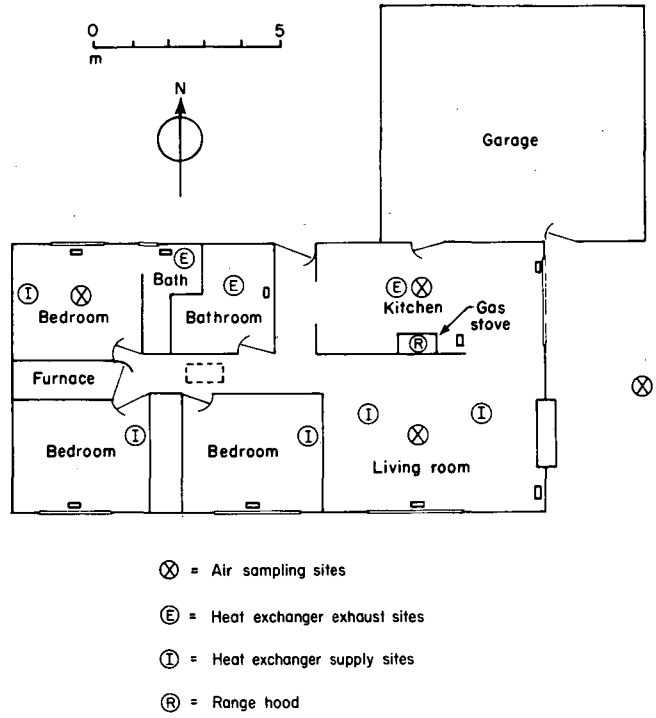

Figure 1. Floor plan of experimental research house.

(XBL 7910-4489A)

fans were used. For all experiments reported, 425 liters (15 ft^3) of natural gas were burned with the oven set at 180°C (350°F), and the two top burners set on high flame. A water-filled pot was placed on each burner. The mean burn time was 35 ± 1 minute. We compared the results of these experiments with those derived from a previously published indoor air quality model[4] and assessed the effectiveness of the two types of mechanical ventilation.

Figure 2 compares the measured and model-derived CO concentration for an infiltration-only experiment. (Note that although the concentration profile modeled represents the whole-house average, the kitchen was the only room actually monitored during range operation.) It was expected that the concentrations in the living room would be near the modeled level and that the concentration in the bedroom would be below the modeled level while the

*This work was supported by the Director, Office of Energy Research, Office of Health and Environmental Research, Human Health and Assessments Division of the U.S. Department of Energy under Contract No. DE-AC03-76SF00098.

†Condensed from Traynor, G.W., et al., (1981), The Effects of Ventilation on Residential Air Pollution Due to Emissions from a Gas-Fired Range, Lawrence Berkeley Laboratory Report LBL-12563.

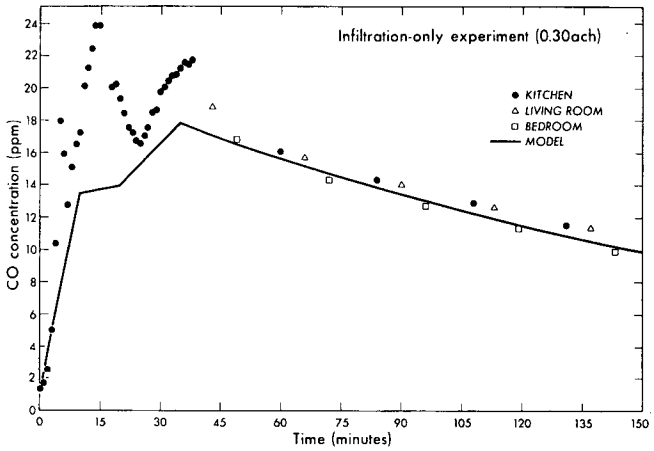

Figure 2. Comparison of measured model-derived CO concentrations in research house (volume = 260 m_3) resulting from burning 425 liters of material gas in a range without mechanical ventilation (0.30 ach). Outdoor CO concentration < 0.1 ppm.

(XBL 8110-1387)

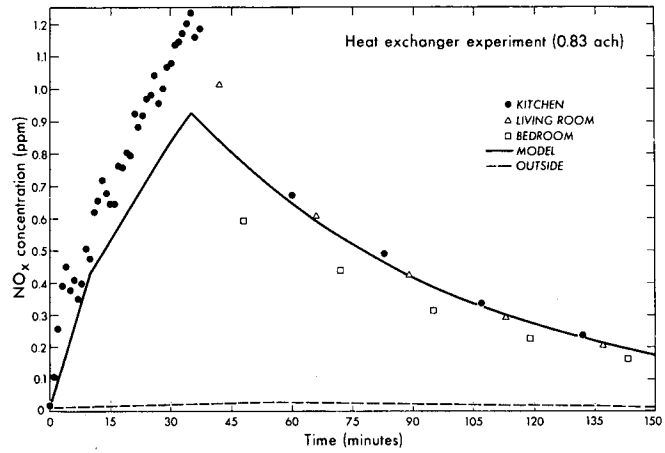

Figure 4. Comparison of measured and model-derived NO_x concentrations in research house (volume = 260 m^3) resulting from burning 425 liters of natural gas in a range with whole-house mechanical ventilation (0.83 ach).

(XBL 8110-1386)

range was in operation, due to incomplete mixing in this time period. When the house air was well mixed, as evidenced by the uniform levels of CO throughout the living space, the average indoor concentration of CO predicted by the model correlated well with measured values (see Figure 2) and probably would correlate well before the house air is mixed, although our data do not show it because the living room and bedroom were not monitored during combustion.

Figure 3 shows the measured and modeled concentrations of CO for an experiment where whole-house mechanical ventilation was used with the gas range in operation. Although the air-exchange rate was almost triple that of the experiment depicted in Figure 2, the CO peak derived from the model was reduced by only 20 percent. This phenomenon occurs because the initial rise in indoor pollutant levels is relatively independent of the air-exchange rate which, over time, plays an increasingly greater role.

Figure 4 compares NO_x concentrations measured in the research house with those derived from the model for an experiment with whole-house mechanical ventilation. Figure 5 shows the measured NO_x concentrations when a range hood was used during gas-stove operation. As is evident, while this spot ventilation increased the air-exchange rate to

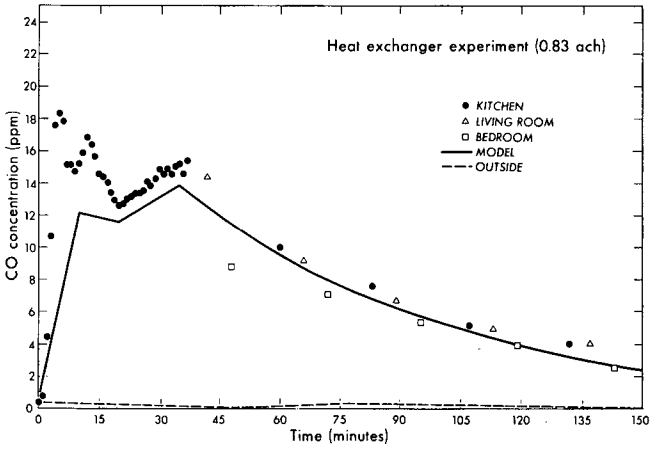

Figure 3. Comparison of measured and model-derived CO concentrations in research house (volume = 260 m^3) resulting from burning 425 liters of natural gas in a range with whole-house mechanical ventilation (0.83 ach).

(XBL 8110-1388)

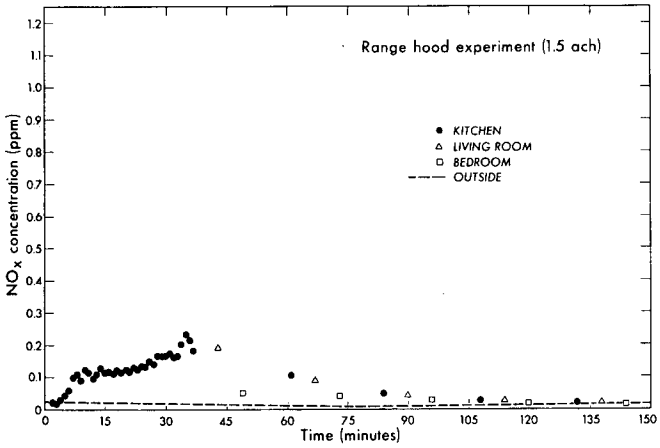

Figure 5. Measured NO_x concentrations in research house (volume = 260 m^3) resulting from burning 425 liters of natural gas in a range using a range hood (1.5 ach).

(XBL 8110-1389)

about twice that obtained with whole-house ventilation (see Figure 3), it reduced NO_x levels in the kitchen to about one-sixth of those observed in the whole-house ventilation experiment. Measurements from six experiments showed that the range hood reduced the average source strengths of the CO, CO_2, and NO_x by 60 to 87 percent. Macriss and Elkins,[9] using NO_2 at comparable range hood flow rates, reported reductions of 40 to 50 percent. This disparity is probably due to an important difference in the criterion used to determine range hood effectiveness. Theirs was based on the reduction of the ratio of NO_2 levels in the kitchen to NO_2 levels in the whole house whereas ours was based on the reduction in source strength.

PLANNED ACTIVITIES FOR FY 1982

Research in FY 1982 will concentrate on two areas. First, further characterization of indoor combustion sources will be made. Specific attention will be given to unvented portable kerosene heaters, wood and coal stoves, and cigarette smoking. Second, further field work will be conducted in occupied and unoccupied dwellings to test the effects of appliance use patterns and occupant behavior on indoor air pollution. Pollutant mixing processes will also be studied.

REFERENCES

1. Cote, W.A., Wade, W.A. III, and Yocum, J.E. (1974), A Study of Indoor Air Quality, U.S. Environmental Protection Agency Report EPA-650/4-74-042, Washington, D.C.

2. Himmel, R.L., and DeWerth, D.W. (1974), Evaluation of the Pollutant Emissions from a Gas-Fired Range, American Gas Association Laboratories Report No. 1492, Cleveland.

3. Yamanaka, S., Hirose, H., and Takada, S. (1979), "Nitrogen Oxides Emissions from Domestic Kerosene-Fired and Gas-Fired Appliances," Atmospheric Environment 13, pp. 407-412.

4. Traynor, G.W. et al., (1981), Indoor Air Pollution from Domestic Combustion Appliances, Lawrence Berkeley Laboratory Report LBL-12886, to be published in Proceedings of the 1981 International Gas Research Conference, Los Angeles, September 28-October 1, 1981.

5. Hollowell, C.D., Budnitz, R.J., and Traynor, G.W. (1977), "Combustion Generated Indoor Air Pollution," in Proceedings of the Fourth International Clean Air Congress, Tokyo, Japan, May 16-20, 1977.

6. Palmes, E.D., Tomczyk, C., and DiMattio, J. (1977), "Average NO_2 Concentrations in Dwellings with Gas or Electric Stoves," Atmospheric Environment 11, pp. 869-872.

7. Melia, R.J.W., et al., (1978), "Difference in NO_2 Levels in Kitchens with Gas or Electric Cookers," Atmospheric Environment 12, pp. 1379-1381.

8. Roseme, G.D., et al., (1979), Residential Ventilation with Heat Recovery: Improving Indoor Air Quality and Saving Energy, Lawrence Berkeley Laboratory Report LBL-9749.

9. Macriss, R.A., and Elkins, R.H. (1977), "Control of the Level of NO_x in the Indoor Environment," in Proceedings of the Fourth International Clean Air Congress, Tokyo, Japan, May 16-20, 1977.

Pollutant Emission Rates from Indoor Combustion Appliances and Sidestream Cigarette Smoke*†

J. R. Girman, J. R. Allen, M. G. Apte, C. D. Hollowell, V. M. Martin, and G. W. Traynor

Indoor combustion appliances and tobacco smoking are primary sources of air pollution in many residential settings. Gas-fired stoves and unvented space heaters, both kerosene- and natural-gas-fired types, emit potentially harmful pollutants such as carbon monoxide (CO), carbon dioxide (CO_2), nitric oxide (NO), nitrogen dioxide (NO_2), sulfur dioxide (SO_2), formaldehyde (HCHO), and respirable particulates. Sidestream tobacco smoking emits CO, CO_2, NO, NO_2, respirable particulates, and a wide range of organic compounds. The degree of the indoor air pollution and, therefore, the degree of health risk to occupants from these sources depends on the type and amount of pollutants entering the occupied space and the type and rate of removal processes occurring, e.g., natural infiltration, mechanical ventilation, and chemical reactions.

Calculating emission rates of these combustion-generated pollutants is an essential step in assessing the degree to which these pollutant sources affect indoor air quality. In this paper, we report the pollutant emission rates derived from our studies of a gas-fired stove, gas-fired unvented space heater, kerosene-fired unvented space heater, and sidestream cigarette smoke. These experiments were carried out in an environmental chamber under controlled ventilation, and our Mobile Atmospheric Research Laboratory[1] was used to measure gas-phase pollutant concentrations.

ACCOMPLISHMENTS DURING FY 1981

Figure 1 illustrates typical pollutant concentration profiles for unvented gas-fired space heaters, and Table 1 lists their emission rates, based on a study currently in progress. These appliances are used principally in the southern and southwestern states. As indicated in Table 1, eight heaters have been tested, ranging in size from 12,700 to 42,200 kJ/hr (12,000 to 40,000 BtuH); O_2 consumption rates are included in this table since there is some concern about its depletion in environments where these heaters are used. The NO_x emission rates from these unvented gas-fired space heaters, which average 12 μg/kJ of N,

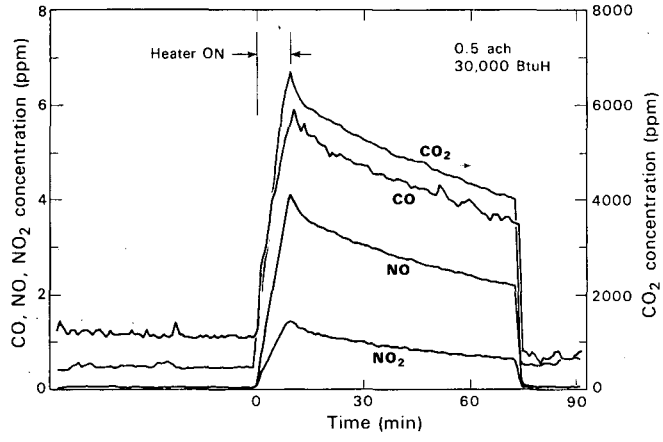

Figure 1. CO_2, CO, NO, and NO_2 emissions from a 31,700-kJ/hr (30,000-BtuH) unvented gas-fired space heater operated in a 27-m^3 environmental chamber without mechanical ventilation (0.5 ach).
(XBL 8110-1377A)

are lower than those of the kerosene space heater or of the gas-fired stove. On the other hand, fuel consumption rates must also be considered when comparing different appliances. The HCHO emission rates from these unvented heaters averaged 0.81 μg/kJ, which is lower than that associated with gas-fired stoves. CO emissions were found to be much more variable than those of other pollutants. Five heaters had low CO emission rates (less than 30 μg/kJ), while the other three heaters had much higher rates. Even in the same heater, CO emission rates were highly variable during repetitive tests. CO_2 emission rates and O_2 consumption rates were relatively constant from heater to heater and test to test.

The variability of CO emissions prompted a series of tests on the sensitivity of emission rates to adjustments of the air shutter. All unvented gas-fired space heaters had previously been tuned with a portable CO analyzer and inspected visually for flame characteristics. With adjustment of the air shutter as the only variable, tests were run on heater 30D by combusting five cubic feet of natural gas in ten minutes under identical ventilation conditions (0.4 ach) and measuring peak CO, NO_2, and NO concentrations. The results of these tests are shown in Figure 2. This plot is similar to an emission vs air/fuel ratio plot with the X-axis representing the percent opening of the air shutter. When the air-shutter opening is increased from 21 percent to 32 percent, the CO emissions increase by a factor of nine. This increase of 21 percent to 32 percent in the air-shutter opening occurs with less than a 10-degree rotation of the shutter, a small adjustment that

*This work was supported by the Director, Office of Energy Research, Office of Health and Environmental Research, Human Health and Assessments Division of the U.S. Department of Energy under Contract No. DE-AC03-76SF00098, and by the Directorate for Health Sciences of the U.S. Consumer Products Safety Commission under Contract No. CPSC-IAG-81-1375.

†Condensed from Girman, J.R., et al. (1981), Pollutant Emission Rates from Indoor Combustion Appliances and Sidestream Cigarette Smoke, Lawrence Berkeley Laboratory Report LBL-12562.

Table 1. Pollutant emission rates from well-tuned, unvented gas-fired space heaters operated at full input.

Heater[a]	ach	No. of Tests	CO μg/kJ	CO_2 μg/kJ	O_2 μg/kJ	HCHO μg/kJ	$N(NO_x)$ μg/kJ	NO_2/NO Volumetric Ratio	Particulates[b] μg/kJ
12D	0.43	3	114	50,000	-67,400	4.20	10	1.46	0.30
20D	0.71	3	29	50,100	-71,700	0.61	14	0.39	0.039
30D[c]	0.59	1	25	49,900	-72,900	0.59	14	0.37	0.006
16A	0.53	1	165	51,500	-71,900	0.55	12	0.85	0.049
40A	0.39	2	63	51,000	-68,900	0.96	14	0.84	0.009
20M	0.38	2	14	50,100	-73,700	0.91	11	0.53	0.079
30M	0.56	1	11	52,600	-73,700	0.43	12	0.34	0.064
40M	0.74	2	13	54,600	-71,300	0.61	12	0.35	0.024

[a]Fuel consumption in thousands of BtuH, e.g., 40 = 40,000 BtuH = 42,200 kJ/hr.

[b]Mass of particulates from 0.0056 to 0.562 μm based upon electric mobility analysis and assuming a particle density of 2.0 g/cm^3.

[c]This heater was subjected to extensive tuning and can be considered to be optimally tuned.

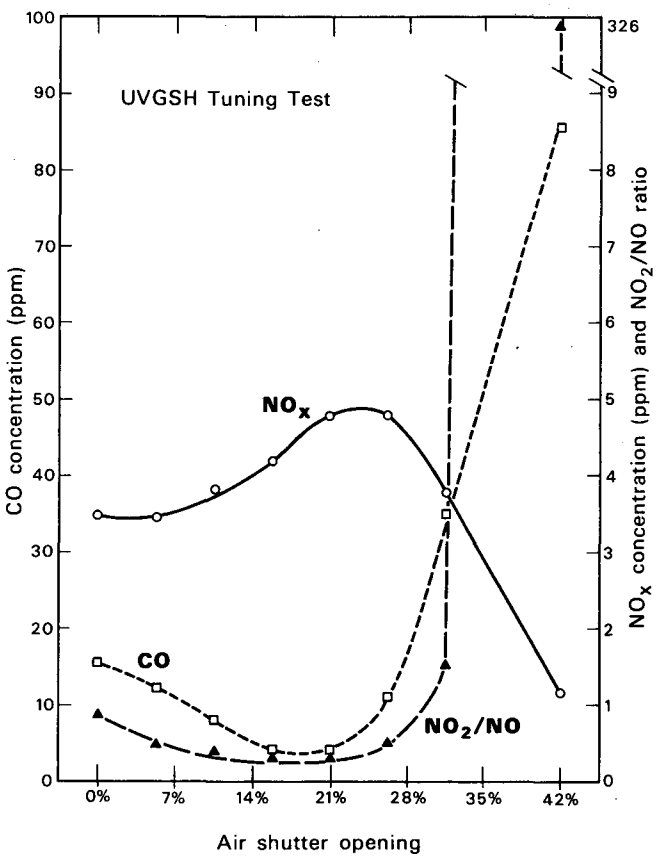

underscores the sensitivity of CO emissions to tuning.

Additional tuning tests were conducted on the 30D to investigate the effect of O_2 depletion on CO emissions. By varying the ventilation rate, steady-state O_2 levels of 20 percent or 18 percent could be achieved. At 20 percent O_2, the steady-state concentration of CO in the chamber could be varied from 4 to 90 ppm by changing the air-shutter opening from 0 to 47 percent open. At 18 percent O_2, the steady-state concentrations of CO could be varied from 7 to 153 ppm by adjusting the air-shutter opening over the same range. This test demonstrated that steady-state O_2 concentrations alone are poor predictors of steady-state CO concentrations.

Conversely, NO_x emissions are not as sensitive to tuning. However, in the excess air regime (air shutter open more than 21 percent), the NO_2 to NO ratio appears to be extremely sensitive to tuning, increasing from 0.3 at a 21-percent opening to

Figure 2. Peak NO_x and CO concentrations and the NO_2-to-NO volumetric ratio vs air shutter opening for a 31,700-kJ/hr (30,000-BtuH) unvented gas-fired space heater after combusting 5 ft^3 of natural gas in a 27-m^3 environmental chamber ventilated at less than 0.5 ach.

(XBL 8110-1376A)

greater than 300 at a 42-percent opening. Thus, although NO_x emissions are not very sensitive to tuning, the fraction of NO_x in the form of NO_2 is very dependent upon the state of tune.

This heater, 30D, as previously tuned and tested, was one of the highest CO-emitting heaters; after applying the results of the tuning curve, however, it was one of the four lowest CO-emitting heaters. Given the unlikelihood that extensive tuning of this nature would be routinely performed in the field, all other unvented heaters used for this experiment were left as tuned previously (using a portable CO analyzer and observing flame characteristics).

Three of these heaters (20M, 30M, 40M), all from the same manufacturer, were the lowest CO emitters, as well as being among the lowest emitters of HCHO and NO_x. Furthermore, emission rate tests showed that these heaters were relatively insensitive to tuning. This insensitivity is illustrated by the results in Table 2, which compares emission rates from the 30D and 40M heaters under two conditions, one with the air shutter fully opened and one with the shutter fully closed. The heaters from this manufacturer incorporate a very different burner design compared to those of the other two manufacturers. Instead of having many small circular ports in a flat, rectangular burner that produce many small "flamelets," this burner has relatively few slots cut across a cylindrically-shaped burner which produce a softer "feathered" flame. It is likely that this burner design accounts for both the lower emission rates and their insensitivity to tuning.

Table 2. Comparison of pollutant emission rates of two poorly tuned, unvented gas-fired space heaters operated at full input.

Heater[a]	ach	CO µg/kJ	CO_2 µg/kJ	O_2 µg/kJ	HCHO µg/kJ	$N(NO_x)$ µg/kJ	NO_2/NO Volumetric Ratio
Fully open air shutter							
30D	0.44	517	43,500	-57,900	20.2	3	289
40M	0.37	8	59,100	-59,100	0.49	12	0.31
Fully closed air shutter							
30D	0.41	159	52,500	-70,800	1.35	11	0.65
40M	0.40	35	49,000	-67,200	0.29	10	0.56

[a]Fuel consumption in thousands of BtuH, e.g., 40 = 40,000 BtuH = 42,200 kJ/hr.

CONCLUSIONS

These data on pollutant emission rates obtained from combustion appliances and sidestream cigarette smoke in an environmental chamber, combined with data on source usage, provide important information for determining the impact of combustion-generated pollutants on indoor air quality under a wide variety of environmental conditions. Other necessary parameters for these determinations are the ventilation rate, reactive decay constants, indoor volume, and outdoor pollutant concentration.

Our laboratory studies have shown that unvented combustion appliances and tobacco smoking, in particular, produce enough pollutants to be of concern, both in single-room environments and, based on calculations, in residential-sized buildings. While our findings suggest that both unvented heaters and sidestream cigarette smoke can pose a health risk in spaces where ventilation is reduced, in the case of unvented gas and kerosene space heaters, the NO_2 emissions are high enough to warrant concern, even under relatively high ventilation conditions.

The burner design of one manufacturer of an unvented gas-fired space heater appears to reduce pollutant emissions significantly and is insensitive to tuning as well, indicating that improvements in burner design should be pursued. Of course, other techniques for reducing or alleviating the effect of pollutant emissions from these sources should also be developed.

Finally, if we are to determine the degree to which occupants are at risk from exposure to combustion-generated pollutants, we need information on (1) occupant usage patterns and (2) specific characteristics of the environments where these heaters are used. Such data are not presently available. A survey of this type should be supplemented by field studies to measure pollutant concentrations in a variety of indoor environments and over a wide range of usage patterns.

PLANNED ACTIVITIES FOR FY 1982

The group is extending its measurements program beyond characterization of emission rates from gas stoves. Measurements of emission from unvented gas appliances will be performed, as well as more extensive measurements than heretofore of emissions from unvented kerosene-fueled space heaters. In addition, consideration is being given to a protocol for characterizing emissions from wood-burning stoves.

Organic Contaminants*†

R. R. Miksch, C. D. Hollowell, and H. E. Schmidt

A significant amount of energy is consumed while heating or cooling outside air as it enters an office building. Recent construction practices have incorporated energy conservation strategies that minimize the amount of outdoor air used for ventilation. In a number of new office buildings occupants have registered complaints of poor indoor air quality.[1,2] As of July 1981, the National Institute of Occupational Safety and Health (NIOSH) had conducted more than eighty investigations of closed office spaces where occupants complained of eye, nose, and throat irritation, as well as drowsiness and headaches.[3] In the majority of these investigations, however, traditional industrial hygiene tests have failed to identify any etiological agent(s) according to established industrial occupational health criteria.

One of several hypotheses is that exposure to organic contaminants contributes to poor indoor air quality. Preliminary data suggest that workers in office environments are exposed to a broad spectrum of compounds present at very low levels relative to permissible exposures but high levels relative to outdoor air. In this paper, preliminary data on the identities and relative amounts of organic contaminants in representative office spaces are discussed, as well as potential sources in new and aged building materials, wet-process photocopiers, smoking, and building maintenance products.

ACCOMPLISHMENTS DURING FY 1981

By sampling air using the porous polymer Tenax-GC and subsequently thermally desorbing trapped organic contaminants, the problems associated with traditional charcoal hygiene tests were largely overcome. Figure 1 shows typical comparative gas chromatograms of equal size air samples taken simultaneously outside and inside a closed office space. Organic contaminants are greater in number and concentrations indoors than outdoors, as indicated by the sizes and number of peaks. For a few samples, comparison of the peak areas with those of external standards indicated that the largest peaks corresponded to air concentrations of a few tenths of a milligram per cubic meter.

Samples were analyzed by gas chromatography-mass spectrometry (GC-MS) to establish identities. Generally, the largest peaks fell into one of three classes of compounds, the largest being aliphatic hydrocarbons, including straight-chain, branched-chain, and derivatives of cyclohexane. These hydrocarbons are derived petroleum distillate-type solvents. The second largest class was alkylated aromatic hydrocarbons, predominately toluene but also including xylenes, trimethyl- and other substituted benzenes, and even methyl- and dimenthyl-napthalenes. These compounds are either solvents themselves or constituents of naphenic-type, petroleum solvent mixtures. The third class observed was chlorinated hydrocarbons, predominately tetrachloroethylene, 1,1,1,-trichloroethane, and trichloroethylene. Miscellaneous other compounds observed were ketones, aldehydes, and benzene.

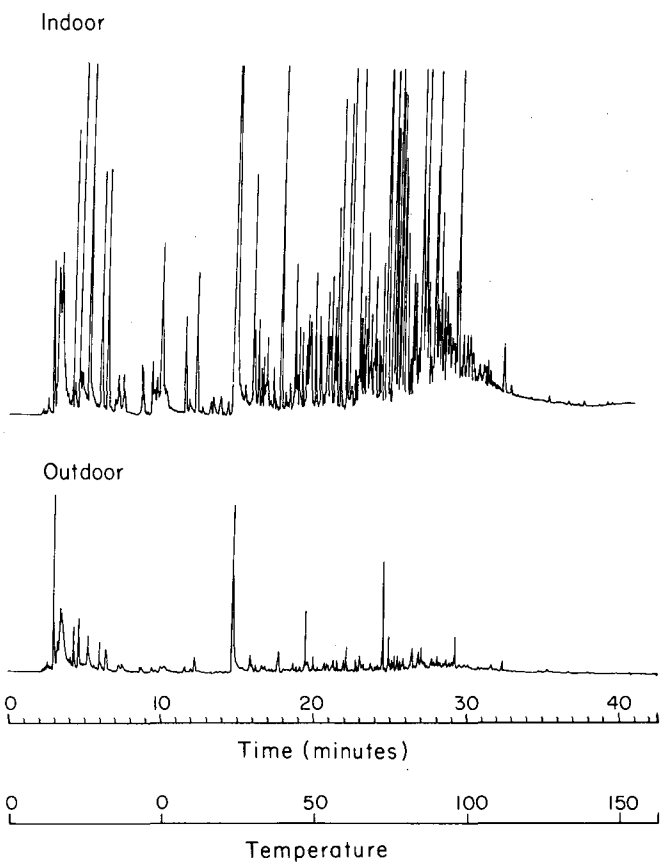

Figure 1. Comparative gas chromatograms for equal size air volumes sampled using the polymer Tenax-GC inside and outside an office where IAQ complaints were registered.

(XBL 808-1727)

*This work was supported by the Assistant Secretary for Conservation and Renewable Energy, Office of Building Energy Research and Development, Building Systems Division of the U.S. Department of Energy under Contract No. DE-AC03-76SF00098.

†Condensed from Miksch, R.R., Hollowell, C.D., and Schmidt, H.E. (1981), Trace Organic Contaminants in Office Spaces, Lawrence Berkeley Laboratory Report LBL-12561.

Several sources of organic contaminants in closed office spaces are (1) new building materials, (2) aged building materials, (3) wet-process photocopiers, (4) tobacco smoke, and (5) building maintenance products. The impact of each of these sources was estimated by considering a hypothetical office with dimensions of 100 X 100 X 10 ft containing 40 workers and using the well-mixed tank ventilation model of Turk.[4] Table 1 summarizes the source characteristics, and Figure 2 displays exposure patterns predicted by the ventilation model for various source-generation patterns.

New building materials are a source of organic contaminants because they contain residual solvents and other compounds remaining after the process of manufacture. Qualitative GC-MS analysis of the headspace vapor standing over representative building materials revealed a great number of compounds, predominantly toluene and aliphatic hydrocarbons. Ketonic solvents and specialty compounds such as butylated hydroxytoluene (BHT) were seen.

Because residual solvents in new building materials will diminish with time as the material "dries out," a trial calculation was performed to estimate how long this process might take for wall-to-wall carpeting in the model office space. Using the following assumptions, we calculated that (1) the emission rate decays exponentially with time; (2) the emission rate initially is 1 mg/ft^2-hr; and (3) the initial solvent load of the carpet is 10 g/ft^2 with a half-life of 300 days, or ten months. The generation pattern will appear constant relative to a daily time frame, and the concentrations and cumulative workday exposures will be inversely proportional to the ventilation rate, as shown graphically in the top third of Figure 2. For the assumed initial emission rate, the nominal organic contaminant concentrations and cumulative exposures are 3.6 mg/m^3 and 29 $mg\text{-}hr/m^3$ at 1.0 air change per hour (ach) and 18 mg/m^3 and 144 $mg\text{-}hr/m^3$ at 0.2 ach.

Among aged building materials, wood and other

Table 1. Characteristics of sources of organic contaminants in a typical office space.[a]

Source	Nominal emission rate (g/hr-office)	Generation pattern	Major known types of organic contaminants emitted
New building materials	10[b]	Continuous	aliphatic hydrocarbons aromatic hydrocarbons ketones esters (formaldehyde) many miscellaneous
Aged building materials	low	Continuous	formaldehyde
Wet-process photocopiers	25[c]	workday	aliphatic hydrocarbons
Smokers	1[d] 0.5[d] 0.25[d] (4)[d]	workday	formaldehyde acrolein nicotine (total particulates) many miscellaneous
Building maintenance products	100[e]	episodic	aliphatic hydrocarbons aromatic hydrocarbons formaldehyde amines chlorinated hydrocarbons many miscellaneous

[a]The typical office being considered had dimensions of 100 x 100 x 10 ft with an occupancy of 40 workers.

[b]Emission rate calculated assuming 1.0 mg/ft^2 for wall-to-wall carpeting after several months.

[c]Emission rate calculated assuming one wet-process photocopier using 1000 g of fluid per week.

[d]Calculated from data in Weber et al.[5]

[e]Emission rate calculated assuming 100 g of product (floor detergent or dusting fluid) applied in 1 hr.

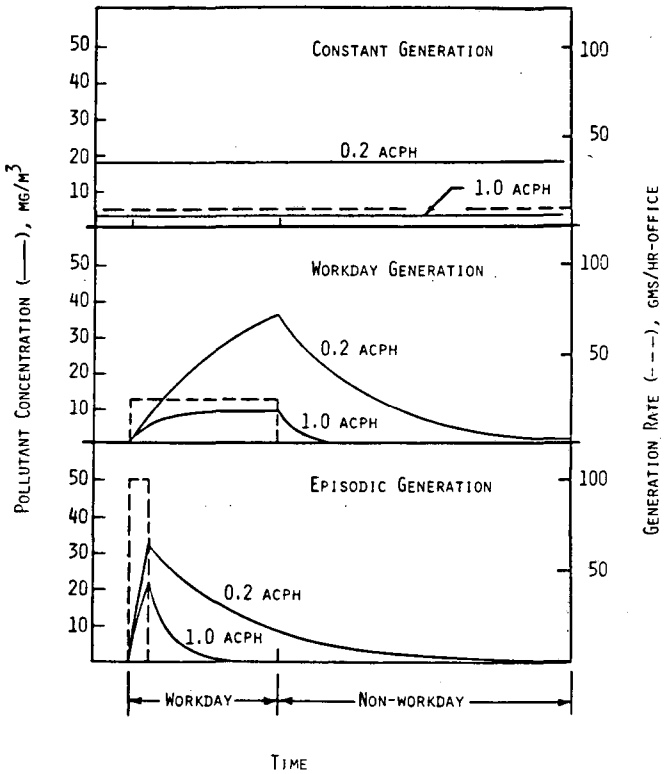

Figure 2. Behavior of mean pollutant exposure levels for different generation patterns predicted by the well-mixed tank model of Turk.[4]

(XBL 818-11301)

products containing urea or formaldehyde are the only well-documented cases where a pollutant, in this case formaldehyde, is emitted. These products are probably not used extensively in new office buildings. Observed formaldehyde levels are low[2,3] and can be reasonably accounted for by smokers (see below). Although aged building materials probably do not generate significant quantities of organic contaminants in most office buildings, they may still affect indoor air quality by adsorbing and desorbing organic contaminants generated from other sources.

Newer, inexpensive wet-process photocopiers can use toner and developer fluids that are very nearly pure petroleum distillate solvents. In the model office with one photocopier operated during the workday, the estimated nominal emission rate is 25 g/hr. As shown in the center of Figure 2, at 1.0 ach the petroleum distillate solvent equilibrates during the workday at a mean concentration of approximately 9 mg/m^3. The cumulative workday exposures are 173 mg-hr/m^3 and 67 mg-hr/m^3 for 0.2 and 1.0 ach, respectively, with an exposure ratio of 2.6.

Tobacco smoke can be a major source of organic pollutants in office spaces, but their effect is difficult to quantify. Data from Weber et al.,[5] on irritating components of passive smoke show 5.3 mg of formaldehyde, 2.3 mg of acrolein, 21.1 mg of total particulate matter, and 1.25 mg of nicotine generated per cigarette. If it is assumed that during the workday in the model office 10 of the 40 workers smoke 20 cigarettes, then, theoretically at 1.0 ach, the concentrations of these pollutants will equilibrate at 0.38, 0.16, 1.5, and 0.1 mg/m^3, respectively. The first two values are higher than observed values.

Building maintenance products comprise a very broad category, and organic contaminants emitted include most solvents and many specialty compounds. The generation pattern is episodic in that products are applied over relatively short time intervals. The lower third of Figure 2 shows the episodic application of 100 g of maintenance product (e.g., dust remover containing aromatic hydrocarbons) over one hour at the beginning of the workday. At ventilation rates of 0.2 and 1.0 ach, respectively, the peak exposures are 32 mg/m^3 and 21 mg/m^3 and the cumulative exposures are 137 and 36 mg-hr/m^3. (The ratio of the latter two values is 3.8.) The exposures could be reduced to zero by conducting maintenance activities immediately after the workday.

CONCLUSIONS

Occupants of new office buildings are exposed to elevated levels, relative to outdoor air, of a large variety of organic contaminants that are judged incapable of inducing adverse health effects by existing hygiene criteria. However, the criteria may be inadequate, given that (1) additive or synergistic effects are not adequately addressed; (2) the criteria are generally based on acute exposure studies whereas here the exposure is chronic; (3) the population at risk is more diverse, including women and elderly workers; and (4) annoyance from odorant effects is not considered.

Several sources considered here (new building materials, photocopiers, tobacco smoke, and building maintenance products) are of roughly equal magnitude with respect to emissions of organic contaminants. Implementation of control strategies must consider the nature and generation pattern of each source. For new building materials, further research may define an acceptable waiting period prior to occupancy or a period of high ventilation rates while they "dry out." Workday pollution from photocopiers and tobacco smoke may be reduced by increased ventilation, but not as efficiently as by source removal. Episodic pollution from building maintenance products can be reduced by increased ventilation, but a better strategy is to offset product use from the workday period.

PLANNED ACTIVITIES FOR FY 1982

For the near future, experimental work on organics other than the aldehydes has been suspended, primarily because of funding limitations. However, considering the importance of organics, the group anticipates work in this area at some time in the future and is maintaining an active relationship with those working on organics, particularly our collaborators at the University of California, Berkeley.

REFERENCES

1. Rand, G. (1979), Amer. Inst. of Arch. J. 68, pp. 38-41.

2. Turiel, I., et al. (1981), "The Effects of Reduced Ventilation on Indoor Air Quality in an Office Building," submitted to J. Air Pollut. Contr. Assoc., Lawrence Berkeley Laboratory Report LBL-10479.

3. Keenlyside, R. (1981), National Institute of Occupational Safety and Health, Cincinnati, Ohio, personal communication.

4. Turk, A. (1963), "Measuring Odorous Vapors in Test Chambers," ASHRAE J. 5, pp. 55-58.

5. Weber, A., Jermini, C., and Grandjean, E. (1977), "Irritating Effects on Man of Air Pollution Due to Cigarette Smoke," Amer. J. Pub. Health 66, pp. 672-676.

A New Passive Monitor for Determining Formaldehyde in Indoor Air*†

K. L. Geisling, J. R. Girman, R. R. Miksch, S. M. Rappaport, and M. K. Tashima

Recent concern that exposure to low levels of formaldehyde (HCHO) may pose a health hazard[1] has prompted many investigations of HCHO levels in homes and office buildings. A serious obstacle in these investigations has been the lack of a simple, accurate, and inexpensive system for sampling HCHO in air. Bubbling air through water or aqueous solutions of sodium bisulfite ($NaHSO_3$) is presently the most common method for monitoring HCHO. However, sampling systems that employ bubblers have many disadvantages: (1) the systems are large and bulky, making them difficult to transport from one sampling site to another; (2) bubbler systems employ pumps, with some type of flow control system, that require frequent calibration and are subject to breakdown; (3) during the long sampling periods required to determine low levels of HCHO, refrigeration is necessary to prevent loss of samples through evaporation; and (4) samples must also be refrigerated during shipping and storage to prevent evaporation. In general, bubbler systems are unwieldy, difficult to operate, expensive, and unreliable.

We have developed a passive sampler that collects HCHO under the principle of diffusion and consists of a glass-fiber filter treated with sodium bisulfite ($NaHSO_3$) contained in a glass vial. Formaldehyde diffuses through the vial and reacts with the $NaHSO_3$ to form a stable addition product. If the concentration at one end of a diffusion path is maintained at zero, Fick's First Law of Diffusion yields an expression relating the quantity of a gas transferred through the diffusion path to the ambient concentration of the gas and the time of exposure. The rate at which the device samples a contaminant species from ambient air is obtained from this expression. The constants in the expression are the cross-sectional area of the diffusion path and the diffusion coefficient. The sampling rate of a passive sampler based on diffusion requires no correction for temperature and pressure variations over the typical range of conditions encountered in indoor air quality audits.[2] Passive sampling devices based on the laws of permeation and diffusion offer many advantages for indoor sampling of a number of reactive gases.[2-4] The sampler reported here is lightweight and small, can be operated by untrained personnel, and is very inexpensive. Once in the field, the passive monitor is merely uncapped, placed in a vertical position, and left for the appropriate sampling period. Following exposure, the sampler is recapped and returned to the laboratory for analysis.

ACCOMPLISHMENTS DURING FY 1981

Because the diffusion coefficient of HCHO in air is not well documented, we designed a series of experiments to establish a calibration curve relating the amount of HCHO transferred through the diffusion tube (and trapped on the treated filters) to its ambient concentration. Glass-fiber filters were treated with 5-percent $NaHSO_3$, dried under N_2, and then placed in the bottom of glass vials whose area-to-length ratio is 0.517 cm (2.5 cm in diameter and 9.5 cm in length). These sampling devices were exposed to five HCHO concentrations ranging from 0.05 to 0.8 ppm for one-week sampling periods. Test atmospheres of HCHO gas were produced by a novel generation system in which trioxane, the cyclic trimer of HCHO, is decomposed over an acid catalyst to monomeric HCHO. Dilute HCHO gas of known concentration was continuously pumped into two chambers, each containing five passive monitors (Figure 1). Air in the chambers was kept well mixed, and the temperature was maintained at 19 to 22°C. The dilute gas stream was drawn out of the chambers at a rate high enough to assure that the

*This work was supported by the Director, Office of Energy Research, Office of Health and Environmental Research, Human Health and Assessments Division of the U.S. Department of Energy under Contract No. DE-AC03-76SF00098.

†Condensed from Geisling, K.L., et al. (1981), A New Passive Monitor for Determining Formaldehyde in Indoor Air, Lawrence Berkeley Laboratory Report LBL-12560.

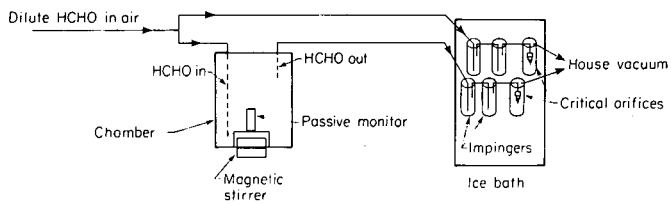

Figure 1. Schematic diagram of the apparatus used for evaluating the formaldehyde passive monitor. For our study, the apparatus was constructed in duplicate, and the two chambers were placed in an insulated box, with each chamber containing five passive monitors.

(XBL 816-2374)

passive monitors withdrew a maximum of 5 percent of the HCHO in the test atmosphere while the gas was present in the chamber. Bubbler samples were collected in parallel to validate the concentration of HCHO in the gas stream from the generation system.

Following exposure, distilled water was added directly to the passive monitors to elute the sodium formaldehyde bisulfite formed on the filters. The resulting solutions (and the bubbler solutions) were analyzed by the wet-chemical, spectrophotometric chromotropic acid method currently recommended by the National Institute of Occupational Safety and Health.[4] The results of the calibration experiments are given in Table 1, and the data are plotted in Figure 2. The equation of the least-squares line for the data is given by the expression:

$$\mu g \text{ HCHO collected} = 0.283 \times (\text{ppm-hr}) + 0.094$$

The correlation coefficient given by the regression analysis is 0.997, indicating that the collection

Table 1. Results of calibration experiments for the HCHO passive monitor.

Known HCHO air conc.[a] (ppm)	Reference method HCHO air conc.[b] (ppm)	Duration of sampling (hr)	HCHO collected[c] (μg)
0.058	0.060 ± 0.002	162.67	2.96 ± 0.22
0.096	0.101 ± 0.003	154.52	4.39 ± 0.17
0.201	0.204 ± 0.006	141.17	8.40 ± 0.26
0.397	0.407 ± 0.008	158.84	17.5 ± 1.7
0.839	0.871 ± 0.025	160.24	39.4 ± 2.4

[a]Based on gravimetrically determined generation rate of HCHO.

[b]Based on 24-hr bubbler samples, average of 14 observations ± absolute standard deviation.

[c]Average ± absolute standard deviation.

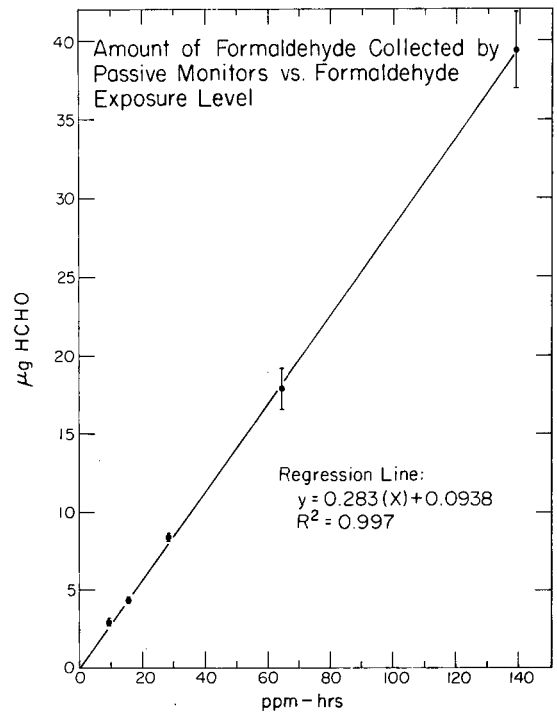

Figure 2. Amount of formaldehyde captured by the passive monitor plotted as a function of HCHO exposure level.

(XBL 816-2372)

of HCHO by the passive monitor is well described by the laws of diffusion. The linearity of the calibration curve also indicates that the rate at which HCHO was trapped by the $NaHSO_3$-treated filters did not vary as concentration increased. It may be inferred, therefore, that the collection efficiency of the passive monitor for HCHO was high enough to provide excellent performance over a wide range of HCHO concentrations.

An important requirement of any field sampling device is that it retain its active element while being stored prior to exposure in the field and that the collected sample remain stable with no losses during storage and shipment after exposure. We have performed tests to determine the pre- and post-exposure storage stability of our HCHO passive monitor for periods of one and two weeks. The data are presented in Tables 2 and 3 and show that the passive monitors stored prior to exposure lost none of their ability to collect HCHO. Also, no significant loss (within one standard deviation) of HCHO was detected for samples stored after exposure.

CONCLUSIONS

The calibration curve developed in our experiments enables a user of this passive monitor to determine time-weighted concentrations of HCHO by measuring the amount collected on the $NaHSO_3$-treated filter in a known exposure time. In

Table 2. Pre-exposure storage stability of passive monitors.

Storage time	HCHO Concentration (ppm)		Concentration ratio stored/non-stored
	Passive monitors stored prior to exposure[a]	Passive monitors exposed immediately after preparation[b]	
1 wk	1.42 ± .07 (n=7)	1.40 ± .05 (n=4)	1.01
2 wk	1.36 ± .10 (n=8)	1.33 ± .07 (n=4)	1.02

[a]Passive monitors were prepared, filled with N_2 and capped, and stored at room temperature before exposure to HCHO. Average HCHO concentration ± absolute standard deviation for n samples.

[b]Average HCHO concentration ± absolute standard deviation for n samples. Passive monitors were exposed with stored samples.

Table 3. Post-exposure storage stability of passive monitors.

Storage time	HCHO Concentration[a] (ppm)		Concentration ratio stored/non-stored
	Passive monitors stored after exposure[b]	Passive monitors analyzed after exposure	
1 wk	1.24 ± .07 (n=7)	1.35 ± .09 (n=5)	0.92
2 wk	1.41 ± .06 (n=8)	1.36 ± .02 (n=4)	1.04

[a]Average HCHO concentration ± absolute standard deviation for n samples.

[b]Stored at room temperature.

addition, lower detection limits of HCHO concentration may be obtained from the calibration curve for various sampling periods. In an occupational environment, an eight-hour sample would be sufficient to detect the permissible exposure limit of 3 ppm set by the Occupational Safety and Health Administration; in a residential environment, a 100-hr sample would allow detection of 0.1 ppm for indoor air quality audits.

The rate at which the passive monitor described here samples HCHO in ambient air is 3.84 ± 0.16 cc/min at STP. This rate was obtained by converting the units of μg/ppm-hr from the slope of the calibration curve. The collection rate of HCHO may be varied to increase or decrease the detection limits by simply modifying the geometry of the passive monitor.

Tests to date have demonstrated excellent results for storage periods as long as two weeks, and we believe that the samplers may be stored for much longer periods.

PLANNED ACTIVITIES FOR FY 1982

The formaldehyde passive monitor will be developed further and field tested during the coming year. In addition, substantial efforts will be devoted to development of a carbon monoxide passive monitor. Finally, we will continue to test and evaluate commercially available passive monitors for their suitability in indoor air monitoring.

REFERENCES

1. Gunby, P. "Fact or Fiction about Formaldehyde," JAMA 243, pp. 1697-1703.

2. Palmes, E. D., et al. (1976), "Personal Sampler for Nitrogen Dioxide," Am. Ind. Hyg. Assoc. J. 37, pp. 570-577.

3. McCammon, C.S. Jr., and Woodfin, J.W. (1977), "An Evaluation of a Passive Monitor for Mercury Vapor," Am. Ind. Hyg. Assoc. J. 38, pp. 378-386.

4. National Institute of Occupational Safety and Health (1977), "NIOSH Manual of Analytical Methods," 2nd ed., Publication No. 77-157A, DHEW (NIOSH), Cincinnati, Ohio.

5. Nelms, L. H., Reiszner, K. D., and West, P. W. (1977), "Personal Vinyl Chloride Monitoring Device with Permeation Technique for Sampling," Anal. Chem. 49, pp. 994-998.

Distribution of Indoor Radon Concentrations and Source Magnitudes: Measurements and Policy Implications*†

A. V. Nero, Jr., M. L. Boegel, S. M. Doyle, B. A. Moed, and W. W. Nazaroff

Substantial effort has been devoted in recent years to studying radon 222 and its daughters in U.S. residences. As a part of our study of the effect of ventilation on indoor concentrations, our group has carried out surveys in conventional and energy-efficient houses, measuring airborne radon concentrations and air-exchange rates concurrently. These surveys have been complemented by measurements of radon emanation rates from building materials commonly used in the United States. Based on this earlier work, this report examines the frequency distribution of indoor radon concentrations and air-exchange rates found in these studies, discusses radon source magnitudes extracted from our data, compares the distribution of source magnitudes with information on emanation rates from source materials, and, finally, considers the ways in which variability in source magnitude might affect regulatory efforts to control indoor concentrations of radon and its daughters.

ACCOMPLISHMENTS DURING FY 1981

Radon Concentrations and Air-Exchange Rates

Three housing groups--consisting of 17 "energy-efficient" houses in the United States and Canada,[1] 29 conventional houses in the San Francisco area,[2] and 52 houses in a community in rural Maryland[3]--were surveyed. In each case radon, and usually radon-daughter, concentrations were measured simultaneously with infiltration rate, radon in grab samples, and infiltration by a tracer-gas-decay technique. To establish a correspondence between the radon concentration and the ratio of source magnitude to air-infiltration rate, we asked occupants to close windows and doors for the night prior to measurements. Our results, presented in Figure 1, show clearly that radon concentrations do not correlate strongly with air-exchange rates in any of these survey groups. Moreover, it is evident that, in these houses, radon concentrations are distributed over a much broader range than are infiltration rates. From these observations, we suggest that the wide distribution of radon concentrations found in this and other work[4] arises largely from variations in source magnitude.

Distribution of Radon Source Magnitudes

For steady-state conditions, the radon source magnitude, i.e., the radon entry rate per unit house volume, may be estimated by taking the product of the radon concentration and the air-exchange rate. Figure 2 displays a frequency distribution of the source magnitudes calculated from the data of Figure 1. Values range over almost

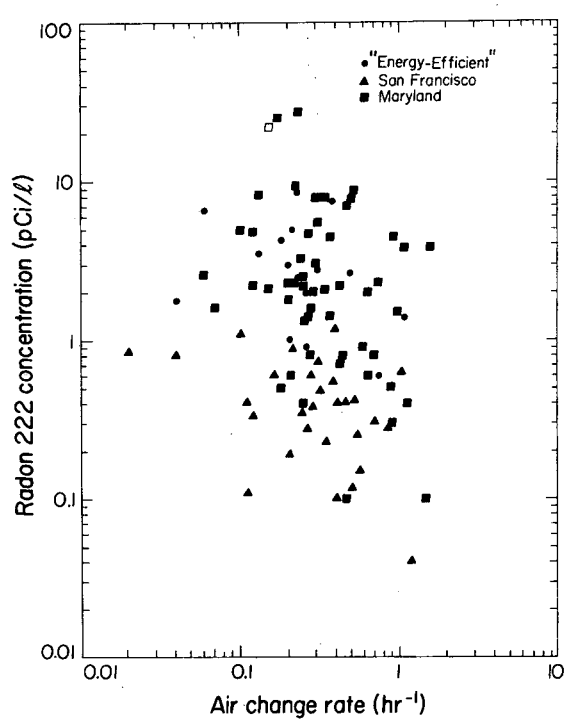

Figure 1. Radon concentrations and air-change rates in U.S. residences. The figure is a composite of results from three survey groups: "energy-efficient" houses in the United States and (one) in Canada; conventional houses in the San Francisco area; and conventional houses in a community in rural Maryland.

(XBL 818-8115)

*This work was supported by the Assistant Secretary for Conservation and Renewable Energy, Office of Building Energy Research and Development, Building Systems Division, and by the Director, Office of Energy Research, Office of Health and Environmental Research, Human Health and Assessments Division and Pollutant Characterization and Safety Research Division of the U.S. Department of Energy under Contract DE-AC03-76SF00098.

†Condensed from Nero, A.V., and Nazaroff, W.W. (1981), Distribution of Indoor Radon Concentrations and Source Magnitudes: Measurements and Policy Implications, Lawrence Berkeley Laboratory Report LBL-12565.

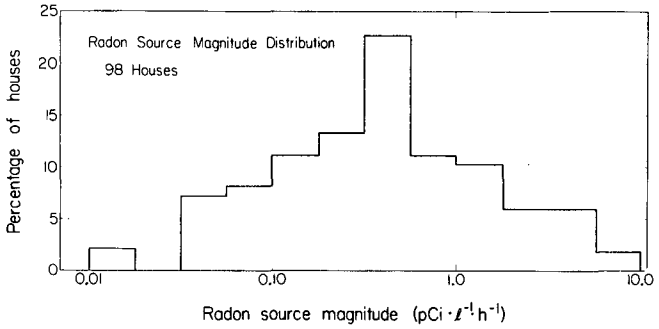

Figure 2. Frequence distribution of radon source magnitude. For each of 98 houses, the radon entry rate per unit volume is calculated from the radon concentration and air-change rate given in Figure 1.

(XBL 818-1146)

three orders of magnitude. The geometric standard deviation of the distribution is similar to that for the radon concentrations in these houses and much larger than that for the infiltration rates. This distribution is similar to that obtained for residences in England.[5]

Because this distribution of source magnitudes is based on analysis of grab samples, it contains some uncertainty associated with the assumption that measured parameters are constant before sampling, which may not be the case. This uncertainty aside, the source magnitudes measured represent instantaneous values only. When measurements are repeated in a single house, the source magnitudes are found to vary significantly, although not nearly as widely as the distribution seen in Figure 2. The distribution of time-averaged source magnitudes can therefore be expected to have a mean and standard deviation similar to those for Figure 2. Furthermore, in an individual house, the source magnitude may correlate with infiltration rate in such a way that the indoor radon concentration does not vary as much with time as the source magnitude.[6] Hence, our observation that most of the variation in radon concentration arises from variations in source magnitude, when derived from grab-sample measurements, may also apply to time-averaged values of these parameters.

Contribution of Building Materials and Soil to Source Magnitudes

The major sources of radon in most buildings are thought to be building materials or underlying soil and rock. Table 1 (adapted from Ingersoll[7]) presents radon emanation rates and radionuclide concentrations for concrete samples from nine metropolitan areas in the United States. The average radon emanation rate from all samples tested was 0.8 pCi $kg^{-1}hr^{-1}$. A concrete slab 0.2 m thick, with an average emanation rate and a typical density of 2000 kg/m^3, would have an emanation rate, expressed per unit area, of approximately 0.04 pCi $m^{-2}sec^{-1}$. For a one-story house, interior height 2.4 m, placed on this concrete slab, the corresponding source magnitude would be 0.07 pCi $l^{-1}hr^{-1}$, an order of magnitude below the average source magnitude of 0.9 pCi $l^{-1}hr^{-1}$ for our 98-house sample.

In contrast to concrete, the soil can contribute a large portion of the observed radon source magnitude. A typical radon flux from the soil is 0.4 pCi m^{-2} sec^{-1} (Ref. 8), which would contribute 0.7 pCi l^{-1} hr^{-1} to the house postulated above, assuming this typical flux gained entry to the interior. Our group has recently begun to study the specific question of radon transport, important if the source of indoor radon is to be understood and if information on radionuclide concentrations or radon fluxes is to be used as a basis for identifying geographic areas where high indoor radon concentrations may be endemic.

Risk Assessment and Control Strategies

The considerable effort now being devoted to

Table 1. Emanation rates and radionuclide concentrations in ordinary concrete.

Origin	No. of samples	Emanation rate per mass (pCi kg^{-1} hr^{-1}) Range	Mean	S.D.	Elemental concentrations (mean) U (ppm)	Th (ppm)	K (%)	Average escape-to-production ratio (%)
Albuquerque, N. Mex.	12	0.70-1.95	1.22	0.35	2.5	6.0	1.5	22
Kansas City, Mo.	12	0.40-0.65	0.53	0.07	1.0	2.0	0.7	25
Philadelphia, Penn.	7	0.35-0.55	0.42	0.08	0.6	1.5	0.7	17
Salt Lake City, Utah	9	0.50-0.75	0.64	0.08	2.0	4.0	0.6	14
San Francisco - Oakland	21	0.65-1.10	0.83	0.12	1.5	3.0	0.6	24
Austin, Texas	8	0.60-0.92	0.73	0.12	1.3	1.5	0.8	24
San Antonio, Texas	8	0.27-0.72	0.46	0.14	3.0	7.5	1.5	8
Chicago, Ill.	12	0.25-1.39	0.66	0.36	1.5	2.0	0.5	25
St. Paul - Minneapolis, Minn.	5	0.54-0.75	0.62	0.09	1.5	4.0	1.5	19
Knoxville, Tenn.	6	0.46-0.78	0.59	0.12	1.0	1.2	0.5	23

assessing the risk from indoor exposure to radon daughters should take explicit account of the wide variation in indoor concentrations. Whereas average exposures are the basis for estimating population risks, knowledge of the frequency distribution is necessary for estimating individual risks. Data presently available suggest that millions of the U.S. population are exposed to concentrations ten times the average. It appears appropriate that regulatory efforts be designed to avoid such excessive exposure of individuals, at the same time achieving an acceptable average exposure of the population as a whole.[9]

Controlling average exposures and avoiding excessively high individual exposure requires attention to major factors affecting indoor concentrations, i.e., ventilation rates and source magnitudes. Because variations in the latter appear to be the principal cause of variations in indoor concentrations, examination of the geographic distribution of source magnitudes and of its relationship to population distribution may be a critical requirement for identifying the portion of the population subjected to excessive exposures and for designing programs to reduce such exposures.

CONCLUSIONS

Indoor radon concentrations measured by our group vary over a large range and do not correlate well with infiltration rate. Calculation of source magnitudes for the houses monitored yield values ranging over three orders of magnitude, and this variation appears to be the main cause of the variation in indoor concentrations. Radon emanation rates from building materials such as concrete do not account for the source magnitudes observed. On the other hand, the radon flux from soil averages ten times as much as that from concrete and could account for the source magnitudes observed. The observed distribution in indoor concentrations suggests that a significant portion of the population is subject to unusually high risks, and variations in source magnitude need to be considered in developing strategies for identifying this portion of the population and for reducing indoor concentrations.

PLANNED ACTIVITIES FOR FY 1982

Selected field studies of concentrations and sources will continue. A major element will be a long-term, automatic study of infiltration rates, radon concentrations, and radon source indicators at a single house. In addition, efforts will continue on examining the potential for characterizing radon source strengths on a geologic or geographic basis.

REFERENCES

1. Hollowell, C.D., et al. (1980), Radon in Energy Efficient Residences, Lawrence Berkeley Laboratory Report LBL-9560.

2. Berk, J.V., et al. (1979), "Radon Measurements and Emanation Studies," in "Energy Efficient Buildings Program," chapter from Energy and Environment Division Annual Report 1979, Lawrence Berkeley Laboratory Report LBL-10704.

3. Moschandreas, D.J., Rector, H.E., and Tierney, P.O. (1981), A Survey Study of Residential Radon Levels, Geomet Technologies, Report ES-877, Rockville, Md.

4. George, A.C., and Breslin, A.J. (1978), "The Distribution of Ambient Radon and Radon Daughters in Residential Buildings in the New York-New Jersey Area," in Natural Radiation Environment III, T.F. Gesell and W.M. Lowder, Eds., 2 Vols., Technical Information Center, U.S. Department of Energy Report CONF-780422, pp. 1272-1292.

5. Cliff, K.D. (1978), "Assessment of Airborne Radon Daughter Concentrations in Dwellings in Great Britain," Phys. Med. Biol. 23, pp. 696-711.

6. Nazaroff, W.W., Boegel, M.L., and Nero, A.V. (1981), Measuring Radon Source Magnitude in Residential Buildings, presented at meeting on Radon and Radon Daughter Measurement, Montgomery, Ala., Aug. 27-28, Lawrence Berkeley Laboratory Report LBL-12484.

7. Ingersoll, J.G. (1981), A Survey of Radionuclide Contents and Radon Emanation Rates in Building Materials Used in the United States, submitted to Health Phys., Lawrence Berkeley Laboratory Report LBL-11771.

8. Wilkening, M.H., Clements, W.E., and Stanley, D. (1972), "Radon-222 Flux Measurements in Widely Separated Areas," in Natural Radiation Environment II, J.A.S. Adams et al., Eds., U.S. Energy Research and Development Administration Report CONF 26-720805, Washington, D.C.

9. Nero, A.V. (1981), Indoor Radon Exposures from Radon and Its Daughters: A View of the Issue, Lawrence Berkeley Laboratory Report LBL-10525.

Instrumentation for a Radon Research House*†

W. W. Nazaroff, A. V. Nero, Jr., K. L. Revzan, and A. W. Robb

We have designed and built a highly automated monitoring and control system for studying radon and radon-daughter behavior in residences. The system has been installed in a research "house," a test space contained in a two-story wood-framed building, which enables us to conduct controlled studies of (1) pollutant transport within and between rooms, (2) the dynamics of radon-daughter behavior, and (3) techniques for controlling radon and radon daughters. The system's instrumentation is capable of measuring air-exchange rate, four-point radon concentration, individual radon-daughter concentrations, indoor temperature and humidity, and outdoor weather parameters (temperature, humidity, wind speed, and wind direction). It is also equipped with modules that control the injection of radon and tracer gas into the test space, the operation of the forced-air furnace, the mechanical ventilation system, and the mixing fans located in each room. A microcomputer controls the experiments and records the data on magnetic tape and on a printing terminal. The data on tape is transferred to a larger computer system for reduction and analysis. As programmed, the computer provides substantial flexibility in experimental design, thus enabling us to collect large amounts of data from diverse experiments with relatively little manual effort.

The test space, three rooms on the first floor of the building with a total floor area of 54 m^2, has been renovated to assure that the thermal and air-leakage characteristics of the envelope conform to current energy-efficient building practices. Heat is provided by a forced-air furnace with supply registers located in each room. Each room has several small blowers mounted on the walls to facilitate mixing. The speed of the blowers is controlled by variable transformers, and their power is switched under computer control. Except for the radon-daughter analyzer, the instrumentation system is located in a fourth first-floor room that is isolated from the test space.

In this report, we describe the essential design and function of the instrumentation system as a whole, singling out those components that measure ventilation rate, radon concentration, and radon-daughter concentrations.

*This work was supported by the Assistant Secretary for Environment, Office of Health and Environmental Research, Human Health and Assessments Division, and the Assistant Secretary for Conservation and Solar Energy, Office of Buildings and Community Systems, Buildings Division, of the U.S. Department of Energy under Contract No. DE-AC03-76SF00098.

†Nazaroff, W.W., Revzan, K.L., and Robb, A.W. (1981), Instrumentation for a Radon Research House, presented at the Symposium on Air Pollution, Health, and Energy Conservation, University of Massachusetts, Amherst, Mass., October 13-16, 1981, Lawrence Berkeley Laboratory Report LBL-12564.

ACCOMPLISHMENTS DURING FY 1981

Microcomputer System

The microcomputer system is a modified commercial product (Intel 80/20-4) that has four circuit boards in a chassis with a power supply. The microcomputer chip is the key element of one board. Two of the remaining boards contain most of the system memory, which is of two types: random-access memory (RAM) for data and temporary program storage and erasable programmable read-only memory (EPROM) for storing programs over long time periods. The fourth circuit board contains special circuits such as a real-time calendar/clock and a 16-channel analog multiplexer coupled to an analog-to-digital converter. The microcomputer system and its interfaces to other components of the instrumentation system are shown schematically in Figure 1.

The uncommitted interface links are available to accommodate additional instruments and/or to control other devices that future experimental goals may require. The system software was designed to provide great flexibility in experimental specification and to be relatively easy and inexpensive to develop and modify. The program through which the user communicates with the system, written in BASIC, enables the user to command the system to automatically execute a series of quite different experiments. An interpreter for the BASIC program resides in EPROM.[1]

Ventilation Measurement

Ventilation rate is measured by tracer-gas decay using sulfur hexafluoride (SF_6). In the simplest case, where the air within the test space is considered to be well-mixed, the time constant in the exponential decay of the tracer-gas concentration gives the ventilation rate. Our system can sequentially sample the concentration at four points with a minimum interval of one minute between samples, the limiting factor being the response of the SF_6 analyzer. Nominally, three of these points would be used to measure the concentration of SF_6 in the three rooms, enabling us to determine the degree of mixing among the rooms. We have also provided four injection lines that are switched on and off by the computer; the flow rate for the tracer is adjusted manually. Three of these lines, their outlets placed near mixing fans, are used to supply SF_6 independently to the three rooms; the fourth line is installed in the furnace return duct to supply the entire test space. The SF_6 concentration is measured by a commercially available, non-dispersive infrared (NDIR) analyzer (Foxboro Wilks, Model Miran 101), calibrated using

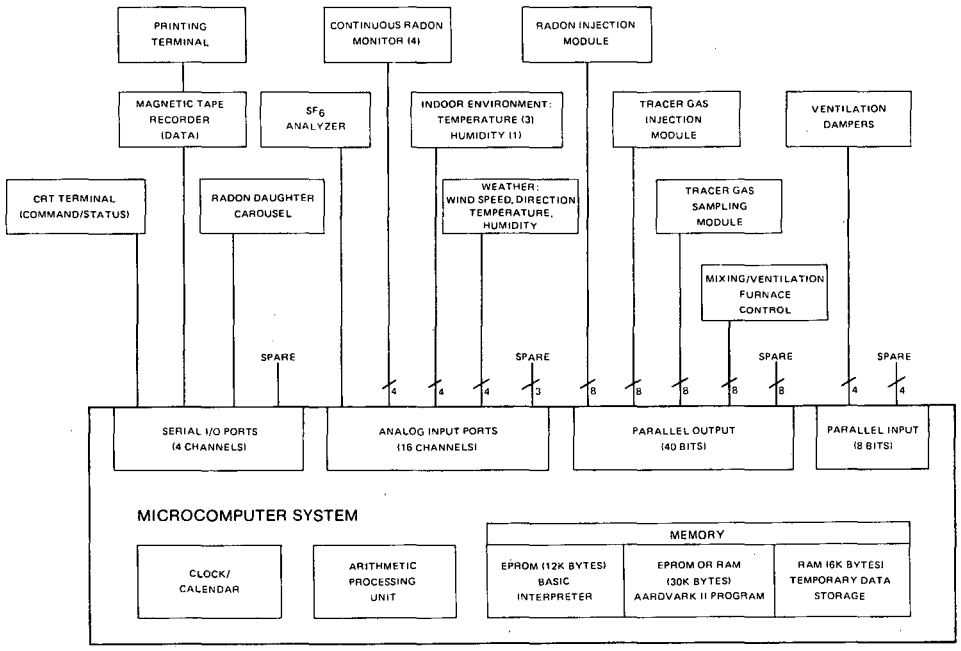

Figure 1. Instrumentation system for a radon research house.

(XBL 821-31)

three compressed-air tanks containing known concentrations of SF_6. In addition to using SF_6 for measuring ventilation rates, we plan to use this tracer gas to examine air movement and mixing within a room and between rooms.

Radon Injection and Measurement

We inject radon into the test space up to a concentration of about 50 pCi/l--the high end of the range of concentrations found in houses. Setting the concentration at this level enables us to measure radon and radon daughters fairly precisely. This concentration is also high enough to assure that contributions of outdoor levels of radon and daughters will not affect indoor levels. The radon we inject is derived from 200 microcuries of ^{226}Ra, precipitated as a stearate. The radium is contained between two filters in a specially designed, stainless-steel holder. Air is blown through the holder and distributed to one or more of four points: one in each of the three rooms and one mounted below the roof eave outdoors.

The radon concentration is measured with a Continuous Radon Monitor (CRM), after the design of Thomas.[2] Filtered air is drawn through a scintillation cell, 170 ml in volume. Alpha particles that are created within the cell from the decay of radon and two of its daughters, ^{218}Po and ^{214}Po, produce light flashes when they strike the phosphor. The light is detected by a photomultiplier tube; the signal is then amplified and the pulses counted. There are four CRMs in this instrumentation system, one for each room with the fourth uncommitted. Each radon monitor is interfaced to the computer through an analog input channel. The output voltage of the CRM is proportional to the total in its counter, which resets automatically after reaching 1023 counts. The radon monitors are calibrated by comparing their response to that of a scintillation cell calibrated with standard reference method ^{226}Ra solution (National Bureau of Standards). The sensitivity of the monitor, defined as the concentration at which the relative standard deviation in the measurement is 50 percent, is 0.2 pCi/l for a three-hour integration interval.

Radon-Daughter Measurement

Radon-daughter concentrations are measured with an automated instrument, the Radon-Daughter Carousel (RDC), which has seven filter holders mounted near the edge of and uniformly spaced around a platter, 25 cm in diameter. Air is drawn through a filter (Millipore, 25 mm diameter, 0.4-0.8 m pore size) nominally at 10 l/min for 10 minutes. The filter is then advanced to the counting station where a solid-state detector and associated electronics count separately the alpha decays from ^{218}Po and ^{214}Po. The sampling and counting stations are fixed; the platter is rotated to select which filter is used for sampling or is counted. The results from two counting intervals are used to calculate the concentrations in air of the radon daughters: ^{218}Po, ^{214}Pb, and ^{214}Bi. With a detector efficiency that is 0.2 (counts/disintegration) and a total measurement

time of 40 minutes, the individual daughter concentrations are measured with a relative standard deviation of 20 percent at concentrations of roughly 0.5 pCi/l.[3] A dedicated microprocessor controls the operation of the RDC. It can be programmed to operate over a wide range of timing schemes. The microprocessor communicates with the main microcomputer system through a serial port.

CONCLUSIONS

This automated instrumentation system is completely operational with the exceptions of the radon-daughter carousel, the radon-source module, and the ventilation dampers, all of which are in the final stages of development. The system has already proved useful in studying the rates of mixing within a room, with and without forced convection. In the first few months of using the system, we experienced a few problems that appear to be related to the quality of the 115 VAC power in the research house. To correct these problems, we plan to add an isolation transformer and a back-up power supply to the system. We are presently planning a wide range of experiments using this system and, because expansion capabilities have been included in the design, we are assured of being able to accommodate future research goals. Although built for a specific research project on indoor radon, the system could easily be reconfigured for use in other indoor air quality research projects.

PLANNED ACTIVITIES FOR FY 1982

The instrumentation package for the radon research house will be completed, including devices for particulate monitoring. The measurement program will begin, including characterization of radon transport and ventilation effectiveness in the house and studies of the effect of ordinary building systems (furnace recirculation and filters) on daughter concentrations.

REFERENCES

1. McGoldrick, P.R., Dickinson, J., and Allison, T.G. (1978), LLL8080 Basic II Interpreter User's Manual, Lawrence Livermore Laboratory Report UCID-17752.

2. Thomas, J..W., and Countess, R.J. (1979), "Continuous Radon Monitor," Health Phys. 36, pp. 734-738.

3. Nazaroff, W.W., Nero, A.V., and Revzan, K.L. (1981), Alpha Spectroscopic Techniques for Field Measurement of Radon Daughters, to be published in the proceedings of Natural Radiation Environment Second Special Symposium, Bombay, India, Jan. 19-23, 1981, Lawrence Berkeley Laboratory Report LBL-10769.

Indoor Air Quality in New Energy-Efficient Houses and Retrofitted Houses

C. D. Hollowell, J. V. Berk, S. R. Brown, J. F. Dillworth,
J. F. Koonce, Jr., J. H. Pepper, and R. A. Young

Of primary interest in buildings designed or retrofitted to be more energy efficient is the effect of such measures on air quality. Since 1978, the Building Ventilation and Indoor Air Quality program at the Lawrence Berkeley Laboratory (LBL) has been conducting studies of indoor air quality in a variety of occupied buildings. This report presents the results of indoor air quality studies in several new energy-efficient houses and houses retrofitted for energy efficiency. The LBL Energy Efficient Buildings Mobile Laboratory, a fully instrumented, automated facility capable of monitoring a wide range of air-quality parameters on site for several weeks, was used for these studies. The mobile laboratory is positioned outside a building whose air quality is to be monitored; air sampling lines installed at several sites within the structure under study terminate inside the laboratory, where the air-monitoring instrumentation is located. As a general practice, we sample the outdoor air to determine what fraction of the pollution indoors originates outside. For indoor sampling, we select three sites to account for the spatial distribution of pollutant sources and incomplete mixing of the interior air, both of which can cause variations in the pollutant concentration from one room to another. Air is sampled sequentially from these four locations with a microprocessor-controlled sampling and data-logging system.

Gaseous pollutants, as well as air-exchange rates and comfort and meteorological parameters, can be measured on a continuous basis with the mobile laboratory. However, several indoor pollutants must be measured on a time-integrated basis because of their physical and chemical properties or low concentrations. Often, these measurements must be made directly at the sampling site rather than in the mobile laboratory. For example, indoor radon is measured for a one-week period using a portable battery-operated device which records the alpha decays from decaying radon atoms.[1] Formaldehyde and total aldehydes are collected over periods up to 24 hours using temperature- and flow-controlled gas bubblers.[2] Other organic contaminants are collected over periods of hours using the porous polymer Tenax-GC as an adsorption medium. Inhalable particulates are divided according to size and collected on Teflon filters, typically for 24-hour periods.[3] Most of these collection devices were developed at LBL; all require subsequent laboratory analysis of their samples to determine composition and concentrations.

ACCOMPLISHMENTS DURING FY 1981

New Energy-Efficient Houses

Table 1 summarizes the indoor air quality data, collected throughout the 1979-80 year at five energy-efficient houses located throughout the United States. The house in Carroll County, Maryland, was an energy-efficient research house which, in addition to other energy-conserving features, incorporated plastic vapor barriers in the wall, ceiling, and floor cavities to minimize infiltration. This house had all-electric appliances and was occupied by LBL field personnel during the sampling period. The house in Mission Viejo, California, was built by a large home building company as a model home incorporating several energy-conserving features. It had all-natural-gas appliances and was occupied by a family of three during the sampling period. Both houses in Minnesota (Northfield and Dundas) were owner-designed and included many energy-conservation features. Because of the very low air-exchange rates achieved in these houses, indoor moisture became a problem. To circumvent this problem and other possible indoor air quality problems, we recommended the installation of air-to-air heat exchangers in both houses. Our air quality measurements were taken with and without the heat exchangers operating. Both houses had all-electric cooking appliances. The Northfield house was occupied by a family of five, and the Dundas house was occupied by a family of two. The Rio, Wisconsin, farmhouse had been retrofitted (storm windows, weatherstripping, and a vapor barrier on the interior walls). It was occupied by a family of five, one of whom was a cigarette smoker, and propane cooking appliances were used. The house was heated with a woodburning stove located in the basement.

As indicated in Table 1, the infiltration rates in all five houses are considerably lower than the national average, ~0.75 ach. No significant carbon monoxide problems were observed in any of the houses, including those with gas-fired appliances and smokers. The high levels of nitric oxide in the Dundas house before the heat exchanger was turned on were associated with the operation of an oil-burning furnace in the basement, and the dramatic reduction made by the heat exchanger was

*This work was supported by the Assistant Secretary for Conservation and Renewable Energy, Office of Buildings Energy Research and Development, Building Systems Division of the U.S. Department of Energy under Contract No. DE-AC03-76SF00098.

†Condensed from Hollowell, C.D., et al. (1981), Indoor Air Quality in New Energy-Efficient Houses and Retrofitted Houses, Lawrence Berkeley Laboratory Report LBL-12566.

Table 1. Indoor air quality measurements in five new energy-efficient occupied houses.[a]

	Caroll County, MD	Mission Viejo, CA	Northfield, MN		Dundas, MN		Rio, WI
			HX off	HX on	HX off	HX on	
Infiltration rate (ach)	0.15	0.4	0.1	0.3	0.1	0.3	0.3
CO (ppm)	1.2	1.4	0.5	0.4	0.7	0.4	2.2
CO_2 (ppm)	598	689	1175	722	1316	478	1125
NO_2 (ppb)	9	41	15	16	19	20	77
NO (ppb)	5	44	5	2	70	5	72
SO_2 (ppb)	3.2	0.9	1.0	1.7	--	--	9.0
O_3 (ppb)	4.3	15.6	1.7	1.7	9.0	9.3	15.0
Particulates--fine ($\mu g/m^3$)	7.8	32.6	6.8	6.8	19.5	8.0	92.4[b] 6.0[c]
Particulates--total ($\mu g/m^3$)	9.9	48.9	14.8	13.8	27.9	14.6	129.6[b] 23.5[c]
Formaldehyde (ppb)	98	214	69	73	80	64	53
Total aldehydes (ppb)	150	227	99	91	122	163	81
Radon (pCi/l)	22.0	5.0	7.5	0.8	1.7	--	6.5

[a]All values represent average concentrations during the monitoring period.

[b]Smoking.

[c]No smoking.

caused by its exhaust inlet being adjacent to the furnace. The high radon levels in some of the houses are most likely attributable to high radon emanation from soil. This hypothesis is being investigated further in our laboratory.[4]

Very high levels of particulates were measured in the Rio, Wisconsin, house, where one of the occupants was a smoker. Although this house also differed from the others in using propane combustion appliances and a woodburning stove, the detailed data clearly confirm that the high levels of particulates were attributable to cigarette smoke.

Retrofitted Houses

Table 2 summarizes the indoor air quality data collected at three houses retrofitted for energy efficiency. The first two houses were part of a Pacific Power and Light Company (PPL) residential weatherization program in Medford, Oregon. A summary of the weatherization measures implemented in these two houses is shown in Table 3. The third house was a 100-year old home in Cranbury, New Jersey, that had been retrofitted just before our visit and "super" retrofitted by house doctors from Princeton University's Center for Energy and Environmental Studies before our final measurements were made.

As shown in Table 2, the concentrations of the gaseous pollutants in both Medford houses were low with no difference between pre- and post-retrofit periods, despite the fact that one of the occupants of house #1 smoked 20-40 cigarettes daily. Both houses had electric appliances exclusively, and, because there were no combustion sources inside the homes except for the cigarettes, these low levels were not unexpected.

On the other hand, there was a definite difference in the levels of particulates between smoking and non-smoking periods in house #1, both pre- and post-retrofit. In terms of the effect of the retrofit shown in Table 3, the indoor concentrations of both the fine and total inhalable particulates during the smoking period increased by approximately 20 percent after retrofitting; particulate levels measured during the non-smoking period did not change as a consequence of the retrofit. The total particulates during the post-retrofit period (77 $\mu g/m^3$) was approximately the same level as the EPA standard for total suspended particulates for a one-year period (75 $\mu g/m^3$).

The only gaseous pollutant that exhibited a change as a result of the retrofit was carbon dioxide, which increased 20 to 30 percent in Medford house #1 but was still well below existing health guidelines or standards. Radon levels were at or below the lower limit of detectability. Formal-

Table 2. Indoor air quality measurements in three retrofitted occupied houses.

	Medford, OR #1		Medford, OR #2		Cranbury, NJ	
	Pre-retrofit	Post-retrofit	Pre-retrofit	Post-retrofit	Pre-retrofit	Post-retrofit
Infiltration rate (ach)	(Fan on) 0.62 (Fan off) 0.33	0.49 0.20	(Fan on) 0.82 (Fan off) 0.33	0.58 0.23	0.44	0.39
CO (ppm)	0.3	0.3	0.3	0.3	2.9	3.1
CO_2 (ppm)	670	847	593	656	767	703
NO_2 (ppb)	7	4	4	5	25	29
NO (ppb)	3	7	8	7	50	46
SO_2 (ppb)	--	--	--	--	3	3
O_3 (ppb)	4	4	5	16	--	--
Particulates-- fine ($\mu g/m^3$)	(Smoking) 31 (No smoking) 9	36 8	12	10	12	8
Particulates-- total ($\mu g/m^3$)	(Smoking) 62 (No smoking) 31	77 35	45	26	25	18
Formaldehyde (ppb)	55	53	68	51	22	19
Total aldehydes (ppb)	84	85	94	71	29	31
Radon (pCi/l)	<1	1.2	<1	<1	3.6	3.8

Table 3. Summary of weatherization measures at the Medford, Oregon, houses.

	House No. 1	House No. 2
Storm windows		
No.	10	9
Area (m^2)	11.8	15.6
Storm doors		
No.	2	3
Weatherstripping		
No. doors	2	0[a]
No. sliding glass doors replaced	2	1
Ceiling insulation		
From	R15	R19
To	R38	R38
Area (m^2)	127	102
Floor insulation		
From	0	0
To	R19	R19
Area (m^2)	127	131
Duct insulation		
From	0	0
To	R9	R9
Ground cover/ moisture barrier	Yes	No

[a]Doors had been weather-stripped before retrofit.

dehyde and total aldehydes were well below the proposed guidelines for formaldehyde and remained the same after the retrofit.

The data from Medford house #2 showed the same trends as Medford house #1. The concentrations of the gaseous pollutants were low, generally lower than or equal to the levels seen in house #1. House #2 also had exclusively electric appliances and, because none of the occupants smoked, there were no combustion sources in this house. As in house #1, the levels of radon were below the lower limit of detectability, and the concentration of formaldehyde again was well below proposed guidelines. The levels of particulate mass in house #2 were low and very similar to those measured during the non-smoking periods in house #1. None of the indoor air quality parameters changed significantly as a result of the retrofit.

Data from the third retrofitted house in Cranbury, New Jersey, are also shown in Table 2. The concentrations of the gaseous pollutants were all low and did not change after the retrofit. Because the infiltration rate did not change, this finding was not unexpected. The average concentrations of the combustion-generated pollutants were lower than expected in a house with all-gas appliances (a gas stove, hot water heater, and washer-dryer, all containing pilot lights) located in the kitchen area. The explanation may be that the occupancy levels were unusually low during the monitoring period: one of the adults was absent for one week of each sampling period, and almost no cooking was done during these times. The low levels of both fine and total particulates approximated those seen in the Medford houses during the no-smoking period.

CONCLUSIONS

In general, our studies of new energy-efficient residences (with air-exchange rates lower than 0.4 ach) indicate that indoor levels of radon, formaldehyde, and particulates sometimes exceed existing guidelines or standards for outdoor air, due to a number of factors such as geographic variation of radon content in soil, indoor furnishings, and occupant activities.

The impact of residential retrofit programs on indoor air quality appears to be minimal, based on this study of three retrofitted houses, where no pollutants reached levels approaching health guidelines or standards. We can conclude that retrofit programs, such as that of Pacific Power and Light Company, improve the thermal integrity of houses and should continue without fear of significantly increasing indoor air pollution. In the Cranbury house, the "super" retrofit had no appreciable effect on the infiltration rate already achieved by the homeowner's prior weatherization, and thus little or no adverse impact on indoor air quality resulted from this "super" retrofit.

PLANNED ACTIVITIES FOR FY 1982

In the near future, detailed measurements using the mobile laboratory will not continue, but substantial efforts will be devoted to development, testing, and field use of simpler monitoring packages, most of which depend on use of passive monitors that are available or under development (such as the formaldehyde monitor discussed earlier).

REFERENCES

1. Boegel, M.L., Nazaroff, W.W., and Ingersoll, J.G. (1979), Instructions for Operating LBL Passive Environmental Radon Monitor (PERM), Lawrence Berkeley Laboratory Report LBID-073.

2. Fanning, L.Z., Allen, J.R., and Miksch, R.R. (1981), Instructions for Operating LBL Formaldehyde Sampler, Lawrence Berkeley Laboratory Report LBL-10629.

3. Loo, B.W., et al. (1979), A Second Generation Dichotomous Sampler for Large-Scale Monitoring of Airborne Particulate Matter, Lawrence Berkeley Laboratory Report LBL-8725.

4. Nazaroff, W.W., Boegel, M.L., and Nero, A.V. (1981), Measuring Radon Source Magnitude in Residential Buildings, presented at meeting on Radon and Radon Progeny Measurement, Montgomery, Alabama, August 27-28, 1981, Lawrence Berkeley Laboratory Report LBL-12484.

Low-Infiltration Housing in Rochester, New York: A Study of Air-Exchange Rates and Indoor Air Quality*†

F. J. Offermann, J. F. Dillworth, D. T. Grimsrud, C. D. Hollowell, J. F. Koonce, Jr., W. W. Nazaroff, J. H. Pepper, A. W. Robb, G. D. Roseme, and R. A. Young

With the increasing cost of energy, builders across the country are constructing houses specially designed to reduce energy consumption. Some conservation measures used, such as increased insulation, improve the thermal resistance of the structure while others, such as installation of continuous vapor barriers and weather stripping, reduce the quantity of air that leaks into and out of a building. Air exchange can account for as much as one-half of the total space-conditioning load of a house. Measures that reduce air leakage can be especially cost effective because of their relatively low cost of implementation.

A problem associated with houses which have low air-exchange rates is that the concentrations of indoor-generated air pollutants tend to be higher than those in well-ventilated houses. Indoor-generated contaminants include combustion by-products (gaseous and particulate species from cooking, heating, and tobacco smoking), odors, micro-organisms from occupants, a broad spectrum of chemicals outgassed by building materials and home furnishings, and toxic chemicals from cleaning products and other materials used by occupants. The concentration of any indoor-generated pollutant is determined by its emission rate (source strength) into and removal rate out of the indoor air space. One of the primary removal mechanisms for indoor-generated pollutants is dilution and flushing with outside air.

To address the issues of residential air-exchange rates and indoor air quality, a study was conducted in a number of houses in Rochester, New York, under the joint sponsorship of the Lawrence Berkeley Laboratory (LBL), the New York Energy Research and Development Authority (NYSERDA), and the Rochester Gas and Electric Company (RG&E). The objectives of the study were (1) to assess the effectiveness of construction techniques designed to reduce infiltration, (2) to monitor indoor air quality and air-exchange rates in selected tight homes, and (3) to evaluate the thermal performance and impact on indoor air quality of mechanical ventilation systems employing air-to-air heat exchangers. Our sample consisted of 60 houses constructed by two builders and included houses with and without special builder-designed weatherization components.

During the summer of 1980, the "effective leakage area" of each house was measured by fan pressurization.[1] During the 1980-81 heating season, ten of these houses were singled out for a detailed study of indoor air quality and air-exchange rates. Nine of these ten houses were relatively tight structures; three contained gas cooking appliances (one of the three had tobacco-smoking occupants), and six contained electric cooking appliances (three of the six had tobacco-smoking occupants). The tenth home, which was built without special weatherization components, was a relatively loose structure that served as a comparison.

Mechanical ventilation systems with air-to-air heat exchangers were installed in each of the nine tight homes, and air quality and air-exchange rates were monitored in each house for a one-week period without mechanical ventilation, followed by a one-week period with mechanical ventilation. The one loose house was similarly monitored for a single one-week period without mechanical ventilation. In eight of these ten homes, a newly developed portable monitoring system, the Aardvark,[2] was used to automatically measure the air-exchange rate, radon (Rn) concentration, and the indoor and outdoor temperatures, as well as the four air-stream temperatures of the air-to-air heat exchangers. The average daily relative humidity, concentrations of formaldehyde (HCHO) and total aldehydes (RCHO), and the average weekly concentrations of nitrogen dioxide (NO_2) were also measured in these homes. The remaining two homes were monitored by LBL's Energy Efficient Buildings Mobile Laboratory, which, in addition to measuring all of the above parameters, measured concentrations of particulates, carbon monoxide (CO), carbon dioxide (CO_2), nitric oxide (NO), ozone (O_3), and sulfur dioxide (SO_2). In this report, we present the results of the leakage area, air-exchange rate, and indoor air quality measurements made in the ten houses. In addition to these results, a comprehensive final report will include energy data collected in the 60 houses and field performance measurements of the nine air-to-air heat exchangers.[3]

ACCOMPLISHMENTS DURING FY 1981

The results of measurements of leakage area, air-exchange rate, and concentrations of Rn, NO_2, HCHO, and RH in the ten houses selected for a detailed study of indoor air quality are summarized in Table 1, together with relevant characteristics of each house (construction, appliances, and occupancy) that affect indoor air quality. In the full sample of 60 houses, the specific leakage area varied from 1.3 to 9.0 cm/m^2 (effective leakage

*This work was supported by the Assistant Secretary for Conservation and Renewable Energy, Office of Buildings and Community Systems, Buildings Division of the U.S. Department of Energy under Contract No. DE-AC03-76SF00098; the New York State Energy Research and Development Authority; and the Rochester Gas and Electric Company.

†Condensed from Offermann, F.J., Hollowell, C.D., Rizzuto, J., and Roseme, G.D. (1981), Low-Infiltration Housing in Rochester, New York: A Study of Air-Exchange Rates and Indoor Air Quality, Lawrence Berkeley Laboratory Report LBL-12567.

Table 1. Summary of air-exchange rate and indoor air quality measurements made in ten houses in Rochester, New York (November 1980-April 1981).

House I.D.[a] Year built	House volume (m^3) / Specific leakage area (cm^2/m^2)	Combustion appliances[b] / Est. smoking activity[c]	Mech. vent. off[d] / Mech. vent. on	Air-exchange rate (ach)		Rn (pCi/l)	HCHO (ppb) indoor/outdoor	NO_2 (ppb) indoor/outdoor	RH (%)
#45	705	GF	11/13-20	0.37	.10	2.1	28/<5	2/14	44
1979	2.0	20	11/21-26	0.61	.23	0.9	29/<5	6/29	40
#1	467	all electric	12/7-15	0.22	.09	0.4	36/<5	1/7	47
1977	2.4	5	12/16-21	0.47	.19	0.1	19/<5	3/10	38
#10	357	all electric	1/6-13	0.30	.09	1.2	7/<5	1/9	35
1976	1.4	0	1/14-20	0.611	.70	0.7	<5/<5	5/25	30
#56	360	GF,GS,GW,GD	1/28-2/4	0.50	.13	0.2	11/<5	10/15	36
1981	3.2	0	2/11-16	0.61	.21	0.0	18/<5	9/18	33
#33	496	GS,GF,GW,FP	2/21-28	0.38	.15	0.3	33/<5	23/9	42
1979	2.5	0	3/4-10	0.78	.16	0.0	19/<5	20/12	33
#37	411	GF,GW	3/14-21	1.17	.65	0.0	17/<5	6/11	29
1974	5.4	5							
#52	357	all electric	3/24-30	0.28	.10	1.1	64/<5	3/12	41
1980	1.4	0	3/31-4/7	0.73	.13	0.4	62/<5	<1/11	42
#60	493	GF,GW	4/10-20	0.33	.10	2.2	57/<5	12/18	52
1979	2.7	0	4/21-28	0.52	.06	1.6	42/<5	13/18	45
#6	402	WS	1/8-22	0.38	.09	1.6	29/<5	5/16	30
1977	2.8	20 + pipe	1/23-30	0.66	.166	0.7	22/<5	5/13	26
#49	425	GF,GS,GW	2/5-19	0.42	.11	0.1	30/<5	11/15	25
1973	3.5	25	2/20-3/2	0.64	.17	0.2	29/<5	16/11	27

[a]All houses were occupied single-family detached dwellings, with full basements.

[b]Key: (FP) fireplace, (WS) woodstove, (GS) gas stove, (GF) gas furnace, (GW) gas water heater, (GD) gas clothes dryer.

[c]Number of cigarettes smoked indoors per day.

[d]Dates of indoor air quality sampling periods (with and without mechanical ventilation).

area in cm^2 /floor area in m^2). Of the 49 houses built by one of the builders, the 36 houses with special weatherization components (e.g., polyethylene vapor barriers in the outside walls and sealing of all joints and electric outlets) had an average specific leakage area of 2.8 cm^2/m^2, which is 50 percent lower than the 5.5 cm^2/m^2 average measured in 13 similar houses without such components. Based on typical weather data for Rochester, New York, these average specific leakage areas correspond to average heating season infiltration rates of 0.54 air changes per hour (ach) and 1.85 ach, respectively, as calculated using a model of infiltration developed at LBL.[4]

The indoor concentrations of Rn, NO_2, HCHO, and RCHO measured during both ventilated and unventilated periods were below the various guidelines presently used to assess indoor air quality.[5] It should be understood that the guidelines to which we refer are, at the present time, the only "standards" available to us. There is an urgent need for comprehensive studies of the health risks associated with indoor air pollution so that such guidelines will have applicability to indoor air quality issues. The indoor concentrations of particulates, CO, CO_2, NO, O_3, and SO_2 measured by LBL's mobile laboratory in houses #6 and 49 were also below existing guidelines.

During the unventilated period, the average indoor Rn concentrations were moderately elevated, ranging from 2.2 to less than 0.2 pCi/l. Indoor concentrations of HCHO ranged from 7 ppb to 64 ppb, exceeding the outdoor concentrations, which were consistently below the detection limit of 5 ppb. In the case of NO_2, however, indoor concentrations measured during the unventilated period were consistently lower than the outdoor concentrations (10 to 30 ppb, typical of urban environments) except in house #33 (which had all gas appliances), where the average indoor NO_2 concentration was 23 ppb, the highest measured in this study. As expected, houses with gas appliances had higher average indoor concentrations of NO_2 (11 ppb) than houses with all-electric appliances (2 ppb). The average relative humidity measured in the nine tight houses during this period ranged from 25 to 52 percent. During the period when mechanical ventilation was used, the average air-exchange rate in these homes increased 80 percent, from 0.35 to 0.63 ach. Under these conditions average indoor Rn concentrations decreased 50 percent, from 1.0 pCi/l to 0.5 pCi/l, average HCHO concentrations decreased 18 percent, from 35 ppb to 27 ppb, and average relative humidity decreased from 39 percent to 35 percent. These decreases are consistent with our expectations because outdoor concentrations of Rn, HCHO, and water vapor were much lower than indoor concentrations. On the other hand, because NO_2 concentrations were generally lower indoors than outdoors, ventilation had the effect of increasing the

average indoor NO_2 concentrations slightly, from 7 to 9 ppb.

CONCLUSIONS

Special house weatherization components such as continuous polyethylene vapor barriers and joint-sealing are effective in reducing leakage area and, hence, infiltration, as evidenced by the direct measurements of leakage area and air-exchange rates made in this study. In the nine relatively tight houses studied, the air-exchange rates measured during the unventilated period were relatively low, 0.2-0.4 ach, while indoor concentrations of Rn, HCHO, and NO_2 were below existing air quality guidelines, findings which suggest that the source strengths of these pollutants were relatively low in these houses. Clearly, the key to having an energy-efficient house with both low air-exchange rates and good indoor air quality is to construct and furnish the house such that indoor pollutant sources are low. Evidence that this is achievable in standard residential housing, at least with respect to the pollutants we monitored, is provided by our findings in these nine houses.

When designing houses to have low air-exchange rates, builders should be selective in choosing building materials that are not potential sources of indoor air pollution. Research has been initiated at LBL and other research organizations to study pollutant emissions from various building materials. Many sources of indoor air pollution, however, are beyond the control of builders: e.g., radon emanation from soil, which is site specific; occupant-related sources such as tobacco smoking; use of unvented combustion appliances and toxic cleaning products; and selection of house furnishings constructed with formaldehyde resins.

Alternatively, mechanical ventilation systems with air-to-air heat exchangers can be installed in tightly constructed houses where it is uncertain whether the uncontrolled ventilation from infiltration, together with that ventilation occasioned by occupant activities (e.g., opening doors and windows, use of exhaust fans etc.), will adequately maintain acceptable indoor air quality. These units provide a controlled supply of ventilation air without seriously compromising the energy efficiency of the house and are effective in reducing concentrations of indoor-generated pollutants, as demonstrated in this study. Some remaining problems to be resolved with regard to these systems are freezing of moisture within heat exchangers and contaminant transfer in heat exchangers designed to transfer both heat and water vapor. In addition, the question of their cost effectiveness for residential use needs to be examined. All of these issues are being addressed in ongoing research at LBL.

PLANNED ACTIVITIES FOR FY 1982

This specific project is completed, but related work is being continued as part of other projects, specifically, the use of the Aardvark system, in an expanded form, for a long-term study of infiltration rates and radon source strengths and the examination of ventilation effectiveness of mechanical ventilation systems using air-to-air heat exchangers.

REFERENCES

1. Grimsrud, D.T., Sonderegger, R.C., and Sherman, M.H. (1981), Infiltration Measurements in Audit and Retrofit Programs, Lawrence Berkeley Laboratory Report LBL-12221.

2. Nazaroff, W.W., Offermann, F.J., and Robb, A. (1981), Automated System for Measuring Air-Exchange Rate and Radon Concentration in Houses, Lawrence Berkeley Laboratory Report LBL-12945.

3. Offermann, F.J., et al. (1981), Residential Air Leakage and Indoor Air Quality in Rochester, New York, Lawrence Berkeley Laboratory Report LBL-13100.

4. Sherman, M.H., and Grimsrud, D.T. (1980), Measurement of Infiltration Using Fan Pressurization and Weather Data, Lawrence Berkeley Laboratory Report LBL-10705.

5. Dudney, C.S., and Walsh, P.J. (1981), Report of Ad Hoc Task Force on Indoor Air Pollution, Oak Ridge National Laboratory Report ORNL/TM-7679.

Performance Measurements for Residential Air-to-Air Heat Exchangers

W. J. Fisk, K. M. Archer, R. Bitton, P. Boonchanta,
B. El-Adawy, R. Haynes, C. D. Hollowell, and G. D. Roseme

Many builders and homeowners are implementing procedures to reduce infiltration, the exchange of outdoor and indoor air. Although reducing infiltration is an effective strategy for conserving energy, it can have adverse effects on the quality of the indoor air. In some tightly sealed homes, humidity can rise to high levels and cause excessive condensation on windows and damage to building materials. More importantly, the levels of indoor-generated air contaminants are likely to be higher in tightly sealed homes. Some of the more common indoor contaminants and their sources are nitrogen dioxide from combustion appliances, radon gas from the soil surrounding basements and foundations, and formaldehyde from building materials and furnishings.[1]

One way to alleviate most indoor air quality problems, without sacrificing all of the energy savings resulting from reduced infiltration, is to install a mechanical ventilation system that incorporates an air-to-air heat exchanger. The purpose of the heat exchanger is to transfer heat from a warm outgoing airstream in winter to a cooler airstream entering the house from outside. In the summer, the process is reversed; the heat exchanger cools and, in some cases, dehumidifies the hot outside air that passes through it and into the house. Thus, ventilation can be accomplished without the high energy loss normally associated with ventilation systems having no heat-recovery devices.

A residential heat exchanger is used with two fans, one to bring outdoor air into the house and the second to exhaust an equal amount of air. In many cases a fan system (fans and fan motors) is supplied with the heat exchanger; however, some manufacturers supply only a "core," the section of a heat exchanger in which heat is transferred between airstreams.

Some models of residential heat exchangers are designed to be used with a duct system for air distribution. Other models are simply installed through the wall or window of a residence. Because window- or wall-mounted heat exchangers are not used with an air distribution system, they may not be as effective as ducted units in ventilating all regions of a residence.

Little information is available on the performance of residential heat exchangers. Two important aspects of heat-exchanger performance that have been investigated by Lawrence Berkeley Laboratory (LBL) are thermal performance and fan-system performance. The thermal performance of a residential heat exchanger is often characterized by its "effectiveness," which is a measure of its ability to preheat or precool ventilation air. If a heat exchanger is 75 percent effective, it can preheat or precool ventilation air by approximately 75 percent of the difference between indoor and outdoor temperatures. Although a number of factors can cause the field performance of a heat exchanger to differ from that indicated by laboratory measurements of effectiveness,[2] effectiveness is a useful criterion for comparing heat exchangers and for indicating approximately their performance in a residence. Because the effectiveness of a heat exchanger decreases as the flow rate of air passing through the heat exchanger increases, effectiveness measurements are generally performed for a range of flow rates.

To characterize the performance of a heat exchanger's fan system, we employ three parameters: airstream flow rate, airstream static pressure drop, and total fan power consumption. For heat exchangers that are supplied with a fan system, the airstream flow rates are a function of the fan speed and the resistance to flow in the duct systems attached to the heat exchanger. An increase in fan speed or a decrease in resistance causes an increase in airstream flow rates. For ducted heat exchangers, the flow rates are typically adjusted by using valves to vary the resistance of the supply and exhaust duct systems. Some ducted heat exchangers also have multi-speed fans for flow-rate control. Window- or wall-mounted heat exchangers, which have no air distribution systems, are typically supplied with a multi-speed fan system for controlling air-flow rates.

The parameter used to describe the resistance of a duct system is the drop in airstream static pressure as it passes through the ducts. This pressure drop increases with an increase in flow rate and can be predicted if the characteristics of the duct system are known.

The third parameter used to describe the performance of a heat exchanger's fan system is the total fan power consumption. An economic analysis of heat-exchanger use being performed at LBL indicates that fan power consumption can be an important economic consideration. Fan placement is also

*This work was supported by the Assistant Secretary for Conservation and Renewable Energy, Office of Building Energy Research and Development, Building Systems Division of the U.S. Department of Energy under Contract No. DE-AC03-76SF00098.

†Condensed from Fisk, W.J., et al. (1981), Performance Measurements for Residential Air-to-Air Heat Exchangers, Lawrence Berkeley Laboratory Report LBL-12559.

important because it determines the fraction of the fan's energy consumption that is delivered to the residence.

In this report, we present a summary of results from measurements of effectiveness on five models of residential heat exchangers. Data describing the fan performance of two of these heat exchangers are also presented. In a previous LBL report,[2] similar performance data are presented for five additional heat exchangers, together with a description of the procedures and facilities used for this testing program.

ACCOMPLISHMENTS DURING FY 1981

Before presenting the test results, the manufacturer of each heat-exchanger model is identified. (Complete descriptions and prices for the heat exchangers are available from the manufacturers.)

Identification of Models Tested

Two of the heat-exchanger models tested are manufactured by Des Champs Laboratories, Inc. in East Hanover, New Jersey (Models 79 M.2 and 79M). These two units essentially are identical, except for the inclusion of a single-speed fan system in Model 79M. A third heat exchanger tested was manufactured by Enercon Industries, Ltd. in Regina, Canada, and a fourth is a heat-exchanger core manufactured by Heatex AB in Hammarsvagen, Sweden. The Enercon heat exchanger is supplied with external fans, but the fan system was not tested. Several Swedish companies use one or more of the Heatex cores in their heat exchangers. The fifth heat exchanger tested is the Mitsubishi VL-1500 unit, which is available from Mitsubishi Electric Sales America, Inc. in Compton, California.

The first four heat exchangers are used with an air distribution system; the Mitsubishi unit is designed for wall or window installation. The Mitsubishi exchanger is also designed to transfer moisture as well as heat between airstreams. Moisture transfer is desirable in hot humid weather but can be a disadvantage in homes with high humidity problems during the winter. In addition, a heat exchanger that transfers moisture may also transfer some indoor contaminants between airstreams. No data on the moisture transport capabilities of the Mitsubishi heat exchanger are presented in this report.

Effectiveness Test Results

A summary of test results for the five heat-exchanger models is presented in Table 1. The effectiveness of the heat exchangers varied significantly among models, ranging from a high of 84 percent to a low of 52 percent for flow rates of 85 to 340 m^3/hr (50 to 200 ft^3/min).

In Table 1, the effectiveness data for the Mitsubishi heat exchanger has been discounted because, for this heat exchanger, the flow rate of the exhaust airstream is greater than that of the supply airstream. The imbalance in flow rates will cause this heat exchanger to save less energy than indicated by the non-discounted effectiveness. The effectiveness data was discounted by 19, 18, and 14 percent, respectively, for the high, medium, and low fan speeds because of corresponding imbalances in flow rate for the three fan speeds. When interpreting the effectiveness data for the Mitsubishi, it should also be noted that this unit was tested with its fan system operating and that heat from the fan motor causes the measured effectiveness to differ from the true effectiveness.

Fan Performance Test Results

As indicated in Table 1, the fans used with the Des Champs Model 79M heat exchanger have a high power consumption, approximately 180 watts. However, the fans are positioned so that most of the energy they consume is delivered to the residence. In our test system, the maximum air flow rate provided by this heat exchanger's fan system was approximately 178 m^3/hr (105 ft^3/min). Higher flow rates would be obtainable if this unit was used with a very low-resistance duct system.

As mentioned earlier, the exhaust airstream for the Mitsubishi heat exchanger has a higher flow rate than the supply airstream. The amount of ventilation air provided by this heat exchanger is equal to the higher, or exhaust, flow rate. This flow rate is presented in Table 1 for the low, medium, and high fan speeds. The fan power consumption for the Mitsubishi heat exchanger, also shown in Table 1, is considerably less per unit of ventilation air than that of other heat exchangers tested by LBL.

CONCLUSIONS

Based on test results presented in this report and in a previous LBL publication,[2] a 70- to 80-percent effectiveness is a reasonable expectation for a residential heat exchanger. The effectiveness of heat exchangers varies significantly, however, and many models have an effectiveness that is less than 70 percent.

The fan power consumption of residential heat exchangers tested by LBL ranges from 0.4 to 2.1 watts per m^3/hr of ventilation air. Fan power requirements can be reduced by using efficient fans and fan motors, minimizing the resistance to air flow through heat exchangers and duct systems, and using fan speed instead of damper valves for the control of air-flow rates.

PLANNED ACTIVITIES FOR FY 1982

Future research will include studies of ice or frost formation within heat-exchanger cores and studies of the ventilation efficiency of heat exchangers. In addition, work will begin on other techniques for the control of indoor pollutant levels. Some of the new work will be conducted in collaboration with other groups, such as measurement of ventilation effectiveness with the radon group.

Table 1. Summary of thermal performance and fan performance test results for five models of residential heat exchangers.

Heat Exchanger	Flow rate m^3/hr (ft^3/min)	Effectiveness (%)	Total fan power consumption (watts)	Static pressure[a] drop (in mm Hg)
Des Champs[b] Model 79M.2	85 (50)	83		
	170 (100)	82		
	340 (200)	79		
Des Champs[c] Model 79M	85 (50)	84	176	12 (0.47)
	170 (100)	81	185	8 (0.32)
	340 (200)	79		
Enercon[b]	85 (50)	71		
	170 (100)	65		
	340 (200)	56		
Heatex AB[b]	85 (50)	60		
	170 (100)	60		
	340 (200)	52		
Mitsubishi[d] VL-1500	65 (38)	65	24	
	110 (65)	60	42	
	144 (85)	56	57	

[a]Static pressure drop in the duct systems attached to the heat exchangers.

[b]No fan system tests were performed for this model.

[c]The maximum flow rate provided by this model's fan system in our fan performance test system was 178 m^3/hr (105 ft^3/min).

[d]This model is used without an air distribution system. Flow rates and fan power consumption are for low, medium, and high fan speeds. Effectiveness data has been discounted because of the imbalance in airstream flow rates for this model.

REFERENCES

1. Hollowell, C.D., Berk, J.V., and Traynor, G.W. (1979), Impact of Reduced Infiltration and Ventilation on Indoor Air Quality in Residential Buildings, Lawrence Berkeley Laboratory Report LBL-8470.

2. Fisk, W.J., Roseme, G.D., and Hollowell, C.D. (1980), Performance of Residential Air-to-Air Heat Exchangers: Test Methods and Results, Lawrence Berkeley Laboratory Report LBL-11793.

ENERGY EFFICIENT WINDOWS AND DAYLIGHTING*

S. E. Selkowitz, S. M. Berman, R. L. Johnson, J. D. Kessel,
J. H. Klems, C. M. Lampert, and M. D. Rubin

Approximately 20 percent of the annual energy consumption in the United States is used for space conditioning of residential and commercial buildings. About 25 percent of this amount is required to offset heat loss and heat gain through windows. In other words, 5 percent of our national energy consumption--3.5 quads annually, or the equivalent of 1.7 million barrels of oil per day--is tied to the energy-related performance of windows.

An important aim of the Windows and Daylighting Group is to develop a sound technical base for predicting the net energy performance of windows and skylights, including both thermal and daylighting aspects. This capability will be used to generate guidelines for optimal design and retrofit strategies in residential and commercial buildings and to assist development of new high-performance materials and designs. One of the strengths of our program lies in its breadth and depth: we examine energy-related aspects of windows at the molecular level from the perspective of electron microscopy at one extreme and field test facilities and in-situ experimentation at the other. We have developed, validated, and now utilize a unique and powerful set of interrelated computational tools and experimental facilities that enable us to address the major research issues in our field. It is critically important that technical data developed by our program be effectively communicated to design professionals and to other public and private interest groups. Although our efforts in technology transfer have been reduced during the past year, we continue to participate actively in activities of all appropriate professional and scientific societies, both national and international, to ensure that our research results are widely disseminated.

ACCOMPLISHMENTS DURING FY 1981

Our work is organized into three major areas: (1) Window Performance--Analysis and Testing; (2) Fenestration Systems--Research, Development, and Field Testing; and (3) Daylighting.

Window Performance--Analysis and Testing

Analytical Modeling. Analytical models of thermal performance form the basis of much of our research program. We have made improvements to our models of window heat transfer that enable calculation of frame conduction effects, infiltration, and convection in gas mixtures and inclined air spaces. We have continued to improve our optical and thermal models for windows having thin-film coatings. An example of such a coating is the heat mirror which reflects long-wave infrared radiation, thereby supressing heat transfer. Based upon last year's work on the solar-optical and thermal properties of heat-mirror coatings, we calculated the thermal loads for residential buildings having windows with heat-mirror coatings. We studied coatings that are applied to plastic glazing materials to increase solar transmittance. Unlike conventional antireflection coatings, these have a complex surface structure consisting of microscopic dendrites. We found that describing these dendrites as a quadratic-pyramid shape accurately indicated the optical properties of such surfaces. The energy savings attributable to the additional solar gain provided by these coatings was also evaluated for residential buildings.

The fundamental optical properties of glazing materials must be known to calculate the thermal properties of the complete window. A procedure was derived for obtaining optical constants from simple photometric properties measured on sheet materials. Polyethylene terephthalate (PET) is the most common substance used as a substrate for thin-film coatings in windows. We calculated the infrared properties of PET from the measured optical constants. Because these PET films have an appreciable infrared transmittance, their properties vary with thickness (Figure 1).

The solar-optical properties of windows change with the sun's angle of incidence. Most building models represent this information as coefficients of a power series. Certain rational functions and Legendre polynomials are examples of functions that

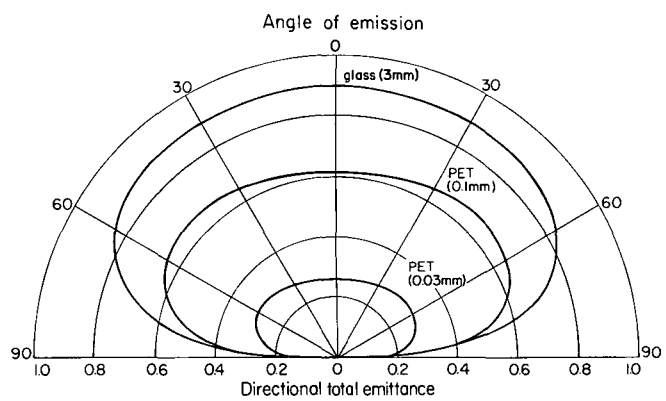

Figure 1. Directional total emittance of window glass (3 mm) and PET films (0.1 and 0.03 mm) at 293 K. The horizontal axis represents the surface of the material; the angle of emission is measured from the normal to this surface.

(XBL 8110-1455)

*This work was supported by the Assistant Secretary for Conservation and Renewable Energy, Office of Buildings and Community Systems, Buildings Division, of the U.S. Department of Energy under Contract No. DE-AC03-76SF00098.

better represent the optical data. We have calculated the coefficients of these approximating functions for a number of standard and advanced windows.

Although it is relatively easy to measure the air-leakage rate of a window system under specified conditions, it is difficult to estimate the impact of window air infiltration on annual energy consumption. We extended the basic models developed by the Energy Performance of Buildings Group to predict annual energy savings of windows in residences as a function of window and building properties and climate.

Performance Testing. In 1977, we established a Building Technology Laboratory in the College of Environmental Design of the University of California, Berkeley, to support our research and development activities, provide independent testing and evaluation of materials and products submitted by subcontractors, and thus permit evaluation of new products being introduced to the market. Testing facilities include a calibrated hotbox (Figure 2), which is being used to test the thermal performance of windows and associated energy-conserving accessories. A sample of devices now on the market or prototypes of devices soon to be on the market was tested to establish a baseline against which future improvements in window performance can be compared. Data from this test facility have also been used to validate our computer models.

The heat-loss and heat-gain rates of windows can be improved with the use of thin-film coatings on glazing materials. To fully characterize glazing-material performance, we have developed capabilities for measuring a range of optical properties of glazing materials and coatings. Infiltration tests on windows are also being made in our laboratory.

The single piece of information most relevant to assessing the benefit to be derived from a window or window improvement is its net energy performance under actual conditions of use in a building. This is a dynamic property, essential for predicting the performance of managed window systems (i.e., windows having thermal/optical properties that can be manually or automatically changed by building occupants). The laboratory testing facilities described above, however, are designed primarily to conduct steady-state measurements of static materials and devices. No experimental methodology currently exists for measuring the net performance of windows in situ.

In 1981, we began constructing a Mobile Window Thermal Test (MoWiTT) facility to fill this experimental gap. Shown in Figure 3, the facility consists of one or more measurement modules with an instrumentation van. Each measurement module consists of twin guarded calorimeters and will permit dynamic study of combined solar, infiltrative, conductive/convective, and radiative heat transfers through a window as a function of window type and orientation. The inner and outer shells of the first measurement module were completed during 1981. In 1982, the module will be assembled, tested, and calibrated.

Modeling of the expected performance of the MoWiTT (see Figure 4) has shown quantitatively the improved measurement ability for both daytime and nighttime measurements that are the results of the MoWiTT's unique features. It should be noted that even the "typical" conventional facility used for comparison is much more accurate and sophisticated than any facility currently existing in the U.S.

We have developed an experimental approach

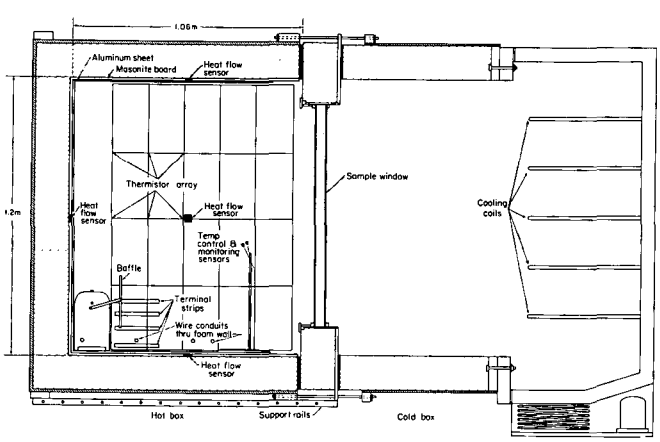

Figure 2. Section through calibrated hotbox showing hot and cold box chambers and sample window.
(XBL 799-2921A)

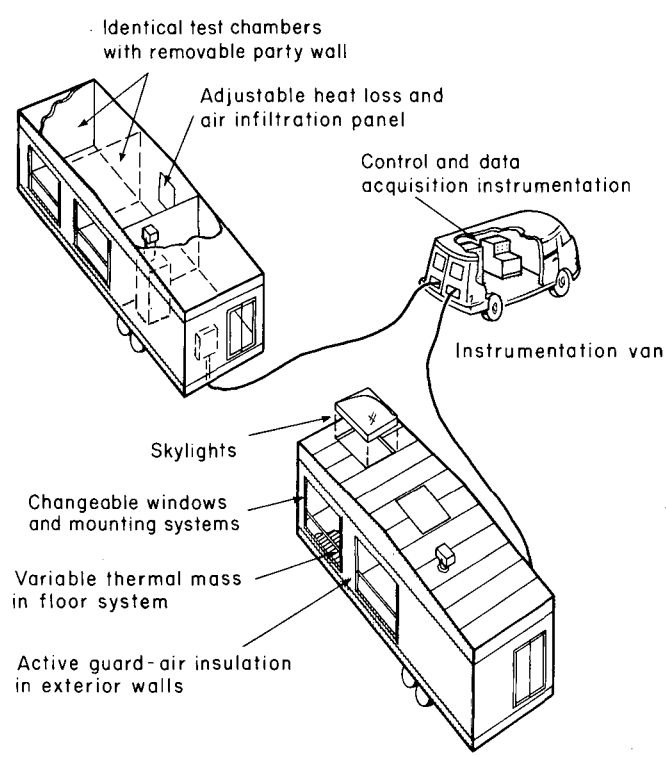

Figure 3. Schematic view of Mobile Window Thermal Test (MoWiTT) facility.
(XBL 811-30)

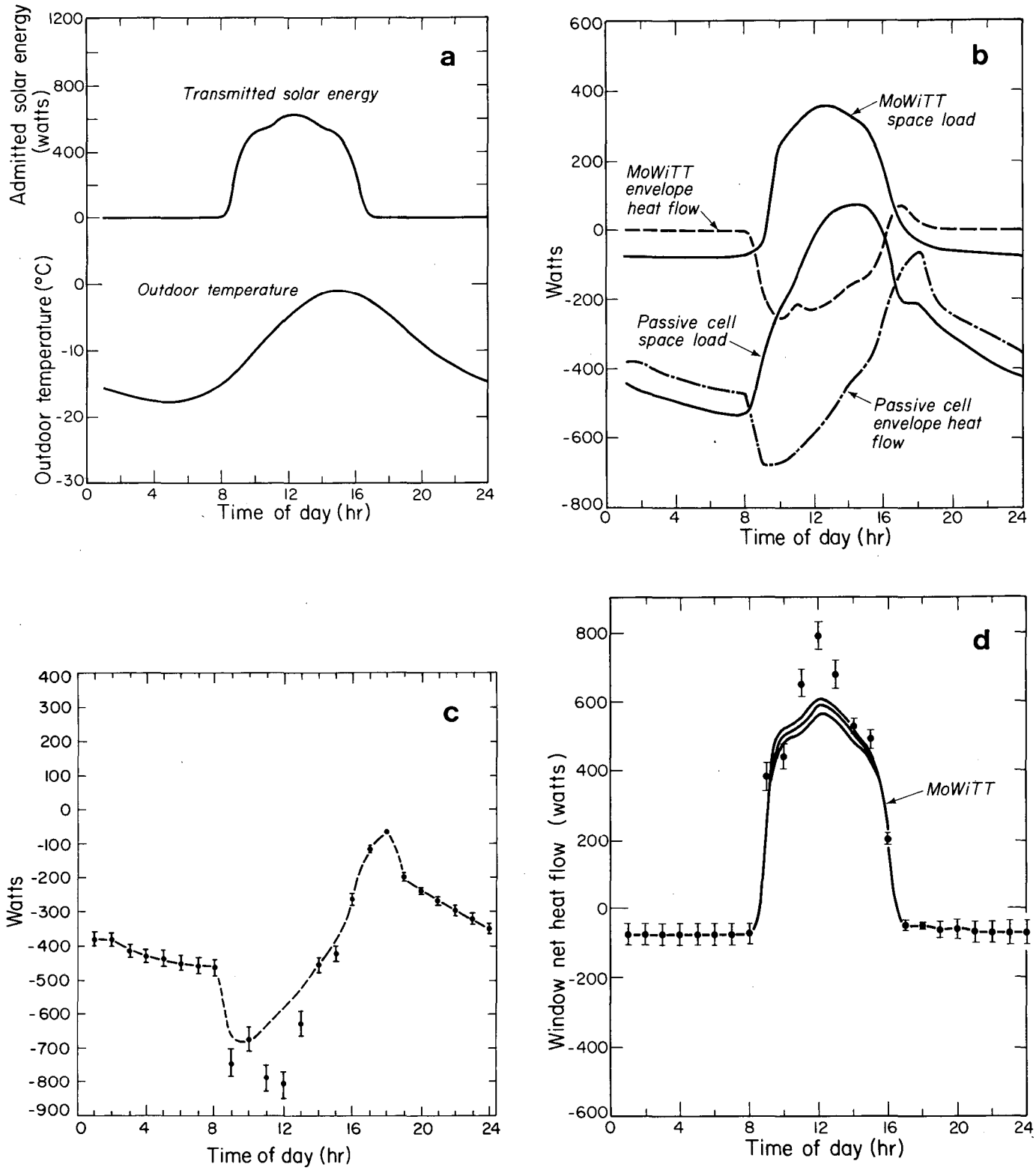

Figure 4. BLAST Simulation of a triple-glazed window measurement comparing the MoWiTT and a passive test cell. (a) Assumed outdoor temperature and solar energy transmitted through the window. (b) Calculated space loads (solid curves) and envelope heat flows (dashed curves) for the MoWiTT and for the passive cell. (c) Measurement of envelope heat flow in the passive cell. Dashed curve: BLAST calculation of the envelope heat flow; points with error bars: envelope heat flow measured with a grid of commercial heat-flow meters. (d) Derived values for the net heat flow through the window. Solid curves are the mean, +1 standard deviation, and -1 standard deviation for measurements by the MoWiTT. Points with error bars are the corresponding quantities for the passive cell with heat-flow meter grid.

(XBL 8110-1402,-1404,-1405, and -1406)

that will enable MoWiTT to be used to measure the thermal impact of daylighting strategies. Electric lighting in a building is simulated as part of the internal load in a MoWiTT test cell. In a naturally lit building, electric lighting requirements will be varied in response to available daylight. We accomplish this in MoWiTT by measuring daylight levels in an accurately constructed scale model of the building to be simulated and then using these data to alter the internal load in MoWiTT. This hybrid thermal/daylighting simulation will be further explored in 1982.

An outgrowth of work on the MoWiTT facility has been the development of a new heat-flow meter. Instead of the usual method of measuring the temperature difference across a known thermal resistance using a deposited thermopile, this heat-flow meter uses AC resistance thermometry to measure the temperature difference. Heat-flow meters of this type can be made economically in sizes large enough to cover entire walls, and we intend to incorporate them into the MoWiTT facility.

During 1981, our efforts have concentrated on developing and testing a prototype heat-flow meter with the characteristics necessary for a unit that will be included in the MoWiTT facility. A promising one-foot-square prototype has been produced and tested in a specially constructed, guarded hot-plate apparatus. The prototype shows excellent linearity and sensitivity, as shown in Figure 5. We will develop this prototype into a final production version and incorporate it into the MoWiTT during 1982.

Fenestration Systems--Research, Development, and Field Testing

To provide real energy savings, window innovations developed by inventors in both the private and public sectors must find their way in significant numbers to the market and then to building installations. The transition from laboratory prototype to local building-supply store is not a simple one. A variety of research activities are needed to help establish the energy-saving potentials of new and existing window and skylight products. Field testing of products frequently leads us back to the laboratory to re-investigate thermal performance and the properties and durabilities of various materials. Our program continues its investigation at several levels into the emerging energy-efficient technologies described below.

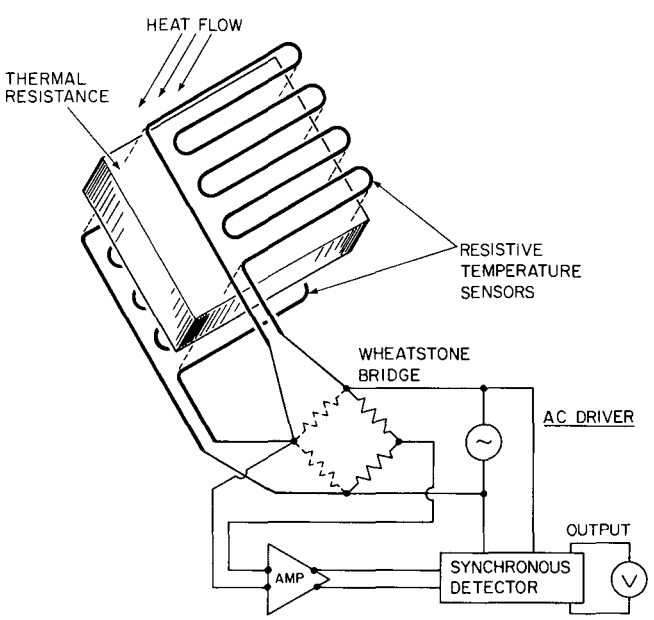

Figure 5. Schematic view of heat-flow meter design based upon resistance thermometry. (XBL 8011-2627)

Transparent Heat Mirrors. A transparent heat mirror is an optical coating applied to a glass or plastic glazing material to transmit the majority of the solar spectrum and reflect thermal infrared radiation emitted by room-temperature surfaces. By reducing the radiative component of thermal losses, the heat-transfer coefficient of a single- or multiglazed window is greatly reduced.

In prior years, our program has supported several heat-mirror research and development projects. Some manufacturers are currently considering introduction of heat mirrors on both glass and plastic materials. However, materials stability and durability, along with design issues, are not yet fully resolved. The coated-plastic substrate would be incorporated into a window unit either by adhesive bonding to glass or by being stretched across the air space in a double-glazed unit, creating an additional air space and, thus, improved insulating values. In 1981, several computer programs developed at LBL were used to provide thermal performance data for numerous window configurations that incorporate heat-mirror coatings (see Window Performance: Analysis and Testing section).

For both the manufacturer and the ultimate buyer, the durability of heat-mirror coatings is an essential attribute. Poor resistance to corrosive attack and abrasive forces, which characterized many of the coatings first developed, still remains an uncertainty that obstructs widespread and rapid utilization. In 1981, we examined some of the generic failure mechanisms of coatings by means of sophisticated analysis equipment available at LBL. A representative result from the scanning electron microscope is shown in Figure 6.

To prove to the architectural and engineering community that heat-mirror coatings will save energy without creating adverse effects, we conduct and support evaluations of windows incorporating heat mirrors in new and existing buildings. In 1981, we identified and specified windows incorporating appropriate heat-mirror coatings for several field test projects. We expect to continue this type of activity in 1982 and to assist in further analyzing and interpreting results.

Optical-Shutter Materials. Thin-film coatings having sun-control properties that can be changed by sunlight, temperature, or an applied voltage represent a long-term development goal of our program. We continue to examine the basic science of photothermochromic and electrochromic materials

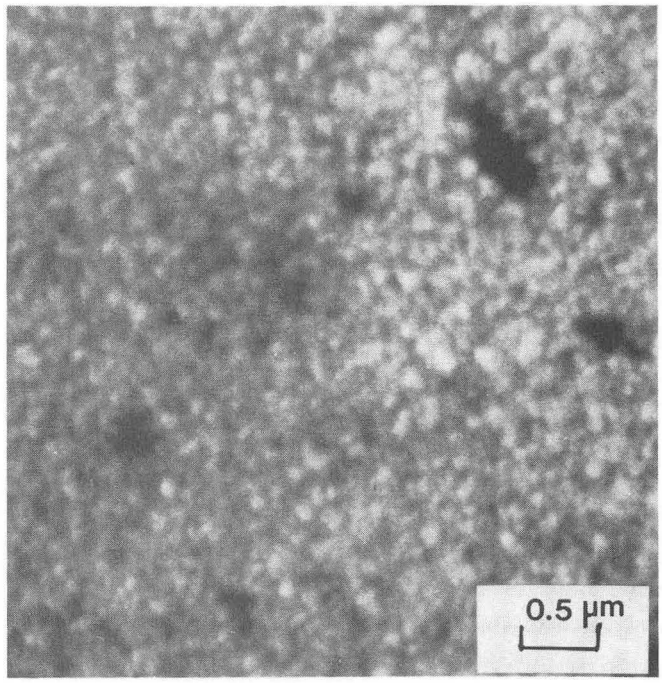

Figure 6. Particulate microstructure of an SnO_2:F transparent heat-mirror coating on glass. This coating was formed by chemical vapor deposition and analyzed by scanning electron microscopy (30° tilt, 20 kV). This film exhibits discontinuity in coverage (dark areas) which can be traced to interfacial contamination.

(XBB 810-10119)

that might have potential as optical shutters for windows.

Selective-Reflectance Coatings. Reflective and/or tinted glass is widely used in many commercial buildings to reduce solar impact and, thus, the energy required for air conditioning. This glazing, however, also reduces the amount of daylight entering interior spaces and potentially increases the use of electric lighting. An optical coating that selectively reflects short-wave infrared rays (which account for approximately one-half of the sun's radiation) but transmits visible light could, ideally, reduce cooling loads by 50 percent without reducing available illumination. Under subcontract, Kinetic Coatings, Inc. of Burlington, Mass., has used novel ion-beam sputtering techniques to produce a coating that is durable and weather-resistant and can be applied to the outside of a window.

Kinetic Coatings has demonstrated that coatings of high quality and good uniformity can be deposited on a thin plastic substrate in a roll-coating process. Coatings tailored to four building applications (residential, new and retrofit; commercial, new and retrofit) were produced and tested in 1980-1981.

As noted earlier, durability of window coatings is a critical issue because coated plastic glued directly to existing windows must withstand UV radiation, temperature cycling, physical abrasion, atmospheric pollutants, and cleaning agents. In prior years, a wide range of selective-reflectance coatings and protective layers were produced and tested for both optical performance and weatherability. Multilayer metal-dielectric coatings deposited on polyester and polypropylene substrates have shown adequate durability in exposure tests conducted to date.

Because coating durability has been the key uncertainty restricting the development of successful energy-conserving products, we have developed a materials-science characterization and test capability during the past few years. We can now examine the physical structure of coated samples by transmission and scanning electron microscopic techniques and analyze the chemical composition of both films and their defects by scanning Auger and x-ray spectroscopic techniques. Figure 7 shows the example data produced by this analysis.

Fenestration Optimization Studies. Selection of materials and design of fenestration systems for optimal annual energy performance is a complex problem that requires consideration of heating and cooling requirements and daylight utilization. A study has been undertaken to define the ideal performance characteristics of both existing and hypothetical glazing in a commercial office building as a function of climate and orientation within a broad set of fenestration parameters. Annual energy performance is being modeled with a modified version of DOE-2.1.

The initial phase of this work has concentrated on the variables of glazing material properties and glazing area. Computer analysis has been completed for three varied climates. Sample results in Figure 8 show energy requirements for a south zone in New

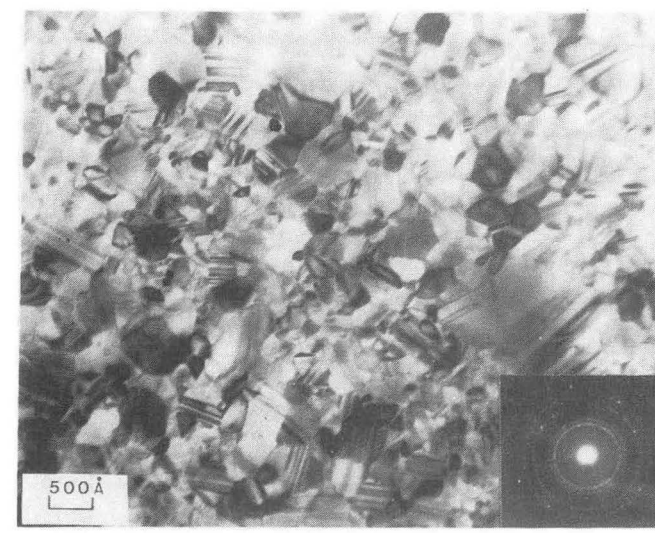

Figure 7. Transmission electron micrograph of improved silver layer microstructure in Al_2O_3/Ag on polyethylene terephthalate substrate (bright field at 100 kV). The continuous polycrystalline nature of the film is noted in both the micrograph and electron diffraction pattern.

(XBB 810-10120)

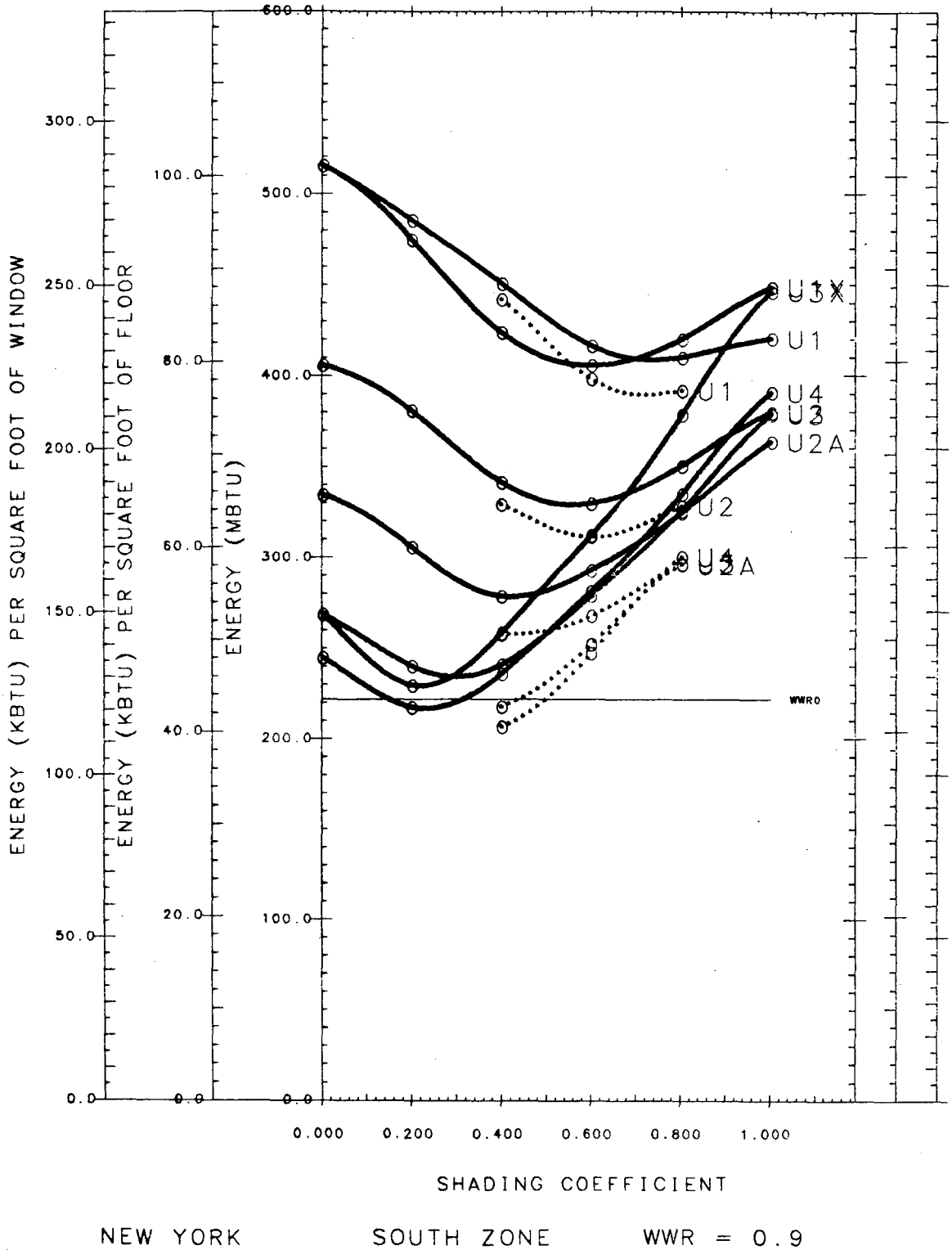

Figure 8. Energy requirements for a south-oriented office module in New York City.

U1 = Normal single glazing, nominal 6.28 W/m^2°C.
U2 = Single glazing with low-emissivity coating, nominal 4.33 W/m^2°C.
U2A = Normal double glazing, nominal 2.78 W/m^2°C.
U3 = Normal triple glazing, nominal 1.8 W/m^2°C.
U4 = Nominal W/m^2°C.
Suffix X -- No drapes deployed as a shading device.
Solid Line -- Energy use with no utilization of daylighting.
Broken Line -- Energy use with daylighting utilization.

(XBL-823-8273)

York City for a broad range of U-values and shading coefficients, with and without the effect of daylighting. Detailed analysis of component loads (heating, cooling, fans, lighting) enables us to understand the complexity of this optimization problem. Although optimal glazing parameters vary with climate, orientation, and window size, we conclude that it is almost always possible to find a glazing system that outperforms an insulated wall on the basis of annual energy consumption.

Air-Flow Window Systems. Another category of a high-performance window system is known as the air-flow window. In this system, a stream of air flowing between the panes of multiple-glazed windows acts as a heat-transfer fluid. Solar gain can be either collected or rejected as required, and daylighting can be fully utilized throughout the year. A design approach that has been used in Europe for many years involves integrating the window into the heating, ventilating, and air-conditioning (HVAC) system and exhausting room air through the glazing cavity. Venetian blinds in the glazing cavity can be adjusted to provide optimum daylight penetration, control the glare of direct sunlight, and function as solar absorbers. By means of the air flow, solar gain is either rejected to the outside or distributed through the HVAC system as required (Figure 9).

Although the first cost of such windows is higher than the cost of conventional windows, the prospect for widespread utilization is attractive.

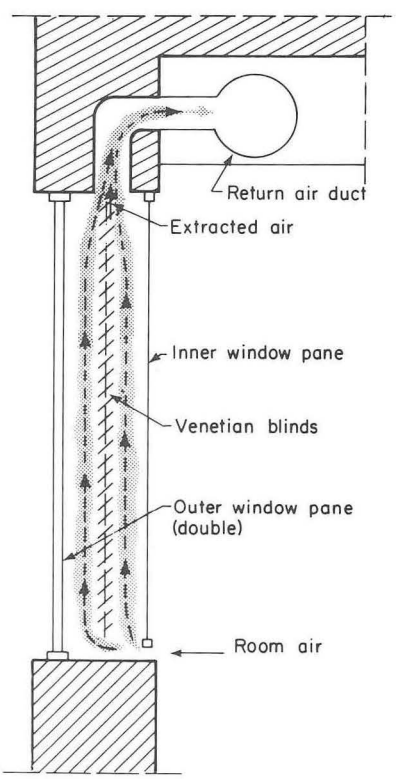

Figure 9. Schematic cross-section of air-flow window system.

(XBL 7912-13366)

The window package fits within the currently accepted architectural vocabulary, utilizes conventional components having well established reliability, and offers multifunctional control of energy performance.

Another approach being investigated was developed at the Environmental Research Laboratory (ERL) of the University of Arizona. This window system, designed primarily for residential application, combines existing commercially available components to achieve control of energy flows and relies on gravity-induced draft for heating and on overpressurization of the building by an evaporative cooler for cooling. ERL has completed summer and winter testing and has written computer-simulation codes.

LBL has supported long-term thermal-performance testing of these two generic types of air-flow windows. Preliminary results are promising. Industry interest has been growing because of the multifunction control options, and it is expected that U.S.-made units will be commercially available in 1982.

Daylighting

Windows and skylights provide daylight in buildings, thus reducing both electric lighting use and peak-power requirements. In addition, because natural lighting has always been valued by architects and building occupants, daylighting studies represent an area where good architectural design and significant energy savings are mutually supportive goals.

Studies of potential annual energy savings from maximum use of daylight in buildings require data on daylight availability, including the frequency and intensity of daylight. No source for such data currently exists for most of the United States. In 1977, the Pacific Gas & Electric Company building in San Francisco was instrumented to collect and record the amount of solar and visible radiation available at all building surfaces. An array of thirteen pyranometers and photometers was installed to feed readings to a data-acquisition system at fifteen-minute intervals (Figure 10).

Preliminary results from this monitoring suggest strong linear correlations between illumination and insolation, a finding that encourages us to believe that daylight availability data can be generated from existing measurements of solar radiation. Figure 11 illustrates one technique for analyzing and displaying the data. Daylight illumination on a vertical east-facing surface is shown as a set of contour lines for all hours of the day throughout the year. A generalized method for developing illumination-availability data from insolation is now being developed, based upon data collected from 1978 to 1981.

Accurate and efficient daylighting design methods must be conveyed to building designers if they are to successfully incorporate daylighting designs in buildings. Several approaches are in progress as part of the overall LBL program in this area. During the past few years, we have supported

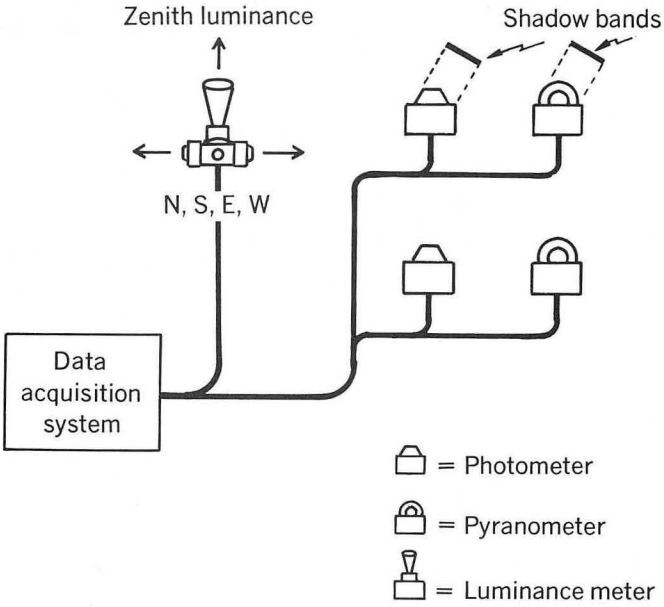

Figure 10. Schematic of photometric and radiometric sensor array on rooftop for determining insolation/illumination correlations.
(XBL 796-10182)

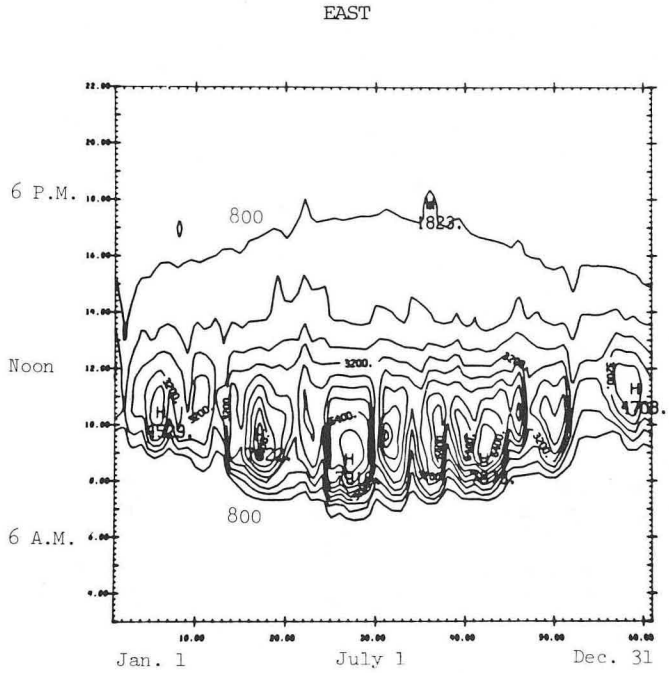

Figure 11. Vertical illuminance on an east-facing surface as measured during 1979 at the PG&E building in San Francisco. Interval between contour lines is 800 footcandles.
(XBL 813-8789)

a research project to develop a versatile and powerful computer program to predict daylight illumination in interior spaces. A working version of the program, SUPERLITE, which can compute illumination for non-rectangular geometries and can treat several types of window-shading devices, was completed in 1980 by researchers at the University of Southern California. Additional modeling capabilities are now being added while validation of the model is underway at LBL. A team at the University of Washington has developed a graphic design method that employs transparent overlays for daylight predictions and is designed to be used by architects at an early stage in the design process. Several parallel modeling efforts were completed at LBL. A simplified model for predicting daylight illumination from clear and overcast skies was developed in 1979, and, while relatively accurate, it required repetitive calculations. In 1980 this model, QUICKLITE, was adapted for use with a programmable hand calculator.

An effort continued in 1980 to incorporate advanced daylighting analysis capabilities into a building energy analysis program (DOE-2). In the previous year, in a cooperative program with the DOE-2 group, we developed and successfully utilized a simplified daylighting preprocessor that calculated hourly average-lighting schedules for each month. We have now completed initial development of an hour-by-hour daylighting model in DOE 2.1B. The daylighting model is being validated and will be extended in 1982 to allow modeling of very complex fenestration and shading systems.

The 24-foot-diameter artificial sky dome (Figure 12), designed and built on the U.C. campus in 1979 to facilitate model studies for daylighting, became operational in 1980 with the simulation of luminance distributions for an overcast sky. In 1981, we designed and installed improved lighting controls in the dome in order to simulate complex luminance distributions for clear skies. Sky-luminance distributions are reproduced on the underside of the hemisphere; light levels are then measured in a scale-model building under the artificial sky. From these measurements, we are able to predict daylighting-illumination patterns in real

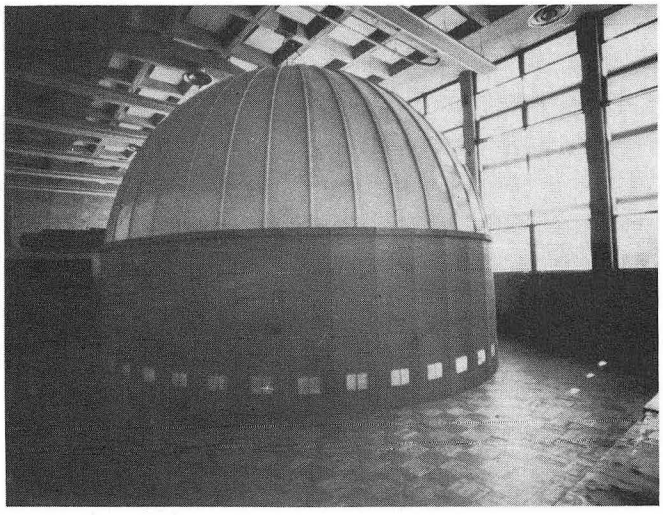

Figure 12. Exterior view of 24-foot-diameter hemispherical sky simulator for daylighting studies.
(XBB 804-5182)

buildings. The artificial sky already has been used for research and teaching purposes, as well as by architects working on daylighting features for new office buildings.

To test the combined effects of sky and direct sun without collimation or horizon errors, four scale-model test platforms were fabricated and mounted on the roof of our building. Because these test cells incorporate a tilting base, the sun's incident angle can be varied over a wide range.

Although direct energy savings from daylighting are the primary interest of building owners, significant savings might also accrue from reductions in peak-power demands. Past studies here indicated that savings that derive from time-of-day utility pricing, as well as from peak-demand charges, can equal or exceed the direct energy savings from daylighting in some buildings. This finding suggests that the economic benefits to utilities and to building owners employing daylighting strategies can be even greater than the benefits predicted from an analysis of direct energy savings alone.

Because direct sunlight is the only natural light source having sufficient intensity and collimation to illuminate interior spaces deep in a building, various design approaches have been studied to exploit beam daylighting in buildings. During the past four years, we have undertaken a small effort to examine the feasibility of mounting reflective and refractive devices in windows to take advantage of direct sunlight. We are also investigating the possiblity of using advanced optical technologies as beam-sunlighting systems. Limited computer simulation and model studies have been conducted; however, additional study is needed if we are to validate their technical feasibility and cost-effectiveness. Initial results suggest that the simplest systems that employ few or no moving parts, such as light shelves, may be the most cost-effective solutions.

We believe that daylighting techniques would be more widely used by architects and builders if technically accurate information was more accessible to them. A second draft of selected learning units in our Daylighting Resource Package, prepared in collaboration with the Illuminating Engineering Society, several universities, and daylighting experts throughout the country, was edited for future dissemination to educators and building designers. We initiated planning for an International Daylighting Conference to be co-sponsored by AIA, ASHRAE, and IES in February 1983.

PLANNED ACTIVITIES FOR FY 1982

Window Performance--Analysis and Testing

Our review of methods for calculating solar heat gain suggests that the simple single-term shading coefficient as presently used is inadequate for calculating solar gain for geometrically complex shading systems. An improved method is proposed to account for variations in angle of incidence and fraction of diffuse solar radiation. Special models will be developed to represent the optical and thermal properties of complex shading devices and non-homogeneous glazing materials. We will evaluate new thin-film devices, such as optical shutters and light-focusing holograms. Heat transfer around edges and through window frames will be studied.

The first module of the MoWiTT facility will be finished and calibrated during the first half of 1982, with initial field operation planned for later in the year. We will begin to compare results from dynamic performance testing with those from steady-state tests.

Fenestration Systems--Research, Development, and Demonstration

An international conference on optical materials for architectural windows and solar applications will be organized by LBL in conjunction with the International Society for Optical Engineering.

Our materials-science program will continue to answer research problems pertaining to heat-mirror coating design and durability. A limited effort will be undertaken to investigate such new materials as durable, transparent, optical-protective coatings and high-transmission films. Material combinations that exhibit improved coating properties and substrate/film stability will be identified. Basic research will examine selected refractory oxides, borides, carbide, and nitride systems for their suitability as heat-mirror or protective materials. We will continue the study and evaluation of optical-shutter materials for windows.

Test data collected on the performance characteristics of air-flow windows will be analyzed; performance characteristics will be compared to those of other heat-collecting window designs; and computer modeling techniques for annual energy analysis will be developed.

The energy optimization studies will be expanded to include additional classes of devices (operable shading and insulating systems), other building types, and additional climates. We will extend our analysis to include peak-load effects in addition to energy savings.

Daylighting

A complete summary of daylighting availability data based upon analysis of three full years of data from our San Francisco site will be completed in 1982. A recommended correlation between radiation and illumination data will be developed.

The simulation capability of our artificial sky will be completed in 1982, and improvements will be made in modeling variable ground reflectances. Plans will be completed to add a sun simulator, although construction will not begin until late in 1982. As the facility's capabilities are improved, we plan to perform an extensive series of tests to compare results from the indoor simulator,

from outdoor tests, and from the computer modeling studies as a means of defining the inherent limitations and constraints of all model-testing studies.

In the area of daylighting computations, the large computer model, SUPERLITE, will be expanded and used for parametric modeling studies of various fenestration and building designs. The new daylighting capabilities of DOE-2 will be fully tested and validated and will initiate development of a more powerful and flexible model that allows modeling of virtually any complex architectural solution.

Initial studies of the energy savings attributable to daylighting will be expanded to include a more comprehensive study of the effects of daylighting and lighting controls on a building's peak-power requirements. An analysis of prior work on glare from windows and its impact on the potential savings from daylighting will also be undertaken.

LIGHTING SYSTEMS RESEARCH*

R. R. Verderber, S. M. Berman, R. D. Clear, and F. M. Rubinstein

The Lawrence Berkeley Laboratory has managed the National Lighting Program for the Department of Energy (and its predecessor agencies) since 1966. For the past five years, the primary goal has been to accelerate the introduction of energy-efficient lighting products and concepts into the marketplace. This strategy was conceived as the initial thrust for accomplishing our goal of bringing about a 50-percent reduction in U.S. energy consumption for lighting by the mid-1990s. This savings of energy, more than 200 billion kilowatt-hours, is equivalent to 381 million barrels of oil annually, or more than one million barrels of oil equivalent per day--an amount greater than could be produced by the proposed synfuel program.

Programs initiated at LBL include development of the solid-state ballast, switching and control systems, and energy-efficient light sources, along with fundamental visibility studies and investigations into the effects of artificial light upon humans. The nature of the above studies required establishing three lighting laboratories: the Physical Lighting Laboratory, the Visibility Laboratory, and the Health and Environmental Laboratory. These laboratories are staffed with individuals representing various scientific disciplines: physicists, engineers, optometrists, and physicians, who interact closely to solve the lighting and visibility problems selected for study.

The commercial application of the technologies initiated by the LBL program (solid-state ballasts, lighting control systems, and adaptive circline lamps) reflects its impact upon the lighting community. However, this early success has introduced new issues that must be addressed to assure the widespread use of these new technologies. This includes the need to study the fundamental properties of plasmas (gas discharges) with regard to driving fields, magnetic fields, and ionizing materials; the effect of new light sources upon visibility and performance; and the effect of new light sources and systems upon humans and existing electronic systems. The new technologies have also suggested additional means to further increase the reliability and efficacy of light sources through fundamental studies of gas discharges at very high frequencies.

To meet these needs, the primary thrust of the lighting program has been altered to explore more basic problems. The three major efforts consist of the technical program (efficient light sources, advanced lighting systems); building applications (lighting system integration, building energy optimization); and the impacts program (visibility, performance, and human responses to artificial lighting).

The accomplishments that have been realized by the 1981 projects and the activities planned for 1982 are described below.

ACCOMPLISHMENTS DURING FY 1981

Solid-State Fluorescent Ballasts

The technical developments underlying the solid-state fluorescent ballast have been completed.[1] Included in this development was a demonstration of the 1977 ballast prototypes in a Pacific Gas & Electric Company (PG&E) office building. The demonstration was designed to reveal any defects in the solid-state ballasts that would become evident in a large-scale installation. Several problems were identified and appropriate modifications made. To verify that these ballasts were then commercially viable, two large demonstrations were initiated in 1980 and completed in 1981. At a Veterans Administration (VA) Medical Center,[2] a

*This work was supported by the Assistant Secretary for Conservation and Renewable Energy, Office of Building Energy Research and Development, Building Equipment Division of the U.S. Department of Energy under Contract No. DE-AC03-76SF00098.

250-ballast demonstration was conducted to determine the energy savings of such a retrofit as well as to measure electromagnetic interference (EMI) levels to determine if they would present a hazard to equipment or personnel.

Figures 1 and 2 present the results of the conducted and radiated EMI, respectively, measured from solid-state ballasts. In both figures, the recommended Federal Drug Administration (FDA) limits are plotted for the susceptibility limit, the narrowband limit, and the broadband limit. The conducted EMI from the solid-state ballasted system is about 20 db above the EMI from the core-coil ballasted system (see Figure 1). However, EMI from the solid-state ballasted system falls well within the susceptibility limits prescribed by the FDA. The radiated EMI, Figure 2, exceeds the FDA susceptibility limit at only two frequencies, 24 and 48 kHz. While this suggests a potential for disturbance, the EMI levels from a TV set (Figure 3) are about the same as levels from the lighting system. Because TV sets are in all the wards and have not been identified as a source of disturbance, it is unlikely that the level from these lamp systems would adversely affect equipment or personnel.

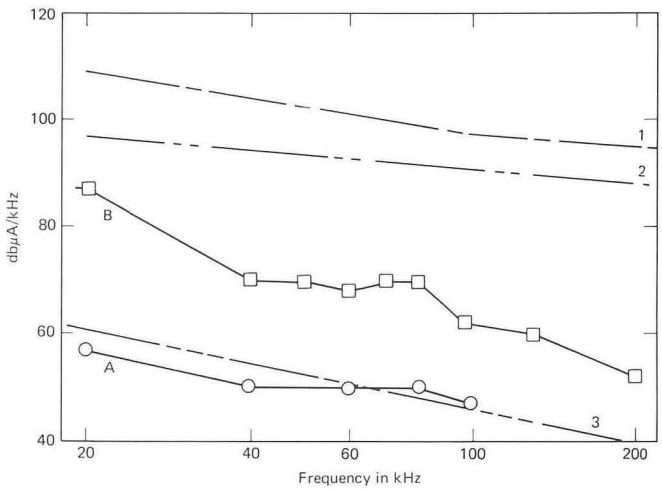

Figure 1. Conducted EMI data for 36 two-lamp fixtures: (A) conventional ballasts, (B) solid-state ballasts, (1) FDA medical device susceptibility limit, (2) FDA narrowband emission limit, (3) FDA broadband emission limit.

(XBL 813-411)

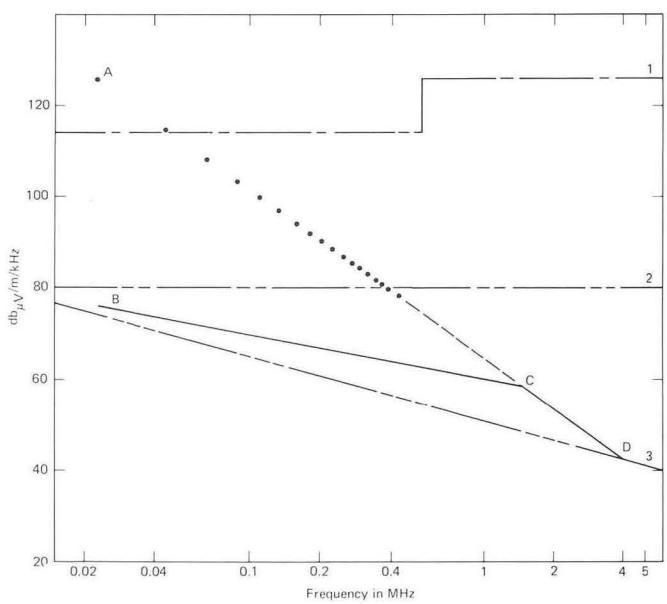

Figure 2. Electric-field radiated EMI for a 4-ft, 2-lamp, solid-state ballasted fixture: (AC) narrowband peaks, (BCD) broadband background noise, (1) FDA susceptibility limit, (2) FDA narrowband limit, (3) FDA broadband limit.

(XBL 813-414)

Neither these data nor the four-year demonstration at the PG&E building revealed any office or hospital area in which a solid-state ballasted lamp affected an in-place system which was not affected by a core-coil ballasted lamp.

The second demonstration[3] involved 2000 solid-state ballasts distributed to about 20 sites throughout the United States. The maintenance staff at each site installed the units and measured the power and light levels before and after installation. Although some of the reports have not yet been returned, initial results indicate about a 10-percent decrease in light level and a 32-percent decrease in power level, which is equivalent to about a 22-percent increase in system efficacy. Each site was to monitor failures; the failure rate of the 120-volt units was negligible. For example, at the PG&E site where 400 ballasts were installed, only one ballast failure has been reported. The much greater failure rate of the 277-volt units has been attributed to spurious voltage spikes and can be eliminated by using transistors having higher voltage ratings.

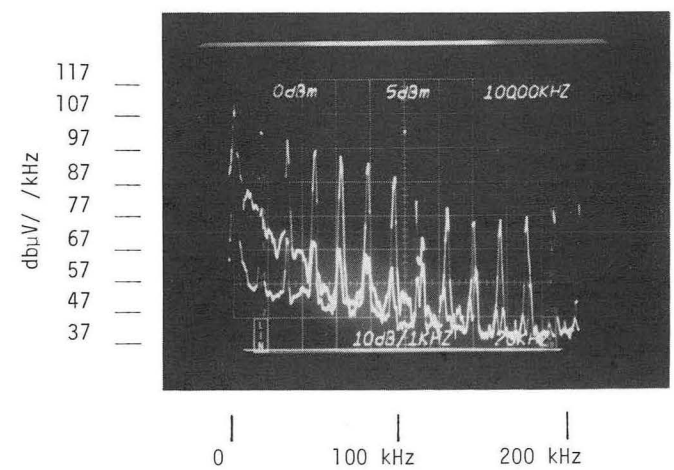

Figure 3. Electric field radiated EMI spectrum analyzer photograph for room television set located 6 feet away.

(XBB 818-8203A)

These two solid-state ballast demonstrations have provided further evidence of the energy savings, reliability, and safety of the concept of solid-state ballasts operating gas-discharge lamps at high frequency.

High-Pressure Sodium (HPS) Ballasts

The first phase of this project, begun in 1980, had the goal of developing solid-state HPS ballasts for 150-watt, 200-watt, and 400-watt HPS lamps. A contractor was selected for each type of lamp. Phase I results showed efficiency improvements as high as 17 percent.[4-7]

The three contracts were continued in order to study the effect of voltage surges on the systems and ways to improve system efficacy. Two contractors have delivered 15 solid-state ballasts that are being tested at LBL.

The low improvement of lamp efficacy (4 percent) at high frequency has been disappointing. However, a review of the HPS lamp theory shows that conductive losses will increase if the lamp-wall temperature is decreased. Thus, operating lamps at higher frequency and lower power, as most contractors are doing, will reduce lamp efficacy.[8]

Ongoing measurements will examine lamp efficacy as a function of input power. These data should provide ballast designers with the information necessary to design systems having optimum performance.

Switching and Lighting Controls

A major objective of the switching and controls project has been to develop a computer program to forecast the energy saved by applying various lighting-control strategies to a given building. Smith, Hinchman & Grylls, an architectural/engineering firm, was contracted by LBL to develop this computer program. The program, written in the FORTRAN programming language, was delivered to LBL in 1981 and has been put on our BKY computer system.

This computer program is an especially powerful tool for estimating the energy-conserving potential of a lighting-control system that responds to natural daylight. Calculations of available daylight in the building space under analysis are required as input data to the program. Such calculations, however, are cumbersome if made by hand and expensive if modelled on a computer. In an effort to minimize the number of required input data, the computer program uses Fourier series curve-fitting to generate a complete daylight-availability curve for a given day from a small number of input data points. The accuracy with which the program predicts the energy saved by daylighting is significantly affected by the degree to which the generated daylight-availability curve matches actual daylighting conditions.

To validate the accuracy of the curve-fitting technique, the subcontractor was requested to compare actual daylighting measurements taken at the

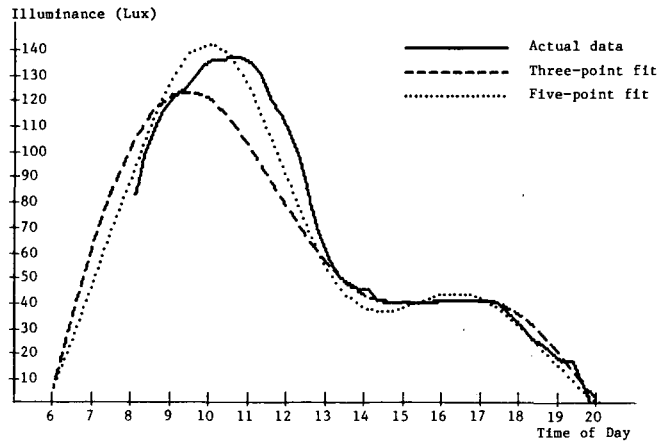

Figure 4. Comparison of predicted light levels with measured light levels at the test site. (XBL 8112-13010)

PG&E building in San Francisco with the Fourier series curve generated from a limited number of input data points. In Figure 4, the measured daylight values are shown by the dotted line. The Fourier series curves generated using three and five input points are shown with the dashed and dotted lines, respectively. Using five input points, the generated curve matches the measured values very closely. The curve generated from only three data points is also a reasonable fit and is probably sufficiently accurate for most purposes.

Energy-Efficient Light Bulbs (EELB)

This program was designed to explore several concepts for an efficient light source that could be used in the same socket as an incandescent bulb. Our aim was to attain lamp efficacies of 40 to 50 lumens per watt, which would be nearly three times as efficient as a 100-watt incandescent lamp (17.5 lumens per watt). The four approaches chosen include the compact fluorescent lamp, the coated filament lamp, the magnetic arc spreading lamp, and the electrodeless fluorescent lamp. Litek International Corporation has completed the first phase of their contract and delivered a final report and ten operating electrodeless lamps.[9]

Nine lamps have been measured by the LBL staff. The results are listed in Table 1. The

Table 1. Performance of electrodeless lamps.

Lamp No.	Light Output (lumens)	Power (watts)	Power Factor (percent)	Efficacy (lumens/watt)
1	1660	29.2	58	56.8
2	1710	31.9	58	53.5
3	1550	30.8	58	50.2
5	1890	34	59	55.7
6	1550	31.3	59	49.6
7	1630	31.9	59	51.2
8	1740	32.2	58	54.2
9	1630	29.3	59	55.7
10	1620	32.1	58	50.3
Average	1660	31.0	58	53

performance of these lamps has exceeded our initial goals, as the average efficacy of the lamps exceeds 50 lumens per watt.

In addition, the lumen output of some lamps exceeds the light output from a 100-watt incandescent lamp (1750 lumens). This has never before been achieved by any reasonable-size fluorescent system.

The high efficacy and high light output result from eliminating the need for filaments: the low-pressure gas discharges are driven at a very high frequency (13.56 MHz). This high-frequency mode of operation, however, introduces a potential for interfering with other electronic systems such as TV sets, radios, and communication devices. LBL will carefully measure the conducted and emitted electromagnetic interference (EMI). We have done some initial cursory testing by operating a lamp within three feet of a TV set. We observed no interference. Extended studies will focus on more quantitative measurements of EMI levels.

Physical Lighting Laboratory

The Physical Lighting Laboratory was completed and furnished with the equipment necessary to accurately measure the absolute light levels from light sources. Much of the effort to date has gone toward calibrating the standard National Bureau of Standards (NBS) light sources and spectral distributions in order to give us the capability of measuring absolute levels of light.

The fundamental study of low-pressure plasma that could improve the efficacy of fluorescent lamps by optimizing the Hg isotope mix has realized considerable progress. The initial task of designing test lamps that can obtain reproducible results with ±1 percent accuracy is near completion. The lamps have been made of quartz to permit the measurement of the 185-nm and the 254-nm radiation emitted by the low-pressure Hg plasma. We have resolved all of the problems that have included seasoning the filament, controlling the minimum lamp wall temperature (gas pressure), and accurately measuring the intensity of the 185-nm and 254-nm lines.

Visibility and Productivity Laboratory

The connection between visibility and productivity continues to be of major interest. In April 1980, the Illuminating Engineering Society (IES) updated its illumination recommendations with the publication of RQQ #6, "Selection of Illuminance Values for Interior Lighting Design." In April 1981, the International Commission on Illumination (CIE) released its publication CIE 19/2, "An Analytic Model for Describing the Influence of Lighting Parameters upon Visual Performance."

In 1981, LBL prepared a critical review of the above documents. This review was presented at the annual IES technical conference in Toronto and has been accepted for publication in the IES Journal.[10]

During the year, LBL, in conjunction with the University of California School of Optometry, has also established a visibility laboratory to study the cause of fatigue associated with video display visual tasks. A microcomputer has been modified and programmed to present visual displays on a variety of terminals and then score performance on tasks associated with the displays. A system has been designed that can vary the types of light sources and the rate of flicker. To expedite the accumulation of data, the lab has three test stations in which three subjects can be tested simultaneously.

Health and Environmental Laboratory

The Health and Environmental Laboratory was designed to study the effects of artificial illumination upon humans. The experimental designs were submitted to the University of California Council, which granted approval to perform these tests on human subjects. Establishing the laboratory included the purchase and programming of a computer system to control the visual task and the lighting system while continually measuring subjects' vital signs.

The testing chamber was constructed at the LBL shops. The chamber will isolate the subject from the environment and influences that would be manifest in an artificial lighting system: light, sound, and electromagnetic radiation. Initial test runs of the equipment have been made.

PLANNED ACTIVITES FOR FY 1982

High-Frequency Performance of Gas-Discharge Lamps

In the next stage of the solid-state ballast program, we will study the performance of gas-discharge lamps over a higher frequency range (above 20-30 kHz). We intend to extend the measurements to several megahertz to determine the optimum frequency range. The selection of the 20-kHz frequency was based upon existing switching transistors. The introduction of power-field effect transistors permits ballast designs above the MHz region.

In addition, to resolve the potential electromagnetic interference (EMI) question, LBL is planning to measure the conducted and radiated EMI for all newly introduced lighting systems. Members of the lighting community involved with high-frequency lighting systems will participate in a two-day working seminar to be held at LBL. The purpose of the seminar will be to establish ways of measuring EMI from these systems and to exchange information on possible problems associated with EMI.

Switching and Lighting Controls

The two current demonstrations will be completed and the data compiled. These data will be used to validate the computer program that has been developed to predict the energy savings that can be realized by different control strategies and techniques. To improve this computer program, a simple program is being devised to input daylighting data.

LBL has developed some programs that can be used with hand-held calculators and will be used as the daylighting input for the controls program.

Physical Lighting Laboratory

After the test lamp is shown to produce results within 1-percent accuracy, a series of experiments will be made with various Hg isotope mixes. Each measurement consists of a series in which one parameter is varied: power input, frequency, lamp wall temperature, ambient temperature, or current. The results from this series of experiments will be compared to theoretical predictions.

Visibility Laboratory

The laboratory equipment and testing facilities will be tested to determine if we are obtaining the proper light and control of the light. Subjects will be selected in accordance with the experimental design, and the lighting system will be varied with regard to type of light (incandescent, fluorescent), type of fluorescence (cool-white, warm-white, tri-stimulous phosphor), intensity, percent flicker, and various visual tasks. By measuring the accuracy of subjects' responses as a function of the illumination and video display tasks, we can perhaps relate the onset of visual fatigue to contrast, acuity, and color sensitivity.

We are planning two other major projects. The first is to develop a rational method for recommending or specifying light levels (visibilities) that are based on visual performance criteria. An important part of this task is to determine how to deal with the severe problems in the present models that estimate visual performance. Our second planned activity is to try to improve existing models of visual performance.

Health and Environmental Laboratory

After all of the equipment meets the staff's requirements, test subjects will be screened. Initial experiments will be qualitative. The more obvious parameters of artificial lighting systems will be varied: type of source (incandescent, fluorescent, high-pressure sodium), illumination level (<50 footcandles, > 100 footcandles), spectral distribution (continuous, tri-stimulous, monochromatic, cool-white, warm-white, and daylight), glare, percent flicker, and audible noise. By monitoring subjects' vital signs, with and without the performance of visual tasks, these experiments will indicate the onset of stress and/or discomfort.

These results will provide the basis for quantitative measurements of the parameters that are shown to have a qualitative influence. Other parameters of interest will be EMI levels and ultraviolet and infrared radiation.

REFERENCES

1. Verderber, R.R. (1980), Electrical Consultant 60, pp. 22-26, and Lawrence Berkeley Laboratory Report LBL-10707.

2. Verderber, R.R., et al. (1981), Energy Efficient Management of Lighting in a VA Medical Center, Lawrence Berkeley Laboratory Report LBL-12659.

3. Verderber, R.R., and Morse, O. (1980), On-Site Demonstration Procedure for Solid-State Fluorescent Ballast, Lawrence Berkeley Laboratory Report LBL-11619.

4. Felper, G. (1980), HID 400-watt Sodium Ballast, Phase I Final Report, Lawrence Berkeley Laboratory Report LBL-11254.

5. Alling, B. (1980), HID Solid-State Ballast Program, Phase I Final Report, Lawrence Berkeley Laboratory Report LBL-11845.

6. Burke, R. (1980), Energy Efficient HID Solid State Ballast, Lawrence Berkeley Report LBID-391.

7. Verderber, R. and Morse, O. (1981), Energy Savings with Solid-State Ballasted High-Pressure Sodium Lamps, Lawrence Berkeley Laboratory Report LBL-12595.

8. Waymouth, J.F., and Wyner, E.F. (1981), "Analysis of Factors Affecting Efficacy of HPS Lamps," Journal of Illuminating Engineering Society, p. 237.

9. Simpson, R., and Jones, R. (1980), Electrodeless Fluorescent Lamp, Lawrence Berkeley Laboratory Report LBL-13480.

10. Clear, R., and Berman, S. (1981), A New Look at Models of Visual Performance, Lawrence Berkeley Laboratory Report LBL-12496.

BUILDING ENERGY SIMULATION GROUP*

J. J. Hirsch, W. F. Buhl, R. B. Curtis, A. E. Erdem, K. H. Olson, and F. C. Winkelmann

The purpose of this project has been to create, test, document, and maintain a user-oriented, public-domain computer program that will enable architects and engineers to perform design studies of whole-building energy use under actual weather conditions. The development of this program, which in its successive public generations has been known as Cal-ERDA, DOE-1.4, DOE-2.0, and, finally, DOE-2.1, has been guided by several objectives:

1. that the description of the building by the user be in quasi-English so that the input can be read and understood easily by non-computer scientists;

2. that, when available, the calculations be based upon well-established algorithms, i.e., the calculational procedures used should be acceptable to the engineering community;

3. that it permit simulation of commonly available heating, ventilation, and air-conditioning (HVAC) equipment;

4. that the computer costs of the program be minimal; and

5. that the predicted energy use of a building be acceptably close to measured values.

These objectives require compromises to be made. Greater accuracy, for example, can be purchased only at the cost of more detailed and time-consuming algorithms and more complex demands upon the user for data about the building being modeled. Considerable experience and user feedback have culminated in a program which has received much acceptance.

As can be seen in Figure 1, DOE-2 is composed of two major segments: the Building Description Language (BDL) processor, which allows the user to give a quasi-English description of building components, and the LOADS, SYSTEMS, PLANT, and ECONOMICS (LSPE) processor, which uses building descriptions to simulate the building energy performance. Details of the development and structure of the DOE-2 program are available in past annual reports[1-3] and other published materials.[4-8]

ACCOMPLISHMENTS DURING FY 1981

The major accomplishment of FY 1981 was the completion of the DOE-2.1A version of the program and the drafting of its accompanying documentation.[9-13] LBL was assisted in this program by the Q-11 Group at Los Alamos National Laboratory (LANL), which was responsible for producing the final DOE-2.1A Reference and Engineers Manuals from LBL-produced drafts. In addition, the "DOE-2 USER NEWS" was published quarterly by the Building Energy Simulation Group (BES) to keep the user community informed about the latest developments, uses, and problems of the program. The DOE-2.1A version is used on many computers with word sizes of 32 bits or larger. It is currently available on DEC-10, DEC-VAX, CDC-Cybers, IBM, Data General MU8000, Honeywell level-6, and Cray-N machines.

The BES Group's ongoing research into calculation methodologies relating to building energy use is divided into two major areas of interest. The first area centers on the modeling of the building-envelope components and systems. The second area of interest is the simulation of heating, ventilating, and air-conditioning (HVAC) equipment and their associated control systems. Selected major new features of DOE-2.1A in these two areas are described below.

Building Envelope Heat-Transfer Modeling

The first step in the simulation of the building is modeling the heat transfer through the building envelope components. During FY 1981, three major areas of envelope heat transfer have been studied: (1) conductive gains through generalized layered walls and Trombe wall systems; (2) daylight transmission through windows as a supplement to artificial lighting systems and thermal effects of alternative glazing systems; and (3) techniques providing fast and accurate calculation of heating and cooling loads (or response) of whole spaces.

Response Factors

Building energy-use analysis programs which take into account transient heat flow must simulate the delayed transmission of heat through layered wall sections. The most popular means of doing so use response factors developed by Mitalas and Stephenson[14,15] and extended by a number of other authors in specific implementations. The response factors are sets of time series describing the response of a one-dimensional multi-layered slab to a unit pulse of heat applied to one face of the slab while the opposite face is held at a constant temperature. Most computations of response factors use the solution of the one-dimensional heat-flow equation in terms of Laplace transforms. In this approach, the differential equations become a series of coupled algebraic equations which are readily solvable. The Laplace transforms of the temperature and heat flux on one side of the slab are linearly related to the Laplace transform of the temperature and heat flux on the other side of

*This work was supported by the Assistant Secretary for Conservation and Renewable Energy, Office of Building and Community Systems, Buildings Division, U.S. Department of Energy under Contract No. DE-AC03-76SF00098.

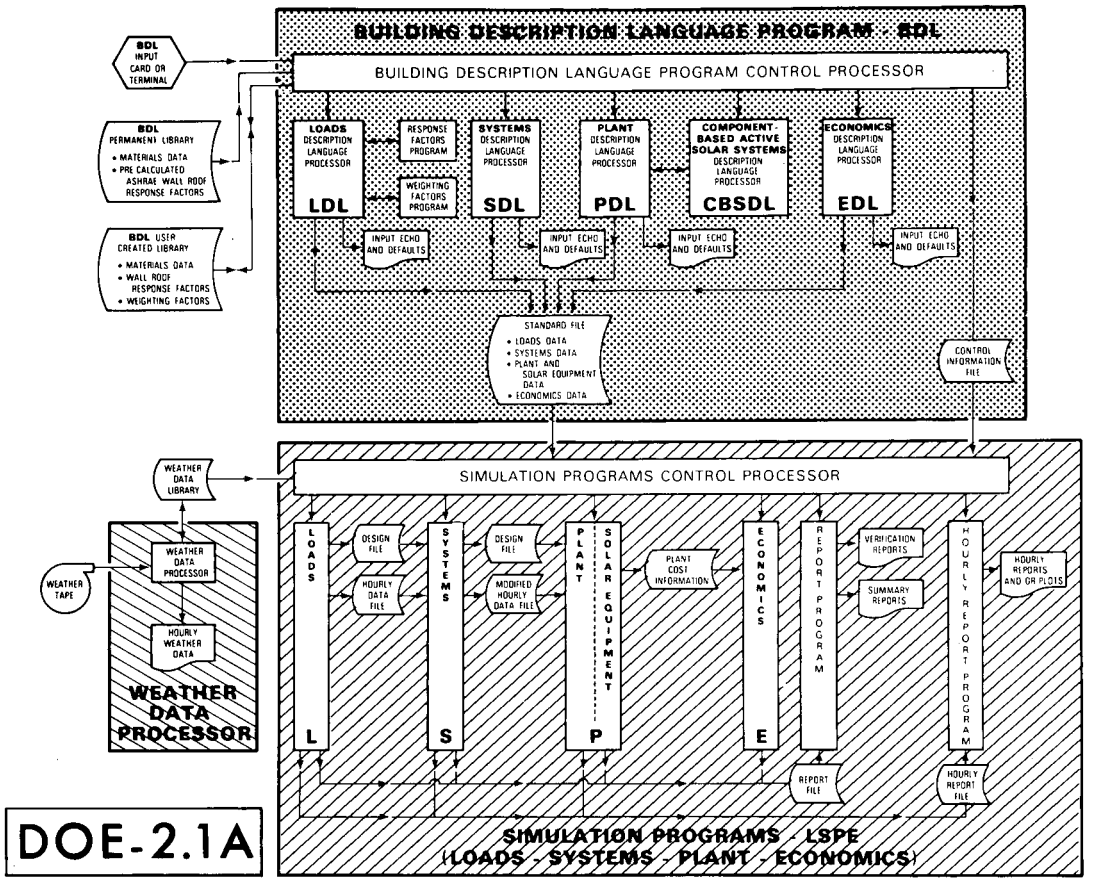

Figure 1. DOE-21A computer program configuration.
(XBL 825-601)

the slab. These linear equations may be written in matrix notation as shown in Equation (1).[13]

$$\begin{bmatrix} T(0,s) \\ q(0,s) \end{bmatrix} = \begin{bmatrix} A(s) & B(s) \\ C(s) & D(s) \end{bmatrix} \begin{bmatrix} T(L,s) \\ q(L,s) \end{bmatrix} \qquad (1)$$

The coefficients A(s), B(s), C(s), and D(s) are simply related to the corresponding coefficients for a single layer by the matrix formula of Equation (2).

$$\begin{bmatrix} A(s) & B(S) \\ C(s) & D(s) \end{bmatrix} = \begin{bmatrix} A_1(s) & B_1(s) \\ C_1(s) & D_1(s) \end{bmatrix} \begin{bmatrix} A_2(s) & B_2(s) \\ C_2(s) & D_2(s) \end{bmatrix} \cdots \begin{bmatrix} A_n(s) & B_n(s) \\ C_n(s) & D_n(s) \end{bmatrix} \qquad (2)$$

where

$$A_j(s) = \cosh\left[x_j \sqrt{\frac{s}{\alpha_j}}\right] ; \quad B_j(s) = \frac{\sinh\left[x_j \sqrt{\frac{s}{\alpha_j}}\right]}{k_j \sqrt{\frac{s}{\alpha_j}}}$$

$$C_j(s) = k_j \sqrt{\frac{s}{\alpha_j}} \sinh\left[x_j \sqrt{\frac{s}{\alpha_j}}\right] ; \quad D_j(s) = \cosh\left[x_j \sqrt{\frac{s}{\alpha_j}}\right]$$

and where s_j is the width of the jth layer, k_j is its thermal conductivity, and α_j is its thermal diffusivity.

The equations represented by Equation (1) must be solved for the fluxes in terms of the temperatures in order to compute the response factors.

$$\begin{bmatrix} q(0,s) \\ q(L,s) \end{bmatrix} = \begin{bmatrix} D(s)/B(s) & -1/B(s) \\ 1/B(s) & A(s)/B(s) \end{bmatrix} \begin{bmatrix} T(0,s) \\ T(L,s) \end{bmatrix} \quad (3)$$

The remaining problem is essentially to determine the inverse Laplace transforms of the coefficients in the square matrix. This requires locating the zeros of the function B(s). It is this process that is so time consuming, especially for multi-layered walls. The function B(s) must be evaluated many times; and, each time, the entire matrix multiplication indicated in Equation (2) must be performed. Hittle and Bishop[16] have found an improved method for locating the roots, but their method still requires performing the matrix multiplication. Peavy[17] argues that the matrix approach is at fault and provides explicit formulas for up to seven layers. Work performed by the BES Group has shown that the matrix approach can be used and the time-consuming matrix multiplication can be avoided. At the same time, there is no limit to the number of layers because the method is general.

If the matrix multiplication in Equation (2) is performed and the resulting matrix elements are subjected to trigonometric manipulation, it can be shown that the functions A(s), B(s), C(s), and D(s) can be cast in the forms:

$$A(s) = \sum_{k=1}^{2^{n-1}} a_k \cosh(\phi_k \sqrt{s}) \; ; \; B(s) = \frac{1}{\sqrt{s}} \sum_{k=1}^{2^{n-1}} b_k \sinh(\phi_k \sqrt{s} \; ;$$

$$C(s) = \sqrt{s} \sum_{k=1}^{2^{n-1}} c_k \sinh(\phi_k \sqrt{s} \; ; \; D(s) = \sum_{k=1}^{2^{n-1}} d_k \cosh(\phi_k \sqrt{s}) \quad (4)$$

where n is the number of layers and the coefficients a_k, b_k, c_k, d_k, and ϕ_k are constants independent of s. As a result, they need to be computed once at the beginning of the calculation and never again. When this algebraic simplification is combined with more sophisticated root-locating algorithms, the time of calculation of the response factors can be reduced by factors of up to 20.

Trombe Walls

The presently available building-energy-analysis programs, which have concentrated on energy transport by conduction and radiation, have been incapable of simulating convective transport because of the difficulty of simulating convection in comparison to conduction and radiation. In many buildings, particularly those that employ "passive" solar design, convection can be an important and even dominant effect.

The BES Group, in collaboration with LANL, has begun to integrate models of certain passive solar elements into the DOE-2.1A building-energy-analysis code. In FY 1981, a model of a Trombe wall was successfully added to DOE-2.1A. The Trombe wall consists of a south-facing window (usually double- or triple-paned) separated from a massive masonry or concrete wall by an air gap (see Figure 2). The combination acts as a crude solar collector, with the heat capacity of the wall providing the heat storage and preventing large temperature swings in the occupied space. Two types of Trombe wall are modeled: vented and unvented. In the case of the unvented Trombe wall, heat enters the occupied space through conduction alone. The vented Trombe wall has vents at the bottom and top of the wall which enable warm air to flow by natural convection directly into the living area.

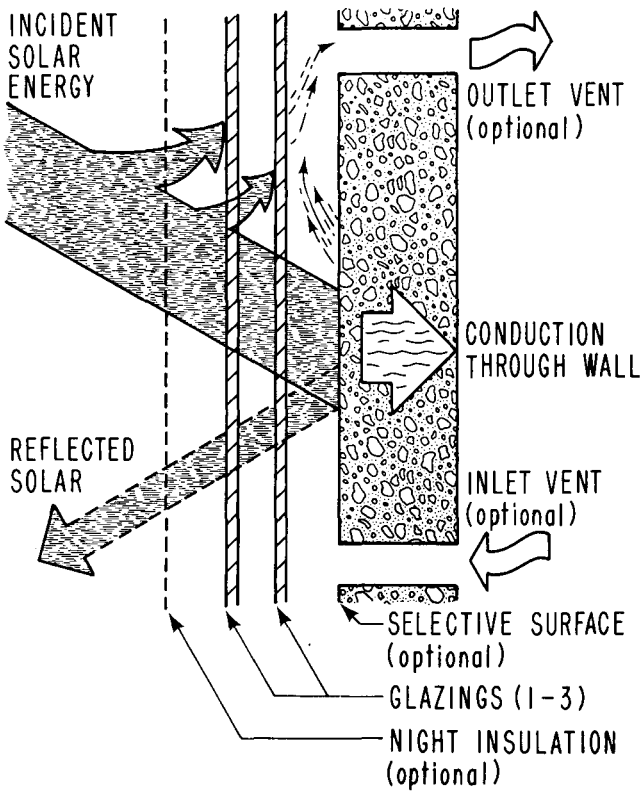

Figure 2. Diagram of heat flows in the DOE-2 thermal storage model.[18]

(XBL 825-597)

The model of the unvented Trombe wall is a straightforward extension of the already-existing capabilities of DOE-2. All that is needed is the convective heat-transfer coefficient across the air gap. Once this is known, the resistances to heat flow of the window and air gap can be combined into one overall resistance, and the heat flow through the wall can then be obtained in the usual manner. A standard empirical formula giving Nusselt number in terms of Grashoff number is used to obtain the convective coefficient. The formula is typical of engineering solutions to convective problems in that it combines experimental results with a parameterization based on a theory (the use of Nusselt and Grashoff numbers). Also typical is the fact that three different formulas must be used for the three cases of turbulent flow, laminar flow, and no flow (pure conduction).

The vented case is much more difficult to simulate. A force-balance equation is written to obtain the air-flow rate. The buoyancy force of the warm air is balanced by the opposing frictional forces caused by the air flowing through the vents and the air gap. Because the buoyancy of the air depends on its density, which is a strong function of the air temperature, the model must simultaneously do an energy balance on the wall and window surfaces to obtain surface and air temperatures. Because the operations are non-linear, they must be solved numerically, and the model must iterate between the two equations until a stable, simultaneous result is obtained for air flow, air temperature, and the surface temperatures.

The problems encountered in modeling the vented Trombe wall are typical of the difficulties arising from modeling convective processes simultaneously with radiative and conductive heat transfer. The experience gained in modeling the Trombe wall will enable development of models for other situations in which convective heat transport is important.

Practically speaking, the existence of a Trombe-wall model in DOE-2 enables the designer to optimize his Trombe-wall design for the building and climate of interest. The parameters that can be varied include wall heat-capacity and thickness, air-gap width, and amount and scheduling of insulation placed over the window. In a residence, the Trombe wall should be designed to deliver a significant amount of heat to the occupied area in the early morning hours when the heating demand is large. Venting can provide immediate delivery of heat during the day, if needed. The designer may want to vary the size of the vents to optimize the split between the amount of heat being delivered by the vents and the amount of heat stored in the wall for later delivery by conduction through the wall. For non-sunlit hours, insulation on the glazing helps solve the greatest deficiency of Trombe walls: the conduction of stored heat back out through the window. Without the flexibility of a Trombe-wall model integrated into a building-energy program, the exploration of the above options is not feasible. Overall energy savings produced by a Trombe wall would then be largely a matter of guesswork.

Daylighting

Lighting accounts for about 20 percent of the total electrical-energy consumption in the United States. Use of natural lighting is a very cost-effective way of reducing this consumption and, at the same time, enhancing the quality of the indoor environment. For several years, architects and engineers have been using scale models, hand-calculator programs, and sophisticated main-frame computer programs, such as LUMEN-II, to determine the level of interior daylight for different building configurations. However, none of these tools determines the annual energy savings from daylighting, information which can have an important effect on design decisions.

For this reason, a daylighting simulation has been added to DOE-2. Designers can now quickly and inexpensively determine the hourly, monthly, and yearly impact of daylighting on electrical-energy consumption and peak electrical demand, as well as the impact on cooling and heating requirements and, perhaps most important, on annual energy cost.

The DOE-2 daylighting algorithms were developed in collaboration with the LBL Windows and Daylighting Group. The calculation has two main stages. In the first stage, a preprocessor calculates in detail a set of "daylight factors" (interior illuminance divided by exterior horizontal illuminance) for later use in the hourly loads cal-

culation. The user specifies the coordinates of one or two reference points in a space. DOE-2 then integrates over the area of each window to obtain the contribution of direct light from the window to the illuminance at the reference points and the contribution of light from sky and ground which enters the window and reflects from the walls, floor, and ceiling before reaching the reference point. Taken into account are such factors as window size, glass transmittance, inside surface reflectances of the space, sun-control devices such as blinds and overhangs, and the luminance distribution of the sky. Because this distribution depends on the position of the sun and the cloudiness of the sky, the calculation is made for standard clear- and overcast-sky conditions and for a series of 20 different solar altitude and azimuth values covering the annual range of sun positions. The resulting daylight factors are stored for later use. Analogous factors for discomfort glare are also calculated and stored.

Stage two is the hourly daylighting calculation performed every hour of the year that the sun is up. The illuminance from each window is found by interpolating the stored daylight factors using the current-hour sun-position and cloud cover, then multiplying by the current-hour exterior horizontal illuminance. If the glare-control option has been specified, the program will automatically close window blinds or drapes to decrease glare below a pre-defined comfort level. Adding the illuminance contributions from all the windows gives the total number of footcandles at each reference point.

The program next simulates the lighting-control system to determine the electrical lighting energy needed to make up the difference, if any, between the daylighting level and the required illuminance.

An example of the daylighting calculation is shown in Figures 3 and 4. The 400-ft^2 module in Figure 3 has a 5-ft x 20-ft east-facing window with a glass transmittance of 80 percent. The window is covered on the inside by fixed drapery having a transmittance of 60 percent. A 4-ft-deep overhang runs the entire length of the window. Wall, floor, and ceiling reflectance is 50 percent. The daylighting reference point is located mid-floor at desk height (30 in.). Overhead lighting of 2 W/ft^2 provides 50 fc of illuminance at full power between 8:00 a.m. and 6:00 p.m. Continuously dimmable lighting control allows the lights to dim linearly to 10 fc at minimum (30 percent) power.

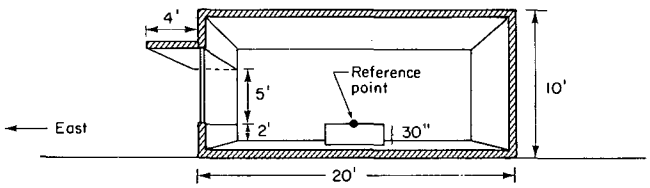

Figure 3. Test model for DOE-2 daylighting calculation.

(XBL 825-596)

The results of a DOE-2 run of a partly cloudy June day in San Francisco are shown in Figures 4a and 4b. Figure 4a shows that the daylight illuminance varies from a minimum of 0.4 fc at 5:00 a.m. to a maximum of 64 fc at 9:00 a.m. Summing over the hours in Figure 4b gives a net reduction in lighting energy use of 59 percent.

To verify that the DOE-2 daylighting calculation gives accurate results, program predictions are being checked against illuminance measurements obtained by the Windows and Daylighting Group, using scale models with various common window configurations. An offshoot of this cross-check will be the development of a method to enable daylight factors measured from models, or calculated by programs such as LUMEN-II, to be used directly in DOE-2, thus making it possible to simulate virtually any daylighting configuration.

Glazing Optimization Study

In collaboration with the Windows and Daylighting Group, a study was undertaken in which annual energy consumption in an office building

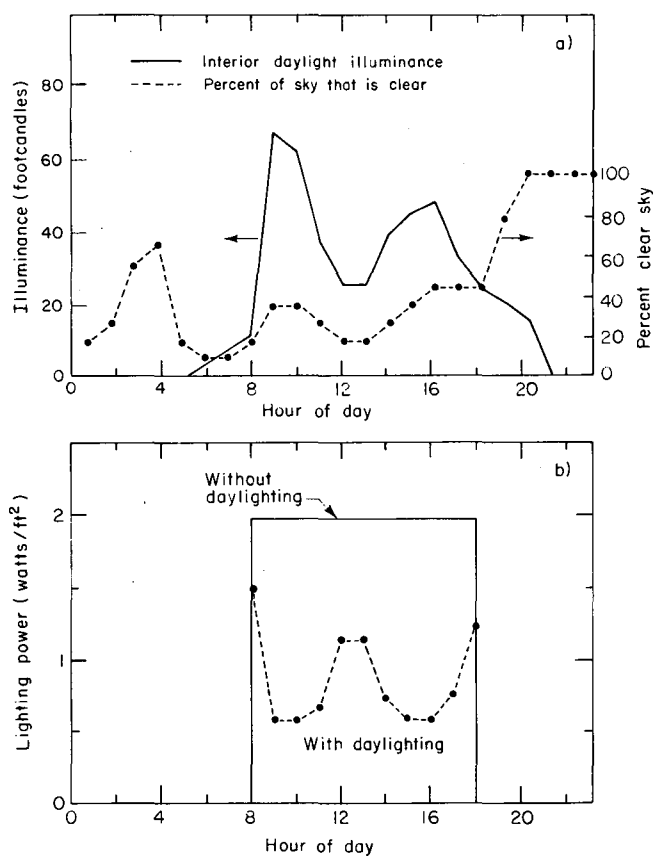

Figure 4. Results of DOE-2 daylighting calculation for a partly cloudy June day in San Francisco, for the test module shown in Figure 3. (a) Daylight illuminance at the reference point and percent of sky that is clear. (b) Power consumption for electric lighting with and without daylighting.

(XBL 825-598)

module was modeled parametrically with DOE-2 for a wide range of glazing properties in three different climates.[19] A primary objective was to develop results that could be readily generalized and applied to optimize glazing for a wide variety of design considerations.

Values for thermal conductance, shading coefficient, and visible transmittance were parametrically varied through representative ranges. Annual energy use in a prototypical module of an office building was calculated as a function of glazing material properties, glazing area, orientation, and climate. A module configuration, representative of commercial office building construction, was evolved through a series of sensitivity studies as the basis for a building-block approach for calculations. The 200-ft by 200-ft building module, which can be considered as a single floor in a multistory building, contains four identical perimeter zones, each 30 ft deep, surrounding a core zone. The windows are furnished with drapes having a shading coefficient multiplier of 0.6. There is an 80-percent probability that the drapes are closed when direct solar transmission exceeds 20 Btu/ft^2-hr.

Annual energy consumption was modeled with DOE-2.1, which was modified to improve the analysis of fenestration performance. Glass conductance was varied from 1.1 Btu/ft^2-hr (single glazing) to 0.32 Btu/ft^2-hr (triple glazing). Shading coefficient was varied from 0 to 1.0 and window-to-wall ratio was varied from 0 to 90 percent. Cities were chosen to represent a wide range of climatic conditions. We selected Bismarck, North Dakota, with a northern heating-dominated climate; New York City, with significant heating and cooling requirements; and Miami, Florida, characterized by low latitude and a cooling-dominated climate.

An example of our results for New York City is shown in Figure 5.

From more than 250 DOE-2.1 energy analyses, four general conclusions were drawn:

1. Glazing of a perimeter zone office will have a major impact on energy consumption for both heating and cooling. The relationship of energy consumption to glazing is a complex function of glazing size, orientation, and climate.
2. In all climate zones and on all orientations, a glazed wall with properly selected glazing can usually provide equivalent or better energy performance than an unglazed wall. Energy efficiency can be achieved while retaining the desirable architectural qualities of windows.
3. Net annual performance can be fully understood only by examining the component loads in detail and by accounting for the performance of heating and cooling equipment and building operation schedules.
4. No rule of thumb consistently allows for selecting optimal glazing properties. In most cases, if a desired energy budget is chosen, several glazing-system approaches will be available to the building designer, providing flexibility in the design of energy-efficient solutions without compromising other design requirements.

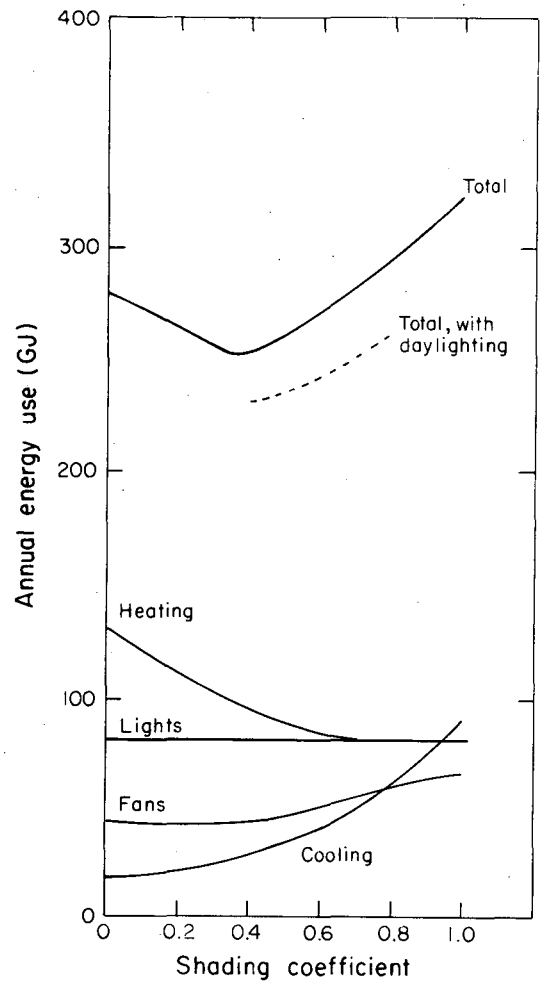

Figure 5. Sample glazing optimization results for a prototype office building located in New York City. The curves, obtained with DOE-2, show how the annual energy use and the energy-use components of a south-facing perimeter zone depend on the shading coefficient of the glazing. The zone has single-pane glass and a window-to-wall ratio of 90 percent.

(XBL 825-595)

In future work, this study will be expanded to include the performance of window systems with a variety of fixed and operable shading devices. The Building Energy Simulation and the Windows and Daylighting groups are currently developing algorithms which will enable the thermal, solar gain, and daylight transmittance properties of such devices to be modeled.

Custom Weighting Factors and Thermal Balance Loads

Research is continuing in these two areas with the objective of providing substantially improved

techniques to calculate the heating and cooling loads of building thermal spaces. In the "custom-weighting-factor" method, a fast-executing transfer-function approach is used. The second method being investigated, called "modified thermal balance," although more accurate, is a more time-consuming technique. The user will ultimately be able to choose the technique best suited to the application at hand.

Custom Weighting Factors

In this approach, the heat gain from lights, solar radiation, people, equipment, and conduction through the envelope are calculated for each hour. Part of each gain will appear immediately as a load on the HVAC system; the remainder will be stored as heat in the walls, floor, furniture, and other mass in the building and will be slowly released to the room air. The time delays involved in this process are accounted for by the weighting factors. Mathematically, the cooling load in hour t in Btu/hr due to the ith source (Q_t) is given by:

$$Q_t^i = V_0 q_t^i + V_2 q_{t-1}^i + W_1 q_{t-1}^i + W_2 q_{t-2}^i \quad , \qquad (5)$$

where

q_{t-j}^i = the heat gain in hour t-j (Btu/hr)

Q_{t-j}^i = the cooling load in hour t-j (Btu/hr)

V_j, W_j = the weighting factors

i = the index for the source of heat gain (lights, solar, etc.).

The net load for a particular hour is the sum of the Q_t^i over all of the sources. A similar transfer-function relationship relates the cooling loads to the actual space temperatures and the heat-extraction rates for that hour and previous hours.

In earlier versions of the program, "ASHRAE weighting factors" were used. These were calculated about 15 years ago by the National Research Council of Canada for buildings of very simple geometry and were adapted by the American Society of Heating, Refrigerating, and Air-Conditioning Engineers (ASHRAE).[13] LANL studies showed that the ASHRAE weighting factors lead to inaccurate results for buildings where direct gain is important. Figure 6 shows temperature measurements for the LANL direct-gain test cell as well as the predictions yielded by using the ASHRAE weighting factors. There is a 7°F space-temperature difference at the peaks between the predicted and the measured data.

A technique for calculating weighting factors specifically for the space configuration under consideration was developed[13] and incorporated into DOE-2.1 in the previous year. In this technique, a detailed thermal-balance calculation is made initially to find the cooling-load profile produced by a unit impulse of heat gain from each of the sources listed above. Equation (5) is applied to these profiles, and the weighting factors are extracted by solving the resulting equations simultaneously.

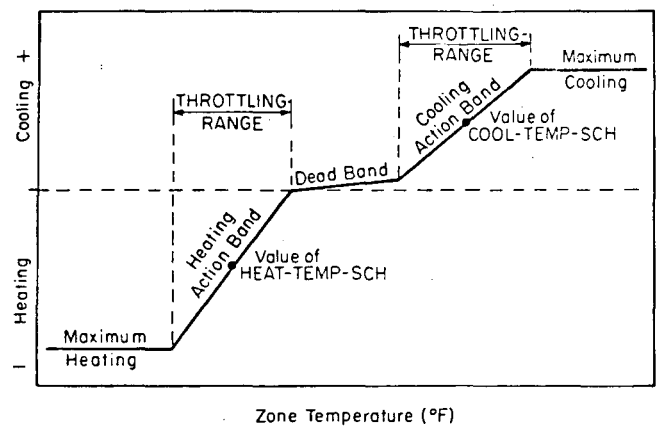

Figure 6. Five possible regions of thermostatic action.

(XBL 825-600)

The addition of the "custom-weighting-factor" (CWF) technique made it possible to accurately account for the storage of heat in the thermal mass of the building and, in particular, enabled direct-gain, passive solar buildings to be modeled with DOE-2. In the initial implementation of CWFs, the user was required to make two separate DOE-2 runs, one to calculate and store CWFs in a library and a second to fetch the CWFs and use them in the LOADS and SYSTEMS simulation. To simplify this procedure, a new feature, called "automatic custom weighting factors," was added to DOE-2 in FY 1981, making it possible to generate and utilize CWFs in a single run.

Modified Thermal-Balance (MTB) Algorithm

The MTB algorithm calculates space heating and cooling loads by considering the radiative coupling between the surfaces of the space. For each wall or window, the thermal-balance equations are written for the inside and outside surfaces. Thermal-balance equations include radiative, conductive, and convective heat-transport methods (the convective term, currently in its simplest form, will be improved later).

Coupling between the surfaces is done through a radiative interchange method. This is in contrast with the weighting-factors method in which the coupling between the components of heating/cooling loads are calculated using a time series for each component type. In the radiative interchange method, for each surface, we lump all other surfaces into a single effective surface and assign a mean radiant temperature to them; then we do radiative interchange with the surface in question and the lumped surface. This calculation is repeated for each surface, and convergence is checked. For the radiative interchange method, we linearize the Boltzmann equation, which is fourth order, with respect to the surface temperature. In this method, inside- and outside-surface temperatures are tracked. The heat storage and transport

through delayed walls, floors, and furniture are handled by using response factors. Solar gains on the outside surfaces are calculated in a similar manner, as in the weighting-factor LOADS program. Solar gain on an inside surface is calculated by computing the amount of solar radiation coming through the windows and hitting the surface.

We believe that the MTB technique may be more accurate in certain situations than the weighting-factor approach. For example, it would enable moveable insulation to be placed over windows at night. The weighting-factor technique does not permit the room transfer functions to be functions of time, which is necessary when the conductance of the windows varies with time. The MTB approach also computes the inside-surface temperature as a function of time. If these temperatures vary widely, the convective, and even the radiative, heat-transfer coefficients can vary enough to cause significant changes in the building conditions. Human comfort strongly depends upon the inside-surface temperatures, and, yet, the weighting-factor approach provides no information in this regard. Further studies will be made of the differences among the weighting-factor, the MTB, and the full thermal-balance techniques to determine which situations require the more complex, and therefore more time-consuming, techniques, if sufficient accuracy is to be maintained.

The main approximations in MTB that require further improvements are:

- The view factors used in radiative interchange are proportional to the surface areas.
- The room temperature used in the expressions is constant; this must be allowed to vary within a given range.
- The convective coupling between the surface and room air is a constant; this must vary with surface temperature and air temperature.

Instead of doing radiative interchange on a surface-by-surface basis, we might use a simultaneous solution of surface temperatures.

HVAC Equipment and Controls

The SYSTEMS and PLANT sub-programs of DOE-2 were originally designed to estimate the energy consumption of the HVAC equipment of large buildings. Many modeling assumptions were based on the philosophy that the most important considerations should be those that have a significant impact upon the energy-consumption values integrated over time. The program made no attempt to simulate the actual performance of the equipment components on an hour-by-hour basis but, rather, predicted overall energy use. This philosophy was supported by the fact that, in the past, the larger HVAC equipment was systematically oversized and tightly controlled. For modeling such systems, it was not necessary to consider performance parameters that depend on inside or outside environmental variables.

As DOE-2 gained popularity, the user community wanted to extend the use of the program to small commercial and residential buildings. At the same time, the engineering community, in an effort to conserve energy, was moving away from recommending oversized systems and constant, year-round control points. These shifts prompted us to make substantial changes in the algorithms of both SYSTEMS and PLANT. The new algorithms tend to be more concerned with modeling hourly performance of actual equipment than with merely estimating the integrated daily or annual energy consumption.

In the SYSTEMS simulation, work during FY 1981 concentrated in two areas: more accurate equipment sizing and more accurate control system interactions. In the PLANT simulation, work was performed in two additional areas: (1) the development of algorithms to simulate "free" cooling using cooling-tower water and (2) study to determine the potential useage of a standby emergency diesel generator for peak shaving.

System Sizing

In DOE-2.1, the sizing of systems (if not specified by the user) is a function of the peak heating and cooling loads, calculated at the reference temperature set in LOADS. If the LOADS temperature is between the design heating and cooling temperatures for a zone, the peak loads will be over-estimated for heating and for cooling; and, consequently, the air flow rate for the zone will not, in fact, correspond to the heat addition or heat extraction actually required at the time of the peaks.

Another problem with the sizing strategy in DOE-2.1 is that plenums and unconditioned zones are also treated at constant temperature in LOADS, usually at the same temperature as the conditioned zones. As a result, there is no contribution to the peak loads of conditioned zones from inter-zone heat transfer between the conditioned and adjacent unconditioned zones. Since an unconditioned zone is likely to be cooler than the conditioned zones in winter and hotter in summer, both the peak heating load and peak cooling load for an adjacent conditioned zone will be underestimated. These two effects will cancel each other only accidentally.

To give the user the opportunity to correct for both of these defects, a new capability has been introduced into the SYSTEMS program. This new capability enables the user to instruct the SYSTEMS program to adjust the heating and cooling peak loads to account for differences between the value of the reference temperature used in LOADS and the value desired for heating and cooling design in SYSTEMS. An adjustment is made for the external and internal wall conductances as well as for the infiltration loads.

HVAC Control Systems

For equipment controlled by a zone thermostat, a linear relationship is assumed to describe the interaction of the thermostat, space temperature, and equipment output. As can be seen in Figure 6, there are generally five regions of interest for

thermostat-equipment interaction: upper and lower bound regions within which maximum cooling and heating, respectively, are supplied; heating- and cooling-action band regions within which proportional control of equipment output is effected; and a dead band region within which the equipment action is constant and usually equal to that at the bottom of the cooling-action band. It is possible that the space temperature and resultant thermostat reaction may change significantly during the basic one-hour time step used in DOE-2. Additionally, the heating- and cooling-action bands may each be composed of multiple regions within which different pieces of equipment function. Thus, the seemingly simple problem of modeling a space-thermostat controlling equipment can become a very complex set of interacting equations and boundary conditions. Improvements were made and incorporated into DOE-2.1A to closely model this problem. Similar improvements were designed and implemented to model the control of space humidity.

Equipment Performance Curves

Another ongoing area of BES Group interest is the collecting of HVAC equipment performance data and the production of empirical correlations suitable for use in simulation models. This is an important area of future work because very little data of high quality is currently available. Results of this work are valuable to other groups interested in HVAC equipment simulation. During FY 1981, generic correlations were produced for the capacity and energy consumption of several types of HVAC systems. This list includes residential and commercial water-to-air/air-to-air heat pumps; rooftop constant-volume/variable-volume, variable-temperature systems; packaged and built-up terminal air conditioners; residential split-system cooling and gas furnaces; and chilled water and direct-expansion coils.

Direct Cooling

Two methods of providing "free" cooling from a central plant cooling tower were researched and implemented in DOE-2.1A. The motivation is to find an inexpensive retrofit of existing chiller-cooling-tower arrangements that will reduce cooling cost. The two "free" cooling concepts take advantage of periods during which the outdoor wetbulb temperature is low enough (between 35° and 50°) to make possible production of cooling-tower exit water that is cold enough to provide building cooling without the use of a chiller.

The first method, known as the strainer cycle, injects the cooling-tower water directly into the building chilled-water loop through a strainer which removes any harmful impurities. Thus, the water-chiller equipment is entirely bypassed.

The second method, known as the thermocycle, uses the water-chiller equipment as a passive heat-exchanger system. The cooling-tower water passes into the chiller-condenser section and cools the refrigerant. A small auxiliary pump, added during the retrofit, sprays the refrigerant onto the evaporator coils, thus cooling the water circulating in the chilled-water loop (see Figure 7).

Peak Shaving and Load Management

During the past several years, modifications have been made to DOE-2 to allow generalized equipment management based on time-of-day, season, and type as well as magnitude of load. This enables the study of different types of peak-shaving strategies to reduce the peak electrical demand by using on-site generation facilities. The first study undertaken examines a technique which would possibly be realized through low-cost retrofits and a small, incremental first-cost for high-rise office buildings.[20]

The national building code requires that a source of emergency power be provided in all high-rise buildings and that it be capable of meeting emergency needs for not less than two hours. The main objective of this study was to point out the viability of using an otherwise-idle emergency generator to achieve peak shaving. It was shown that this concept has the potential for reducing the life-cycle cost of such buildings under certain electrical-demand charging structures.

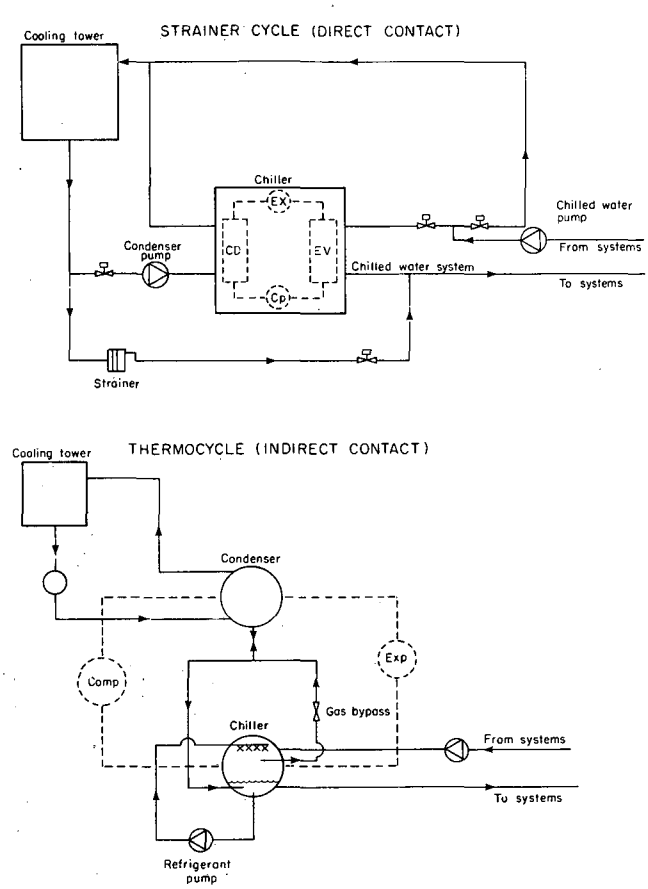

Figure 7. Direct cooling configurations.
(XBL 825-599)

PLANNED ACTIVITIES FOR FY 1982

Future plans for the program lead in two separate directions. On the one hand, the existing program will be maintained and supported, and its documentation will be clarified and supplemented as areas of confusion are uncovered. Several additions will be made to the existing program to supplement its capabilities. These include: (1) expanded output report capability, (2) an improved window simulation in collaboration with the Windows and Daylighting Group at LBL, (3) an expanded user-library capability, (4) further research into the thermal balance LOADS program alternative, (5) improved economic calculations, (6) expanded energy cost alternatives, (7) simulation of evaporative coolers, (8) improved infiltration algorithm, and (9) metric input and output options.

The second direction for FY 1982 activity is exploratory; i.e., we will probe the development of a building energy-use analysis program that can be easily adapted to new developments in the building and conservation sciences.

REFERENCES

1. Energy & Environment Division Annual Report, FY 1978, Lawrence Berkeley Laboratory Report LBL-8619.

2. Energy & Environment Division Annual Report, FY 1979, Lawrence Berkeley Laboratory Report LBL-LBL-11650.

3. Energy & Environment Division Annual Report, FY 1980, Lawrence Berkeley Laboratory Report LBL-11990.

4. Diamond, S. C., and Hunn, B. D. (1980), The DOE-2 Verification Project: Phase I Results, Los Alamos National Laboratory Publication LA-UR-80-357.

5. Schnurr, N. M., et al. (1979), Applications of DOE-2 to Direct-Gain Passive Solar Systems: Implementation of a Weighting Factor Calculative Technique, Los Alamos National Laboratory Publication LA-UR-79-2227.

6. Roschke, M. A., Hunn, B. D., and Diamond, S. C. (1978), A Component Based Simulator for Solar Systems, Los Alamos National Laboratory Publication, LA-UR-78-1494.

7. Carroll, W. L. (1980), Annual Heating and Cooling Requirements and Design Day Performance for a Residential Model in Six Climates: A Comparison of NBSLD, BLAST 2, and DOE-2.1, Lawrence Berkeley Laboratory Report LBL-9270.

8. Curtis, R. B. (1981), The Theoretical Basis of the DOE-2 Building Energy-Use Analysis Program, Lawrence Berkeley Laboratory Report LBL-12300.

9. LBL Building Energy Analysis Group (1980), DOE-2 Users Guide, Version 2.1, Lawrence Berkeley Laboratory Report LBL-8689, Rev. 1.

10. LBL Building Energy Analysis Group (1980), DOE-2 BDL Summary, Version 2.1, Lawrence Berkeley Laboratory Report LBL-8688, Rev. 1.

11. LBL Building Energy Analysis Group (1980), DOE-2 Sample Run Book, Version 2.1, Lawrence Berkeley Laboratory Report LBL-8688, Rev. 1.

12. LANL Group Q-11, Solar Energy (1980), DOE-2 Reference Manual (Part 1, Part 2), Version 2.1, Lawrence Berkeley Laboratory Report LBL-8688, Rev. 1, and Los Alamos National Laboratory Publication LA-7689-M, Version 2.1.

13. LBL Building Energy Analysis Group, and LANL Group Q-11, Program Support, (1980), DOE-2 Engineers Manual, Version 2.1., Lawrence Berkeley Laboratory Report LBL-11353.

14. Stephenson, D. G., and Mitalas, G. P. (1967), Cooling Load Calculations by Thermal Response Factor Method, ASHRAE Transactions, 73, Part 1.

15. Stephenson, D. G., and Mitalas, G. P. (1967), Room Thermal Response Factors, ASHRAE Transactions, 73, Part 1.

16. Hittle, D. C., and Bishop, R. (1981), An Improved Root-Finding Procedure for Use in Calculating Transient Heat Flow through Multilayered Slabs, CERL Preprint.

17. Peavy, B. A. (1978), Determination and Verification of Thermal Response Factors for Thermal Conduction Application, U. S. National Bureau of Standards Report NBSIR 77-1405.

18. Moore, J. E., et al. (1981), Thermal Storage Wall Model Development in the DOE-2 Computer Program, Los Alamos National Laboratory Publication LA-UR-81-981.

19. Johnson, R., et al. (1981), Glazing Optimization Study for Energy Efficiency in Commercial Office Buildings, Lawrence Berkeley Laboratory Report LBL-12764.

20. Choi, S., Hirsch, J., and Birdsall, B. (1981), Use of a Diesel Engine-Driven Emergency Power Generating System for Peak Shaving in Buildings, Lawrence Berkeley Laboratory Report LBL-12299.

BUILDINGS ENERGY DATA GROUP*

A. H. Rosenfeld, J. P. Harris, B. L. Gardiner, C. A. Goldman, A. K. Meier, B. C. O'Regan, J. C. Ribot, H. D. Ross, B. D. Wagner, T. J. Usibelli, and L. W. Wall

The Buildings Energy Data (BED) Group compiles and analyzes research results from the LBL Energy Efficient Buildings program and integrates these results with measured data from conservation programs and buildings science research. Buildings science research is traditionally organized by technology (windows, artificial lighting, thermal storage, infiltration, etc.) or by professional specialty (testing of indoor air quality, modeling of building performance, etc.). These divisions are awkward for those needing conservation information concerning a particular building type (home, school, office) or analytical function (design, retrofit, energy management). A major goal of the BED group is to provide research results that cut across traditional research fields. We find that this reformulation of research data is useful to decision-makers in utilities and government agencies, as well as to our own researchers.

The group's work is organized into two main projects and a small effort in primary data collection. The Building Energy Use Compilation and Analysis (BECA) project involves the compilation, critical assessment, and periodic publication of measured data on the energy performance and cost-effectiveness of low-energy new homes (BECA-A), existing "retrofitted" homes (BECA-B), energy-efficient commercial buildings (BECA-C), and appliances and equipment (BECA-D). A second project maintains and updates a data base on the performance and cost of individual technologies for saving energy in buildings and tracks new technologies as they progress through research, development, field testing, and commercial production. We use this data base, often in collaboration with outside organizations, to develop "supply curves of conserved energy." Conservation supply curves provide a consistent accounting framework for estimating the potential for conservation. When used in conjunction with an energy-demand forecasting model based on end-use analysis, they can help to establish the technical potential for cost-effective conservation. Finally, we participate in direct data-gathering activities on a limited scale. This generally occurs in response to our awareness of a serious but solvable data gap or as a result of close contact with a utility, energy service firm, or other non-research organization.

ACCOMPLISHMENTS DURING FY 1981

During the past year, BED continued to develop and refine data bases on the measured performance and cost-effectiveness of energy-saving homes and commercial buildings, as well as the performance and cost characteristics of individual technical measures. Using these data, along with DOE-2 computer simulations, we have completed major studies of technical potentials for conservation and solar use in California residences and in all U.S. buildings. We have initiated a conservation potentials study for the Pacific Northwest region in cooperation with the Bonneville Power Administration and are assisting the San Diego Gas and Electric Company in a similar effort.

In 1981, we continued a joint project with the Pacific Gas and Electric Company to (1) demonstrate "house-doctor" audit/retrofit techniques, (2) train an initial group of utility and private-industry house doctors, and (3) measure resultant energy savings and cost-effectiveness in a sample of northern California homes. Using passive samplers developed at LBL, we began work with the California Energy Commission on a pilot project to conduct field measurements of infiltration and indoor air quality in 20 new California homes that were built to meet or exceed the California Title-24 energy-conservation standards.

Finally, in 1981 we helped edit and publish proceedings from the 1980 Summer Study on Energy-Efficient Buildings, convened the previous August by the American Council for an Energy-Efficient Economy (ACEEE) and sponsored by DOE and the Solar Energy Research Institute. The Summer Study attracted widespread participation by utilities, government agencies, energy researchers, and private industry. Participants focused on the long-term technical potential for conservation in buildings and the changes in government policy and utility practice needed to achieve that potential.

A summary of major results from each of the BED project areas during 1981 is outlined below.

BECA-A: New Residences

We have collected data on the thermal performance and economics of new passive solar, active solar, and super-insulated homes throughout North America. A house's energy performance can be characterized in terms of both the thermal integrity of the shell and the building's overall performance. The thermal integrity parameter deals solely with the heat conductance, infiltration, and solar gain of the building shell, whereas the overall performance parameter accounts for the fuel type and efficiency of the heating and cooling systems, internal gains from appliances and occupants, and shell performance. Submetered energy consumption, weather data, and inside room temperatures were used to calculate energy performance after correcting for internal loads and occupancy.

*This work was supported the Assistant Secretary for Conservation and Renewable Energy, Office of Buildings and Community Systems, Buildings Division of the U.S. Department of Energy under Contract No. DE-AC03-76SF00098 and by the Bonneville Power Administration, the San Diego Gas and Electric Company, and the California Policy Seminar.

Incremental costs (materials and labor) of the energy-saving features were also collected.

We found that residential space-heating energy use in new homes can be economically reduced to around 10 percent of the national average for the existing housing stock [i e., to 1-4 Btu/ft^2-DD(^{o}F) per year]. For comparison, this low level of heating energy consumption is less than that used for water heating (about 25 MBtu/household per year) in all but the coldest parts of the nation.

Figure 1 plots several cost-effective low-energy homes, comparing them with proposed federal "energy budget" guidelines and with current building practice. The super-insulated homes in our data base tend to use less heating energy than do the passive solar homes and perform better in cold climates. Thermal performance does not appear directly correlated to cost, perhaps because passive solar homes cost more to design than super-insulated homes and may offer additional amenities. More refined estimates of thermal performance and comparisons among buildings will require better measurements of internal loads and occupant behavior.

BECA-B: Residential Retrofits

BECA-B assesses the technical performance and economics of energy-conserving retrofit measures in existing homes. The data collected thus far represent measured energy savings and retrofit costs for more than 60 North American residential retrofit projects. The sample size within each project ranges from 1 to 33,000 homes. The single homes reflect individual research or demonstration sites while the larger samples are from utility-sponsored programs.

Figure 2 relates energy savings (on the vertical axis) to two important economic variables: total cost of the retrofit projects (horizontal axis), and the cost of conserved energy (represented by sloping lines drawn from the origin). The data in Figure 2 suggest that a $1000 investment in retrofits will, on the average, reduce a house's heating energy consumption 25 percent, while a $2000 investment will reduce consumption 40 percent. For the 58 projects shown in Figure 2, the median energy savings are 23 percent. The median cost of conserved energy is $3.50/MBtu, which is substantially less than average 1981

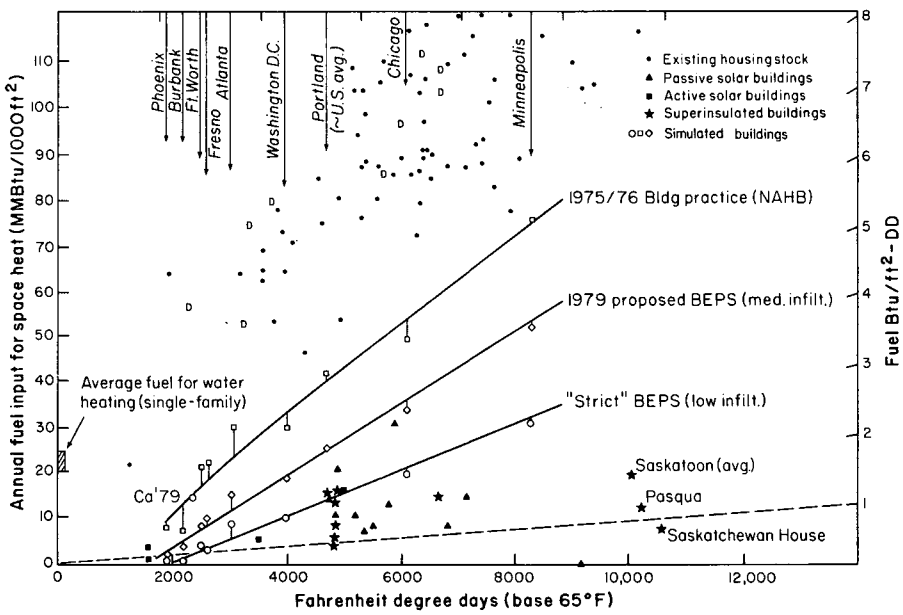

Figure 1. The relationship between degree-days and space-heating energy requirements for new, low-energy homes. For reference, the existing housing stock (dots in the upper portion of the figure), recent building practice, and proposed federal energy budget guidelines are also plotted. To emphasize the performance of building shells rather than the choice of heating fuel and system, usage in electric resistance heated homes is multiplied by 1.5, corresponding to average fuel furnace system efficiencies of 67 percent. Note that even in relatively severe climates, well above the U.S. average, space-heating energy requirements can be reduced to roughly one-tenth of those in existing homes and below the average amount of energy used for water heating. Average added cost of the energy-saving features ranges from $100 (for passive solar design) to $17,000 (for some active solar houses), with an average added cost of $5,000.

(XBL 826-775)

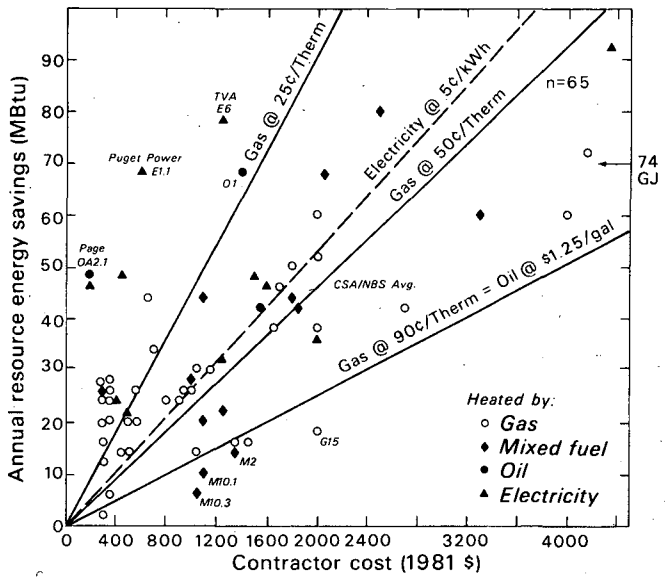

Figure 2. Annual energy savings vs contractor cost for retrofitted homes. Annual savings, in resource energy after retrofits, are plotted against the contractor cost of retrofits for 65 data sources. The sloping reference lines represent the boundary of cost-effectiveness for typical residential energy prices. Since conservation investments are typically "one-time," the future stream of energy purchases for 15 years is converted to a present value, assuming a 7 percent real discount rate. A conservation retrofit is cost-effective if the data point lies above the purchased-energy line for the type of fuel saved. (XBL 822-156)

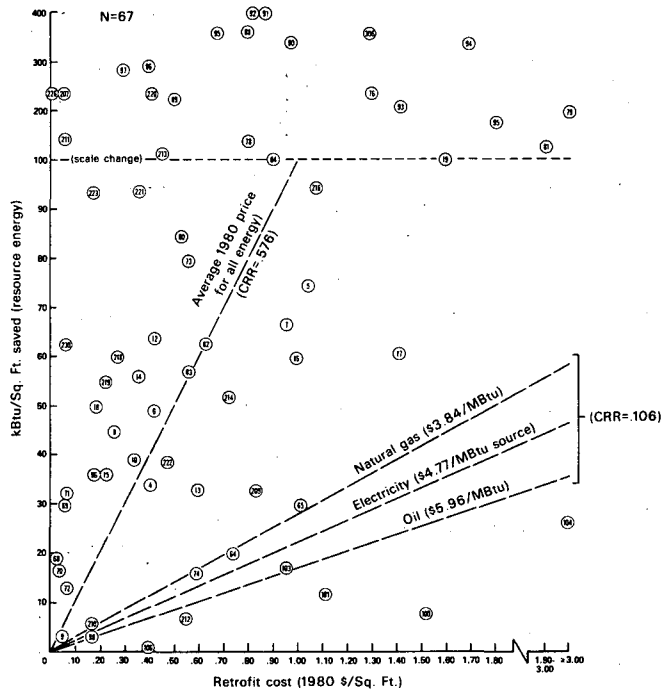

Figure 3. Annual energy savings (resource kBtu/ft^2) vs retrofit cost (1980 $/ft^2) for commercial building retrofits. Note the scale changes on both horizontal and vertical axes, indicating considerable scatter in the data. Lines drawn from the origin show boundaries for cost-effectiveness in saving electricity, oil, and gas, assuming 1980 average energy prices, 10-percent real interest, and 30-year amortization (CRR = 0.106/year). Those points above and to the left of a boundary line are cost-effective under that criterion. The fourth line shows the cost-effectiveness boundary for a two-year amortization period and 10-percent real interest (CRR = 0.576/year), using 1980 weighted average prices for all forms of energy used in commercial buildings. These data are not weather-corrected. Electricity is counted in terms of resource energy, i.e., 11,500 Btu/kWh. Source: Ross and Whalen, 1981. (XBL 826-776)

prices for energy supplied to residential customers ($4/MBtu for natural gas, $9/MBtu for oil, and $15/MBtu for electric resistance heat). The data suggest that, considering the technology available today plus current and projected energy prices, there may be decreasing returns for residential retrofit investments above $2000.

BECA-C: Commercial Buildings

A large number of U.S. commercial buildings have been retrofitted for improved energy efficiency, but in only a few cases are there adequate records to compare pre- and post-retrofit energy use. Such data are necessary to establish the cost-effectiveness of the conservation measures or practices and to identify which factors are associated with successful retrofits. The BECA-C project compiles and analyzes available data on commercial building retrofit projects. Beginning in 1982, the data base will be extended to new, energy-efficient commercial buildings.

Results from the initial BECA-C data base, consisting of 222 sites evaluated by Ross and Whalen,[1] are summarized in Figure 3. Average energy savings for the buildings are 19 percent of pre-retrofit consumption. As Figure 3 illustrates, there was considerable variance in energy savings and in the cost-effectiveness of retrofit investments. About 10 percent of the buildings in the data base used more energy after retrofit than before, indicating that there is still some risk to investing in conservation. The negative results were probably due to poor operation and maintenance practices or, in at least one case, to product failure (a window film failed to adhere). The average conservation investment to achieve this level of savings was $0.65/ft^2. Boundaries of cost-effectiveness for various assumed energy prices and capital recovery rates (CRR) are also illustrated in Figure 3. Retrofit projects that are cost-effective, using various criteria, lie above and to the left of the appropriate boundary line.

Only one-fourth of the buildings in the total

sample had sufficient data for a complete economic analysis; that is, they had adequate records of both retrofit costs and energy consumption prior to and following the retrofits. Nearly 90 percent of the buildings achieved simple paybacks of three years or fewer.

We also compared the savings predicted through audits to the measured savings in 18 buildings for which data were available. The average energy savings predicted during audits (23 percent) were somewhat higher than the average measured savings (17 percent), but the discrepancy between predictions and measurements for individual buldings was often quite large (including both over- and under-predictions). While this causes concerns for the accuracy of current audit techniques, we cannot yet draw simple conclusions from this limited sample of buildings.

House-Doctor Demonstration Project

The EEB program is conducting a cooperative project with Pacific Gas and Electric Company (PG&E) to determine the energy savings attributable to "house-doctoring." House-doctoring is an extended energy audit, including installation of simple, cost-effective conservation measures and use of infiltration monitoring equipment to identify and immediately seal major air leaks. We trained six PG&E weatherization specialists in house-doctoring techniques and chose Walnut Creek, Calif., as the site for a controlled experiment. At PG&E's expense, 10 homes were retrofitted with the more costly measures (principally ceiling and wall insulation) recommended by the house-doctor audit. Another 10 homes were audited and "house-doctored," but not otherwise retrofitted. A final group of 10 homes received only the standard, PG&E informational audit. Results were compared with energy used in a randomly selected control group of 10 homes, and with a comparison group consisting of all Walnut Creek homes.

Some results of the project are shown in Figure 4. We compared the costs and energy savings of house-doctoring to results obtained in the other groups. While all groups showed a decline in energy use (weather-adjusted), we found no statistically significant increase in savings from house-doctoring activities. We attribute this, in part, to the relatively mild winter climate in Walnut Creek and to the inadvertent selection of houses having unusually low air-change rates prior to house-doctoring. This meant that even a large percentage reduction in infiltration would only slightly decrease energy consumption. The project encountered other technical and institutional obstacles, which may have affected savings in the house-doctored homes compared to the other groups. These included (1) the difficulty of getting newly recruited house doctors to perform efficiently with very limited training and field experience and (2) the absence of strict limits on control-group houses being retrofitted outside the project. All of these factors complicated the analysis and limit our ability to generalize results. However, a series of similar experiments conducted by Princeton University in the colder climate of New York and New Jersey showed somewhat larger, cost-effective net savings from house-doctoring vs control groups.[2]

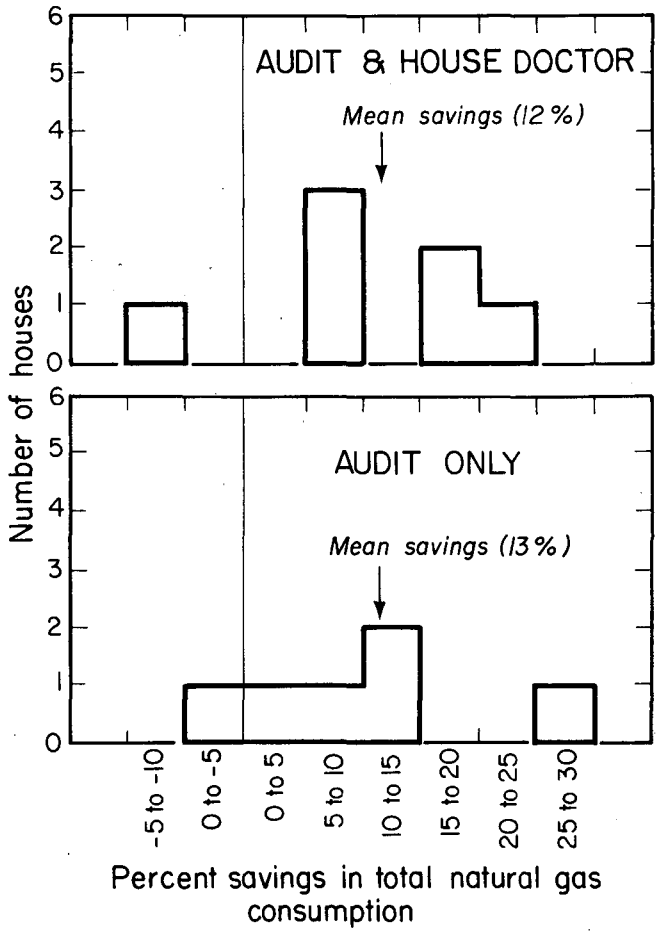

Figure 4. Results of Walnut Creek, Calif., house-doctoring compared to a control group. The distribution of energy savings (expressed in percent of original use) resulting from house-doctoring are shown. House-doctoring in this experimental project did not add any statistically significant energy savings. (XBL 826-700)

Air Quality in New Title-24 Homes

Under the auspices of the California Energy Commission, we have collaborated with the University-wide Energy Research Group in monitoring air quality in 16 homes built to meet or exceed the California Title-24 energy-code requirements. Limited resources forced us to focus on those homes which we expected to have the poorest indoor air quality, namely, newly built, low-infiltration homes having natural-gas appliances. New construction materials and natural-gas combustion are major sources of residential indoor air pollution, and tight houses will tend to maintain higher pollutant concentrations.

All 16 houses had infiltration rates below the prevailing Title-24 standards (0.5 air changes per hour). We monitored concentrations of formaldehyde

(typically caused by outgassing from new building materials and furniture), nitrogen dioxide (a combustion product), and radon (a decay product of naturally occurring radium in soil, groundwater, and some building materials).

Results to date indicate that new houses having low air-change rates do not necessarily experience poor indoor air quality. Figure 5a shows the weak correlation between the infiltration rate and radon concentrations; Figure 5b shows the weak correlation between the infiltration rate and nitrogen oxide concentrations. The average nitrogen dioxide level, 10.4 ppb, was well below the EPA limit of 50 ppb for outside air; moreover, indoor concentrations of NO_2 for many homes were lower than the outside ambient concentration. The radon levels ranged from 0.32 to 2.24 pCi/l. This corresponds to a range of 0.0016 to 0.0110 Working Levels (WL), again well below proposed American and Swedish standards for existing houses.

These results do not necessarily mean that all new, tight homes have good air quality. Localized "pockets" of radon in the soil, poorly vented gas appliances, or building materials and furnishings that release formaldehyde and other organics could create unhealthy air-quality conditions in those houses. Our data suggest only that indoor air-quality problems are not inevitable, even in fairly well sealed, energy-efficient houses.

Conservation Technologies Data Base and Potentials

The conservation data base and potentials project complements and helps integrate other BED activities by analyzing what might happen if today's best achievable practice--not the average--were applied, hypothetically, to the entire building stock. This provides a useful perspective on the BECA data concerning conservation results currently being achieved in new and retrofitted buildings. In turn, data from the BECA project provide an empirical benchmark to assure that the estimates of technical potential for conservation remain realistic.

Our objective is to establish and refine a data base defining the "envelope" of technical opportunities for improved energy efficiency. This in turn provides a more meaningful basis for setting policy goals and estimating how conservation might affect future energy demand. Only after establishing the technological frontier for conservation in buildings can we systematically identify those opportunities offering the greatest potential savings at the lowest cost.

Information on conservation technologies is obtained from performance and cost data, compiled through the BECA project, for conservation measures already commercially available. Data on newly emerging or prospective technologies are collected from research programs at LBL and other establishments, as well as through contacts and collaboration with innovative designers, manufacturers, builders, and utilities.

To date, a detailed data base on conservation technologies by end use has been developed only for residences; future work will extend this data base to commercial buildings. Results have been published for two major studies: an analysis of conservation potential in the 1980 stock of California residences and appliances,[3] and an assessment of conservation potential in the year 2000 for all

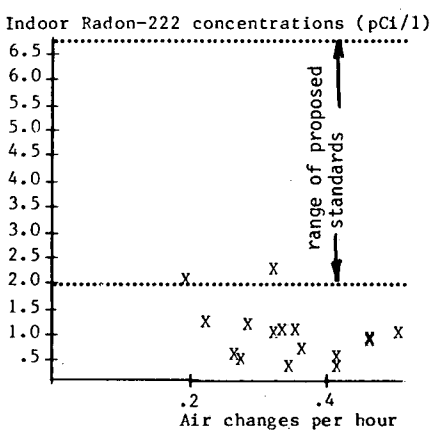

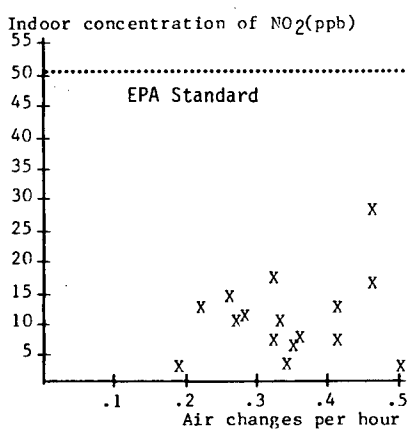

Figures 5. (a) The relationship between air-infiltration rates and radon concentrations in new, tight homes meeting California's Title-24 building standards. Figure 5a shows that there is only a weak correlation between air-change rate and radon concentrations, suggesting that other factors may be more important. For comparison, the range of proposed standards (U.S., Canada, Sweden) is between 1.9 and 6.7 pCi/l. (b) The relationship between air-infiltration rates and nitrogen oxide (principally dioxide) concentrations in the same sample of homes. There is again a weak correlation between air-change rate and nitrogen oxide concentrations, suggesting that factors such as age of construction materials and furniture may be more significant determinants of the concentrations. For comparison, the EPA long-term ambient standard for nitrogen dioxide is 50 ppb.

(XBL 825-10211)

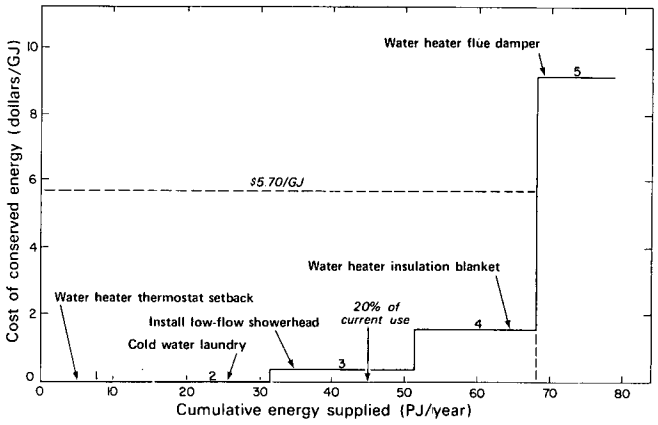

Figure 6. A supply curve of conserved natural gas for residential water heating in California. Each step corresponds to a conservation measure. The y-coordinate is the cost of conserved energy (here, natural gas), and the x-coordinate is the annual savings after 10 years. A conservation measure is cost-effective if its cost of conserved energy is less than the price of the energy it displaces (in this case natural gas, at $5.70/GJ). For each measure, we calculate the average energy savings and the fraction of the homes eligible for the measure. We assume a 5-percent real discount rate in the cost-of-conserved-energy calculation. Total gas used for residential water heating in California in 1978 was 216 PJ. (Adapted from A. Meier et al. (1981), Supply Curves of Conserved Energy for California's Residential Sector (Lawrence Berkeley Laboratory Report LBL-13608 (preprint). Also to appear in Energy.) (XBL 8011-3984B)

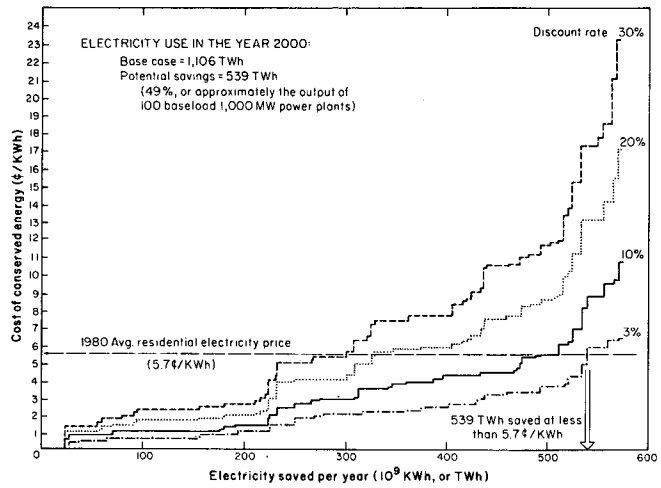

Figure 7. Year 2000 supply curve of conserved electricity for the United States' residential sector. Each step represents a conservation measure whose height is the cost of conserved electricity. A conservation measure is cost-effective if its cost of conserved energy is less than the price of the electricity it displaces (in this case, 5.7 ¢/kWh). The baseline forecast of residential electricity consumption in the year 2000 is 1,110 TWh/year. Investing in conservation measures with costs of conserved electricity less than than the current cost of electricity (5.7 ¢/kWh) would save 49 percent of the forecasted electricity consumption. (Adapted from Solar Energy Research Institute, A New Prosperity: Building a Sustainable Energy Future, 1981.) (XBL 826-774)

U.S. buildings, with an emphasis on residential buildings.[4]

To translate the data on individual conservation technologies into aggregate estimates of potential energy savings, we have developed supply curves of conserved energy. Supply curves (see Figures 6 and 7) begin with the ranking of individual measures in order of cost effectiveness. On a supply curve, the cost per unit of conserved energy is measured on the vertical axis, and the cumulative annual energy savings is measured on the horizontal axis. In this way the potential "supplies of conserved energy" can be compared with other energy sources, in terms of unit cost.

Figure 6 is a supply curve of conserved fuel as of 1980 for one end use: water heating in California homes. For each conservation measure, the data base used to generate this supply curve lists cost and performance characteristics, size of the applicable stock, and the statewide annual energy savings that could potentially be achieved.

A conservation measure is cost effective if the cost of conserved energy (CCE) is less than the value of the energy it displaces. One can estimate the economical "reserves" of conserved energy by selecting a comparison price for the energy displaced. In Figure 6, we show a comparison price of $7.00/GJ, representing the 1980 tail-block price of residential natural gas in California.

Similar conservation supply curves (not shown) for all California residential gas and electricity uses indicate that about 22 percent of residential electricity consumption potentially could be saved in 10 years at less than $0.08/kWh, and that 34 percent of residential gas use might be saved at less than $7.00/GJ.

In our analysis of for the entire U.S. residential sector, many additional measures were included, and a longer time horizon was studied (20 years instead of 10). The supply curve of conserved residential electricity for the year 2000 is shown in Figure 7. We relied on the Oak Ridge residential energy demand model[5] for projections of growth in population, housing stock, and appliances. For the base case, we assumed that new units would operate at the same efficiency as today. The results of the analysis of year 2000 energy use and conservation potentials are summarized in Table 1 and illustrated graphically in Figure 8. Even though the conservation measures are restricted to those currently on the market and the life cycle is cost justified at today's average energy prices, the conservation potential for the

Table 1. Comparison of annual energy use in U.S. residential and commercial buildings: 1980 and 2000 baseline forecast; 2000 technical potential. Annual consumption is in quads (= 10^{15}Btu) of resource energy.

	Estimated 1980 energy use[a]			Projected energy use in 2000					
				EIA baseline forecast[b]			Technical potential[c]		
Building subsector	Fuel	Electricity	Total	Fuel	Electricity	Total	Fuel	Electricity	Total
Residences									
Existing 1980 residences: heating and cooling	7.04	2.65	9.69	5.50	1.98	7.48	1.37	0.66	2.03
New residences: heating and cooling	-	-	-	1.59	1.96	3.55	0.54	0.81	1.35
Water heating	1.29	1.00	2.29	1.46	2.11	3.57	0.55	0.92	1.47
Appliances	0.47	4.16	4.63	0.68	6.67	7.35	0.43	4.13	4.56
SUB-TOTAL	8.80	7.81	16.61	9.23	12.72	21.95	2.89	6.52	9.41
Commercial buildings									
Existing 1980 stock	4.4	5.6	10.4[d]	3.2	4.9	8.1	1.6	2.4	4.0
New construction	-	-	-	0.4	4.4	4.8	0.1	2.7	2.8
SUB-TOTAL	4.4	5.6	10.4	3.6	9.3	12.9	1.7	5.1	6.8
BUILDING SECTORS TOTAL	13.2	13.41	27.01[d]	12.83	22.02	34.85	4.59	11.62	16.21

[a]Estimates based on Oak Ridge National Laboratory Buildings Energy Use Data Book, Report ORNL-5552, Dec. 1979.

[b]Based on mid-range projections by the Energy Information Administration, U.S. Department of Energy, in the 1979 Report to Congress.

[c]Estimated SERI/LBL consumption target, assuming implementation of all feasible conservation and solar measures that are cost effective.

[d]Includes 0.40 from other sources.

Source: SERI (1981), as revised for 2nd edition.

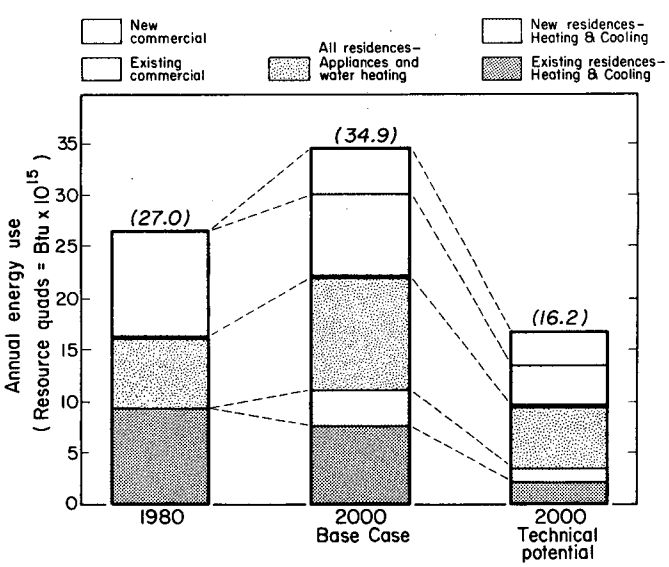

Figure 8. A graphical comparison of energy use in 1980 (left), the forecast by the ORNL model for the year 2000 (center), and the technical potential for 2000, assuming all cost-effective conservation and solar measures have been implemented.

(XBL 826-698)

year 2000 would reduce demand 30 percent below today's residential energy use--despite the additional energy required by 40 million new homes.

PLANNED ACTIVITIES FOR FY 1982

Building Energy Use Compilation and Analysis

We plan to expand all the BECA data bases and to improve analytical techniques for comparing results for different climate zones and structural types. As we continue to collect data for new energy-efficient homes, the BECA-A data base will be broadened to include energy requirements for cooling, hot water, lighting, and other appliances, as well as multi-year records. We expect to develop better methods to account for the relative importance of internal gains in heavily insulated, low-infiltration buildings.

Future additions to the BECA-B data base will emphasize multi-family retrofit projects and the addition of several years of post-retrofit data. We will also examine more carefully the most successful and least successful measures and programs to determine what factors affect conservation results. Finally, data will be collected and analyzed to determine how well pe-retrofit predic-

tions of energy savings and costs compare with actual values, both for individual measures and for the building as a whole.

Submetered data will be added to address questions of component performance and to allow more precise comparisons between predicted and actual performance. Multi-year energy savings data on a subset of buildings will provide insights to performance degradation over time due to physical factors or occupant behavior. A BECA-D data base on efficient appliances and equipment will be established, along with a specialized data base on unoccupied or "controlled-occupancy" buildings, to be used for validating building simulation computer models. Publications based on each of the BECA data bases will be submitted at least biannually, or more often as data warrant.

Primary Data Collection

The house-doctoring project is virtually complete, but we shall continue to monitor utility bills in 1982 because a second winter will greatly increase the reliability of our data. We are also preparing guidelines for subsequent experiments which will avoid some of the difficulties we encountered.

We expect to finish the analysis of indoor air quality in the Title-24 homes in 1982. Other small-scale projects to collect data on indoor air quality and other building characteristics may be initiated if opportunities become available.

Conservation Technologies Data Base and Potentials

We plan to refine and expand the data and methodologies for evaluating conservation technical potentials. The emphasis will be on filling gaps in the data and replacing engineering or computer-model estimates with measured data. We shall extend the supply-curve approach to non-residential buildings, including potential reductions in electrical peak demand as well as energy. Technology performance and cost data will be translated into a format suitable for cross-checking or updating the engineering-cost tradeoff curves used in the Oak Ridge model and other similar end-use/engineering models. Finally, we will develop a second-generation computer model for generating conservation supply curves. This model will include: better methods of treating interactions among measures and across end uses, easier comparisons of conservation potentials to baseline forecasts of energy consumption, a multi-year perspective rather than "snapshot" supply curves, greater flexibility to include economic variables, and an ability to vary the degree of aggregation of individual measures.

Other Activities

As an extension of the BECA project, we are now assisting in planning a second Summer Study to be held in August 1982, again under ACEEE sponsorship. Its theme will be "Documenting Results of Energy Conservation in the Buildings Sector." Sponsors are expected to include DOE, LBL, Bonneville Power Administration, Texas Utilities, the Gas Research Institute, and the Electric Power Research Institute. A commercially published book, based on the conference proceedings, should be the most extensive, up-to-date collection of quantitative data on energy conservation in buildings.

REFERENCES

1. Ross, Howard, and Whalen, Sue (1981), "Conservation Progress in Retrofitted Commercial Buildings," Buildings Division, U.S. Department of Energy.

2. Dutt, Gautarn, et al. (1982), "The Modular Retrofit Experiment: Exploring the House Doctor Concept," Princeton University, Center for Energy and Environmental Studies, PU/CEES Report No. 130.

3. Wright, J., et al. (1981), Supply Energy through Greater Efficiency: The Potential for Conservation in California's Residential Sector. Lawrence Berkeley Laboratory Report LBL-10738, to be published by The University of California Press.

4. Rosenfeld, A.H., et al. (1981), Chapter 1: "Buildings," in Solar Energy Research Institute, A New Prosperity: Building a Sustainable Energy Future, Brick House Press, Andover, Mass. (Also published in preprint form as Lawrence Berkeley Laboratory Report LBL-11300, 1980).

5. Hirst, Eric, and Carney, Janet (1978), The Oak Ridge Engineering-Economic Model of Residential Energy Use, Oak Ridge National Laboratory Report ORNL-CON 24.

ENVIRONMENTAL RESEARCH PROGRAM

INTRODUCTION

The environmental impacts of different kinds of energy are the primary concern of this program. These impacts include short- and long-term effects on regional and local economies and ecosystems, water availability and quality, air quality, land use, and human health. During FY 1981, research groups in this program have concentrated on atmospheric aerosol research, applied physics and laser spectroscopy, environmental impacts of various types of combustion, the environmental effects of oil shale, retorting, fresh-water ecology and acid precipitation, the continuing survey of instrumentation for environmental monitoring, and the use of trace analysis in investigating historical ecological impacts.

The Atmospheric Aerosol Research Group has focused its studies on aerosol characterization, formation, and transformation and on the effects of aerosols on precipitation, visibility, and climate. During the ten-year history of the group, its members have contributed to the better understanding of several aspects of aerosol chemistry and physics. At present, the main research interests of the group involve chemical processes that occur in clouds and fogs, aerosol nitrogen chemistry, and the role of particulate carbon in visibility and climate. To accomplish its research objectives, the group has developed novel analytical methods, such as a laser transmission method for optical characterization of particles and thermal-evolved gas analysis for the characterization of carbonaceous and nitrogenous aerosol species. Members of the group were also the first to apply photoelectron and Raman spectroscopy to aerosol characteristics.

The Applied Physics and Laser Spectroscopy Research Group applies the knowledge of advanced laser spectroscopy and condensed matter physics to energy and environmental problems. Emphasis is on the development of physical methods, as opposed to conventional chemical analysis techniques. The ultrahigh sensitivity, narrow line width, and tunability of lasers and the minimal sample preparation required make it possible for team members to apply such techniques to energy production and to test novel methods for energy conversion, such as photovoltaic solar cells and superionic electrical energy storage devices. The accumulated experience of the group during the last five years will be employed in gaining a better handle on such significant environmental problems as the global carbon dioxide problem and acid rain. In both cases, emphasis will be placed on remote sensing.

LBL's role in oil shale research has primarily been one of studying associated environmental problems and the development of schemes for treating large quantities of solid and liquid wastes resulting from oil shale retorting. During FY 1981, the work of the Oil Shale Research Group was entirely redirected toward aspects of wastewater treatment and characterization. However, two previously initiated projects on other aspects of retorting were continued and neared completion during the year. These projects are the partitioning of metals from raw shale to different waste streams during retorting and the comparative evaluation of various modified in-situ retort abandonment strategies to minimize groundwater pollution. The research of this group is a joint endeavor with the Sanitary Engineering and Environmental Health Research Laboratory of the University of California, Berkeley. Professor J.F. Thomas, Group Head of Sanitary and Environmental Engineering in the Department of Civil Engineering, became the Principal Investigator of this group after the departure of Dr. J.P. Fox.

Approximately 90 percent of the energy consumption in the United States is attributable to combustion processes. The research effort of the Combustion Research Group has been directed toward achieving control over complex combustion processes by acquiring a fundamental understanding of the complex chemical and physical processes which determine combustion efficiency, emissions, and safety. Development of suitable analytical techniques for measuring intermediate and product species formed during the oxidation of fossil fuels and for characterizing turbulence has been a major effort. The characterization and understanding of turbulence and high-temperature chemistry are of high priority in this program. Areas of application which dominate these studies are engine research, pollutant abatement in utilities, control of unwanted fires, and ignition phenomena.

Ecotoxicology is the science that seeks to determine the pathways, fate, and effects of toxic substances in the natural environment. The projects of the Lake Ecotoxicology Research Group focus on one particular type of natural environment, freshwater lakes. Research has proceeded in two converging directions: the development of laboratory microcosms for lake ecotoxicology and the study of acid precipitation in the western United States. The group has demonstrated that lake microcosms can be designed and operated to provide realistic toxic-substance test systems and

has applied microcosms to analyze effects of acid precipitation. Field studies on acid precipitation and its effects in the Sierra Nevada and the Colorado Rockies have been another major focus of the group.

Three major projects have occupied members of the Trace Element Analysis Group: continuation of the survey of instrumentation for environmental monitoring, the study of the iridium anomaly approximately synchronous with terminal Eocene extinction, and the characterization of New World obsidian sources and the cost-effective determination of provenience of selected artifacts. The Environmental Instrumentation Survey, which was started in 1971, updated two previously published sections of the Survey and completed a new section on calibration and sampling. Arrangements were made for commercial publication of the Radiation volume. Research continued on the relationship between iridium anomalies and terminal Eocene extinctions. A substantial portion of the work concerning characterization of obsidian sources involved the study of obsidian artifacts from Guatemala and Ecuador, the heartland of the Mayan culture.

During FY 1981, the research groups of the Environmental Research Program conducted studies which are described in the short reports that follow. In many cases, more detailed reports have been or will be published.

ATMOSPHERIC AEROSOL RESEARCH

SO_2 Oxidation of Soot Particles Exposed to Water*

W. H. Benner, E. Ljungstrom, and T. Novakov

The oxidation of SO_2 in the atmosphere leads to the formation of sulfuric acid, which, if incorporated into cloud and rain water and not neutralized by ammonia, can acidify the water. The oxidation of SO_2 can produce gas-to-particle transformations and can lead to haze formation. In the ambient atmosphere, SO_2 is oxidized by a variety of homogeneous and heterogeneous chemical reactions. The research reported here focuses on several heterogeneous (i.e., gas-droplet/particle) reaction pathways.

It has been shown that aqueous suspensions of activated carbons oxidize S(IV) [S(IV) = $SO_2 \cdot H^2O$ + $SO_3^{=}$ + HSO_3^-] to sulfate[1] and that dispersed wet soot particles oxidize absorbed SO_2 to sulfate.[2] These previously reported experiments indicated the importance of liquid water in the reaction system, but the amount of water required to cause the wet oxidation of S(IV) was unknown. Specifically, it was not known if soot particles suspended in air having RH less than 100 percent would produce sulfate when exposed to SO_2. Fog-chamber experiments were conducted to answer these questions. In addition, these previously reported experiments were conducted with surrogate soot particles, namely, commercially available activated carbons. Recently, adequate amounts of ambient particles were obtained, and experiments to determine their capacity to oxidize S(IV) were begun.

*This work was supported by the Assistant Secretary for the Environment, Office of Health and Environmental Research, Pollutant Characterization and Safety Research Division of the U.S. Department of Energy under Contract No. DE-AC03-76SF00098 and by the Environmental Protection Agency.

ACCOMPLISHMENTS DURING FY 1981

The experimental procedures used to measure the rate of heterogeneous oxidation of S(IV) have been described in detail previously.[1,2] Therefore, only a summary of the procedures is included here. An aqueous suspension of activated carbon was nebulized, and the resulting mist was passed through a diffusion drier to evaporate the water from the resuspended particles of activated carbon. The relative humidity (RH) of this particle-laden air stream was controlled by adding humidified and/or dry air to it. The particle-laden air stream and SO_2 were introduced into the bottom of a chamber (Fig. 1), and the mixture was forced upwards through the chamber at a flow rate which permitted a 30-minute contact time between particles and SO_2. The effluent from the chamber passed through additional diffusion driers which further dried the particles and removed SO_2 from the air stream, thereby quenching the reaction between particles and SO_2. Particles were collected simultaneously on a prefired quartz fiber filter and a Fluoropore filter. Carbon on the quartz filter was determined by a combustion technique, and the aqueous extract of the Fluoropore filter was analyzed by ion chromatography for sulfate.

When Nuchar[3] was exposed to 0.75 ppm SO_2 in the chamber, the carbon-normalized rate of sulfate formation on the particles (Fig. 2) is shown to be dependent on RH. The rate is maximum at 100 percent RH and decreases by a factor of 2 when the particles are exposed to 20 percent RH. The data points plotted at 100 percent RH in Figure 2 were obtained from chamber runs in which fog droplets were introduced into the chamber; this was necessary to maintain the RH at 100 percent. These data at 100 percent RH represent a totally wet particle, i.e., one completely encapsulated with water, in

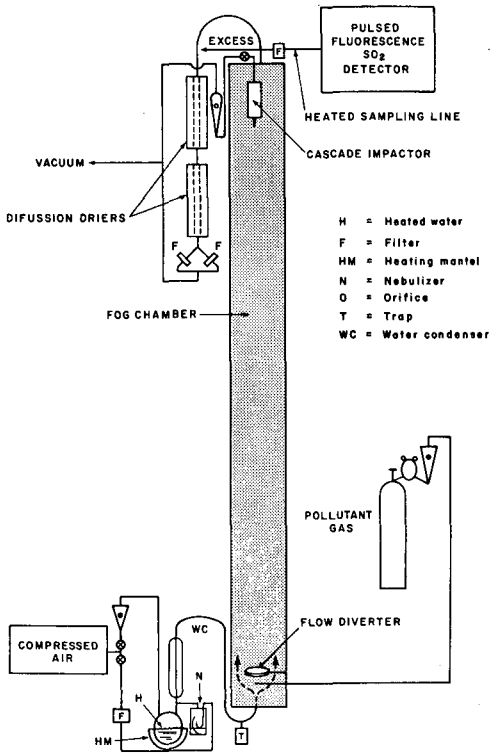

Figure 1. Laboratory fog chamber and associated equipment. (XBL 822-89)

contact with SO_2. In such a droplet, SO_2 is first adsorbed into the layer of water which surrounds the particle; then dissolved S(IV) species diffuse to the surface of the soot particle where oxidation proceeds. The sulfate ions which form by catalytic oxidation of S(IV) on the particle surface desorb from the surface and diffuse back into the liquid phase. This process regenerates the catalytic site on the particle so that another S(IV) species can be subsequently oxidized at the same site. When the particles are exposed to RH less than 100 percent, the amount of water on the particles is decreased; and a corresponding decrease in the rate of sulfate formation is observed (Fig. 2).

Exposure of a previously nebulized particle to 20 percent RH is probably inadequate to remove water from the pores of the particles. In several experiments, the particles were heated to desorb water to see if pore water played an important role in the oxidation of S(IV) by soot particles. These data are plotted at 0 percent RH in curve 1, Figure 2. These data were not collected from fog-chamber experiments but from a separate experiment. In this experiment, a particle-laden filter was placed in a filter holder, and both were heated to 50°C while -35°C dew-point air was drawn through the filter for one hour to dry the particles. Then the filter was cooled to room temperature, and SO_2 (0.75 ppm final concentration) in -35°C dew-point air was drawn through the filter for 30 minutes (equivalent to SO_2-particle reaction time in the chamber). It can be seen that the rate of sulfate formation was substantially decreased when the particles were rigorously dried. This finding indicates that residual pore water plays an important role in promoting S(IV) oxidation by soot particles.

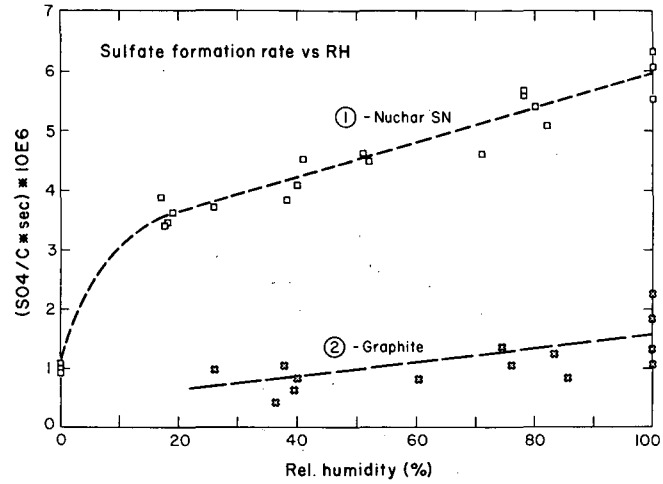

Figure 2. Sulfate formation on particles exposed to 0.75 ppm SO_2 at various values of RH. (XBL 822-88)

Curve 2 in Figure 2 was obtained using ground graphite particles. From previous experience, it was known that graphite particles are nearly inactive in terms of S(IV) oxidation. When a water droplet containing a soot particle is exposed to SO_2, a small amount of S(IV) is oxidized in solution by air oxidation. When a droplet contains Nuchar, the catalytic oxidation of S(IV) on the soot particle predominates over the noncatalyzed oxidation of S(IV) by dissolved O_2. The graphite data are included to show the upper limit of the noncatalyzed oxidation of S(IV).

The relative importance of soot-SO_2 oxidation pathway in the ambient atmosphere is dependent in part on the wetness of the particles, as shown in Figure 2. As a soot particle travels about in an air mass, it is likely to experience exposure to large variations in RH. Figure 3 shows the effect of a step-like change in RH on the rate of sulfate formation. The data presented in Figure 3 were collected from duplicate experiments in which filters, preloaded with Aktivköhle (a commercially available activated carbon), were exposed to SO_2 and RH in a small glass flow chamber. All the filters, each having a known loading of Aktivköhle, were first equilibrated in the chamber with ~40 percent RH air. Then SO_2 was introduced into the flow stream, and, after selected times, a filter was removed from the chamber. Each filter was analyzed for sulfate. At the indicated times, a step-like increase or decrease in RH was produced. The rate of sulfate formation was calculated for each interval indicated by the horizontal bars in Figure 3. For example, a filter was removed from the chamber after a 120-minute exposure. In the calculation of the rate of sulfate formation for the 30- to 120-minute period, the amount of sulfate which formed during the first 30 minutes of the 120-minute exposure was subtracted from the total sulfate on the filter removed at 120 minutes. The amount of sulfate which formed during the first 30 minutes on the filter removed at 120 minutes was calculated using the rate of sulfate formation determined from the previous filter (0- to 30-minute exposure) and normalizing to carbon concentration. Similar calculations were made for each interval.

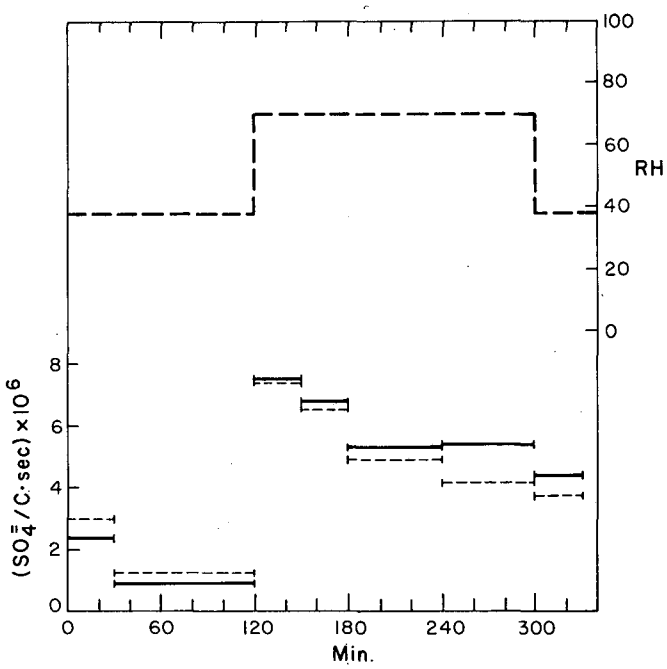

Figure 3. Sulfate formation on particles exposed to 0.75 ppm SO_2 and step-like changes in RH.
(XBL 822-87)

Figure 3 shows that the rate of sulfate formation decreased with time during the initial period of 40 percent RH. This indicates that the catalytic sites were becoming saturated, probably because there was inadequate liquid water into which the sulfate formed could desorb. At exposure time of 120 minutes, the RH was increased to ~70 percent, and a concurrent step-like increase in the rate was noted. The rate decreased over the subsequent 180-minute period, indicating again that saturation of the catalytic sites was occurring. At exposure time of 300 minutes, the RH was decreased to ~40 percent, but a concurrent drop in the rate was not observed. The small decrease in rate that occurred between the 240- to 300-minute period and the 300- to 330-minute period could not be justifiably related solely to the RH change because the rate appeared to follow the pattern established during the 120- to 300-minute period, in which the rate continuously declined. It is also possible that enough sulfate formed during the first 300 minutes of the 330-minute exposure time so that the particles had become hygroscopic and did not lose much of the water they adsorbed during exposure to 70 percent RH. Thus, the rate of sulfate formation was higher during the 300- to 330-minute period compared to the 0- to 30-minute period because more water was present on the particles during the 300- to 330-minute period. Future research is planned to prove or disprove this conjecture by measuring the amount of water on the particles after exposure to SO_2 and RH. The data presented in Figure 3 do not contradict the findings presented in Figure 2. In Figure 2, the rate of sulfate formation is that rate measured during the first 30 minutes of exposure to SO_2 and RH, while Figure 3 indicates what happens during long-term exposure.

Most of the particles we have used in the S(IV) oxidation studies have been commercially available activated carbons (Aktivköhle, Nuchar). Recently an electrostatic precipitator was used in Los Angeles to collect gram quantities of ambient particles. S(IV) was added to an aqueous suspension (0.5 g/10 ml) of these particles (pre-extracted in 0.1 M NaOH), and the S(IV) concentration was followed versus time. The preliminary results presented in Figure 4, curve 5, show that S(IV) can be oxidized by ambient particles. The implication of this finding is that ambient particles can heterogeneously oxidize SO_2. For the purpose of comparison, the rates of sulfate formation for other types of soot particles are also presented in Figure 4, and it can be seen that the ambient particles display the slowest capacity to oxidize S(IV). Presently, it is thought that the rate of sulfate formation determined for ambient particles is a lower limit for the rate because the rigorous pre-extraction in 0.1 M NaOH may have changed the catalytic sites on the particles. The extraction in 0.1 M NaOH was necessary to eliminate interference from an unknown ion that coeluted with S(IV) in the ion chromatographic determination of S(IV).

PLANNED ACTIVITIES FOR FY 1982

The results of the ongoing fog-chamber studies continue to point out the importance of liquid water in the soot-SO_2 reaction system. Future fog-chamber studies are planned to elucidate the role that water, trapped in the pores of soot particles, plays in oxidizing SO_2. The studies will be conducted with surrogate soot particles. Since we demonstrated that suspensions of ambient particles can oxidize S(IV), further experimentation is planned so that the importance of the oxidation of SO_2 by ambient particles can be evaluated. Eventually a reaction rate law will be developed so that this reaction can be incorporated into atmospheric transformation models.

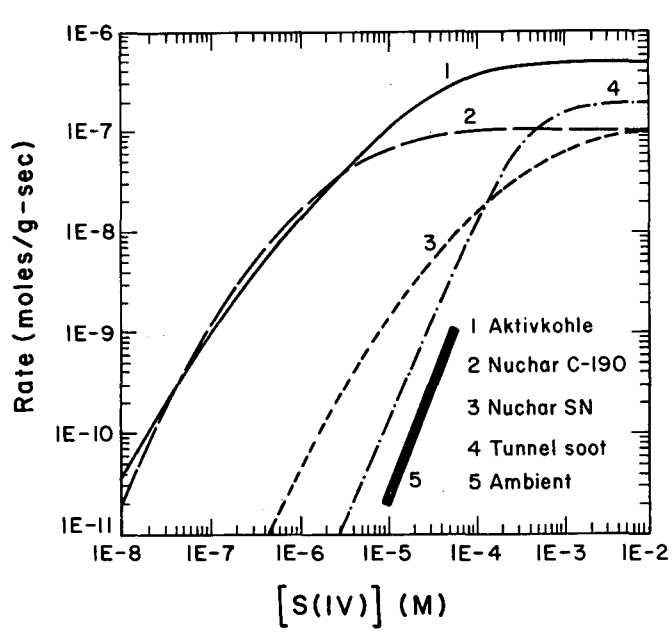

Figure 4. Rate of sulfate formation vs [S(IV)] for several aqueous suspensions of soot particles.
(XBL 822-86)

REFERENCES AND FOOTNOTE

1. Brodzinsky, R., et al. (1980), "Kinetics and Mechanism for the Catalytic Oxidation of Sulfur Dioxide on Carbon in Aqueous Suspension," Journal of Physical Chemistry 84, p. 3354.

2. Benner, W.H., Brodzinsky, R., and Novakov, T. (1982), "Oxidation of SO_2 in Droplets Which Contain Soot Particles," Atmospheric Environment, in press.

3. Nuchar is a commercially available activated carbon used as a surrogate for ambient soot particles. See Ref. 2 for a justification for using Nuchar.

Aqueous Reactions of Nitrite with Bisulfite Ions in Sulfate Aerosol Formation*

S. B. Oblath, S. G. Chang, S. S. Markowitz, and T. Novakov

The role of the oxides of nitrogen (NO_x) in the production of atmospheric sulfate aerosols has been of concern to environmental chemists for a number of years, both in homogeneous and heterogeneous systems.[1,2] In aerosol droplets, the NO_x reactively dissolve to form mixtures of nitrite and nitrate ions, which can then undergo a number of ionic reactions with aqueous SO_2. An understanding of these reactions is important to a complete evaluation of the process of sulfate aerosol formation.

For several years, we have been involved in a study of the reactions of nitrite ion with sulfur dioxide in aqueous solution as a model system for the aerosol droplets. Our work[3-5] and studies by other researchers[6] have shown that a variety of processes can be involved in these reactions. Under conditions which are likely to be found in a polluted atmosphere, the reactions can be briefly summarized as follows:

1. Nitrite and bisulfite ions react to form either nitrous oxide or hydroxylamine disulfonate, depending on the acidity.

2. Hydroxylamine disulfonate undergoes hydrolysis to hydroxylamine monosulfonate (HAMS) and sulfate ion.

3. Hydroxylamine monosulfonate reacts with nitrite ion to form nitrous oxide and sulfate ion.

Because processes 1 and 3 above are both sources of nitrous oxide and the rates of formation from the HAMS reaction have not been fully investigated,[7] we have undertaken a kinetic study of the reaction between nitrite ion and HAMS. The results of this study will allow the source of N_2O to be clearly established for any conditions normally encountered in aerosol droplets.

*This work was supported by the Assistant Secretary for Environment, Office of Health and Environmental Research, Division of Biomedical and Environmental Research Division, and the Morgantown Energy Research Center, through the Assistant Secretary of Fossil Energy, of the U.S. Department of Energy under Contract No. DE-AC03-76SF00098.

ACCOMPLISHMENTS DURING FY 1981

The kinetics of the reaction of a nitrite ion with hydroxylamine monosulfonate was investigated[8] by monitoring the loss of a nitrite ion (initial 0.5 to 5 m$\underline{M}$) at 354 nm with a Cary 219 visible spectrophotometer. Concentrations of other species, always in at least 10 times excess, were determined by addition of a known weight of pure salt. The acidity was maintained in the pH range of 3.9 to 4.8 by use of phthalate, oxalate, or tartrate buffer systems. Temperature was maintained by use of constant temperature baths, and ionic strength was held constant by addition of sulfate salts. Except where noted elsewhere, a temperature of 20°C and an ionic strength of 1.2$\underline{M}$ were used throughout the study.

The results of initial studies showed the reaction rate to be first order in nitrite ion, in agreement with previous workers.[7] In addition, the previous workers had shown the reaction rate to be independent of the HAMS concentration. At lower concentrations of HAMS, the reaction should become dependent on this species. Our experiments demonstrate this, as shown in Figure 1. Up to about 0.05 $\underline{M}$, the reaction shows a well-behaved first-order HAMS dependence, which then begins to approach a zero-order dependence. The solid line in the figure is a nonweighted least-squares fit to the data.

Additional investigation showed the reaction to be second-order, with respect to H^+, in both the HAMS-dependent and -independent regimes. It was independent of sulfate ion concentration or ionic strength of the solution. The temperature dependence is shown in Figure 2, and an activation energy of 30 kJ/mole was found. There was only a small difference (about 3 kJ/mole) in the values for each of the two regimes. The buffer species were found to affect the rate of reaction, and the results are shown in Figure 3. The buffer concentration refers to the sum of the acid and conjugate base forms.

The kinetic information can be summarized in the following rate law for the reaction extrapolated to zero buffer concentration:

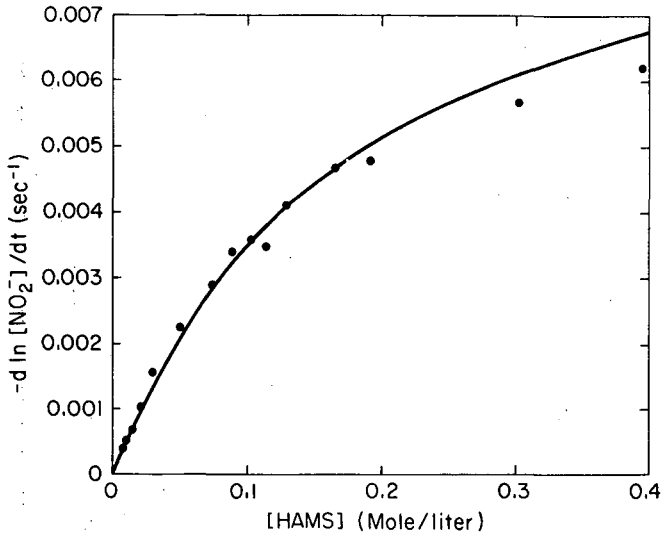

Figure 1. Dependence of the HAMS-nitrite ion reaction rate on HAMS concentration. (XBL 812-8163)

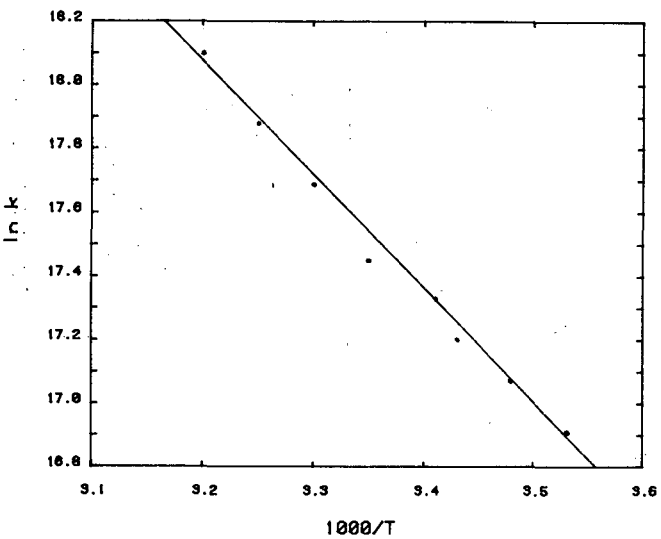

Figure 2. Arrhenius plot for the HAMS-nitrite ion reaction constant in the HAMS independent regime. (XBL 812-8161)

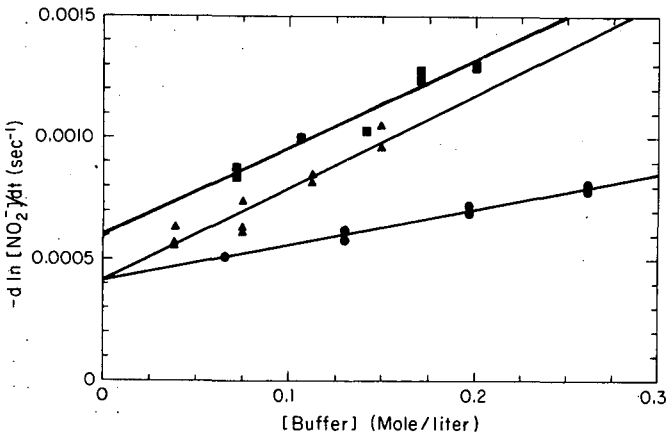

Figure 3. Buffer dependence in the HAMS-nitrite ion reaction. ■ indicates phthalate buffer, ▲ indicates tartrate buffer, ● indicates oxalate buffer. (XBL 815-3010)

$$\text{Rate} = \frac{k[NO_2^-][H^+]^2[\text{HAMS}]}{1 + k'[\text{HAMS}]} ,$$

where k = 1.5 x 10^7 l^3/mole^3-sec and k' = 5.5 l/mole at 20°C. The effect of the buffer may then be included as

$$\text{Total rate} = \text{Unbuffered rate}(1 + k_B[\text{Buffer}]) ,$$

where k_B is 7.5, 3.1, and 8.0 l/mole for phthalate, tartrate, and oxalate, respectively.

The following mechanism is proposed to account for the observed behavior:

$$HONO + H^+ \rightarrow NO^+ + H_2O$$

$$NO^+ + \text{HAMS} \rightarrow \text{products } (N_2O + SO_4^=) .$$

We presume that the second reaction is a nitrosation of hydroxylamine monosulfonate. When HAMS is present in high concentrations, the second step becomes rapid and step 1 is rate determining. When HAMS is present in low concentrations, the second step is rate limiting. Using a steady state approximation, the calculated rate law is of the form

$$\text{Rate} = \frac{k_1k_2[H^+][HONO][\text{HAMS}][\text{HAMS}]}{k_{-1} + k_2[\text{HAMS}]} ,$$

which is the same form as the observed, unbuffered rate law.

The effect of the buffer species, which has been observed in the study with phthalate, oxalate, and tartrate species and previously for acetate buffers,[7] can also be explained. All these buffer species contain a carboxylate (R-COO⁻) functionality, which is believed to form a complex with NO^+ ion.[9] Assuming that the weakly bound nitrosyl complex can react with HAMS in a manner similar to NO^+, the two processes will run concurrently; and the rate will be enhanced as the concentration of buffer species--and thus the nitrosyl complex--is increased. The tendency to form the complex, as well as its ability to react, will be the main factors in determining how efficiently the buffer enhances the rate of reaction.

The rates of reaction between HAMS and nitrite ion to form N_2O as presented in this report can be compared to those for the direct reaction of nitrite and bisulfite ions described previously.[4] We have found that both the reaction of HAMS and the rate of hydrolysis of hydroxylamine disulfonate to HAMS[10] are slow compared to the rate by direct NO_2^- - HSO_3^- reaction, under the mildly acidic conditions expected in a polluted atmosphere. When reactions such as these are considered in wet scrubber processes for flue gas, which are run at higher temperatures and concentrations, the formation of N_2O by reaction of HAMS with nitrite ion may become more important.

PLANNED ACTIVITIES FOR FY 1982

The next area to be investigated will be the possible reactions of both the hydroxylamine disulfonates and monosulfonates with nitrate ion, which is present in this reaction system because of the reactive dissolution of NO_x. It would also be interesting, from the point of view of scrubber chemistry, to investigate the reactions in the presence of various metal ions and chelating agents proposed for use in simultaneous (NO_x + SO_2) wet scrubbers, to see what effects they have on these reaction rates.

REFERENCES

1. Calvert, J.G., et al. (1978), "Mechanism of the Homogeneous Oxidation of Sulfur Dioxide in the Troposphere," Atmospheric Environment 12, p. 197.

2. Britton, L.G., and Clarke, A.G. (1980), "Heterogeneous Reactions of Sulphur Dioxide and SO_2/NO_2 Mixtures with a Carbon Soot Aerosol," Atmospheric Environment 14, p. 829.

3. Oblath, S.B., et al. (1981), "Kinetics of the Formation of Hydroxylamine Disulfonate by Reaction of Nitrite with Sulfites," Journal of Physical Chemistry 85, p. 1017.

4. Oblath, S.B., et al. (1981), "Kinetics of the Initial Reaction of Nitrite Ion in Bisulfite Solutions," submitted to Journal of Physical Chemistry; Lawrence Berkeley Laboratory Report LBL-12581.

5. Chang, S.G., Toossi, R., and Novakov, T. (1981), "The Importance of Soot Particles and Nitrous Acid in Oxidizing SO_2 in Atmospheric Aqueous Droplets," Atmospheric Environment 15, p. 1287.

6. Martin, L.R., Damschen, D.E., and Judeikis, H.S. (1981), "The Reactions of Nitrogen Oxides with SO_2 in Aqueous Aerosols," Atmospheric Environment 15, p. 191.

7. Seel, V.F., and Pauschmann, H. (1962), "Zum Kinetic der Umsetzung von Hydroxylaminemonosulfonat mit Nitrite," Zeitschrift fur Naturforschung 17b, p. 347.

8. Oblath, S.B., et al. (1981), "Reaction of Nitrite Ion with Hydroxylamine-N-Sulfonate in Aqueous Solution," submitted to Journal of Inorganic Chemistry, Lawrence Berkeley Laboratory Report LBL-13255.

9. Hughes, E.D., Ingold, C.K., and Ridd, J.H. (1958), "Nitrosation, Diazotisation, and Deamination. Part 1. Principles, Background, and Method for the Kinetic Study of Diazotisation," Journal of the Chemical Society (London), p. 58.

10. Naiditch, S., and Yost, D. (1941), "The Rate and Mechanism of the Hydrolysis by Hydroxylamine Disulfonate Ion," Journal of the American Chemical Society 63, p. 2123.

Carbon Particles in the Arctic*

H. J. Rosen and T. Novakov

Recent studies in the Arctic show the presence of unexpectedly high aerosol concentrations,[1] which appear to have a large anthropogenic component.[2] To investigate the chemical composition, origins, and climatic impact of the aerosol, a collaborative sampling program was started by LBL and NOAA in October 1979. This program has emphasized the analyses of the carbonaceous aerosol and its optical properties, but it also has the capability to determine other major aerosol components. Preliminary results from this study show that large concentrations of combustion-generated particles are present in the Arctic and that they may have a significant impact on the heat balance over this region.[3,4]

*This work was supported by the National Oceanic and Atmospheric Administration through the U.S. Department of Energy under Contract No. DE-AC03-76SF00098.

ACCOMPLISHMENTS DURING FY 1981

An aerosol sampler was designed and constructed at Lawrence Berkeley Laboratory to collect parallel filter samples on 47-mm quartz fiber and Millipore substrates at a flow rate of approximately 1.5 cfm. The sampler was put into operation on 18 October 1979 and coupled to a wind controller on 7 January 1980 to minimize local contamination by collecting samples only when the wind was blowing from the clean air sector. Approximately 100 filter pairs have been collected at sampling time intervals ranging from 2 to 7 days. All these filters have been analyzed to determine the total carbon content of the aerosol, the absorption coefficient of the aerosol, and the concentration of elements with $Z > 11$ by the x-ray fluorescence technique. The absorption coefficients reported here are at 0.5μ and have been corrected in a preliminary way for filter penetration effects. Only selected filters have been analyzed by Raman spectroscopy and optico-thermal analysis.

Chemical Composition of the Arctic Aerosol

Excluding the obvious natural aerosol components (e.g., sea salt and soil), the predominant components of the Barrow aerosol are carbon- and sulfur-containing particles. The carbonaceous aerosol has a large graphitic component which has been identified by Raman spectroscopy.[2] There is considerable indirect evidence that a major part of the Arctic aerosol is produced from combustion processes. However, the strongest and most direct substantiation of this fact is provided by the Raman spectra shown in Figure 1.[2] These spectra demonstrate the presence of substantial quantities of graphitic species which have a structure similar to carbon black and can only be produced by combustion processes. Associated with these species are large optical absorption coefficients ($\simeq 10\ m^2/g$). If one ignores the possible contribution of natural burning processes (e.g., forest fires), which is expected to be small during these times of year in the Northern Hemisphere, this component can be attributed directly to anthropogenic combustion processes.

Both the total carbon and total sulfur contents of the aerosol have also been determined. The total carbon concentrations were measured by combusting the aerosol samples in oxygen at 800°C and measuring the evolved CO_2.[5] The total sulfur content was determined by x-ray fluorescence analysis. In Figures 2 and 3, the concentrations of these two components during various times of year are compared to those found in urban environments. It is clear from these figures that the

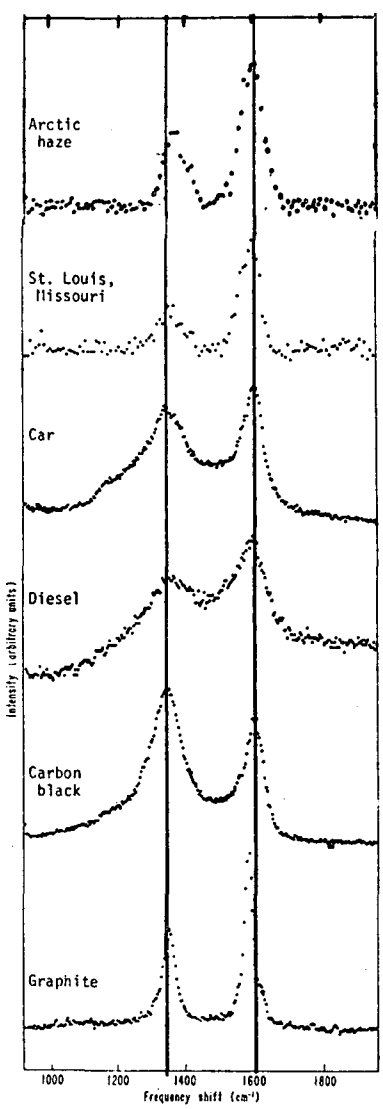

Figure 1. Raman spectrum of Arctic haze particulates compared to those of urban particulates, various source emissions, carbon black, and graphite. (XBL 767-3091B)

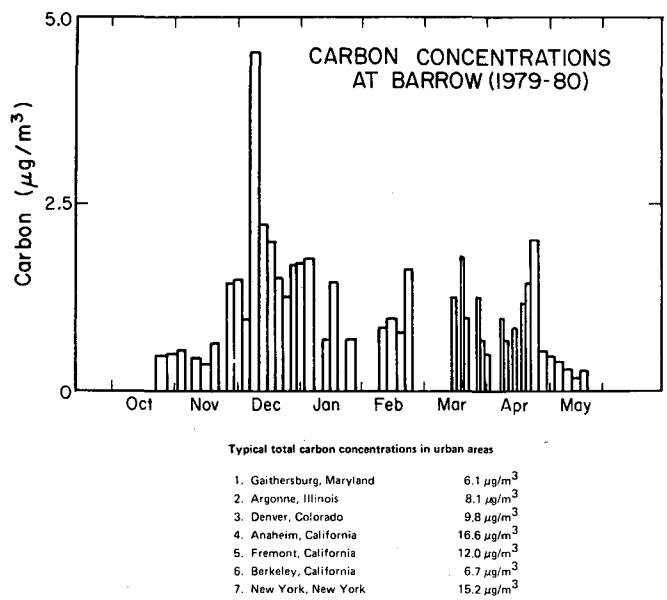

Figure 2. Comparison of total carbon concentrations at Barrow, Alaska, to those found in various urban locations. (XBL 8112-1694)

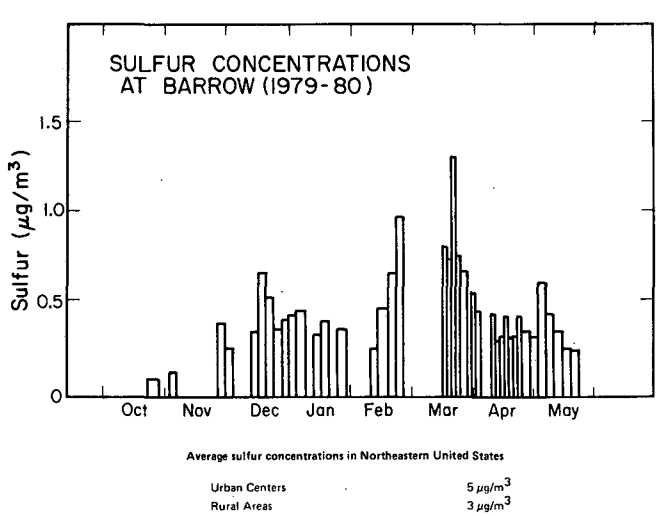

Figure 3. Comparison of sulfur concentrations to those found in urban centers and rural areas. (XBL 8112-1693)

concentrations of these aerosol components are large from the early winter to spring. These levels, of course, are less than those found in urban areas, but surprisingly not by large factors.

Model Calculation of the Effect of Absorbing Aerosols on the Heat Balance over the Arctic

Using the absorption coefficients measured at ground level at Barrow, Alaska,[2] a simple model calculation of the possible effects of the Arctic aerosol on the heat balance can be made. In the calculation, we assume a uniform aerosol distribution from ground level to the height h (see Fig. 4) and use the two-stream approximation of Chylek and Coakley.[6] With these assumptions the effective albedo of the earth-atmosphere system can be written as

$$I_R/I_0 = A - 2\tau_A A + \tau_B(A - 1)^2 \quad , \qquad (1)$$

where

A = albedo of surface
τ_A = optical depth due to absorption
τ_B = optical depth due to backscattering
I_0 = incident energy
I_R = reflected energy

Over snow-covered regions, $A \simeq 0.8$, and the scattering or cooling term is negligible compared to the absorption or heating term of all reasonable τ_A, τ_B. Equation (1) then becomes

$$I_R = I_0 A - 2\tau_A I_0 A \quad ,$$

and the change in light reflected due to aerosols is

$$I_R - I_R^A = 2\tau_A A I_0 \quad .$$

This change in irradiance is calculated for a plane perpendicular to the incoming radiation. If we calculate the change in irradiance parallel to the earth's surface, we get

$$\Delta = (I_R - I_R^A)\cos\theta = 2\tau_A I_0 \cos\theta \quad ,$$

but τ_A can be written as $b_A h/\cos\theta$ and

$$\Delta = 2 b_A h A I_0 \quad ,$$

where b_A is the absorption coefficient. I_0 is the average incident radiation from the sun, and we will approximate it by

$$I_0 = I_0^S f_1 f_2$$

where

$$I_0^S = \text{solar constant} = (1350\ \text{W/m}^2)$$

and f_1 is the fractional cloud cover and f_2 is the fractional length of day. Then,

$$\Delta = 1350(2)\ b_A h A f_1 f_2 = 2700\ b_A h A f_1 f_2\ \text{W/m}^2 \quad .$$

For this calculation, let $A = 0.8$, $f_1 = 0.5$, and $h = 5 \times 10^3$ m; then,

$$\Delta = 5.4 \times 10^6\ b_A f_2 \quad .$$

We now use our measurements of the absorption coefficient at Barrow and values of f_2 obtained from the Smithsonian Meteorological Tables to calculate the results shown in Figure 5. Since one-half the sun's irradiance is above and below 0.75 μ, the absorption coefficients reported at 0.5 μ have been corrected to this wavelength, assuming a $1/\lambda$ dependence characteristic of graphitic carbon. The results shown in Figure 5 indicate rather substantial changes in the heat balance during the months of February through May and possibly during June. During these months, approximately 6 W/m^2 more energy is absorbed by the earth-atmosphere system due to the presence of the haze. This energy change is about equivalent to the change in the radiation balance at midlatitudes expected from a four-percent increase in the solar constant and is comparable to the change in the

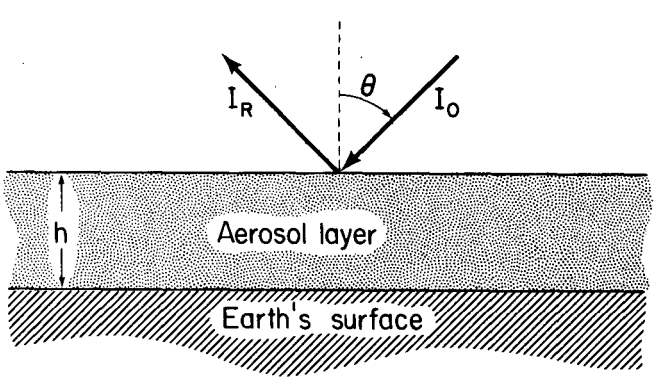

Figure 4. Schematic of earth-atmosphere system used in model calculation. (XBL 8112-1692)

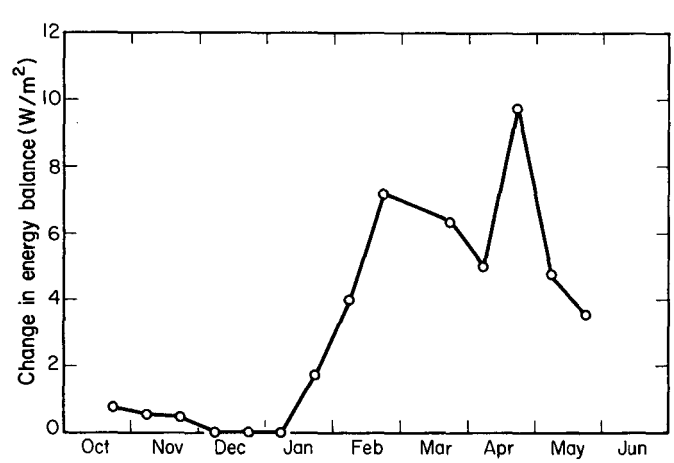

Figure 5. Change in energy balance predicted from simple model calculation. (XBL 8112-1691)

terrestrial radiation balance due to a doubling of CO_2. It is difficult to translate this into a ground-level temperature change; however, there have been many models that predict a one-percent increase in the solar constant would lead to ~1°K increase in the surface temperature of the earth. This calculation is obviously oversimplified and should only be viewed as being indicative of the possible large climatic effect of the Arctic aerosol.

PLANNED ACTIVITIES FOR FY 1982

The program described above will be extended to other Arctic sites stretching from the Canadian Arctic to the Norwegian Arctic. The program will emphasize determining the optical properties of the Arctic haze and its sources by geographical area and combustion technology. Such information is necessary for determining the present impact of the Arctic haze on the heat balance and predicting future trends.

The authors would like to thank Bob Giauque and Linda Sindelar for doing the x-ray fluorescence analysis of the samples.

REFERENCES

1. See, for example, Kerr, R.A. (1981), "Pollution of the Arctic Confirmed," Science 212, p. 1013.

2. Rosen, H., Novakov, T., and Bodhaine, B. (1981), "Soot in the Arctic," Atmospheric Environment 15, p. 1371.

3. Bodhaine, B., and Winchester, J.W. (1981), "Importance of Carbon Particles in the Atmosphere," report at ARL-GMCC-NOAA Workshop, Boulder, Colorado, March 4, 1981.

4. Porch, W.M., and MacCracken, M.C. (1981), "Parametric Study of the Effects of Arctic Soot on Solar Radiation," accepted for publication in Atmospheric Environment.

5. Mueller, P.K., Mosley, R.W., and Pierce, L.B. (1971), "Carbonate and Noncarbonate Carbon in Atmospheric Particulates," in Proceedings, Second International Clean Air Congress, Academic Press, New York.

6. Chylek, P., and Coakley, J.A. (1974), "Aerosols and Climate," Science 183, p. 75.

Application of Thermal Analysis and Photoelectron Spectroscopy for the Characterization of Particulate Matter*

R. L. Dod and T. Novakov

Carbon-, nitrogen-, and sulfur-containing species account for most of the mass of aerosol particles. Despite years of effort by many investigators, the exact chemical forms of carbon, sulfur, and nitrogen in these particles are not known nor are the formation mechanisms of these species known with certainty. There are many reasons for this situation, including the complexity of the system and the dependence of the apparent chemical composition on the analytical methods used. For example, wet chemical analyses of sulfur and nitrogen species report only ions in solution. These ions, however, may be originally water soluble (e.g., sulfate and ammonium from ammonium sulfate), or they may be ionic products of hydrolyzable species such as amides.[1] Of course, insoluble species will not be detected by wet chemical techniques.

In contrast, methods such as photoelectron spectroscopy (ESCA) analyze the entire sample content without sample preparation. However, ESCA is a surface technique, and the sample is exposed to vacuum and x-ray bombardment during analysis. ESCA results, therefore, may not be representative of the bulk composition; some volatile species may be lost because of the vacuum, and in principle the x-ray bombardment may cause chemical changes of some species.

Because of these possible problems, it seemed desirable to employ a technique that will analyze the bulk properties of particles without chemical treatment or preseparation of the sample and to compare these results with ESCA results. Thermal analysis in the evolved-gas-analysis (EGA) mode is one such technique.[2,3]

ACCOMPLISHMENTS DURING FY 1981

The analytical results of our previous ESCA work[4] can be summarized as follows. Sulfur is found to be predominantly in a +6 oxidation state, i.e., sulfate. Other chemical states of sulfur have also been observed, although these seldom approach sulfate concentrations. Generally, at high pollutant concentrations, sulfate is practically the only sulfur species present. Nitrogen can be present in an oxidized and a reduced form. The oxidized form has been identified as nitrate, while the reduced form consists of ammonium and a group of species consisting of particulate amines

*This work was supported by the Assistant Secretary for the Environment, Office of Health and Environmental Research, Pollutant Characterization and Safety Research Division of the U.S. Department of Energy under Contract No. DE-AC03-76SF00098 and by the National Science Foundation.

and amides, N_x. These N_x species were first discovered by ESCA[5] and are easily distinguished from ammonium by a ~2 eV chemical shift of the N(1s) peak.

Attempts were made to prove the existence of the particulate amines by other techniques with only limited success. At best, indirect evidence[6] was obtained from the fact that nitrate and ammonium cannot account for total particulate nitrogen determined by combustion. However, the observed nitrogen deficiency was much less than indicated by ESCA. An attempt to detect N_x by infrared spectroscopy[7] failed because of interfering absorption bands.

To detect N_x species by EGA, we used the results of our earlier ESCA analyses,[5] which demonstrated that exposing a sample to vacuum and x-ray bombardment or heat results in the volatilization of most of the nitrate and ammonium salts. Thus, in a sample exposed to vacuum, the only major nitrogenous species will be N_x. This is illustrated in Figures 1a and 1b. The NO_x thermograms of the original and vacuum-exposed samples are shown in Figures 1c and 1d. The ESCA spectra show that the principal species are volatile nitrate and ammonium, probably present as ammonium nitrate and ammonium sulfate, and non-volatile N_x. The corresponding thermograms show a reduction in intensity in the triplet located between 150 and 300°C, assigned to ammonium nitrate and ammonium sulfate. Peaks at ~350 and 450°C and the peak at ~550°C are unchanged, however. The first two probably correspond to N_x, while the last peak is most likely due to a metal nitrate.

We have used the ESCA results to provide empirical information about the apparent stoichiometry of sulfate, ammonium, and nitrate ions and other elements and species. Wet chemical analyses performed at several laboratories seemed to contradict some of the conclusions reached from ESCA studies. For example, total reduced nitrogen, as determined by ESCA, often agrees with the determination of ammonium by wet chemical methods. A consequence of this discrepancy is that, in analyses where wet analysis would indicate ammonium sulfate, ESCA would suggest ammonium bisulfate, based on the assumption that particulate N_x species are not associated with sulfate. This assumption may not be valid because it has been demonstrated[1] that a large fraction of N_x present in the original sample may be hydrolyzed to ammonium and removed by water extraction.

An insight into this apparent inconsistency may be achieved by combined ESCA and EGA analysis. Figure 2 shows the ESCA spectrum of the N(1s) region of a sample collected in Gaithersburg, Maryland. In addition to a small nitrate peak, a pronounced ammonium peak is also seen. This sample contains a very small concentration of N_x, evidenced only by a slight asymmetry of the ammonium peak, and enough ammonium to almost completely neutralize the sulfate as determined by ESCA. The conclusion is that here the sulfate is in the form of ammonium sulfate. The NO_x thermogram of the same sample and the positions of NH_4NO_3 and $(NH_4)_2SO_4$ thermogram peaks are shown in Figure 3.

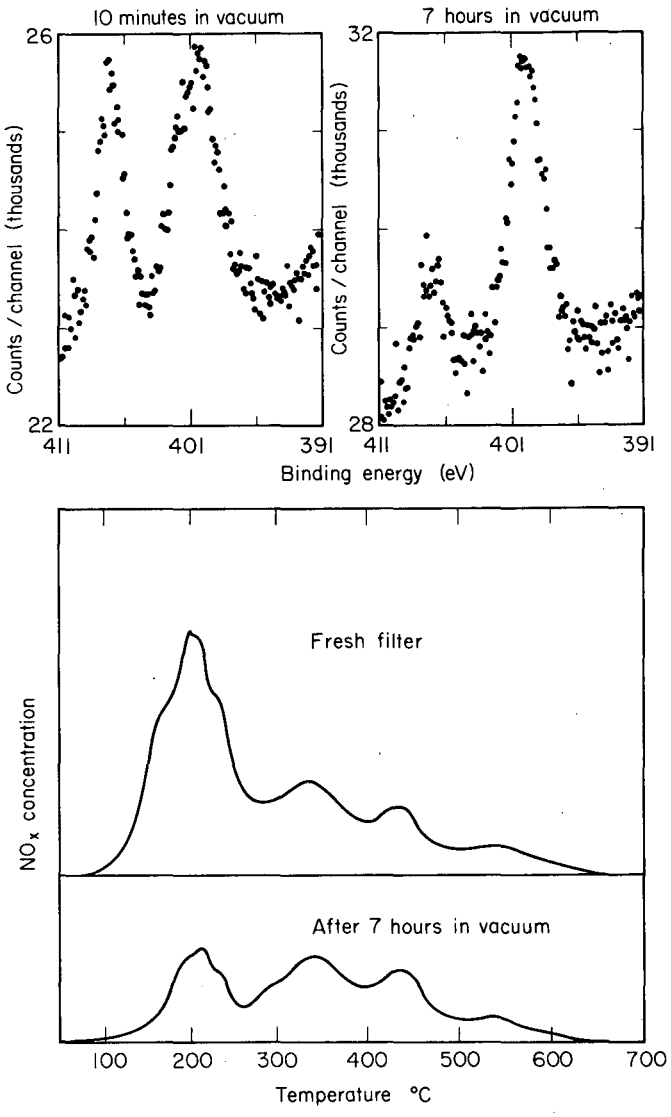

Figure 1. ESCA spectra and NO_x thermograms from an ambient particulate sample from Riverside, California, before and after exposure to vacuum. (XBL 8111-1625)

This thermogram suggests that the principal counterion for sulfate is ammonium, not N_x, and that the sulfate is present as $(NH_4)_2SO_4$. This is consistent with the ESCA observations.

This situation is quite different for an Anaheim sample whose N(1s) ESCA spectrum is shown in Figure 4. Here, in addition to NO_3^- and NH_4^+, the N_x peak is clearly seen. Volatility in ESCA vacuum indicates that the nitrate in this sample is present as NH_4NO_3, and therefore a significant portion of the ammonium is associated with the nitrate. The remainder of the ammonium is insufficient to provide counterions for the sulfate. This ESCA result suggests an ammonium-deficient sulfate compound such as ammonium bisulfate. We note that if the entire reduced nitrogen were hydrolyzed, there would be sufficient ammonium to conclude that the sulfate is present as ammonium sulfate.

The thermogram of this sample is shown in Figure 5. The ammonium nitrate peak and the

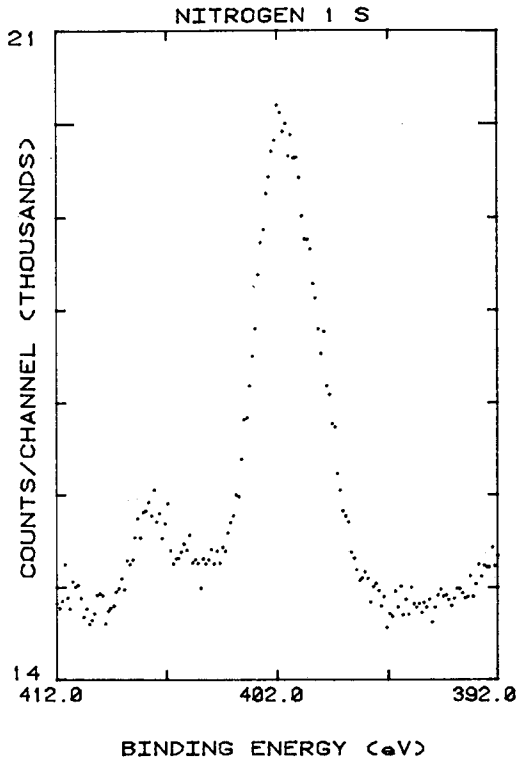

Figure 2. N(1s) ESCA spectrum of 24 April 1979 ambient particulate sample from Gaithersburg, Maryland. (XBL 8112-12921)

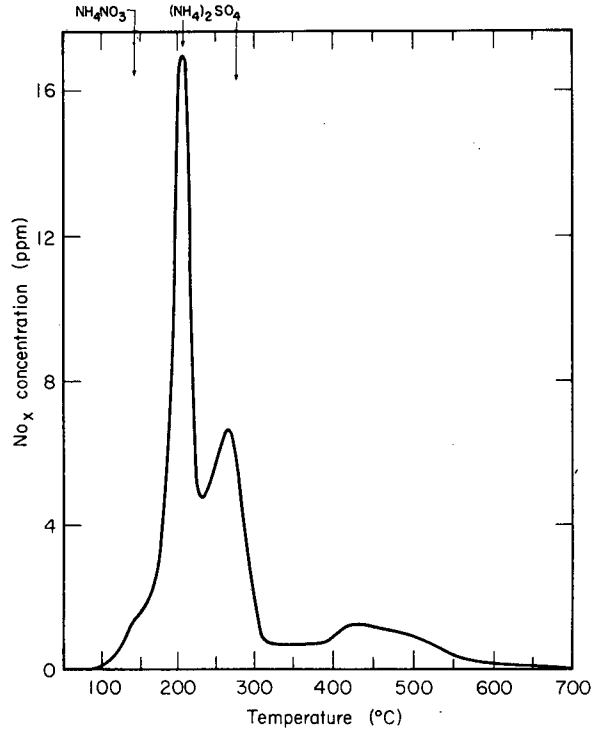

Figure 3. NO_x thermogram for 24 April 1979 ambient particulate sample from Gaithersburg, Maryland. (XBL 8111-1622)

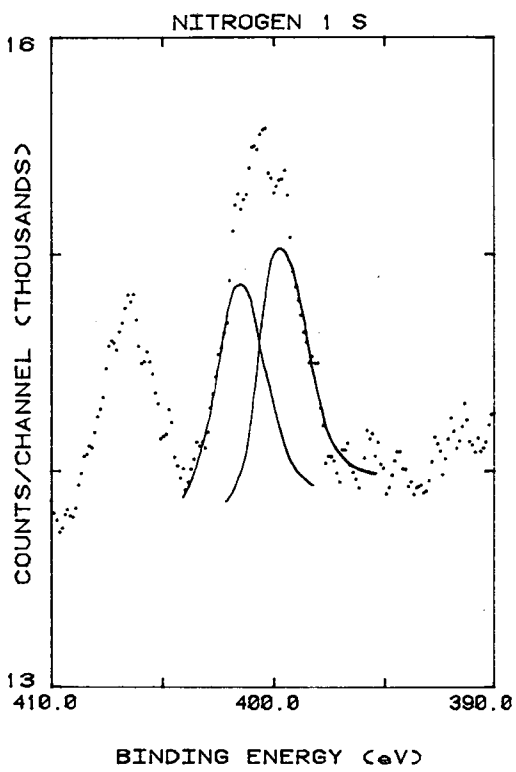

Figure 4. N(1s) ESCA spectrum of 27 July 1979 ambient particulate sample from Anaheim, California. (XBL 8112-12920)

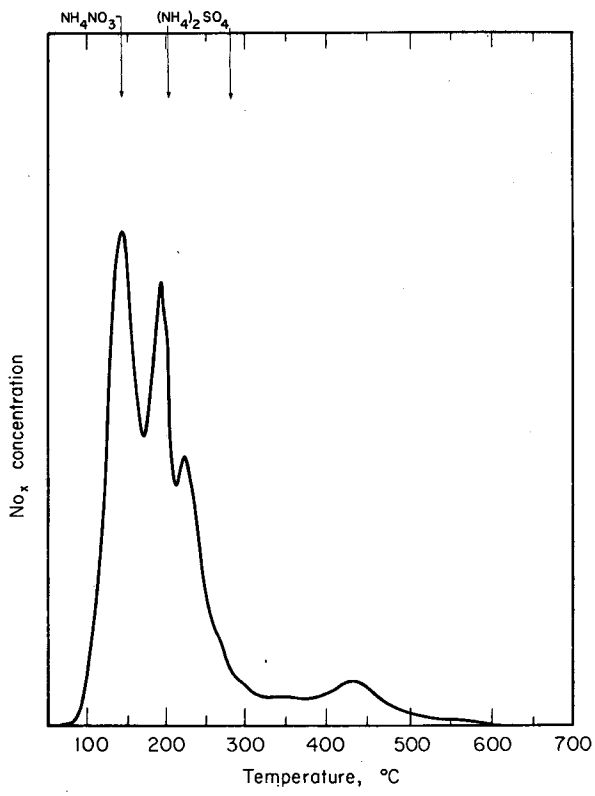

Figure 5. NO_x thermogram of 27 July 1979 ambient particulate sample from Anaheim, California. (XBL 8111-1621)

first peak of ammonium sulfate match closely the positions of standard compounds. However, the peak at 270°C is noticeably shifted from the second ammonium sulfate peak, although the overall appearance of the doublet is similar to that of ammonium sulfate. A tentative explanation of this observation is that the sample does not contain pure ammonium sulfate, but rather that some of the ammonium ions are replaced by a charged organic nitrogen complex. This complex should produce the right chemical shift (relative to ammonium) in the ESCA spectrum, decompose at a lower temperature than ammonium bisulfate, and hydrolyze to ammonium in water solution.

PLANNED ACTIVITIES FOR FY 1982

Analysis of more standard materials and collected particulate samples will be carried out in order to more fully understand the relationship of nitrogen species to carbon. In addition, the thermal analysis apparatus will be modified to permit detection of evolved sulfur, thus providing additional information from which conclusions may be drawn about the association (or lack thereof) of the nitrogenous species with sulfate.

REFERENCES

1. Gundel, L.A., et al. (1979), "Characterization of Particulate Amines," in Nitrogenous Air Pollutants, D. Grosjean, Ed., Ann Arbor Science, Ann Arbor, p. 211.

2. Dod, R.L., Rosen, H., and Novakov, T. (1979), "Optico-Thermal Analysis of the Carbonaceous Fraction of Aerosol Particles," in Atmospheric Aerosol Research Annual Report 1977-78, Lawrence Berkeley Laboratory Report LBL-8696, p. 2.

3. Dod, R. et al. (1980), "Application of Thermal Analysis to the Characterization of Nitrogenous Aerosol Species," in Energy and Environment Division Annual Report 1979, Lawrence Berkeley Laboratory Report LBL-11650, p. 8-25.

4. Novakov, T. (1978), "Identification and Determination of Particulate Compounds: Electron Spectroscopy," in Analysis of Airborne Particles by Physical Methods, H. Malissa, Ed., CRC Press, West Palm Beach, p. 191.

5. Chang, S.G., and Novakov, T. (1975), "Formation of Pollution Particulate Nitrogen Compounds by NO-Soot and NH_3-Soot Gas-Particle Surface Reactions," in Atmospheric Environment 9, p. 495.

6. Spicer, C.W. (1977), "Photochemical Atmospheric Pollutants Derived from Nitrogen Oxides," Atmospheric Environment 11, p. 1089.

7. Chang, S.G., and Novakov, T. (1977), "Identification of Surface Nitrogen Complexes on Graphite Particle Surfaces," Atmospheric Aerosol Research Annual Report 1976-77, Lawrence Berkeley Laboratory Report LBL-6819, p. 57.

Theoretical Studies of the Thermal Decomposition of Carbonaceous Aerosol Particulates*

A. D. A. Hansen and T. Novakov

The carbonaceous fraction of atmospheric aerosol particles is a complex mixture of many forms and compounds of carbon, including volatile organics, high molecular weight organics, quasi-"graphitic" microcrystallites, and inorganic carbonates. The development of analytical methods to separate these components is essential to an understanding of their origins and thus, ultimately, to the development of effective air pollution controls. One analytical method is evolved gas analysis (EGA), which classifies the components according to their thermal decomposition characteristics. This report presents a theoretical approach to the interpretation of EGA of the graphitic carbon component of aerosol particles.

*This work was supported by the Assistant Secretary for the Environment, Office of Health and Environmental Research, Pollutant Characterization and Safety Research Division of the U.S. Department of Energy under Contract No. DE-AC03-76SF00098 and by the National Science Foundation.

ACCOMPLISHMENTS DURING FY 1981

Experimental

In our EGA system, the sample is slowly heated in a pure oxygen stream. The evolved gas is passed to a continuous CO_2 detector over an oxidizing catalyst to ensure that volatilized or partly combusted material is completely converted to CO_2. The concept is similar to that of the flash desorption method[1] and was first used to study aerosol particles by Malissa et al.[2] Subsequent work[3,4] has developed this technique into a powerful tool for the study of carbonaceous and nitrogenous materials. In the present apparatus, the sample is a 1-cm diameter quartz fiber filter punch with 10 to 50 μg carbon content. The sample is heated at 10°C/min in an oxygen stream of ~175 ml/min at atmospheric pressure which flows past the sample at about 1 cm/sec. The maximum recorded CO_2 concentration downstream is typically 50 ppm, corresponding to a maximum decomposition rate of the order of 0.05 μg C/sec.

Most aerosol samples yield complex traces of CO_2 evolution versus temperature due to the presence of many different classes of compounds. However, certain samples may be chosen or selectively pretreated so that the "thermogram" shows a single peak corresponding to the oxidation of the graphitic carbon fraction. This material has been observed in substantial quantities in all urban atmospheres sampled to date[5] and is expected to have significant effects on atmospheric physics and chemistry.[6,7] In the present work we concentrate on the interpretation of the analysis of this component of carbonaceous aerosols.

Table 1. Oxidation parameters of various carbonaceous materials.

Sample	Activation energy (kcal/mole)	Pre-exponential factor (sec^{-1})	Peak temperature (°C)
(a) Combustion source aerosols			
Jet Engine	20.8	3.6×10^4	590
Oil-fired furnace	25.9	1.2×10^5	575
Diesel test stand engine	27.9	2.2×10^6	570
Acetylene soot	31.1	1.6×10^7	540
(b) Fine particle carbons			
Ground graphite #1	25.3	1.9×10^4	690
"Channel black" activated carbon	25.6	1.4×10^5	595
"Nuchar" activated carbon	34.7	1.2×10^9	480
Ground graphite #2	53.7	3.7×10^{11}	680
(c) Carbon oxidation studies in literature[a]			
Spectrographic graphite	54.3	5×10^6	
Graphitized carbon black	38.0	5.5×10^6	
Catalyzed carbon composites	16-46		

[a]From References 8-10.

Results

The CO_2 thermogram for a diesel exhaust sample is shown in Figure 1a. When displayed as an Arrhenius plot (Fig. 1b), it shows the characteristics of a thermally activated process with a slope corresponding to an activation energy of 26.8 kcal/mole. The reaction rate, i.e., the rate of CO_2 evolution, increases rapidly with temperature until the amount removed is comparable to the original mass. After a peak, the remaining material rapidly burns off to completion. Other samples may show similar slopes but differing peak temperatures (Table 1, parts a and b), suggesting the combustion of materials of similar reactivity but differing porosity or particle size. The range of apparent activation energies for the decomposition of the graphitic carbon fraction of combustion-source aerosols is within the range of values reported in the literature[8-10] for the oxidation of various carbons (Table 1, part c).

Theoretical

We develop a model by considering the combustion of n carbon atoms all equally exposed to oxygen at time t, temperature $T(t) = Qt$. Their rate of removal may be written as

$$-\frac{dn}{dt} = nA'T^{\alpha}\exp(-E/T) \quad . \tag{1}$$

The activation energy E is expressed here in degrees Kelvin, and the exponent α models the rate of collision of oxygen with the carbon. Since the temperature interval in which the carbon burns off is usually fairly narrow, the T^{α} variation is small, and we absorb this term into the pre-exponential activity factor A. Substituting $x = E/T$, Equation (1) is written as

$$\frac{d}{dx}(\log n) = \frac{AE}{Q}x^2e^{-x} \quad , \tag{2}$$

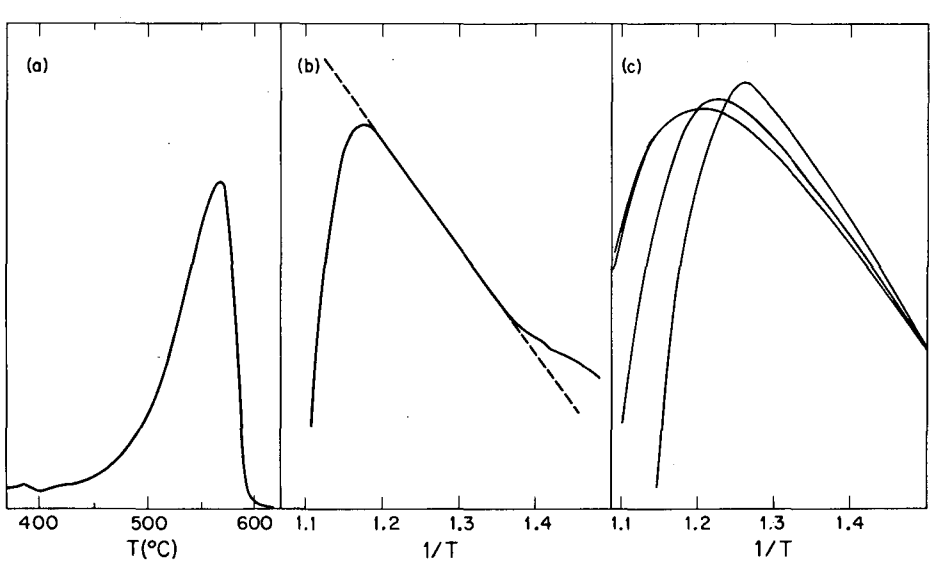

Figure 1. (a) Rate of CO_2 evaluation versus temperature for sample of diesel exhaust particulates. (b) Arrhenius plot of data shown in (a): log(d[C]/dt) versus reciprocal of temperature (units 10^{-3} $^{o}K^{-1}$). (c) Theoretical model: Arrhenius plot of Equation (9) for varying values of activity enhancement factor k - left to right, k = 0, k = 0.1, k = 1, k = 3. (XBL 822-82)

whose solution is written in the form appropriate to the Arrhenius plot as

$$\log\left(\frac{-dn}{dt}\cdot\frac{1}{n_o}\right) = \log A - x - F(x) \quad , \tag{3}$$

where

$$F(x) = \frac{AE}{Q}\,(x^2 + 2x + 2)\,e^{-x} \quad . \tag{4}$$

The linear term in Equation (3) is the normal rate term common to thermally activated reacting systems; the term F(x) arises because the reacting material is consumed as a function of time and temperature. In practice, there may be mechanisms by which the average apparent value of A changes as a function of time, temperature, or size of particle remaining. For example, it is known[11,12] that the oxidation of carbon crystallites progresses much more rapidly parallel to the basal planes than perpendicular to them. Initially, a relatively small fraction of the carbon atoms will be close to exposed basal plane edges. As burn-off proceeds, this fraction may be expected to increase. Also, the surface-to-volume ratio of the particle will in general increase with the burn-off, thus exposing atoms previously inaccessible to oxygen in the interior of the particle. The oxidation process may be partly assisted by the catalytic activity of metallic impurities. If these impurities are not themselves lost from the reacting surfaces, then as burn-off proceeds their numbers will increase relative to the quantity of carbon remaining and the apparent activity will increase.

We can represent these variations by replacing A by $A\cdot P(n)$ where n is the number of carbon atoms remaining. Equation (2) then becomes

$$\frac{d}{dx}(\log n) = \frac{AE\,P(n)}{Q}\cdot x^2 e^{-x} \quad , \tag{5}$$

whose solution is

$$\log\left(-\frac{dn}{dt}\right) = \log n + \log P(n) - x \quad . \tag{6}$$

where n as a function of x is determined by the relation

$$\int_{n(x)}^{n_o} \frac{dn}{n\,P(n)} = F(x) \tag{7}$$

with F(x) as before defined by Equation (4). A linear increase in average apparent activity with increasing burn-off can be represented by

$$P(n) = 1 + k\left(\frac{n_o - n}{n_o}\right) , \tag{8}$$

yielding the solution

$$\log\left(-\frac{dn}{dt}\cdot\frac{1}{n_o}\right) = \log A - x - (1 + k)\,F(x) - 2\log\{1 + k\exp[-(1 + k)\,F(x)]\} \quad . \tag{9}$$

A plot of this function is shown in Figure 1c for various values of k, reducing to the solution [Eq. (3)] for k = 0. The effect of the activity increase modelled by Equation (8) is to increase the sharpness of the burn-off to zero at high temperatures but does not affect the slope of the linear portion. Many experimental results show burn-off curves that correspond to this result [Eq. (9)] with values of k in the range 0.5 to 2, suggesting that mechanisms of apparent activity enhancement may be operational. Since the burn-off rates are low, it is not believed that exothermicity or reactant/product film diffusion effects are significant. The effects of interactions of other carbonaceous species with the thermal decomposition of the graphitic fraction were minimized by selecting samples showing low concentrations of these other materials or by pre-extraction with suitable solvents. The restrictive effects of pore diffusion limitations cannot be calculated without detailed knowledge of the particles' microstructure. However, it is known that the graphitic microcrystallite grain size is typically 3 nm,[13] and BET surface area measurements on the samples yield figures in the range 10 to 100 m^2/gm. The maximum specific burn-off rates in these experiments are in the range 10 to 100 $\mu g/m^2\cdot sec$, which, with the above results, suggests that the material is indeed effectively highly microporous.

PLANNED ACTIVITIES FOR FY 1982

The catalytic effects of metals on the oxidation of graphitic carbon have been extensively reported in the literature.[14] The largest effects are seen on carbons of initially high chemical and structural purity and are usually observed as a lowering of the activation energy accompanied by a compensating decrease in the pre-exponential factor A. Microscopic studies[15] have shown situations in which small catalyst particles channel into graphitic surfaces. In the present experiments, the samples contain substantial quantities of metallic impurities, notably lead, iron, vanadium, etc. Work is in progress to study the effect of pre-extraction of the samples with inorganic solvents and to systematize the variations of oxidation parameters (Table 1) with regard to measurements of the types and concentrations of impurities, morphological studies, etc. In addition to graphitic carbon, ambient aerosol samples contain carbonaceous species that volatilize, pyrolyze, or decompose in other non-oxidative processes. These processes and the resultant instrumental response will be studied theoretically and experimentally in our EGA apparatus with pure compounds, mixtures, and ambient samples.

REFERENCES

1. Hagstrum, H.D. (1953), "Instrumentation and Experimental Procedure for Studies of Electron Ejection by Ions and Ionization by Electron Impact," Review of Scientific Instruments 24, p. 1122.

2. Malissa, H., Puxbaum, H., and Pell, E. (1976), "Zur Simultanen Relativkonduktometrischen Kohlenstoff- und Schwefelbestimmung in Stauben," Zeitschrift fur Analytische Chemie 282, p. 109.

3. Dod, R.L., Rosen, H., and Novakov, T. (1978), "Optico-Thermal Analysis of the Carbonaceous Fraction of Aerosol Particles," in Atmospheric Aerosol Research Annual Report, 1977-78, Lawrence Berkeley Laboratory Report LBL-8696, p. 2.

4. Dod, R.L., et al. (1980), "Application of Thermal Analysis to the Characterization of Nitrogeneous Aerosol Species," Atmospheric Aerosol Research Report FY 1979, Lawrence Berkeley Laboratory Report LBL-10735, p. 35.

5. Novakov, T. (1981), "Microchemical Characterization of Aerosols," in Nature, Aim and Methods of Microchemistry, H. Malissa, M. Grasserbauer, R. Belcher, Eds., Springer-Verlag, Vienna, p. 141.

6. Chylek, P., and Coakley, J.A. (1975), "Aerosols and Climate," Science 183, p. 75.

7. Brodzinsky, R., et al. (1980), "Kinetics and Mechanism for the Catalytic Oxidation of Sulfur Dioxide on Carbon in Aqueous Suspensions," Journal of Physical Chemistry 84, p. 3354.

8. Marsh, H., Taylor, D.A., and Lander, J.R. (1981), "Kinetic Study of Gasification by Oxygen and Carbon Dioxide of Pure and Doped Graphitizable Carbons," Carbon 19, p. 375.

9. Walker, P.L. (1980), "Fundamental Rate Constants for Carbon Gasification by Oxygen," Carbon 18, p. 447.

10. Ehrburger, P., Lahaye, J., and Bourgeois, C. (1981), "Characterization of Carbon-Carbon Composites," Carbon 19, p. 7.

11. Walker, P.L., Ruskino, F., and Austin, L.G. (1959), "Gas Reactions of Carbon," Advances in Catalysis 11, p. 133.

12. Grisdale, R.O. (1953), "The Properties of Carbon Contacts," Journal of Applied Physics 24, p. 1288.

13. Rosen, H., et al. (1978), "Identification of the Optically Absorbing Component in Urban Aerosols," Applied Optics 17, p. 3859.

14. See, for example, the review by Walker, P.L., Shelef, M., and Anderson, R.A. (1968), "Catalysis of Carbon Gasification," in Chemistry and Physics of Carbon, P.L. Walker, Ed., Vol. 4, Dekker, New York, p. 287.

15. Thomas, J.M. (1966), "Microscopic Studies of Graphite Oxidation," in Chemistry and Physics of Carbon, P.L. Walker, Ed., Vol. 1, Dekker, New York, p. 121.

Application of Selective Solvent Extraction to Carbonaceous Aerosols*

L. A. Gundel and T. Novakov

Considerable effort has been directed toward demonstrating that many polar organic compounds in ambient particulate matter result from photochemical reactions which involve gas-phase hydrocarbons and ozone.[1] These aerosol components are "secondary" organics since their origin is gas-to-particle conversion rather than direct emission in the particulate phase from sources. Directly emitted particles contain "primary" organic compounds and elemental or "black" carbon.[2,3] Knowledge of the relative contributions of primary and secondary carbon to the aerosol burden will influence the choice of control strategies for particulate matter; and, therefore, development of accurate characterization and quantitation techniques is important.

The selective solvent extraction-carbon analysis technique, as developed by Grosjean[4] and applied by Appel et al.,[5] was intended to assess the relative contributions of primary and secondary carbon to ambient particulate matter. This technique has been applied to carbonaceous aerosols collected in the Los Angeles basin during periods of high photochemical activity, as indicated by high ozone concentrations.[5-7] Concentrations of primary and secondary particulate organics were equated with concentrations of nonpolar and polar carbon compounds, respectively. An upper limit to the elemental carbon concentration was obtained from the difference between total carbon and total organic carbon (nonpolar and polar).

If the extraction technique measures amounts of photochemically generated secondary particulate

*This work was supported by the Assistant Secretary for the Environment, Office of Health and Environmental Research, Pollutant Characterization and Safety Research Division of the U.S. Department of Energy under Contract No. DE-AC03-76SF00098 and by the National Science Foundation.

carbon, it should yield very different results in fractions of polar carbon for particles collected during smog episodes in Los Angeles than in particles collected in locations with low photochemical activity, such as Berkeley.

We have used this technique to characterize urban particulate matter from Berkeley and New York City and from combustion sources (automotive, diesel, and natural gas). What previous workers[5-7] have labelled as primary, secondary, and elemental carbon fractions are here referred to as nonpolar, polar, and unextractable carbon, respectively. The fraction of total carbon which is extracted from the filters but not recovered in extracts is labelled the volatile fraction.

ACCOMPLISHMENTS DURING FY 1981

Sampling Methods

Particulate material was collected at 40 SCFM by high-volume samplers (Sierra Instruments) on quartz fiber filters (Pallflex 2500 QAS) which had been fired at 800°C for 12 hours before use. Filter samples were wrapped in aluminum foil, manila envelopes, and plastic bags for storage at -5°C.

Twenty-nine 24-hour samples were collected at two sites in Berkeley between December 1977 and November 1979. The Lawrence Berkeley Laboratory (LBL) site was located on a hillside at the eastern edge of Berkeley, above the city center. The other site was located on the roof of an industrial building across from a major freeway which runs along the San Francisco Bay shore. Average total carbon loadings were 8 and 15 $\mu g\ m^{-3}$ for the LBL and freeway sites respectively. Two 24-hour high-volume samples were collected in New York City during February 1978, with average total carbon loading of 11 $\mu g\ m^{-3}$.

Samples were also collected in the Caldecott Tunnel (a highway tunnel) and in a parking garage near the University of California campus to sample fresh vehicle exhaust. Emissions from an idling diesel-powered passenger bus and a natural gas boiler were also collected. For sources, the sampling time was adjusted to give loadings in the range of 30 to 50 $\mu g\ C\ cm^{-2}$.

Analytical Strategy

Our results have been obtained using methodology developed by Grosjean[4] and Appel et al.,[5] who postulated that all soluble organic carbon is extracted by successive treatment of a portion of a filter with benzene and a (1:2, v:v) methanol-chloroform mixture, but only primary or nonpolar organic carbon is extracted by treatment of a different portion of the filter with cyclohexane. We follow the procedure of Appel et al.[6,7] to determine the total amount of recoverable organic carbon in filter samples as the sum of the carbon content of the benzene and methanol-chloroform extracts per cm^2 of filter. Amounts of nonpolar (primary) carbon are obtained from the carbon content of cyclohexane extracts per cm^2 of filter. Amounts of polar (secondary) carbon are determined from the difference between amounts of recoverable organic carbon and nonpolar carbon. Earlier workers[5-7] calculated upper limits to the elemental carbon concentration as the difference between total carbon and recoverable organic carbon. In this study, amounts of unextracted carbon are obtained from the carbon content per cm^2 of the benzene, methanol-chloroform-extracted filters. Amounts of volatile carbon are obtained from the difference between total carbon and the sum of recoverable organic carbon and unextractable carbon as discussed below.

The Soxhlet extraction and carbon determination procedures were essentially the same as those used by B.R. Appel et al.[6,7] except that we determine the carbon content of both extracts and extracted filters. This permits comparison of the extract's carbon content with the carbon lost by the filter during the extraction step.

Optical attenuation[8] measurements were performed on some of the filter examples, before and after extraction. The amount of black (elemental or graphitic) carbon in particulate samples has been shown[8-10] to be proportional to the optical attenuation, ATN, which is defined as 100 ln I_0/I, where I_0 and I are the intensities of helium-neon laser light transmitted through blank and loaded filters, respectively. X-ray fluorescence (XRF) was used to determine trace metal content of filters before and after extraction for highway tunnel particulate matter.

Particle Loss During Extraction

Particle loss from filters during extraction is a source of error in measurement of amounts of unextracted carbon from extracted filters. One way to assess the loss magnitude is to measure the optical attenuation[8] of the filter samples before and after extraction, since ATN is proportional to the concentration of unextractable black carbon in the particles.[8-10] Cyclohexane and benzene extraction do not affect the attenuation values for a group of 8 source and 10 ambient filter samples. The methanol-chloroform extraction step leads to an average decrease of 8 percent in attenuation values for the ambient samples. This represents an average loss of 3 percent of the total carbon. The source filters remain unchanged.

We have also studied the problem of particle loss by following the concentrations of selected heavy elements by XRF analysis of several sections of a tunnel filter after each step of the extraction. An average of 53 percent of the carbon was lost after extraction. Pb and Br losses were 44 and 97 percent, respectively. Small percentages of Cr (6), Cu (0), and Fe (11) were removed. Losses of Pb and Br in benzene alone are less than 5 percent in this experiment; losses of the other metals are even smaller. Pb, Br, and some Fe appear to be removed by solubilization. The low losses of Cr, Cu, and Fe indicate that particle loss during extraction is small, certainly less than 10 percent. No corrections for particle loss have been applied to the data.

The Volatile Fraction

Cyclohexane and benzene extracts of ambient and source particles contain less carbon than has been removed from the filters during extraction. For both cyclohexane and benzene, the carbon loss is 13 percent of the total carbon for ambient particles and somewhat higher for combustion source samples (garage and tunnel, 15 percent; diesel, 73 percent). This carbon deficiency is not due to particle loss but may be accounted for by the escape of volatile compounds during extraction and evaporation of solvent from the extracts prior to carbon determination. Because the loss of nonpolar compounds is partly offset by a slight (~3 percent of total carbon) excess carbon content in the polar extracts, the concentration of volatile carbon is defined as the difference between total carbon concentration and the sum of the concentration of organic (nonpolar + polar) and unextracted carbon. Volatile carbon accounts for approximately 10 percent of the total carbon for Berkeley-LBL, New York City, tunnel, and garage samples (Fig. 1). The natural gas boiler particles sampled here contain no volatile carbon.

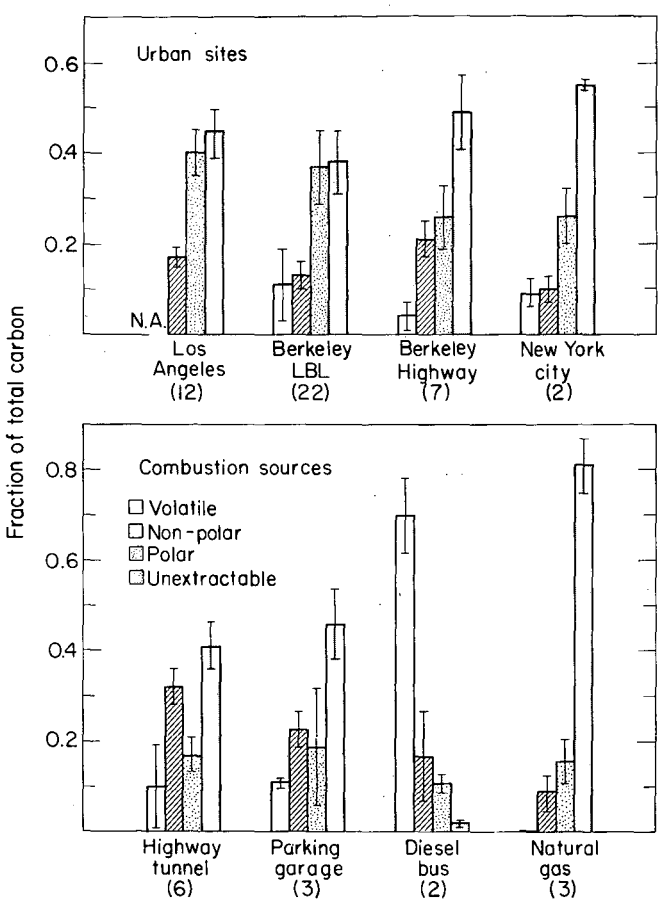

Figure 1. Selective solvent extraction results for carbonaceous particles collected from urban sampling sites and from combustion sources. The number in parentheses below the site or source label represents the number of filter samples analyzed. Error bars represent standard deviation. Los Angeles data are taken from Reference 8.

(XBL 818-1252)

When ambient air is drawn at 20 SCFM for 24 hours through two prefired quartz or glass fiber filters arranged in a series without physical contact, the second or downstream filter has a carbon content of 10 to 15 percent of the total carbon content of the particulate-laden filter.[11] High-volume sampling at 40 SCFM with two filters shows similar effects. Extraction of the back-up high-volume filter by cyclohexane or benzene removes about 70 percent of the adsorbed material, but very little (~5 percent) of the total carbon is recovered in the extract. These results suggest that volatile compounds adsorbed onto the filter material during sampling may account for at least part of the carbon lost during extraction.

Extraction Results for Urban Sampling Sites

We have applied the selective solvent extraction method to filter samples of particulate matter collected in Berkeley and New York City. Our results can be compared with those obtained by analysis of twelve 14-hour, high-volume filters which contained particulate material collected at three locations in the Los Angeles basin during four days of a photochemical episode in July 1975.[6,7] Average ozone concentrations were 20, 25, 240, and 0 ppb for Berkeley-LBL, Berkeley-freeway, Los Angeles, and New York respectively.

The top half of Figure 1 displays the results of these studies. Data are presented as volatile, nonpolar, polar, and unextractable fractions of total carbon content. The data of Appel et al.[6,7] are included in the figure. The major finding of this study is that the carbonaceous components of particulate matter collected during periods of low ozone concentration are similar to particulate matter collected in the Los Angeles basin during periods of high ozone concentration, as characterized by selective solvent extraction. Nonpolar, polar, and unextractable fractions from extractions of Berkeley-LBL and Los Angeles samples are 0.13, 0.37, 0.38, and 0.17, 0.40 $\lesssim$ 0.44 respectively. These sets of data do not have a statistically significant difference, even though the unextractable fraction for the Los Angeles data has not been corrected for the probable presence of volatile carbon. Aerosol particles collected in both areas have roughly three times as much polar as nonpolar carbon; close to half the carbon is insoluble.

No seasonal variations in nonpolar, polar, or unextractable carbon fractions are observed in Berkeley-LBL particulate material. The Berkeley-LBL results seem to be independent of the total carbon loading since there is no significant difference between extraction data for particles collected under clear (3 to 6 $\mu g\ C\ m^{-3}$) and hazy (15 to 34 $\mu g\ C\ m^{-3}$) conditions.

Ambient particulate material collected close to a heavily used freeway in Berkeley contains a higher nonpolar carbon fraction than does particulate material collected at LBL (Fig. 1). Fractions of volatile, polar, and unextractable carbon are statistically indistinguishable at the two sites, although the total carbon loading at the freeway site is roughly double that observed at the LBL site. The polar to nonpolar ratio is 1:1.

Winter New York City samples appear to contain a larger fraction of unextractable carbon than samples collected in California. The nonpolar to polar carbon ratio is about the same for New York City as for the other urban sites in this study.

Extraction Results for Combustion Sources

The vehicular exhaust samples contain particulate matter with more nonpolar than polar carbon (Fig. 1). The nonpolar fraction is significantly larger for vehicle particles than for Berkeley-LBL, Los Angeles, and New York City aerosols. The polar fraction is smaller for sources than for urban sites. The polar to nonpolar ratio is close to 0.6:1 for these sources, compared to approximately 3:1 for urban sites. Unextractable carbon levels are comparable for urban site, tunnel, and parking garage particles (38 to 55 percent). Natural gas soot contains mostly unextractable carbon (81 percent), while diesel bus samples are mainly volatile carbon (70 percent). Although ambient particulate carbon collected under nonphotochemical conditions is similar to the particulate carbon collected during a photochemical episode, both differ from sources when characterized by selective solvent extraction.

Conclusions

We have found that the carbonaceous components of particles from New York City, Los Angeles, and Berkeley are very similar when characterized by the selective solvent extraction-carbon analysis technique. Photochemical activity, as indicated by ozone level, was much less intensive in Berkeley and New York City than in Los Angeles, although fractions of polar and nonpolar carbon are very similar for the two locations. Automotive and diesel primary combustion particles differ from ambient particles by enrichment in amounts of nonpolar carbon; however, significant fractions of polar carbon are also associated with all combustion sources studied here.

Because of this, the polar fraction of ambient carbonaceous particles cannot be entirely secondary in origin. Part of what has been called secondary carbon in the past is source related. Because of the similarity of Berkeley-LBL and episodic Los Angeles organic particulate matter, the contribution of ozone-related photochemical processes to production of particulate matter cannot be uniquely identified by application of selective solvent extraction. This finding is consistent with the results of long-term sampling in several cities by Hansen et al.,[3] who have found that a fairly constant fraction of the total particulate carbon is black carbon, regardless of the location, season, ozone concentration, or time of day. Ambient particulate material from Los Angeles, Berkeley, and New York City contains larger fractions of polar organic carbon than combustion-source particles; this suggests that other transformation processes may exist in addition to photochemical gas-to-particle conversion.

PLANNED ACTIVITIES FOR FY 1982

This study has found that the selective solvent extraction technique cannot successfully distinguish secondary from primary carbon in ambient particles. We will apply thermal[12] and optical[8] analyses to determine primary, secondary, and black carbon in carbonaceous particles. Selective solvent extraction will continue to be used for sample pretreatment in these studies.

REFERENCES

1. For a review, see Grosjean, D. (1977), "Aerosols," in Ozone and Other Photochemical Oxidants, National Academy of Sciences-National Research Council, Committee on Medical and Biological Effects of Environmental Pollutants, Washington, D.C., Chap. 3.

2. Novakov, T. (1981), "Microchemical Characterization of Aerosols," in Nature, Aim and Methods of Microchemistry, H. Malissa, M. Grasserbauer, and R. Belcher, Eds., Springer-Verlag, Vienna, p. 141.

3. Hansen, A.D.A., et al. (1980), "The Use of an Optical Attenuation Technique to Estimate the Carbonaceous Component of Urban Aerosols," in Atmospheric Aerosol Research FY 1979, Lawrence Berkeley Laboratory Report LBL-10735, p. 16.

4. Grosjean, D. (1975), "Solvent Extraction and Organic Carbon Determination in Atmospheric Particulate Matter: The Organic Extraction-Organic Carbon Analyzer (OE-OCA) Technique," Analytical Chemistry 47, p. 797.

5. Appel, B.R., Colodny, P., and Wesolowski, J.J. (1976), "Analysis of Carbonaceous Materials in Southern California Atmospheric Aerosols," Environmental Science and Technology 10, p. 359.

6. Appel, B.R., et al. (1977), Characterization of Organic Particulate Matter, Final Report to California Air Resources Board, Contract No. ARB 5-682.

7. Appel, B.R., et al. (1979), "Analysis of Carbonaceous Material in Southern California Atmospheric Aerosols, 2," Environmental Science and Technology 13, p. 98.

8. Mueller, P.K., Mosley, R.W., and Pierce, L.B. (1972), "Chemical Composition of Pasadena Aerosol by Particle Size and Time of Day. IV. Carbonate and Non-Carbonate Carbon Content," Journal of Colloid and Interface Science 39, p. 235.

9. Rosen, H., et al. (1978), "Identification of the Optically Absorbing Component in Urban Aerosols," Applied Optics 17, p. 3859.

10. Yasa, Z., et al. (1979), "Photoacoustic Investigations of Urban Aerosol Particles," Applied Optics 18, p. 2528.

11. Gundel, L., Dod, R., and Novakov, T. (1981), "Determination of Black Carbon by Thermal Analysis," in Environmental Pollutant Studies, Lawrence Berkeley Laboratory Report LBL-11986, p. 26.

12. Dod, R.L., et al. (1980), "Investigations of Sampling Artifacts in Filtration Collection of Carbonaceous Aerosol Particles," Atmospheric Aerosol Research, FY 1979, Lawrence Berkeley Laboratory Report LBL-10735, pp. 8-35.

13. Dod, R.L., Rosen, H., and Novakov, T. (1979), "Optico Thermal Analysis of the Carbonaceous Fraction of Aerosol Particles," Atmospheric Aerosol Research Annual Report, 1977-78, Lawrence Berkeley Laboratory Report LBL-8696, p. 2.

The Relation Between Concentrations of Polynuclear Aromatic Hydrocarbons and Black Carbon*

L. A. Gundel, H. J. Rosen, and T. Novakov

In addition to black carbon, particulate organic carbon in ambient aerosols contains primary and secondary organic compounds. In this article, we study the relationship between black carbon concentration and one class of primary organic compounds, polynuclear aromatic hydrocarbons (PAH), in urban carbonaceous particles. These compounds and their oxidized derivatives may constitute part of the health hazards associated with ambient and source aerosols.[1-3] Earlier work on this project[4] has established that a linear relationship exists between concentrations of several polynuclear aromatic hydrocarbons and black carbon for ambient aerosol particles collected in Berkeley during the summer of 1980. Here we investigate that relationship for particles collected in three other sampling locations in the United States during the same season.

ACCOMPLISHMENTS DURING FY 1981

Experimental Methods

The samples used in this study were 24-hour loaded quartz and cellulose acetate filter pairs (47-mm diameter) collected simultaneously as part of the LBL sampling program during the summer of 1980.[5] The sampling locations were Gaithersburg, Maryland; Argonne, Illinois; and New York, New York.

Optical attenuation (ATN) measurements[6] for the loaded cellulose acetate filters have been used to determine blank carbon (BC) concentrations since ATN has been shown to be proportional to black carbon concentration[5-7] for ambient particles. ATN is defined as ATN = 100 ln I_0/I, where I_0 and I are the intensities of light transmitted through blank and loaded filters respectively. ATN has units of optical density per 10^6 m air. Black carbon concentration in μg m^{-3} is related to ATN by ATN/[BC] = 21.3.[7,8]

For determining PAH concentrations of each filter sample, one section (1.94 cm^2) of the quartz filter was extracted in 0.400 ml peroxide-free spectral quality tetrahydrofuran by sonication at 25°C for 15 minutes.[9] A 50-μl aliquot of the extract was injected onto a liquid chromatographic column, which had been chosen for its selectivity for separation of PAH compounds[10] (VYDAC 201TP, 10-μm particle size, 25-cm length, 0.48-cm i.d.). The hydraulic system was purchased from Waters, Inc. A mixture of acetonitrile and tetrahydrofuran (19:1,v:v) in water was used as the mobile phase at a flow rate of 3.0 ml min^{-1}. Composition of the acetonitrile-tetrahydrofuran mixture varied from 70-98 percent in 30 minutes using Waters' gradient #9. The separated PAH compounds were detected with a Schoeffel Model SF970 fluorescence detector with excitation wavelength set at 280 nm. All fluorescence at wavelengths ≥389 nm was recorded as the sample eluted from the column. PAH standard compounds were supplied by Pfaltz and Bauer, Aldrich Chemical Co., and Nanogens, Inc. Peak heights were used for measurement of concentrations of PAH in extracts of ambient particulate loaded filters.

Identification of PAH compounds from retention times of fluorescent peaks in chromatograms of ambient extracts was accomplished by comparison to retention times of PAH standards. The fluorescence ratio technique[11] was used to confirm the assignments. Identification by this technique requires that the ratios of peak intensities for several combinations of excitation, λ_{ex}, and emission, λ_{em}, wavelengths match for an extract peak and a known PAH peak with the same retention time.

The Relationship Between PAH Concentration and Black Carbon Concentration

Five fluorescent compounds have been identified in the extracts of particulate matter collected at every site: benzo(b)fluoranthene (BbF), benzo(k)fluoranthene (BKF), benzo(a)pyrene

*This work was supported by the Assistant Secretary for the Environment, Office of Health and Environmental Research, Pollutant Characterization and Safety Research Division of the U.S. Department of Energy under Contract No. DE-AC03-76SF00098 and by the National Science Foundation.

(BaP), benzo(ghi)perylene (BghiP), and indeno(1,2,3-cd)pyrene (IcdP). Some PAH compounds which fluoresce weakly under the same conditions were not detected: chrysene, benzo(e)pyrene, dibenz(a,h) anthracene, and perylene. The PAH compounds found in this study have been detected in urban particulate matter collected in other cities[12] and in particulate samples from combustion sources.[13]

Figure 1 shows average values for PAH and total carbon concentrations for Berkeley,[4] Gaithersburg, Argonne, and New York. Relative PAH concentrations appear similar for Berkeley and Gaithersburg. The New York City sampling site displays higher PAH and total C concentrations, as expected for a location which is heavily influenced by combustion sources.[5]

Table 1 shows the slopes and average correlation coefficients for linear least squares fits of [PAH] to [BC]. A linear relationship exists between [PAH] and [BC] for Berkeley and Gaithersburg. Average correlation coefficients are 0.82 and 0.91. The data from Argonne divide neatly into two groups which display different linear relationships. The average difference in slopes is about 5. Both the high and low [PAH] data are highly correlated with [BC]. Correlation coefficients are 0.92 and 0.90, respectively. The correlation between [PAH] and [BC] is weak for New York City, with r = 0.54. These results indicate that concentrations of PAH are highly related to black carbon concentrations for all sampling sites, except New York City; but the same linear relationship does not exist for all sites. This may be due to different contributions from combustion sources and to different weather and PAH degradation processes.

The authors thank A.D.A. Hansen for providing optical attenuation and total carbon concentration data.

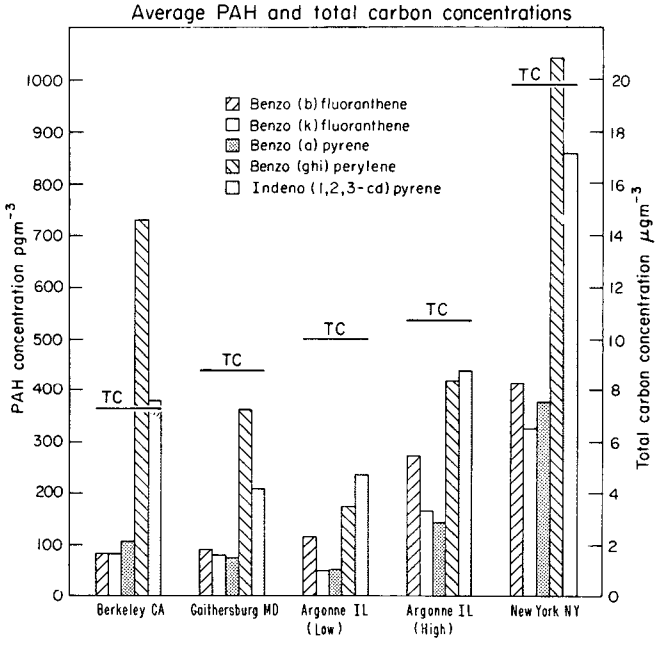

Figure 1. Average values of PAH and total carbon concentrations for carbonaceous particles collected at several locations in the United States. Berkeley data are taken from Reference 4. Argonne data are divided into low and high [PAH] as discussed in the text. (XBL 822-93)

PLANNED ACTIVITIES FOR FY 1982

The relationship between PAH and black carbon concentrations will be studied for carbonaceous particles collected in Austria and Yugoslavia. Adsorption of PAH onto ambient and model black carbons will be investigated.

Table 1. Relationship between PAH and black carbon concentrations for carbonaceous particles collected in July and August 1980 for several sampling sites.

	Slope x 10^6 of [PAH] vs. [BC]					Average Values			
Site	BbF	BkF	BaP	BghiP	IcdP	r [PAH] vs. [BC]	[Total C] gm^{-3}	[BC] gm^{-3}	Number of Samples
Berkeley	37.6	35.4	81.6	465	262	0.82	7.3	1.6	9
Gaithersburg	100	128	116	751	246	0.91	8.8	1.6	7
Argonne (low)	32.0	30.3	24.6	80.9	71.9	0.90	10.0	2.5	4
Argonne (high)	237	172	107	322	290	0.92	10.7	2.2	5
New York	80.7	74.5	97.8	167	213	0.54	19.8	3.7	8

REFERENCES AND FOOTNOTE

1. Wang, Y.Y., et al. (1978), "Direct Acting Mutagens in Automobile Exhaust," Cancer Letters 5, p. 39.

2. Pitts, J.N., Jr., Grosjean, D., and Mischke, T. (1977), "Mutagenic Activity of Airborne Particulate Organic Pollutants," Toxicology Letters 1, p. 65.

3. Schuetzle, D., et al. (1981), "The Identification of Polynuclear Aromatic Hydrocarbon Derivatives in Mutagenic Fractions of Diesel Particulate Extracts," International Journal of Environmental Analytical Chemistry 9, p. 93.

4. Gundel, L., Rosen, H., and Novakov, T. (1981), "Relation Between Concentrations of Polynuclear Aromatic Hydrocarbons and Black Carbon," in Environmental Pollutant Studies, Lawrence Berkeley Laboratory Report LBL-11986, pp. 5-32.

5. Hansen, A.D.A., et al. (1980), "The Use of an Optical Attenuation Technique to Estimate the Carbonaceous Component of Urban Aerosols," in Atmospheric Aerosol Research FY 1979, Lawrence Berkeley Laboratory Report LBL-10735, p. 16.

6. Rosen, H., et al. (1978), "Identification of the Optically Absorbing Component in Urban Aerosols," Applied Optics 17, p. 3859.

7. Gundel, L., Dod, R., and Novakov, T. (1981), "Determination of Black Carbon by Thermal Analysis," in Environmental Pollutant Studies, Lawrence Berkeley Laboratory Report LBL-11986, pp. 5-26.

8. This differs from the values given in Reference 7 (19.0) because ATN measured on cellulose acetate filters is 1.12 times ATN measured on quartz in Reference 7.

9. Golden, C., and Sawicki, E. (1975), "Ultrasonic Extraction of Total Particulate Aromatic Hydrocarbons (TpAH) from Airborne Particles at Room Temperature," International Journal of Environmental Analytical Chemistry 4, p. 9.

10. Ogan, K., and Katz, E. (1980), "Retention Characteristics of Several Bonded-Phase Liquid Chromatography Columns for Some Polycyclic Aromatic Hydrocarbons," Journal of Chromatography 188, p. 115.

11. Das, B.S., and Thomas, G.H. (1978), "Fluorescence Detection in HPLC Determinations of Polycyclic Aromatic Hydrocarbons," Analytical Chemistry 50, p. 967.

12. For a summary see: Ontario Ministry of the Environment (1979), Polynuclear Aromatic Hydrocarbons, Air Resources Branch, ARB-TDA-Report Number 57-79, p. 146.

13. Daisey, J.M., Leyko, M.A., and Kneip, T.J. (1979), "Source Identification and Allocation of Polynuclear Aromatic Hydrocarbon Compounds in the New York City Aerosol," in Polynuclear Aromatic Hydrocarbons, P.W. Jones and P. Lever, Eds., Ann Arbor Science, Ann Arbor, p. 201.

Determination of Low-Z Elements Simultaneously by Charged Particle Activation Analysis*

M. McKinney, S. S. Markowitz, and T. Novakov

This work is a continuation of the work of Clemenson et al.[1,2] for developing rapid nondestructive techniques for determining carbon, nitrogen, and oxygen in atmospheric aerosols. X-ray fluorescence or neutron activation analysis can then be used to determine nearly all the higher Z elements. Combustion analysis could be used for these elements, but they may not be sufficiently sensitive for certain applications and the sample would be destroyed.

Nondestructive techniques have been developed for determining these elements by Macias et al.,[3] Failey et al.,[4] and Gladney et al.[5] These methods, however, require lengthy use of accelerator or reactor time, and the latter method requires large samples. Previously, Clemenson et al.[1,2] developed methods of determining carbon, nitrogen, and oxygen separately by activation analysis using different charged particles in different experiments. We want to develop a method for simultaneously determining carbon, nitrogen, and oxygen in atmospheric aerosols by irradiating the sample with one type of charged particle.

*This work was supported by the Assistant Secretary for the Environment, Office of Health and Environmental Research, Pollutant Characterization and Safety Research Division of the U.S. Department of Energy under Contract No. DE-AC03-76SF00098 and by the National Science Foundation.

ACCOMPLISHMENTS DURING FY 1981

The experiments were carried out using the stacked-foil technique, and the samples and standards were irradiated and counted within 2 to 3 minutes at the 88-inch Cyclotron. The 14-MeV ^{3}He beam was degraded to 10 MeV, and both the aerosol sample, on a silver filter, and the 1/2-mil nylon standard were bombarded at the same energy and with the same number of microcoulombs.

The samples were irradiated for 0.5 minutes at 0.5-μA beam intensity and were analyzed by detecting the 511-keV positron annihilation radiation in coincidence using 3-inch NaI crystals and Ortec single-channel analyzers. The decay curve was analyzed into 2.0-, 20.4-, and 110-minute components, due to $^{14}N(^{3}He,d)^{15}O$, $^{12}C(^{3}He,^{4}He)^{11}C$, and $^{16}O(^{3}He,p)^{18}F$, respectively, by using the CLSQ code. The amounts of carbon, nitrogen, and oxygen were determined by the "relative" method of analysis. The carbon determinations agreed well with combustion analysis, but the nitrogen determinations were substantially higher. This was presumably caused by sulfur and silicon in the aerosol which produced ^{31}P with a 2.5-minute half-life, which interfered with the nitrogen determination.

For this reason we chose another activating particle, deuterons. Previously, Clemenson[2] determined carbon from the $^{12}C(d,n)^{13}N$ reaction. We hope to simultaneously determine oxygen from the $^{16}O(d,n)^{17}F$ reaction and nitrogen from

the $^{14}N(d,2n)^{14}O$ reaction. The first two elements are determined by analysis of the decay curve of the 511-keV coincident γ-rays with half-lives of 1.1 and 10 minutes. The nitrogen is determined by detecting the unique 2.3-MeV positron annihilation radiation.

PLANNED ACTIVITIES FOR FY 1982

We will continue with the development of deuterium activation analysis of atmospheric aerosols. Also, H. Benner of our group has adapted a combustion technique for determining oxygen in the levels found in aerosols, and we wish to check our activation results with this technique.

REFERENCES

1. Clemenson, M., Novakov, T., and Markowitz, S.S. (1979), "Determination of Nitrogen in Atmospheric Aerosols by Proton Activation Analysis," Analytical Chemistry 51, p. 572.

2. Clemenson, M., Novakov, T., and Markowitz, S.S. (1980), "Determination of Carbon in Atmospheric Aerosols by Deuteron Activation Analysis," Analytical Chemistry 52, p. 1758.

3. Macias, E.S., et al. (1978), "Proton Induced γ-ray Analysis of Atmospheric Aerosols for Carbon, Nitrogen, and Sulfur Composition," Analytical Chemistry 50, p. 1120.

4. Failey, M.P., et al. (1979), "Neutron Capture Prompt γ-ray Activation Analysis for Multielement Determination in Complex Samples," Analytical Chemistry 51, p. 2209.

5. Gladney, E.S., Curtis, D.B., and Jurney, E. (1979), "Simultaneous Determination of Nitrogen, Carbon, and Hydrogen by Thermal Neutron Prompt γ-Ray Spectrometry," Analytical Chimica Acta 110, p. 339.

APPLIED PHYSICS AND LASER SPECTROSCOPY RESEARCH

N. M. Amer,* M. S. Cooper, R. W. Gerlach, R. P. Hall, W. B. Jackson,† R. L. Johnson,‡
S. E. Kohn,§ S. J. Kulik, M. A. Olmstead, A. Skumanich, D. R. Wake, and Z. A. Yasa

The research philosophy of our group is to apply the knowledge of advanced laser spectroscopy and condensed-matter physics to energy and environmental problems. Because of the narrow line width and tunability of lasers, unsurpassed sensitivity and specificity can be achieved in detecting trace contaminants of the environment. The advanced state of condensed-matter physics makes it possible to apply such knowledge to energy production and to test novel methods for energy conversion such as photovoltaic solar cells, superionic electrical energy storage devices, and the recovery and extraction of oil from abandoned wells and oil shale with lyotropic liquid-crystal emulsifiers.

Laser Photoacoustic and Photothermal Measurements and Characterization‖

Laser photoacoustic and photothermal spectroscopies provide a powerful tool for detecting trace contaminants in air and water, as well as for investigating the fundamental properties of gaseous, liquid, or solid phases of matter. One of the goals of this project is to develop ultrasensitive, multiparameter, elemental, and molecular detectors for the characterization of pollutants released in the process of energy production and utilization, with emphasis on remote sensing. Another aim is to maintain a state-of-the-art capability in photoacoustic and photothermal detections by fully understanding the physics of these techniques. Concurrent with these efforts, we are actively developing new or modified laser systems compatible with our particular needs.

Photothermal Spectroscopy of Scattering Media**

Insensitivity to scattering has generally been accepted as an inherent characteristic of photoacoustic detection. The physical reasoning underlying this assumption has been that the photoacoustic signal arises from heat generated following optical absorption and thereby is a measure of the cross section of such absorption. However, the thermal energy generated by the absorption of light is a function of the intensity distribution within the sample, which depends on its scattering characteristics. Consequently, deviation from Beer's Law should, in principle, affect the thermal signal generated. We will show that, for highly scattering media, the photoacoustic signal is strongly dependent on the scattering parameters. On the other hand, for optically thin solids and liquids, the photoacoustic signal is insensitive to light scattering up to a scattering coefficient($\lambda\alpha$) of $\sim 1/\ell$ where ℓ is the sample thickness, λ is the fraction of light scattered, and α is the total attenuation coefficient of a coherent beam.

Most photothermal detection techniques respond to the surface temperature averaged over the sample surface and/or a weighted integral of sample temperature over its volume. We analyze the coupled heat diffusion and radiative transfer equations. We rigorously show that, for a wide range of experimental conditions, the coupled equations can be solved exactly, yielding a photoacoustic signal

$$S \propto 1 - (R + T) \qquad (1)$$

where R is the reflectance (diffuse and specular) and T is the transmittance (diffuse and coherent) of the sample of interest. Hence, Equation (1) proves the intuitive conclusion that the photoacoustic signal is proportional to the absorptance of the sample.

In the case of gas-cell-microphone detection of solids, Equation (1) is valid for (a) $\ell_{th} \gg \ell_{opt}$, or (b) $\ell_{th} \gg \ell_{opt}$, where ℓ_{th} is the thermal diffusion length and ℓ_{opt} is the optical thickness

*Group leader.
†Present address: Xerox Research Center, Palo Alto, Calif.
‡Present address: Department of Electrical Engineering, Texas A&M University, College Station, Texas.
§Present address: Aerospace Corporation, Los Angeles, Calif.

‖This Work was supported by the Director, Office of Energy Research, Pollutant Characterization and Safety Research Division, U.S. Department of Energy, under Contract No. DE-AC03-76SF00098.
**Complete version of this work appeared in Appl. Optics 21, 21 (1982) and Lawrence Berkeley Laboratory Report LBL-13275.

of the sample. This conclusion also holds for transverse photothermal deflection and for piezoelectric photoacoustics of solids.

For the case where $\ell_{th} \leq \ell$ or $\ell_{th} \leq \ell_{opt}$, an approximate Schuster-Schwarzchild analysis of the radiative transfer equations is used to obtain an analytical expression for the photoacoustic signal. In the general case, the scattering characteristics of the medium enters the expression in a complicated form. An interesting limiting case is $\ell_{th} \ll \ell_{opt}, \ell$ for which

$$S \propto (1 - \lambda)\, \alpha \left[1 + \frac{2(1 + r_i)}{(1 - r_i)} R \right] \qquad (2)$$

where $(1 - \lambda)\alpha$ is the absorption cross section and r_i is the internal reflection coefficient for diffuse light at the sample-gas boundary. It can be seen that the photoacoustic signal is proportional within a thermal length to the sample absorption cross section, with the proportionality constant considerably increased from its value of 1 for no scattering. This is due to the increase in photon flux at the sample-gas boundary.

The solution for the coupled heat diffusion and radiative transfer equations can be employed in one of two ways to evaluate the scattering contribution to the photoacoustic signal:

a. One may write the solution in terms of R and T which can then be determined experimentally using integrating sphere techniques. Combining the measurement of R and T with the detected photoacoustic signal yields information on such sample properties as its internal reflectance which is otherwise experimentally inaccessible, or

b. One may solve the radiative transfer equation for R and T in terms of the scattering coefficient $\lambda\alpha$, the attenuation coefficient, and the internal reflectance. By inserting this solution in the general solution for the photoacoustic signal, one obtains the dependence of the photoacoustic signal on the scattering and the absorption of the sample.

Using a two-flux model for R and T, the results of evaluating the solutions for various absorption constants and internal reflectance coefficients are shown in Figure 1. Physically for $\lambda\alpha\ell < 0.1$, the effective light path length within the sample is equal to the sample thickness and the photoacoustic signal is independent of scattering. When $\lambda\alpha\ell \sim 1$, the mean path length of the light increases as the scattering increases, as does the absorption. At still higher scattering, the signal saturates because all the light is scattered without further increase in the effective path lengths. For very high scattering samples, the reflectance becomes larger as the scattering increases leading to a decrease in the light intensity within the sample. Hence, the signal decreases. Figures 2 and 3 qualitatively define the relationship between measured and actual absorption, thus providing correction factors for various materials.

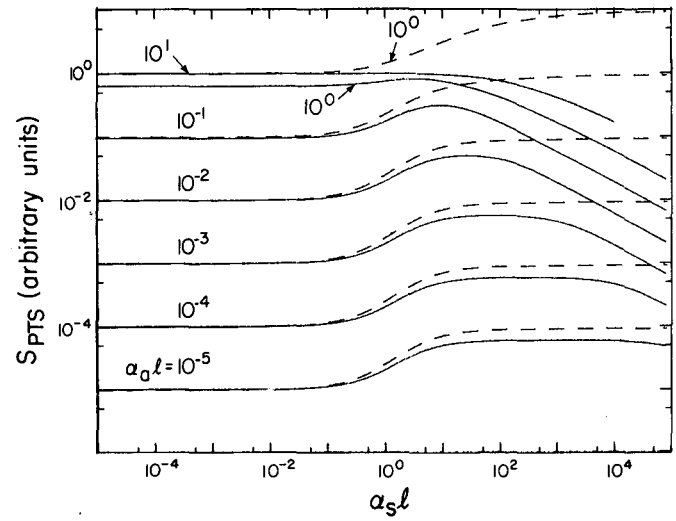

Figure 1. Energy absorbed vs. scattering coefficient. (XBL 818-1270)

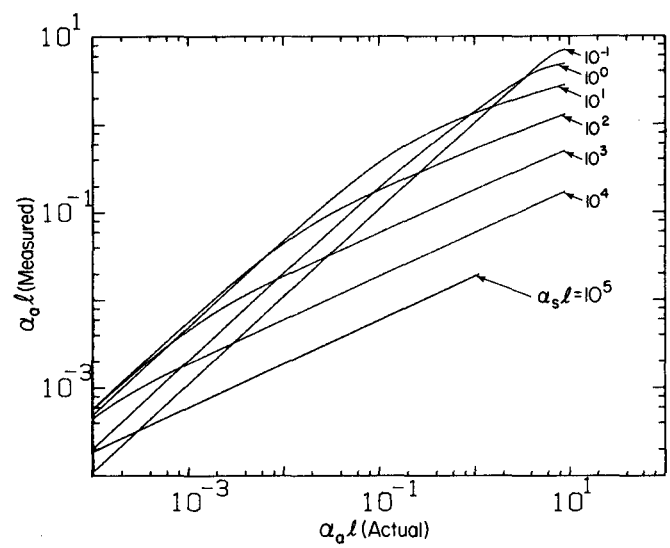

Figure 2. Measured and actual absorption for thermally thin samples. (XBL 818-1263)

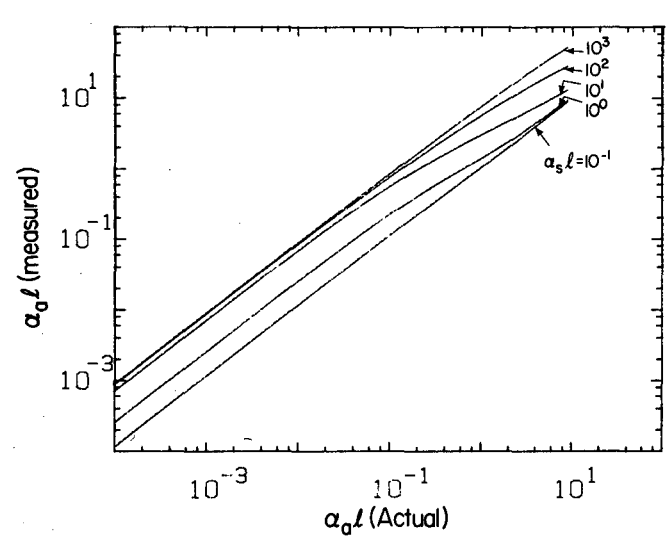

Figure 3. Measured and actual absorption for thermally thick samples. (XBL 818-1266)

Our results provide a complete picture of the role of light scattering in photoacoustic detections. We show that, whereas under certain conditions photoacoustic spectroscopy is insensitive to scattering, under others it can significantly affect photoacoustic spectra.

Loss Mechanisms in Resonant Spectrophones*

In studies of phase photoacoustic spectroscopy, the gas whose spectrum is being investigated is generally one of several present in the sample, often only in trace amounts. The response of the spectrophone is determined by the characteristics of the sample gas as a whole and depends on the various thermal and molecular relaxational properties of the gases present. In particular, for an acoustically resonant spectrophone, important characteristics will include the sound velocity, heat capacity, thermal conductivity, viscosity, and the energies and relaxation times of the molecular vibrations. The sound velocity determines the resonant frequencies of the cavity, while the other parameters govern the loss mechanisms that determine the quality factors of the resonances and also cause small shifts in the resonant frequencies. In an earlier study, the resonant frequencies and quality factors of acoustical resonances were determined for various buffer gases at atmospheric pressure, and the results were compared to theoretical predictions based on classical surface viscous and thermal losses. Significant discrepancies were observed for all non-noble gases. It is the goal of this work to investigate the pressure-dependent behavior of the spectrophone and to incorporate molecular relaxation effects into the theoretical interpretation of that behavior. We have made a number of extensions and improvements in experimental and analytical technique (Fig. 4). The spectrophone used was a stainless steel cylinder polished to a 1/3 micron surface finish to guarantee well-defined boundary layers whose losses could be calculated accurately from theory. The spectrophone and vacuum system were bakable to reduce impurity effects due to outgassing. Whereas, in the earlier experiment, a large concentration of the optically absorbing component (9000 ppm of CH_4) was used, we kept the absorber concentration small (50 ppm of C_2H_4) so as not to disturb the properties of the buffer gas. Use of an electro-optic modulator system allowed access to modes at much higher frequencies, thus enabling the study of lighter gases. We have measured the resonant frequency and quality factor as a function of pressure from atmospheric pressure down to 10 torr or lower for each buffer gas. Data analysis consisted largely of nonlinear, least-squares curve fitting of the resonant response curves. This provided more accurate determinations of the resonant frequency and Q than the half-power point method used in the previous experiment.

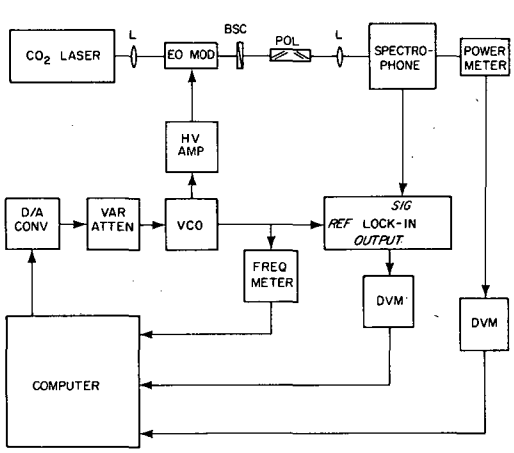

Figure 4. Experimental arrangement.

(XBL 816-2337)

Buffer gases studied included monatomic (He, Ne, Ar, Kr, Xe), diatomic (H_2, H_2, O_2), and polyatomic (CO_2, N_2O, SF_6) gases. In all cases except SF_6, which is already a strong absorber, 50 ppm of C_2H_4 was added to provide optical absorption at CO_2 laser wavelengths. For each gas, the Q and resonant frequency of the first radial mode were determined as a function of pressure, and the Qs and frequencies of other modes were determined at atmospheric pressure. In some cases, other modes were also studied at sub-atmospheric pressures. The resulting data on f_{res} and Q vs pressure were compared to theoretical curves generated by summing the surface viscous and thermal losses, the bulk viscous and thermal (Stokes-Kirchhoff) losses, and the losses due to molecular relaxation effects. For the latter, it was assumed that all vibrational levels relaxed with a single relaxation time which was adjusted to give the best fit to the data.

It was found that, for monatomic gases, the classical surface losses accounted almost entirely for the observed Q factors at all pressures (Fig. 5). For the diatomic molecules N_2 and O_2,

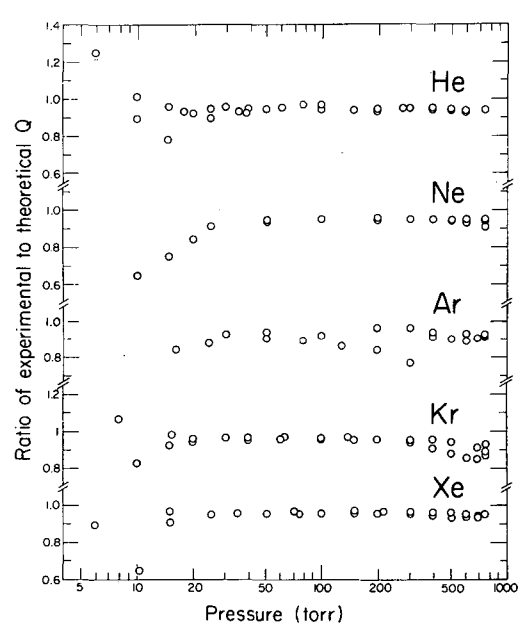

Figure 5. Ratios of experimentally observed to theoretical quality factor as a function of pressure. (XBL 816-2341)

*Complete version of this work appeared in Appl. Optics 21, 81 (1982) and Lawrence Berkeley Laboratory Report LBL-13223.

the relaxation times are so long that they do not produce much relaxational damping at or below atmospheric pressure, and the classical surface losses again largely account for the observed Q. For H_2, the vibrational energy is so high that the acoustic wave does not significantly excite molecular vibrations, but it is necessary to include rotational relaxation to explain the observed Q's (Fig. 6). For polyatomic gases, we found that the observed pressure dependence of Q could be well explained by the combined effects of classical losses plus vibrational relaxation, provided the assumed relaxation times were adjusted to fit the data (Fig. 7).

It has already been noted that molecular relaxation effects will also give rise to a frequency shift as a function of pressure. However, even for monatomic gases, for which molecular relaxation effects should be absent, we observed pressure-dependent frequency shifts. For all of the noble gases, we observed a downward shift in frequency at low pressure which appeared consistent with a $p^{-1/2}$ pressure dependence. We interpret this as being due to a reduction in the speed of sound in the thermal boundary layer, whose thickness varies as $p^{-1/2}$. The gas in this layer is in good thermal contact with the walls, and hence sound propagation is no longer adiabatic, as in the bulk of the gas, but tends toward isothermal behavior as one approaches the wall. We have calculated to first order that the frequency shift is

$$\left(\frac{\delta\omega}{\omega}\right)_{bl} = d_h\left(\frac{1}{L} + \frac{1}{R}\right)\left(1 - \sqrt{\gamma} - \frac{1}{2}\ln\gamma\right) \qquad (3)$$

where $d_h = (2\kappa/\omega\rho C_p)^{1/2}$ is the thermal boundary layer thickness, L and R are the cell length and radius, and $\gamma = C_p/C_v$. This is reasonably consistent with observed frequency shifts.

For Xe, we also observed a downward shift in frequency with increasing pressure above 100 torr. This shift is accounted for by a change in the speed of sound due to deviation of the equation of state from that of an ideal gas, and is given by

$$\left(\frac{\delta\omega}{\omega}\right)_{vir} = \frac{p}{R_g T}\left[B + \frac{T}{h}\frac{dB}{dT} + \frac{T^2}{2h(h+1)}\frac{d^2B}{dT^2}\right] \qquad (4)$$

where B is the second virial coefficient, $h = C_v/R_g$, and R_g is the gas constant (Fig. 8).

Having accounted for these shifts, which may be present for any gas, we next proceed to the

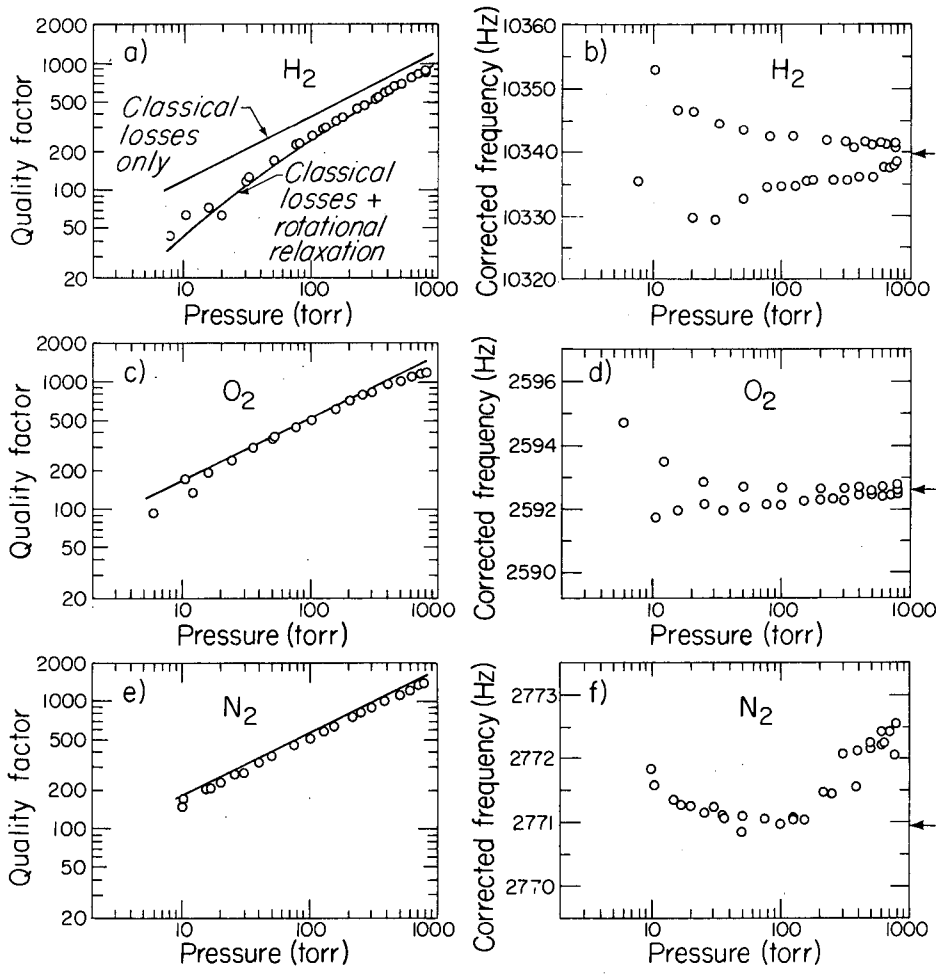

Figure 6. Quality factor and resonance frequency as a function of pressure for diatomic gases. (XBL 816-2343)

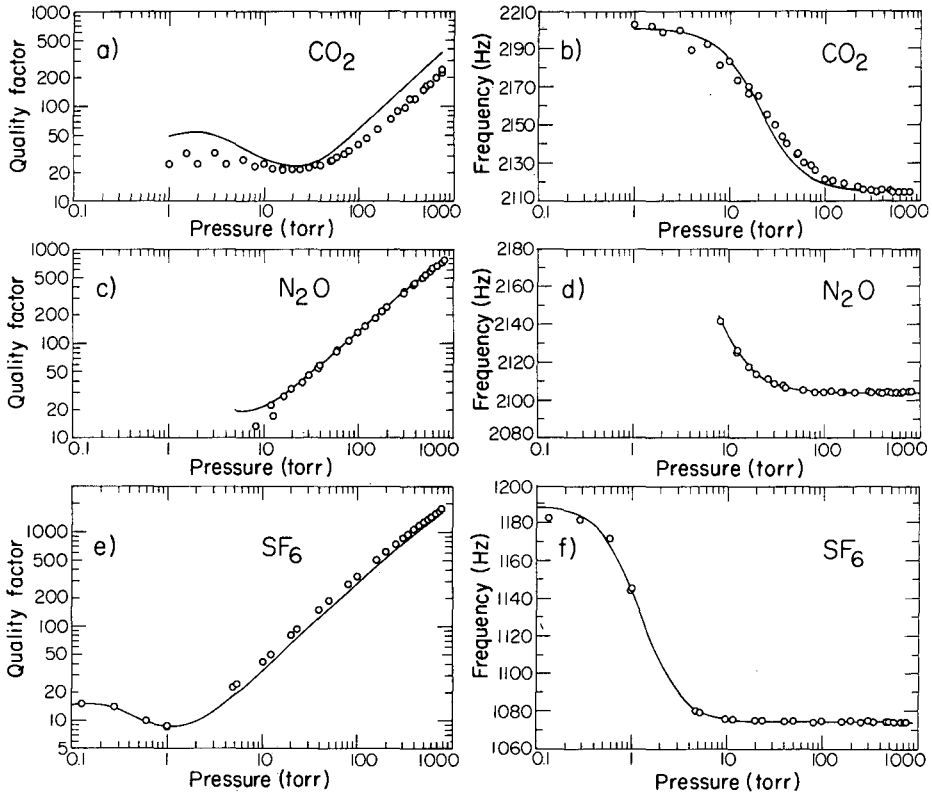

Figure 7. Quality factor and resonance frequency as a function of pressure for polyatomic gases. (XBL 816-2342)

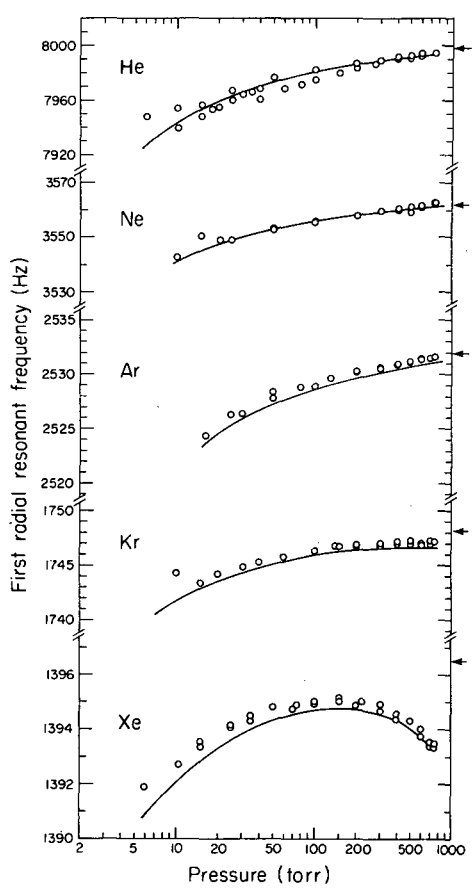

Figure 8. Frequency of first radial mode as a function of pressure for noble gases. (XBL 816-2340)

relaxing gases. The diatomic gases produced no observable relaxational frequency shifts in the pressure range of our experiment. For the polyatomics, the frequency vs pressure data could be fitted with theoretical curves by assuming a single effective relaxation time. The times thus arrived at are consistent with those obtained from the dependence of Q on p.

Another interesting effect observed was a coupling between modes due to boundary layer effects. Although the gas absorbed too weakly to allow direct excitation of modes having longitudinal dependence, these could be indirectly excited in cases where they were nearly degenerate with radial modes. We believe this is due to a coupling between these modes caused by viscous effects on the end walls. Isolated longitudinal modes, far from any radial modes, are never observed, except for the strong absorber SF_6.

In conclusion, we have gained some insight into the physics of resonant spectrophones. This should be useful in their application over a wide range of pressures with a wide variety of buffer gases and, potentially, also in the determination of molecular relaxation times.

Photothermal Buckling Spectroscopy: An *in vacuo* Detection Technique*

Recently, we conceived a new method for the detection of heat generated upon the absorption of light. This approach should be uniquely suited for the in vacuo measurement of low optical absorption coefficients in coatings and their films. Preliminary results in our laboratory proved the feasibility and the sensitivity of this concept.

The basic idea is that optical heating will induce the expansion and buckling of the illuminated surface. One can then relate the amplitude and phase of this buckling to the optical absorption coefficient in a relatively straightforward manner, which would be similar to what we developed for photothermal deflection spectroscopy. Two optical detection schemes can be employed to measure the surface buckling: interferometric and beam deflection (Fig. 9).

In a very preliminary effort to test the feasibility of this approach, we were successful in obtaining the absorption spectrum of didymium glass mounted in an ultrahigh vacuum chamber (10^{-11} torr) equipped with the appropriate optical windows. Because the laser sources providing the pump and probe beams were located outside the vacuum chamber, the measurement was performed remotely. We were able to demonstrate a sensitivity of 10^{-2} to 10^{-3}Å surface motion.

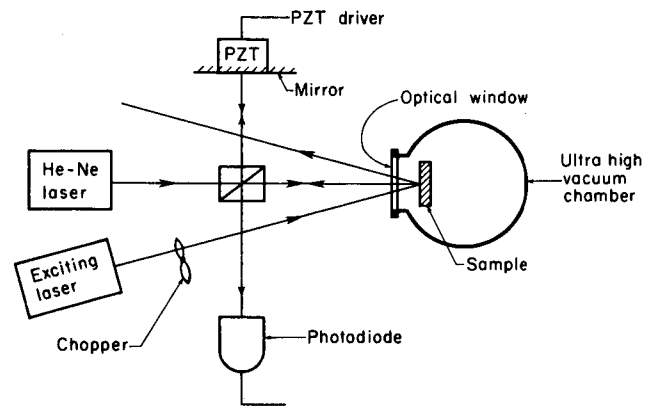

Figure 9. Photothermal buckling detection device. (XBL 823-3661)

*Complete version appears in Lawrence Berkeley Laboratory Report LBL-13522 (1981); submitted to Optics Letters.

Amorphous Photovoltaic Semiconductors*

Amorphous photovoltaic semiconductors, such as hydrogenated amorphous silicon, hold promise for meeting DOE cost and efficiency guidelines for thin film solar cells prior to 1990. To achieve the higher conversion efficiencies required, it is necessary to better characterize the unique optical and transport properties of these materials. Photoacoustic and photothermal spectroscopies can be used to elucidate the optical and electronic properties of a-Si:H. Of particular interest is the investigation of the optical properties near the so-called bandgap. By combining luminescence studies, photoconductivity, and optical absorption, a full and accurate characterization of the de-excitation of these photo-excited amorphous semiconductors can be achieved.

Experiments investigating the optical properties of hydrogenated amorphous silicon are currently under way. The experiments are designed to yield new information on the details of the optical absorption, the nature of the bandgap, and the electronic and transport properties of this promising material.

Direct Measurement of Gap-State Absorption in a-Si:H by Photothermal Deflection Spectroscopy †

In amorphous semiconductors, the optical absorption of defects and impurities is most readily observed above the band edge because it is not obscured by the much larger band-to-band absorption. Consequently, sub-gap absorption spectra should provide information about the number and energy level of defects in these materials. Although such measurements have been made on chalcogenide glasses, none of these made on hydrogenated amorphous silicon (a-Si:H) are reliable because of experimental limitations. The films are typically 1 μm thick and are not optically homogeneous, making conventional transmission and reflection measurements of absorption coefficients, α, unreliable below 50-100 cm^{-1}. Derivation of the absorption from photoconductivity requires reliance upon the experimentally unverified assumptions that the efficiency-mobility-lifetime product, $\eta\mu\tau$, is independent of photon energy. We have recently developed the highly sensitive ($\alpha\ell \sim 10^{-8}$) technique of photothermal deflection spectroscopy (PDS), which directly measures the optical absorption, is highly insensitive to scattering, and does not rely on the above assumption. We have found an absorption tail extending in the forbidden gap down to 0.6 eV. We show that the source of this absorp-

*This work was supported by the Assistant Secretary for Conservation and Solar Energy, Office of Solar Energy, Photovoltaic Energy Systems Division, U.S. Department of Energy under Contract No. DE-AC03-76SF00098.

†Complete version of this work appears in Lawrence Berkeley Laboratory Report LBL-13273 (1981); submitted for publication in Physical Review B (Rapid Communications).

tion is silicon dangling-bond defects which are located ~1.4 eV below the conduction band. Furthermore, we find that doping introduces defects at the same energy level and with approximately the same cross section.

Figure 10 shows the effect of increasing the rf power density on the absorption tail of undoped material while keeping the substrate temperature fixed. As the rf power increases, the strength of the sub-gap absorption tail increases in a monotonic fashion. A progressive decrease in the slope of the exponential edge as the rf power increases is also observed.

The effects of doping and compensation on the absorption spectra are summarized in Figure 11, which shows the results for PH_3 and B_2H_6 doped films. The sub-gap absorption tail rises as the doping level is increased, while the slope of the exponential edge decreases as the dopant concentration is increased.

To separate those effects due to dopant incorporation from the effects of shifts in the Fermi level, we measured α for a series of compensated films prepared by fixing the PH_3 concentration and gradually increasing the B_2H_6 concentration. The magnitude of the sub-gap absorption decreases as the degree of compensation increases. Concurrently, there is a pronounced shift to lower energies and a broadening of the exponential region.

If the gap state absorption is due to dangling bonds, one would expect a positive correlation between the magnitude of the absorption and the number of dangling bonds, as determined by electron spin resonance. In the case of the undoped material, by plotting the equilibrium spin density, N_s(ESR), vs the defect density, N_s(ABS), we obtain an excellent agreement over three orders of magnitude, as shown in Figure 12. Because ESR is a quantitative measure of the density of defects, the agreement suggests that the sub-gap tail is due to defects with spins.

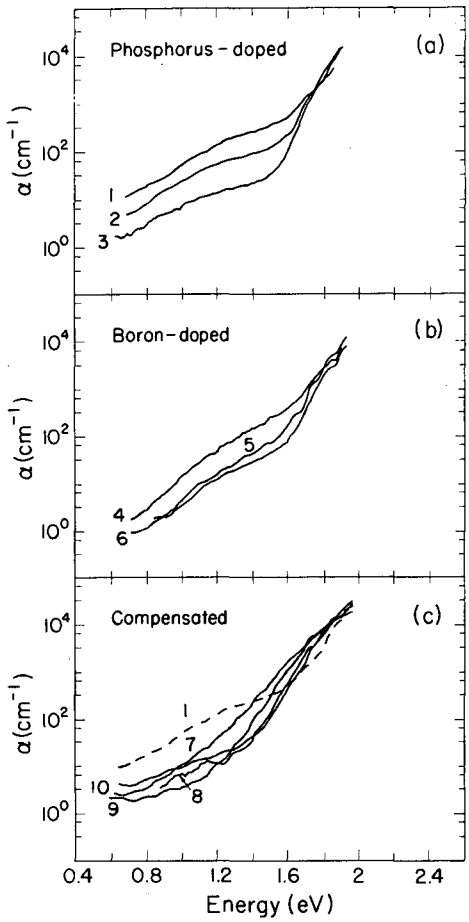

Figure 11. Absorption coefficient vs energy for various dopants. (a) PH_3 doping concentration of the films is $1:1\times10^{-3}$, $2:3\times10^{-4}$, and $3:1\times10^{-5}$. (b) B_2H_6 doping concentration is $4:10^{-3}$, $5:3\times10^{-4}$, and $6:10^{-4}$. (c) Compensated samples. All have 10^{-3} PH_3 and the B_2H_6 concentrations are 1:0, $7:2\times10^{-4}$, $8:4\times10^{-4}$, $9:2\times10^{-3}$, and $10:4\times10^{-3}$. (XBL 818-1142A)

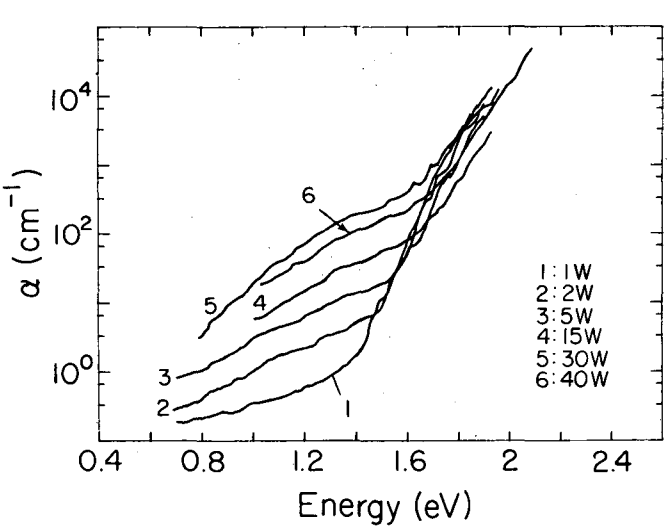

Figure 10. Absorption coefficient vs energy for undoped a-Si:H for various rf powers, substrate temperature T_s = 230°C. (XBL 818-1141A)

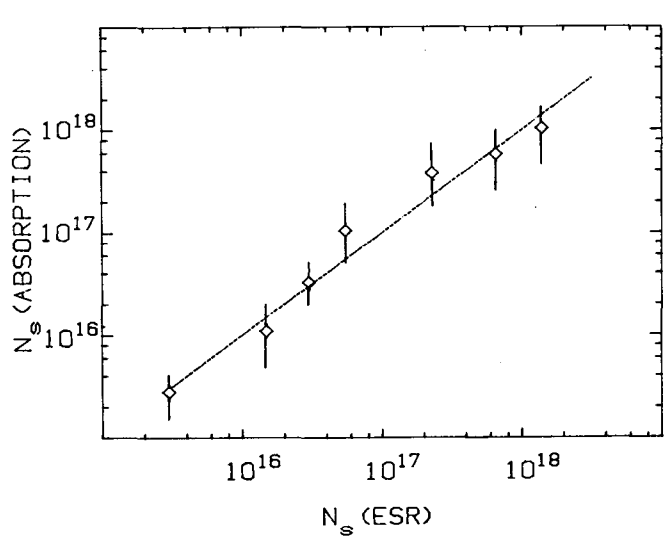

Figure 12. Number of defects deduced from absorption vs number of spins measured by ESR. (XBL 818-1139)

For doped a-Si:H, there is no equilibrium spin density. However, the defect density may be estimated from the light-induced ESR (LESR) or from the quenching of luminescence. Again, the agreement is excellent (Fig. 13).

Using the agreement between absorption, ESR, LESR, and luminescence-deduced defect densities along with other data, the following picture emerges. As the rf power density and the substrate temperature increase for the undoped a-Si:H, a maximum in the density of states (10^{15} to 10^{18} states/cc), caused by dangling silicon bonds appears ~1.3 eV below the conduction band. The evidence that the absorption is due to dangling silicon bonds is the fact that the ESR and LESR lines used to calculate N_s(ESR,LESR) have g = 2.0055, which is known to be due to dangling silicon bonds. This result supports the theoretical prediction of Joannopoulos which places the Si dangling bond ~1.3 eV below the conduction band. The fact that the energy of the absorption tail is the same as that of the maximum in the density of states, as determined by deep level transient spectroscopy and field effects measurements, strongly suggests that this maximum is in fact due to Si dangling bonds. Because films with the lowest absorption tails have the highest luminescence, we conclude that dangling bonds quench the luminescence rather than cause it, as previously had been hypothesized. Furthermore, we estimate the optical cross section of the dangling bond to be 1.2×10^{-16} cm^2.

Doping with PH_3 introduces 10^{17} to 10^{18} defects/cc ~1.3 eV below the conduction band. The energy and cross section of these defects are nearly identical to that of dangling bonds. The absence of equilibrium ESR and the presence of a g = 2.0055 LESR line can be explained by the pairing of electrons at the defect center.

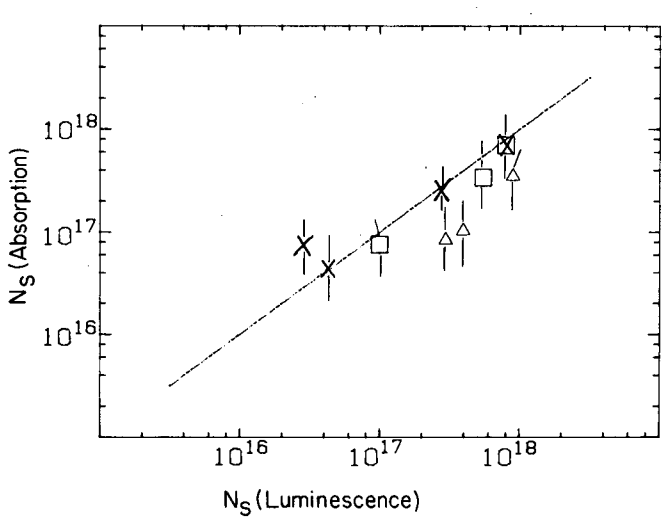

Figure 13. Number of defects deduced from Equation (1) vs number of spins estimated by luminescence. □ - phosphorous doped samples, Δ - boron doped samples, X - compensated samples. (XBL 818-1140)

The Energy Dependence of the Efficiency-Mobility-Lifetime Product ($\eta\mu\tau$) in a-Si:H*

Although incorporating hydrogen in amorphous silicon can significantly reduce the density of states within the gap, little is known about the energy distribution of the remaining states or their effect on the transport properties of the material. We present results combining our absorption data with photoconductivity measurements to derive $\eta\mu\tau$ as a function of photon energy in the range of 0.7 to 2.1 eV. We find that, for phosphorus-doped samples, the $\eta\mu\tau$ product is fairly constant between 2.1 and 0.9 eV. For the undoped film, this product is constant down to 1.5 eV, where it drops by a factor of ~5. Below 0.9 eV, $\eta\mu\tau$ drops rapidly.

The results of our secondary photoconductivity (SPC) measurements on undoped films are shown in Figure 14. Qualitatively, the overall shape is independent of both the frequency and the presence of dc bias light. The dependence of SPC on the chopping frequency at lower photon energies is due to the increase in response time. The dc bias light curve follows the dc measurement but is enhanced at ~0.9 eV and quenched at ~1.2 eV.

In Figure 15, we present both dc SPC measurements and the absorption for the same film. The most remarkable feature is that the shape of the absorption and shape of the SPC curves are roughly the same until ~0.9 eV, where the SPC measurement begins to decrease.

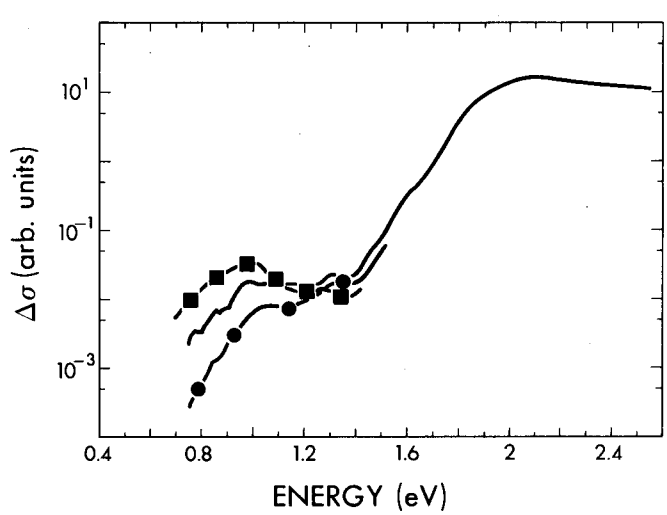

Figure 14. Secondary photoconductivity vs photon energy for an undoped film. DC SPC without dc bias light (——), 27 Hz SPC with dc bias light (-■-), 27 Hz SPC without dc bias light (-●-). Conductivity has been normalized by the light intensity. (XBL 8110-1416)

*Complete version appears in Lawrence Berkeley Laboratory Report LBL-13477 (1981); submitted to Physical Review B.

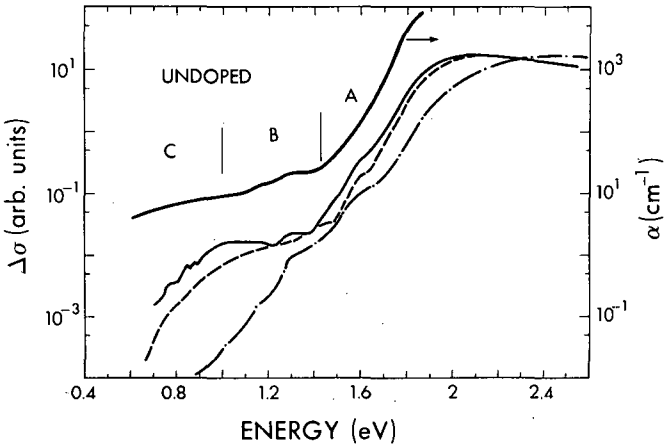

Figure 15. Photoconductivity (primary and secondary) and absorption vs photon energy for an undoped film. (——) (lower solid line), dc SPC measured in this experiment (no dc bias light). (---) ac SPC measured in a Schottky barrier with dc bias light. (-·-) PPC on the same Schottky barrier with dc bias light. (——) (upper solid line), absorption as measured by photothermal deflection. (XBL 8110-1717)

Figure 16 shows absorption and SPC of phosphorus-doped film along with PPC measurements of a phosphorus film in a Schottky barrier configuration. Unlike the undoped case, the absorption follows the SPC closely throughout the energy range 0.9 eV < $\hbar\omega$ < 2.5 eV for doped films. The energy dependence of $\eta\mu\tau$ is shown in Figure 17.

By combining our measurements with results of other experiments, we arrive at the following model, which depicts the approximate density of

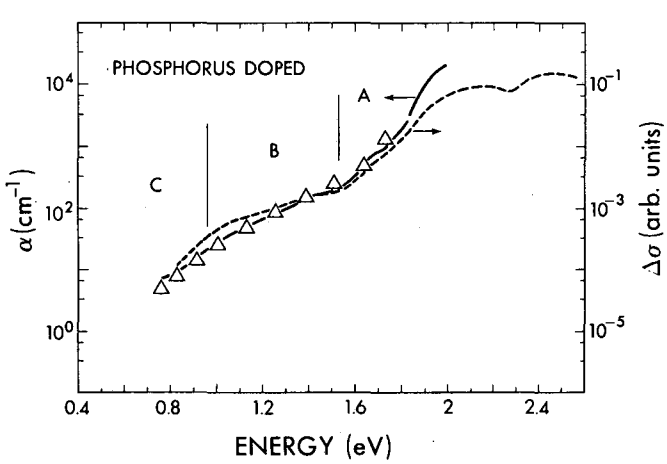

Figure 16. Photoconductivity (primary and secondary) and absorption for a 0.19 percent phosphorus doped film. (- - -) SPC 18 Hz (this experiment). (Δ) PPC on a Schottky barrier. (——) absorption as measured by photothermal deflection. (XBL 8110-1418)

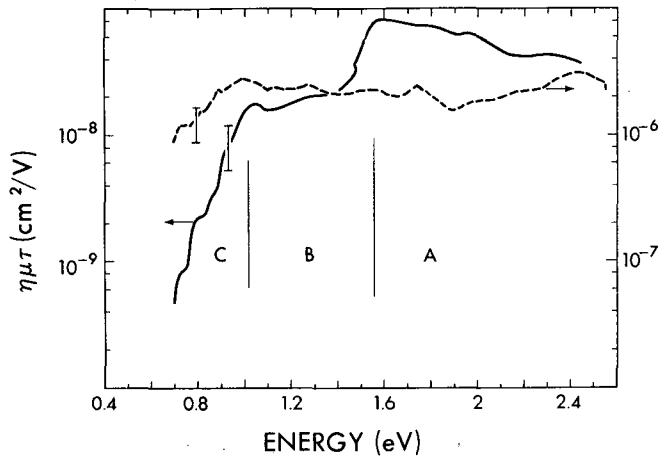

Figure 17. $\eta\mu\tau$ product vs photon energy for an undoped film (——) and for a phosphorus-doped film (-----). Error bars indicate maximum relative error. Absolute magnitudes of error may be larger. (XBL 8110-1414)

states for doped and undoped material (Fig. 18). The absorption measurements have shown that the density-of-states maximum above the valence band is in large part due to dangling silicon bonds for the undoped material and that the maximum is strongly correlated with the LESR signal for the phosphorus-doped material. A maximum 0.3 eV below the conduction band is not shown in the density of states. There is evidence from field-effect and luminescence measurements supporting the existence of this maximum.

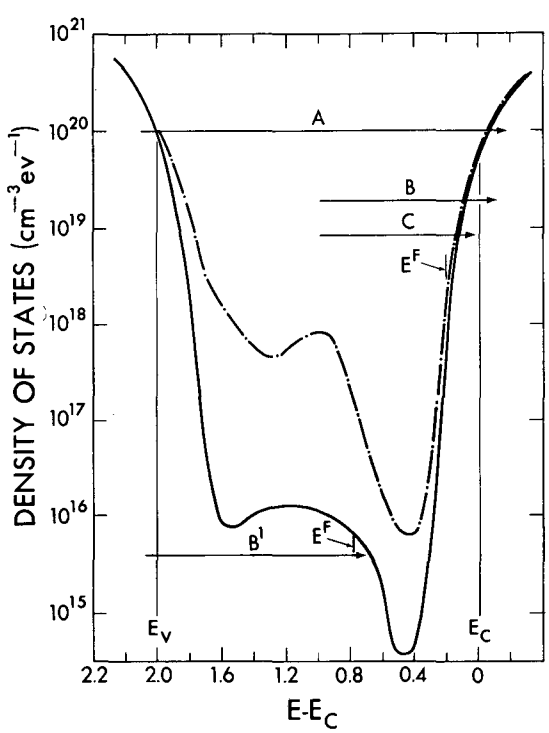

Figure 18. Density of states for undoped and P-doped films as measured by DLTS. Shown are various transitions giving rise to photoconductivity for the different energy regions. States are localized for energies between E_V and E_C. (XBL 8110-1415)

Liquid Crystal Research*

The liquid-crystalline state of matter is characterized by a spontaneous anisotropic order and by fluidity. The anisotropic order leads to anisotropy in the physical properties of the medium, and the fluidity makes it easily susceptible to external perturbations in the form of electric or magnetic fields, temperature, or pressure. In addition, we have demonstrated that certain gaseous organic pollutants change the liquid-crystalline structure. This change, which is readily detectable, is the basis for an inexpensive and sensitive (10^{-6}) personal dosimeter for some organic pollutants. Once their physical properties are well understood, the class of liquid crystals known as lyotropics offers the potential for employing such a material for the efficient recovery of oil from abandoned wells and from oil shale.

Physical Properties of Liquid-Crystalline Monolayers

Lyotropic liquid-crystalline monolayers are interesting for several reasons. First, not unlike other 2-d systems but unlike one-dimensional systems, these monolayers exhibit a variety of phases; many of these phases are similar to those observed in three dimensions. Also, these 2-d systems may have important technological applications in such diverse fields as oil recovery, catalysis, electronics, and liquid crystal displays. Additionally, 2-d systems are interesting in their own right and are not yet well characterized, either experimentally or theoretically. Furthermore, they are of unique biological importance.

We have chosen to investigate this system using the non-perturbing technique of light scattering. Scattering from the monolayer molecules themselves is very small. However, the presence of the monolayer causes reduction of the interfacial tension and greatly alters the behavior of small wavelength capillary waves at the liquid-monolayer-liquid interface. In thermal equilibrium, r.m.s. fluctuations of the interface are on the order of a few angstroms. These fluctuations consist of the superposition of a large number of traveling wave frequencies, ω, and wavelengths, q. Any given wave of fixed q will act somewhat like a moving diffraction grating and will cause part of the laser beam to be scattered into an angle determined by q with frequency shifts of $\pm\omega$. Thus, the scattering is caused by a change in index of refraction between the two bulk liquids. In this experiment, the laser beam enters and leaves the upper non-polar liquid through a coupling prism at right angles to the beam (Fig. 19). A small fraction of this beam is scattered, relative to the reflected beam, into angles $\lesssim 1$ degree. Some light is also elastically scattered into small angles by

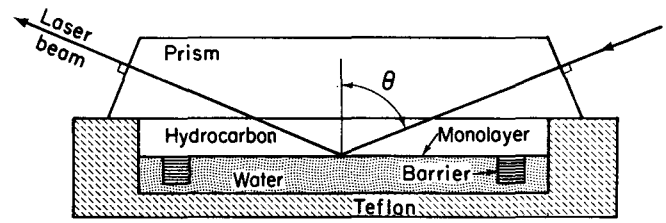

Figure 19. Details of the scattering configuration (side view). (XBL 812-160)

the liquids and optical components. Next, a precision small-angle rotation is made on the beam, causing the main beam to go off axis and allowing light scattering by the negative of this angle to enter a small pinhole and finally a photomultiplier. Here, the elastically and inelastically scattered light beats together on the photocathode, generating a photocurrent containing the difference or ripple frequency. A real-time digital autocorrelator and microcomputer determines the frequency and the damping coefficient from the time correlation function.

To obtain the interfacial tension from ω and q, an accurate hydrodynamic theory of the fluctuation-driven ripples is needed. As an illustration, the dispersion relation for harmonic waves on the clear surface of a single liquid is

$$\omega^2 = \gamma q^3/\rho + gq$$

where

$\gamma(T)$ = surface tension at a given temperature

ρ = liquid mass density (3-d)

g = acceleration due to gravity

Since we investigate only very small q values, we may ignore the gravity term, and a measurement of ρ, ω, and q will give the surface tension in this simple case. The actual experimental situation is complicated by a second liquid, bulk (3-d) liquid shear viscosities, the visco-elastic constants of the 2-d monolayer, and the fact that not all waves are harmonic. Therefore, we have extended the anharmonic theory of fluctuation-driven ripples of a single fluid to our system. The predicted power spectra can be fit to the Fourier transformer of the measured time correlation function. To be discussed later is the fact that hydrodynamics also gives the form of the power spectra for "longitudinal" waves in which the monolayer molecules move in the plane of its interface. A schematic of experimental equipment is shown in Figure 20.

Our recent results are shown in Figures 21 and 22. At low coverage, we observe a two-dimensional liquid-like behavior, while at high coverage a two-dimensional solid-like phase is found. Between these two phases, an intermediate regime exists

*This work was supported by the Director, Office of Energy Research Pollutant Characterization and Safety Research Division of the U.S. Department of Energy under Contract No. DE-AC03-76SF00098.

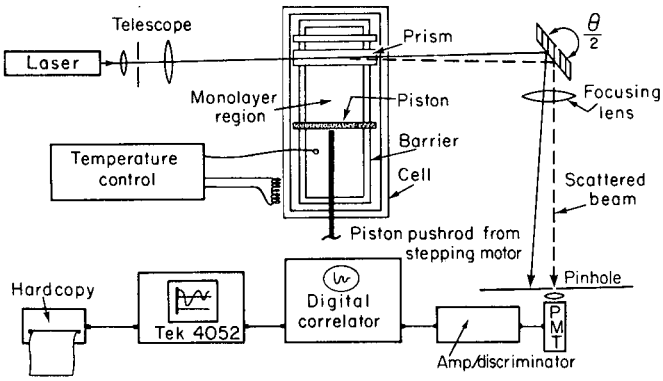

Figure 20. Schematic of experimental equipment (top view). (XBL 812-161)

where the frequency of the surface waves appears to remain constant. This preliminary observation suggests that this regime is a co-existence region where islands of 2-d solid phase exist in a "sea" of 2-d liquid. This is further supported by the damping coefficient measurements shown in Figure 22. Here, the intermediate regime exhibits large scattering of the data, implying that these solid islands move in and out of the probing laser beam. nature of the liquid-to-"coexistence region" phase transition, as opposed to the smoother nature of the "coexistence region"-to-solid transition.

Additional data are required before we can attempt to contrast our results with current theories on two-dimensional melting and phase transition.

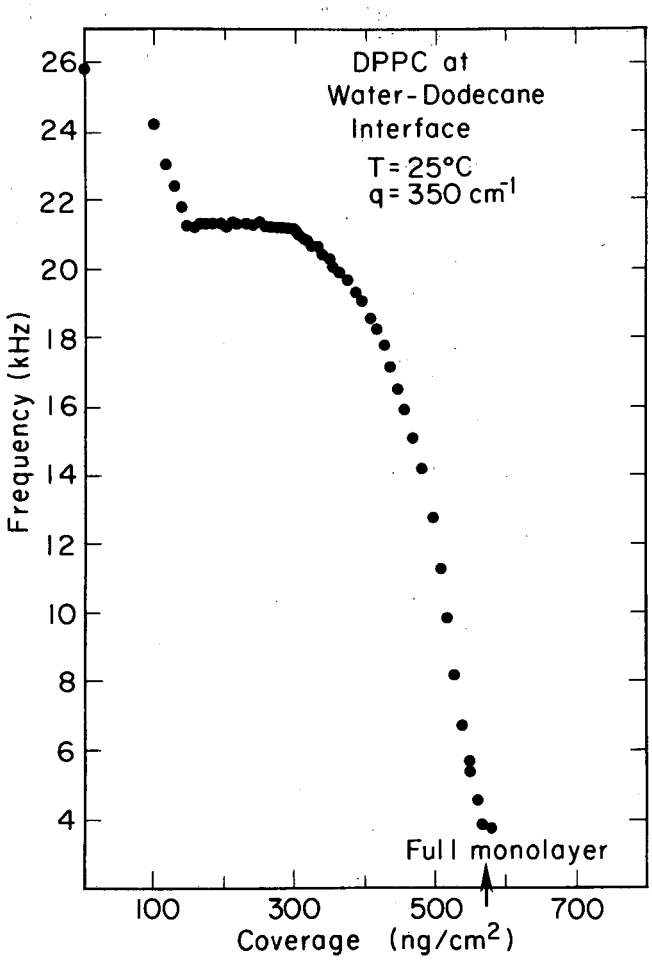

Figure 21. Ripplon frequency as a function of coverage. (XBL 823-3663)

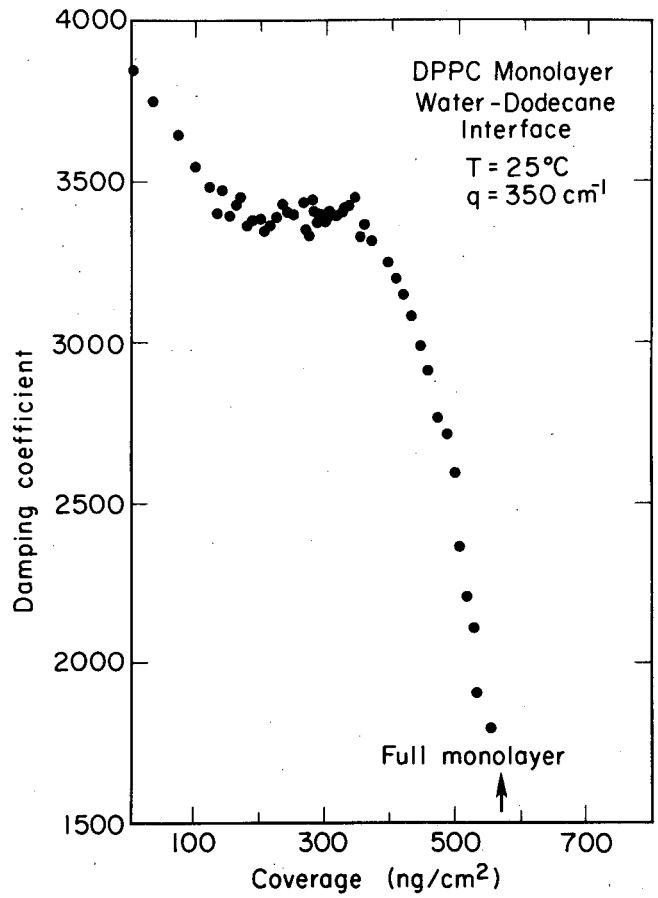

Figure 22. Damping coefficient as a function of coverage. (XBL 823-3662)

Novel Laser Systems*

Our research activities, at times, require the development of new laser systems to meet a specific need. Of current interest to us is the generation of sub-picosecond tunable laser pulses for use in probing elementary excitation in amorphous photovoltaic semiconductors. A brief description of our achievements during FY 1981 is described below.

New Approaches for the Generation of Ultrashort Tunable Laser Pulses

Reciprocal Mode-Locking. Recently, we developed a new approach to ultrashort pulse generation: reciprocal mode-locking. This method combines the advantages of synchronous pumping and passive mode-locking. A dye laser, internally pumped within the extended cavity of the ion laser, is mode-locked when its cavity length is matched to that of the pump laser. The output of the pump laser is passively mode-locked by the combination of the saturable absorption and the lasing action of the dye, which is in turn synchronously pumped and mode-locked.

This new approach to ultrashort pulse generation has several significant advantages over present mode-locking schemes:

1. It eliminates the need for an active mode-locking device;
2. It significantly reduces the need for careful matching of the cavity lengths of the dye and pump lasers;
3. When compared to conventional passive mode-locking schemes, reciprocal mode-locking yields significantly wider tuning range and higher average power; and
4. It enables the use of high-transmission (10 percent) output couplers.

Initially we reported the generation of 10-psec pulses with a 300-Å tuning range and 80-mW average power. Based on recent results, we have succeeded in shortening these pulses down to one psec, widening their tuning range to 600-Å and increasing their average power to 200 mW.

Tightly Focused Double Mode-Locking Scheme. The cavity configuration shown in Figure 23 has been built for the generation of widely tunable, high-average-power ultrashort pulses at two independent wavelengths.

The R6G dye jet is cw-pumped by the 5145-Å output of an Ar^+ ion laser. A second dye jet

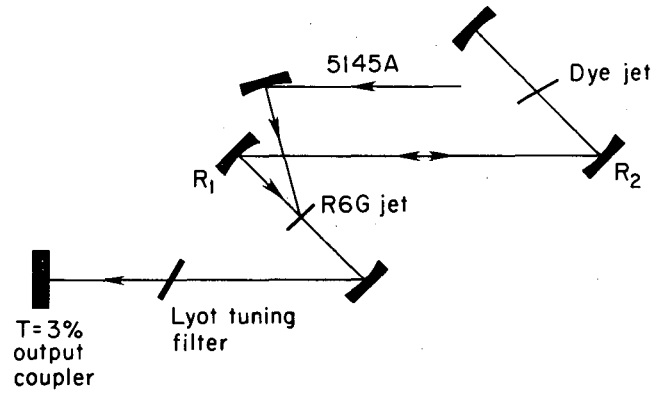

Figure 23. Cavity configuration for generating widely tunable, high-average-power, ultrashort pulses at two independent wavelengths.
(XBL 823-3660)

(cresyl violet, cv) is introduced in the dye laser cavity. The duration of the pulses and their tuning range is strongly dependent on the ratio $F\sigma_a/\sigma_c$, where σ_c is the emission cross section of R6G at the lasing wavelength and σ_a is the absorption cross section of cv at that wavelength. F is the ratio of the beam area in R6G to that in cv. Hence $F \sim (R_1/R_2)^2$. Therefore, improved performance (shorter pulses and wide turning ranges) is expected by setting R_2 as small as possible.

The independent tunability of the two wavelengths is to be obtained by a compensated wedged quartz waveplate which can be translated and rotated. To minimize dispersion due to cavity mismatch, the thickness of this plate is kept small.

This scheme has resulted in 0.5 psec pulses at two independently tunable wavelengths. The average output power is ~150 mW, and the tuning range is 500Å. The relative ease of generating these ultrashort pulses makes this scheme ideal for sub-picosecond time-resolved spectroscopy.

PLANNED ACTIVITIES FOR FY 1982

In the area of laser photoacoustic and photothermal spectroscopy and detection, emphasis will be placed on the implementation of these highly sensitive techniques in a remote sensing configuration. Of immediate interest to us is the question of the role of atmospheric turbulence and speckling on such a configuration. The species to be remotely detected are those involved in the generation of acid rain, e.g., SO_2 and NO_x. The theory of photothermal buckling will be developed, and this technique will be extended to liquids. Elemental photoacoustic and photothermal detection will continue, and multiphoton photoacoustic spectroscopy will be initiated.

Research on amorphous photovoltaic semiconductors will focus on the elucidation of the nature of

*This work was supported by the Office of Energy Research, Pollutant Characterization and Safety Research Division of the U.S. Department of Energy under Contract No. DE-AC03-76SF00098 and by the LBL Director's Fund.

the gap states in amorphous silicon. Experiments aimed at resolving the picture of the density of states are planned. Work has been initiated to investigate the optical nature of the Staebler-Wronski effect, which degrades the performance of hydrogenated amorphous silicon solar cells. A time-resolved study of the role of defects on excess carrier recombination in amorphous silicon will continue, and direct measurements of carrier lifetime are planned. We also plan to initiate research in the area of the optical and electronic properties of crystalline and amorphous semiconductor surfaces.

Applications of liquid crystals to energy-related problems will continue to be explored. Work on specific gaseous organic liquid crystal detectors will continue, and the challenging question of the nature of mechanisms involved will be pursued. Work on the ferro-liquid crystal magnetometer will resume, with emphasis on the physics of the underlying mechanism responsible for the observed effect. The elucidation of the physical properties of lyotropic monolayers will continue, and the information obtained from this work will be evaluated in the context of emulsification.

Finally, activities in the area of developing new laser systems will center on further shortening the tunable pulses we now generate. The goal is to reach $\leq$100 femtosecond during FY 82. To achieve that goal, counterpropagating beam schemes will be employed.

OIL SHALE RESEARCH

A Mathematical Model for Leaching of Organic Carbon from In-Situ Retorted Oil Shale*

W. G. Hall, R. E. Selleck,† and J. F. Thomas

The rich oil shale deposits in Colorado's Piceance Creek Basin are being considered for early commercialization by vertical modified in-situ retorting (VMIS). In this process, large underground chambers of oil shale, several hundred feet in cross section and up to 700 feet high, are pyrolyzed in place. This type of processing may result in environmental problems, including the disruption of groundwater aquifers, leaching of retorted shale, and subsidence described by Persoff and Fox.[1]

A major environmental concern is leaching of retorted shale. Most of the oil shale beds in the Piceance Creek Basin are infiltrated with groundwater aquifers. During in-situ retort preparation and retorting, groundwater levels adjacent to the development site are lowered below the retorts by pumping. After oil recovery is complete, groundwater may reinvade the abandoned retorts and leach soluble organic and inorganic compounds. These materials may be transported through surrounding aquifers to wells, springs, and surface streams.

Several methods have been proposed to control this problem.[1] These include grouting, intentional leaching, and various hydrological modifications. The purpose of the present investigation, initiated in June 1978, is to study selective leaching as a means of minimizing the impact of abandoned in-situ retorts on water quality. In this approach, water would be injected into the retort, collected, and treated in a surface facility. This appeared feasible because experimental work revealed that most of the leachable material is readily removed with a few pore volumes of water.

Our approach was to first define the kinetics of leaching spent shale by using data collected from batch and column leaching experiments. The kinetic data were then incorporated into a mathematical model of the leaching and transport mechanisms.

*This work was supported by the Assistant Secretary for Environment, Office of Environmental Compliance and Overview, Environmental Control Technology Division and the Assistant Secretary for Fossil Energy, Deputy Assistant Secretary for Oil, Gas, and Shale Technology, Office of Oil Shale of the U.S. Department of Energy under Contract No. DE-AC03-76SF00098.

†University of California, Berkeley, California.

ACCOMPLISHMENTS DURING FY 1981

A mathematical model of the mass transfer and transport mechanisms involved in leaching of solute from spent shale was developed and verified. Kinetic constants for use in the model were derived from batch and continuous-flow column experiments.

Leaching and Transport Model

Water passing through a bed of spent shale leaches out soluble material and transports it through the pores of the bed. The solute is a complex mixture of organic and inorganic compounds. Since the modeling of multi-component mass transfer and diffusion was beyond the scope of this study, it was assumed that the organic portion of the solute could be characterized by total organic carbon (TOC) and electrical conductivity (EC). Both of these can be easily measured.

Bed porosity is distributed between macro- and micro-pores. The former lie between the particles and the latter are found within the particles. The micro-pores remain after the thermal conversion and the removal of raw organic compounds from the mineral matrix.

Mass transfer between solid and liquid phases may be represented by a series of mechanisms, each in the series applicable to solute movement within a particular domain. Domains include: the solid shale, liquid within micro-pores, interfaces between phases, and fluid in the macro-pores. It is likely that the rate of overall mass transfer will be governed by transfer within a single domain. Investigations were directed toward the identification of this domain and the development of a model applicable to the movement of solute from the solid to the liquid phase.

The spent shale was modeled as a bed containing porous cylinders in random contact. The macro- and micro-pores are initially saturated with water. Mass transfer between the solid and liquid phases was assumed to be complete and the solute of interest to be contained completely within the fluid at the start of leachate flow. This assumption was based on observations of solute build-up in leachates from column and batch studies, during which transfer rates were high at first and then

dropped quickly. The change in rates appears to reflect transfer of material from sites in the solid phase located at increasing distances with time from the phase interface.

The physical model is thus an interconnected network of micro- and macro-pores filled with water and containing the total mass of the solute of interest. The micro-pores act as reservoirs for solute, which is transferred to the fluid in the macro-pores by molecular diffusion. Transport of solute in the macro-pores is by viscous flow involving dispersive and diffusive mechanisms. Mass transfer between phases after the initial flux during filling is not included in the model.

Mass Transport Equations

The leaching and transport of solute in a bed of spent shale can be modeled by a mass transport rate equation:

$$\frac{\partial c}{\partial z} = - U_p \frac{\partial c}{\partial z} + D_a \frac{\partial^2 c}{\partial z^2} + r_r - \frac{\partial q}{\partial t} \cdot \frac{1}{m} \qquad (1)$$

in which:

- c = concentration of solute in liquid phase in the macro-pores
- t = time
- U_p = velocity of leachate in macro-pores
- Z = distance in direction of flow
- D_a = dispersion coefficient
- r_r = rate of chemical reaction
- q = concentration of solute in liquid phase in micro-pores
- m = ratio of macro-pores to micro-pore volume

The terms on the right side of the equation are the contributions to the net change of the solute concentration with time due to convection, dispersion, chemical reaction, and mass transfer, respectively.

Equation (1) can be coupled with the Fickian diffusion equation:

$$\frac{\partial q}{\partial t} = D_m \nabla^2 q \qquad (2)$$

in which:

- D_m = diffusion coefficient
- ∇^2 = Laplacian operator

Equations (1) and (2) are solved for the following assumptions and initial conditions by a method similar to that used by Rosen[2].

1. Axial dispersion is neglected.
2. Chemical reactivity of the solute is zero.
3. Diffusion within the micro-pores is the rate-limiting mechanism.
4. Shale particles are modeled as cylinders having a radius "b."
5. All solute is initially contained in the liquid phase.

Equation (1) is normalized to Equation (3) by setting $\theta = t - Z/U$ and $X = Z/mU$.

$$\frac{\partial c}{\partial x} + \frac{\partial q}{\partial \theta} = 0 \qquad (3)$$

A solution to Equation (2) for diffusion from a cylinder was derived from Crank[3] and substituted into Equation (3). The resulting equation was then solved by Laplace transform techniques to yield Equation (4).

$$u(X,T) = 1 - \mathcal{L}^{-1}\left\{\frac{1}{s} \exp\left[-\alpha x \sum_{1}^{\infty}\left(\frac{s}{s + [O_i]^2}\right)\right]\right\} \qquad (4)$$

in which

- $U(X,T)$ = Leachate concentration in macro-pores in a fixed bed expressed as a function of length and time parameters, X and T, respectively.
- X = Z/mU
- T = D_m/b^2
- α = $4\ D_m/b^2$
- s = Transform variable
- $[O_i]$ = Ith zero root of zero-order Bessel function
- $\mathcal{L}^{-1}$ = Inverse of Laplace transform.

Solutions to Equation 4 were obtained by numerical inversion programs from the LBL Computer Center Library.[4,5] Leachate solute concentration break-through curves for various length and time parameters are shown in dimensionless form on Figure 1.

Leaching Experiments

Batch and column experiments were undertaken with spent shale produced in run S-55 of the Laramie Energy Technology Center 10-ton, simulated in-situ retort in Wyoming. Spent shale was leached in Lucite columns 11.5 cm in diameter by 1.2 m long. Taps for leachate sample withdrawal were located at 15 cm intervals along the axis. A column was packed with spent shale, filled with water, allowed to remain quiescent until TOC levels in the leachate and shale approached quasi-equilibrium. Distilled water was then pumped downward through the shale bed. Downward flow minimized the effects of density counter-currents caused

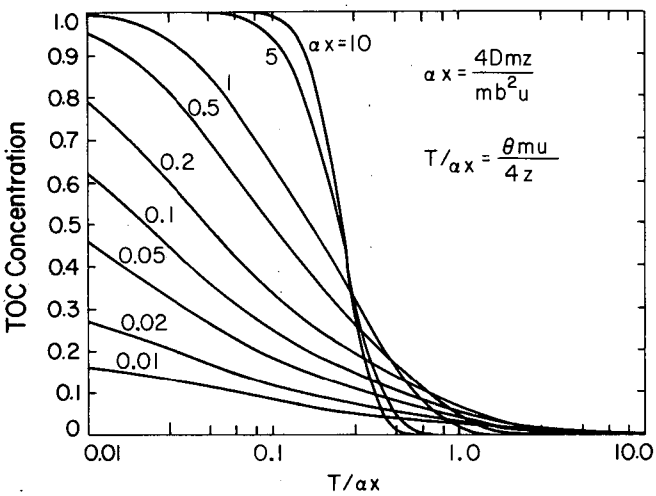

Figure 1. Dimensionless leachate solute concentrations in a bed of spent shale as functions of time and length parameters, x and T.

(XBL 821-71)

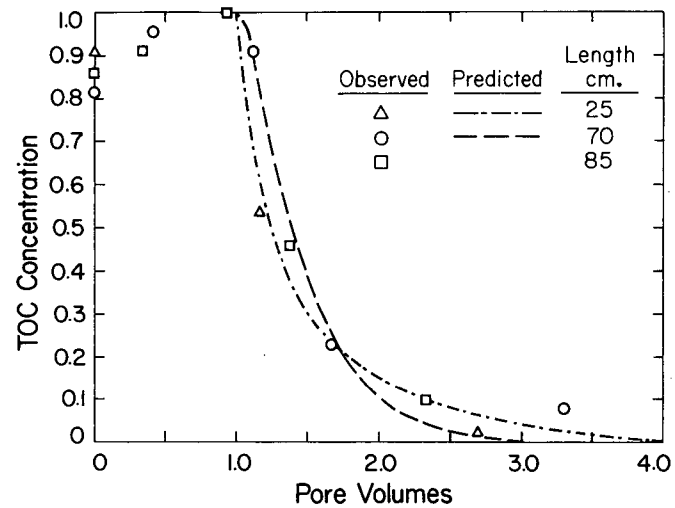

Figure 2. Observed and predicted TOC concentrations in leachates from columns packed with spent shale.

(XBL 821-72)

by local dissolved salt concentration gradients.

In general, TOC and EC concentrations decreased rapidly with time. The shorter the distance of leachate travel at any given time and the greater the time at any particular distance, the lower is the concentration.

Observed TOC concentrations are plotted against pore volumes of leachate passage for column leaching lengths of 25, 70, and 85 cm (Fig. 2). Pore volume of passage if defined as the product of time and pore velocity divided by column length. Concentrations were normalized by dividing by the highest observed effluent concentration. Predicted concentrations for 25- and 70-cm distances are also shown on the figure. These curves were calculated from the dimensionless break-through curves of Figure 1 for the experimental variables listed in Table 1 for run D-8.

Analyses of Results

This model was applied to the six separate column runs described in Table 1 in which the average cylinder radius of the spent shale was varied from 0.4 to 0.8 cm and the average macro-pore velocity from 4.4 to 20 x 10^{-3} cm/sec. The resulting diffusion coefficients calculated from best-fit analyses of observed column effluent TOC data and the dimensionless break-through curves are tabulated in Table 1. The diffusion coefficients range from 0.9 to 4.8 x 10^{-5} cm^2/sec and may be compared with a molecular diffusion coefficient of 1.0 x 10^{-5} cm^2/sec, a typical value for the diffusion of organic compounds at dilute concentrations in water. The calculated coefficients for all of these column runs are an order of magnitude of the latter value. This indicates that the model is realistic for the first few pore volumes of leachate.

Table 1. Diffusivities of TOC in spent shales and experimental variables used in small column experiments.

Run No.	m Pore ratio	Z Dist. cm	b Radius cm	U Velocity cm/sec x 10^3	D_m/b^2 sec^{-1} x 10^4	D_m cm^2/sec x 10^5
D-4	3.1	25	0.4	4.4	1.8	2.9
D-4	3.1	85	0.4	4.4	1.2	1.9
D-5	3.1	85	0.4	14.0	3.0	4.8
D-6	2.9	70	0.4	20.0	0.6	1.0
D-7	2.9	55	0.4	18.0	2.2	3.5
D-7	2.9	70	0.4	18.0	n.d.	n.d.
D-8	3.0	25	0.5	7.4	0.4	1.0
D-8	3.0	70	0.5	7.4	n.d.	n.d.
D-8	3.0	85	0.5	7.4	0.6	1.5

n.d. - not determined.

TOC levels in the leachate at the start of a run were approximately 40 mb/l. Small increases in concentrations were noted in some columns before the passage of one more volume of water as shown on Figure 2. The leachate TOC was approaching an equilibrium with that in the solid. The same increase would be noted in a static batch test because each element of moving water has the same leaching history relative to each stationary piece of shale. The model, as proposed, could include this stationary phase but modifications would have to be made to allow for diffusion into the macro-pores.

After one pore volume of fluid had passed, the TOC concentrations dropped rapidly to levels below 5 mg/l in the next one to two volumes of fluid. Thereafter, the concentrations decreased very slowly. After the passage of more than 50 pore volumes of water, the effluent TOC concentrations of about one mg/l were still being observed.

It is hypothesized that the decidedly asymmetric tail of the break-through curve is due to the transport of small amounts of solute into the micro-pores from the solid phase and that this mechanism had become the rate-limiting process. Further studies into the kinetics of leaching solute from spent shale must include this mechanism for a complete characterization of the leaching process.

PLANNED ACTIVITIES FOR FY 1982

Work planned for the next fiscal year includes the completion of the investigation and the preparation of the final report.

REFERENCES

1. Persoff, P., and Fox, J.P. (1980), "Control Strategies for Abandoned In-Situ Oil Shale Retorts," Energy and Environment Division Annual Report 1979, Lawrence Berkeley Laboratory Report LBL-10486.

2. Rosen, J.B. (1952), J. Chem. Phys. 20, 387.

3. Crank, J. (1975), Mathematics of Diffusion, Second Edition, Clarendon Press, Oxford.

4. Willis, R., C# BKY LAPINV, LBL Computer Center Library Programs, Lawrence Berkeley Laboratory, Berkeley.

5. International Mathematics and Statistics Library (IMSL), FLINV, LBL Computer Center Library Programs, Lawrence Berkeley Laboratory, Berkeley.

Development of Low-Cost Grouts from Spent Oil Shale*

P. Persoff

In vertical modified in-situ (VMIS) retorting, the resource is processed in the ground. The area to be developed is dewatered by pumping, and large chambers of rubblized oil shale are formed by mining out 20 to 40 percent of the in-place shale and blasting the remainder into the created void. The mined-out material is brought to the surface for retorting. The in-place material is pyrolyzed to recover oil, leaving large abandoned retort chambers underground.

This type of processing may cause environmental problems, including ground subsidence and the leaching of the spent shale by re-invading groundwater. Resource recovery is low because about half of the raw shale must be left intact as pillars to support the overburden. These problems may be mitigated by filling abandoned retorts with a grout which would occupy the void space created by mining and blasting, improve the structural stability of the abandoned retorts, and reduce the retort's permeability to groundwater flow. If the backfilled retorts are sufficiently strong, it may be possible to design retorts so that the pillars can eventually be retorted for additional resource recovery after grouting is complete.

Because oil shale is a low-grade hydrocarbon resource (25 gallons per ton is typical for VMIS) and because 20 to 40 percent of this material is removed to create permeability needed for VMIS retorting, the void space to be filled by grout is large, about 9 to 13 cubic feet per barrel of oil recovered (including oil recovered from surface retorting). Thus, low cost is the first requirement for any candidate grout material. Transportation costs limit the use of common, cheap grouting materials, such as fly ash or bentonite, to about 10 percent of the grout formula. The surface retorting accompanying VMIS development, however, will produce large quantities of spent shale on

*This work was supported by the Assistant Secretary for Environment, Office of Environmental Compliance and Overview, Environmental Control Technology Division of the U.S. Department of Energy and by the Assistant Secretary for Fossil Energy, Deputy Assistant Secretary for Oil, Gas, and Shale Technology, Office of Oil Shale, of the U.S. Department of Energy under Contract No. DE-AC03-76SF00098.

site, about 1.4 tons per barrel of oil recovered by surface retorting. Properties of spent shale vary widely, depending upon the raw shale source and the surface retorting process used; but, in some cases, the spent shale has properties which may commend it as a grouting material.[1] Grouting with spent shale would also dispose of much of the spent shale.

The purpose of this project, which was started in September 1978, is to evaluate low-cost grouts incorporating spent shale for grouting abandoned retorts to achieve impermeability.

ACCOMPLISHMENTS DURING FY 1981

A second series of low-cost grouts (arbitrarily designated Series R) was prepared containing only water and materials which either are waste materials or can readily be replaced by waste materials. During FY 1980, a first series of grouts, Series Q, was prepared and tested; results of that work are presented in the FY 1980 Annual Report.[1] Permeability measurements of the cured grouts indicate that permeability, while higher than observed for compacted spent shales, may be low enough to control leaching by groundwater. However, consolidated drained triaxial tests indicate that the grouted retort stiffness is probably too low to permit enhanced resource recovery.

In Series R grouts, the bulk of the solid material (89.75 to 99.75 percent) was spent oil shale. The remainder was fly ash, gypsum, and fluidizer. These last two ingredients may be replaced by waste gypsum from phosphoric acid manufacture and a commercial waste liquor, respectively. Separate tests[2] were made to evaluate the suitability of these waste materials as replacements for the grout ingredients.

Materials

Lurgi spent shale was collected in the electrostatic precipitator from Lurgi run no. 9, in 1976. This material was selected because both of the commercial VMIS ventures, Rio Blanco and Cathedral Bluffs, are considering the Lurgi process for surface retorting of mined shale. Lurgi spent shale is a fine powder with a median particle size of about 3 micrometers (for more information, see the FY 1979 Annual Report[3]).

Class F fly ash was obtained from the Craig, Moffat County, Colorado, power plant, the nearest source of fly ash to the site of VMIS developments. Class C fly ash was obtained from two sources: the Wyodak, Gillette, Wyoming, and the Comanche, Pueblo, Colorado, power plants. These sources are more distant, but class C fly ash is cementing while class F is not (it must react with $Ca(OH)_2$ to cement[4]). Analysis of the class C ashes by x-ray diffraction showed that their cementing property is due to the presence of tricalcium aluminate (C_3A). This compound is an ingredient of portland cement which hydrates very rapidly, causing a "flash set" unless its set is retarded. In portland cement, this retarding action is obtained by adding a few percent gypsum, which reacts with the C_3A to form ettringite, thus adding to the strength. Grouts made with class C fly ash were also given 5 percent gypsum per weight of fly ash.

Waste gypsum was supplied by the Chevron Chemical Company phosphoric acid plant near Salt Lake City. This plant processes "phosphate rock" [$Ca_3(PO_4)_2$] into phosphoric acid; waste gypsum ($CaSO_4$) is disposed of in slurry ponds. Two commercially available fluidizers were tested. As shown below, they differed slightly in their fluidizing effect but markedly and surprisingly in the properties of the grouts produced.

Grout Formula Design

Grout formulae were designed to meet two criteria: fluidity and stability. Fluidity refers to the ability of the grout to flow, specifically, to penetrate small voids in an abandoned retort. Stability refers to resistance to "bleeding," i.e., separation of a clear supernatant fluid by sedimentation. These two criteria are contradictory in the sense that, although increasing the water-solids ratio (wsr) results in greater fluidity, it also causes greater bleeding. We wanted a nonbleeding grout that was still sufficiently fluid. Our criterion for fluidity was that the time of efflux from a standard Corps of Engineers grout flow cone[5] be 18-22 seconds. Experience with intrusion grouting of pre-packed aggregate concrete has shown this to be reasonable.[6] Grouts containing only spent shale and water with wsr low enough to be nonbleeding were too thick to measure by the flow cone method. In Series Q grouts, we satisfied both criteria by replacing one-third of the spent shale by -30 +50 mesh sand. However, because grout penetration is limited to pores larger than three times the diameter of the largest particle, sanded grouts cannot penetrate through pores smaller than 1 mm (approximately). For complete penetration, we considered it preferable to have a grout consisting of all fines. In Series R grouts, we satisfied both criteria by using 0.25 or 0.50 percent by weight fluidizer, as shown below.

Grout Preparation

The formulae of Series R grouts are shown in Table 1. Grouts were prepared by batch mixing the dry ingredients, including the fluidizers which were supplied as powders, with the minimum amount of water to produce a grout fluid enough for flow cone measurement. Water was then added in incre-

Table 1. Low-cost spent shale grouts (Series R).

	R-1	R-2	R-3	R-4	R-5
Lurgi spent shale, g	100	100	100	90	90
Class F fly ash (Craig), g	-	-	-	-	10
Class C fly ash (Wyodak), g	-	-	-	9.5	-
Reagent gypsum, g	-	-	-	0.5	-
Fluidizer A, g	0.50	0.25	-	-	-
Fluidizer B, g	-	-	0.25	0.25	0.25
Distilled water, ml	69.4	74.6	71.8	68.9	63.3
Flow cone time, sec	16.6	16.1	17.9	22.2	22.4

ments until the flow cone time was reduced to the target value. As shown in Table 1, actual values fell slightly outside this range. Series Q grouts were mixed at low speed (125 rpm), according to ASTM C 305. In preparing Series R, however, we found that high speed mixing (1300 rpm) with a Jiffy mixer (Jiffy Co., Irvine, Calif.) produced a more fluid grout with the same formula. All Series R grouts were mixed 3 minutes at 1300 rpm after each incremental addition of water. Grouts were expected to be thixotropic, but we found that, after the final addition of water, additional mixing for 3 minutes or standing for 10 minutes did not affect the flow cone time. Lack of thixotropy was probably due to the inclusion of the fluidizers. For two of the grouts, rheologic measurements were made with a Contraves rheometer model 15-T; these measurements showed that the grouts were Casson fluids with yield stress values about 60 dyne/cm^2. All grouts were tested for bleeding by allowing a 250-ml graduate full of grout to stand for four hours; bleeding was less than one percent in all cases.

Experimental

Sample Preparation. Grout samples for permeability measurements were prepared by pouring the fluid grout into waxed cardboard cylinders, 2 inches in diameter by 4 inches high. Cardboard molds were used instead of metal because the specimens were expected to be so weak that they would be damaged by removing a metal mold. The samples were cured at 70°F in 100 percent humidity for times ranging from 5 to 7 months. This range of cure times is due to the fact that all grouts were prepared and cast over a three-day period, while testing took much longer, up to a week per sample. Specimens for structural tests were prepared using grout and aggregate to simulate grouted in-situ spent shale. The aggregate used was simulated in-situ spent shale from Laramie Energy Technology Center's 10-ton retort run S-55, which was crushed and sieved to +1/4 -3/8 inch, saturated with water and surface dried. In preliminary work, we tried to pump the grout into pre-packed aggregate but found that we could not eliminate trapped air by this method. Therefore, we followed ASTM C 31 for the preparation of test specimens: the grout and aggregate were mixed in a bowl and packed into the mold in three lifts, each lift being rodded 25 times with a 1/4 inch rod to eliminate trapped air. As with the permeability specimens, waxed cardboard cylinder molds were used. The aggregate occupied about 50 percent of the total sample volume, compared to 60 to 80 percent theoretically occupied by in-situ spent shale.

Permeability Measurements. The permeability of spent shale grout, like that of a saturated soil, depends upon the confining pressure it encounters. To determine the relationship between permeability and confining pressure, permeability was measured in a U.S. Bureau of Reclamation load cell, as shown in Figures 1 and 2. With this apparatus, any desired confining pressure (P_2 in Figure 1) can be applied to the specimen, and a hydraulic gradient can be applied across the length of the specimen. A back pressure (P_3 in Figure 1) was applied downstream of the specimen so that dis-

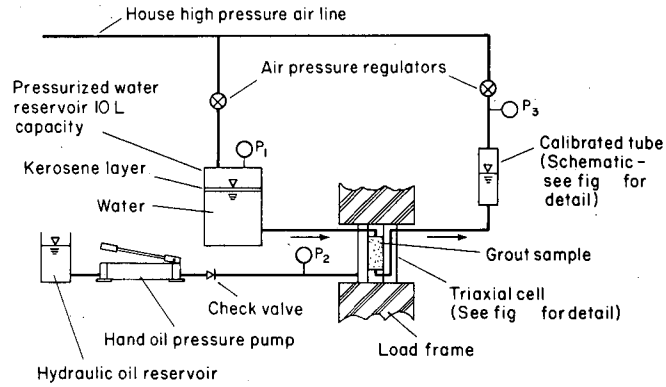

Figure 1. Permeability measuring system used for R-series grouts.

(XBL 821-34)

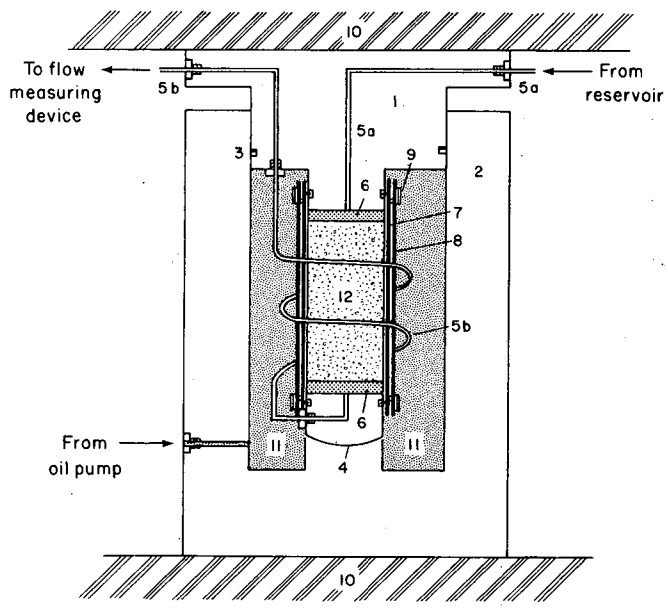

Figure 2. Triaxial loading cell used in permeability measurements. The grout sample (12) is subjected simultaneously to all-around confining pressure and to a hydraulic gradient.

(1) Head of triaxial cell.

(2) Body of triaxial cell.

(3) Piston ring.

(4) Spherical socket in body of cell mates with bottom head.

(5) a. Path of water at P_1 flowing to specimen.
b. Path of water at P_3 flowing from specimen.

(6) Porous stones at each end of sample

(7) Inner jacket, cut from bicycle inner tube.

(8) Outer jacket, cut from bicycle inner tube.

(9) Hose clamp bears on O-ring, isolating sample from confining fluid.

(10) Load frame provides axial confining pressure equal to lateral confining pressure.

(11) Confining fluid (hydraulic oil) at P_2.

(12) Grout sample.

(XBL 821-35)

solved air would not come out of solution while water was percolating through the specimen. This would have caused bubbles to block some of the pores (equivalently, the specimen would have become desaturated), causing measured permeability to be low. The rate of fluid exiting the specimen against the backpressure was measured using a volume change device described by Chan and Duncan.[7] When ready for testing, samples were taken from the curing room, and the molds were stripped off. A knife was used to trim the ends flat and parallel, and porous stones were placed on the ends. Two flexible, impermeable jackets cut from bicycle inner tubes were placed on the specimens, which were than saturated by submerging them in de-aired water under a vacuum for 10 days before being assembled to the apparatus as shown in Figure 2. Permeability was measured on two specimens for each of five formulae, at confining pressures of 60, 120, and 240 psi. Results of the permeability measurements are shown in Figure 3.

Consolidated Drained Triaxial Tests. Consolidated drained triaxial tests were made to determine the response of grouted retorts to long-term loading. As noted above, the samples for triaxial testing were composed of grout and spent shale aggregate. Triaxial testing served two purposes: the data were needed to predict the ability of grouted retorts to support the overburden, and data also were used to predict the confining pressure that would be seen by a grouted retort. The latter influences the permeability as shown in Figure 3. Consolidated drained tests were considered to best simulate the long-term condition, when any increase in pore pressure would have time to dissipate.

The test method is described in Houston.[8] Briefly, the specimens were prepared by capping the ends with a gypsum plaster, as described in the FY 1980 Annual Report.[1] This made the ends flat and parallel without trimming because trimming could have dislodged pieces of aggregate. The samples were then saturated in de-aired water under a vacuum and encased in filter paper and flexible membranes for the consolidated drained triaxial test. Consolidated drained tests were made at confining pressures of 40 and 80 psi. Unconfined tests were also conducted, i.e., 0 psi confining pressure. The maximum axial stress, corresponding to the failure point, for each grout-aggregate combination is plotted against confining pressure in Figure 4. The cohesion (c) and angle of internal friction (ø) were determined from the slopes and intercepts of the curves in Figure 4 using the relationships

$$\frac{d\sigma_{1_f}}{d\sigma_3} = \tan^2 \; 45^\circ + \frac{\phi}{2}$$

$$q_u = 2c \tan \; 45^\circ + \frac{\phi}{2}$$

where

σ_{1_f} = axial stress at failure (psi)

σ_3 = confining pressure (psi)

c = cohesion (psi)

q_u = unconfined compressive strength, the y-intercept (psi)

ø = angle of internal friction.

Since the lines are not straight, the average value of $d\sigma_{1_f}/d\sigma_3$ in the range 0 to 40 psi confining pressure was used to determine ø. The modulus

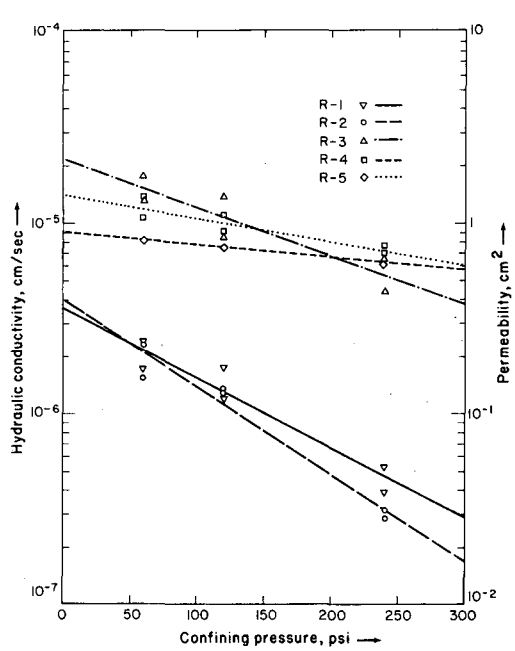

Figure 3. Relationship between confining pressure (P_2) and permeability for R-series grouts. (XBL 821-21)

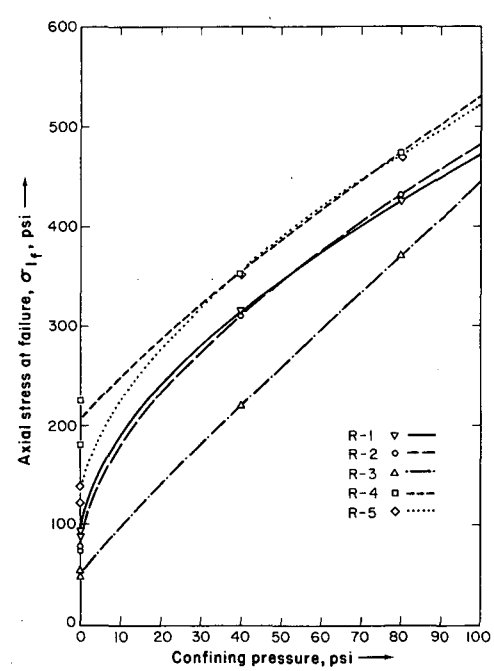

Figure 4. Relationship between confining pressure (P_2) and axial load at failure ($_{1_f}$) for simulated grouted cores. Curves are fit to data points by power law. (XBL 821-22)

of elasticity was determined from the maximum slope of the plot (not shown) of deviator stress vs strain. The strain was zeroed after the confining pressure was applied. The values of the structural parameters are summarized in Table 2.

Discussion of Results

The structural properties of the grouted cores (modulus, cohesion, and unconfined compressive strength) can be related to the grout formulae and to the way permeability of the grouts changed with confining pressure. As shown in Tables 1 and 2, addition of 10 percent fly ash to the grout produced substantial increases in unconfined compressive strength and cohesion. The increase in strength was greater with class C fly ash and gypsum (this combination is not only a pozzolan, but also a true hydraulic cement) than with class F fly ash, which is a pozzolan but not a cement. Pozzolans develop strength by reacting with free lime [$Ca(OH)_2$]. Tests for free lime by ASTM C 114 showed that Lurgi spent shale contains no measurable free lime. It is not clear whether the strength increase in R-5 over R-3 was due to pozzolanic reaction with a trace of free lime, some other reaction, or to a lower water-solid ratio.

The fluidizer used also apparently contributed to the strength. Grout R-3, with 0.25 percent of fluidizer B, had an unconfined compressive strength of 53 psi, while R-2, made with 0.25 percent of fluidizer A and a slightly higher water-solids ratio, had an unconfined compressive strength of 78 psi. Grout R-1, made with 0.5 percent of fluidizer A and slightly lower water-solids ratio, had still higher strength.

Figure 3 shows that, as confining pressure increases, permeability decreases for all grouts. This suggests that, under confining pressure, the grout samples consolidate, forming a denser, more compact structure with smaller pores. More support is given to this interpretation by the fact that grouts R-4 and R-5, which have higher moduli of elasticity (see Table 2), also have lines of lesser slope in Figure 3; that is, because they were stiffer, they consolidated less and permeability decreased less.

An unexpected and as yet unexplained result is the effect of fluidizer on grout permeability. As noted above, grouts made with fluidizer A were somewhat stronger than those made with fluidizer B. Figure 3 also shows that these grouts had much lower permeability than any of the grouts made with fluidizer B, with or without fly ash.

Table 2. Structural parameters of simulated grouted cores.

Grout	Unconfined compressive strength, psi	Cohesion, psi	Angle of internal friction, degrees	Modulus of Elasticity, ksi, at confining pressure		
				0 psi	40 psi	80 psi
R-1	93	19	47	16	14	10
R-2	78	15	48	9	18	12
R-3	53	12	42	9	10	10
R-4	203	55	38	51	23	30
R-5	131	27	47	33	21	26

Ratigan and Goodman[9] reported subsidence model calculations assuming various stiffnesses, as defined by elastic modulus values, of grouted retorts ranging from 0 (i.e., no grout) to 750 ksi (1 ksi = 1000 psi). These calculations indicated that little increased resource recovery would be possible if grouted retort stiffness is less than 50 ksi. Comparison of the results in Table 2 with these calculations shows that none of the grouts tested is stiff enough to provide enough overburden support to appreciably increase resource recovery. Simulated grouted cores, using grout R-4, did have a modulus of elasticity of 50 ksi when tested unconfined, but a lower modulus when tested under confining pressures, suggesting that the higher value could not be used in design.

This work shows that, for grouts which are compliant enough to consolidate under confining pressure (this includes all grouts tested), higher modulus prevents development of low permeability. Because these grouts are not strong enough to provide increased resource recovery, the best approach seems to be to design for lowest permeability. Thus the best grout of those tested here appears to be R-1 or R-2, using fluidizer A and no fly ash. Because the effect of the fluidizer choice is so important, other fluidizers should be screened. Variation between batches may also be important.

PLANNED ACTIVITIES FOR FY 1982

The numerical groundwater flow model development by Mehran et al.[10] will be used to determine the effect of retort grouting on the post-abandonment groundwater flow regime. Other retort abandonment strategies will also be evaluated, including placing a grout curtain around the retort block, intentionally leaching the retorts, and locating retorts in a "dry" zone, i.e., in aquitards rather than aquifiers.

The cured grouts will also be examined by scanning electron microscopy to determine whether any interparticulate bridging can be observed which might explain the effect of fluidizer on permeability.

REFERENCES

1. Persoff, P. (1981), "Development of Low Cost Grouts from Spent Oil Shale," in Energy and Environment Division Annual Report, 1980, Lawrence Berkeley Laboratory Report LBL-11989.

2. Mehta, P.K., and Persoff, P. Use of Waste Materials as Grout Ingredients, manuscript in preparation.

3. Mehta, P.K., and Persoff, P. (1980), "Hydraulic Cement Production from Lurgi Spent Shale," Energy and Environment Division Annual Report, 1979, Lawrence Berkeley Laboratory Report LBL-10486.

4. American Society for Testing and Materials (1978), Book of Standards, Part 14, Standard C 618-78.

5. U.S. Department of the Army (1977), U.S. Army Corps of Engineers Handbook for Cement and Concrete, Standard CRD-C 79.

6. Anonymous (1979), "Preplaced Aggregate Concrete for Structural and Mass Concrete," American Concrete Institute Journal, Oct. 1979, p. 796.

7. Chan, C.K., and Duncan, J.M. (1966), A New Device for Measuring Volume Changes and Pressures in Triaxial Tests on Soils, Institute of Transportation and Traffic Engineering, University of California, Berkeley.

8. Houston, W.N. (1981), Consolidated Drained Triaxial Test, CE 270L Class Notes, University of California, Berkeley.

9. Ratigan, J.L., and Goodman, R.E. (1981), "Structural Requirements for the Abandonment of In-Situ Retorts" in Energy and Environment Division Annual Report, 1980, Lawrence Berkeley Laboratory Report LBL-11989.

10. Mehran, M., Narasimhan, T.N., and Fox, J.P. (1980), An Investigation of Dewatering for the Modified In-Situ Retorting Process, Piceance Creek Basin, Colorado, Lawrence Berkeley Laboratory Report LBL-11819.

Analytical Methods for Quantitating Performance of Oil Shale Wastewater Treatment*

C. G. Daughton,† B. M. Jones, R. H. Sakaji, and J. F. Thomas

The disposal, discharge, or reuse of solid and liquid wastes from oil shale retorting each would necessitate different degrees of waste treatment. Analytical methods for measuring the degree of contaminant removal are essential for treatment research, process control parameters used for the design and operation of treatment facilities, and the establishment of regulatory guidelines. These methods not only must be accurate, precise, and appropriate for the complex and heterogeneous matrices of oil shale wastes, but, equally important, they should have detection limits that permit their application to the experimental scale, while being sufficiently simple for routine use in a commercial treatment plant.

Conventional "standard methods" developed for domestic wastes often yield meaningless design and monitoring data when applied to industrial wastes. This is especially true for "bulk" or colligative properties whose values do not necessarily reflect the degree of attained treatment. For example, the biochemical oxygen demand (BOD) test cannot be used as a measure of pollutant concentration. The BOD of a biologically treated wastewater may well indicate complete treatment when, actually, a large portion of contaminants (i.e., biorefractory compounds) remain unchanged. The BOD test totally relies on the degree of acclimation of the microbial seed and may yield erroneous and inconsistent results for exotic industrial wastes that contain biorefractory compounds; the presence of compounds that can uncouple oxidative-phosphorylation can yield erroneously high values, while insufficient acclimation of the seed can yield artificially low values.

Other "bulk" property methods such as chemical oxygen demand (COD) and dissolved organic carbon (DOC) can be applied to quantitate biorefractory compounds. Tremendous qualitative differences can exist, however, between quantitatively identical values obtained by any bulk-property method. For example, removal of a large portion of DOC (e.g., 80 percent) may be an inadequate degree of treatment if the toxicity, color, and odor of the wastewater are strictly associated with the remaining percentage. The major problems with the application of routine "standard methods" to retort wastewaters have been discussed.[1,2]

The value of nonspecific quantitative data that colligative properties yield can be amplified by qualitative data obtainable from physical manipulation of the samples. There are two basic approaches to quantitating particular chemical classes or particular compounds in heterogeneous mixtures. Compounds can be quantitated by methods of detection that are specific for chemical classes or particular compounds; many of these methods involve colorimetric reactions or derivatization methods that enable specific compounds to be detected by other means such as absorption or emission spectroscopy. Compounds of interest to the analyst ("analytes") each require a specific method of detection. The second approach employs an appropriate means of detection after a prelim-

*This work was supported by the Assistant Secretary of Environment, Office of Environmental Compliance and Overview, Environmental Control Technology Division of the U.S. Department of Energy under Contract No. DE-AC03-76SF00098.
†Sanitary Engineering and Environmental Health Research Laboratory, University of California, Berkeley.

inary step that separates the analyte from the mixture. A separation or "fractionation" pretreatment enables the use of routine bulk-property methods as means of detection that need not be specific. For example, total organic carbon can be used to quantitate organic carboxylic acids if these compounds can be separated from the other organic compounds of a mixture. Qualitative differences can therefore be distinguished between apparently identical values for a given bulk property.

ACCOMPLISHMENTS DURING FY 1981

We have emphasized two approaches in developing analytical methods for quantitating the performance of treatment schemes for oil shale wastewaters. The first approach is improvement and validation of standard methods for bulk properties and development of new methods. We have improved and validated methods for the estimation of microbial biomass in activated sludge by the determination of cellular protein and for the quantitation of dissolved ammonia by a phenol-hypochlorite colorimetric method. A new approach to the determination of dissolved oil in retort wastewaters was developed; this involved separation of the hydrophobic organic solutes from the aqueous mixture by reverse-phase partitioning, followed by detection using infrared spectroscopy.

The second approach has been the development of simple, rapid, chemical-class fractionation procedures that can amplify the limited information yielded by measurement of bulk properties. This approach provides qualitative information that complements the quantitative values of bulk property determinations. For example, DOC and COD values alone are of limited use; identical values for a given property obviously can result from solutions of different compounds. By physically separating solutes into different chemical classes, the subsequent determination of bulk properties can be more informative. A simple means of fractionating aqueous organic solutes is based on relative polarities of the solutes. This can be easily accomplished without the usual risks associated with chemical or physical alteration or contamination of the aqueous sample (e.g., introduction of solvents, acids or bases, or application of heat) by passage of the sample through a miniature reverse-phase liquid chromatography cartridge. The aqueous effluent can then be subjected to conventional analyses.

The following sections delineate the protocols that we have developed for the determination of microbial biomass, ammonia, and dissolved oil and for the fractionation of chemical classes in retort waters.

Microbial Biomass

Microbial biomass concentration is an important parameter to determine for research on the biological treatment of retort waters. It is also an indirect indicator of organic solute removal. The problems associated with routine methods, such as volatile suspended solids and turbidity, have been discussed[1]; these approaches are often thwarted because of the intense and variable color, abiotic particulates, and tarry materials of retort water. A method suitable for research must also have a detection limit sufficiently low to avoid consuming excessive quantities of experimental samples. An alternative approach that gives a more direct approximation to biomass involves the determination of cellular protein, which generally constitutes about 50 percent of the dry cell mass of bacteria.

Theory: Determination of Biomass as Protein. The three major steps in determining cellular protein are: (a) cell harvest, (b) cell digestion (i.e., protein liberation), and (c) quantitation of whole cell protein. Cell harvest concentrates the cells when they are present at low concentrations and separates them from solutes in the extracellular fluid (e.g., free protein and colored substances) that may interfere with the subsequent detection step. Cell harvest is usually done by centrifugation, followed by collection and washing of the pellet. We have employed a more convenient method that uses filtration, washing, and collection of the retentate. Because it is very difficult to remove the retained cells quantitatively, it is necessary to digest the cells while they are still retained by the filter. Basic problems with these steps include representative subsampling of flocculent bacterial cultures, loss of cells during sampling because of sorption to pipette tips and membrane filter holders, cell lysis during washing, and retention by the filter of compounds that interfere with the protein assay. Digestion in alkaline solution solubilizes the whole cell protein. The filter must be able to withstand the digestion and not interfere with the detection of protein. Protein quantitation can be done by numerous methods, most of which involve formation of a reaction product that absorbs light. Two of the most prevalent methods are the Bradford assay,[3] which involves the protein-binding capability of Coomassie Brilliant Blue dye resulting in a shift in the absorption maximum of the dye, and the Lowry assay,[4] which makes use of the chemical reduction of phosphotungstic-phosphomolybdic acid (Folin phenol reagent) by phenols, which include tryptophan and tyrosine amino acids of protein, to yield heterophosphomolybdate blue. The addition of cupric ions in alkali gives a peptide-cupric Biuret reaction which enhances and gives a more reproducible color development with the Folin reagent.

The dye-binding assay suffers from interference by alkali, which necessitates neutralization of the digested samples prior to dye addition, from the necessity of subsampling the digestate, and from the particulate nature of the protein-dye complex which causes erratic absorbance readings when a micro-flow-through cell is used in place of cumbersome cuvettes in a spectrophotometer. Although the Lowry assay has a higher inherent detection limit than the dye-binding assay, procedural stipulations allow the use of much smaller sample sizes during harvest. A major advantage of using the Lowry assay is that the entire procedure can be performed in a single tube, thereby minimizing dilution errors and glassware usage. For these reasons, the Lowry assay has a lower detection limit in practice for this particular application. A major disadvantage is that the color of retort water, in volumes as small as one microliter, can

give μ positive interference; this necessitates thorough rinsing of all extracellular fluid that was entrained by the filter.

Cell harvest can be achieved with many different filters that have nominal pore diameters of 0.2 to 0.45 μm. During digestion, glass-fiber filters and cellulose ester and polycarbonate membranes release silicates, particulates, and phenols that interfere with the Lowry assay. Polycarbonate membranes can be used, however, for the dye-binding assay. Nylon membranes cannot be used for the Lowry assay because of irreversible sorption of the reduced phosphomolybdate complex from solution. The chemical inertness of Teflon membranes has allowed their use in our protocol. Their hydrophobicity, however, necessitates their wetting by methanol to allow passage of aqueous sample, and they must also be restrained under the surface of the digestion solution to ensure contact of the retained cells with the alkali.

Protocol: Determination of Biomass as Protein. This protocol has been discussed in detail.[5] A Teflon membrane filter (25-mm diameter, 0.45-μm pore diameter) is placed in a glass filtration unit. The filter is wetted with 1 ml of methanol and immediately, upon vacuum filtration of the methanol, an appropriate accurately measured volume of dispersed culture is applied to the filter. The retained cells are rinsed with phosphate buffer and methanol to remove tarry materials. The membrane is pushed to the bottom of a screw-capped Pyrex culture tube by a glass rod that rests on the retentate side of the membrane. The glass rod remains inside the tube in order to hold the membrane under 0.5 ml of aqueous 1 N NaOH. The tubes are sealed with Teflon-lined screw caps and placed in a fluidized sand bath at 100°C for 10 minutes. An advantage of a sand bath over a water bath is that the tops of the tubes remain cool, encouraging refluxing; this prevents the leakage of steam through the caps, which would lead to irreproducible losses in the volumes of the digestates. To each of the cooled digestates, 2.5 ml of a solution prepared by addition of 25 parts of 5 percent sodium carbonate to one part of a mixture of 0.25 percent $CuSO_4 \cdot 5H_2O$ and 0.5 percent sodium tartrate is added. After mixing, followed by incubation for 10 minutes at ambient temperature, 0.5 ml of 1.0 N Folin-Ciocalteu Phenol reagent (Sigma Chemical Co.) is added and the solutions immediately mixed. After 30 minutes of incubation at ambient temperature, the absorbance of the samples at 750 nm is read against a reagent blank. Protein values are determined by interpolation from a standard curve prepared from bovine serum albumin standards that were developed in parallel with the samples after digestion.

Dissolved Ammonia

Ammonia and its equilibrium ion, ammonium, are present in wastewaters from oil shale retorting at concentrations generally greater than several hundred parts per million. Only three approaches are available to a routine wet-chemistry laboratory for quantitating the aqueous equilibrium pair as total ammonia: (a) colorimetry, (b) titration, and (c) by direct ammonia-selective electrode. We have validated methods for colorimetry and titration for several oil shale wastewaters.[6] Gas-sensing electrodes, however, proved to be extremely unreliable, probably because fouling of their membranes by retort waters lead to unstable response curves.

Theory: Determination of Ammonia. Ammonia quantitation by titration requires distillation of the ammonia from the water to eliminate the interferences of carbonate alkalinity and color. This is a straightforward method that relies on the pK_a of the ammonium-ammonia equilibrium. If a sample is maintained at a sufficiently high pH and temperature, the equilibrium pair can be stoichiometrically distilled as ammonia gas; if the adjusted pH is too high, digestion of organically bound nitrogen may occur and contribute a positive interference. Organic amines also contribute positive interferences. For this reason, results should be referred to not as "ammonia," but rather as "distillable bases."

Ammonia quantitation by colorimetry without distillation involves the formation of an ammonia reaction product whose molar extinction coefficient is sufficiently high to alleviate interference by the endogenous chromogenicity of the retort water. Routine colorimetric methods include Nesslerization and various adaptations of the indophenol-blue procedure, which is also called the phenate, phenol-hypochlorite, or Berthelot method. This method is based on the Berthelot color reaction catalyzed by nitroprusside[7]:

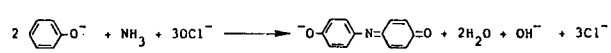

Ammonia is converted to monochloramine between pH 9.7 and 11.5. Monochloramine reacts with phenoxide to form indophenol blue via intermediates, which probably include quinonechloramine.[8] Losses to dichloramine, nitrite, etc. occur above pH 11.5.

The colorimetric phenate method has the major advantage of sample throughput and specificity, although the formation of indophenol can be suppressed by relatively high millimolar concentrations of primary and secondary amines, sulfides, thiols, and certain other reducing agents.[8] In our laboratory, an analyst can perform about 50 determinations per day vs 20 for the distillation/titration method. The colorimetric method is also conducive to automation by segmented-flow or flow-injection analysis. The success of this method, when applied to highly colored retort waters, results from the dilution of the sample by the reagents, which effectively eliminates interference by endogenous chromophores. The disadvantage of the colorimetric method is that several range-finding dilutions may be required to bring the absorbance of an unknown sample within the standard curve range. Precision and accuracy are sacrificed when dilutions are performed, but more significantly, the large ratio of exposed surface to volume of samples contained in measuring devices exacerbates the loss of ammonia by degassing; this problem is magnified by the necessity of measuring small volumes (e.g., microliters). We have found that the most satisfactory solution to this problem is the use of glass capillaries for accurate volume measurement and transfer.

Representative results from the colorimetric procedure are presented with those from the distillation/titration procedure (Table 1) for raw retort waters and for treated retort waters. Mean concentrations determined on different days for a sample type varied because subsamples were obtained from different lots and because of degassing during storage. In addition, with the colorimetric or distillation/titration method, recoveries of ammonia from either biologically spent Oxy-6 retort water or from Oxy-6 gas condensate fortified with 100 to 50,000 ppm ammonia-N have been confined to the 93- to 110-percent range. Slopes of the standard-additions curves were 1.00 (r^2 = 0.9999, n = 11).

Protocol: Determination of Ammonia. Samples are diluted to give total ammonia-N concentrations in the ranges of 10-100 ppm or 100-1000 ppm. Five ml of phenol/nitroprusside reagent (5 g phenol and 25 mg nitroferricyanide dihydrate diluted to 500 ml with water) is added to 20- x 50-mm Pyrex culture tubes with Teflon screw caps. Samples or standards (prepared from ammonium sulfate) are withdrawn with 20-µl TC glass capillaries; the entire capillary is carefully added, and the tube is sealed and shaken vigorously. Immediately after adding 5 ml of alkaline hypochlorite (2.5 g sodium hydroxide and 4.2 ml of 5 percent sodium hypochlorite diluted to 500 ml), the tubes are resealed, shaken vigorously, and immersed in a 37°C bath for 15 minutes. The tubes are cooled to room temperature, and the absorbance vs a reagent blank is read at 635 nm or 520 nm for the low- or high-concentration ranges, respectively.

Chemical Class Fractionation

Ambiguous results are a major drawback of measuring nonspecific "bulk" properties to determine the success of a particular treatment scheme. For example, two different treatment processes may remove entirely different classes of compounds, while the DOC or COD removed by each process may be identical. The value of these parameters could be amplified by physically separating various chemical classes prior to measurement of any bulk property. Usual approaches include "isolation" processes such as liquid-liquid partitioning, ion exchange, or sorption (e.g., onto charcoal or macroreticular resins) and "concentration" methods such as lyophilization and ultrafiltration.[9,10] The isolation schemes usually depend on various sequences of pH adjustment in the acidic, neutral, and basic ranges, followed by extraction with water-immiscible solvents and back-extractions into aqueous phases or passage of the sample through series of exchange resins or sorbents. The fractionated classes are generally permutations of acid, neutral, or basic organic compounds. The solutes are then recovered from the various fractions by selectively removing the water or organic solvent. These procedures risk the chemical or physical alteration or contamination of the sample by the introduction of solvents, acids, bases, and heat. Although these methods are capable of separating many different chemical classes, depending on the complexity of the fractionation scheme, they are too time consuming for use in routine experiments.

Table 1. Evaluation of methods for determination of ammonia in oil shale process waters.

Day of analysis	Method	Sample	x[a]	s	% rsd	n[b]
I	phenate	rw[c]	1131	18.0	1.59	10
II	phenate	rw	1136	31.2	2.75	9
III	phenate	rw	1089	12.8	1.18	10
IV	phenate	gc[d]	7339	102	1.39	10
V	phenate	gc	7214	215	2.98	10
VI	phenate	gc	6757	177	2.62	20
VII	phenate	gc	6759	95.4	1.41	10
VIII	dist/titr[e]	gc	6759	70.1	1.04	5
IX	phenate	gc	149[f]	1.94	1.30	9
X	dist/titr	gc	134[f]	5.86	4.37	5
XI	phenate	TV[g]	2279	31.5	1.38	10

[a]Mean concentration (mg/L NH_3-N).
[b]Number of replicates.
[c]Oxy-6 retort water.
[d]Oxy-6 gas condensate.
[e]Distillation/titration.
[f]Stripped with hot air.
[g]Retort water from a near-commercial surface process.

We have developed a method for separating a wastewater into polar (hydrophilic) and nonpolar (hydrophobic) fractions by passing the sample through a reverse-phase chromatographic cartridge. The method is rapid, and no alteration or contamination of the sample occurs. This crude fractionation step greatly increases the information that can be derived from the subsequent application of colligative detection methods. Moreover, these fractions can be subjected to experimental treatments for comparison with parallel treatment of the raw unfractionated water.

Theory: Chemical Class Fractionation. Reverse-phase chromatography uses a stationary phase that is less polar than the mobile phase, which is commonly water modified with organic solvents. Solvent "strength" (i.e., capacity to elute sorbates or retained compounds) increases with increasing hydrophobicity of the solvent. A typical reverse-phase stationary material is composed of silica particles whose inherently polar surface silanol groups are covalently bonded to aliphatic octadecylsilyl (C-18) groups, which create an immobilized hydrophobic layer around each silica particle.

When an aqueous sample that contains organic solutes is passed through a reverse-phase cartridge, the effluent generally will be unchanged. If the stationary phase is pretreated with a water-miscible organic solvent such as methanol, the less-polar solutes will partition into the hydrophobic stationary phase; the more-polar solutes will remain in the aqueous effluent. The methanol serves to "wet" or "activate" the reverse-phase material. The solutes that partition into the activated stationary phase from the mobile aqueous phase can be eluted with an organic solvent of sufficient strength.

The general principle of reverse-phase separation can be demonstrated by the following experiment. An aqueous mixture of bromophenol blue and p-nitrophenoxide ion is prepared. Bromophenol blue is a relatively hydrophobic intensely purple sulfonphthalein dye substituted by two dibromophenyl groups. p-Nitrophenoxide is a relatively polar bright yellow ionized phenol. The mixture of these two compounds is deep violet. When this mixture is

applied to an unactivated C-18 cartridge, the effluent is deep violet and nothing is retained by the stationary phase. In contrast, when the cartridge is activated, the effluent is bright yellow and the stationary phase becomes deep purple; a water-miscible organic solvent can easily elute the bromophenol blue from the stationary phase. Complete physical separation of the two solutes is thereby effected.

Similarly, the application of retort water to a cartridge containing unactivated C-18 material gives an effluent that is unchanged. Activation of the cartridge with methanol allows retention of a large percentage of the organic solutes. Raw retort water generally is dark brown and has a pungent, tarry smell; these odoriferous characteristics are common to nitrogenous heterocycles. This characteristic odor totally masks the high concentrations of ammonia. The aqueous effluent from an activated C-18 cartridge, however, smells strongly of ammonia, whose odor had been totally obscured by the intense odor of the heterocycles. If the water is removed from this fraction, ammonia is concomitantly removed, and its absence enables the intense odor of fatty acids to be noticed. The aqueous effluent is generally colorless or pale yellow. The reverse-phase packing material has retained nearly all of the color. A large percentage of the retained compounds can be eluted with organic solvent (e.g., methanol). If the organic solvent is removed from the organic eluate, the residuum possesses the odor and color of raw retort water.

Protocol: Chemical Class Fractionation

a. General Procedure. Miniature C-18 cartridges are available from several manufacturers (e.g., C-18 Sep Paks from Waters Assoc., Inc., Milford Mass.). These cartridges contain about 400 mg of packing material. Activation is achieved by applying 5 ml of methanol to the cartridge, followed by rinsing with 5 ml of water. The sample is then passed through the cartridge at a sufficiently slow rate (e.g., 5-30 ml/min); the total quantity applied must be predetermined from breakthrough experiments. The initial milliliter of aqueous effluent is discarded because of its dilution by the water that remained from activation of the cartridge. Subsequent aqueous effluent can be collected for analysis or for subjection to treatment schemes.

The retained organic compounds can be eluted after residual aqueous sample is rinsed from the cartridge. The solvent used for initial elution must be mutually miscible in water and in whatever strong solvent may be subsequently used. Compounds of different polarities will be eluted depending on the strength of the organic solvent. Methanol elutes nearly all of the compounds that have not been irreversibly bound to the stationary phase; less polar solvents will not elute the more polar compounds. We have used this protocol routinely in our biological and physicochemical treatment research.[11,12]

b. Oil and Grease Procedure. The problems with the determination of oil and grease in retort water by the standard gravimetric liquid-liquid partitioning method have been discussed.[1] Consequently, we have adapted our general fractionation procedure to the determination of dissolved oil and grease (Fig. 1).[13] The analytes, which are hydrophobic, are retained by the stationary phase; the aqueous effluent is discarded. At this point in the protocol, the basic procedure is modified because the method of detection precludes use of a "switchover" solvent of mutual miscibility. The aqueous residuum in the cartridge must therefore be removed by mechanical means, best achieved by lyophilization. The nonpolar compounds (oil and grease) can then be eluted with Freon (1,1,2-trichloro-1,2,2-trifluoroethane) and quantitated by infrared spectroscopy by measuring absorbance from the C-H stretch at 2930 cm^{-1} (Fig. 2). True aliphatic oil can be determined by passing the Freon

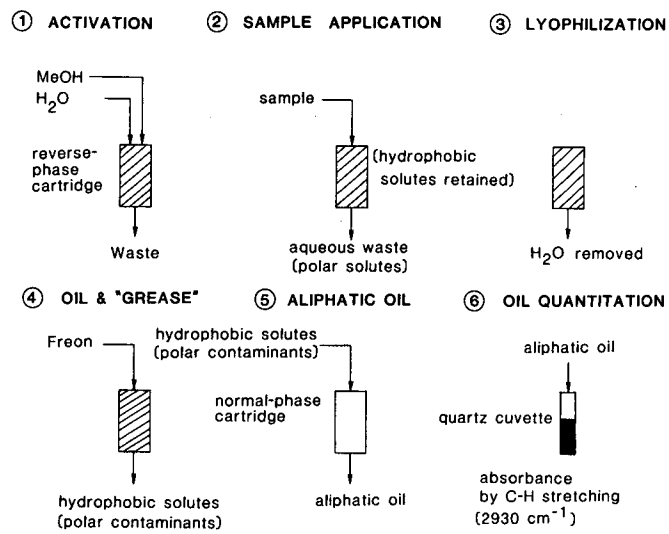

Figure 1. Reverse-phase chromatographic/infrared spectroscopic method for wastewater oil.
(XBL 817-10839)

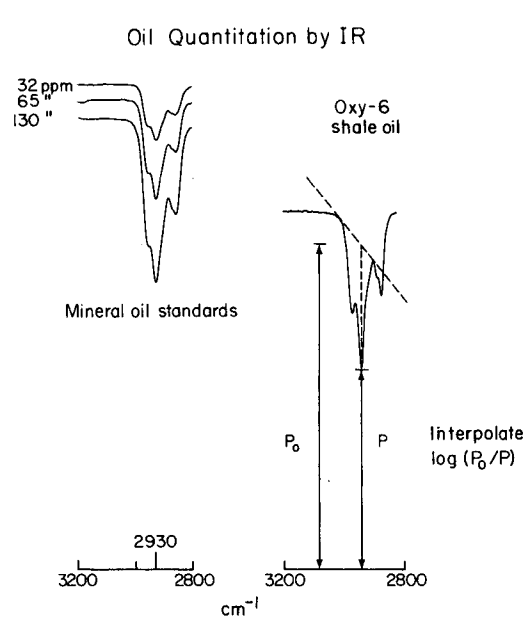

Figure 2. Quantitation of oil in oil shale retort water by IR absorbance and comparison to mineral oil standards. (XBL 814-688)

eluent through a normal-phase activated silica cartridge, which would remove solutes that contained functional groups. An additional advantage of the reverse-phase fractionation method for determining oil and grease is that routine methods such as DOC and COD can be used to quantitate the retained compounds. This can be done indirectly by analyzing the unfractionated sample and the aqueous effluent and calculating the difference.

PLANNED ACTIVITIES FOR FY 1982

Routine methods are essential for the quantitation of organic nitrogen in retort waters. Kjeldahl digestions are the standard method but are very time consuming and yield incomplete recoveries of heterocyclic nitrogen. We plan to investigate the quantitation of organic nitrogen by pyrochemiluminescence.

We are currently developing an organic carbon analyzer that uses low-temperature, UV-persulfate oxidation coupled with coulometric titration. This would have decided advantages in speed and accuracy over commercial units that employ either high-temperature combustion or non-dispersive infrared detection.

ACKNOWLEDGMENTS

We thank J. Cantor, G. Langlois, and K. Yu, laboratory technicians of the LBL-SEEHRL Oil Shale Wastewater Treatment Program, for their capable assistance.

REFERENCES

1. Daughton, C.G., Jones, B.M. and Sakaji, R.H. (1981), "Analytical Problems in Monitoring Retort Water Treatment," in Energy and Environment Division Annual Report 1980, Lawrence Berkeley Laboratory Report LBL-11989.

2. Wallace, J.R. (1981), "The Analysis of Oil Shale Wastes: a Review," Denver Research Institute Report, EPA 600/7-81-084 (NTIS PB81-190522).

3. Bradford, M.M. (1976), "A Rapid and Sensitive Method for the Quantitation of Microgram Quantities of Protein Utilizing the Principle of Protein-Dye Binding," Anal. Biochem. 72, pp. 248-254.

4. Lowry, O.H., et al. (1951), "Protein Measurement with Folin Phenol Reagent," J. Biol. Chem. 193, pp. 265-275.

5. Yu, K., et al. (1981), "Protein Assay Protocol," in LBL-SERL Oil Shale Wastewater Treatability Project.

6. Cantor, J., et al. (1981), "Quantitation of Ammonia in Oil Shale Process Wastewaters," in LBL-SEEHRL Oil Shale Waste Treatment Program, Lawrence Berkeley Laboratory Report LBID-465.

7. Scheiner, D. (1976), "Determination of Ammonia and Kjeldahl Nitrogen by Indophenol Method," Water Res. 10, pp. 31-36.

8. Ngo, T.T., et al. (1982), "Interference in Determination of Ammonia with the Hypochlorite-Alkaline Phenol Method of Berthelot," Anal. Chem. 54, pp. 46-49.

9. Leenheer, J.A. and Farrier, D.S. (1979), "Applications of Dissolved Organic Carbon Fractionation Analysis to the Characterization of Oil Shale Processing Waters," in EPA Oil Shale Symposium: Sampling, Analysis and Quality Assurance, Denver, CO, March, 1979, pp. 273-285.

10. Jolley, R.L. (1981), "Concentrating Organics in Water for Biological Testing," Environ. Sci. Technol. 15, pp. 874-880.

11. Jones, B.M., et al. (1982), "Microbial Aspects of Oil Shale Wastewater Treatment," in Energy and Environment Division Annual Report 1981, Lawrence Berkeley Laboratory Report LBL-13500.

12. Sakaji, R.H., et al. (1982), "Processes for the Physico-Chemical Treatment of Oil Shale Wastewaters," in Energy and Environment Division Annual Report 1981, Lawrence Berkeley Laboratory Report LBL-13500.

13. Daughton, C.G., Jones, B.M., and Sakaji, R.H. (1981), "Oil Shale Wastewater Treatment: Analytical Methods Development" (invited paper), 53rd Annual California Water Pollution Control Association Conference, Long Beach, California, April 29-May 1, 1981.

Microbial Aspects of Oil Shale Wastewater Treatment*

B. M. Jones, R. H. Sakaji, J. F. Thomas, and C. G. Daughton†

To effectively investigate the microbial oxidation of contaminative organic solutes of a waste stream, the chemical and physical properties of the wastewater should be accurately characterized and the anticipated flow streams should be clearly delineated. The chemical characteristics of the major wastewaters from the pilot-scale retorting of oil shale have been tremendously variable, both within and among individual waste streams. The type of retorting process, the water-collection configuration, and the source of oil shale contribute to this variability. To minimize the problems of intra-sample variation and to allow for interlaboratory comparison and confirmation of experimental results, our research has concentrated on composited samples of modified in-situ (MIS) retort water and gas condensate from Occidental Oil Shale Company's retort burn #6 (Oxy-6).[1,2]

Gas condensate contains extremely high concentrations of dissolved gases such as ammonia and carbon dioxide. In contrast, retort water is characterized by a more complex spectrum of polar and nonpolar organic solutes of higher concentrations. The major classes of organic compounds include alkanes, carboxylic acids, polyhydric phenols, and nitrogenous and oxygenated heterocycles.[3] The extreme levels of contaminative organic solutes, the presence of surfactants, suspended oil, tars, and particulates, the possibility of toxicity to microorganisms, the high level of dissolved inorganic salts and gases, and the undesirable color and odor of these wastes frustrate both the application of established pollution control technologies and the determination of treatment performance by standard analytical methodologies.[4,5]

In addition to being highly contaminated with organic and inorganic constituents, these waters will be produced in voluminous quantities. An ironic complication that would confound water management schemes is that oil shale retorting often requires steam, yet oil shale deposits are in semi-arid regions of Colorado, Utah, and Wyoming. Industrial water requirements and wastewater disposal are major environmental issues associated with the development of a commercial oil shale industry. Treatment goals, reuse options, and technical strategies have required a fresh research perspective and innovative technical solutions.

Biological treatment is the conventional technique that is applied for the removal of organic contaminants from a wastewater stream. An acclimated microbial community can effect the conversion of dissolved organic solutes into cellular biomass, heat, and gases. This scheme can fail, however, if

(a) The resultant cells are not separable from the liquid,

(b) Nutrients essential for growth are not available in the solution,

(c) Components of the medium are toxic to the microorganisms,

(d) The microorganisms that are present are enzymatically incapable of mineralizing the organic material, or

(e) A large portion of the compounds present is inherently resistant to microbial alteration.

Oxy-6 retort water can easily support microbial growth without the addition of any nutrients. Our experiments have shown, however, that conventional biological treatment without extensive enrichment for and acclimation of appropriate organisms is incapable of degrading more than 50 percent of either the chemical oxygen demand (COD) or the dissolved organic carbon (DOC); the remaining solutes may have been altered, but total mineralization was not accomplished. We have found[1] that increasing the concentration of Oxy-6 retort water in a basal salts medium from 10 to 50 percent depresses the cellular yield (protein synthesized per unit volume of retort water); in contrast, cellular yields from media with higher concentrations of retort water (50 to 83 percent) remained constant. We concluded that this retort water exerts a slightly toxic effect and have chosen to work with 50-percent dilutions of retort water in subsequent experiments to facilitate inter-experiment comparison. To effect more extensive catabolism of the remaining organic solutes, alternative aspects of microbial metabolism must be explored.

ACCOMPLISHMENTS DURING FY 1981

The major foci of our work on the microbial alteration and degradation of oil shale process waters have been the determination of optimum treatment efficiencies obtainable and the elucidation of factors that limit biooxidation. Attempts to alleviate these limitations included nutrient addition, extensive microbial enrichment and acclimation, implementation of novel aspects of microbial metabolism, and chemical and physical pretreatment. The limiting microbial nutrients in Oxy-6 retort water have been identified as endogenous inorganic orthophosphate and bioavailable carbon. We have investigated novel aspects of microbial metabolism for the degradation of nor-

*This work was supported by the Assistant Secretary of Environment, Office of Environmental Compliance and Overview, Environmental Control Technology Division of the U.S. Department of Energy under Contract No. DE-AC03-76SF00098.

†Sanitary Engineering and Environmental Health Research Laboratory, University of California (Berkeley), Richmond, California 94804 (associated faculty).

mally recalcitrant organic solutes. The integration of biological treatment with physical or chemical pretreatment of retort water has met with qualified success.

To understand the limitations of microbial catabolism of the organic solutes in oil shale process water, we have conducted an ongoing series of experiments using batch culture. Batch culture favors the examination of the dynamics of bacteriological growth and concomitant substrate removal. Its major advantage over continuous culture is the small scale, which allows for many simultaneous experimental treatments. Our experiments generally involved incubating the wastewater, supplemented with basal salts and experimental additions, in the presence of an acclimated microbial community derived from sewage, soil, and industrial sources in 250-ml baffled Erlenmeyer shake flasks at 30°C. Microbial growth was monitored via turbidity, a facile nondestructive indicator of cellular growth; and, when growth had apparently ceased (stationary phase) and specific nutrients became limiting, the cultures were sampled for protein (biomass) and the extracellular fluids were analyzed for DOC concentration.

Nutrient Limitation

The three major macronutrients required by microorganisms are carbon, nitrogen, and phosphorus. Retort water is characterized by high concentrations of carbon and nitrogen, whereas determinations of phosphorus have rarely been obtained. To demonstrate if inorganic orthophosphate (P_i), the universally utilized form of phosphorus, was the primary nutrient limiting further growth in Oxy-6 retort water, cellular yields (i.e., mass of protein produced per mmol of P_i consumed) were determined. Shake flasks containing 50-percent retort water, supplemented with various concentrations of P_i and nonlimiting amounts of Mg, were inoculated with acclimated bacteria that had been grown on retort water without added P_i, to ensure that storage of intracellular polyphosphates had not occurred. Protein and DOC concentrations were determined immediately after inoculation and when stationary phase had been attained. Limitation of growth by P_i in 50-percent dilutions of Oxy-6 retort water was verified by the linear increase in biomass concentration with increasing concentrations of P_i up to approximately 0.10 m$\underline{M}$ P_i (Fig. 1). Concentrations of P_i greater than 0.10 m$\underline{M}$ did not increase cellular densities at stationary phase nor enhance substrate removal; approximately 50 percent of the initial DOC remained in solution at stationary phase. By extrapolation of the curve for protein production versus P_i amendment, the endogenous P_i concentration was calculated. This "bioassay" for endogenous P_i gave a concentration of 0.03 m$\underline{M}$ P_i for unmodified raw water (Fig. 1). After supplying P_i in nonlimiting concentrations, the addition of other essential nutrients (Fe and Mg), trace metals, and vitamins did not enhance organic carbon removal. The absence of another essential nutrient was limiting microbial growth.

To investigate this secondary nutrient limitation and to examine the dynamics of microbial

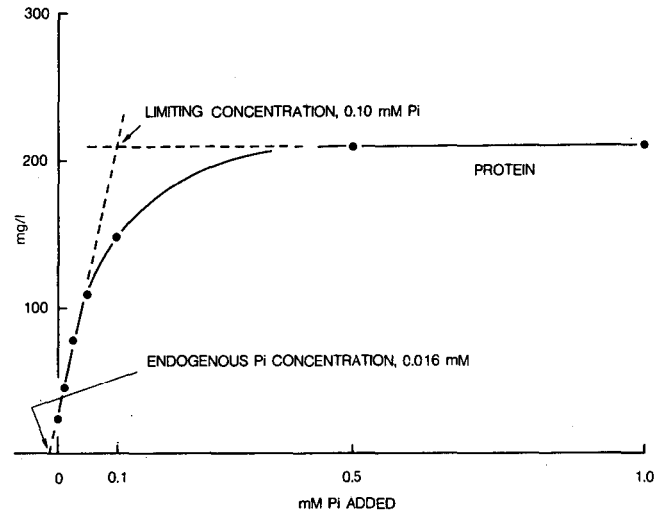

Figure 1. Effect of inorganic orthophosphate on protein synthesis: microbial growth on 50-percent retort water. (XBL 817-10840)

growth in Oxy-6 retort water, we initiated a long-term batch culture experiment. Three liters of 50-percent Oxy-6 retort water, supplemented with 20 m$\underline{M}$ P_i, was inoculated with acclimated microbial seed, aerated with humidified compressed air, stirred, and incubated at 30°C. The parameters of turbidity, absorbance (450 nm), pH, and concentrations of COD, DOC, and cellular protein were monitored throughout the study (Fig. 2). The microbial assemblage grew exponentially after a short lag phase, as indicated by turbidity and protein concentration. The biomass of the outgrown culture decreased slightly. During exponential growth, there was a concomitant decrease in organic solute concentration, as measured by COD or DOC. With the onset of stationary phase, the solute concentration reached a lower, constant value. Initial COD and DOC concentrations were reduced 51 and 54 percent, respectively, and continued monitoring for five days revealed neither further reductions in sub-

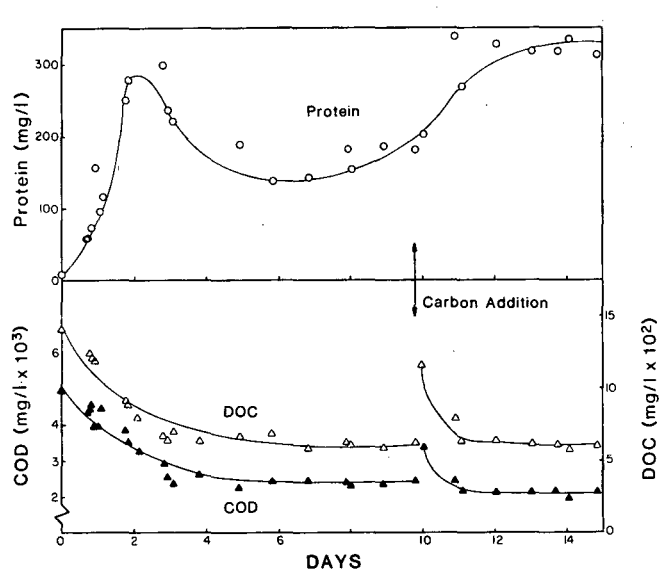

Figure 2. Effect of carbon amendment on bacterial growth (50-percent retort water). (XBL 821-7910)

strate concentrations nor the induction of microbial growth on new substrates (diauxic growth). At the conclusion of biological treatment, neither the dark color nor the distinctive odor, both thought to be associated with nitrogenous heterocycles of the nonpolar fraction of solutes,[5] was reduced, although the odor was altered.

Upon cessation of growth and concomitant solute removal, the solutes in the expended extracellular fluid ("spent retort water") were apparently biorefractory. We have assumed that the organic solutes in the wastewater fall into two classes[6]: "soft," or easily degradable, and "hard," or inherently resistant to biological oxidation. The "soft" fraction probably consists of alkanes and carboxylic acids. This hypothesis has been corroborated by the demonstration of the rapid microbial degradation of benzoic and a homologous series of both aliphatic mono- and dicarboxylic acids in oil shale retort water.[7] The nonpolar substituted heterocycles and polyhydric phenols presumably compose a major portion of the recalcitrant or refractory solutes.[8]

From our experimental results and according to our hypothesis, bioavailable carbon was the essential nutrient that was responsible for the secondary limitation to microbial growth; the carbon remaining in solution at the exhaustion of the initial microbial activity appeared to be biorefractory. To demonstrate that carbon became the limiting growth factor in the long-term batch culture experiment, easily degradable carbon sources were added to the outgrown culture. Two successive additions of carboxylic acids (sodium acetate and disodium succinate, each as 25 m$\underline{M}$ carbon) elicited renewed microbial growth (Fig. 2). We concluded that, after satisfying the P_i requirement, the remaining organic solutes were recalcitrant to biological oxidation. Toxicity and trace nutrient availability were probably not significant factors.

The addition of carboxylic acids to the outgrown culture resulted in an immediate and expected increase in substrate concentration, as measured by COD and DOC. These concentrations were reduced by microbial activity and the DOC concentration returned to its value before the carbon addition. In contrast, for both carbon supplements, the COD values were reduced to values below the preaddition concentration. We have postulated that the remaining biorefractory organic compounds may have been partially oxidized, but not mineralized, to yield a lower COD, i.e., the "specific COD" decreased.[4]

The partial oxidation of the organic compounds without their mineralization was indicative of either incomplete microbial enzyme complements or the accidental "fortuitous" alteration (cometabolism) of resistant compounds without the derivation of carbon or energy by enzymes whose synthesis was intended for the catabolism of other compounds. If carbon and energy requirements are supplied by an easily degradable substrate (in this case carboxylic acids), it is possible that recalcitrant substrates may have been adventitiously altered without microbial nutritional benefit. Mineralization of refractory compounds can be effected by sequential cometabolic attack by a series of bacterial species. To encourage cometabolism, we added biodegradable analogs of substances that presumably constitute the major fraction of the refractory solutes. The addition of phenol (20 m$\underline{M}$ as C) to the batch culture stimulated a small delayed growth response; alteration of the recalcitrant compounds, however, was not evident. Results from the addition of quinoline (30 m$\underline{M}$ as C), a nitrogenous heterocycle, were inconclusive. In subsequent work with defined culture media, we selectively enriched for enzymatically competent bacteria by supplying quinoline as a sole carbon source. The resultant community appeared to alter quinoline and produce a highly pigmented byproduct. When transferred into spent retort water, this inoculum was unable to effect any detectable changes in the solute composition. Although our results have not been definitive, the concepts of cometabolism and analog enrichment for the eventual degradation via sequential alterations of recalcitrant solutes remain as novel approaches to biological treatment of retort water.

Preliminary experiments on the biotreatment of Oxy-6 gas condensate have yielded suprising results. We had speculated that the organic species of gas condensate would be predominantly lower-molecular-weight volatile organic compounds derived from retort off-gases. We had predicted that these species would be amenable to biodegradation. Repeated attempts using many sources of inocula have failed to establish any microbial growth in gas condensate. Toxicity was not a factor because the addition of easily degradable fatty acids to gas condensate yielded dense microbial growth. We have hypothesized that the organic solutes in Oxy-6 gas condensate are similar to compounds in the recalcitrant fraction of Oxy-6 retort water.

Nitrogenous Heterocycle Degradation

If biological treatment of retort water could be optimized, it would be an expedient means of upgrading oil shale wastewaters for reuse. We are concentrating our research efforts on enhancing the microbial degradation of the recalcitrant nonpolar solutes, which we suspect are predominantly heterocyclic compounds. A major factor in this recalcitrance may be that the requisite ring-cleaving enzymes are inducible only for the abstraction of nitrogen from the heterocycles. Such nitrogen-abstraction enzymes would normally be repressed by the presence of an easily utilizable inorganic nitrogen source such as ammonia or nitrate. If this supposition is correct, the high concentration of ammonia in retort water may be a major factor for the recalcitrance of the nitrogen heterocycles. Another consideration is that, although the collective concentration of nitrogen heterocycles in retort water may be high, large numbers of these compounds may be present at concentrations significantly lower than their respective enzyme affinity constants.[8,9]

A survey of the literature has revealed that the metabolism of nitrogen heterocycles has been only superficially investigated. The availability of exogenous nitrogen and carbon and energy sources

has direct influence on the metabolism of these compounds.[10-12] Elimination of available ammonia would be one approach to encouraging the induction of the requisite enzymes for nitrogen heterocycle ring cleavage. This possibly could be accomplished by steam or air-stripping. These processes, however, may be incapable of removing sufficient quantities of ammonia to reach growth-limiting values. Low concentrations of ammonia can support microbial growth since the cellular demand ratio for carbon to nitrogen is relatively high (12-25:1)[13]; the possibility of the presence of nitrate exacerbates the problem. An alternative approach has been delineated.[8] This method involves the selective enrichment for bacteria that can utilize nitrogenous heterocycles analogous to those in the wastewater as sole sources of nitrogen in defined media. The ideal model substrates would be compounds from retort water that partition into reverse-phase chromatographic packing material.[5] These compounds are effectively separated from the ammonia, which is totally unretained, and are the exact solutes that require degradation. The resultant microbial cells would contain high levels of derepressed enzymes for nitrogen abstraction. The cellular mass could then be harvested and added to spent or raw retort water. The synthesis of nitrogen-abstraction enzymes would be repressed by the ammonia in the raw retort water, but the previously synthesized enzymes would be active in degrading nitrogenous heterocycles, unless their activity were completely inhibited by the presence of ammonia. We have been unable, however, to grow sufficient quantities of cells on nitrogen heterocycles for introduction into retort water. These preliminary results should not be viewed as totally discouraging because it has been reported that the isolation of bacteria on xenobiotics as nitrogen sources is relatively rare.[12]

Organic Solute Distribution

When the organic solutes of Oxy-6 retort water were separated into polar and nonpolar fractions, via reverse-phase chromatography,[5] 55 percent of the DOC was associated with the polar fraction and 45 percent with the nonpolar. As previously discussed, approximately 50 percent of the DOC was consistently removed from unfractionated Oxy-6 retort water by exhaustive biological treatment. As a corollary to the previously presented model of the two classes of organic compounds in Oxy-6 retort water, we have proposed that the recalcitrant species in Oxy-6 retort water would be associated predominantly with the nonpolar fraction; the polar solutes would be the exclusive sources of carbon and energy for the microbial community in the unfractionated raw water.[14]

To investigate this contention, polar and nonpolar organic fractions of Oxy-6 retort water were prepared by reverse-phase partitioning. The nonpolar solutes were redissolved in ASTM Type I water, and both fractions were diluted to yield 50 percent of their concentrations in raw retort water. Each fraction was supplemented with P_i, inoculated with bacteria acclimated to 50-percent unfractionated retort water, incubated, and analyzed for DOC content at time zero and at stationary phase. Although the results from replicate experiments were not as unambiguous as we had anticipated, the majority of the recalcitrant solutes appeared to be associated with the nonpolar fraction (Table 1). Each fraction supported microbial growth and neither was totally degraded; approximately three times more carbon, however, was utilized from the polar than from the nonpolar fraction. This evidence supported our hypothesis that the biorefractory solutes were predominantly nonpolar solutes, such as nitrogenous and oxygenated heterocycles.

One possibility for the limitation of microbial growth on the nonpolar fraction was that the buffering capacity and essential inorganic nutrients of the raw water were separated from the retained solutes because they were strictly associated with the aqueous polar effluent. The addition of supplementary ammonium chloride, trace metals, and phosphate buffer for pH control did not

Table 1. Bacterial removal of DOC from Oxy-6 retort water fractionated by reverse-phase separation (four experiments).

Fraction[a]	Dissolved organic carbon concentration (mg/l)							
	I[b]		II[c]		III[d]		IV[d]	
	Initial	Δ[e]	Initial	Δ	Initial	Δ	Initial	Δ
Control (unfractionated)	1575	865	1496	656	1471	838	1432	817
	1.0[f]	55[g]	1.0	44	1.0	57	1.0	61
Polar	752	455	746	513	835	642	819	643
	0.48	63	0.50	69	0.57	77	0.57	79
Nonpolar	807	199	646	200	NR[h]	NR	NR	NR
	0.51	24	0.43	31				
Nonpolar + N[i]	NR	NR	646	256	657	208	632	314
			0.43	39	0.45	32	0.44	50
recombined polar + nonpolar	NR	NR	1408	777	1516	842	1427	1029
			0.94	55	1.0	56	1.0	72

[a]Each control and fraction of Oxy-6 retort water was diluted 50% prior to inoculation.

[b]Recycled reverse-phase cartridge was not rinsed before elution.

[c]Recycled reverse-phase cartridge was rinsed with 2 ml ASTM Type I water; rinse discarded

[d]New reverse-phase cartridge was rinsed with 2 ml ASTM Type I water; rinse pooled with polar fraction.

[e]DOC removed by biooxidation.

[f]Portion of DOC in fraction compared with initial unfractionated DOC.

[g]% of DOC removed by biooxidation compared with initial DOC.

[h]Experiment not run.

[i]Supplemented with 2.5 mM ammonium chloride.

encourage further mineralization of the nonpolar solute fraction. In addition, recombination of the two separated fractions did not enhance DOC removal as compared with unfractionated retort water. Furthermore, the carbon in Oxy-6 gas condensate was almost exclusively composed of nonpolar compounds (82 percent nonpolar, 18 percent polar); neither fraction was able to support microbial growth. These results support our proposal that the organic compounds in gas condensate are analogous to the recalcitrant species in retort water.

In a parallel set of experiments, the sorption of polar and nonpolar constituents by spent shale was investigated.[15] These results indicated that TOSCO II spent shale preferentially sorbs nonpolar organic compounds from Oxy-6 retort water and has a very low sorptive affinity for the easily biodegradable polar components.[16] A dosage of 750 mg/ml of spent shale removed 52 percent of the DOC from the nonpolar fraction whereas virtually no sorption (3 to 4 percent) of polar organic solutes occurred. These findings verify our hypothesis that spent shale sorption and biological oxidation are complementary processes for the treatment of oil shale retort water.[14,16,17]

Integration of Biological and Physico-Chemical Treatment

It is unlikely that one method will be totally effective for oil shale wastewater treatment. A particular method may be extremely effective for the removal of specific classes of organic compounds; when applied to a heterogeneous mixture such as retort water, however, it may be able to remove only a fraction of the contaminative solutes. To effectively treat these waters, a combination of treatment methods that have complementary capabilities will be required in either sequential or simultaneous applications. The integrated processes should be evaluated carefully because the final degree of treatment can be additive (the sum of the individual processes), antagonistic (lower than either of the processes), or synergistic (greater than the sum of the processes).

The sequential and simultaneous integration of biological and sorbent treatments were investigated to determine if these two processes removed complementary classes of organic solutes which would result in an additive degree of treatment. Acclimated bacteria incubated in shake-flask cultures containing first-pore-volume effluent of Oxy-6 retort water (50 percent) from a column of TOSCO II spent shale[16] were able to effect the removal of 65 percent of the remaining organic solutes. This represents a total removal of 80 percent of the DOC by the sequential application of spent shale and biological oxidation. In addition, the cellular yields (g protein/mol C removed) from the shale-pretreated water were significantly higher than in control cultures of raw water (3.8 g/mol vs 2.7 g/mol). This suggests that the spent shale may have reduced the osmolality or removed some of the toxic compounds from the retort water, enabling the bacteria to expend less energy on maintenance and more on cellular reproduction. The total DOC removal from the third pore volume of effluent was 65 percent, and the growth yield was 3.5 g/mol. When the sequence of these two processes was reversed, the removals of DOC were equivalent. Batch sorbent equilibrium experiments[16] were conducted using 750 mg/ml of TOSCO II spent shale added to spent retort water. The total DOC removal was 75 to 78 percent. These results indicated that the two processes, spent shale and biological treatment, removed complementary fractions of DOC because the individual removals were additive regardless of the combined process sequence.

The possibility of a synergistic relationship between treatment processes was investigated by the simultaneous application of biological and sorbent treatment methods. Preliminary observations of enhanced DOC removals from the direct combination of these two processes led us to speculate that the sorptive surfaces may serve to concentrate the refractory compounds normally present in excessively low concentrations and thereby allow for enzymic transformations of the compounds followed by desorption of the metabolites. Since the sorbent surfaces would be renewed, they could be considered as serving a catalytic role. To test the premise of enhanced solute removal by simultaneous application of treatment methods, small dosages of TOSCO II spend shale, Anvil Points raw shale, or I.C.I. powdered activated carbon (PAC) were added to inoculated raw or spent retort water (in a manner analogous to powdered activated carbon treatment, i.e., PACT process). The results from the simultaneous use of spent shale and biological treatment have not been reproducible. Catalytic dosages of spent shale (10-100 mg/ml) resulted in zero to six percent enhancement of DOC removal above that obtained from summing the effects of biological and sorbent treatments along (Table 2). Higher dosages of spent shale (500 mg/ml) in combination with microbial treatment resulted in eight percent enhanced DOC removal and yielded 74-percent overall removal of DOC; this is within the range of removals observed for the sequential application of these treatment methods. Unactivated raw shale was an ineffective sorbent; DOC reduction attributable to a synergistic relationship between treatment

Table 2. Percent DOC removal from 50 percent dilutions of Oxy-6 retort water by combined biological/sorbent treatment.

	% DOC Removal from Inoculated Retort Water			
Sorbent	Total	Sorption	Biodegradation	Enhancement[a]
PAC[b]				
0.13 mg/ml	52[c]	1	51	nil
1.3 mg/ml	62	10	47	4
6.6 mg/ml	85	36	50	nil
Spent shale[d]				
10 mg/ml	54	nil	51	2
100 mg/ml	57	10	50	nil
500 mg/ml	74	16	50	8
Raw shale[e]				
25 mg/ml	52	nil	47	5

[a]Total % removal minus removals from biodegradation and sorption.

[b]Powdered activated carbon (I.C.I.), 12-40 mesh.

[c]Percent reduction from raw 50% Oxy-6 retort water.

[d]TOSCO II spent shale, 60-80 mesh.

[e]Anvil Points raw shale, 60-80 mesh.

processes was five percent. Catalytic dosages of PAC (0.13 mg/ml to 1.3 mg/ml) were responsible for enhanced DOC removals of zero to four percent. Higher dosages of PAC (6.6 mg/ml) in direct combination with an acclimated microbial inoculum did not result in a synergistic effect, but 85 percent of the DOC was removed and the color of the wastewater was substantially reduced. This is the greatest degree of treatment we have observed for an MIS retort water. In essence, the simultaneous application of treatment processes, however, did not produce a significant degree of enhanced treatment above the additive effects of the processes.

PLANNED ACTIVITIES FOR FY 1982

A major research topic will be the biodegradation of nitrogenous heterocycles. The selective enrichment for competent microorganisms will continue by seeking new sources of inocula, and the concepts of cometabolism and analog enrichment for the alteration and eventual degradation of biorefractory compounds will be pursued. Work will continue on the induction of nitrogen-abstraction enzymes; specific nitrogenous heterocycles and recalcitrant retort water organic solutes will be provided as sole sources of nitrogen, carbon, and energy for acclimated bacteria. In addition, the possibility of growth limitation by the propensity of nitrogenous heterocycles to sequester essential growth factors and trace metals will be addressed. The successful integration of physicochemical and biological treatment methods will be investigated; the effect of environmental factors on the treatability of the waters will be identified.[16] Biological treatment methods will also be evaluated for wastewaters produced from the surface retorting of oil shale.

ACKNOWLEDGMENTS

We thank J. Cantor, G. Langlois, and K. Yu, laboratory technicians of the LBL-SEEHRL Oil Shale Wastewater Treatment Program, for their capable assistance.

REFERENCES

1. Jones, B.M., Sakaji, R.H., and Daughton, C.G. (1981), "Treatment of Wastewater from Modified In-Situ Oil Shale Retorting," in Energy and Environment Division Annual Report 1980, Lawrence Berkeley Laboratory Report LBL-11989.

2. Daughton, C.G., and Sakaji, R.H. (1980), Communication to D. Sheesley and R. Poulson, "Oxy-6 Retort Water: Preparation of Composite Sample", 9 July 1980.

3. Torpy, M.F., and Raphaelian, L.A. (1981), "Organics Constituent Analysis and Biological Treatment of Oxy-6 Water-Research Program Study," in Oil Shale Wastewater Treatability Workshop; Mathtech, Inc., Arlington, VA., 5 March 1981, pp. 125-126.

4. Daughton, C.G., Jones, B.M., and Sakaji, R.H. (1981), "Analytical Problems in Monitoring Retort Water Treatment," in Energy and Environment Division Annual Report 1980, Lawrence Berkeley Laboratory Report LBL-11989.

5. Daughton, C.G., et al. (1982), "Analytical Methods for Quantitating Performance of Oil Shale Wastewater Treatment," in Energy and Environment Division Annual Report 1981, Lawrence Berkeley Laboratory Report LBL-13500.

6. Jones, B.M., et al. (1981), "Removal of Contaminative Constituents from Retort Water: Difficulties with Biotreatment and Potential Applicability of Raw and Processed Shales," in Oil Shale Wastewater Treatability Workshop; Mathtech, Inc., Arlington, VA., 5 March 1981, pp. 127-131.

7. Rogers, J.E., et al. (1981), "Microbiological Degradation of Organic Components in Oil Shale Retort Water: Organic Acids," Appl. Environ. Microbiol., 42, pp. 830-837.

8. Daughton, C.G. (1981), "Biodegradation of Heterocycles in Synfuels Wastes," DOE Invention Case #IB-417.

9. Raphaelian, L.A., and Harrison, W. (1981), Organic Constitutents in Process Water from the In-Situ Retorting of Oil from Oil-Shale Kerogen, Argonne National Laboratory Report ANL/PAG-5.

10. Naik, M.N., et al. (1972), "Microbial Degradation and Phytotoxicity of Picloram and Other Substituted Pyridines," Soil Biol. Biochem., 4, pp. 313-323.

11. Watson, G.K., and Cain, R.B. (1975), "Microbial Metabolism of the Pyridine Ring," Biochem. J., 146, pp. 157-172.

12. Cook, A.M. and Hütter, R. (1981), "s-Triazines as Nitrogen Sources for Bacteria," J. Agric. Food Chem., 29, pp. 1135-1143.

13. Cook, A.M., Daughton, C.G., and Alexander, M. (1978), "Phosphonate Utilization by Bacteria," J. Bacteriol., 133, pp. 85-90.

14. Jones, B.M., Sakaji, R.H., and Daughton, C.G. (1982), "Oil Shale Wastes: Fundamental Approaches to Treatment," in Proceedings of the 2nd DOE Workshop for Processing Needs and Methodology for Contaminated Water Streams from Synfuels, Germantown, Maryland, 1982 (in press); Lawrence Berkeley Laboratory Report LBL-13033.

15. Sakaji, R.H., Jones, B.M., and Daughton, C.G. (1981), "Raw and Spent Shale for the Treatment of Oil Shale Process Waters," in Energy and Environment Division Annual Report 1980, Lawrence Berkeley Laboratory Report LBL-11989.

16. Sakaji, R.H., et al. (1982), "Processes for the Physicochemical Treatment of Oil Shale Wastewaters," in Energy and Environment Division Annual Report 1981, Lawrence Berkeley Laboratory Report LBL-13500.

17. Jones, B.M., et al. (1981), "Factors Limiting Biodegradation of Oxy-6 Process Water Constituents," in Fourth Annual DOE Oil Shale Conversion Symposium, Denver, Colorado, 24-26 March 1981; Lawrence Berkeley Laboratory Report LBL-12420.

Processes for the Physico-Chemical Treatment of Oil Shale Wastewaters*

R. H. Sakaji, B. M. Jones, J. F. Thomas, and C. G. Daughton†

Physicochemical treatment methods for oil shale process wastewaters are often unsuccessful or infeasible because the concentrations of organic and inorganic solutes necessitate the excessive use of chemicals or energy for their removal. The economic burden caused by the use of this type of treatment technology to control environmental discharges may make the extraction of oil from oil shale economically infeasible. Combining biological treatment with physicochemical treatment or using cogenerated by-products of the oil shale operation as treatment agents may yield environmental control technologies that may be both successful and economical.

The major emphases of our research in this field have been physicochemical treatment processes that utilize: (a) cogenerated wastes and materials (e.g., spent and raw shale), (b) environmental factors of the western oil shale region (e.g., UV radiation), and (c) feasible conventional methods (e.g., steam stripping). Importance is placed on the evaluation of those physicochemical methods that remove organic or inorganic solutes that are complementary to those removed by biological treatment or that enhance the performance of biological treatment.

Wastewaters generated by the oil shale industry vary markedly in their characteristics due to the different retorting processes used to extract the oil. The wastewaters generally have high dissolved organic carbon (DOC) concentrations which contribute the characteristic color and odor. The concentration of DOC ranges from 2200 to 19,000 mg of carbon per liter.[1] The high alkalinity and pH of these wastewaters can be attributed to the high dissolved inorganic carbon (DIC) and ammonia-nitrogen concentrations, which vary from 1960 to 19,200 mg/l and 1700 to 13,200 mg/l, respectively.[1]

Our studies have shown repeatedly that only 50 percent of the DOC is amenable to initial biodegradation[2] and that the remaining fraction of DOC is recalcitrant to initial biological oxidation by acclimated bacteria. To improve the performance of the biological treatment units, some form of physicochemical treatment may be required. For example, there are indications that the refractory organic compounds are nitrogenous heterocycles.[2] The presence of easily utilized ammonia-nitrogen may repress those enzyme systems that may be capable of extracting the ring-bound nitrogen. Steam stripping is capable of decreasing the high ammonia-nitrogen concentrations to levels that should result in the derepression of these enzyme systems.

A major limitation to biological treatment may be the large numbers of organic solutes which compose the DOC concentration, each of which may be present at a concentration below its requisite enzyme affinity value. Sorption and concentration of these solutes at a solid-liquid interface may make these compounds more available for biodegradation. Physicochemical treatment processes may also remove compounds that are toxic to bacteria or may simply reduce the mass loadings of pollutants to downstream treatment units, thus improving their performance.

ACCOMPLISHMENTS DURING FY 1981

A major portion of this year's research was the investigation of various sorbents for the removal of organic solutes. Spent and raw shales are by-products from the retorting and mining of oil shale in surface and modified in-situ operations. Our investigations involved the evaluation of these compounds as sorbents for the removal of DOC from the oil shale process wastewaters. Raw and spent shales are not readily available to true in-situ retorting operations because the oil shale is left in the ground for retorting. This means that treatment of wastewaters generated at in-situ retorting operations may require the use of a more conventional sorbent, such as activated carbon. Treatment of the wastewaters by recirculation through either new (raw) or used (spent) retorts may encourage sorption of organic solutes resulting in a leachate either of better quality or more amenable to further upgrading.

We have shown that sample fractionation by reverse-phase chromatographic partitioning results in the removal of 50 percent of the DOC from Oxy-6 retort water.[3] This partitioning process removes the more hydrophobic solutes from the aqueous sample. Our batch and continuous-flow sorption studies have shown that the sorbed compounds belong predominantly to the biorecalcitrant fraction.

*This work was supported by the Assistant Secretary of Environment, Office of Environmental Compliance and Overview, Environmental Control Technology Division of the U.S. Department of Energy under contract No. DE-AC03-76SF00098.
†Sanitary Engineering and Environmental Health Research Laboratory, University of California (Berkeley), Richmond, California 94804 (associated faculty).

Sorption is therefore a process that is complementary to biological treatment, and it may serve to concentrate organic solutes at the sorbent surfaces to levels above the enzyme affinity values.

As a result of last year's operational problems with a prototype steam stripper,[4] design of a pilot-scale steam stripper was initiated. The problems encountered in the previous design included: maintaining the dimensional similitude between the packing material and the inside diameter of the column, obtaining mass balances for the stripping gas and contaminative constituents around the system, maintaining isothermal conditions in and through the packed bed, and decreasing the heat loss through the packed bed. The problems encountered with this preliminary design were addressed in the design of the pilot-scale unit now under construction at SEEHRL.

Raw Shale for Wastewater Treatment

Use of the readily available raw oil shale as a sorbent for wastewater treatment has been proposed,[5] and initial results from continuous-flow column studies appear promising. Analogous to the octadecyl-bonded silica used in the reverse-phase partitioning fractionation scheme,[3] raw shale contains a hydrophobic compound, kerogen, embedded in its inorganic marlstone matrix. The kerogen could be capable of partitioning hydrophobic solutes from retort water. Raw shale used to upgrade retort water could be subsequently disposed of by retorting to extract the crude shale oil. Studies on the use of raw shale from the Anvil Points mine, Fischer assayed at 35 gpt, as a partitioning sorbent encountered technical problems that prevented the completion of the experimental work. The major technical barrier to successful implementation of this process appeared to be proper wetting (activation) of the raw shale surface.[3,5] This would be accomplished by using a solvent that is miscible in both water and kerogen.

Spent Shale and Activated Carbon as Sorbents

We have shown previously that spent shales from different retort processes can effect the removal of DOC or dissolved inorganic carbon (DIC).[6] The ability of processed shales to remove either DOC or DIC is dependent on the retorting conditions. Spent shales produced from retorting at lower temperatures sorb DOC, whereas high-temperature retorting yields shales that are more efficient for the removal of DIC.[6] The ability of spent shales to act as sorbents is apparently dependent on the conditions that the surface of the shale has experienced during retorting. Spent shales from low-temperature retorting retain the residual char. In contrast, high-temperature retorting results in carbonate decomposition and combustion of the char, which can significantly alter the shale surface characteristics. The studies that were completed this past year evaluated the removal of solutes from Oxy-6 retort water (Occidental Oil Shale, Inc. retort #6, a modified in-situ retorting operation) by spent shale from the TOSCO II low-temperature (500°C) surface retorting process and by Calgon F-400 powdered activated carbon.

TOSCO II spent shale and Calgon F-400 were evaluated as sorbents in closed systems (batch studies). Organic solute removal was quantitated as DOC. The use of DOC as a measure of the organic solutes in retort water was an inadequate but necessary approximation to evaluate the sorption process. The information yielded by this general parameter is limited because each organic solute has different sorption characteristics. Equilibrium curves were obtained under ambient temperature conditions. Because adsorption is an exothermic process, less adsorption would be expected at warmer temperatures. Fluctuations in room temperature may have had some effect on sorbent evaluation. Sorption studies conducted under isothermal conditions (30°C) demonstrated that less material was sorbed than predicted by equilibrium curves constructed at ambient temperature.

Development of Equilibrium Curves. Development of the equilibrium curves began by determining the time required for the retort water organic solutes to reach equilibrium with each sorbent in a closed system. To establish these times, a series of flasks containing replicate quantities of TOSCO II spent shale or PAC (Calgon F-400) and Oxy-6 retort water was placed on a wrist-action shaker. At predetermined time intervals, a flask was removed and the solids were separated by filtration. The filtrate was analyzed for DOC to estimate the unsorbed solutes (C). These values were plotted as C/C_o vs. time, as in Figure 1, where C_o was the DOC concentration at time zero.

The initial rate of sorption was very rapid, as indicated by the steep slope of the curve labeled nonpolar (Fig. 1). As the sorbent became saturated with solute, the rate of sorption slowed, and the slope of the curve decreased. The major portion of the sorption process was completed after 24 hours, at which time sorption was slow and probably limited by the diffusion of the solutes into the pores. In replicate experiments, an apparent increase in the rate of solute removal was noted after 48 hours. This was attributed to biological

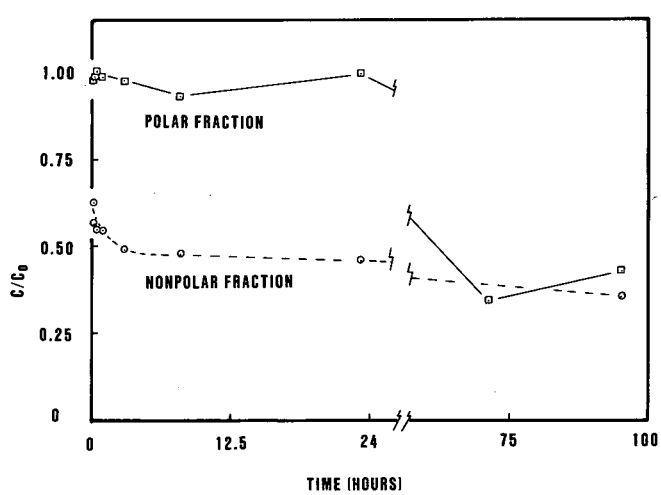

Figure 1. Batch equilibrium time study: reverse phase fractions of Oxy-6 DOC.

(XBL 822-7938)

oxidation because the experiments could not be conducted under aseptic conditions, and the spent shale was an excellent source of inoculum. Consequently, equilibrium curves were developed assuming 24-hour equilibrium times.

This time-course study was repeated using retort water that had been fractionated by the reverse-phase partitioning scheme.[3] The aqueous effluent, which contained the polar fraction of DOC, was used without alteration. The organic solutes that were retained (i.e., the nonpolar fraction) were eluted with methanol and redissolved in ASTM Type I water after evaporation of the methanol. The results of this time-course study are shown in Figure 1. No sorption of the polar fraction of DOC was detected. The solutes that were removed by the spent shale seemed to belong exclusively to the nonpolar fraction of the DOC. The DOC concentration in the polar fraction began to decline after 24 hours, presumably because of the growth of bacteria.[2] The rate of DOC sorption from the nonpolar fraction was very fast initially, but slowed down significantly after 24 hours, as had occurred in the unfractionated samples. Unlike the unfractionated sample, however, the DOC remaining did not continue to decrease after 48 hours. These results indicated that the spent shale: (a) sorbed only those compounds that were nonpolar, (b) did not sorb the polar fraction of DOC, and (c) removed compounds that were complementary to those removed by biological oxidation (i.e., the biorefractory solutes).

Equilibrium curves for Oxy-6 retort water with

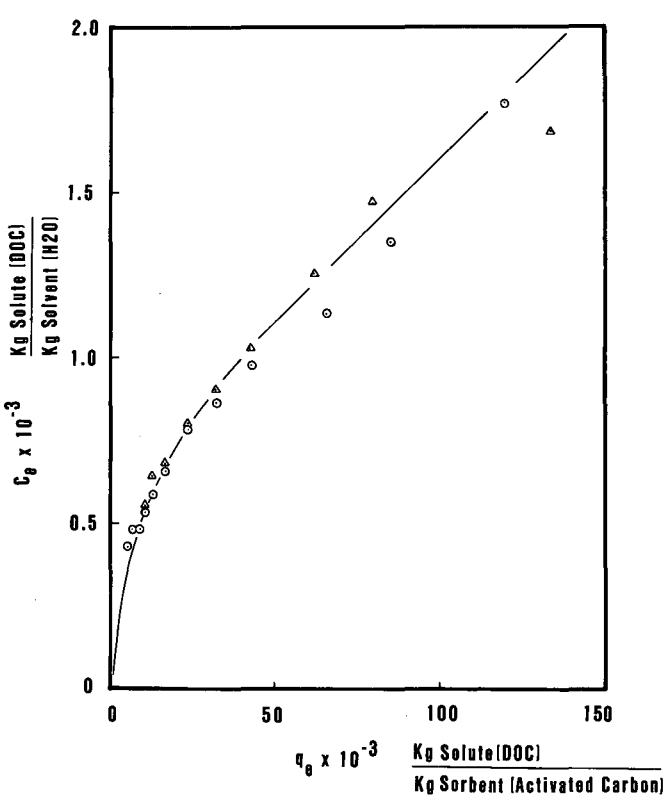

Figure 2. Sorption equilibrium curve: activated carbon (Calgon F-400). (XBL 822-7939)

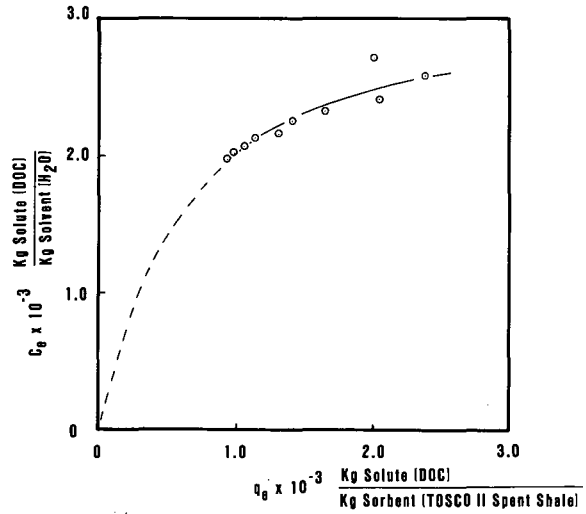

Figure 3. Sorption equilibrium curve: spent shale (TOSCO II). (XBL 822-7940)

TOSCO II spent shale and Calgon F-400 activated carbon were obtained under ambient temperature by adding different quantities of sorbent to a constant volume of retort water. After shaking for 24 hours, each sample was filtered and the filtrate was analyzed for DOC. The results are plotted for activated carbon (Fig. 2) and for spent shale (Fig. 3). The x-axis is the quantity of DOC sorbed per unit mass of sorbent (kg DOC sorbed/kg sorbent):

$$\frac{\text{(initial DOC-final DOC) x (volume of liquid)}}{\text{mass of sorbent}}$$

The y-axis is the equilibrium concentration of DOC or final DOC in the bulk solution. These curves should not be confused with equilibrium curves developed under isothermal conditions, which are commonly referred to as isotherms.

Since the solutes were a complex heterogeneous mixture, the results were fitted to the Freundlich equation, $q_e = mC^{1/n}$. The coefficients m and 1/n are determined from a log-log plot of q_e vs C_e where m represents the maximum saturation capacity and 1/n represents the adsorption intensity. The values for spent shale and activated carbon were 1/n = 2.97 and m = 104,700, and 1/n = 2.08 and m = 64,570, respectively. These results indicated that neither sorbent would be a favorable choice since 1/n values were greater than one.[7] These results can be partially attributed to the nonspecificity of DOC as a measure of solute concentration and to the inability of either spent shale or activated carbon to sorb more than 50 percent of the DOC.

Continuous-Flow Column Study. A fixed-bed column (2 in. i.d. x 3 ft) was filled with TOSCO II spent shale (25-120 mesh), and Oxy-6 retort water was applied at a surface loading rate of 0.1 gpm/f^2. The concentration of DOC in the column effluent was plotted against the percent throughput to exhaustion, which was defined as 0.95 C_o (Fig. 4). The results showed that 43 percent of the DOC

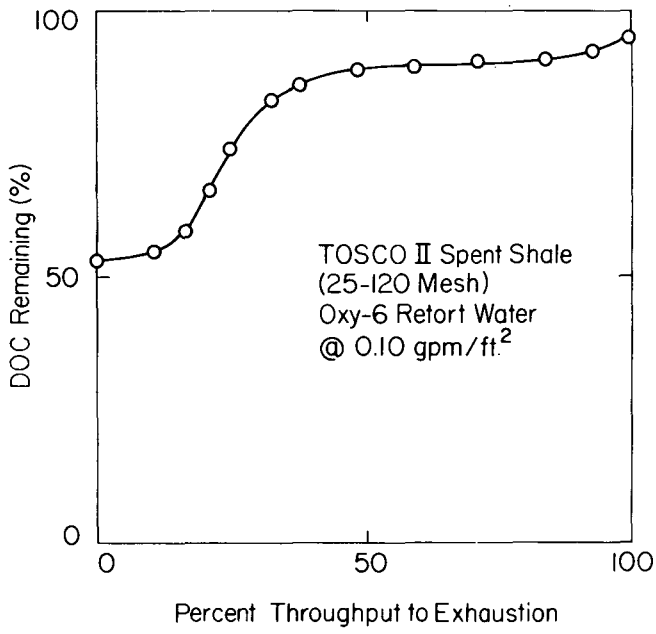

Figure 4. Continuous-flow treatment of retort water by fixed-bed spent shale: breakthrough curve. (XBL 816-968)

was removed from the first pore volume of effluent by the spent shale column but that the sorptive capacity of the bed quickly decreased; only 21 percent of the DOC was removed in the third pore volume. While the DOC removal was not sustained, as predicted by the low sorptive capacity obtained from the equilibrium studies, the column did continue to remove a small portion of the DOC over an extended period of time, as noted by the tail on the breakthrough curve.

Batch Sorption Study. Batch studies using spent shale or activated carbon and bacterial populations (acclimated to Oxy-6 retort water) were conducted to determine if the addition of a sorbent could result in the concentration of organic solutes on the sorbent surface resulting in further removal of DOC by biological oxidation.[2] Flasks containing a known quantity of sorbent and a known volume of retort water were inoculated with an acclimated microbial population and incubated at 30°C. Since the sorptive process is 95 percent complete after one hour and because the biological removal of organic solutes is significant in these cultures after 24 hours, the removal by sorption was quantitated by analyzing samples after one hour. Results from this study indicated that sorption after one hour is 20 percent less effective than was predicted by the equilibrium curves. This was believed to be due to the short time given the system to come to equilibrium and the use of a 30°C water bath, which was higher than ambient temperature. These studies were replicated, using Oxy-6 retort water that had been subjected to biological treatment. Results from these studies indicated that the same percentage removal of DOC by sorption was achieved in batches of both untreated and biologically treated retort water. The processes of sorption and biological oxidation removed complementary fractions of DOC.

Steam Stripping

The high concentrations of ammonia in oil shale process wastewaters will undoubtedly require removal of ammonia for discharge or reuse of the water. This characteristically high ammonia concentration may be the result of residual ammonium nitrate/fuel oil explosive or, more likely, from the pyrolysis and degradation of kerogen, which is 2 percent nitrogen by weight. When kerogen is pyrolyzed, the amino groups are released as gaseous ammonia that dissolves in the condensed water/oil emulsion at the cooler end of the retort.

Ammonia at low concentrations is toxic to aquatic organisms, and high concentrations can inhibit biological treatment. In addition, resource recovery of ammonia as ammonium sulfate may provide an economic benefit in some ammonia removal operations.

Ammonia removal is commonly accomplished by one of several methods in both the domestic water and wastewater treatment industries. These methods include nitrification/denitrification, breakpoint chlorination, ion exchange, ambient-temperature air stripping, and steam stripping. There are technical and economic barriers to using most of these processes. For example, nitrification/denitrification by biological treatment would not be feasible because of the large reactors required to remove the high concentration of ammonia. Additionally, an exogenous carbon and energy source would have to be added to the wastewater stream because carbon would become a limiting nutrient. Breakpoint chlorination is economically infeasible because of the high chlorine demand. Studies[8] have also shown that the organic solutes foul ion exchange resins to such an extent that the capacity and ability to regenerate the resin is lessened. There are also technical and economic limitations to the use of ambient-temperature countercurrent air stripping. The addition of alkali to increase the pH of the wastewater is required to shift the equilibrium of the ammonium ion-dissolved ammonia gas reaction to favor the dissolved gas form. The high buffering capacity of the wastewater requires an uneconomical quantity of caustic. Caustic addition in the form of lime also produces a large quantity of calcium carbonate sludge that requires dewatering and disposal. Steam stripping is commonly used by the petroleum industry for the removal of carbon dioxide, hydrogen sulfide, and ammonia from refinery wastewaters. Using conditions of elevated temperature, the steam stripper achieves ammonia removal because the pK_a of the ammonium ion-ammonia gas equilibrium and the solubility of ammonia are concomitantly decreased. Steam stripping will also remove carbonate alkalinity because carbon dioxide will be stripped together with the ammonia.

To study the steam stripping process, the last half of FY 1981 was spent designing a "pilot-scale" steam stripper. The stripper was designed for isothermal and adiabatic operation at temperatures exceeding 100°C because optimum operating temperature from the experience of oil refineries is 110°C.[9] The insulated Pyrex stripping column is 16 ft x 2 in. i.d. and packed with 1/4-in. ceramic saddles. The stripper has been designed to prevent

condensation of the stripping gas in the column. The design of this steam stripper will enable us to investigate several operational variables that were uncontrolled in the first experiments. These include the use of dry saturated steam instead of wet steam and the use of a live steam generator that will prevent the reflux and recycle of organic solutes and may lead to their alteration. We will also study the use of dry saturated steam at temperatures above 100°C to determine the optimum operating conditions for this process. Refluxing or reboiling in actual plant operation requires a higher steam usage than a nonrefluxed system because more heat is required to reheat the reflux to stripper operating temperatures.[9] Because the reflux is also enriched in the dissolved gases, more stripping is required to remove recycled components. The design of the steam stripper was completed late in FY 1981, and construction began at the close of the fiscal year.

PLANNED ACTIVITIES FOR FY 1982

Steam Stripping

Construction of the steam stripper will be completed early in 1982 with startup and operation to begin by mid-year. Startup will consist of testing structural integrity and the steam generation system, along with calibration of equipment such as pumps, temperature controllers, pressure gauges, and steam generation system.

Ozonation

Ozonation is used in the wastewater and water treatment industry as a powerful oxidant.[10,11] Ozone reacts rapidly with a majority of organic compounds and can result in the removal or reduction of color. Biological oxidation of organic solutes in oil shale process wastewaters does not significantly decrease or alter the color of these wastewaters.[2] We plan to evaluate the use of ozone to fully or partially oxidize the biorefractory organic solutes. Partial oxidation of polymerized or heterocyclic organic solutes may increase their susceptibility to biological oxidation. While the use of ozone may be economically unattractive as a treatment process in itself, small concentrations of ozone may be used as an aid to increase the oxidation of organic solutes by another treatment process. The two major technical limitations are that (a) the instability of ozone requires that it must be generated on-site and (b) the high ozone demand caused by the ammonia must be eliminated for the treatment to become effective. This would require that the wastewater be stripped of ammonia prior to ozonation.

Environmental Factors

The investigation of the effects of environmental UV irradiation of oil shale process wastewaters is a major priority. Ponding of these wastewaters for prolonged periods of time at high altitudes may result in the photolytic alteration of organic solutes. This may retard or enhance biodegradability. Alteration of these organic solutes may result in the synthesis of new compounds, the decomposition of existing compounds, the polymerization of organic solutes making them amenable to removal by sedimentation but less conducive to biodegradation, isomerization of organic solutes, or the alteration of organic compounds making them more susceptible to biooxidation.[12] The photoalteration of organic solutes may contribute significantly to improving or impeding the treatability of these wastewaters.

Photolytic alteration of the organic solutes may require the addition of a photosensitizing agent,[12] a molecule that is capable of absorbing UV radiation and transferring its dissipated energy to a molecule that does not absorb the radiation directly.

Freeze-thawing of ponded wastewaters may be viewed as an aid to treatment. Crystallized frozen water may exclude many of the dissolved ions and organic solutes from its lattice and concentrate them in the lower regions of the pond. While the presence of dissolved materials in the wastewaters decreases or depresses the freezing point of water, the solubility of many compounds decreases. These compounds may precipitate under the correct conditions and settle to the bottom of the ponds. When the surface melts, the partially purified water can be removed for further treatment.

The major goal of this project is to develop strategies and economically feasible methods that are environmentally acceptable for the treatment of commercial oil shale wastes. A major objective toward meeting this goal is the screening and identification of complementary treatment processes. Studying the integration of treatment units will enable us to develop processes that effect additive or synergistic removals of organic and inorganic solutes. This will enable us to develop meaningful strategies and options for successful water management programs. This task is facilitated by the use of experimental- and bench-scale treatments.

ACKNOWLEDGMENTS

We thank J. Cantor, G. Langlois, and K. Yu, the laboratory technicians of the LBL-SEEHRL Oil Shale Wastewater Treatment Program, for their capable assistance. We also thank Dr. Frank Pearson (SEEHRL) and Dr. Badawi Tleimat (Sea Water Conversion Laboratory) for their contributions to the steam stripper design.

REFERENCES

1. Fox, J.P., Farrier, D.S., and Poulson, R.E. (1978), "Chemical Characterization and Analytical Considerations for an In-Situ Oil Shale Process Water," Laramie Energy Technology Center Report LETC/RI-78/7.

2. Jones, B.M., et al. (1982), "Microbial Aspects of Oil Shale Wastewater Treatment," in Energy and Environment Division Annual Report 1981, Lawrence Berkeley Laboratory Report LBL-13500.

3. Daughton, C.G., et al. (1982), "Analytical Methods for Quantitating Performance of Oil Shale Wastewater Treatment," in Energy and Environment Division Annual Report 1981, Lawrence Berkeley Laboratory Report LBL-13500.

4. Pearson, F., et al. (1981), "Steam Stripping of Gas Condensate and Retort Water," in Energy and Environment Division Annual Report 1980, Lawrence Berkeley Laboratory Report LBL-11989.

5. Sakaji, R.H., Jones, B.M., and Daughton, G.C. (1981), "Raw and Spent Shale for the Treatment of Oil Shale Process Wastewaters," in Energy and Environment Division Annual Report 1980, Lawrence Berkeley Laboratory Report LBL-11989.

6. Fox, J.P., et al. (1980), "Spent Shale as a Control Technology for Oil Shale Retort Water," in Energy and Environment Division Annual Report 1979, Lawrence Berkeley Laboratory Report LBL-10746.

7. Treybal, R.E. (1980), Mass Transfer Operations, 3rd Ed., McGraw-Hill, New York.

8. Harding, B.L. (1977), "Removal of Ammonia and Alkalinity from Oil Shale Retort Waters by the Use of Weak Acid Cation Exchange Resins," in Second Pacific Chemical Engineering Congress, Denver, Colo., Aug. 28-31, 1977, Vol. 1.

9. American Petroleum Institute (1969), API Manual on Disposal of Refinery Wastes, Volume on Liquid Wastes, 1st Ed., Washington, D.C.

10. Culp, R.L., Wesner, G.M., and Culp, G.L. (1978), Handbook of Advanced Wastewater Treatment, Van Nostrand Reinhold Co., New York.

11. Weber, W.J., Jr. (1972), Physicochemical Processes for Water Quality Control, Wiley-Interscience, New York.

12. Glasstone, S., and Lewis, D. (1960), Elements of Physical Chemistry, 2nd Ed., Van Nostrand, New York.

COMBUSTION RESEARCH

Collision Dynamics Studies of Selected Hydrogen/Oxygen Reactions*

N. J. Brown, J. A. Miller†, and O. Rashed

A detailed understanding of the kinetics of the hydrogen/oxygen flame system over a range of temperatures and densities typical of combustion systems is important. Reactions of the hydrogen/oxygen system play a unique role in combustion chemistry because they are a subset in all hydrocarbon oxidation schemes. The specific chemistry of the radical species HO_2, which is formed as an intermediate during oxidation, is important in understanding: (1) ignition limits, (2) chain-branching, (3) heat release, and (4) radical shuffling mechanisms in combustion systems. The reaction $H_2 + HO \rightarrow H_2O + H$ is also important because it is responsible for much of the heat release and product formation in hydrogen/oxygen combustion.

Our current research is concerned with investigating the unimolecular dissociation of the HO_2 molecule at the low- and high-pressure limits and the state-to-state kinetics of the $H_2 + OH \rightarrow H_2O + H$ reaction. The existence of an analytical representation of an ab initio potential energy surface for HO_2 and the four-atom system, $H_2 + OH$, provides us with a unique opportunity to investigate the dynamics of these important combustion reactions.

ACCOMPLISHMENTS DURING FY 1981

The methods of classical dynamics are used to investigate the high-pressure-limit unimolecular dissociation of HO_2: $HO_2(^2A'') \rightarrow H(^2S) + O_2(\Sigma\bar{g})$.[1] The potential energy surface is the analytical representation given by Melius and Blint[2] of their ab initio calculation. Volume-weighted orthant sampling is used to sample the phase space of the critically excited (above threshold) HO_2 molecule. The high-pressure-limit dissociation of HO_2 is investigated as a function of energy and initial angular momentum of the reactant molecule.

Four types of trajectories are identified: trajectories which do not result in dissociation during the 50-psec time interval considered, isomerizing trajectories whereby the hydrogen atom migrates to and is bound to the second oxygen atom, dissociating trajectories which are preceded by isomerization, and directly dissociating trajectories. Dissociative trajectories are each analyzed for dissociation time, isomerization time (when appropriate), final relative velocity, final kinetic energy, final O_2 rotational energy, final O_2 vibrational energy, magnitude of final molecular angular-momentum, magnitude of final orbital angular momentum, and final impact parameter. A set of trajectories is a collection of trajectories with a specified total energy and angular-momentum distribution. Average product energies and distributions of final-state properties are determined for each class of dissociating trajectories in each given set.

Aspects of microcanonical phase-space sampling are investigated in detail. Our method of sampling the surface $H(p_i,q_i) = E$ in phase space is derived from the orthant-sampling procedures previously employed by other investigators.[3,4] We have modified these methods in our own study and have compared results from four sampling procedures: volume-weighted orthant sampling, equally weighted orthant sampling, volume-weighted orthant sampling without projection within the orthant, and volume-weighted orthant sampling without momenta scaling.

Reaction properties are remarkably insensitive to the sampling procedures employed. Four sets of trajectories having identical initial-energy and angular-momentum ranges, but which were generated with different sampling procedures, yield overall dissociation rate coefficients which lie within 10 percent of each other. The distributions of dissociation times for sets which differ only in sampling procedure are shown in Figure 1. These and the average product energy distributions are virtually identical for the four sets. The agreement among rate coefficients and product attributes for the four sampling procedures is reassuring and indicates that our results are not biased by non-uniformities in sampling.

Lifetime distributions are determined for the microscopic unimolecular processes: overall dissociation, direct dissociation, and isomerization. The random lifetime assumption is obeyed very accurately for all reactions, provided that the random lifetime assumptions of RRKM theory is interpreted correctly. The existence of a two-channel (isomerization and direct dissociation) unimolecular process is a sufficient condition for the existence of two distinct reactivity bands in phase space; each band consists of a set of continuously connected phase points which react through the specified channel. The existence of such a boundary separating the two bands leads to "apparent" non-RRKM

*This work was supported by the Director of the Office of Energy Research, Office of Basic Energy Sciences, Chemical Sciences Division of the U.S. Department of Energy under Contract No. DE-AC03-76SF00098.

†Combustion Research Facility, Sandia National Laboratories, Livermore, California.

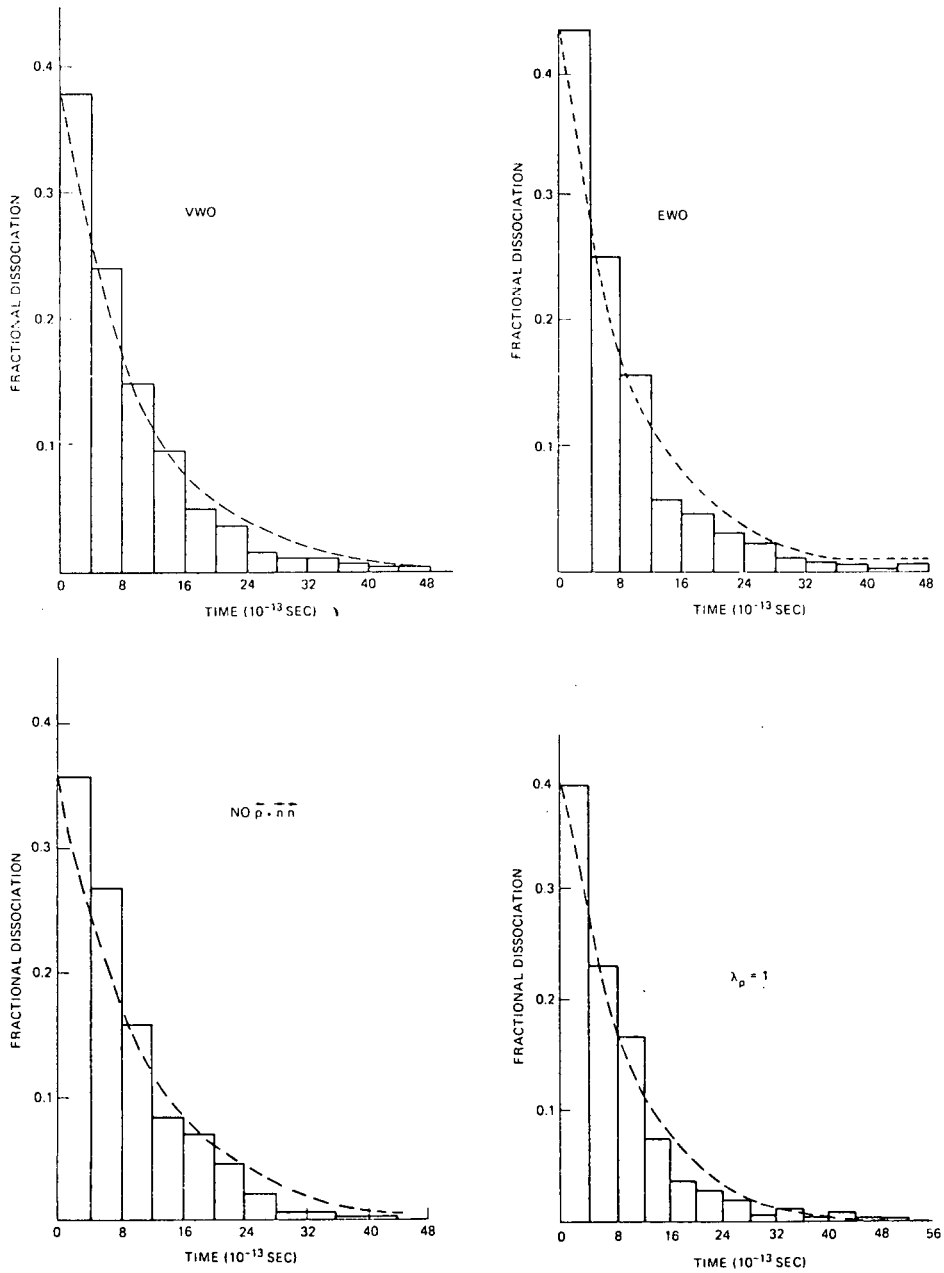

Figure 1. Lifetime distributions and random lifetime curves, based on the first bin-intercept method, for different sampling procedures, E = 55 kcal/mole, J $\leq$ 10. (XBL 823-8144)

behavior analogous to the "intrinsic" non-RRKM behavior attributed by Bunker to "bottle necks" in phase space.

A major emphasis of this investigation is the effect of molecular rotation on the unimolecular dissociation of HO_2. In the analysis, HO_2 is approximated as a prolate symmetric top, and the magnitude of total angular momentum is expressed as a multiple of $\hbar$, referred to as J. The most important result of our work is the conclusion that molecular rotation cannot be accounted for simply in terms of a centrifugal barrier. This is illustrated in Figure 2, where overall dissociation rate coefficients are plotted as a function of energy above threshold for two different J ensembles. Specific unimolecular rate coefficients, when cast in terms of available energy, are systematically smaller for high-J ensembles than for low ones. Additionally, for high J, there exist many long lived complexes (>50 psec), some of which may never dissociate. This is not the case for low-J ensembles with the same amount of available energy. It cannot be emphasized too strongly that this is not a centrifugal barrier effect. The energy dependence of the microcanonical rate coefficients indicates that the rotational degrees of freedom associated with K in the symmetric top expression for rotational energy is partially inactive. Whereas anharmonicity is a very strong mechanism for cou-

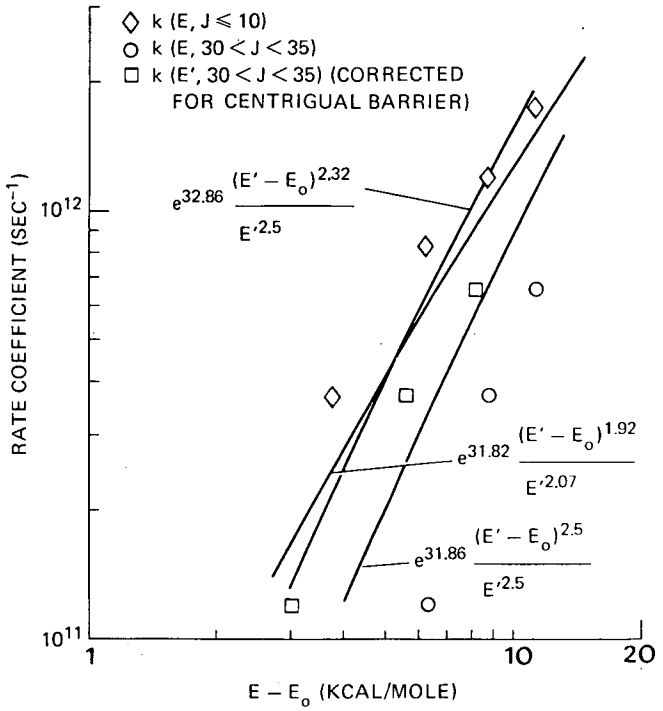

Figure 2. Rate coefficients as a function of energy. ◇ k(E, J ≤ 10), o k(E, 30 < J < 35), □ k(E', 30 < J < 35). E' is the available energy, $E' = E - B^{\ddagger}_{eff}J^2$. k(E',J ≤ 10) differs very little from k(E, J ≤ 10) and thus is not plotted. The three curves represent, respectively, the best fit $k(E') = \alpha[(E' - E_0)^m/E'^n]$ to the seven k(E') results.
(XBL 823-8145)

pling the various vibrational degrees of freedom, vibrational-rotational interaction is relatively weaker for coupling the rotational degrees of freedom to the vibrational degrees of freedom.

A new study initiated this year is a classical dynamics study of the reaction $H_2 + OH \rightarrow H_2O + H$. This work is closely coordinated with the Theoretical Combustion working group and has as its primary objective the determination of the effect of initial rotational energy on reactivity. The potential energy surface used in this study is the analytical form of Schartz and Elgersma[5] of the ab initio Walsh and Dunning[6] surface. Reaction probabilities and final product energies will be calculated as a function of relative kinetic energy and reactant rotational and vibrational energies.

PLANNED ACTIVITIES FY 1982

We will investigate the low-pressure-limit unimolecular dissociation of HO_2. Low-pressure-limit kinetics are second order, and the rate-limiting process is intermolecular energy transfer. Helium and neon will be considered as energy-transfer-effecting collision partners. Potential energy surfaces which account for the rare-gas/HO_2 interaction will be constructed, and collisions will be investigated as a function of surface properties, total system energy, relative kinetic energy, and total molecular angular momentum. Results will be compared with theoretical models used to estimate weak collision attributes. Numerical differentiation, as opposed to analytical differentiation, will be attempted in the solution of the equation of motion.

The energy range of the high-pressure-limit investigation of HO_2 will be extended to allow for a second dissociation channel: $HO_2 \rightarrow OH + O$, and the character of reactivity bands in phase space will be examined. A suprisal analysis of the final-state properties' distribution, which fully accounts for angular momentum and energy conservation, will be made.

The effect of initial rotational energy in each of the reactant molecules will be determined in the study of H_2 and OH dynamics. The partitioning of energy in the product H_2O molecule will be determined and analyzed.

REFERENCES

1. Miller, J.A., and Brown, N.J. (1982), "The Dynamics of Unimolecular Dissociation of HO_2: Phase Space Sampling, Microcanonical Rate Coefficients and Rotational Effects," accepted for publication, J. Phys. Chem.

2. Melius, C.F., and Blint, R.J. (1979), "The Potential Energy Surface of the HO_2 Molecular System," Chem. Phys. Lett. 64, p. 183.

3. Bunker, D.L., and Hase, W.L. (1973), "On Non-RRKM Unimolecular Kinetics: Molecules in General, and CH_3CN in Particular," J. Chem. Phys. 59, p. 4621.

4. Wolf, R.J., and Hase, W.L. (1980), "Trajectory Studies of Model H-C-C → H + C = C Dissociation. 1. Random Vibrational Excitation," J. Chem. Phys. 72, p. 316.

5. Schatz, G.C., and Elgersma, H. (1980), "Quasi-Classical Trajectory Study of Product Vibrational Distributions in the $OH + H_2 \rightarrow H_2O + H$ Reaction," Chem. Phys. Lett. 73, p. 21.

6. Walch, S.P., and Dunning, T.H. (1980), "A Theoretical Study of the Potential Surface for $OH + H_2$," J. Chem. Phys. 72, p. 1303.

Combustion Instabilities Leading to Flashback*

L. Vaneveld, K. Hom, and A. K. Oppenheim

Following our FY 1981 studies[1] of turbulent combustion instabilities leading to flashback, we investigated secondary effects, namely, those due to (1) buoyancy and (2) contraction at combustor outlet. As before, experiments were performed in an oblong, rectangular-cross-section, combustion tunnel, where the effects of a bluff-body flame holder were reproduced by a rear-facing step behind a streamlined inlet nozzle.

In our previous investigation using this facility,[2] three distinct types of unstable behavior were noted: humming, buzzing, and chucking, each distinguishable by a characteristic frequency and a particular flow pattern. Humming is associated with the highest frequency (~170 Hz) because it is evidently controlled by a standing longitudinal sound wave that accentuates the vortex-pairing pattern of the "free shear layer" behind the edge of the step. In fact, we have demonstrated that a similar effect can be induced externally by a loudspeaker operating within the same frequency band. Buzzing and chucking manifest the instabilities of the flow system. Buzzing is associated with a flapping motion of the flame up and down across the combustion chamber at a much lower frequency (~70 Hz), while chucking is characterized by the motion of the flame back and forth at a somewhat lower frequency (~50 Hz). This leads eventually to periodic flashback followed by the re-establishment of the flame in the form of a tongue jetting forth behind the edge of the step and following the outer contour of the recirculation vortex.

The mechanism of all these phenomena has been rationalized in terms of interaction processes between two vortex systems: the trailing vortices behind the edge of the step and the recirculation vortex with its satellites in the wake behind its base. In the humming mode, this interaction is at a minimum and the flow field is controlled primarily by the trailing-vortex system. The buzzing mode sets in when the recirculation vortex overcomes the large-scale structure of the trailing vortices so that the flame is stretched as it moves up and crinkled as it moves down. The chucking mode is generated by the combined action of two counter-rotating recirculation vortices whose growth is promoted by the augmentation of the exothermic process of combustion as the equivalence ratio in the initially lean mixture is increased.

*This work was supported by the Director of the Office of Energy Research, Office of Basic Energy Sciences, Engineering, Mathematics, and Geosciences Division of the U.S. Department of Energy under Contract No. DE-AC03-76SF00098 and by the U.S. National Aeronautics and Space Administration under Grant No. NSF 3227, through the Engineering Office of Research Services, University of California, Berkeley.

The experimental results have been interpreted on the basis of numerical modeling analysis using the random vortex method.[3]

ACCOMPLISHMENTS DURING FY 1981

Transition to Flashback

To provide an insight into the flow field at the side walls, the step was moved into the test section. The transition to flashback was triggered by a sudden increase in the flow rate of fuel, executed by the use of a pre-set, solenoid-controlled secondary valve in the fuel line. As in our previous studies, all the experiments were performed with lean propane-air mixtures, initially at room temperature and atmospheric pressure.

A sequence of cinematographic schlieren records, displayed at a time interval of 18 msec between frames, is shown in Figure 1. The initial disturbances of a still predominantly stable combustion mode are depicted in the left column. The first four frames on the right show the flapping motion of the flame characteristic of the buzzing mode. This leads to chucking, culminating in flashback depicted in the three bottom frames. The inlet velocity was initially 13.3 m/sec and finally 13.4 m/sec, corresponding to the Reynolds number of 2.2×10^4.

The concomitant pressure transducer record revealed that a relatively low frequency (~40 Hz) of stable combustion was dramatically increased in amplitude and frequency (~60 Hz) by the onset of a periodic sequence of buzzing, chucking, and flashback.

Effects of Buoyancy

A corresponding sequence of events recorded with the step mounted at the roof of the test section is depicted in Figure 2. Here, the stable combustion mode was evidently associated with a number of disturbances at various frequencies, while the transition included distinct buzzing as well as chucking modes. Buzzing modes are depicted in the last three frames in the left column and the top three on the right; chucking modes are shown in the remaining four, which also display a progressively escalating flashback. The pressure amplitude of the flashback was of the same order as before, but the frequency was somewhat lower (~45 Hz).

As demonstrated by these records, there is no essential difference between the transition to flashback with the step at the top and the step at the bottom of the combustor, indicating that the effects of gravity are of secondary importance. Nonetheless, we have been able to establish a definite trend due to this effect because, as shown in Table 1, the tendency towards flashback was

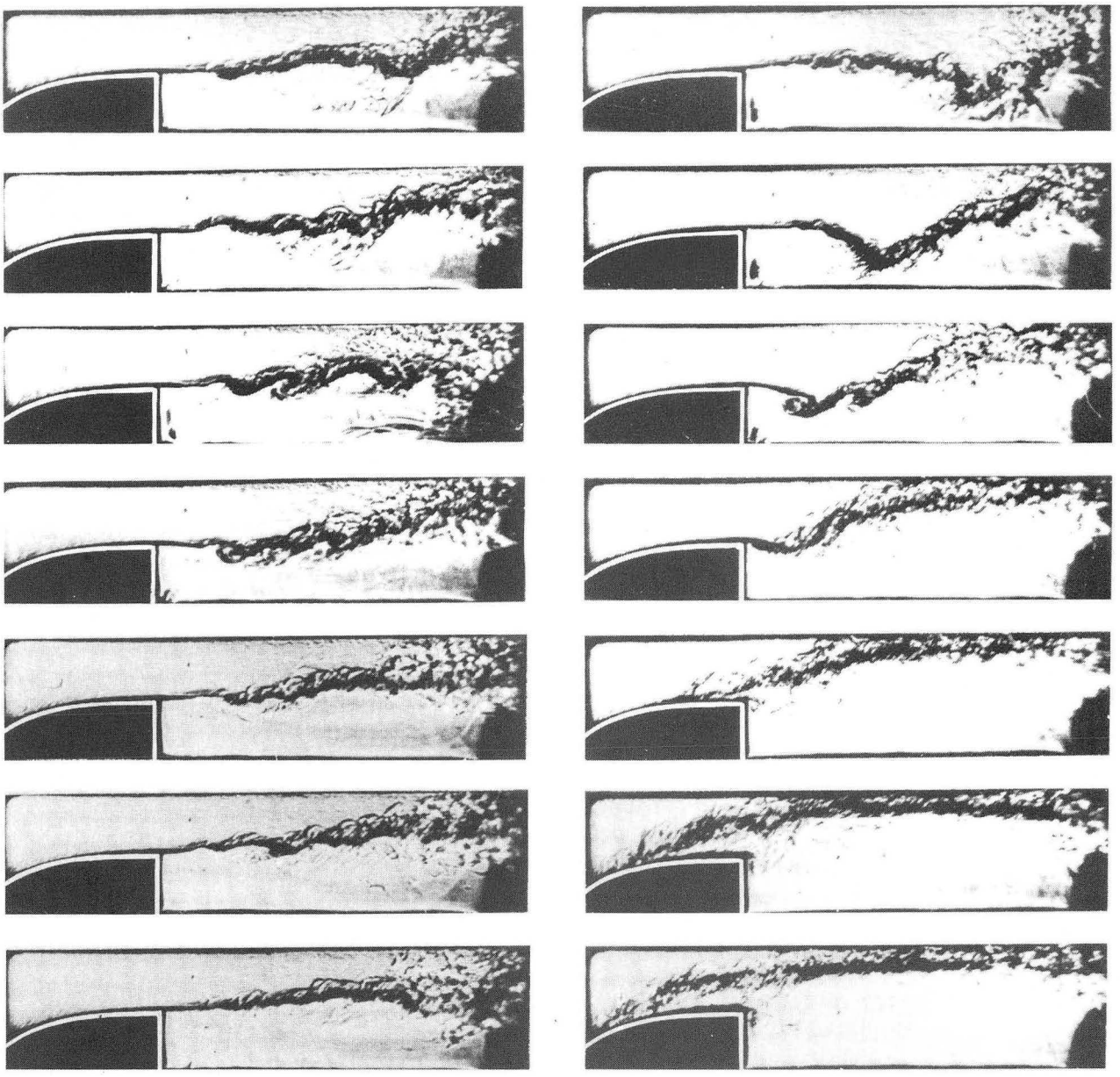

Figure 1. Transition to flashback-step at the bottom. Inlet flow velocity: 13.2-13.4 m/sec (Re = 2.2 x 10^4). Time interval between frames: 18 msec. (XBB 8112-11635)

definitely impaired with the step at the top. The equivalence ratios at flashback listed in Table 1 were obtained in a series of experiments where these critical values were recorded under a variety of operating conditions: with the choke-valve in the exhaust line fully opened or closed and with the cooling-water spray on and off.

In all cases, the values of critical equivalence ratios were definitely higher with the step at the top than with the step at the bottom, manifesting the effects of the mechanism whereby gravity can, in the first case, impair and, in the second, enhance the growth of the recirculation zone that triggers the flashback.

Effects of Contraction at Combustor Exit

The effects of contraction at the exit of the combustion chamber were modeled by fitting the test section with another step downstream so that, with the step at the inlet, it formed a trough. The results of an experiment embodying a complete set of processes associated with transition from stable combustion to flashback in this configuration of the combustion chamber at the relatively low inlet velocity of 9 m/sec are presented in Figure 3. Starting with the stable combustion mode shown in the first three frames, there is a short transition period of humming, humming-enforced vortex pairing, followed immediately by buzzing, and buzzing-

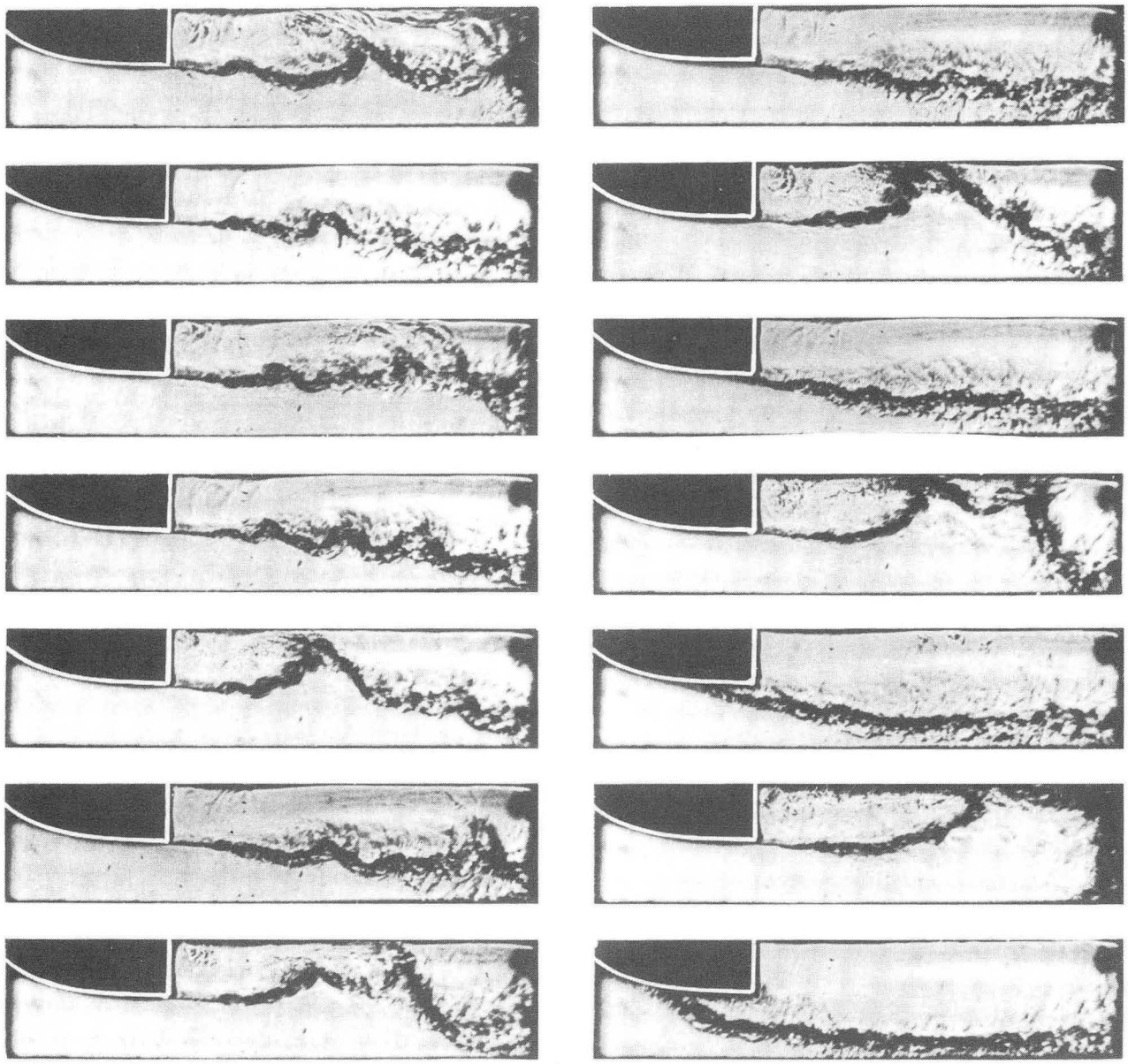

Figure 2. Transition of flashback-step at the top. Inlet flow velocity: 13.3-13.4 m/sec (Re = 2.2 x 10^4). Time interval between frames: 11 msec. (XBB 8112-11636)

Table 1. Equivalence ratios at flashback for different orientations of the step and various flow restrictions downstream.

	Exhaust Choke On		Exhaust Choke Off	
	Water On	Water Off	Water On	Water Off
Step on Bottom	0.783	0.824	0.812	0.934
	0.785		0.786	0.875
Average	0.784	0.824	0.799	0.905
Step on Top	0.803	0.840	0.809	0.921
	0.819	0.835	0.812	0.928
	0.819		0.833	
	0.816		0.830	
Average	0.814	0.838	0.821	0.925
Change	+0.030	+0.014	+0.022	+0.020

produced flame stretching and flapping. Then, as shown in the first three frames on the right, this was transformed into a chucking mode that induced the flashback displayed in the last frame. The characteristic frequency of the flashback was 55 Hz.

CONCLUSIONS

1. By comparing the results of experiments leading to flashback with a bluff-body flame holder in the form of a step that was mounted either at the bottom or at the top of a combustion chamber, a small but nonetheless quite definite effect of buoyancy was established. Irrespective of various flow obstructions introduced downstream, the critical equivalence ratio for flashback was consistently lower with the step at the bottom, indicating that buoyancy was then enhancing the growth

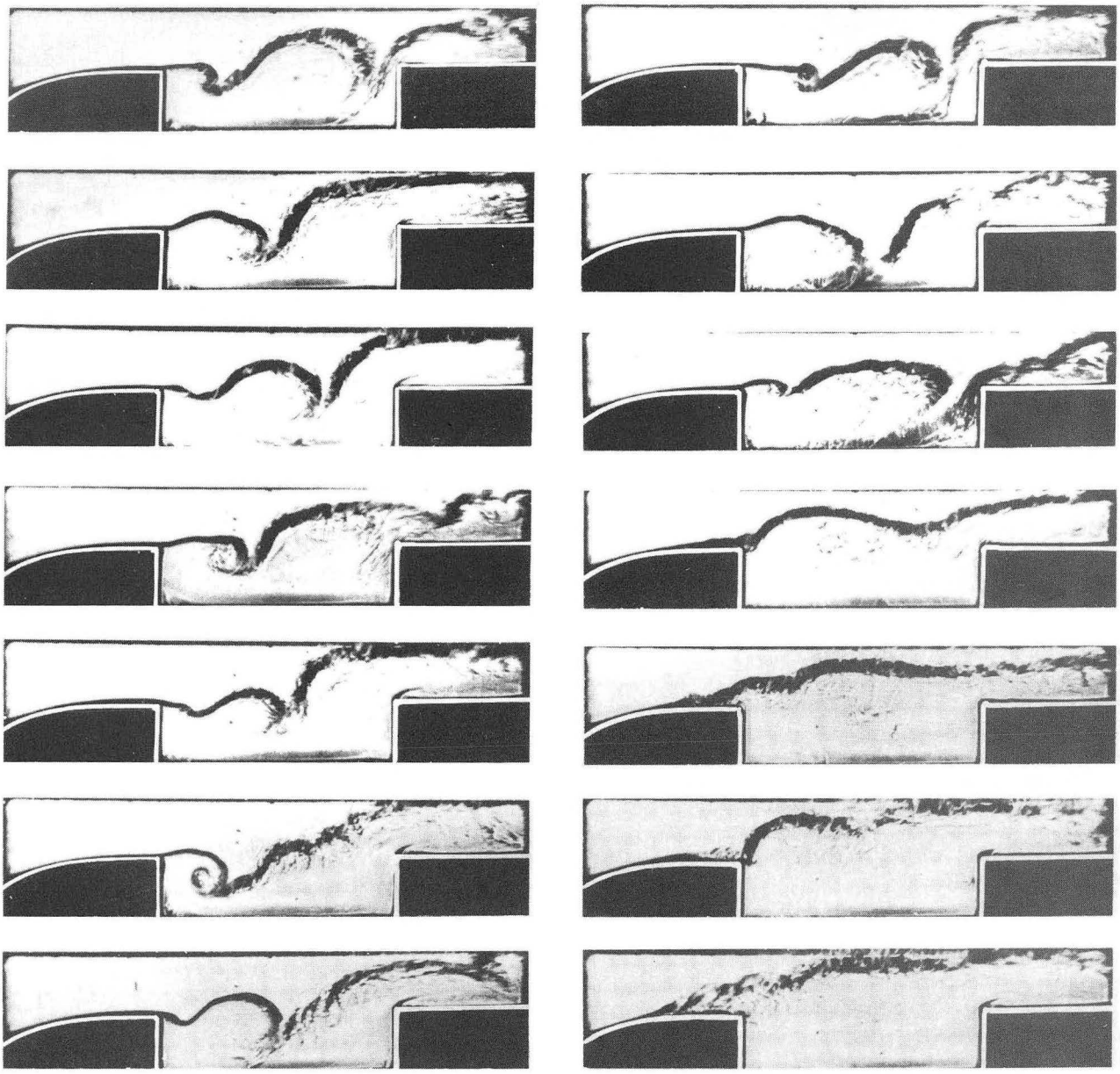

Figure 3. Transition to flashback in a trough-shaped combustor. Inlet flow velocity: 9.0-9.12 msec (Re = 1.5×10^4). Time interval between frames: 20 msec. (XBB 8112-11637)

of the recirculation zone that pushed the flame upstream, causing flashback.

2. The contraction at the end of the combustion chamber had a promoting influence on the process of vortex pairing, reinforcing the influence of the trailing vortices over that of the recirculation vortex system and thus curbing significantly the tendency to flashback. Nonetheless, all the characteristic features of combustion instabilities leading to flashback in the absence of contraction could be established in its presence, provided that the flow velocity was sufficiently low.

A paper reporting these studies was presented at the AIAA 20th Aerospace Sciences Meeting on January 11, 1982 in Orlando, Florida.[4]

PLANNED ACTIVITIES FOR FY 1982

Following the study reported here, the test section was dismantled and replaced by a highly versatile system where the flame is stabilized behind a splitter plate with a burner situated upstream in one of the inlet channels. The new test section is provided with quartz windows on all sides to permit an unobstructed view of the flow field in both vertical and horizontal directions. Proper provisions also have been incorporated for the control of the boundary layer. The study currently under way is concerned with a fully

developed turbulent flame in the shear layer behind the splitter plate, following ignition of a premixed charge due to mixing with a co-current stream of hot combustion products.

After the completion of these studies, we plan to use this facility to study combustion instabilities in a pre-mixed gas stream behind a bluff-body stabilizer mounted in the center of the combustor. Of particular interest will be the mechanism of blow-off, as well as that of flashback. The parameters whose influence is to be taken under consideration in this connection will be the geometry of the bluff-body flame holder, i.e., the relative thickness of the plate, the shape of its trailing edge vs the rack configuration, and its thermal properties (i.e., the adiabatic wall vs constant temperature under the control of a water-cooling system).

REFERENCES

1. Energy and Environment Division Annual Report, FY 1980, Lawrence Berkeley Laboratory Report LBL-11990, pp. 6-2 to 6-4.

2. Keller, J.O., et al. (1981), On the Mechanism of Turbulent Flashback, Paper presented at the AIAA 19th Aerospace Sciences Meeting, St. Louis, Mo., January 1981.

3. Ghoniem, A.F., Chorin, A.J., and Oppenheim, A.K. (1980), Numerical Modeling of Turbulent Flow in a Combustion Tunnel, Lawrence Berkeley Laboratory Report LBL-11520.

4. Vaneveld, L., Hom, K., and Oppenheim, A.K. (1982), Secondary Effects in Combustion Instabilities Leading to Flashback, Paper presented at AIAA 20th Aerospace Sciences Meeting, Orlando, Florida, January 11-14, 1982.

Ignition Studies*

A. K. Oppenheim, F. C. Hurlbut, F. Robben, R. B. Peterson, P. A. Coico, and H. E. Stewart

These studies occupy a central position in our research on controlled combustion. The major premise of this effort is that a new technology of combustion systems where the chemical reactions of oxidation are fully controlled can be developed as a consequence of proper exploitation of active radicals. The knowledge required for this purpose involves not only a thorough understanding of the chemistry of radical production and their reactions but also a complete command over the fluid mechanics of the gaseous flow fields where these reactions take place.

Our contributions in this respect consist of

1. Rationalization of the technological significance of enhanced ignition and the methodology of controlled combustion, the principal motive of our program of research.

2. Study of the fluid-mechanical properties of turbulent jets, the major means for the delivery and distribution of active radicals in the combustible medium.

3. Analysis of the exothermic effects of combustion processes, the mechanism whereby the chemical reaction of oxidation affects the flow field.

4. Development of molecular-beam mass spectrometry, the direct measuring technique for the determination of the time-resolved evolution and decay of active radicals in the course of ignition.

The accomplishments made over the last year in each of these areas are reviewed here.

ACCOMPLISHMENTS DURING FY 1981

Technological Significance

The relevance of our research to technological progress in internal combustion engines formed the subject of two papers. The first concerned explicitly enhanced ignition,[1] and the second exposed the significance of controlled combustion to the development of novel engines that would provide satisfactory service as clean and efficient energy conversion systems.[2]

The principal concepts we developed are summarized as follows:

1. The technology of internal combustion engines has been advanced to such high levels, with all the concomitant attributes of outstanding engineering and highly developed production facilities, that one should expect its progress to continue over a long period, irrespective of potential competition for alternative power plants, at least as far as automobile propulsion is concerned.

2. The most prominent demands upon the progress of this technology stem from the concern over the environmental impact and the shortage of fuel. On a long range, the tasks imposed by these demands cannot be accomplished by engine improvements derived from better engineering designs without due

*The work was supported by the Director of the Office of Energy Research, Office of Basic Energy Sciences, Engineering, Mathematics, and Geosciences Division of the U.S. Department of Energy under Contract No. DE-AC03-76SF00098.

consideration being given to all the scientific avenues available for this purpose.

3. Controlled combustion is the most promising direction in the progress of engine technology because it could concomitantly minimize emissions, maximize efficiency, and optimize tolerance to a wide scope of fuels. Controlled combustion could satisfy all demands by processes occurring in the engine cylinder without the use of a chemical processing plant in the exhaust system. The most attractive way to accomplish this is by using a homogeneous combustion process.

4. After establishment of uniform initial conditions, the principal means for achieving a homogeneous combustion process are enhanced ignition and enhanced autocatalysis. Both involve proper exploitation of active radicals. The acquisition of knowledge required for the development of systems where the evolution of active radicals and their influence are appropriately monitored form the major objective of our studies.

Turbulent Jets

Because turbulent jets are the principal means for the delivery and distribution of active radicals, their mechanism is of particular significance to the subject of our research. Consequently, the formation of such jets was analyzed by the use of the random-vortex method, a technique whose engineering applications have been pursued by us in collaboration with its creator, Professor A.J. Chorin.[3,4] Our first publication on this subject, concerned with numerical modeling of turbulent combustion in premixed gases, has been published recently in the Proceedings of the Eighteenth Symposium (International) on Combustion,[5] while the details of the methodology we developed for this purpose are in press as one of the forthcoming Transactions of The Royal Society of London.

The result of last year's studies are presented in the report on "Numerical Modeling of Turbulent Combustion" elsewhere in this volume.

Exothermic Effects

Because the exothermic effects are obviously of central importance to the initiation and control of the combustion process, they have been subjected to most extensive and careful studies we conducted over a number of years. Our fundamental paper on the thermochemistry of ignition, treating the evolution of the exothermic process in the presence of heat losses to surroundings, has been published recently in the Proceedings of the Seventh International Colloquium on Gasdynamics of Explosions and Reactive Systems.[6] The principal features of the theory we developed there are described in 1979 Energy and Environment Division Annual Report.[7]

The problem is formulated in such a manner that the solution lends itself to presentation in terms of an integral curve on a multi-dimensional phase space whose coordinates are the concentrations of all the species participating in chemical reaction and the temperature. The particular effects we studied thereby were those of a given finite initial concentration of radicals. The families of integral curves corresponding to various initial temperatures and radical concentrations revealed the existence of an attractor, a surface of demarcation specifying a threshold in minimum initial radical concentration to exert a significant influence upon the development of the combustion process. The order of magnitude in the threshold value is approximately one percent of the initial concentration of fuel which, for a typical lean hydrocarbon-air mixture, means an absolute molecular fraction of radicals initially in the combustible mixture of about 5.10^{-4}, a sufficiently low level to be of practical interest. Thus, a firm theoretical background has been established for the experimental program of our research.

On the other side of the spectrum of exothermic effects in ignition is the strong ignition limit, a threshold for explosive onset of the combustion process. This process is initiated coherently over a sufficiently large mass of the combustible substance, producing enough exothermic energy to generate a blast wave. We presented our experimental shock-tube study of this threshold for a bi-fuel, methane-hydrogen-oxygen system at The Combustion Specialists Meeting in Bordeaux.[8]

In the area of blast waves, the ultimate manifestations of exothermic effects, our collaborative studies with Soviet scientists, Barenblatt and Zeldovich, have culminated in a paper on self-similar waves headed by fronts where variable amounts of energy are deposited or withdrawn, published in the Journal of Fluid Mechanics.[9] An extension of this work, concerned with self-similar blast waves associated with variable energy deposited in the flow field, was published in Proceedings of the Seventh International Colloquium on Gasdynamics of Explosions and Reactive Systems.[10] A related study of the effects of internal, radiative and conductive, heat transfer on the structure of self-similar blast waves is scheduled for publication in the Journal of Fluid Mechanics.[11]

The theoretical approach we developed for the analysis of exothermic effects in combustion yielded an extraneous dividend, the determination of such effects in diffusion flames. In a manuscript, submitted to the forthcoming Combustion Symposium in Haifa,[12] we analyze the contours of gaseous, unconfined, planar, and axi-symmetric jet diffusion flames and the structures of the flow fields they acquire under the influence of exothermicity. For the sake of clarity, the problem is formulated in the simplest possible way. The flame is treated as essentially laminar, the reaction rates are considered infinite, and the medium is assumed to behave as a perfect gas with constant specific heats, its Schmidt and Prandtl numbers being unity and its viscosity proportional to the temperature, while the buoyancy effects are neglected. Under such circumstances the problem lends itself to treatment by the Shvab-Zeldovich technique. The results, derived as an inverse to self-similar solutions in the incompressible domain obtained by a Dorodnitsyn-Howarth transformation of the governing equations for compressible flow, are expressed in terms of algebraic formulae. When applied to hydrogen-air and a number of hydrocarbon-air mixtures, these formulae were in

amazing agreement with experimental data obtained under zero-gravity conditions.

Mass Spectrometer

The most ambitious aspect of our experimental research program is the development of a molecular-beam mass spectrometer with sufficiently high time resolution and sensitivity to record the evolution and concentration histories of active radicals over their relatively short life span in the course of ignition. The current status of this work has been described in a recent LBL report.[13]

The salient features of the apparatus have been described in the 1980 Energy and Environment Division Annual Report.[14] Bringing this system into a fully functional state at the high level of performance for which it was designed was to be more difficult and time demanding than expected. Nonetheless, preliminary tests established that a satisfactory modulation of the molecular beam by the use of a high-speed chopper has been achieved, as manifested by the relatively symmetric shutter function (Fig. 1) we were able to obtain from our measurements. The molecular beam we formed by the use of a sharp-edge orifice was fully supersonic at a Mach number of 2.34, as evaluated from the time-of-arrival record presented in Figure 2.

The major problem confronting us at the moment is due to wall effects whose proper control requires a more careful alignment of the skimmer with respect to the beam-forming nozzle than expected at the onset. Currently, proper adjustments for this purpose are being made. As a consequence of our concentrated effort and because all elements of the apparatus, including a computer-controlled data-acquisition system, are functioning quite satisfactorily, the whole apparatus should soon become fully operational.

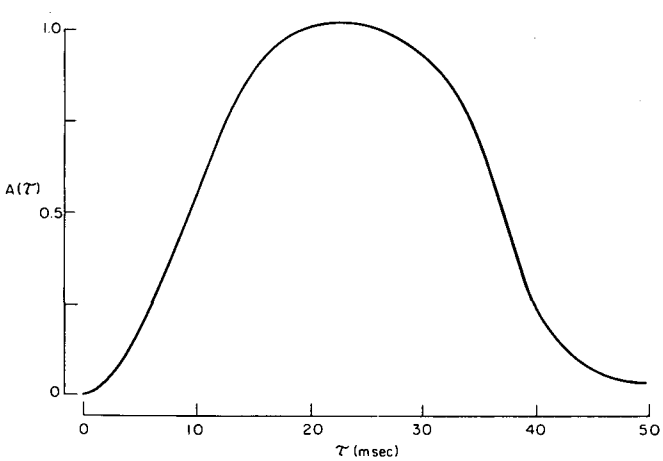

Figure 1. Experimental record of the shutter function of the molecular beam mass spectrometer. Chopping speed: 2-pulses per second; Normalized distance between orifice and skimmer: x/d = 60; Nitrogen beam at a pressure of 500 torr.
(XBL 818-11335)

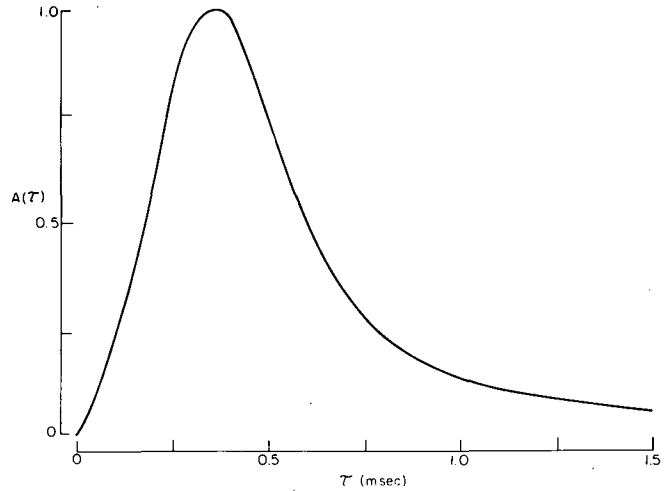

Figure 2. Experimental record of the time of arrival function of the molecular beam mass spectrometer. Chopping speed: 400 pulses per second; Other conditions same as in the case of Figure 1.
(XBL 818-11336)

PLANNED ACTIVITIES FOR FY 1982/83

The primary experimental apparatus for the proposed research is the high-frequency-response molecular-beam mass spectrometer we developed especially for this purpose. The sequence of goals we propose to achieve by its use is as follows:

1. Time-resolved measurements of the generation of radicals produced at a known rate by the photolysis of nitrous oxide in an inert atmosphere.

2. Time-resolved measurements of the generation of radicals by the photolysis of hydrogen peroxide in an inert atmosphere.

3. Study of the effects of radicals generated by photolysis in reactive media.

4. Study of selected equivalent reactions initiated by the essentially thermal effects of a reflected shock wave.

5. Study of ignition by plasma jets and by combustion jets.

Work towards each goal will consist of two stages: an exploratory investigation yielding qualitative information, followed by a definitive study yielding quantitative data. We expect that first stages of some latter goals will be introduced into our research program earlier and out of sequence, depending on the demand and schedule. We expect that in FY 1983, Goal 1 will be achieved and the first stage of Goal 5 will be started.

REFERENCES

1. Dale, J.D., and Oppenheim, A.K. (1981), Enhanced Ignition for I.C. Engines with Premixed Gases, SAE Paper 810146, presented at SAE International Congress and Exposition, Detroit, Michigan, February 23-27, 1981.

2. Dale, J.D., and Oppenheim, A.K. (1982), A Rationale for Advances in the Technology of I.C. Engines, presented at the SAE International Congress and Exposition, Detroit, Michigan, February 22-26, 1982.

3. Energy and Environment Division Annual Report, FY 1979, Lawrence Berkeley Laboratory Report LBL-11650 (1980), pp. 6-38 to 6-41.

4. Energy and Environment Division Annual Report, FY 1980, Lawrence Berkeley Laboratory Report LBL-11990 (1981), pp. 6-31 to 6-33.

5. Ghoniem, A.F., Chorin, A.J., and Oppenheim, A.K. (1981), "Numerical Modeling of Turbulent Combustion in Premixed Gases," in Eighteenth Symposium (International) on Combustion, The Combustion Institute, Pittsburgh, pp. 1375-1383.

6. Guirguis, R.H., et al. (1981), "Thermochemistry of Methane Ignition," Progress in Astronautics and Aeronautics, AIAA, New York 76, pp. 134-153.

7. Energy and Environment Division Annual Report, FY 1979, Lawrence Berkeley Laboratory Report LBL-11650 (1980), pp. 6-7 to 6-11.

8. Cheng, R.K., and Oppenheim, A.K. (1981), "Strong Ignition Limits for Methane-Hydrogen Mixtures," in Colloque International Berthelot-Vieille-Mallard-Le Chatelier, First Specialists Meeting (International) of The Combustion Institute, French Section of The Combustion Institute 2, pp. 342-348.

9. Barenblatt, G.I., et al. (1980), "Self-Similar Explosion Waves of Variable Energy at the Front," Journal of Fluid Mechanics 99, Part 4, pp. 841-858.

10. Guirguis, R.H., Oppenheim, A.K., and Kamel, M.M. (1981), "Self-Similar Blast Waves supported by Variable Energy Deposition in the Flowfield," Progress in Astronautics and Aeronautics, AIAA, New York 75, pp. 178-192.

11. Ghoniem, A.F., et al. (1981), "Effects of Internal Heat Transfer on the Structure of Self-Similar Blast Waves," Journal of Fluid Mechanics, in press.

12. Klajn, M., and Oppenheim, A.K. (1982), "Influence of Exothermicity on the Shape of a Diffusion Flame," submitted for presentation at the 19th International Symposium on Combustion, Haifa, Israel, August 8-13, 1982.

13. Hurlbut, F.C., and Oppenheim, A.K. (1981), Molecular Beam System for the Study of Transient Combustion Processes, Lawrence Berkeley Laboratory Report LBL-13178.

14. Energy and Environment Division Annual Report FY 1980, Lawrence Berkeley Laboratory Report LBL-11990 (1981), pp. 6-8 to 6-10.

Optical Measurement of Combustion Products by Tunable Atomic Line Molecular Spectroscopy*

E. Cuellar and N. J. Brown

Considerable research effort has been devoted to obtaining a detailed, microscopically based understanding of the chemistry of combustion. Such a detailed understanding generally has not been possible except for the simplest of systems. This difficulty reflects the complexity of combustion processes, where numerous elementary chemical reactions, each proceeding at its own specific rate, are interwoven with physical transport processes, often resulting in steep temperature and concentration gradients.

The course of chemical reactions in combustion systems such as flames can be conveniently examined using suitable probes of the composition and temperatures of the gases from various parts of the flame which can then be analyzed at a remote station. A major disadvantage of such intrusive probes, however, is that the flow can be disturbed in unpredictable ways, resulting in erroneous measurements of concentrations as the species being measured are created or destroyed in the probe. Optical probes, on the other hand have the distinct advantage of being nonintrusive and do not significantly disturb the species being measured. For example, laser induced fluorescence (LIF) probes have been used to measure minority species and transient molecules present in combustion systems.[1] Since most combustion reactions occur at relatively high temperatures and pressure, laser fluorescence studies require knowledge of collisional quenching rates and of rates of energy transfer between internal energy states. A further difficulty associated with LIF measurements in combustion is the lack of a well characterized spectroscopic data base, including transition probabilities, for many of the molecules of interest.

Optical absorption measurements are much easier to interpret because transition probabilities and quenching and energy transfer rates need

*This work was supported by the Assistant Secretary for Environment, Office of Environmental Compliance and Overview, Environmental Safety and Engineering Division of the U.S. Department of Energy under Contract No. DE-AC03-76SF00098.

not be known to obtain quantitative results. Tunable diode lasers, for example, have been used to measure NO and CO in combustion systems.[2] However, the limitation of the dual beam optical systems necessary to measure minority species and the weaker oscillator strengths of vibrational-rotational transitions compared with electronic transitions limit the detectability of this laser absorption technique to several hundred parts per million (ppm).

We are interested in the development and application of a novel optical absorption technique, called tunable atomic line molecular spectroscopy (TALMS), as a tool in combustion diagnostics. This technique has been pioneered at the Lawrence Berkeley Laboratory by Dr. Tetsuo Hadeishi and his co-workers and has been used in the analytical determination of atomic species[3] and small molecules which exhibit sharp rotational electronic structure.[4] This technique is based on the Zeeman effect and utilizes a unique method for background correction, making it highly sensitive and selective. It is therefore well suited for the quantitative detection of minor species present in combustion environments and has a demonstrated lower limit of detection for some species in the parts per billion (ppb) range.[4] A detailed description of TALMS was presented earlier.[5]

ACCOMPLISHMENTS DURING FY 1981

Tunable atomic line molecular spectroscopy was utilized to detect and measure S_2 formed by the thermal decomposition of H_2S (Ref. 6) and in the equilibrium vapor of elemental sulfur.[7] A Cr(I) atomic emission line was found to be nearly resonant with an electronic transition of S_2. The Cr line was split into Zeeman components by the application of an external magnetic field, and a differential absorption measurement was obtained as a function of magnetic field strength. Several closely spaced lines belonging to different branches which result from the triplet splitting in the (7,2) band of the $B^3\Sigma\bar{u}$ - $X^3\Sigma\bar{g}$ system of S_2 were resolved. The high selectivity of the TALMS technique and its capability for resolving closely spaced spectroscopic structure are shown in Figure 1.

We have initiated a comparative study of optical and probe measurements of nitric oxide (NO) produced by oxidation of atmospheric nitrogen (via the Zeldovich mechanism) in a methane-air premixed laminar flame. Ultraviolet absorption methods have yielded NO concentrations which are 50 to 80 percent larger than those obtained using metallic probes and chemiluminescent gas analyzers.[8] Others[9] have reported probe-determined NO concentrations which were 20 to 30 percent higher than optical absorption measurements. The discrepancies have raised questions about the reliability of probe measurements, and processes occurring within the probes have been suggested which form or destroy NO. More recent studies[10] comparing NO measured optically with NO measured after sampling with metallic and quartz probes have indicated agreement to within 25 percent. However, the lack of sensitivity of these optical absorption techniques required signal enhancing by doping with NO. The

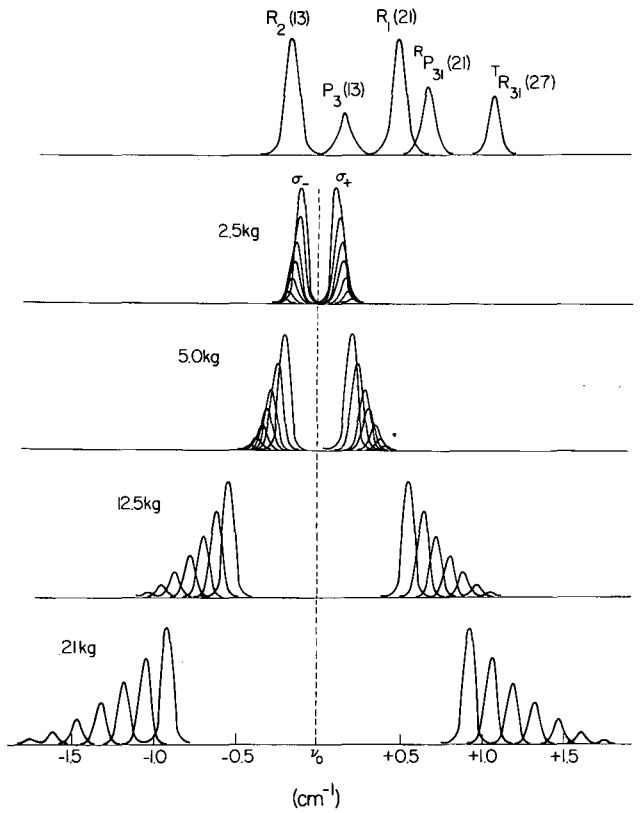

Figure 1. Calculated absorption spectrum of S_2 in the neighborhood of 3018 Å. Also shown is the overlap of the $\sigma_\pm$ Zeeman components of the Cr emission line with the S_2 absorptions at four magnetic field strengths. (XBL 818-1112)

Zeeman effect based background correction of the TALMS technique allows for detection of thermal NO in the 1 ppm range without the need for doping.

A schematic of the experimental system is shown in Figure 2. The spectrometer has been described earlier[5] and remains essentially unchanged. The flat flame burner is mounted on an x-y-z translation stage and is placed in the optical path of the spectrometer. The burner is a water cooled porous plug burner constructed from a 6-cm sintered bronze disk. Methane and air are metered through calibrated rotameters and are premixed in a stainless steel mixing chamber packed with glass beads. The burner was characterized by obtaining a stability map of CH_4-air stable flat flames, as well as temperature and velocity profiles. A stable flat flame was observed at a total flow rate of 30 standard liters per minute at a range of equivalence ratios from 0.75 to 1.5. Velocity profiles were obtained using hot film and hot wire anemometry, and vertical and radial temperature profiles at a range of linear velocities and equivalence ratios were measured using a platinum/platinum 13 percent rhodium thermocouple.

An uncooled quartz microprobe with a 300 micron orifice was used to extract samples from the flame. A chemiluminescent gas analyzer (CLA) was constructed and calibrated and used to measure the concentration of NO sampled with the quartz probe.

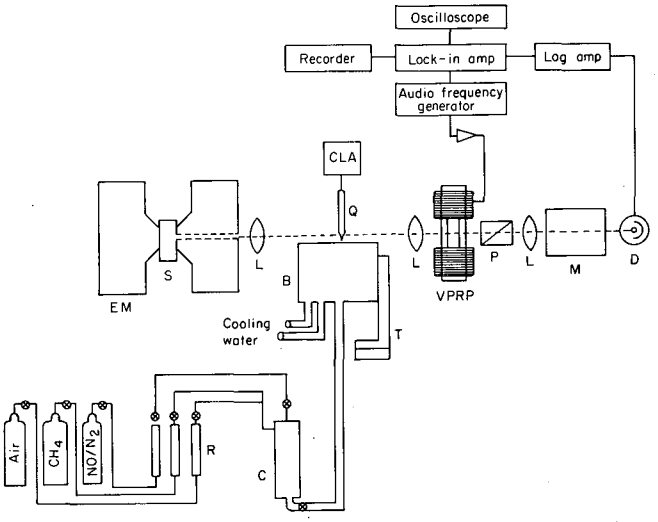

Figure 2. Schematic diagram of the experimental apparatus: EM electromagnet, S atomic light source, L quartz lens, B porous plug burner, T x-y-z translation stage, Q quartz probe, CLA chemiluminescent gas analyzer, VPRP variable phase retardation plate, M monochromator, D photomultiplier tube, C mixing chamber, R rotameters.
(XBL 822-4489)

Radial profiles of NO concentrations at two different heights above the burner and at an equivalence ratio ϕ = 1.0 are shown in Figure 3.

The most significant difference between this chemiluminescent gas analyzer and commercially available CLAs is the addition of a mass flow meter in the sample stream to control the relative composition of the gas in the reaction chamber. By adjusting the flow of the sample stream so that 5 percent of the gas in the reaction chamber is due to the probed sample while 95 percent is due to ozonated oxygen stream, the effects of third body quenching can be significantly reduced. The response of the instrument was found to be linear in NO concentrations to at least 2500 ppm.

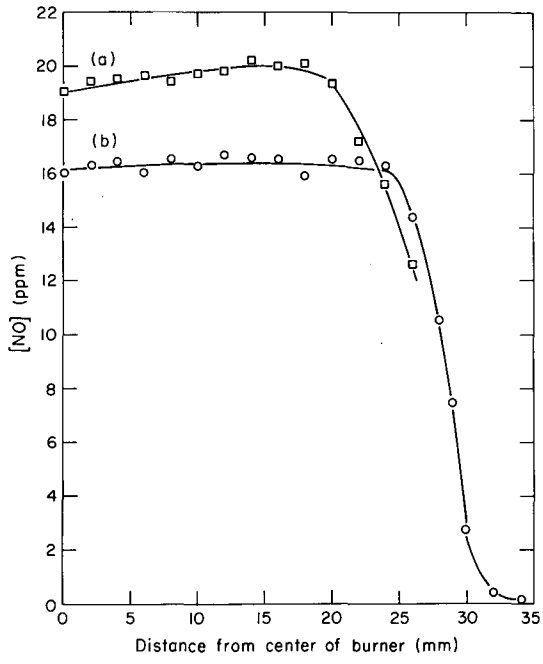

Figure 3. Radial profiles of nitric oxide concentrations measured with an uncooled quartz probe and a chemiluminescent gas analyzer. The NO concentrations are not corrected for third body quenching effects. (a) 15.0 mm above the burner, (b) 5.0 mm above the burner. (XBL 822-4490)

Chemiluminescent gas analyzers are usually calibrated with known NO/N_2 mixtures. When sampling from combustion systems, additional species are introduced into the reaction chamber: H_2O, CO_2, CO, O_2, and hydrocarbons. The relative efficiencies of these third bodies in quenching the chemiluminescent reaction must be taken into account in order to obtain meaningful quantitative results on NO concentrations.[11] We have measured the relative quenching efficiencies of various third bodies by mixing fixed amounts of NO (80, 230, and 510 ppm) with a carrier gas consisting of N_2 and varying amounts of CH_4, CO_2, CO, O_2, H_2, and Ar. Results obtained for CH_4, CO, and O_2 are shown in Figure 4. Carbon monoxide and hydrogen have quenching efficiencies nearly equal to that of nitrogen, while argon is significantly less effective than nitrogen.

PLANNED ACTIVITIES FOR FY 1982

The chemiluminescent analyzer interference study described above will be extended to include other third body collision partners; the most important of these is water. All of these results have been obtained using the configuration described above, where only 5 percent of the gas mixture in the reaction chamber is introduced

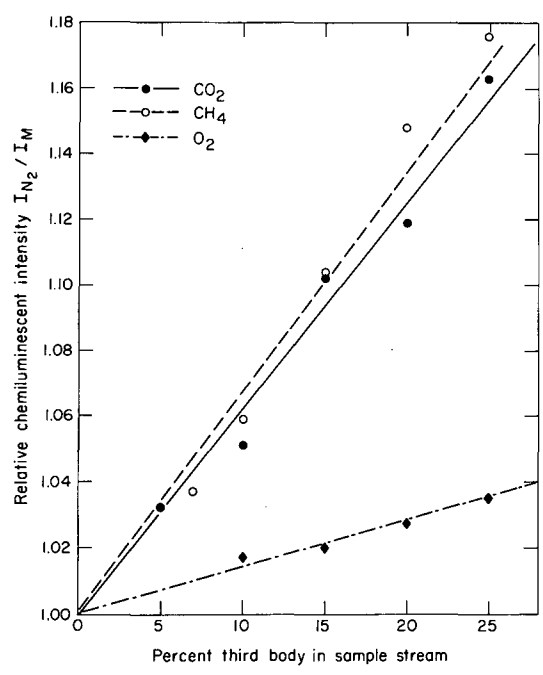

Figure 4. Relative chemiluminescent intensity as a function of third body concentration in the sample mixture. (XBL 822-4491)

through the probe. The effectiveness of this technique in reducing the third body quenching will be evaluated by obtaining data under conditions where approximately 50 percent of the reaction mixture is due to the probe sample.

The comparative study of probe and optical measurements (using tunable atomic line molecular spectroscopy) of NO will be continued. Concentration profiles such as those shown in Figure 3 for an equivalence ratio of $\phi = 1$ will be obtained at other equivalence ratios, ranging from $\phi = 0.75$ to $\phi = 1.5$. Preliminary optical measurements have demonstrated the ability to detect small quantities of NO doped into the cold flow of the burner, but upon ignition the NO signal disappears. Possible explanations include loss of sensitivity due to shifting of the rotational population distribution of NO or combustion reactions affecting the added NO. The important question of high temperature calibrations will be addressed. One way to accomplish this is by doping the burner with known amounts of NO and extrapolating to zero doping levels. A second approach is to measure the line shape of the NO absorption at elevated temperatures and thus obtain the extinction coefficient of NO as a function of temperature.

The number of important molecules that can be detected by TALMS continues to grow. Two such molecules are hydrogen sulfide and benzene.[12] The former is an important molecule in the combustion of sulfur-containing fuels and the latter has been implicated in the formation of polynuclear aromatic hydrocarbons (PAHs) in fuel rich combustion.[13] In addition, CH_2O and SO_2 can be detected by TALMS.[4] Formaldehyde is an important product formed by incomplete combustion, and sulfur dioxide is the most abundant sulfur-containing species formed in the combustion of sulfur-containing fuels and is a serious contributor to the problem of acid rain.

REFERENCES

1. Crosley, D.R. (Ed.), (1980), Laser Probes for Combustion Chemistry, A.C.S. Symposium Series No. 134, American Chemical Society, Washington, D.C.

2. Falcone, P.K. (1981), Absorption Spectroscopy of Combustion Gases Using a Tunable Diode Laser, Ph.D. Thesis, Mechanical Engineering Department, Stanford University, Stanford, California.

3. Hadeishi, T. (1972), "Isotope-Shift Zeeman Effect for Trace-Element Detection: An Application of Atomic Physics to Environmental Problems," Appl. Phys. Lett. 21, p. 438.

4. Koizumi, H., Hadeishi, T., and McLaughlin, R.D. (1979), "Detection of Small Molecules by Magnetically Tuned Frequency-Modulated Atomic Line Sources," Appl. Phys. Lett. 34, p. 382.

5. Cuellar, E. (1980), Detection of S_2 by Tunable Atomic Line Molecular Spectroscopy, Lawrence Berkeley Laboratory Report LBL-11323.

6. Cuellar, E., and Brown, N.J. (1981), "Combustion Diagnostics by Tunable Atomic Line Molecular Spectroscopy," in First Specialists Meeting (International) of the Combustion Institute, 2, p. 545, and Lawrence Berkeley Laboratory Report LBL-12127.

7. Cuellar, E., and Brown, N.J. (1982), "Detection of S_2 by Magnetic Tuning of a Cr(I) Atomic Emission Line," accepted for publication, J. Phys. Chem., and Lawrence Berkeley Laboratory Report LBL-13249.

8. Few, J.D., McGregor, W.K., and Glassman, H.N. (1977), "Resonance Absorption in Combustion Exhaust" in Experimental Diagnostics in Gas Phase Combustion Systems, B.T. Zinn, Ed., Progress in Astronautics and Aeronautics 53, p. 187.

9. Meinel, H., and Krauss, L. (1978), "Monitoring of Nitric Oxide in Flames by UV Differential Resonance Absorption," Comb. and Flame 33, p. 69.

10. Zabielski, M.F., et al. (1981), "The Optical and Probe Measurements of NO: A Comparative Study," in Eighteenth Symposium (International) on Combustion, p. 1591.

11. Mathews, R.D., Sawyer, R.F., and Schefer, R.W. (1977), "Interferences in Chemiluminescent Measurement of NO and NO Emissions from Combustion Systems," Env. Science and Tech. 11, p. 1092.

12. T. Hadeishi, private communication.

13. DiLorenzo, A., et al. (1981), "UV Absorption, Laser Excited Fluorescence and Direct Sampling in the Study of the Formation of Polycyclic Aromatic Hydrocarbons in Rich CH_4/O_2 Flames," in Eighteenth Symposium (International) on Combustion, p. 485.

Combustion in a Turbulent Boundary Layer*

T. T. Ng, R. K. Cheng, F. Robben, and L. Talbot

The interaction between turbulence and combustion involves highly complex fluid-mechanical and chemical processes. Since these processes are stochastic, a good understanding of the mechanisms of turbulent combustion requires detailed statistical measurements of scalar and velocity properties. These statistical data would be most valuable to the theorists for developing numerical models of turbulent combustion.

To date, most experimental studies of premixed turbulent combustion have concentrated on measurements in flames. However, the study of turbulence-combustion interactions in other simple and well-defined experimental configurations with known incident turbulence fields is of significance because the effects of combustion heat release on the turbulent structures may be readily identified. The objective of the present program is to study premixed turbulent combustion in one of the classical turbulent fluid-mechanical configurations: the heated turbulent boundary layer.

The turbulent boundary layer is generated over the floor of a 10-cm-square, 75-cm-long working section of a wind tunnel. The last 25 cm of the floor is the test section and is open to the atmosphere to permit laser diagnostic access. The floor of the test section is lined with nine heating strips. The wind tunnel is driven by a 1.12-kW blower providing maximum air flow of 20 m/sec and is mounted on a traverse table which is interfaced with a computer-controlled data-acquisition system. The data-acquisition system is based on a PDP 11/10 mini-computer and is programmed to enable automatic scanning of the boundary layer by the stationary laser diagnostics. Laser Rayleigh scattering and single component laser doppler velocimetry systems were used to measure statistics of density and two velocity components. The raw data of these measurements are stored on 7-track magnetic tapes and are processed using the LBL CDC 7600 computer. In addition to these statistical measurements, qualitative information on the heated and reacting boundary layer are obtained with high speed schlieren movies showing the development of the thermal and flame structures.

ACCOMPLISHMENTS DURING FY 1981

The Heated Boundary Layer

General features of the heated turbulent boundary layer were studied with free-stream velocity, U_∞, of 19 m/sec and wall temperature, T_W, of 1000 K.[1] The data obtained include mean and root-mean-square (rms) fluctuations of two velocity components, the Reynolds stress ($-\overline{u'v'}$), and mean and rms fluctuations of density in both the heated and unheated flows. Under these experimental conditions, the turbulent velocity boundary layer is fully developed, and the thermal boundary layer is completely embedded inside the velocity boundary layer. Density and velocity profiles for the heated and unheated flows are found to be self-preserving and are compared with the self-preserving analysis developed by Townsend.[2] Although his velocity equation seems to be quite satisfactory for correlating our experimental data, the correlating constants are higher.

The velocity rms fluctuations appear to be unaffected by the wall heating, but the Reynolds stresses are reduced near the heated wall. A tentative explanation has been proposed for this apparent reduction in turbulence production with no overall change in turbulent kinetic energy. This explanation is suggested by the cyclic development of the thermal structures in the heated boundary layer shown on the schlieren movies. The shape and trajectories of the thermal structures seem to be consistent with the large-scale turbulent structures of the velocity boundary layer. These turbulent structures are associated with interactions between the turbulent fluid moving into and out of the wall region. In this heated flow, the interaction would be between cold fluid from the outer region with more viscous hot fluid close to the wall. This hot and cold fluid interaction should be less energetic than in a nonheated flow and thus result in a lowering of the Reynolds stress.

The Reacting Boundary Layer

The effects of combustion heat release within the boundary layer was studied for U_∞ = 10 m/sec and T_W = 1200 K, using ethylene/air mixture with equivalence ratio, ϕ, of 0.35 (Refs. 3 and 4). Measurements were made in isothermal, heated wall, and reacting flows. Data obtained include profiles of mean and rms fluctuations of density and two velocity components and the Reynolds stress. In addition, several higher order cross correlations [$\overline{(u'v')^2}$, $\overline{u'v'^2}$, $\overline{v'u'^2}$ and $\overline{u'k_1} = \overline{u'(u'^2 + v'^2)}$] were deduced to study the various aspects of turbulent kinetic energy transfer in the boundary layer. The procedure for measuring these cross-correlation parameters is an extension of the standard procedure to measure Reynolds stress using a single-component LDV system.[5]

Shown in Figure 1 are two series of schlieren records of the reacting boundary layer. Near the leading edge, as shown on the photographs on the right, the combustion process is confined to a small region close to the hot surface. Farther downstream, as shown on the photographs on the left, combustion takes place in elongated flame structures oblique to the wall rather than in a continuous flame sheet. These structures seem to

*This work was supported by the Director, Office of Energy Research, Office of Basic Energy Sciences, Chemical Sciences Division of the U.S. Department of Energy under Contract No. DE-AC03-76SF00098.

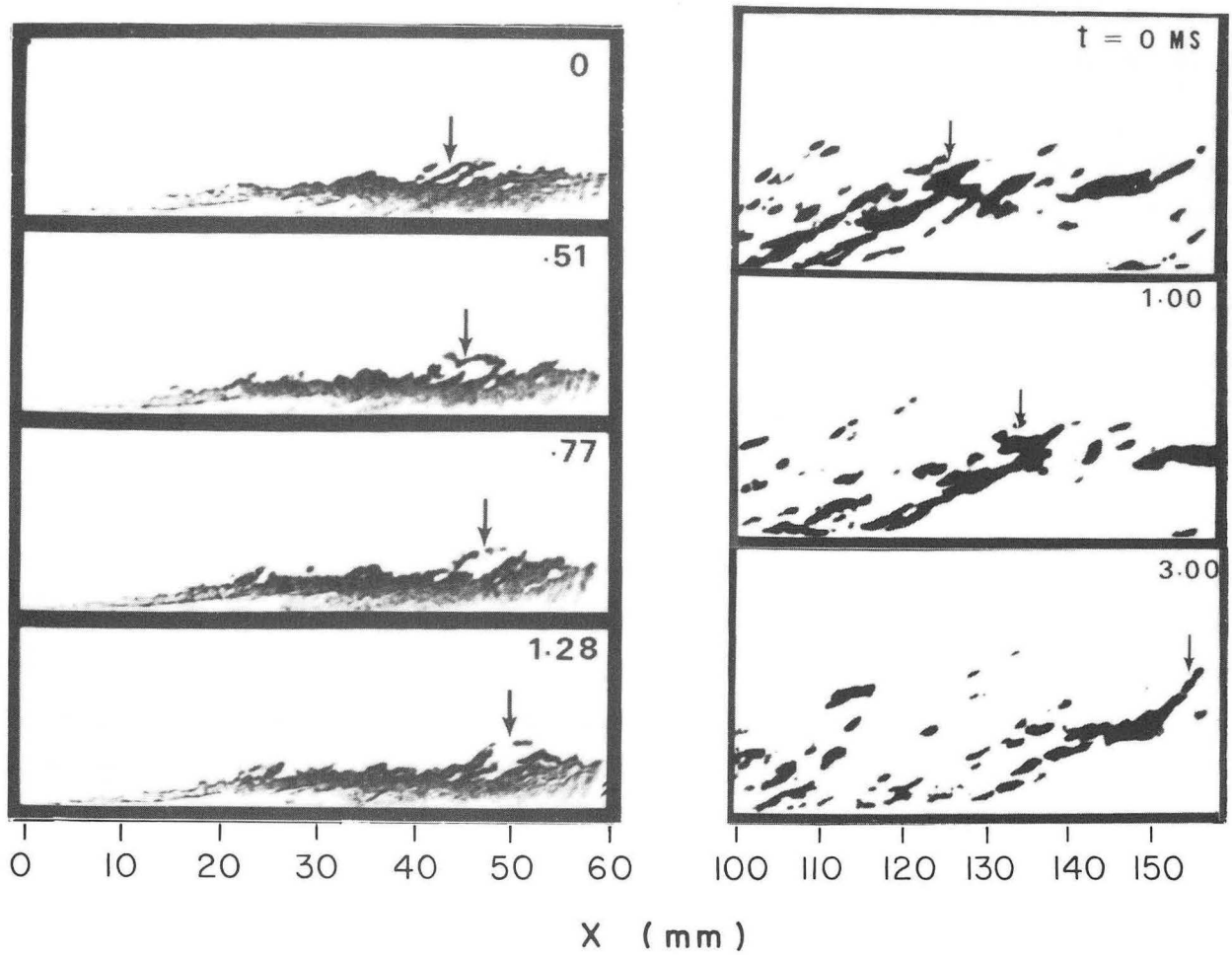

Figure 1. Schlieren records of a reacting turbulent boundary layer. Leading edge of the heated section is at x = 0. U_∞ = 10.0 m/sec, T_W = 1200 K, and ϕ = 0.35, using ethylene/air mixture. (XBB 817-6450A)

be consistent with the large-scale turbulence structures of the velocity boundary layer, indicating that these fluid-mechanical structures govern the combustion processes.

Combustion heat release causes the boundary layer to expand. As a consequence, the mean density and velocity profiles show no overall similarity as in the isothermal and heated wall flows. These profiles also demonstrate a reversal of heat transfer direction between the heated wall and the fluid as the flame structures develop. Near the leading edge, the heat transfer direction is from the wall to the fluid. However, the direction is reversed at locations farther downstream.

Shown in Figure 2 are the streamwise and cross-stream rms velocity fluctuation profiles in a reacting boundary layer at various locations along the test section. In general, combustion increases the velocity fluctuations in the outer part of the boundary layer away from the heated wall. The shape of the fluctuation profiles of density and velocity changes downstream from the leading edge of the heating section. These changes are consistent with the development of the flame structures over the test section. Combustion heat release reduces the Reynolds stress throughout the boundary layer. This reduction in Reynolds stress associated with an increase in turbulent kinetic energy indicates that other turbulence production mechanisms should be important.

Figure 3 shows the effects of combustion on the turbulent kinetic energy diffusion pattern. The change in streamwise turbulent kinetic energy diffusion is significant, as indicated by the difference between the $u'k_1$ profiles of the isothermal and reacting flows. This would mean that the boundary-layer assumptions need to be modified for this reacting flow.

Also deduced and studied are the density and velocity probability density functions (pdf) in the reaction regions where the density and velocity fluctuations are at their peaks. All the density pdf's are bimodal whereas the velocity pdf's are single-peaked. The differences between the density and velocity pdf's perhaps indicate that the fluctuations are associated with the orientations of individual flame fronts within the flame structures. Because density is a scalar quantity, the two peaks of the pdf's are associated with the density in front of and behind the flame fronts. The

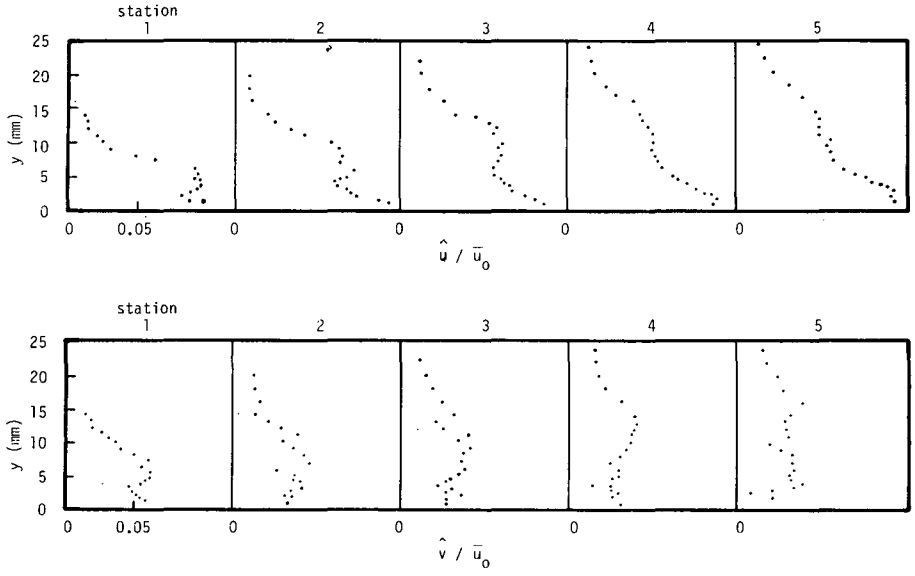

Figure 2. Streamwise and cross-stream rms fluctuation profiles ($\hat{u}$ and $\hat{v}$, respectively) of the reacting turbulent boundary layer over 5 axial stations. Station 1: x = 33 mm, Station 2: x = 62 mm, Station 3: x = 90 mm, Station 4: x = 123 mm, and Station 5: x = 148 mm.
(XBL 8112-12939)

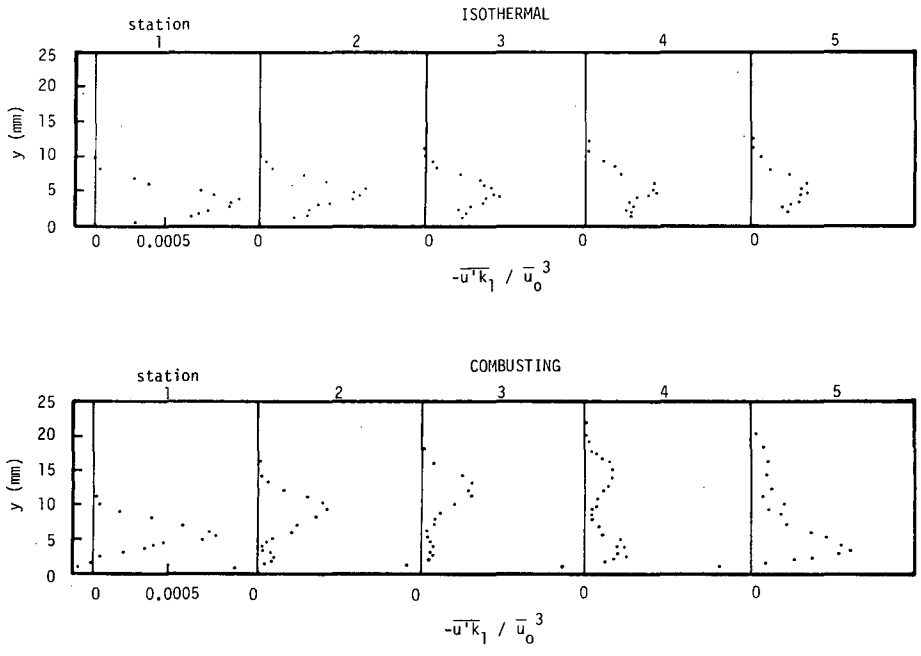

Figure 3. Composition of streamwise turbulence diffusion in isothermal and reacting turbulent boundary layer at 5 axial stations. Station 1: x = 33 mm, Station 2: x = 62 mm, Station 3: x = 92 mm, Station 4: x = 123 mm, and Station 5 x = 148 mm.
(XBL 8112-12942)

orientations of the flame fronts within the flame structures should be quite random. The velocity fluctuations induced by these flame fronts therefore should also be quite random. Consequently, the streamwise and cross-stream velocity pdf's do not show a bimodal distribution.

PLANNED ACTIVITIES IN FY 1982

Further analysis and interpretation of the data of the reacting flow will be made. These results should provide a more comprehensive description of the turbulence-combustion interaction in the turbulent boundary layer.

Instantaneous Reynolds stress will be measured in the isothermal, heated wall and reacting flows using a two-component (two-color) LDV system. These data will be useful for analyzing the turbulence production mechanisms near the wall. The effects of wall heating and combustion heat release on these mechanisms will provide a better understanding of the influence of the large-scale turbulence structures on the development of the flame structures.

Cross-correlation between density and velocity fluctuations will be measured by a system combining the Rayleigh scattering and the single-component LDV systems. These results will be used to study turbulence scalar transport within the various boundary-layer flows. Also, the density and velocity cross-correlation data can be used as a means to obtain conditional sampling of velocity fluctuations. The fluctuation intensities in front of and behind the flame fronts in the flame structures will show whether or not the velocity fluctuations are influenced by combustion heat release. Some higher-order density and velocity cross-correlations can also be obtained by using suitable data analysis methods. These quantities are pertinent to turbulence energy and momentum transport.

REFERENCES

1. Cheng, R.K., and Ng, T.T. (1981), Some Aspects of Strongly Heated Turbulent Boundary Layer Flow, Lawrence Berkeley Laboratory Report LBL-13549, to be published in Physics of Fluids.

2. Townsend, A.A. (1965), J. Fluid Mech. 22, p. 779.

3. Ng, T.T. (1981), Experimental Study of a Chemically Reacting Turbulent Boundary Layer, Ph.D. Thesis, Department of Mechanical Engineering, University of California, Berkeley.

4. Ng, T.T., et al. (1982), Combustion-Turbulence Interaction in a Strongly Heated Turbulent Boundary Layer, Lawrence Berkeley Laboratory Report LBL-13893, accepted for presentation and publication at the 19th Symposium (International) on Combustion.

5. Ng, T.T. (1982), Measurements of Velocity Fluctuation Correlations Using a Single-Component Laser Doppler Velocimetry System, Lawrence Berkeley Laboratory Report LBL-13702, submitted for publication in AIAA Journal.

Velocity Statistics in Premixed Turbulent Flames*

R. K. Cheng, T. T. Ng, F. Robben, and L. Talbot

The characteristics of premixed turbulent combustion are important to the design of most practical combustion systems. The size and power characteristics of a combustor can be optimized because the flame propagation speed and volumetric power density are much higher in turbulent combustion flows than in laminar combustion flows. Although considerable progress has been made in recent experimental and theoretical investigations, the interaction between turbulence and combustion is still not very well understood. There are two basic experimental approaches to the study of turbulent-combustion. The first is to measure gross properties of the turbulent flame and correlate these properties with turbulent properties of the incident flow. The second approach, which this present study adopts, is to understand the physical processes of turbulent combustion interaction through detailed statistical measurements and flow visualization techniques.

Because of the high gradients and extreme conditions associated with combustion flows, statistical measurements of temperature, velocity, and chemical species concentrations are only feasible using laser-based diagnostic techniques. Such data provide information leading to a better understanding of the physical processes of turbulence-combustion interaction. In addition, a statistical data base for turbulent combustion is necessary to assist theorists in formulating and evaluating numerical models of turbulent combustion which would aid the design of future combustion systems with higher efficiencies and lower pollutant emissions.

The objective of the present program is the measurement of velocity statistics in a premixed turbulent flame of simple configuration using laser Doppler velocimetry (LDV). The flame configuration is a V-shaped ethylene/air sheet flame stabilized in turbulent flow with grid- or perforated-plate-

*This work was supported by the Director, Office of Energy Research, Office of Basic Energy Sciences, Chemical Sciences Division of the U.S. Department of Energy under Contract No. DE-AC03-76SF00098.

induced turbulence. Also obtained are schlieren records showing the shape of the instantaneous flame sheet to facilitate the interpretation of the turbulence statistics in the flame.

ACCOMPLISHMENTS DURING FY 1981

Flame propagation in grid-induced turbulence was studied for four conditions with free-stream velocity, U_∞, of 5.0 and 7.0 m/sec and equivalence ratio, ϕ, from 0.66 to 0.8. In addition, flame propagation with the turbulence generated by two different perforated plates was studied for U_∞ = 7.0 m/sec and ϕ = 0.75. A single-component LDV system was used to measure two components of mean and root-mean-square (rms) velocities and the Reynolds stress ($-\overline{u'v'}$). The streamwise macroscale, the probability density functions, and the streamwise velocity spectral density distributions were also deduced from the data.

Figure 1 shows a typical velocity vector field of a V-shaped turbulent flame. The gross effect of the flame on the flow field changes the flow directions ahead of and behind the flame. In the free stream ahead of the flame, the flow is deflected outward. Through the flame region, because of combustion-induced gaseous expansion, the flow is accelerated and deflected inwards. Also, a small increase in the free-stream turbulence level was observed.[1]

Shown in Figure 2 is a schlieren record of a V-shaped flame stabilized in perforated-plate-

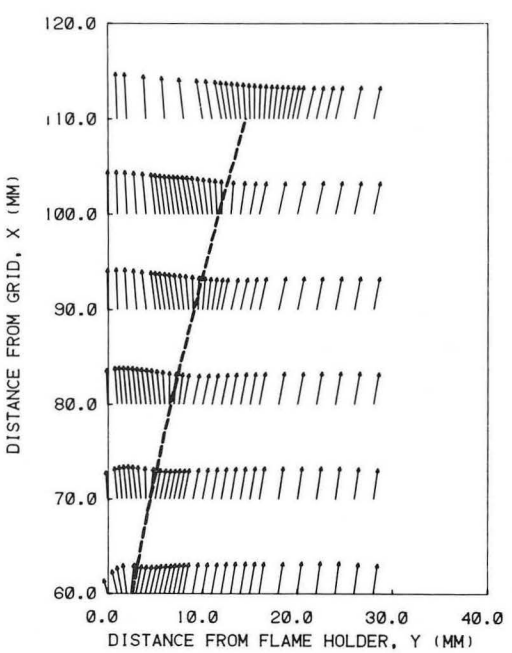

Figure 1. Two-dimensional velocity vector field of a V-shaped turbulent flame in grid-generated turbulence. Flame origin at x = 50 mm and y = 0 mm. u = 7.0 m/sec, ϕ = 0.75. ----- mean flame position, ... cold boundary, —— velocity vectors. (XBL 819-4960)

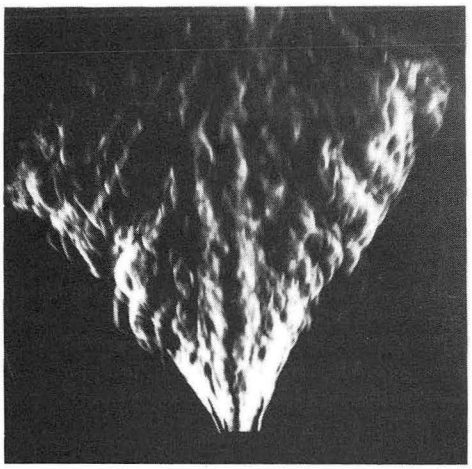

Figure 2. Schlieren image of a V-shaped turbulent flame in perforated-plate-induced turbulence. (XBB 817-6368)

induced turbulence. The instantaneous flame sheet is characterized by the flame convolutions. Under identical initial conditions, the size of the flame region in perforated-plate-induced turbulence is larger than that in grid-induced turbulence because the flame convolutions are developed and amplified more rapidly in the former flow. However, the mean flame angle and free-stream deflections seem to be unaffected by the different incident turbulence.

Increases in both streamwise and cross-stream rms velocity fluctuations are significant inside the flame region. This is caused by local acceleration and flow deflection associated with the movement of the flame sheet about the stationary LDV probe. The fluctuations in the hot region are comparable to or less than that of the incident turbulence. This result shows that turbulent kinetic energy is not increased by combustion heat release for the conditions of these experiments.

As shown in Figure 3, the increase in Reynolds stress inside the flame region is also significant and could be interpreted to mean an increase in turbulence production inside the flame region. However, using an argument based on a simple model of the interaction between the flow and the instantaneous flame front, we are able to demonstrate that the increase in Reynolds stress seems to be consistent with flame-induced acceleration and flow deflection. Furthermore, the magnitude of the Reynolds stress in the flame region is highly correlated with the rms fluctuations. This correlation further indicates that the Reynolds stress is a consequence of the fluctuating flame sheet and may not be intrinsic to fluid-mechanical turbulence production.[2]

PLANNED ACTIVITIES FOR FY 1982

A two-component (two-color) LDV system will be used to measure instantaneous Reynolds stress in the flame region. The data will be analyzed to discriminate between the Reynolds stress ahead of and behind the flame sheet. These results will enable us to further investigate whether the Reynolds stress is intrinsic to fluid-mechanical turbulence production.

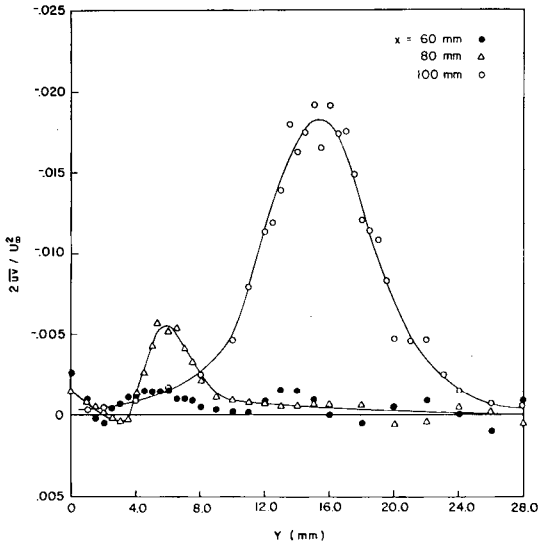

Figure 3. Reynolds stress ($-\overline{u'v'}$) profiles at 3 axial locations across a V-shaped turbulent flame in grid-induced turbulence. Flame origin at x = 50 mm, y = 0 mm, U_∞ = 70 m/sec, ø = 0.75.
(XBL 819-2021)

The cross-correlation between density and velocity will be measured by combining the Rayleigh scattering and the single-component LDV systems. This system will be used to obtain conditional sampling of the velocity fluctuations in the flame region. The data will be reduced to obtain the rms fluctuations ahead of and behind the flame sheet. Comparison of these separate rms fluctuations will show whether turbulence is affected by combustion heat release.

REFERENCES

1. Cheng, R.K., and Ng, T.T. (1981), "Experimental Study of the Flowfield of a V-Shaped Premixed Turbulent Flame," in First Specialist Meeting (International) of the Combustion Institute, The French Section of the Combustion Institute 1, p. 13.

2. Cheng, R.K., and Ng, T.T. (1981), Velocity Statistics in Premixed Turbulent Flames, presented at the 1981 Fall Meeting, Western States Section/The Combustion Institute, Tempe, Ariz., Oct. 19-20, 1981, Lawrence Berkeley Laboratory Report LBL-13367, submitted for publication in Combustion and Flame.

Lean Engine Combustion Studies*

R. F. Sawyer, A. K. Oppenheim, J. W. Daily, R. Greif,
K. Hom, H. E. Stewart, J. B. Woodard, and D. Hirvo

The operation of an internal combustion engine under lean, premixed conditions has the potential advantage of increased efficiency and reduced emissions. Studies of important phenomena relating to lean combustion have been conducted utilizing unique single-pulse, compression-expansion facilities. These devices, which feature square pistons and two glass walls, provide complete optical access to the combustion process, including that part which occurs as the piston is withdrawn.

The initial version of this machine (CE-1) was pneumatically driven and hydraulically controlled. The major drawback of this configuration has been control of the piston trajectory, which cannot be made to fully match that of a reciprocating piston engine. An improved version of the machine has been designed, constructed, and demonstrated. The piston of the second compression-expansion machine (CE-2) is driven by a crankshaft and controlled by a fast-acting clutch-brake mechanism, permitting one- to four-stroke operation. The cross-section of the combustion chamber is larger than that of CE-1 and matches that of the standard CFR laboratory test engine. The head is provided with conventionally operated overhead intake and exhaust valves.

ACCOMPLISHMENTS DURING FY 1981

The crankshaft-operated, compression-expansion machine has been brought into operational condition, including the control system and computer-based data logging system. Preliminary investigations have been conducted of the optical measurement of hydrocarbons using in-situ optical-absorption methods.

The CE-1 version was utilized to obtain simultaneous data on single-event flame propagation, wall heat transfer, and their interaction in a constant-volume chamber. Pressure variation, wall temperature variation, and high-speed schlieren movies were recorded for the combustion of methane and air for various equivalence ratios. Flame locations are shown in Figure 1. Flame speed and wall heat flux variation with respect to time were calculated from the data (Figures 2 and 3). The results indicate that there are important geometry effects on flame speed due to side-wall interaction. The wall heat-flux data show effects due to the location of the flame relative to the location of the heat-transfer measurement. Peak heat-flux

*This work supported by the Assistant Secretary for Conservation and Renewable Energy, Office of Transportation Programs, Division of Transportation Energy of the U.S. Department of Energy under Contract DE-AC03-76SF00098.

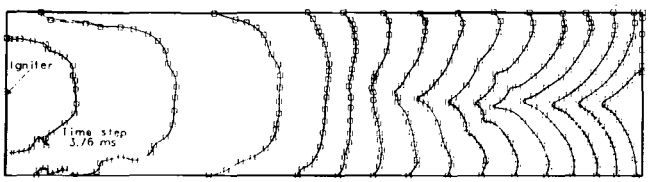

Figure 1. Flame-front location from schlieren movies for time steps of 3.76 msec starting at ignition; total elapsed time to last location shown is 56.4 msec; equivalence ratios 1.1.
(XBL 825-10198)

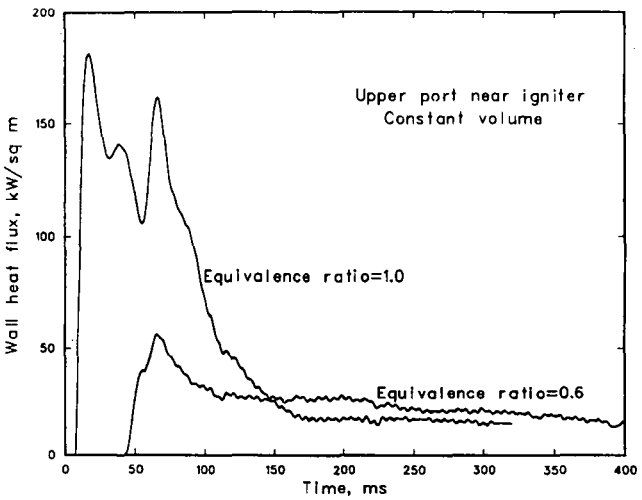

Figure 2. Wall heat flux variation with time at upper port near igniter; constant volume combustion; equivalence ratios 1.0 and 0.6.
(XBL 825-10199)

values occur when the flame front passes the location of measurement. High ignition energies are found to overdrive the rate of flame propagation.

PLANNED ACTIVITIES FOR FY 1982

Flame propagation studies for lean methane/air mixtures will be extended to a thorough investigation of the ignition-expansion and compression-ignition-expansion cases. Ethylene/air mixtures will be investigated to provide a fuel with chemical kinetic properties substantially different from methane and to provide data for comparison with modelling studies.

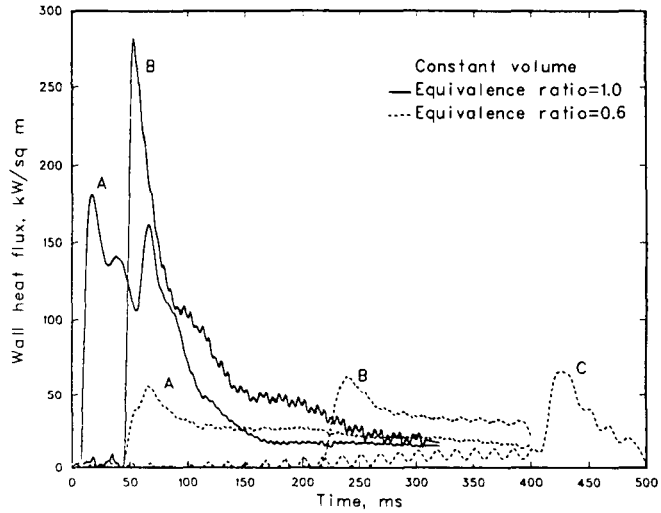

Figure 3. Wall heat flux variation with time for three locations in apparatus: A. upper port near igniter, B. upper port far from igniter, C. bottom port far from igniter; constant volume combustion; equivalence ratios 1.0 and 0.6. (XBL 825-10200)

Heat-transfer studies will be conducted in conjunction with the flame-propagation studies in the CE-1 apparatus and in a constant volume cell, CV-2. Experimental studies will focus upon validation of a theoretical model of the boundary-layer heat-transfer process occurring in the presence of a propagating flame. This model, in turn, will provide fundamental data and boundary conditions useful to the development of larger computational models for engine combustion.

Ignition studies will be transferred from the constant-volume facility (CV-1) to the new square-piston facility, CE-2. Flow visualization using high-speed schlieren cinematography will add the effects of piston motion and valve-induced flows to current ignition observations.

A Staged Fluidized Bed Combustor for the Study of Pollutant Formation and Destruction*†

R. F. Sawyer, J. F. LaFond, and J. R. Hart

Stationary combustion sources account for about one-half of the oxides of nitrogen emitted into the atmosphere. Two mechanistic paths are responsible for the production of nitric oxide during combustion; one involves the oxidation of atmospheric nitrogen (thermal NO) and the other the oxidation of nitrogen chemically bound to fuel molecules (fuel NO). Coal and coal-derived fuels are particularly high in their fuel nitrogen content and therefore represent a special concern as sources of oxides of nitrogen. Reducing maximum flame temperatures has proven an effective method of controlling thermal NO but has little effect on the formation of fuel NO.

Staged combustion is an abatement technique that appears capable of reducing both forms of nitric oxide while also minimizing emissions of other pollutants, both criteria and non-criteria. A two-stage fluidized-bed combustor, consisting of a fuel-rich fluidized bed followed by a fuel-lean fluidized bed, has been constructed. The fluidized beds provide additional control over temperature and residence time in comparison with conventional combustors.

ACCOMPLISHMENTS DURING FY 1981

A laboratory two-stage fluidized-bed combustor has been constructed for the study of the formation and destruction of pollutant species (Figure 1). Characterization of the facility for several configurations and a range of fuel flow rates (fuel/air mixture ratios) has been accomplished in terms of stable operating conditions, temperatures, pressures, and gas composition through the device. A variety of operating parameters are available, including number of stages, bed depths, bed materials, fuel, oxidizer, and dopant flow rates and residence times. Not all of these parameters are independent for stable operation.

Initial studies used propane as the fuel, air as the oxidizer, and NO as a dopant to simulate fuel nitrogen. Species monitoring included CO, CO_2, NO, and total hydrocarbons. Stable two-stage operation was obtained with a fuel-rich mixture in the first stage, followed by air injection and completion of combustion in the second stage. A maximum reduction of 66 percent of the input NO dopant was obtained under two-stage operation (Figure 2).

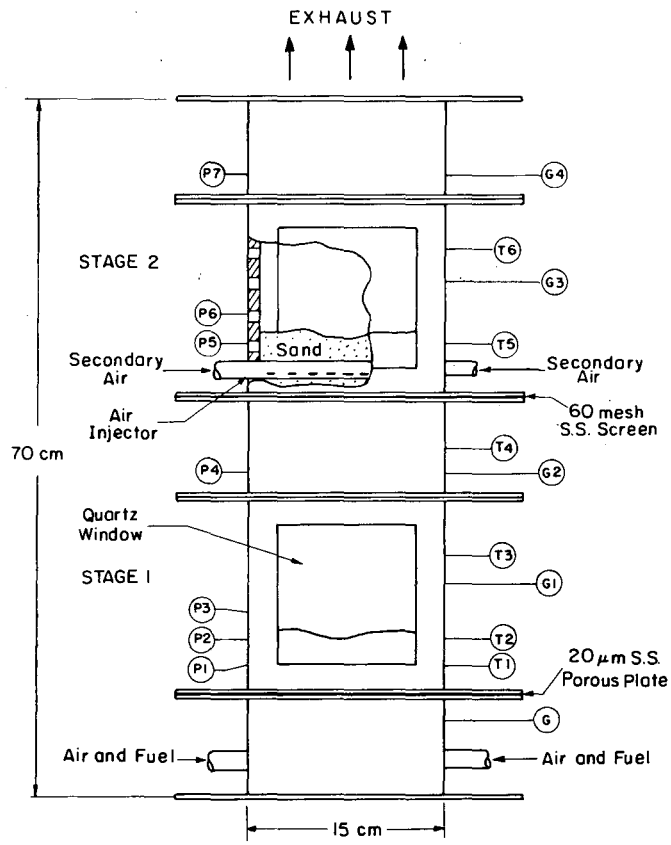

Figure 1. Two-stage fluidized-bed combustor. (XBL 819-6572)

The facility has the additional capabilities of operating either or both beds in a two-dimensional spouted mode, optical access for flow visualization, and addition of a third stage. In addition to the study of pollutant formation and destruction, the apparatus is suited to the investigation of the combustion of low-quality fuels and the incineration of toxic wastes.

PLANNED ACTIVITIES FOR FY 1982

Funding for work on staged combustion has been terminated. The use of this facility will be redirected to investigations of toxic waste incineration during FY 1982. Conditions desirable for minimizing nitric oxides are in many ways similar to those for the destruction of toxic substances, which often are organic materials containing nitrogen, phosphorous, and halogens. Model halogen compounds will be employed as surrogates for toxic halogenated hydrocarbons.

*This work was supported by the Assistant Secretary for Fossil Fuels, Office of Utilization of the U.S. Department of Energy under Contract DE-AC03-76SF00098 and by the Morgantown Energy Technical Center of the U.S. Department of Energy under Contract No. PR-14037.

†Condensed from LaFond, J.F., Hart, J.R., and Sawyer, R.F. (1981), A Staged Fluidized-Bed Combustor for the Study of Pollutant Formation and Destruction, Western States Section, the Combustion Institute, Paper No. 81-53; also Lawrence Berkeley Laboratory Report LBL-13020.

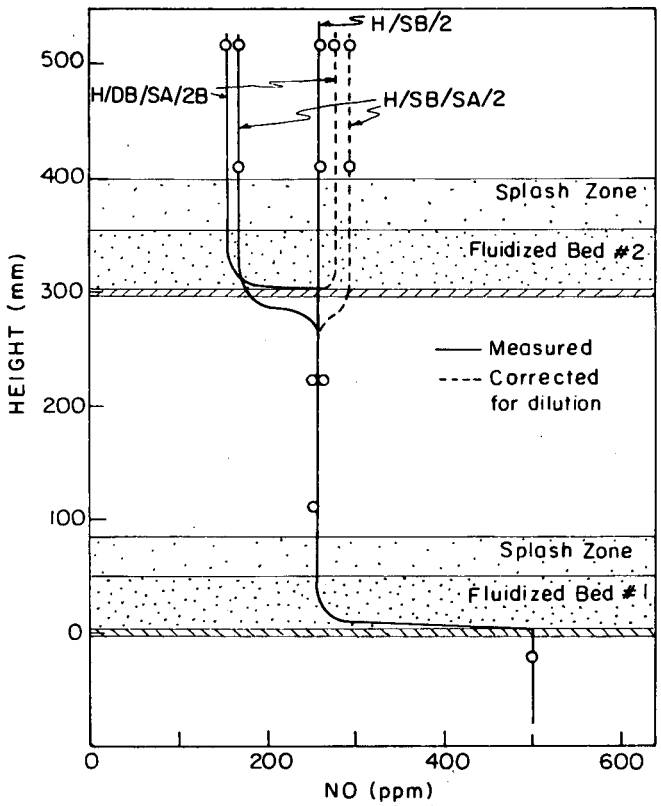

Figure 2. Vertical NO profiles. Single-bed, with and without overfire air, and double-bed configurations, ϕ_1 = 1.48. (XBL 819-6570)

Chlorine and Bromine Inhibition of a Polyethylene Opposed-Flow Diffusion Flame*†

W. J. Pitz and R. F. Sawyer

The importance and contribution of the inherent flammability of polymeric materials to problems of fire safety is well recognized. A series of studies have been undertaken utilizing an opposed-flow diffusion-flame burner because this geometry allows both steady, diffusion-controlled burning and extinction to be observed under well-controlled laboratory conditions. Fuel composition, oxidizer composition, and oxidizer blowing rate are available as experimental parameters.

*This work was supported by the National Bureau of Standards under Contract 805180, the Department of Mechanical Engineering of the University of California at Berkeley, and the U.S. Department of Energy under Contract No. DE-AC03-76SF00098.

†Condensed from Pitz, W.J. and Sawyer, R.F. (1981). "Chlorine and Bromine Inhibition of a Polyethylene Opposed Flow Diffusion Flame." Submitted for presentation at the Second International Specialists Meeting of the Combustion Institute on Oxidation, Budapest, Hungary.

ACCOMPLISHMENTS DURING FY 1981

The opposed-flow diffusion flame was employed to investigate the effect of halogenated inhibitors on the extinction of a polyethylene flame. Three levels of inhibitor effectiveness were examined: none (nitrogen), moderate (chlorine), and substantial (bromine). Chlorine was added to the oxidizer and fuel sides of the diffusion flame to assess differences in inhibitor behavior in contrasting environments. Fuel-side addition was achieved by using chlorinated polyethylene, which has atomic chlorine substituted into its polymeric structure. Conditions of flame extinction were observed in all the above cases and used to evaluate inhibitor effectiveness. Fuel-added chlorine showed much greater inhibitor effectiveness than oxidant-added chlorine (Fig. 1). The increased relative effectiveness may have resulted from promotion of char formation on the chlorinated polyethylene surface.

A numerical boundary-layer model developed previously was employed to extract overall reaction

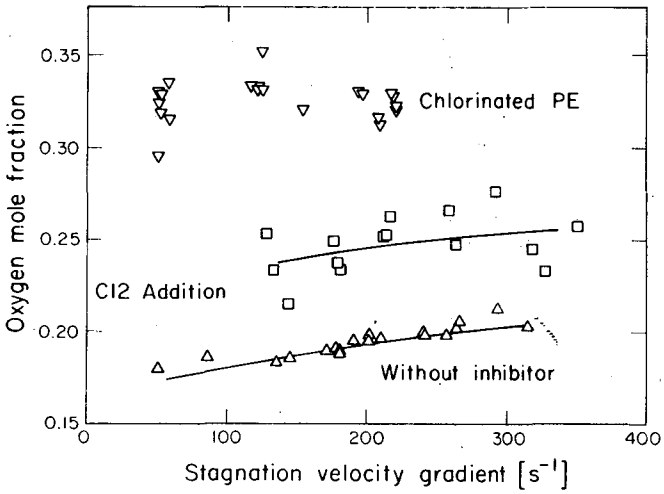

Figure 1. Comparison of extinction conditions for fuel-added and oxidant-added chlorine and for no inhibitor (——— prediction with E_A = 100 kcal/gmole). (XBL 825-676)

rates from the extinction data. The temperature dependencies of the overall reaction rates obtained seemed unaffected by inhibitor addition. The change in overall reaction rate with inhibitor addition was reflected by a change in overall pre-exponential coefficient.

PLANS FOR FY 1982

Final reporting of this work will be accomplished, and this work will then be concluded.

Spouted-Bed Combustion*†

R. F. Sawyer, K. Ohtake, and J. R. Hart

Spouted beds have been used as solids-gas contacting devices in such applications as drying grains and solids blending and for the cooling, coating, and granulation of solids. Spouted-bed reactors have been used in coal gasification, coal carbonization, petroleum cracking, and ore roasting. Recent laboratory studies have focused on the heat-recirculation characteristics of spouted-bed reactors and their ability to burn low quality fuels.

ACCOMPLISHMENTS IN FY 1981

A two-dimensional spouted-bed laboratory combustor has been designed and constructed with the objective of studying the interaction among gas flow, particle flow, and combustion. The laboratory facility, designed for a maximum thermal power of 20 kW, has a quartz front wall, providing full optical access to particle flows and combustion processes (Fig. 1). Initial studies employed premixed propane and air and a fixed bed height, bed material, injector slot width, and combustor geometry.

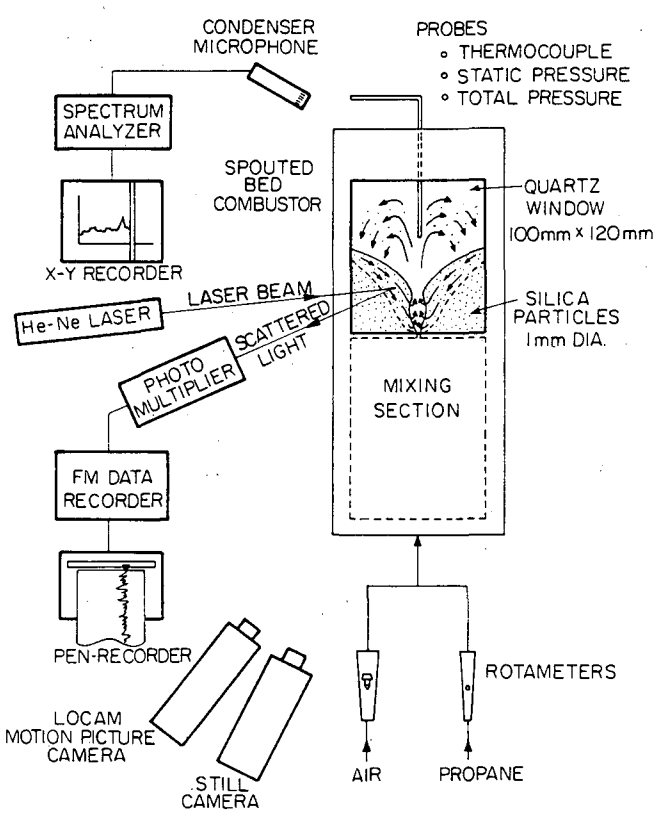

Figure 1. Spouted-bed combustor facility. (XBL 823-5395)

*This work was supported by the U.S. Department of Energy under Contract No. DE-AC03-76SF00098.

†Condensed from Hart, J.R., Ohtake, K., and Sawyer, R.F. (1982), "Flow and Combustion Characteristics of a Two Dimensional Spouted Bed," submitted for presentation at the 1982 Spring Meeting, Western States Section/The Combustion Institute, Salt Lake City, Utah.

As in previous investigations of axisymmetric spouted beds, the ratio of particle-mass circulation rate to jet-mass flow rate was observed to be about ten. Combustion increases this ratio by about 10 percent. A pulsating mode of operation was noted, with a characteristic frequency of about ten Hz controlled by the particle flow. In the present configuration, internal heat recirculation is approximately balanced by heat losses so that lean and rich flammability limits are extended only slightly beyond those of premixed laminar flames (Fig. 2).

PLANS FOR FY 1982

Further characterization of spouted-bed combustion will be undertaken to determine mass circulation rates, including particle velocities in the spout and fountain regions. Particle size, particle composition, bed depth, and slot width will be added as experimental parameters. Initial investigations will be made of the burning of solid fuels.

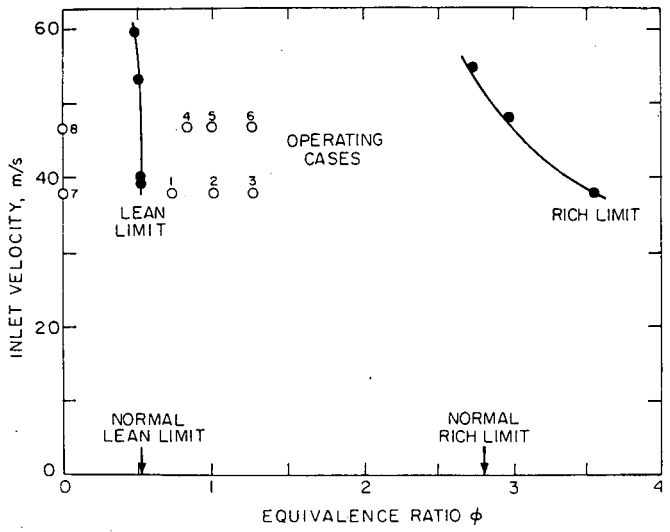

Figure 2. Spouted-bed combustion limits.
(XBL 823-5396)

Characteristics of Fly Ash from Laboratory Combustion of Pulverized Coal*

G. M. Parsons, P. Sherman,† R. Greif, and F. Robben

Pulverized coal combustion produces fly ash particles that comprise a wide range of size and toxic trace element distributions. The smaller fly ash particles have a significant enrichment of volatile trace elements. A commonly used model for the formation and distribution of elements in fly ash particles is the vaporization condensation model. Trace elements are volatilized in the hot combustion zone and, depending on the cooling rate, condense to form small particles or coalesce to form large particles. The larger surface-to-volume ratio of smaller particles leads to an enrichment of volatile trace elements upon condensation. Pollution control devices presently being used or being considered all have high overall mass collection efficiencies which, however, decrease considerably for the smaller particles. The smaller particles also have much longer atmospheric residence times than do the larger particles. This longer residence time, coupled with volatile (usually toxic) enrichment and the ease of ingestion into the lungs, may make the small particulate output from utility boilers more important than their weight fraction would indicate.[1,2]

*This work was supported by the Assistant Secretary for Environment, Office of Environmental Research and Development, Environmental Control Technology Division of the U.S. Department of Energy under Contract No. DE-AC03-76SF00098.

†Department of Aerospace Engineering, University of Michigan, Ann Arbor, Mich.

ACCOMPLISHMENTS DURING FY 1981

A small amount of Pittsburgh seam pulverized coal was entrained in an air/methane/oxygen mixture and burned in an enclosed bunsen type burner fitted with a chimney. This arrangement was able to simulate the temperature-time history of a pulverized-coal burner. Particulate sampling was done with a Lawrence Berkeley Laboratory automated dichotomous air sampler which divides the particulates into two size ranges, those with Stokes diameters in the range between 2.5 and 15 μm and those with Stokes diameters less than 2.5 μm. The mass collected was determined by electron beam attenuation (Beta gage) and the elemental composition by x-ray fluorescence.

The burner chimney controls the rate at which the mixture cools; the residence time is sufficient for the coal particles to burn out in the first 1/4 to 1/3 of the chimney length. Two chimney configurations were used: an uninsulated ceramic tube 44 mm in diameter and 355 mm long and a similar tube provided with a layer of insulation to reduce the heat loss and thereby operate at higher temperatures. At the downstream end of each chimney, secondary air is injected to rapidly cool the combustion products in a short (75-mm-long) section. The initial cooling rate of the insulated chimney is less than that of the uninsulated chimney, but, upon quenching, the cooling rate becomes greater for the insulated chimney. The chimney without insulation will be referred to as the low-exit-temperature chimney while the chimney with insulation will be referred to as the high-exit-temperature chimney.

The normalized percentages of 18 elements in the small size fraction for the different burner and chimney conditions has been tabulated. The elemental concentration on a given filter is first normalized to the silicon concentration on that filter; the percent in the small size fraction is then calculated for each run. The percent in the small size fraction is defined as the ratio 100S/(S+L), where S is the normalized elemental concentration on the small size fraction filter for a given run, and L is similar except for the large size fraction filter. The normalization is made to account for any sample material that may be lost from the filter between the time the sample is taken until the time it is analyzed. The usefulness of the normalization to silicon is based on the assumption that the concentration of silicon in the fly ash is independent of particle size. It was found that concentration of silicon in the small size fraction did change slightly with the peak temperature, but there was no noticeable change with the chimney exit temperature. The normalization was found to reduce the scatter of the elemental concentration data.

In Figure 1 the percent of total sample weight in the small size fraction is shown as a function of the peak temperature. From the linear least squares fit, it is seen that the weight percentage in the small size fraction increases with increasing peak temperature. No correlation was found between the percentage of the total sample weight in the small size fraction and the chimney exit temperature.

In Figure 2 a comparison is made between the volatile element arsenic and the refractory element aluminum. Both elements are first normalized to silicon and then plotted as a function of chimney exit temperature. The line through the small size fraction arsenic data is a least-squares-fit line. The concentration of arsenic in the small size particles appears to be a function of chimney exit temperature, while the concentration of aluminum does not.

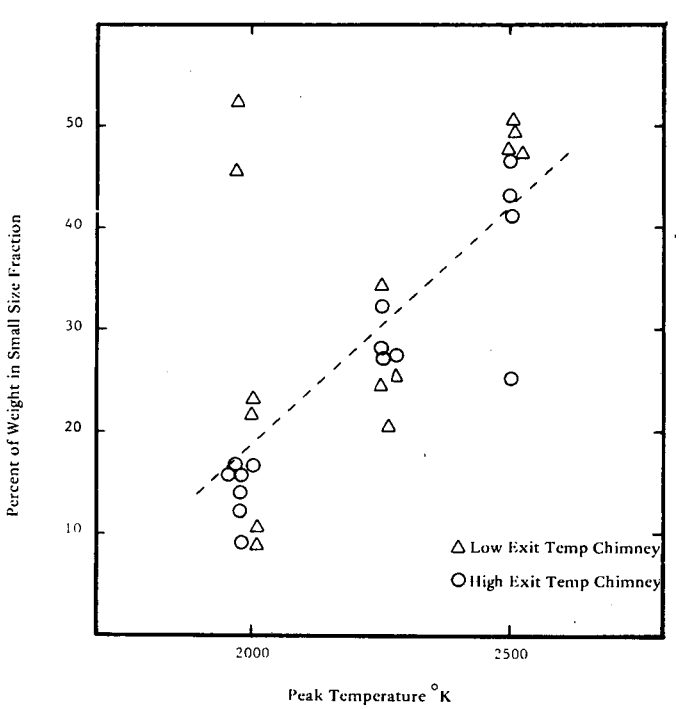

Figure 1. Sample weight in small size fraction.
(XBL 824-8917)

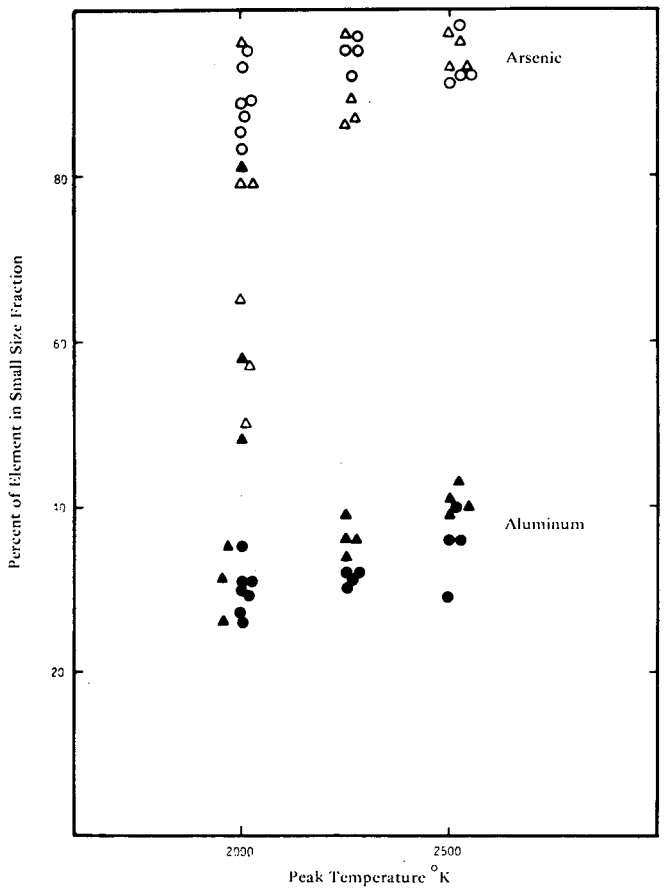

Figure 2. Comparison of aluminum and arsenic: ▲△ low exit temperature chimney, ●○ high exit temperature chimney.
(XBL 824-8919)

Figure 3 is plotted to again compare the behavior of arsenic and aluminum. The percent of aluminum and arsenic in the small size fraction is shown as a function of peak temperature. This figure clearly shows the enrichment of arsenic (~90 percent) and the depletion of aluminum in the small size fraction (~30 percent). The small increase in aluminum concentration in the small size fraction with increasing peak temperature is not large enough, compared to uncertainties, to be significant.

In addition to arsenic, elements showing significant enrichment in the small size fraction are iron, zinc, potassium, and chromium. Other elements having significant enrichment in the small size, but a large degree of scatter at low peak temperatures, are rubidium, vanadium, nickel, selenium, and sulfur. Calcium and titanium appear to be enriched in the small sizes but not to as great an extent. The results are inconclusive for antimony and manganese. As noted previously, aluminum was depleted in the small size fraction.

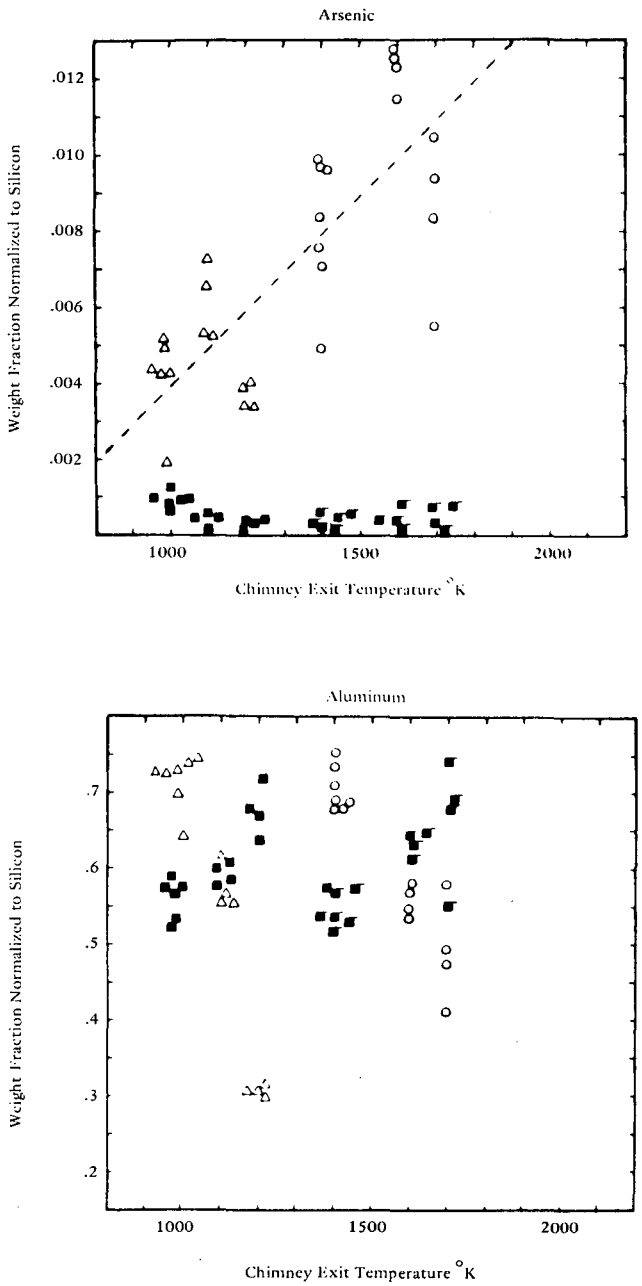

Figure 3. Comparison of arsenic and aluminum: Δ low-exit-temperature chimney, small size fraction; ○ high-exit-temperature, small size fraction; ■ low-exit-temperature chimney, large size fraction; ■ high-exit chimney, large size fraction. (XBL 824-8918)

Others[3,4] found similar enrichments of arsenic, rubidium, vanadium, zinc, and nickel in samples from utility boilers. Agreement was also found for the depletion of aluminum and the slight increase in titanium and iron concentrations in small particles. The enrichment of iron in the small particles increased with increasing peak temperature; this was not found in the utility boiler tests because of their constant operating conditions.

The results of this experiment appear to be in agreement with a vaporization-condensation model for the chemistry of small fly ash particles.[2] According to the model, some of the volatile elements in the coal are vaporized in the high temperature region of the flame. Changes in the chemical state or decreases in temperature cause the vapor to become saturated and condensation may occur. From this model, one would anticipate that the concentration of elements in a particle of a given size would depend on both the peak combustion temperature and the temperature at which quenching occurs (chimney exit temperature). The peak temperature dictates which elements are volatilized. General agreement with Smith[4] is found except in the case of iron. We found iron to be slightly enriched in the small size fraction, whereas Smith found iron to behave like aluminum and subsequently show a depletion in small size particles.

PLANNED ACTIVITIES IN FY 1982

No further work is planned in this area.

REFERENCES

1. Flagan, R.C., and Friedlander, S.K. (1976), "Particle Formation in Pulverized Coal Combustion--A Review," Symposium on Aerosol Science, the 82nd National Meeting of AIChE.

2. Flagan, R.C., and Taylor, D.D. (1980), "Laboratory Studies of Submicron Particles from Coal Combustion," in Eighteenth Symposium (International) on Combustion, The Combustion Institute, Pittsburgh, p. 1227.

3. Markowski, G.R., et al. (1980), "A Submicron Aerosol Mode in Flue Gas from a Pulverized Coal Utility Boiler," Env. Sci. and Tech. 14, p. 1400.

4. Smith, R.D. (1980), "Trace Element Chemistry of Coal during Combustion and the Emissions from Coal-Fired Plants," Prog. Energy Combust. Sci. 6, p. 53.

Two-Point Rayleigh Scattering Measurements in a V-Shaped Turbulent Flame*

M. Namazian, L. Talbot, and F. Robben

The desire for more efficient and lower pollutant-generating combustion devices has stimulated a variety of research efforts aimed at increased understanding of turbulent combustion. Considerable progress has been made in recent years in both theoretical and experimental studies of the turbulent flame. However, a physically realistic perception of the turbulent flame has not yet been achieved. The difficulty stems from the complexity of the problem and the limitations of the available experimental techniques to investigate the problem.

The development of the laser anemometry technique has resulted in a significant advance in understanding turbulent flames by enabling detailed velocity measurements to be made. However, velocity fluctuations are coupled with the density, and, therefore, detailed density fluctuation measurements are also required.

The Rayleigh scattering method,[1] which has been developed in recent years, offers a powerful technique for the measurement of the density and the temperature of gases. This technique has been successfully applied to turbulent flames by a number of investigators[2-5] to measure the density fluctuations at one point. However, detailed statistical spatial characteristics of the combustion zone are difficult to obtain from analysis of a time series of single-point measurements. Alternatively, statistical analysis of a time series of simultaneous measurements at two separated points[6,7] can be a powerful method to determine the spatial and temporal structure of the combustion zone.

The objective of this work is to apply the Rayleigh scattering technique for density measurements at two points in turbulent flames. We used two independent sets of scattered-light collection optics and a method of splitting the laser beam and varying the separation of the two sampled points. Representative results have been obtained in a grid-generated turbulent flame corresponding to the wrinkled laminar flame region, as defined by the Reynolds and Damkohler numbers. Spatial and time-space correlations of the density were obtained 85 mm downstream from the grid in three orthogonal directions. The density fluctuation structures of this flame and their development are discussed.

*This work was supported by AFOSR under Contract F-44620-76-C-0083 through the Office of Research Services, College of Engineering, University of California, Berkeley. Additional equipment and facility support was provided by the Office of Energy Research, Basic Energy Sciences, Chemical Science Division of the U.S. Department of Energy under Contract No. DE-AC03-76SF00098.

ACCOMPLISHMENTS DURING FY 1981

The two-point Rayleigh scattering system was developed and measurements were performed in a V-shaped turbulent flame. Figure 1 shows a schematic diagram of the premixed type combustor and collection optics used for this study.

The two-point measurements were performed in three directions (Fig. 1), x along the jet, y normal to the jet and normal to the flame holder, and z normal to the jet and parallel to the flame holder. In this report, we refer to the two measurement points as points 1 and 2. Point 1 was always set at 35 mm above the flame holder (i.e., 85 mm above the grid) in the axial plane of the combustor normal to the flame holder. Point 2 was then moved in the x, y, or z direction by δ, the distance between sampled points. For each fixed δ, regardless of the direction of separation of the points, a profile of the measurements across the flame front was obtained by moving the combustor in the y direction.

Throughout this study, the equivalence ratio of the ethylene-air mixture was 0.6 and the jet velocity was 7 m/sec, repeating one of the conditions for earlier results obtained by Bill et al.[8] These conditions produced a flame with a half-angle of 12°, and Reynolds number based on the mesh size of 2280.

Two types of optical systems were used in this study, referred to as the one-beam and the two-beam systems. The one-beam system was used when the separation between sampled points was in the horizontal direction (i.e., y and z), and the two-beam system was used when the separation between the two

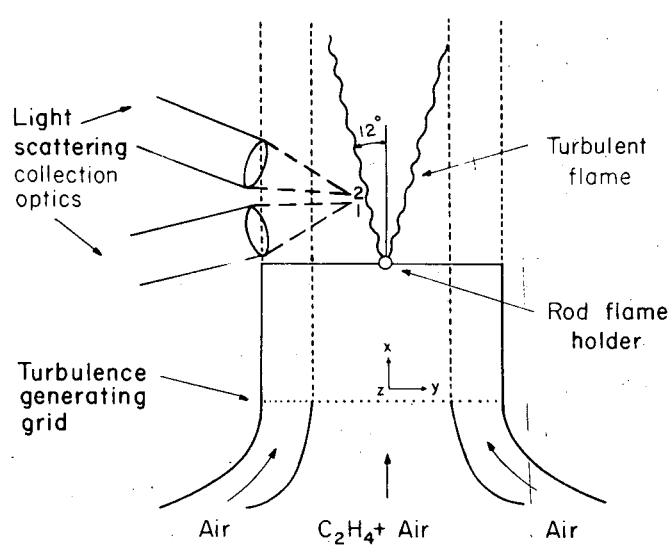

Figure 1. Schematic of experimental apparatus for two-point Rayleigh scattering measurements.
(XBB 823-8761)

sampled points was in the vertical direction. Figure 2a shows the one-beam system with the argon-ion laser beam focused at the test section through a 200-mm lens. The focused beam had a waist diameter of 60 μm and was used to produce the two sampled points by collecting the scattered light from two sections of the beam, each 100 μm long. The collected light was filtered by a narrow-band-pass filter centered at 488 nm and then measured by a photomultiplier.

Figure 2b shows the two-beam system. The laser beam was separated into a blue and a green beam, using a dichroic color separator. Each beam was then brought to focus through separate halves of a lens which had been cut into two pieces, as shown in Figure 2b. When the two parts of the lens were positioned together (forming the original shape of the lens), the two beams would focus nearly at the same point, labeled as point 1 on Figure 2b (the focal points are not exactly identical due to the difference in wave lengths). However, when the upper half of the lens is moved up by δ, the focusing point of the incident beam also moves up by the same amount to point 2, as shown on Figure 2b. The collection systems were then positioned such that the Rayleigh scattering at points 1 and 2 was sampled.

The signals of the two photomultipliers were amplified with low-noise amplifiers equipped with low-pass filters set at 10 kHz. The output signals were sampled simultaneously with a PDP 11/10 computer with dual sample and hold and direct memory access operation. There were 2048 samples of each signal taken at a 10 kHz rate and stored on magnetic tape for post processing. The same PDP 11/10 computer was used to move the combustor so that the flow field positions were scanned automatically.

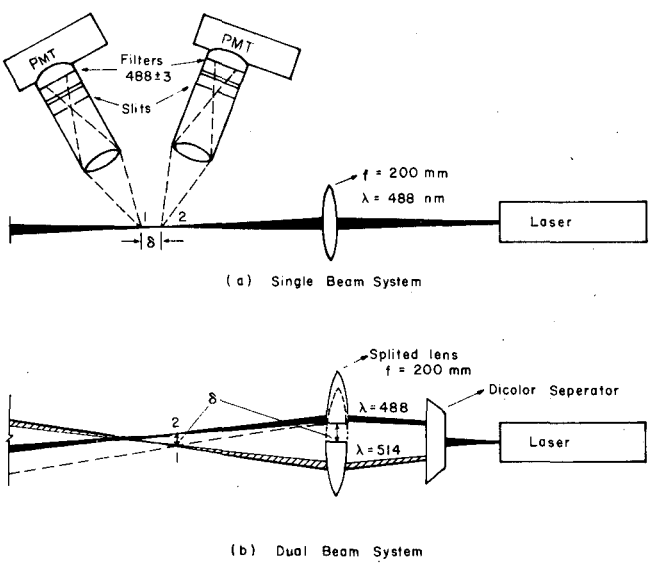

Figure 2. The optical set-up for two-point Rayleigh scattering technique. Single-beam system provides separation between points in horizontal direction and dual-beam system in vertical direction. (XBL 823-8762)

The stored data were reduced on the Lawrence Berkeley Laboratory CDC 7600. The effects of photomultiplier noise and background were removed using the method described by Bill et al.[8] The data presented were also numerically filtered from DC to 50 Hz to remove low-frequency fluctuations which presumably arose from disturbances of the flame by room air current. This filtering is justified because the lowest frequency associated with combustor diameter and free stream velocity is 150 Hz.

Part of the information contained in the measured densities at two points separated by δ can be obtained from the spatial correlation coefficient $R(\delta)$. This quantity provides a measure of the relative strength of the density fluctuation structures whose length scale in the measurement direction is greater than δ. The structures with length scales smaller than δ do not contribute to $R(\delta)$. $R(\delta)$ is defined by

$$R(\delta) = \frac{[\rho_1'(t)\ \rho_2'(t)]}{[\rho_1'(t)^2]^{0.5}\ [\rho_2'(t)^2]^{0.5}}$$

where δ is the distance of separation of the measurement positions denoted by subscripts 1 and 2 and ρ' is the density fluctuation. In Figure 3, values of $R(\delta)$ are shown for the cases of δ lying along the three axes x, y, and z. The values of the spatial correlations are very similar in these three orthogonal directions. This indicates that the spatial structure of the turbulent flame under these conditions is such that the associated length scales are the same in the x, y, and z directions. Further, an integral length scale derived from the area under these curves is found to be approximately 2 mm. By way of comparison, the width of the turbulent flame zone was approximately 4 mm.

Further information on these turbulent flame structures can be obtained from the space-time correlation coefficient $R(\delta,\tau)$, defined by

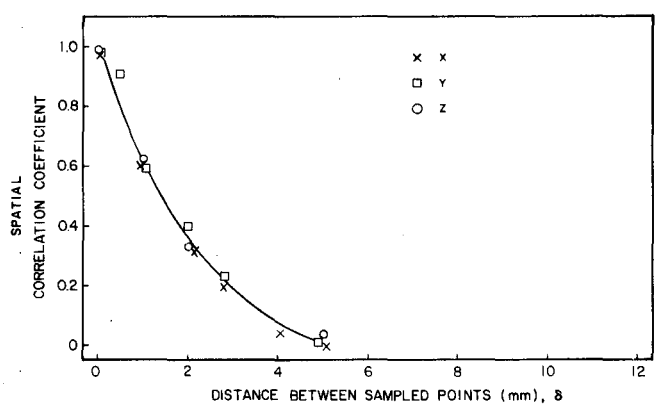

Figure 3. The density spatial correlation in a turbulent flame in three orthogonal x, y, and z directions. Measurement point 35 mm downstream from the flame holder. (XBL 823-8763)

$$R(\delta,\tau) = \frac{[\rho_1'(t)\ \rho_2'(t + \tau)]}{[\rho_1'(t)^2]^{0.5}\ [\rho_2'(t)^2]^{0.5}}$$

where τ is the time delay for which the correlation is calculated. Note that, for $\tau = 0$, $R(\delta,0)$ is just the previously defined spatial correlation coefficient, and for $\delta = 0$, $R(0,\tau)$ is just the ordinary autocorrelation coefficient. In Figure 4, $R(\delta,\tau)$ is shown as a function of τ for several values of δ lying in the x, or flow, directions. Each curve has a maximum whose delay is proportional to δ, the separation between sampled points. The proportionality factor is about 7 m/sec, the same as the flow velocity. Previous measurements[8] indicate that the axial flow velocity through the flame does not change significantly for these conditions. This indicates that the turbulent density structures in the flame are simply convected downstream by the flow, as is suggested by the Taylor hypothesis.

The maximum value of the space-time correlation decreases as the separation between sampled points increases, as shown in Figure 4. This falling maximum implies that the structures decay as they are convected by the flow. Further, the correlation is broader in time as δ is increased, indicating additional structural changes other than simple decay.

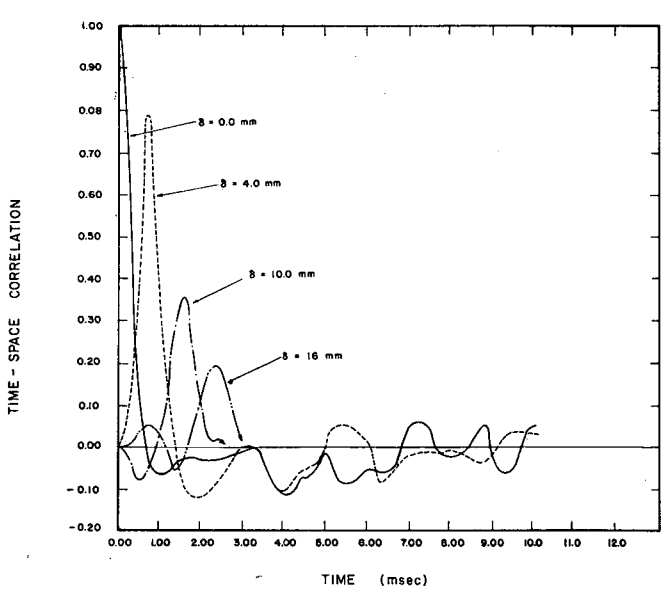

Figure 4. Time-space correlation vs the delay time for separation of δ in the vertical direction. (XBL 823-8764)

We thank R.K. Cheng and T.T. Ng for their assistance throughout the course of this work. The authors also wish to acknowledge the contribution of W.M. Kleiser to this work.

PLANNED ACTIVITIES FOR FY 1982

During FY 1982, two-point measurements in different locations of the flame will be obtained in order to study the development of the length scales. Different flow velocities and equivalence ratios will be studied.

There is still much additional information in a field of two-point measurements, beyond that of the correlation functions, which can be extracted with the use of more sophisticated analytical methods. Our aim is to use these methods, such as the joint probability density function of two signals, to exploit this newly developed two-point Rayleigh scattering technique.

REFERENCES

1. Robben, F., Cattolica, R., and Pitz, R. (1975), Tech. Digest, Applications of Laser Spectroscopy, Optical Society of America Topical Meeting.

2. Pitz, R.W., et al. (1976), "Temperature and Density in Hydrogen--Air Flame from Rayleigh Scattering," in Combustion and Flame 27, p. 323.

3. Cheng, R.K., Bill, Jr., R.G., and Robben, F. (1981), "Experimental Study of Combustion in a Turbulent Boundary Layer," in Eighteenth Symposium (Int'l) on Combusion, p. 1021, The Combustion Institute.

4. Smith, J.R. (1978), "Rayleigh Temperature Profiles in a Hydrogen Diffusion Flame," in Proc. of the Soc. of Photo-Optical Instrumentation Engineers 158, p. 84.

5. Ng, T.T., Cheng, R.K., and Robben, F. (1982), "Combustion-Turbulence Interaction in the Turbulent Boundary," accepted for presentation at the Nineteenth Symposium (Int'l) on Combustion.

6. Streenivasan, K.R., Antonia, R.A., and Danh, H.Q. (1977), "Temperature Dissipation Fluctuations in a Turbulent Boundary Layer," I. Physics of Fluids 20, No. 8.

7. Ho, C.M., Jakus, K., and Parker, K.H. (1976), "Temperature Fluctuations in a Turbulent Flame," Combustion and Flame 27, p. 113.

8. Bill, R.G., Jr., Namer, I., Talbot, K., Cheng, R.K. and Robben, F. (1981), "Flame Propagation in Grid-Induced Turbulence," Combustion and Flame 43, p. 229.

Numerical Modeling of Turbulent Combustion*

A. J. Chorin, A. F. Ghoniem, and A. K. Oppenheim

Studies of numerical modeling of turbulent combustion were concerned with three topics:

1. Evaluation of the properties of turbulent flow fields behind a rearward-facing step,
2. Analysis of unconfined jets,
3. Extension of the random walk method to numerical modeling of diffusional processes, in particular heat conduction.

The work involved the cooperation of three graduate students: D.Y. Chen, Y.W. Dai, and A. Heydari.

ACCOMPLISHMENTS DURING FY 1981

Properties of Turbulent Flow Fields in Channels with Rearward-Facing Steps

Following our studies of two-dimensional flow behind a rearward-facing step of height equal to 1/2 the channel width,[1] we treated cases with step heights of 1/4 and 1/3. The scope of our studies, moreover, was extended by subjecting the numerical solution to statistical analyses. The results we obtained for inlet Re = 10^4 are exemplified by Figures 1 and 2, which display the properties of the flow field behind a step height equal to 1/4 of the channel width for inlet Re = 10^4. Shown in Figure 1 are the computer-graphed vorticity fields, which depict vectorially the motion of all the vortex blobs used in the computations of time intervals expressed in terms of $T \equiv \tau u_\infty/H$, where τ is the time, u_∞ is the inlet velocity, and H is the channel width with the computational time increment t = 0.1 T. Profiles of the corresponding mean velocity components and of the concomitant fluctuating parameters, evaluated over the computational time interval from N_k = 141 to N_k = 198, are shown in Figure 2.

Numerical Modeling of an Unconfined Turbulent Jet

In the case of flow through a channel, there is a natural attribution of computational vortex elements due to their efflux at the open end. As a consequence, after attaining a saturation level, their number remains constant. This is not so for an unconfined jet, where the number of vortex blobs increases indefinitely. In a two-dimensional field, the number of computations involved at each time step is proportional to the square of the number of vortex blobs. Thus the use of time saving devices is of particular importance in this case.

After a number of unsuccessful trials with various methods conceived to reduce the computational time, we have finally succeeded in developing a technique that lessens this time by at least a factor of two. The modification of the algorithm it involves is presented schematically in Figure 3 by the block describing the operation performed on the set of vortex blobs prior to the implementation of the Biot-Savart Law specified in the next block. Its operating principle is described below.

The field is partitioned by a grid into a set of square cells. To update the velocity vector of a vortex blob in a given cell, the Biot-Savart Law is applied to all the other vortex blobs within the cell, as well as to those in the neighboring 8 cells. The area of the 9 cells is thus considered as the near field and its vorticities denoted by subscript nf. The vortex blobs located in cells outside of this area are considered as the far field, the corresponding vorticities being denoted by subscript ff. Their effect is taken into account by a representative pair of vortices, whose strength and location for each cell is evaluated as follows:

$$\Gamma_*^{\pm} = \sum_{\text{cell}} \Gamma_i^{\pm}$$

and

$$Z_*^{\pm} = \frac{1}{\Gamma_*^{\pm}} \sum_{\text{cell}} \Gamma_i^{\pm} Z_i^{\pm}$$

where Γ is the circulation, Z is the position vector, and index $\pm$ indicates that the summation is carried out within each cell separately for the positive and negative vortex elements. Thus if $|\Gamma_*^+| = |\Gamma_*^-|$ while $Z_*^+ = Z_*^-$, one has a doublet, rather than zero.

This procedure has the following properties:

1. It restricts the number of computational operations involved in the evaluation of the velocity field to twice the number of cells plus the number of vortices in the 9 cells of the near field.
2. It yields a velocity field that satisfies the integral invariants of the flow (Batchelor[2] or Leonard[3]):

$$\int \xi dA = \text{const.}$$

and

$$\int \xi \underline{r}\, dA = \text{const.}$$

3. It protects the vorticity distribution from the mal-effects of numerical diffusion while preserving the identity of the vortex blobs.

*This work was supported by NASA on Grant NAG 3-131 and by the U.S. Department of Energy under Contract No. DE-AC03-76SF00098.

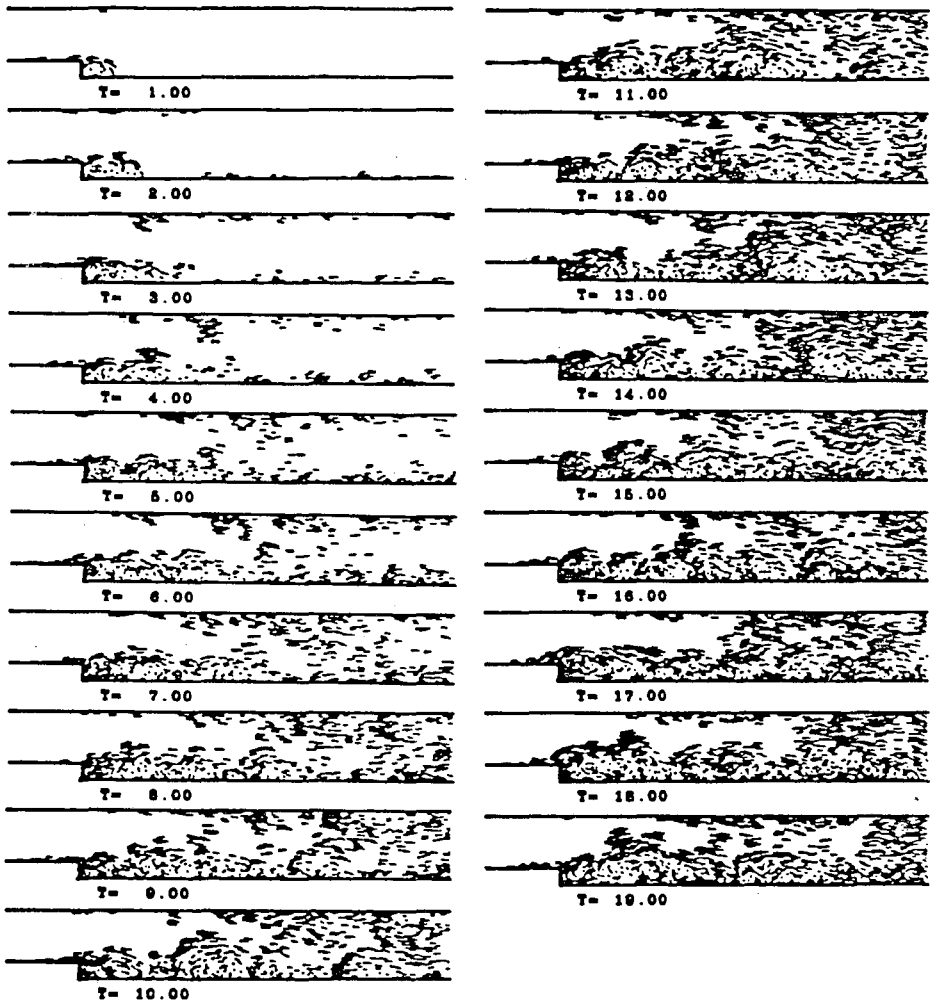

Figure 1. Development of vorticity field in a channel behind a 1/4 step ($Re = 10^4$). (XBL 823-8336)

The development of a turbulent jet, modeled by the random vortex method, is shown in Figure 4, where sequences of vorticity vector fields are displayed on the left and the concomitant velocity vector fields on the right. The time steps in Figure 4 are, respectively, N_k = 40, 90, 140, and 210. The first three time steps were obtained in the usual manner; the fourth was computed using the time-saving technique described above. The evident agreement between the fourth step and the first three steps provides a clear demonstration of the applicability of this technique.

Extension of the Random Vortex Method to Diffusional Processes

The main reason for extending the random vortex method to diffusional processes other than the transfer of momentum is to provide means for treating problems where a number of different transport processes take place concomitantly. Of these, the most interesting involve the transport of momentum and energy as, for example, natural convection with strong interaction between temperature and density or turbulent combustion with significant effects of thermal expansion. It should be noted that the most attractive feature of random walk methods is their essentially Lagrangian character. Consequently, these methods lend themselves particularly well to the treatment of problems dealing with diffusional flow processes, where chemical reactions proceed along particle paths, as in the case of turbulent combustion, the principal objective of our work.

Principal features of our method were developed with particular application to conductive heat transfer in one dimension. They were based on the following concept. The dependent variables of a diffusion equation fall into three differential orders. In a one-dimensional space these are:

1. The primary variables, e.g., the velocity, u, or the temperature, T.

2. The secondary variables, the gradients of the primary variables, e.g., the vorticity, Γ, or the heat flux, q.

3. The integral variables, i.e., either the line integrals of primary variables around the boundary of an area element or the area integral of the secondary variable over this

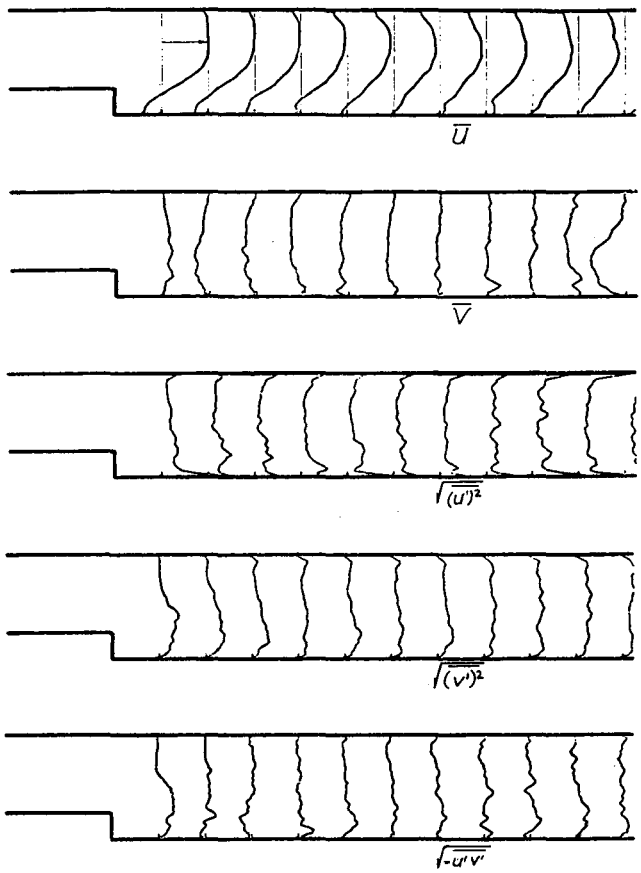

Figure 2. Profiles of mean velocities and fluctuating parameters in a channel behind a 1/4 step (Re = 10^4), evaluated over a time interval N_k = 141-198. (XBL 823-8335)

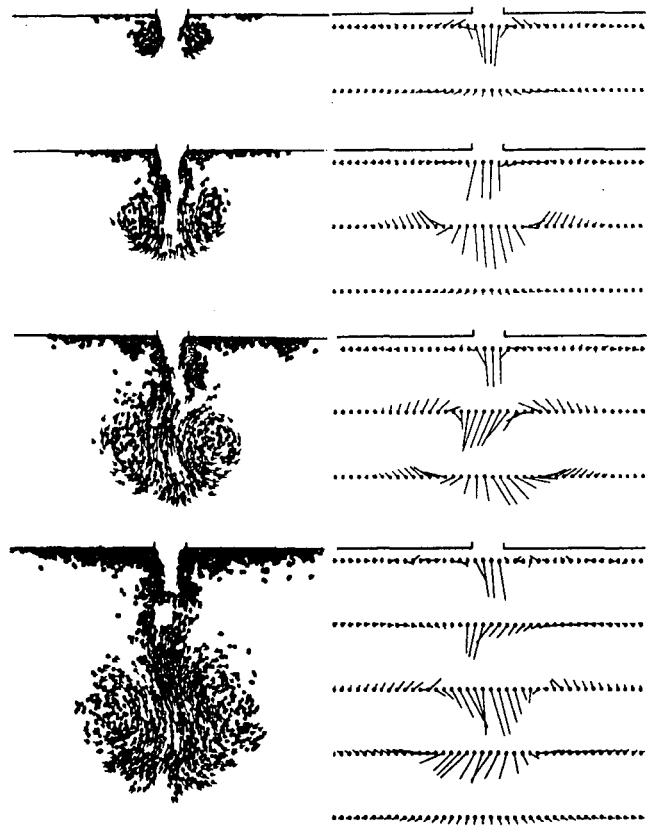

Figure 4. Formation of an unconfined turbulent jet. Vorticity and velocity vector fields at N_k = 40, 90, 140, and 210, the last obtained by the use of the simplified technique. (XBL 823-8333)

element (the two being equivalent according to the Stokes Theorem), i.e., the circulation, Γ, or the internal energy, e.

The fundamental relationships between these variables are presented in Table 1, demonstrating the analogy between the diffusion of momentum and that of energy.

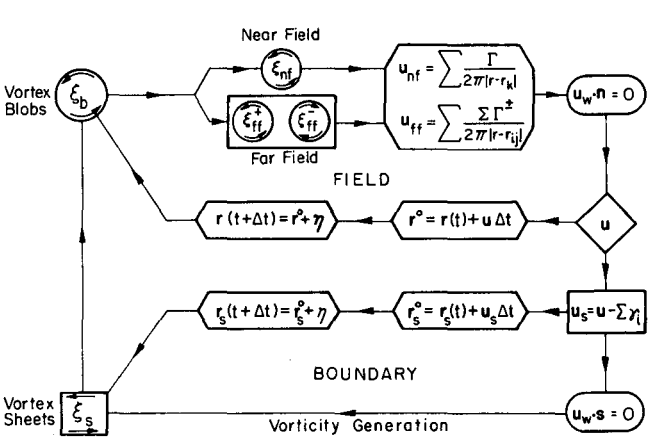

Figure 3. Block diagram of the random vortex algorithm. (XBL 821-5009)

Table 1. Analogy between diffusional processes.

Conserved quantity	Momentum	Energy
Primary variable	u	T
Diffusion equation	$\frac{\partial U}{\partial t} = \nu \frac{\partial^2 U}{\partial_y{}^2}$	$\frac{\partial T}{\partial t} = \alpha \frac{\partial^2 T}{\partial_y{}^2}$
Diffusing element	$f = \int \rho u dA$	$e = \int \rho c T dA$
Conserved quantity	**Vorticity**	**Heat**
Secondary variable	$\xi = -\frac{\partial u}{\partial y}$	$q = -k\partial T/\partial y$
Diffusion equation	$\frac{\partial \xi}{\partial t} = \nu \frac{\partial^2 \xi}{\partial_y{}^2}$	$\frac{\partial q}{\partial t} = \alpha \frac{\partial^2 q}{\partial_y{}^2}$
Diffusing element	$\gamma = \int \xi dA$	$w = \int \xi q dA$

Note: dA = dy; w = de/dt.

The fundamental idea of the stochastic random walk solution is presented in Table 2. It is based on the fact that exact solution of the differential equation of diffusion, subject to initial conditions expressed in terms of a Dirac delta function, is identical to the probability density function of a Gaussian random variable with zero mean. Thus, the solution is constructed by a sequence of random displacements of a set of discrete quantities of the diffusing elements. The solution is then evaluated by local sampling or by global sampling, depending on the variable of primary interest in the problem.

The three fundamental differential orders of the dependent variables lead to a hierarchy of diffusion problems presented in Table 3. Depending on the particular type of problem, the diffusion equation can be formulated in terms of either the primary variable or the secondary variable. The boundary conditions are, as a rule, implemented in terms of the integral constraints. The elements of the solution are evaluated by means of either the Dirac delta or the Heaviside step function, whichever is more appropriate.

Typical examples of solutions we obtained are presented in Figure 5. In each case, the numerical results are shown in comparison to the exact solution. Shown in the upper left corner is the solution of Problem 2 of Table 3 with $\phi = 1$, obtained using $N_s = 10$ elements after 50 computational time steps comprising one run. On its right is a corresponding solution of the same problem, obtained with the same number of $N_s = 10$ elements and using ensemble averaging over 5 runs, each performed with a different set of random numbers.

Table 2. Fundamental idea.

Differential equation	$\frac{\partial \phi}{\partial t} = \alpha \frac{\partial^2 \phi}{\partial_y^2}$
Initial and Boundary Conditions	$\phi(y,0) = \delta(0)$; $\phi(\pm\infty,t) = 0$
Constraint	$\Phi = \int_{-\infty}^{\infty} \phi dy = 1$
Fundamental Solution	$\phi = \frac{1}{\sqrt{2}\pi\sigma} \exp[-(y/\sigma)^2]$; $\sigma = \sqrt{2\alpha t}$
Stochastic Solution	$\Sigma\delta\Phi = 1$
	$y_i(t + \Delta t) = y_i(t) + \eta_i$
	$E(\eta_i) = 0$; $E(\eta_i^2) = 2\alpha\Delta t$
Local Sampling	$\phi = \frac{1}{\delta y} \Sigma\delta\Phi_i\delta(y - y_i)$
Global Sampling	$\Phi = \Sigma\delta\Phi_i H(y - y_i)$

H - Heaviside step function
δ - Dirac delta function
E - Expected value
η - Random variable
σ - Standard deviation

Table 3. Hierarchy of diffusion problems.

No	1	2	3	4
Differential Equation	$\frac{\partial \phi}{\partial t} = \alpha \frac{\partial^2 \phi}{\partial_y^2}$	$\frac{\partial \phi}{\partial t} = \alpha \frac{\partial^2 \phi}{\partial_y^2}$	$\frac{\partial \phi'}{\partial t} = \alpha \frac{\partial^2 \phi'}{\partial_y^2}$	$\frac{\partial \phi}{\partial t} = \alpha \frac{\partial^2 \phi}{\partial_y^2} - 1$
Boundary Condition	$\phi(y,0) = \delta(0)$	$\phi'(y,0) = \delta(0)$	$\phi''(y,0) = \delta(0)$	$\phi(0,t) = 0$
Constraint	$\Phi = 1$	$\phi = 1$ or $f(t)$	$\phi' = 1$ or $f(t)$	$\phi''(0,t) = 1/\alpha$
Diffusing Element	$\delta\Phi_i$	$\delta\phi_i$	$\delta\phi_i'$	$\delta\phi_i$
Elements of Solution	$\phi = \frac{1}{\delta y} \Sigma\delta\Phi_i\delta(y - y_i)$	$\phi' = \frac{1}{\delta y} \Sigma\delta\phi_i\delta(y - y_i)$	$\phi' = \Sigma\delta\phi_i' H(y - y_i)$	$\delta\phi_i = \alpha\phi''(0,t)\alpha t$
	$\Phi = \Sigma\delta\Phi_i H(y - y_i)$	$\phi = \Sigma\delta\phi_i H(y - y_i)$	$\phi = \Sigma\delta\phi_i'(y - y_i) H(y - y_i)$	$\phi = \Sigma\delta\phi_i H(y - y_i)$
Examples	Instantaneous deposition of energy	Prescribed temperature on the boundary (Couette flow)	Prescribed heat flux on the boundary	Uniformly distributed source of energy (Poiseuille flow)

Note: $\phi' = \partial\phi/\partial y$ etc.

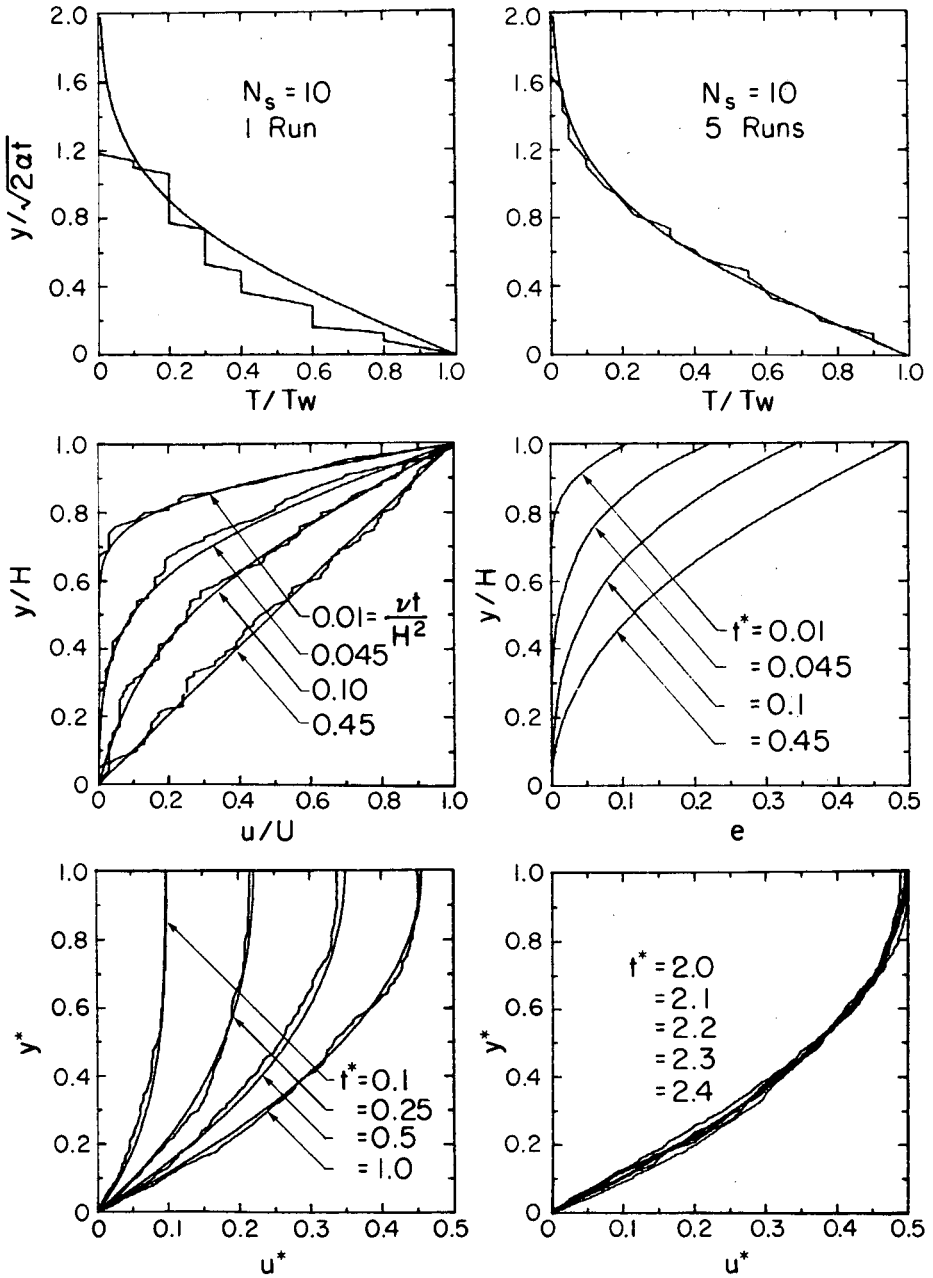

Figure 5. Temperature profiles of self-similar solutions for heat conduction (or diffusion of momentum) in a semi-infinite solid and a slab. (XBL 825-677)

The remainder of the solutions displayed in Figure 5 refer to non-self-similar cases. Presented on the left in the middle row is the solution of Problem 2 with f(t) = 1, while the boundary conditions are applied on both sides of the field, i.e., $\phi = 1$ on one side and $\phi = 0$ on the other, as appropriate for a Couette flow. Next to it is a solution of Problem 3 with f(t) = 1, obtained immediately by the integration of the previous solution. The results are indistinguishable from the exact solution, demonstrating the significant influence of numerical integration upon the accuracy, an example of the effect of proper selection of the variable subjected to random walk. The bottom row displays solutions of Problem 4 of Table 3 showing, on the left side, the development of the field where $t^* = 1$ corresponds to 1000 computational steps and, on the right, the steady-state solution obtained at much longer times, as specified on the graph.

PLANNED ACTIVITIES FOR FY 1982

We will continue the calculations until steady conditions of a fully developed turbulent flow field are established. We intend to accomplish this by using a Cray computer. Arrangements are

now being made to use the system at the NASA Ames Research Center for this purpose.

At the same time, we are planning to model turbulent combustion using our algorithm described by Ghoniem et al.[1] This will be done first using the plume generated by an unconfined jet to study the consequences of multi-point initiation of combustion in comparison to single-point ignition. Then, in a similar manner to the case of the 1/2 step reported by Ghoniem, combustion in the turbulent flow field behind a 1/3 step and a 1/4 step will be studied. The major objective of this study will be to investigate the mechanisms of instabilities, especially the influence of mixture enrichment on flashback.

Finally, we hope to develop further our novel random-element method that has been developed in connection with an elementary application to one-dimensional heat conduction. At first, the method will be extended to two-dimensional heat conduction and then, in conjunction with the random vortex method, to convection in a turbulent flow field. This should eventually enable us to examine the effects of heat transfer in turbulent combustion, thus enlarging significantly the general scope of our studies.

REFERENCES

1. Ghoniem, A.F., Chorin, .J., and Oppenheim, A.K. (1980), Numerical Modelling of Turbulent Flow in a Combustion Tunnel, Lawrence Berkeley Laboratory Report LBL-11520, Phil. Trans. Roy. Soc. London, A394, pp. 303-325 (1982).

2. Batchelor, G.K. (1967), An Introduction to Fluid Mechanics, Cambridge University Press, London, pp. 528-531.

3. Leonard, A. (1980), "Vortex Methods for Flow Simulation," J. of Comp. Phys., 37, 3, pp. 289-335.

The Formation and Reduction of Nitrogen Oxide in the Combustion of Condensed Fuels*

D. Lucas and N. J. Brown

Combustion of fossil and synthetic fuels is often accompanied by the criteria and non-criteria emissions associated with high concentrations of chemically bound nitrogen and sulfur. The emissions of nitrogen and sulfur oxides from such systems can result in acid rain, increased photochemical smog, and other atmospheric pollution phenomena. The reduction of these emissions can be achieved by combustion control and/or post-combustion treatment of the product gases.

A portion of our research effort is concerned with the conversion of fuel nitrogen molecules to nitric oxide, especially in the presence of fuel sulfur compounds. The conversion of fuel nitrogen compounds to NO has been studied extensively, but relatively little research has investigated the coupling between nitrogen and sulfur combustion chemistries. These synergistic effects can be quite important, and most existing methods for reducing nitrogen oxide emissions do not consider conditions where the concentrations of fuel sulfur compounds are high. Another objective of our research is to investigate a method for controlling nitrogen oxide emissions in the post-combustion environment that employs ammonia to selectively reduce nitric oxide in lean combustion products, again with emphasis on the influence that sulfur compounds exert on this process.

Nitrogen and sulfur combustion chemistry was investigated in a turbulent flow reactor, which is shown schematically in Figure 1. The main sections of the reactor are constructed from 5-cm-inside-diameter, low-alloy-steel tubing, with combustion occurring in a 10-cm-diameter section. The larger section is water cooled to allow temperature control of the downstream products without altering the flow rates. The fuel is a #1 diesel oil from the Shell Oil Company, with a measured hydrogen/carbon ratio of 1.85 and less than 0.1 percent (by weight) nitrogen. Higher concentrations of fuel nitrogen and sulfur are obtained by mixing known amounts of pyridine and thiophene, respectively, into the fuel oil before placing it into the delivery tank. The oil is sprayed into the air flow through a commercial high-pressure atomizing nozzle (Monarch Type R, 30° radius, 0.05 1/min). Rapid mixing from the fuel/air mixture was aided by the use of perforated and blocking discs upstream of the nozzle and by packing the air supply lines with steel wool. Swirl introduced into the air supply was found to be detrimental to the combustion, as evidenced by increased flame length and greater sooting tendencies. A quartz tube at the end of the combustion section allows visual inspection of the flame to confirm that the visible flame front terminates at least 50 cm upstream from the ammonia addition section.

For the selective reduction studies, ammonia (Matheson CP grade)/nitrogen mixtures are introduced into the combustion products through four symmetrically oriented, uncooled quartz injectors.

*This work was supported by the Morgantown Energy Technology Center through the Assistant Secretary for Fossil Energy of the U.S. Department of Energy under Contract No. DE-AC03-76SF00098, and by the State of California Air Resources Board under Contract No. A6-196-30.

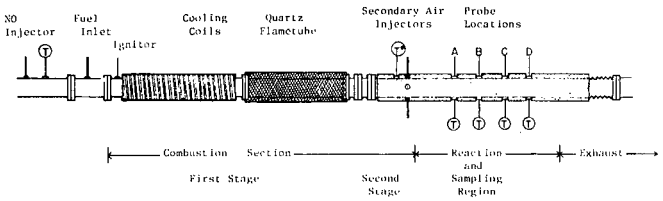

Figure 1. Schematic diagram of the laboratory-scale combustion tunnel. (XBL 812-8257)

The heavily insulated reaction and sampling section begins immediately downstream from the injectors and extends for ~60 cm, where it joins the laboratory exhaust system. There are four different axial locations at which quartz microprobes and/or Chromel/Alumel thermocouples may be inserted into a desired radial location. An aspirated thermocouple is used to correct all reported temperatures for radiation losses. When no ammonia is added, complete combustion and thorough mixing of the product gases are confirmed by measuring temperature and composition profiles in the reaction region. Various analytical techniques are used to measure species concentrations, including chemiluminescent analyzers (NO, N_x), fluorescence detection (SO_2), NDIR (CO, CO_2), GC (various species), and wet chemical methods (NH_3). At the reactant velocities normally used, about 17 m/sec, an axial temperature gradient of 1 K/cm was observed. Radial temperature gradients of 20 to 25 K were measured when the thermocouple was moved from the centerline position to one 80 percent from the distance to the combustor wall. Concentrations of CO, CO_2, and NO were found to be independent of probe position, with the CO and CO_2 measurements within experimental error of their expected values. Mixing characteristics from the ammonia injectors were determined by introducing NO through the injector system and then measuring the NO radial and axial profiles downstream. It was found that mixing was essentially complete within 20 cm from the injection site. Concentration profiles of NO and NH_3 measured when reduction occurs indicate that the reaction is essentially finished (>95 percent) by the final probe station. The data presented are from the centerline position of the final probe position, 59 cm downstream from the ammonia injection site.

ACCOMPLISHMENTS DURING FY 1981

The reduction of NO by NH_3 addition to the post-combustion gases has been measured as a function of temperature, added NH_3 concentration, and concentration of fuel sulfur. The equivalence ratio in this study was varied by changing the fuel rate to minimize changes in the overall flow rate. Fuel nitrogen was varied through the volumetric addition of pyridine to the fuel oil. Selected samples were analyzed by the Microchemical Analysis Laboratory of the University of California at Berkeley. Complete conversion to NO of a fuel with 1.02 percent, by weight, pyridine would results in an NO concentration of ~1200 ppm in the exhaust gases at an equivalence ratio of 0.89. The actual measured concentration before reaction with NH_3 is termed $(NO)_i$. The temperatures listed, T* values, are measured at the centerline immediately upstream from the ammonia injectors. The relative amount of ammonia added is defined by $\beta = (NH_3)_i/(NO)_i$.

Before determining the effect of fuel sulfur on the NH_3 reduction process, the conversion of fuel nitrogen to NO was measured as a function of fuel sulfur concentration, equivalence ratio, and exhaust gas temperature (T*). With no pyridine or thiophene added to the fuel, thermal NO concentrations of 40 to 45 ppm were measured. This thermal concentration was subtracted from the $(NO)_i$ values when calculating the fuel nitrogen conversion efficiency. For fuels with no sulfur added, the conversion of pyridine to NO followed expected trends for the different equivalence ratios, with conversion efficiencies of 40 to 45 percent measured for equivalence ratios between 0.78 and 0.95. Table 1 lists the results obtained for three different fuel sulfur concentrations and various T* values at a fixed equivalence ratio of 0.89. The addition of fuel sulfur tends to increase the amount of NO formed from a fixed amount of fuel nitrogen, with more NO formed as the concentration of thiophene increases. As might be expected, the formation of NO does not have a strong dependence on T*, which is measured well downstream from the flame. However, because T* is controlled by cooling of the combustor around the flame zone, it was necessary to determine that this control did not affect the flame conditions. Within experimental error, measured SO_2 concentrations indicate that quantitative conversion of the fuel sulfur occurs when no NH_3 is present. However, when both sulfur compounds and NH_3 are present, serious errors in the measurements of both species can arise from the formation of sulfur-ammonia compounds, which most likely occurs at the lower temperatures in the probes, sampling lines, or analyzers.

The temperature dependence of the reduction process for various fuel sulfur concentrations is

Table 1. Conversion of pyridine to NO as a function of thiophene concentration at an equivalence ratio of 0.89.

T/K *	Fuel S[a] (%)	$[SO_2]_i$[b] (ppm)	$[NO]_i$[c] (ppm)	% Fuel N Conversion to NO
1170±5	0.04	---	515±10	40
1188			510	39
1224			520	40
1252			515	40
1282			515	40
1176±5	0.33	148±15	610±10	48
1200			600	47
1230			615	48
1268			627	49
1293			650	51
1167±5	0.63	---	635±15	49
1194			630	49
1245			665	52

[a]Added as thiophene.

[b]Measured at terminal probe station with no NH_3 addition.

[c]Added as pyridine (1.02 percent fuel N).

shown in Figures 2, 3, and 4. Nitric oxide concentrations are normalized to the initial NO levels measured. Figure 2 illustrates the temperature dependence when no thiophene is added to the fuel. As more ammonia is added (increasing β), greater reduction of NO is obtained. Also, the optimum temperature for reduction increases with increasing β. The effect of increased fuel sulfur is shown in Figure 3. There is a noticeable shift to higher optimum temperatures when the fuel sulfur increases. However, while the temperature at which the optimum reduction occurs does change, the maximum amount of reduction for a given β is essentially unchanged. A plot of NO reduction as a function of β at a fixed temperature is shown in Figure 4. At β values less than 1, the fuel sulfur has little effect on the reduction process. Above $\beta \simeq 1$, the change in the reduction process with increasing fuel sulfur at a constant temperature is more obvious. Preliminary results indicate that this trend continues at even higher fuel sulfur concentrations.

The presence of fuel sulfur has two different, though interrelated, manifestations: there is an increase in the conversion of fuel nitrogen to NO as the fuel is burned, and the optimum temperature for the NH_3 reduction process shifts to higher values. The observed increase in NO production in the presence of fuel sulfur is in agreement with the results of Wendt et al.,[1] who added thiophene to rich turbulent diffusion flames doped with NH_3 or pyridine. By doping the fuel with benzene in place of thiophene, they showed that the burning characteristics of the fuel oil were not affected by the addition of an aromatic fuel additive in low concentrations but rather by the presence of organic sulfur. They reported the NO produced to be quite dependent on the method of mixing the fuel and air, with more NO produced in the less turbulent diffusion flames. It is very difficult, however, to quantitatively characterize "mixing" in a turbulent diffusion flame. In our study, the

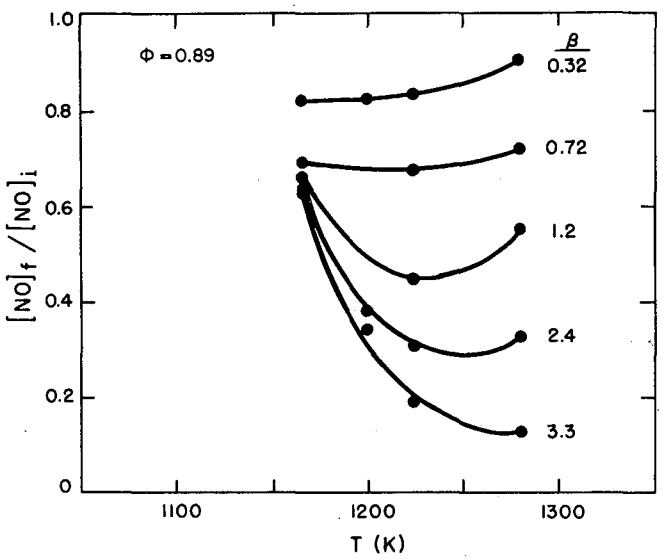

Figure 3. NO reduction with thiophene addition (0.63 percent fuel S). (XBL 812-8278)

flow conditions were held constant, and there were no visible differences in the flames when thiophene was present. The addition of thiophene changes the equivalence ratio only slightly, less than the uncertainty introduced by the fuel and air metering systems. The dependence of the selective reduction of NO by NH_3 on temperature and β has been reported previously.[2] When no thiophene is added to the pyridine/oil mixture (0.04 percent fuel sulfur), the results in terms of NO reduction are essentially identical to those obtained when NO is injected in the air supply (replacing the pyridine in the fuel) to produce a downstream NO concentration of ~500 ppm.[3] It should be remembered that the reduction process takes place in homogeneous, lean mixtures of post-combustion gases at temperatures well below those encountered in the

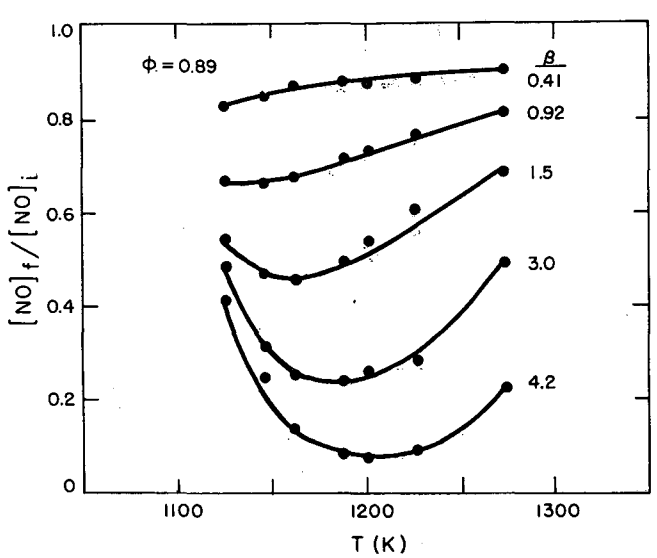

Figure 2. NO reduction as a function of temperature with no thiophene added to fuel (0.04 percent fuel S). (XBL 812-8279)

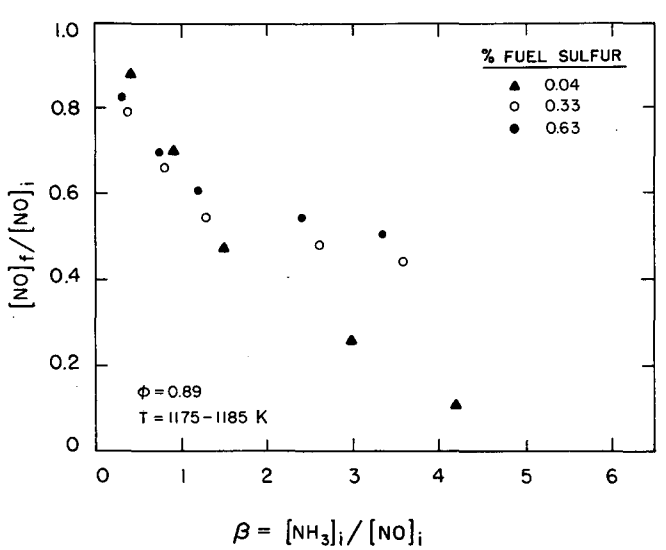

Figure 4. NO reduction at a constant temperature as a function of added NH_3. (XBL 812-8280)

flame. Sulfur compounds in the post-combustion gases could affect the reduction process by reacting with the ammonia or an ammonia-derived species, effectively lowering the concentration of the reducing agent (lower β). This would result in less NO reduction and in a decrease in the temperature for achieving the optimum NO reduction. Neither of these is observed. Lower concentrations of NO_2 and NH_3 are measured when both species are present, but this is most likely attributable to reactions in the sampling system. The observed shift in the optimum temperature suggests a change in the reaction pathway when sulfur compounds are present. One possibility is the existence of fuel-rich pockets immediately around the ammonia injectors: the added ammonia can cause the mixture to become locally rich, reducing the SO_2 to other species such as SH, SO, or H_2S, thereby altering the NH_i (i = 0,1,2, or 3) concentration profiles and the temperature dependence of the reduction process. Alternatively, the sulfur species themselves could react with the NO or NH_i species present. Sulfur dioxide has been identified as the major product of the combustion of sulfur species in lean environments; however, other sulfur species present in significantly smaller concentrations could also be important.

REFERENCES

1. Wendt, J.O., Morcomb, J.T., and Corley, T.L. (1979), "Influence of Fuel Sulfur on Fuel Nitrogen Oxidation Mechanisms," in Seventeenth Symposium (International) on Combustion, pp. 671-678.

2. Muzio, L.J., Arand, J.K., and Maloney, K.L. (1977), "Gas Phase Decomposition of Nitric Oxide in Combustion Products," in Sixteenth Symposium (International) on Combustion, pp. 199-208.

3. Lucas, D. and Brown, N.J. (1981), "Characterization of the Selective Reduction of NO by NH_3," to be published in Combustion and Flame, also Lawrence Berkeley Laboratory Report LBL-12549.

Tests and Criteria for Fire Protection of Cable Penetrations*

R. B. Williamson and F. L. Fisher

The spread of fire in nuclear reactors depends critically on the barrier qualities of the cable penetrations of fire-resistant walls and floor/ceiling assemblies. The ASTM E-119 Fire Endurance Test Method has been used to qualify the unpenetrated walls and floor/ceiling assemblies, but, if such assemblies contain cable penetrations, special attention is required. This is the focus of this project.

The potential spread of fire in nuclear reactors is controlled by fire-resistant wall and floor/ceiling assemblies that define fire areas or zones. One of the overriding considerations in the safe operation of nuclear reactors is that all systems and their associated circuits used to achieve and maintain safe shutdown are safe from fire damage. This objective is achieved in part by identifying "redundent systems" necessary for safe shutdown and then assuring that both of these systems will not be subject to damage from a single fire. This can be accomplished by locating redundent systems in different fire areas separated by fire-rated barriers, or in some instances, by separating them by "substantial physical separation."[1] However, although the latter approach has not yet been quantified, it has been recognized that:

> "Unpierced fire barriers offer the best protection of separating redundent trains of safety-related or safe shutdown equipment. However, these barriers must be pierced for both control and power cables. These penetrations must be sealed to achieve a degree of fire resistance equivalent to that required of the barrier that is unpierced."
>
> Paragraph N_1 Comment Resolution
> Pg. 76008.

The actual fire conditions represented by the E-119 test method are termed "post-flashover" conditions in which fire fully involves a compartment, although the test itself is conducted in a "furnace" that is not closely controlled by the standard. Under actual conditions, as opposed to laboratory test furnaces, post-flashover fires are characterized by a positive pressure differential between the upper half of the fire compartment and the unexposed face of the wall and floor/ceiling assemblies that make up its boundaries. The initial portion of this post-flashover period is also characterized by excess amounts of fuel that have been pyrolyzed by the fire within the compartment. The positive pressure and excess pyrolyzates are clearly proven by the flames that commonly are observed to emerge from the doors and windows of both actual and laboratory post-flashover building fires.

A new ASTM standard, E-841[2], for evaluating "Penetration Fire Stops" is essentially the same as Standard E-119 except that it is written

*This work was supported by the U.S. Nuclear Regulatory Commission through Sandia National Laboratories, Alburquerque, New Mexico under Contract No. 46-6967 and through the U.S. Department of Energy under Contract No. DE-AC03-76SF00098.

specifically to cover assemblies such as cable and pipe penetration devices in fire-rated construction. The new standard calls for the presure differential in the test furnace to be measured and specifies who shall establish the pressure differential. Figure 1 shows the flames that pour through an opening with positive pressure in a fire test. Below the flames in Figure 1 are two other openings that are below the neutral pressure plane and thus have a negative differential pressure between the inside of the furnace and the unexposed face. Two penetrations in the foreground, one above and one below the neutral pressure plane, have been filled with Al_2O_3 wool. The fuel for the flames shown in Figure 1 was polyethylene, contained in steel troughs fixed to the fire-exposed surface of the wall. This experiment, which was conducted in the fire-resistant furnace located at the Richmond Field Station (RFS), was instrumental in the development of the E-814 standard.

ACCOMPLISHMENTS DURING FY 1981

A new concept was discovered during 1981 that may have far reaching consequences for the evaluation of all penetrations of fire-resistive barriers. The concept is to evaluate penetrations through walls or floor/ceiling assemblies in a true post-flashover compartment fire exposure. Many problems associated with E-119 test furnaces result because they are "furnaces," not compartments. Thus, if we return to an actual compartment geometry and create a true post-flashover compartment fire, the pressure differentials, excess pyrolyzates, and other characteristic features of post-flashover fires will be automatically created.

The experimental approach during FY 1981 was to begin instrumenting a pre-flashover room test facility at RFS for post-flashover experiments. Special attention was paid to developing realistic fire conditions while retaining control of the fire itself. Experiments performed at LBL showed how large quantities of excess pyrolyzates could lead to run-away fire conditions in a traditional E-119 furnace. Figure 2 shows the interior of the E-119 furnace at RFS with six sources of excess pyrolyzates dominating the conditions in the furnace. Most fire-resistant furnaces, such as the panel furnace at RFS, are designed for efficient venting of the exhaust gases; this means that the excess pyrolyzates that do not burn in the furnace can burn above the exhaust stacks of the furnace. Figure 3 shows a view of the flames in the exhaust gases above the stacks of the RFS furnace. At the time Figures 2 and 3 were taken, there was more heat being released in the furnace than was necessary to maintain the standard E-119 time-temperature curve. Because there was no way in that experiment to control the rate of pyrolysis, the furnace was essentially out of control unless more air was added. When more air was added by opening the dampers, the neutral pressure plane moved up.

In many nuclear plants there are unusually high pressure differentials across certain fire-resistant barriers to prevent the escape of radioactive materials. The new concept described above is particularly suited to test cable

Figure 1. Flames are produced at openings where positive pressure and a source of fuel are present on the fire-exposed surface of open cable penetrations. (CBB 825-4667)

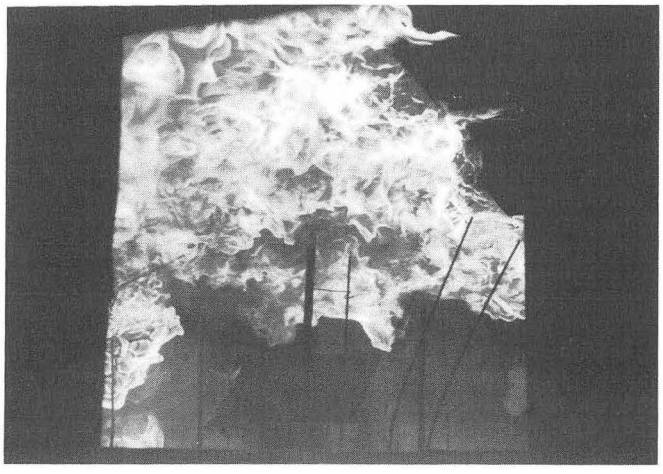

Figure 2. A view of the interior of an ASTM E-119 fire test furnace at RFS. Excess pyrolyzates cover the entire face of the wall and dominate the heat release. (CBB 813-2409)

Figure 3. Excess pyrolyzates from the ASTM E-119 furnace can burn above the stacks if there is insufficient air within the furnace. this is an undesirable condition for furnace operation.
(CBB 813-2413)

penetrations. The positive pressure difference across the specimen can be induced by creating a negative pressure, with respect to atmospheric pressure, in a special plenum on the unexposed face of the specimen rather than a positive pressure, with respect to atmospheric pressure, in the compartment. It is even possible to have a complete "compartment" on the unexposed side of the penetrated barrier. The methods for performing this type of evaluation were explored during the summer of 1981.

Another accomplishment during FY 1981 was the further development of the probabilistic network approach to modeling fire spread. A paper entitled "Coupling Deterministic and Stochastic Modeling to Unwanted Fire" was presented at the Symposium on Fire Risk sponsored by the Society of Fire Protection Engineers at the University of Maryland, March 4-6, 1981. One of the principal features of this approach is that fire-resistive elements can be tested under different conditions, and their expected performance under potential fire conditions can be interpreted in a quantitative fashion.

PLANNED ACTIVITIES FOR FY 1982

The principal research task for this year will be fire test experiments on cable penetrations using excess pyrolyzates and positive pressure induced in a compartment fire exposure. Another activity will be examination of the unexposed-face criteria during the experiments to determine how they relate to the possible spread of fire under actual fire conditions. The emphasis will be on instrumenting the experimental compartment for post-flashover fire tests of cable penetrations and on validating the concept of using a compartment instead of a furnace.

A set of experiments will be performed to explore methods of producing a controlled post-flashover fire condition on the end wall and ceiling of the test compartment. This will entail placing different types of burners and possibly solid and liquid fuels within the compartment. Simple cable penetrations will be constructed for some of these experiments, and movies and still photographs will be taken to illustrate the concept of using the compartment for cable penetration fire tests.

REFERENCES

1. U.S. Federal Register (1980), "Fire Protection Program for Operating Nuclear Power Plants," 10CFR Part 50, 45, No. 225, Nov. 19, 1980, pp. 76602-76616.

2. Annual Book of ASTM Standards (1981), American Society for Testing and Materials, Philadelphia.

LAKE ECOTOXICOLOGY RESEARCH

Optimum Microcosm Design for Ecotoxicology*

J. Harte, D. J. Levy, G. P. Lockett, J. M. Oldfather, J. T. Rees, E. I. Saegebarth, and R. A. Schneider

Our criteria for optimization of microcosms are realism, replicability, and simplicity. Realism requires that the ecologically significant parameters (e.g., nutrient concentrations and plankton densities) measured in the microcosm behave similarly to (i.e., track) those in the natural system being modeled. Replicability requires that microcosms initiated as identically as possible will develop in time nearly identically. Simplicity requires that realism and replicability be achieved with a minimum of expense and complex gadgetry; simplicity is an essential requirement if microcosms are to be of widespread use in toxic-substance testing procedures and are to replace the simple, but often unreliable, single species bioassay currently used as a biological screening tool.

Using particular lakes as a source of microcosm water and as comparison field sites, we are identifying the factors that influence microcosm realism and replicability. Moreover, we are identifying the appropriate control variables which can be adjusted in the laboratory to optimize the microcosms. In earlier work, we identified the problem of algal wall-growth, exacerbated by the large surface-to-volume ratio of microcosms compared with lakes, as a major cause of poor tracking, and we developed a simple effective solution to this problem.[1] In FY 1980, however, a series of tracking studies was completed that showed that even with wall-growth prevented, poor tracking of pelagic diatom populations resulted under certain circumstances. In a paper submitted for publication,[2] the possible causes of this problem were identified and discussed. These causes included: (1) neglect in the microcosms of sources of nutrient to the water column, including upwelling from the benthic sediments and runoff from the watershed surrounding the lake, (2) a discrepancy in water temperature between microcosm and lake, and (3) an inappropriate level of water agitation or turbulence in the microcosms which could influence either the sinking rate of diatoms or the viability of populations of zooplankton and small crustacea that graze on the diatoms. In FY 1981, a systematic study of these factors was begun.

*This work was supported by the Environment and Energy Analysis Division of the Electric Power Research Institute and the Office of Toxic Substances of the Environmental Protection Agency through the U.S. Department of Energy under Contract No. DE-AC03-76SF00098.

ACCOMPLISHMENTS DURING FY 1981

A new microcosm facility was designed and constructed in FY 1981 (Fig. 1). In this facility, the microcosms are housed in two separate rooms, each capable of containing 12 tanks, each up to 50 liters in volume. Temperature control is achieved by a closed circulation system in which water of the desired temperature flows through copper piping in contact with an outer jacket of water surrounding the microcosm containers. Greater precision of temperature control, colder temperatures needed for wintertime studies, and reduced energy consumption characterize this system in comparison to the previous air-controlled coldroom facility. Other features of the new microcosm facility include a greater and more uniform illumination intensity then before, a clock-regulated illumination schedule, and a relatively dust-free environment to reduce the potential for air-borne colonization of the tanks.

Also in FY 1981, cylindrical benthic compartments were designed and constructed for use in

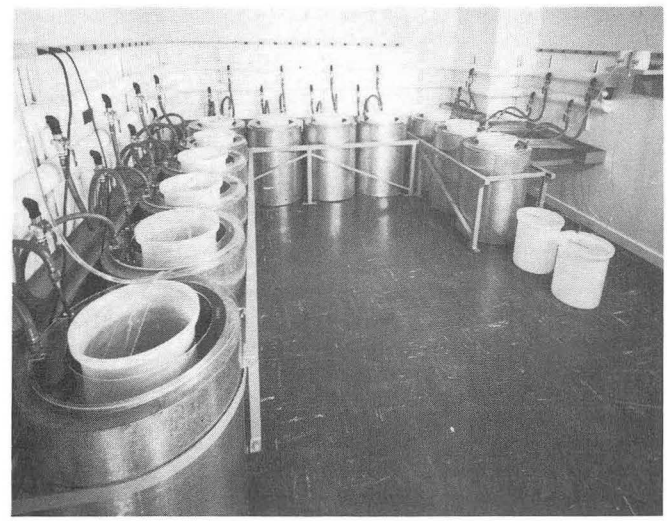

Figure 1. The Lake Microcosm Facility, located at Lawrence Berkeley Laboratory, is the site for acid precipitation studies. This facility simulates natural lake temperatures and ambient lighting during controlled experiments using actual lake water and sediments. (BBC 818-7888)

evaluating benthic microcosms. To allow investigation of the influence of benthic surface area on microcosm realism, these chambers were built in two sizes with similar heights but different diameters. In one mode of operation, the sediments will fill the chambers to within about 1 cm from the top. However, screw-on extenders extend the chamber top about 15 cm above the sediment surface, thus providing partial shielding of the sediments from the water agitation present in the microcosm water column. Covering the chambers and extenders with a removable screw-on cap permits measurement of sediment-zone oxygen profiles and respiration rates. Because the chambers were also designed to double as sediment coring devices, the cores need not be removed and disturbed on transfer from the lake to the microcosms.

The monitoring of Briones Reservoir continued, with increased emphasis on quantifying the spatial heterogeneity of the plankton populations. In addition, further data on light, temperature, and chemical depth profiles were gathered. This information is expected to be of use in interpreting microcosm behavior under the typical circumstances in our laboratory, where the lake waters used to stock the microcosms are taken from a range of depths and mixed together in the tanks.

Using the new microcosm facility, two experiments were made in FY 1981 to determine the influence of the water agitation rate on the realism of pelagic (water-column) microcosms. In the first, conducted in late spring and early summer, two sets of triplicate microcosms were studied. In one set, the water was stirred continuously and vigorously by motor-driven propellers; in the second set, the water was undisturbed. Using the rate of gypsum block dissolution as a crude measure of water agitation, the level of agitation in the first set was approximately the same as in the upper water column (epilimnion) of the lake. A second experiment, in the autumn, studied four levels of agitation: no mixing; gentle aeration; slowly rotating, motor-driven broad paddles; and rapidly rotating, motor-driven propellers.

In both experiments, the greater the rate of agitation, the lower the population of the major grazers of phytoplankton (primarily daphnia) and the higher the population of the diatoms. During the spring-summer period, when diatom populations are at their peak, the more agitated systems tracked Briones Reservoir, the source of the microcosm water, considerably better than did the still-water systems (see Fig. 2). Results from the second experiment are now being analyzed. The data from these and earlier experiments suggest the tentative conclusion that an important influence of agitation rate on plankton dynamics acts through the influence of water agitation on grazer populations; higher levels of agitation suppress these populations and lead to enhanced phytoplankton populations. The mechanism by which agitation affects grazer populations is not understood.

In FY 1981, a paper was prepared for publication describing the results of a mathematical analysis of microbial decomposition activity in lake water. In experiments carried out over the

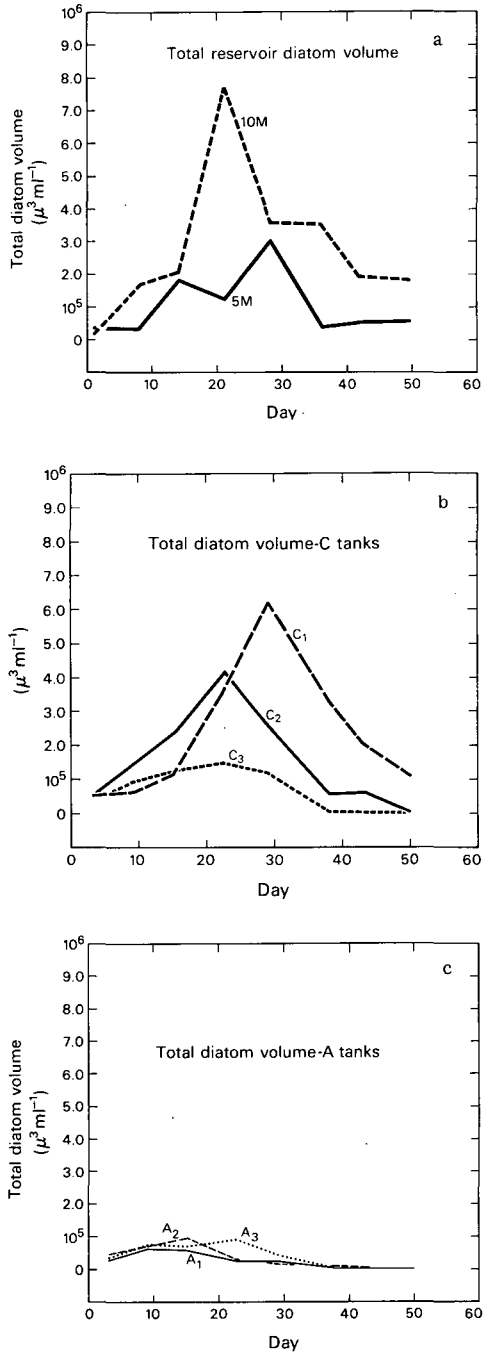

Figure 2. a - Diatom population density in Briones Reservoir. b - Diatom population density in the well-agitated microcosms. c - Diatom population density in the unagitated microcosms.
(XBL 8110-1465, XBL 8110-1464, XBL 8110-1460)

past several years, we had observed unexpected and highly replicable behavior in lake microcosms to which organic matter was added.[4] The organic matter stimulated the growth of microbe populations and the production of inorganic nutrients by decomposition of the organic matter. By introducing the notion of a microbe carrying capacity into a mathematical model of the microbe-detritus-nutrient system and by assuming that microbes utilize all inorganic nitrogenous products of decomposition for their population growth until that capacity is

reached, a successful description of the observed phenomena was obtained (Fig. 3). The success of this approach provides a relatively simple procedure for measuring microbial carrying capacities in aquatic systems. Moreover, by organic additions, it makes possible the determination of the ambient and stimulated rates of decomposition in these waters. Finally, by using the model to analyze the results of experiments in which organic matter and a toxic substance are added to a microcosm, practical damage indices can be extracted to measure the effect of a toxin on decomposition rates and microbial carrying capacities.

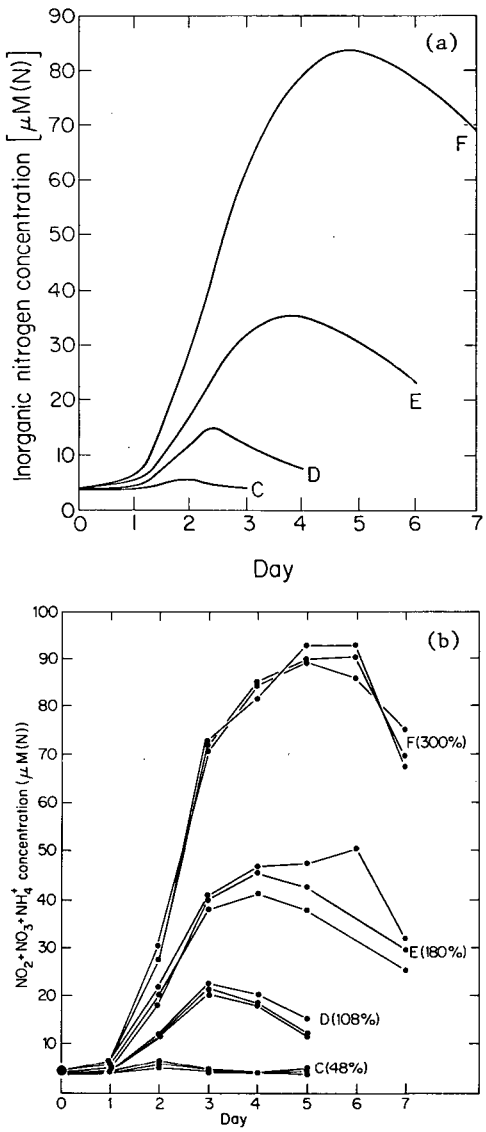

Figure 3. a - Results from an organic addition experiment showing inorganic nitrogen concentration as a function of time after the organic matter addition. b - Model prediction of the experimental results in 3-a. (XBL 794-1355, XBL 819-1280)

PLANNED ACTIVITIES FOR FY 1982

In FY 1982, we will test the benthic chambers described above and determine whether adequate tracking of Briones Reservoir can be achieved during the winter, when the reservoir is not thermally stratified into two isolated water layers (epilimnion and hypolimnion). During winter, the benthic zone exerts its greatest influence on the surface waters; we observed that tracking of purely pelagic (water-column) microcosms is poorest at this time. Because of the great sensitivity of high-elevation lakes to acid rain, benthic microcosms from selected lakes in the California Sierra and in the Rocky Mountains will also be initiated and their realism determined.

Also in FY 1982, high-elevation lake microcosms will be used to measure the effects of acids and toxic metals on microbial decomposition activity. Using the microbial-detritus interactions described above, we will extract from experimental data obtained in the microcosms quantitative measures of impairment of decomposition activity and of changes in microbial carrying capacity induced by the perturbations.

If this approach is successful and alterations in decomposition activity are observed, we will also determine the mechanism by which enzyme-induced decomposition rates are affected by these toxins. Two alternative possibilities are (1) the toxin affects the ability of microbes to produce the appropriate enzyme (e.g., it kills the microbe), and (2) the toxin prevents the enzyme from functioning properly. By measuring the activity of enzymes such as phosphatase that are limnologically important and can be active extracellularly, it will be possible to choose between these alternatives.

REFERENCES

1. Harte, J., et al. (1980), Assessment of Optimum Aquatic Microcosm Design for Pollution Impact Studies, Electric Power Research Institute Final Report EPRI-1224-1, Palo Alto, California.

2. Harte, J., Levy, D., and Reese, J. (1980), "Pelagic Diatom Dynamics in Freshwater Microcosms," accepted for publication in Internationale Revue der Gesamten Hydrobiologie.

3. Harte, J. (1981), "Modeling Lake-Water Mineralization Processes," submitted to Journal of Theoretical Biology.

4. Harte, J., and Levy, D. (1981), "Investigation of the Responses of Lake Waters to Organic Additions," submitted for publication.

Acid Precipitation: Microcosm Applications and Field Studies*

J. Harte, G. P. Lockett, R. A. Schneider, and K. Tonnessen

Acid precipitation, composed primarily of dilute sulfuric and nitric acid originating from the burning of fossil fuels, has been the subject of intense research in the northeastern United States, southeastern Canada, and Scandinavia for more than a decade.[1,2] It was in those regions that the occurrence of acid precipitation (that is, precipitation with a pH substantially below 5.65, the value expected from kinetic equilibrium of precipitation with atmospheric carbon dioxide) and the nature of some of its ecological effects were first carefully documented. Recently, studies have shown that acid precipitation occurs in many other regions of the world as well.[3-5]

Further studies of the distribution of acid precipitation throughout the world can be of considerable use in helping to locate sources, to determine global and regional transport patterns for atmospheric pollutants, and to gain more insight into the chemical composition of natural background precipitation. Moreover, such studies can alert researchers to the potential for ecological damage and economic losses resulting from acid precipitation.

Our research has focused primarily on two regions, the western slope of the high Colorado Rockies and the western slope of the California Sierra Nevada. In addition, acid precipitation research was carried out in the Tibetan Plateau of China. The goals of these efforts are

1. To document instances of acid precipitation in areas not investigated by others.

2. To determine the degree of sensitivity (buffering capacity) of high mountain watersheds and lakes in these areas.

3. To predict chemical and ecological effects of acid precipitation in these regions.

4. To find the sources of the observed acid precipitation events.

A combination of laboratory and field methods is used to achieve these objectives, with emphasis on the use of microcosms to carry out experiments under controlled conditions.

*This work was supported by the Environment and Energy Analysis Division of the Electric Power Research Institute and the Office of Toxic Substances of the Environmental Protection Agency through the U.S. Department of Energy under Contract No. DE-AC03-76SF00098.

ACCOMPLISHMENTS DURING FY 1981

Acid Precipitation Effects in the Sierra Nevada

Research conducted in FY 1981 was designed (1) to investigate the baseline characteristics of high-altitude lakes located on the western slope of the Sierra Nevada which may be particularly susceptible to future damage due to acid deposition and (2) to evaluate the effect of acid stress on these systems in the laboratory by using microcosms (simulated lake systems) containing Sierra lake water and sediments.[6,7] Changes in pH, alkalinity, trace-metal concentrations, and phytoplankton and zooplankton populations (unicellular plants and animals) were measured in treatment systems, with and without sediment compartments, and in control tanks maintained under controlled conditions.

This study provides evidence on the capacity of a number of different lake types to buffer (neutralize) such acid inputs. The extent to which toxid metals are leached from sediments in lake microcosms, following acidification, provides information on the potential for such toxic metal loadings in actual lakes subjected to acid inputs. These experiments are designed to evaluate the effects of both decreased pH and metal increases on the microscopic flora and fauna.

A field survey of 30 lakes on the western slope of the Sierra was also completed, and water and sediment samples were analyzed in the laboratory. Based on the chemical data collected on water quality in these high altitude lakes, baseline conditions have been established. Many of these granite-based lakes may be classified as "sensitive," based on the following set of criteria: (1) lake pH is generally circum-neutral, with some lakes having a pH as low as 6.0; (2) water column alkalinity is low (5-200 eq/l), indicating a limited ability of these lakes to buffer or neutralize acid inputs; (3) ambient levels of dissolved metals in the water column are detectable for elements which might prove toxic to aquatic organisms at increased concentrations (e.g., aluminum, iron, and manganese).

To date, three experimental systems have been tested in the laboratory in the temperature- and light-controlled Aquatic Microcosm Facility. One Bay Area reservoir (Briones) and two Sierra lakes (Tenaya and Mosquito) have been modelled in 15-liter tanks containing water and sediment collected from the field (see Figs. 1-3).

During each experiment, treatment systems were acidified to pH 4 and then tracked through time to determine changes in pH, alkalinity, dissolved metals (Ca, Mg, Al, Cd, Cu, Fe, Mn, Pb, Zn), and biological populations (phytoplankton and zooplankton). Ambient water quality and sediment type

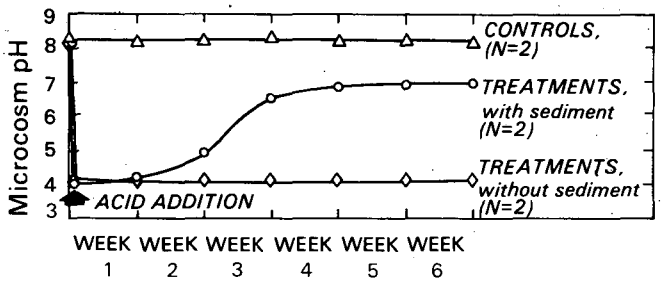

Figure 1. Measured pH changes in the Briones experiment. (XBL 8111-1580)

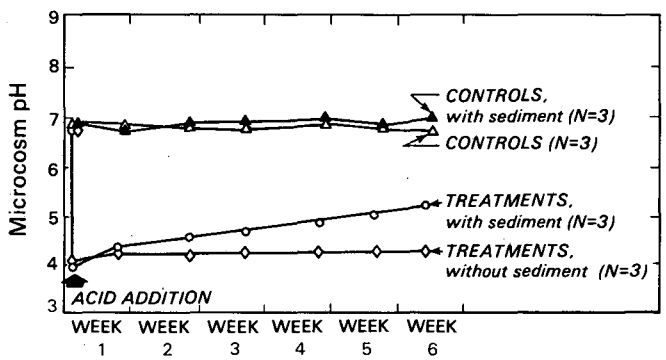

Figure 2. Measured pH changes in the Mosquito Lake experiment. (XBL 811-22)

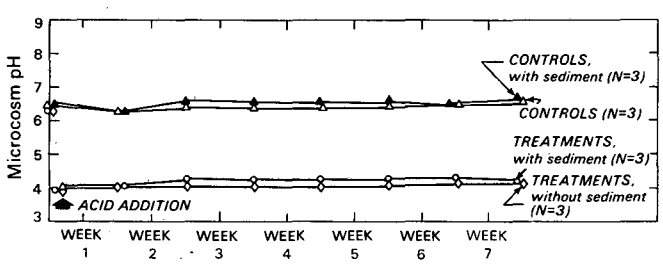

Figure 3. Measured pH changes in the Tenaya Lake experiment. (XBL 8111-1581)

proved to be the most important variables in determining the system response to acid inputs.

In two of the three lakes tested, the pH of the system recovered to near normal levels in the weeks following acidification. In one of the lake systems (Tenaya), no buffering occurred in the tanks with or without sediments.

Fluctuations in metal levels following acidification of the experimental systems differed among lakes. Levels of dissolved aluminum, manganese, and iron were observed to be most affected by changes in pH, with 10- to 100-fold increases in concentrations in the water column of these metals being detected following acidification. These metal resuspension phenomena may provide further evidence of lake basin vulnerability to acidic inputs.

Population levels of phytoplankton and zooplankton species were monitored following experimental acidification. Many vulnerable species were adversely affected by the drop in pH levels in the experimental tanks. In many cases, population "blooms" in the control systems were not observed in the acidified systems. Diversity of species through time increased significantly in the control systems while remaining at a low level in the acid-stressed systems.

Acid Precipitation and Its Effects in the Colorado Rockies

An investigation of the incidence of acid precipitation, its chemical composition, and its likely effects has continued at a research site near the Rocky Mountain Biological Laboratory, Gothic, Colorado. The site, on the western slope of the Colorado Rockies, is a high-elevation watershed spanning an elevation from 11,000 feet up to 12,400 feet. Approximately 60 rain and snow events were analyzed in 1981. For the second year, we have measured acidic precipitation, with a low pH of 3.6 seen in a winter snow storm in January, 1981. The major anions and cations, and also the trace-metal concentrations, have been measured in the rain samples from the summer of 1981. Several features of the precipitation data are noteworthy. First, the winter snow pH measurements showed far more variability from storm to storm than did the summer rain events. Second, there was no simple relation between the magnitude of a storm and its pH, contrary to results obtained in the eastern U.S. that suggest that the most intensely acidic events are those of least magnitude. The dependence of event pH on the time interval between that event and the preceeding one showed a systematic seasonal dependence. The nitrate-to-sulfate ratios for the summer rain storms were generally greater than one and were greatest for those events of lowest pH. These results have implications for our current source-determination studies.

In other work in Colorado, we continued our monitoring of the high-elevation ponds and lakes in the watershed. The data obtained from this monitoring effort have been used to evaluate the feasibility of conducting microcosm studies on site. The microcosm studies will enable us to predict future effects of acid precipitation on decomposition rates in these aquatic systems. In addition, the field monitoring is providing a set of baseline data against which future changes due to acid precipitation can be detected.

Acid Precipitation in China

Interest in acid precipitation in remote areas was stimulated by the recent discovery of acid precipitation in remote regions of the Northern Hemisphere such as Hawaii and the Indian Ocean, along with unexpectedly high concentrations of aerosols of probable anthropogenic origin in the Arctic. These findings have led some to suggest that acid precursors of anthropogenic origin may be widely distributed throughout the Northern Hemisphere, while others have suggested that the natural background pH of precipitation may be well below the theoretically expected value of 5.65.

In June 1981, one of us travelled to Qinghai Province in central China to characterize the chemical composition of precipitation in that region and to assess the resilience to acid precipitation (buffering capacity) of high-elevation lakes and streams in the eastern Tibetan Plateau. Precipitation samples were taken in two types of location: small cities with intensive coal burning and highly variable air degradation and the remote and sparsely populated Amne Machin Mountains (Chi-shih Shan) on the eastern Tibetan Plateau in Qinghai Province.[5]

In this study, precipitation samples were collected on an event basis and the pH measured immediately with a pH meter and electrode. In addition, some of the precipitation samples were preserved and later analyzed for anion and cation (including trace-metal) composition. Lake, pond, and stream waters and glacial ice in the high mountains were also sampled and pH measurements made. In some of these samples, ionic concentrations and phytoplankton densities were also measured.

A total of seven precipitation events with sufficient volume for analysis occurred during the study period. Two of these were in populated areas (Machin and Wen-Chuan) and five in the remote mountains. Because of limited capacity for handling samples for ionic analysis, only three of the samples were acidified and returned to the United States.

Table 1 presents representative results of the precipitation analyses. The most interesting features in Table 1 are the extraordinarily low pH of the sample from Machin, the high ratio of nitrate to sulfate in that sample, the absence of significant acidity in the remote samples, and the relatively high calcium concentrations in all samples for which anion and cation concentrations were measured. The high nitrate-to-sulfate ratio in all samples from a predominantly coal-burning region is surprising. The low pH event suggests the possibility that numerous Chinese cities are being subjected to very intense acid precipitation. Although the surface waters and soils of Qinghai Province we measured were highly alkaline, thus reducing the ecological risk, the potential for human health effects is great. Clearly, further studies of acid precipitation in China are warranted.

PLANNED ACTIVITIES FOR FY 1982

Precipitation and surface-water monitoring will continue at the Rocky Mountain site, and on-site microcosm experiments will begin. The microcosm studies will first serve to determine if these high-mountain lakes can be successfully "tracked" with microcosms and then will be used to determine likely effects of acid precipitation on nutrient cycling rates. Measurements will also be made of cation exchange capacity in the watershed soils surrounding the lakes and ponds. Using data that will be available from our monitoring program by autumn of 1982, we will develop and apply a model to predict the chronology of acidification in the watershed and, in particular, to determine the approximate time scale for depletion of watershed

Table 1. Precipitation analysis for Qinghai Province, China.

	Sample						
	1	2	3	4	5	6	7
Date	6/8/81	6/12/81	6/14/81	6/15/81	6/17/81	6/18/81	6/20/81
Time of measurement	2.00h	19.30h	19.00h	18.00h	1.00h	20.00h	20.00h
Location	Machin	Amne Machin mountains					Wen-chuan
Approximate latitude and longitude	34°30'N 100°10'E	34°50'N 99°E					35°40'N 99°10'E
Elevation (m)	3660	4270	4640	4330	4570	4570	3870
Nature of sample	rain	hail & rain	hail	hail & rain	rain	rain	hail
Amount of precipitation (mm)	0.5	1	12	3	3	3	0.5
pH	2.25	6.3	5.45	6.50	5.90	6.60	8.90
$[H^+]$ ($\mu\underline{M}$)	5600.	0.50	3.6	0.32	1.3	0.25	0.0013
[Ca] ($\mu\underline{M}$)	43		48		19		
[Al] ($\mu\underline{M}$)	4.0		2.5		3.0		
$[NO_3^-]$ ($\mu\underline{M}$)	6480		354		246		
$[SO_4^{2-}]$ ($\mu\underline{M}$)	183		29		51		

buffering capacity at prescribed rates of acid input.

Given the presence of acid precipitation at a specified site, what information is needed and how should it be used to pinpoint the sources of acidity? Relevant considerations are precipitation nitrate:sulfate ratios, weak-acid:strong-acid ratios, composition of the weak acids, and trace metals (e.g., the vanadium:manganese ratio, which is an indicator of the relative importance of petroleum versus coal as a source). In addition, event-basis information on storm direction, storm elevation, and a variety of factors that can influence the amount of alkaline dust in the atmosphere along the storm pathway needs to be considered.

In FY 1982, we will work with the detailed time series of precipitation chemistry data that exists for the western slope of the Colorado Rockies at Gothic, Colorado, augmented by meteorological data to be obtained from the National Weather Service. We will examine event-basis correlations among (1) the results of precipitation analyses, (2) the meteorological conditions characterizing the storm events, and (3) the appropriate characteristics of potential sources. These potential sources are coal-fired electric power plants in the Great Basin, smelters in the Salt Lake City area, California sources (particularly from the LA area), worldwide pollutants distributed throughout the upper atmosphere and scavenged by high-altitude storms, and natural background.

From this effort, we will increase our knowledge of sources of acid precipitation in the West, and, more generally, we will acquire a working understanding of some of the types of meteorological problems that need to be addressed in developing a greater understanding of atmospheric pollution from fossil-fuel consumption.

REFERENCES

1. Cogbill, C.V., and Likens, G.E. (1974), "Acid Precipitation in the Northeastern United States," Water Resources Research 10, 6.

2. Oden, S. (1968), "The Acidification of Air and Precipitation and Its Consequences on the Natural Environment," Swedish Nat. Sci. Res. Cont. Ecol. Comm. Bull. 1, pp. 1-68.

3. Lewis, W.M., and Grant, S.C. (1980), "Acid Precipitation in the Western United States," Science 207, pp. 176-177.

4. McColl, J., and Bush, D.S. (1978), "Precipitation and Throughfall Chemistry in the San Francisco Bay Area," J. Environ. Qual. 7, pp. 352-364.

5. Harte, J. (1981), "An Investigation of Acid Precipitation in Qinghai, Province, China," to be submitted to Environmental Science and Technology.

6. Tonnessen, K., and Harte, J. (1980), "The Potential for Acid Precipitation Damage to Aquatic Ecosystems of the Sierra Nevada, California (USA)," in Proceedings of an International Conference on the Ecological Impact of Acid Precipitation, D. Drablos, and A. Tollan, Eds., SNSF Project, Oslo, Norway, p. 338.

7. Tonnessen, K. (1981), "The Potential Impact of Acid Precipitation on Aquatic Ecosystems of the Western Slope of the Sierra Nevada," in Proceedings of California Symposium on Acid Precipitation, California Air Resources Board (in press).

TRACE ELEMENT ANALYSIS

The Survey of Instrumentation for Environmental Monitoring*

M. S. Quinby-Hunt, C. W. Case, R. D. McLaughlin,
G. A. Morton, D. Murphy, A. V. Nero, Jr., and A. T. Quintanilha

Applications of present and future energy technologies generate by-products that may pollute man's environment to varying degrees. An accurate analysis of such by-products is required if corrective measures or preventative actions are to be taken. There are, at present, numerous sophisticated instruments and techniques that can rapidly and accurately characterize and quantify the varieties and levels of pollutants associated with our technology.

To help those concerned with energy-related pollution, the Environmental Instrumentation Survey was started in 1971 with the aim of collecting information pertinent to this environmental monitoring into a single source. This survey attempts to review three fundamental aspects of the problem: (1) environmental information, (2) analytical techniques, and (3) commercial instrumentation (see Table 1). The first section provides an overview of the sources, characteristics, and effects of large numbers of pollutants and includes information on regulatory means of control. The second section describes and compares the analytical techniques used, including approved, on-going, and developing methods for sensitive, rapid, and accurate identification and quantitation of such pollutants. Problems which may be encountered with each technique are also reviewed. The third section covers instrumental techniques and provides information on commercially available instruments. Instrument notes give detailed descriptions of modes of operation, performance, and other information such as features, options, and cost. The information provided has proved to be extremely valuable to many workers in industrial, state, federal, and other laboratories.

Seven looseleaf binders which cover Air, Water, Radiation, and Biomedical Monitoring are currently available. Wiley-Interscience has recently agreed to publish the RADIATION volume, and plans are currently being made for commercial publication of the entire Survey, thereby significantly increasing its distribution.

ACCOMPLISHMENTS DURING FY 1981

The following new section and updates were completed and published in 1981.

*This work was supported by the Assistant Secretary for Environment, Office of Health and Environmental Research, Pollutant Characterization and Safety Research Division, U.S. Department of Energy under Contract No. DE-AC03-76SF00098.

Radiation

We have successfully negotiated a contract with Wiley-Interscience to publish the RADIATION volume. The work consists of three parts: "Ionizing Radiation and Its Measurement," "Nuclear Technology and the Environment," and "Special Radionuclides." Many of the nineteen chapters that make up this volume have already been edited for publication in book form.

Before contracting with Wiley, we published two updates on "Monitoring Radiation by Radiation Type." Phase I includes a new introduction and updated information on radiation background, fallout, spent fuel processing, and updated instrument notes for some of the sections. Phase II describes monitoring of alpha, beta, gamma, and x-radiation and includes instrument notes for the monitoring sections of the volume, including "Special Radionuclides." The material to be published by Wiley will include an additional update of "Special Radionuclides." This section contains chapters on monitoring radon and its daughters, uranium, thorium, plutonium, radium, strontium, krypton, and tritium.

Water

New sections on bacteria, residues (dissolved and suspended solids), halides, and cyanide and an update on asbestos were completed. These sections contain descriptions of instrumental techniques, including ion chromatography, ion-selective electrodes, and electron microscopy methods for monitoring asbestos.

Air (Particulates)

A new section on calibration and sampling, with new instrument notes for calibration and updated notes for mass and size determinations, was completed.

PLANNED ACTIVITIES FOR FY 1982

Our future work will involve several major updates of the volumes on WATER and AIR (Particulates and Gases) and the preparation of a new ENERGY volume. In addition, we expect to have the RADIATION volume edited and ready for publication during FY 1982.

Table 1. Fundamental aspects of the environmental instrumentation survey.

Environmental Information	Analytical Techniques	Commercial Instrumentation
Characteristics and forms of pollutants or environmental constituents	Approved techniques	Instrument notes including:
Sources and pathways in the environment	On-going methods	Class--laboratory/field
Effects	Developing methods	Description
Controls		Modes of operation
Regulatory situation		Range
		Multiparameter capability
		Sampling
		Performance and specifications in the same units
		Operation
		Requirements
		Options
		References
		Cost
		Address

Sections on personal dosimetry and neutron monitoring are currently being rewritten, and a new section on electronics is in preparation.

Air (Particulates)

The first phase of the section on air particulate composition will be prepared. It will include sections on inorganic and organic composition and revisions of the earlier sections on atomic absorption spectroscopy, x-ray fluorescence, and neutron activation analysis.

Energy

The initial material to be included in the ENERGY volume will be prepared. The introduction will address some of the regulatory and environmental problems encountered by those concerned with both conventional and developing energy technologies.

Water

A new section is being prepared on sampling techniques. This section discusses general sampling techniques for saline and fresh water, including waste water, and special techniques for energy producing technologies. Instrument notes will also be included.

The following sections concerned with organic pollutants will be written and updated: pesticides, phenolics and synthetic fuel pollutants, petrochemicals, and oils and greases. The turbidity section will be updated. A new section on biomass monitoring will be prepared.

Iridium Anomaly Approximately Synchronous with Terminal Eocence Extinctions*

W. Alvarez, F. Asaro, H. V. Michel, and L. W. Alvarez

Iridium and other siderophile elements depleted in the earth's crust occur in anomalously high concentrations at the same stratigraphic level as the marine micropaleontological extinctions that define the Cretaceous-Tertiary boundary at about 66.7 m.y.B.P. This anomaly has been found worldwide. Published data from six laboratories document 12 sites in marine sediments[1-6] and one site in terrestrial sediments from New Mexico[7]; several other occurrences have been discussed.[8] Geochemical details of the anomaly indicate that it was caused by impact on the earth of an extra-terrestrial object, probably having the composition of a carbonaceous chondrite and a diameter of about 10 km.[2,8-10] An impact of this magnitude should occur roughly every 100 m.y.,[11] and theoretical calculations of impact dynamics are compatible with this hypothesis.[12] Suggested killing mechanisms for an extinction following a bolide impact include suppression of photosynthesis during a period of darkness before settling of the dust injected into the atmosphere by the impact,[2] a temperature increase resulting from direct energy coupling to the atmosphere and/or an enhanced greenhouse effect from water vapor transferred from an oceanic impact site to the stratosphere,[13] and poisoning by toxic chemicals introduced into ocean and atmosphere by a cometary impact object.[14]

The impact hypothesis for the terminal Cretaceous extinctions suggests that evidence for impact of an extraterrestrial object might be found at the stratigraphic horizons of other mass extinctions. In fact, there is already one case where evidence for an impact is known at, or at least close to, such an extinction. The North American tektites on land and the associated micro-tektites studied in sea-bottom cores, principally by Glass and his coworkers,[15,16] provide direct evidence for a major impact. The strewnfield extends halfway around the earth and contains at least 10^{10} metric tons of impact melt in the form of far-traveled glassy spherules.[16] Five radiolarian species die out at the microtektite level,[15] but the event occurred about 2 m.y.[17] before the Eocene-Oligocene boundary, as defined in the Deep-Sea Drilling Project (DSDP) reports.[18] The boundary defined in this way may or may not be synchronous with the major turnover of mammal taxa that defines the Eocene-Oligocene boundary in terrestrial sequences in North America, Europe, and Asia,[19] a question beyond the scope of this paper. Dates suggested for the boundary are 32.5 ± 0.9 m.y.[17] and 38.0 m.y.[20] The best value for the fission track and K/Ar ages of North American tektites is 34.2 ± 0.6 m.y.,[17] and the microtektites give fission track ages of 34.6 ± 4.2 m.y.[21]

*This work was supported by the Department of Energy under Contract DE-AC03-76SF00098, the California Space Institute under Award CS24-81, and the NASA Ames Research Center under Contract A-71683 B.

ACCOMPLISHMENTS DURING FY 1981

The possible relation between the Eocene-Oligocene extinctions and a major impact has been considered by other workers.[16,22] To determine whether the impact that produced the North American strewnfield also gave rise to an iridium anomaly, we measured 30 elements by high-precision techniques of neutron activation analysis (NAA) in 9 samples from DSDP site 149 in the eastern Caribbean. Table 1 shows the elemental abundance of Ca, Cr, Ni, and Ir. A preliminary report on this work, including the recognition of a distinct iridium anomaly, has appeared as an abstract in the program for the October 1981, Snowbird, Utah, Conference.[23] A post-deadline paper on the same subject was presented at that conference by R. Ganapathy.

DSDP site 149 cored a "radiolaria-rich nannoplankton chalk" in the Middle Oligocene of core 30, and a "semi-indurated calcreous-rich radiolarian ooze" in the Upper Eocene of core 31.[18] The basal Oligocene is missing between cores 30 and 31,[18,24] a gap possibly amounting to 7 m.[15] This was the discovery site for the North American microtektites,[25] but unfortunately the peak of microtektite abundance was apparently lost in the unrecovered interval between cores 30 and 31. The microtektite abundance rises rapidly at the top of core 31, but is back to near zero at the base of core 30 (Fig. 1). Despite the missing section, this core offered an opportunity to look for an extraterrestrial component.

An iridium anomaly has been found in exact coincidence with the known microtektite level in DSDP site 149 in the Caribbean Sea. The maximum Ir abundance was 0.4 ppb, and the best value of background for 6 samples not in the microtektite region was 0.00 ± 0.05 ppb. The Ir is probably not in the microtektites but was deposited simultaneously with them. This could occur if the Ir were deposited from a dust cloud resulting from a bolide impact, as has been suggested for the anomaly associated with the Cretaceous-Tertiary boundary.

The principal conclusions of this report are

1. The association of iridium anomalies with major impact events, inferred for the Cretaceous-Tertiary boundary, is strengthened by recognition of an iridium anomaly at a microtektite horizon.

2. Although not all impacts which produce detectable iridium enrichments are necessarily related to extinctions,[26] the association of iridium anomalies with extinctions is strengthened by the synchronous disappearance of five species of radiolaria with the appearance of the iridium and microtektite anomalies near the Eocene-Oligocene boundary.

Table 1. Selected DSDP 149 chemical data.*

Core	Section	Interval (cm)	Ca (%)	Cr (ppm)	Ni (ppm)	Ir (ppb)
30	2	20-21	25.1 ± 0.7	27.0 ± 0.9	56 ± 6	<0.36 (-0.06 ± 0.18)
30	2	100-101	23.5 ± 0.8	27.7 ± 0.5	53 ± 6	<0.21 (0.05 ± 0.08)
30	2	140-141	19.7 ± 0.7	34.0 ± 0.5	76 ± 8	<0.22 (0.02 ± 0.10)
31	1	1-2	5.4 ± 0.5	30.4 ± 1.1	86 ± 10	0.41 ± 0.16
31	1	3-4	3.6 ± 0.5	30.8 ± 1.1	98 ± 10	0.34 ± 0.10
31	1	14-15	2.6 ± 0.6	32.7 ± 1.1	103 ± 10	<0.42 (0.14 ± 0.14)
31	1	26-27	1.2 ± 0.4	29.7 ± 0.7	93 ± 9	<0.34 (0.06 ± 0.14)
31	1	40-41	6.1 ± 0.6	27.1 ± 0.7	77 ± 8	<0.24 (-0.01 ± 0.12)
31	1	84-85	6.9 ± 0.5	25.3 ± 0.9	75 ± 9	<0.26 (-0.15 ± 0.13)

*The indicated precisions of measurement are standard deviations in the counting of gamma rays. Ca was calibrated vs a $CaCO_3$ primary standard; Cr and Ni were calibrated vs a secondary standard; STANDARD POTTERY (27), with abundances of 102 ± 4 and 278 ± 7 ppm respectively (28); and Ir was calibrated vs a secondary standard, DINO-1 (prepared from the Danish Cretaceous-Tertiary boundary layer) with an Ir abundance of 31.5 ± 0.6 ppb. The accuracies of the measurements are comparable to the precisions. When backgrounds comparable to gamma-ray peak intensities are subtracted, negative differences are sometimes obtained. If the difference is negative or smaller than 2 standard deviations, the sum of 2 standard deviation plus the value (if positive) is given as the upper limit for a 95% confidence level. The differences, expressed in ppb, are also shown in parentheses.

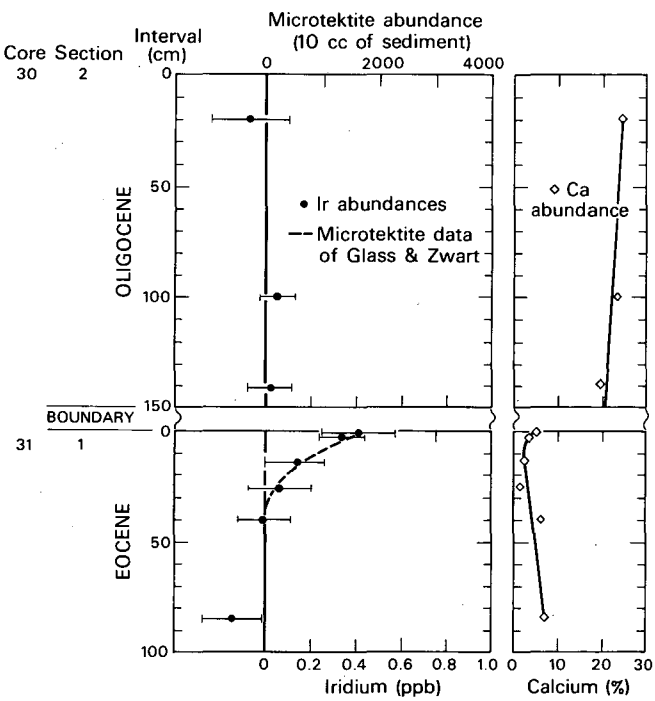

Figure 1. Iridium and calcium whole-rock abundances in cores from DSDP Site 429. Error bars in the Ir data are one standard deviation. One standard deviation in the Ca measurements is smaller than the size of the points. (XBL 819-1356)

3. Detailed studies of the latest Eocene are needed to determine whether or not the terminal Eocene mass extinction of land mammals is synchronous with the tektite-iridium horizon.

PLANNED ACTIVITIES FOR FY 1982

Further analyses are planned on DSDP cores having a complete Eocene-Oligocene sequence containing microtektites. This will provide information on the size of the impacting bolide. More work is needed on terrestrial Cretaceous-Tertiary boundaries and the other extinction horizons.

Neutron irradiations were kindly provided by Tek Lim, supervisor of the small U.C. Berkeley research reactor, and his staff. We are very thankful to B.P. Glass for helpful discussions. The DSDP samples were supplied through the assistance of the National Science Foundation.

REFERENCES

1. Alvarez, W., et al. (1979), "Experimental Evidence in Support of an Extraterrestrial Trigger for the Cretaceous Tertiary Extinctions," EOS 60, p. 734, and "Anomalous Iridium Levels at the Cretaceous Tertiary Bounday at Gubbio, Italy: Negative Results for a Supernova Origin," Geol. Soc. Am. Abstr. Programs 11, p. 350.

2. Alvarez, L.W., et al. (1980), "Extraterrestrial Cause for the Cretaceous-Tertiary Extinction," Science 208, p. 1095.

3. Smit, J., and Hertogen, J. (1980), "An Extraterrestrial Event at the Cretaceous-Tertiary Boundary," Nature 285, pp. 198-200.

4. Kyte, F.T., Zhou, Z., and Wasson, J.T. (1980), "Siderophile-Enriched Sediments from the Cretaceous-Tertiary Boundary," Nature 288, pp. 651-656.

5. Ganapathy, R., Gartner, S., and Jiang, M. (1981), "Iridium Anomaly at the Cretaceous-Tertiary Boundary in Texas," Earth and Planetary Science Letters 54, p. 393.

6. Ksu, K.J., et al., "Environmental and Evolutionary Consequences of Mass-Mortality at the End of the Cretaceous," Science (in press).

7. Orth, C.J., et al., (1981), "An Iridium Abundance Anomaly at the Polynological Cretaceous-Tertiary Boundary in Northern New Mexico," Science 214, p. 1341-1343.

8. Alvarez, W., et al. (1982), "New Data on the Cretaceous-Tertiary Extinction," in Abstracts of AAAS Annual Meeting, Washington, D.C., Jan. 1982.

9. Ganapathy, R. (1980), "A Major Meteorite Impact on the Earth 65 Million Years Ago: Evidence from the Cretaceous-Tertiary Boundary Clay," Science 209, pp. 921-922.

10. Asaro, F., et al. (1980), "Results of a Dating Attempt--Chemical and Physical Measurements Relevant to the Cause of the Cretaceous-Tertiary Extinctions," in Proceedings of the ACS Symposium on Nuclear and Chemical Dating Techniques, Houston, Texas, March 23-28, 1980, Lawrence Berkeley Laboratory Report LBL-11613.

11. Shoemaker, E.M. (1980), private communication to Luis Alvarez (Ref. 2).

12. Ahrens, T.J. et al. (1981), "Effect of the Atmosphere and Ocean on the Impact of the Cretaceous-Tertiary Bolide," in Abstracts of Conference on Large Body Impacts and Terrestrial Evolution: Geological, Climatological, and Biological Implications, Snowbird, Utah, Oct. 19-22, 1981.

13. Emiliani, C., Kraus, E.B., and Shoemaker, E.M. (1981), "Sudden Death at the End of the Mesozoic," Earth and Planetary Sci. Letters 55, p. 317.

14. Hsu, K.J. (1980), "Terrestrial Catastrophe Caused by Cometary Impact at the End of the Cretaceous," Nature 285, pp. 201-203.

15. Glass, B.P., and Zwart, M.J. (1979), "North American Microtektites in Deep Sea Drilling Project Cores from the Caribbean Sea and Gulf of Mexico," Geol. Soc. of Am. Bulletin, Part 1 90, pp. 595-602.

16. Glass, B.P., Swincki, M.B., and Zwart, P.A. (1979), Proceedings of the 10th Conference of Lunar and Planetary Science, pp. 2535-2545.

17. Glass, B.P., and Crosbie, J.R. (1981), Geological Society of America, private communication to W. Alvarez.

18. Edgar, N.T., et al. (1973), "Site 146/149," Initial Rep. D.S.D.P. 15, p. 130.

19. Brunet, M. (1977), "Les Mammiferes et le Probleme de la Limite Eocene-Oligocene en Europe," Geobios, Mem spec'l, pp. 11-27; Savage, D.E. (1981), personal communication.

20. Ness, G., Levi, S., and Couch, R. (1980), "Marine Magnetic Anomaly Time-Scales for the Cenozoic and Late Cretaceous: a Précis, Critique, and Synthesis," Reviews of Geophysics and Space Physics 18, pp. 753-770.

21. Glass, B.P., et al. (1973), Earth and Planetary Sci. Letters 19, pp. 184-192.

22. Urey, H.C. (1980), "Cometary Collisions and Geological Periods," Nature 242, p. 32, and O'Keefe, J.A. (1980), "The Terminal Eocene Event: Formation of a Ring System Around the Earth?" Nature 285, pp. 309-311.

23. Asaro, F., et al. (Ref. 12).

24. Maurrasse, F. (1976), "Radiolarian Stratigraphy and North American Microtektites in Caribbean RC9-58: Implications Concerning Late Eocene Radiolarian Chronology and the Age of the Eocene-Oligocene Boundary," in Transactions of the VII Caribbean Geological Conference, French Antilles, June 30-July 12, 1974, pp. 185-203.

25. Donnelly, T.W., and Chao, E.C.T. (1973), "Microtektites of Late Eocene Age from the Eastern Caribbean Sea," Initial Rep. D.S.D.P. 15, pp. 1031-1037.

26. Kyte, F.T., Zhou, Z., and Wasson, J.T. (1981), "High Noble Metal Concentrations in a Late Pliocene Sediment," Nature 292, pp. 417-420.

27. Perlman, I. and Asaro, F. (1971), "Pottery Analysis by Neutron Activation," in Science and Archaeology, Ed. R.H. Brill, MIT Press, Cambridge, MA, p. 182-195 and (1969), Archaeometry 11, pp. 21-52.

28. Michel, H.V. and Asaro, F. (1980), unpublished data.

Precise Characterization of New World Obsidian Sources and the Cost-Effective Determination of Provenience of Selected Artifacts*

F. H. Stross, F. Asaro, and H. V. Michel

During the past decade and a half, careful chemical analysis has provided highly useful information on the distribution and exchange of obsidian, the volcanic glass, in ancient cultures. In the course of the relevant studies, the importance of this substance as a highly prized and widely used raw material for the production of a host of functional and ornamental artifacts has become increasingly evident, and today the study of obsidian could be considered a discipline in itself. Pertinent information derived by the physical sciences has come to parallel and complement that obtained by the conventional methods of archaeology.

Physical-chemical methods for analyzing pottery, obsidian, and quartzite developed by Lawrence Berkeley Laboratory have proved very useful in archaeological studies.[1] Consequently, a number of academic institutions have requested assistance in their archaeological studies, and this collaborative work during the last year has emphasized studies of obsidian in the New World. These studies are based on accurate and detailed measurements of the composition of sources from which the raw material for excavated artifacts was obtained. Since these artifacts are excavated in great numbers, it has also become important to devise for them, in contrast to source rocks, the most cost-effective techniques of chemical measurement possible. From the artifact measurements, the origin of the artifacts (provenience) can be determined. Collaboration with other institutions and disciplines has insured that the provenience information is effectively integrated into contexts.

ACCOMPLISHMENTS DURING FY 1981

A substantial portion of the work reported here concerned obsidian from the heartland of the Maya culture. Important source areas in Guatemala have been analytically described earlier[2]; this report adds significant areas to these records. Included are the large region often designated as Rio Pixcayá or San Martin Jilotepeque, northwest of Guatemala City, and some smaller source areas within a 50-mile radius of Guatemala City. Artifacts from two well-known sites, Tikal and Quiriguá, both in Guatemala, were analyzed by special techniques developed for their economy.

Source investigations were also made of Ecuadorian obsidian, and artifacts from the Quito Valley were assigned to sources. Procedures also have been developed to intercalibrate analytical data published by other laboratories with our own when direct comparisons, for one reason or another, are not possible.

Neutron Activation Analysis (NAA)

Measurements are made by precise and accurate NAA[1]; data are usually included for 20 elements,[3,4] and errors are carefully evaluated. The measurements are made on specially prepared samples, and the procedures for both sample preparation and measurement are rigidly controlled. As an example, the element abundances of an obsidian artifact originating from Ixtepeque (one of the most important Guatemalan sources, located in southeastern Guatemala) were found to agree within 1.7 percent, for the 16 most precisely measured elements, with the analysis of Ixtepeque obsidian measured three years earlier.

Measurements are calibrated with the standard "Standard Pottery." The element abundances of the latter were determined by using primary standards, and their values and errors have been published.[1,5] The accuracy, expressed in percent, for a particular element, which is usually close to the precision, may be determined by taking the square root of the sum of the squares of the precision, expressed in percent, and the accuracy[5] of that element in Standard Pottery, expressed in percent. These measurements by NAA are very useful for characterization of sources of obsidian but are too expensive for analysis of large numbers of artifacts.

X-Ray Fluorescence (XRF)

This type of measurement can be made with high precision and accuracy.[6] The present work on artifacts, however, was not done in this manner because emphasis was on non-destructive measurements and lowest possible cost. The accuracy of the latter measurements was approximately 10 to 15 percent, and, with some additional effort, accuracies of 6 percent or better should be attainable.

When comparing data measured against the same standard as in the NAA measurements, precision can be used to indicate the extent of agreement. When comparing data measured against different standards, the accuracy should be used to test the agreement.

General Procedure (Artifacts)

Artifacts are first measured for Rb, Sr, and Zr by XRF with a ^{109}Cd source and then for Ba with

*This work was supported by the Council on Research and Creative Work of the University of Colorado and the Museo del Banco Central del Ecuador through the U.S. Department of Energy under Contract No. DE-AC03-76SF00098.

a ^{241}Am source. The artifacts are divided into chemical groups from these measurements, although other elements determined by XRF (Fe, Mn, Zn, Y, and Nb) are sometimes used if their abundances are unusually high. Representative members of each chemical group and any samples not falling into a group are analyzed destructively by an abbreviated NAA sequence for Mn, Na, Dy, K, and Ba. The number of artifacts for which this is necessary is approximately 10 to 15 percent of those analyzed by XRF. These measurements must conform almost exactly to a known group before source assignments are made. For any sample that does not conform to a known group by the abbreviated NAA sequence, the NAA sequence is completed for all of the usual elements. Generally, 10 to 15 percent of the samples undergoing an abbreviated NAA sequence would need to have the NAA completed. All members of chemical groups determined by XRF whose representative members conform exactly with a known source by the abbreviated NAA sequence are assigned to that source. Any artifacts of uncertain origin will have had a complete NAA sequence and will a priori represent a new source or a new variation in a known source.

Laboratory Intercalibration

A number of laboratories[2,7-10] have made chemical measurements on obsidian from Mesoamerican sources, primarily by NAA and XRF. It is often difficult for one laboratory to use the source data of another for many reasons, including the following: abundances are sometimes only given in terms of counting rates of gamma or x-rays, corrections are not made for background or interferring radiations, measurements are calibrated against different standard materials, or measurement errors are made. The best solution would be for all laboratories that study obsidian source material to make accurate measurements against the same standard or against different but well-known standards. When this is not feasible, it is possible to intercalibrate those laboratories which make reproducible, but not necessarily accurate, measurements. Intercalibration of two laboratories does not imply that the results of one laboratory are better than those of the other. It is simply a way of relating the experimental results to each other. The LBL measurements by NAA have been intercalibrated with those of Ericson and Kimberlin[11] and Hurtado de Mendoza and Jester.[7] Our XRF data have been intercalibrated with Zeitlin et al.[9] and with Cobean et al.[8] The interalibration procedures and formulae are being published.[3] The XRF calibrations are rather complex because backgrounds sometimes are not subtracted from the peaks nor are interferences removed by other laboratories.

Sources

Because it is necessary to define the source compositions as completely and accurately as possible, both NAA and XRF measurements are made for the listings that are to be published. Whenever possible, several samples are analyzed to determine if the source is essentially homogeneous over a large area[2] or shows systematic variations, possibly mixing of two different obsidian magmas[7] prior to eruption or fractionation of magma between eruptions.

No strict definition of the concept of source area appears to exist at present. The source areas mentioned are listed in accord, i.e., with usage adopted in the literature and with a recognizable geographic context. These sources in Southern Guatemala include:

1. Those previously referred to as San Martin Jilotepeque, Rio Pixcayá, and Aldea Chatalun, all in the department of Chimaltenago.

2. A source in Sacatepéquez, referred as San Bartolomé Milpas Altas.

3. A source in Santa Rosa by the Laguna de Ayarza, referred to as Media Cuesta.

4. A possible source in the department of El Progreso, by the Puente Chetunal.

The published composition records and the intercalibrated literature data[3,4] supplement the compositions of El Chayal, Ixtepeque, and Tajumulco sources, which had already been published.[2] In addition, two sources located in Ecuador[12,13] have been analyzed: Mullumica a primary source in the high Andes, and Rodeo Corrales, a secondary source not far from Mullumica but in a different drainage system. Possible primary sources for the Rodeo Corrales obsidian are the nearby mountain peaks of Quiscatola and Yanaurco Chico, which have obsidian of identical composition. Mullumica is interesting because it appears to be one of the few obsidian outcrops in which more than one magma may have been incompletely mixed,[14] as mentioned above.

Our final objective is to determine the provenience of artifactual material excavated and to make whatever deductions are possible from this information. In this work, artifacts from the site of Tikal, in the Department of Petén,[4] and from Quiriguá,[3] Department of Izabal, were studied. Also studied were artifacts from Ecuador; these were classified into six groups,[12] for which only two sources are known.[13] Most of the other groups may reflect the heterogeneity resulting from the incomplete mixing of magmas mentioned previously.

Conclusions

Whenever possible, attempts are made to correlate the distribution of proveniences, indicative of an exchange network, with the corresponding archaeological time period. This usually is done by dating associated datable material such as charcoal, normally by radiocarbon methods. When several cultures are involved, the character of the artifacts also becomes important, as in the case of Tikal artifacts.[4]

Tikal imported most of its obsidian from highland Guatemala (e.g., El Chayal, Ixtepeque, and Rio Pixcayá), probably in the form of large polyhedral cores. During the Classic period (approximately A.D. 300 to 900), it also received from central Mexico a very small proportion of obsidian as fin-

ished point knives, green obsidian polyhedral cores, and rare eccentrics and other forms.

The presence at Tikal of central Mexican green obsidian has been known for years, but the presence of central Mexican gray obsidian was discovered by the program of analyzing point-knives.[4] Evidence now demonstrates that obsidian from different sources was preferred for different types of artifacts. The location where the artifacts are found (e.g., in a midden or in a ceremonial deposit) also becomes important because this may become an indicator of the relative wealth of a specific time period.

In Quiriguá, on the other hand, no non-Guatemalan obsidian (outside of a minute proportion of green-obsidian point knives) was found. This suggests trade with Mexican areas was less important in Quiriguá than in Tikal. The Ecuadorian studies are not far enough advanced to permit any conclusions beyond those of provenience indicated above.

PLANNED ACTIVITIES FOR FY 1982

The University of Florida at Gainesville, University of Texas at San Antonio, Trent University (Alberta, Canada), Cornell University, University of California, Santa Barbara, and Greenwood and Associates (Los Angeles) already have indicated their desire to undertake collaborative work with this Laboratory along the lines indicated.

REFERENCES

1. Perlman, I., and Asaro, F. (1969), "Pottery Analysis by Neutron Activation," Archaeometry 11, pp. 21-52.

2. Asaro, F. et al. (1978), "High-Precision Chemical Characterization of Major Obsidian Sources in Guatemala," American Antiquity 43, pp. 436-443.

3. Stross, F.H. et al. (1981), Precise Characterization of Guatemalan Obsidian Sources and Source Determination Artifacts from Quirigua, Lawrence Berkeley Laboratory Report LBL-12252 (Revised, November, 1981).

4. Moholy-Nagy, H., Asaro, F., and Stross, F.H. (1981), Tikal Obsidian: Sources and Artifacts, Lawrence Berkeley Laboratory Report LBL-13143.

5. Perlman, I., and Asaro, F. (1971), "Pottery Analysis by Neutron Activation," in Science and Archaeology, R.H. Brill, Ed., M.I.T. Press, Cambridge, Mass., pp. 182-195.

6. Giauque, R.D., Garrett, R.B., and Goda, L.Y. (1977), "Energy Dispersive X-Ray Fluorescence Spectrometry for Determination of Twenty-Six Trace and Two Major Elements in Geochemical Specimens," Anal. Chem. 49, pp. 62-67.

7. Hurtado de Mendoza, L., and Jester, W.A. (1978), "Obsidian Sources in Guatemala: A regional Approach," Am. Antiquity 43, pp. 424-435.

8. Cobean, R.H. et al. (1971), "Obsidian Trade at San Lorenzo Tenochtitlan, Mexico," Science 174, pp. 666-671.

9. Zeitlin, R.N., and Heimbuch, R.C. (1978), "Trace Element Analysis and the Archaeological Study of Obsidian Procurement in Precolumbian Mesoamerica," in Lithics and Subsistence--The Analysis of Some Tools Used in Prehistoric Economics, D. Davis, Ed., Vanderbilt University, Publications in Anthropology #20.

10. Jack, R.N., and Heizer R.F. (1968), "'Finger-Printing' of Some Mesoamerican Obsidian Artifacts," Contributions to the University of California Archaeological Research Facility 5, pp. 81-100.

11. Ericson, J., and Kimberlin, J. (1977), "Obsidian Sources, Chemical Characterization, and Hydration Rates in West Mexico," Archaeometry 19, 2, pp. 157-166.

12. Asaro, F., Michel, H.V., and Burger, R.L. (1981), Chemical Source Groups in Ecuadorian Obsidian, Lawrence Berkeley Laboratory Report, LBL-13247.

13. Asaro, F., H.V. Michel, and Burger, R.L. (1981), Major Sources of Ecuadorian Archaeological Obsidian and Provenience Assignments of Artifacts, Lawrence Berkeley Laboratory Report, LBL-13246.

14. Bowman, H.R., Asaro, F., and Perlman, I., "On the Uniformity of Composition in Obsidians and Evidence for Magnetic Mixing," Jour. Geology 34, pp. 312-327.

Organic Compounds in Coal Slurry Pipeline Water*

A. S. Newton, H. M. Villarreal, W. E. Walker, and J. P. Fox

The transport of coal by slurry pipeline is an established engineering practice. The methods, equipment, and operating procedures are well developed and have been demonstrated in the successful operation of the Black Mesa Pipeline through which 5 million tons of coal per year are transported from Kayenta, Arizona, to the Mohave Generating Station on the Colorado River at Laughlin, Nevada. At the source near Kayenta, the coal is converted to a slurry of about 50 percent coal in water by wet grinding in rod miles. The slurry is temporarily stored in stirred tanks and then pumped under high pressure through 287 miles of pipe to the receiving station at the Mohave Generating Station, where it can be stored temporarily. For use, it is passed through continuous centrifuges, and the moist cake is dried, repowdered, and burned to generate electricity. The separated liquid centrate still contains several percent coal fines.

The centrate is further treated in a clariflocculator in which a clear overflow and a heavy underflow are obtained by the addition of small amounts of additive flocculants. The overflow is a good quality water, and it is used at the Mohave Generating Station as make-up water and cooling-tower water. None is released to the environment. The underflow, a heavy black material, is pumped to sealed evaporation ponds. When dry, the residues are collected and burned in the boilers. Some trouble has been experienced in drying the underflow, and this part of the process has not been completely successful. Test wells between the Mohave Generating Station and the Colorado River have shown that there is no contamination of the ground water due to the operation of the coal slurry separation facilities.

Because of the possibility that the production of finely divided coal in water under reducing conditions can produce organic contaminants in the water, a study was initiated in August 1979 to measure the extent to which a clear centrate from coal slurry might be contaminated with organic compounds and, if so, to determine if these compounds were toxic, requiring further treatment before disposal into the environment. In FY 1980, it was shown that no compounds were formed which could be detected in the coal slurry water, except phenol and possibly a few substituted phenols. Experiments with perdeuterated hydrocarbons showed that addition of these compounds to water before slurry formation resulted in almost complete absorption of these compounds by the coal. The addition of phenols to water before slurry formation resulted in the same amount of phenol in the slurry water as was found when no phenol was added.

*This work was supported by the Assistant Secretary for Environmental Protection, Safety, and Emergency Preparedness, Office of Environmental Compliance and Overview, Environmental Control Technology Division of the U.S. Department of Energy under Contract No. DE-AC03-76SF00098.

ACCOMPLISHMENTS DURING FY 1981

This year, work continued on the identification and quantification of organic compounds in coal slurry water. Results last year indicated differences in behavior of various types of coal in regard to the degree of absorption of polynuclear aromatic hydrocarbons, PNA's, and phenolic compounds from water. One reason for such a variation is a difference in rates of equilibration between water and each of the respective coals. In earlier studies, the coal slurry water was separated from the coal soon after formation of the slurry, and equilibration may not have been achieved. In a working slurry pipeline, the coal is in contact with the water a minimum of three days and may be in longer contact in holding tanks at each end of the line.

Therefore, emphasis was placed on results after three days' contact between coal and water. A sample of overflow water from the clariflocculator at the Mohave Generating Station was obtained through the cooperation of Dan Cobb, engineer at the Mohave Generating Station, Southern California Edison Company.

Coal was slurried for 2 hours with water in a laboratory-size rod mill to make a 20-percent slurry of coal in water. Before slurry formation, perdeutero compounds were added to the water to a concentration of 100 ppb. After slurry formation, the mill was allowed to stand for 3 days, with occasional stirring to simulate the time in a pipeline. The centrate was then separated with a Beckman Model J-21B centrifuge with a JS-7.5 swinging bucket rotor.

The centrifugation was made at 0°C and a rotor speed of 7500 RPM for 30 minutes. This yielded a clear centrate in all cases. To the centrate was added a perdeutero phenol internal standard to a concentration of 10 ppb and a 1.0-ppb normal anthracene internal standard. One liter of the centrate was made 1 N in NaOH and extracted with three 100-ml portions of n-hexane (nanograde). The combined extracts were dried with sodium sulfate and concentrated to about 2 ml in a rotary evaporator. The concentrate from the rotary evaporator was further concentrated to 0.1 ml by evaporation with a stream of N_2. A 1-µl portion of this was injected into the GC/MS. Quantification was accomplished by comparing the signal at m/z = 178 of the added anthracene standard with the parent ion of each of the respective added perdeutero compounds. The emergence times and sensitivities of each of the added components were determined by calibration with standard mixtures, with each standard containing a known concentration of each of the added com-

pounds. Since the GC/MS trace of the hexane extract showed no response from the perdeutero compounds added, a maximum possible concentration was calculated by observing the minimum detectable peak signal in each run (set by the scan parameters) of the added anthracene internal standard peak and the ratio of the signal intensity of the parent peak of each compound to that of anthracene, each at a concentration of 100 ppm in the standard solution.

The results are shown in Table 1. For each coal, it is evident that less than 0.02 ppb of PNA's or aromatic hydrocarbons can exist in the water. At this ratio of coal to hydrocarbons, all the hydrocarbons are adsorbed onto the coal, if they are ever formed, and are disposed of when the coal is burned.

The overflow water from the Mohave Generating Station was treated similarly. Since no perdeutero compounds had been added, a search was made of all peaks in the reconstructed ion chromatogram (RIC). A few peaks were observed which are normal low-level contaminants of field samples, e.g., octyl and butyl phthalates, squalene, and C_{20} to C_{30} normal hydrocarbons, usually from a lubricating oil contamination. Naphthalene at 0.04 ppb, vanillan at 0.4 ppb, camphor at 0.3 ppb, and di-t-Butyl benzoquinone at 0.8 ppb were observed. These are not normally found as contaminants. All of these may be from the proprietary flocculants added to the clariflocculator.

Table 1. Adsorption of added perdeuterated neutral organic compounds from waters during slurry formation with various coals.

Compound[a]	ppb of compound in coal slurry water[b]		
	Wyodak Coal	Illinois No. 6 Coal	Black Mesa Coal
Acenaphthene-D_{10}	<0.009	<0.013	<0.013
1,2-Diphenylethane-D_{14}	<0.005	<0.007	<0.007
Phenanthrene-D_{10}	<0.005	<0.010	<0.010
Pyrene-D_{10}	<0.003	<0.010	<0.010
p-Terphenyl-D_{14}	<0.003	<0.013	<0.013
17-Tetracosane-D_{50}	<0.01	<0.02	<0.02
1,2-Benzanthracene-D_{12}	<0.003	<0.015	<0.015
Chrysene-D_{12}	<0.003	<0.015	<0.015
Perylene-D_{12}	<0.008	<0.02	<0.02

[a]The compounds are listed in their order of emergence from a 25-m, J&W DB-5 bonded quartz column. The perdeuterated compounds were added to the water before slurry formation to a concentration of 100 ppb.

[b]The water was in contact with the coal for 3 days after slurry formation. The concentrations given are all maxima, the values depending on the final volume of the hexane extract and the GC/MS sensitivity of an added internal standard.

All coal slurry waters and the Mohave overflow water contained phenols in the ppb concentration range. The phenols were separated by methylating the basic solution with dimethyl sulfate, extracting the resulting methyl ethers with n-hexane (nanograde), and concentrating the resulting hexane by evaporation to about 1 ml. The resulting concentrate is analyzed by GC/MS as before, using the methyl ether of perdeutero phenol as an internal standard.

The results are shown in Table 2; it is apparent that, in the range of 1-100 ppb, phenols are found in coal slurry waters from all of the coals tested. The general agreement of the phenol concentrations in the Mohave Generating Station clariflocculator overflow with the phenol concentrations in our laboratory study indicates that the laboratory results can be used to evaluate the problem of organic contaminants in coal slurry water.

CONCLUSIONS

This study shows that organic compounds, other than phenols, do not occur in environmentally significant levels in coal slurry waters from the subbituminous coals tested. Phenols do occur at the concentration levels of 1-100 ppb (μg/l). This concentration level is below the "safe" level set by EPA. If these slurry waters are chlorinated, these phenols will be converted to various polychloro phenols.

Table 2. Phenolic compounds found in coal slurry waters.

	Concentration of phenolic in coal slurry water (ppb)			
	Wyodak Coal	Illinois No. 6 Coal	Black Mesa Coal	Mohave Clariflocculator Overflow
Phenol	4.2	8.3	13.2	8.5
O-Cresol	5.7	13.2	11.5	10.1
P-Cresol	6.8	15.7	27.2	14.2
2,6-Dimethylphenol	2.6	3.4	7.1	2.9
O-Ethyl Phenol	6.5	17.6	18.4	54
P-Ethyl Phenol	2.4	10.1	4.6	6.8
3,5-Dimethyl Phenol	0.3	1.2	2.1	1.0
C_3-Phenol[b]	<0.01	<0.04	2.9	1.5

[a]Phenols are listed in the order of the emergence of their methyl ethers from a 25-m, J&W DB-5 bonded quartz capillary column.

[b]The C_3-isomer is unidentified except by molecular weight.

The Development and Application of X-Ray Fluorescence Analytical Techniques*

R. D. Giauque and L. E. Sindelar

X-ray fluorescence (XRF) techniques are being developed and applied to support programs which require trace multielement chemical analysis. Emphasis is placed on improving the sensitivity capability of XRF and establishing accurate methods which compensate for matrix effects. XRF methods are applied to support (1) oil shale, (2) atmospheric aerosol, (3) waste management, and (4) geochemical research programs. A primary purpose of these programs is to study the distribution, speciation, and fate of numerous trace elements.

ACCOMPLISHMENTS DURING 1981

An XRF method for the determination of forty elements of atomic number 22 (Ti) and higher, in oil shale and geochemical specimens, has been developed. Pulverized specimens are mixed 2:1 with microcrystalline cellulose powder which serves as a binder. Pressed disks of mass thickness 95 mg/cm^2 are prepared. Specimens of this mass thickness permit (1) high analytical sensitivities to be realized for elements which have characteristic x-rays of energy greater than 7 keV ($Z > 27$) and (2) experimental attenuation measurements to be made at 9.88 keV (GeKα) and 11.91 keV (BrKα) to ascertain corrections for matrix effects for all radiations of interest. Absolute calibration of the semiconductor x-ray spectrometer is achieved using two individual-element thin-film standards, one for each secondary excitation radiation. Relative response of the x-ray spectrometer to characteristic x-rays from most elements is achieved using nebulized deposits of multielement standard solutions.[1] AgK excitation radiation is used for the determination of the elements which have characteristic x-rays of energy between 4.5 and 17.5 keV (Ti $\rightarrow$ Mo and Hf $\rightarrow$ U). Similarly, the elements Ru $\rightarrow$ Ce are determined using TbK excitation radiation. Sensitivities realized for most elements are in the 1 to 5 ppm range. Total analysis time required for each specimen is approximately forty minutes. Table 1 lists some results for NBS Standard Reference Material 1633, Trace Elements in Coal Fly Ash, and serves as an illustration of the capability of this method.

Table 1. NBS SRM 1633 coal fly ash.

Element	XRF (μg/g$\pm 2\sigma$)	NBS (μg/g$\pm 2\sigma$)
Ti	6300±600	---
V	169±62	214±8
Cr	123±22	131±2
Mn	440±34	493±7
Fe	54700±2800	---
Ni	102±12	98±3
Cu	131±10	128±5
Zn	211±10	210±20
Ga	44±2	---
Ge	26±2	---
As	64±2	61±6
Se	9.4±1.0	10.4±0.5
Br	5.7±0.8	---
Rb	113±4	(112)
Sr	1400±50	(1380)
Y	66±2	---
Zr	295±8	---
Nb	24±2	---
Mo	20±2	---
Sn	5.0±2.0	---
Sb	6.0±2.4	---
Cs	6.9±2.4	---
Ba	2570±160	---
La	80±8	---
Ce	148±8	---
Pb	73±4	70±4
Th	28±4	(24)

PLANNED ACTIVITIES FOR 1982

The previously described XRF method is being applied to investigate the geochemistry of oil shale from the Geokinetics In-Situ Retort No. 16 near Books Cliff, Utah. Four spent cores and one raw-oil-shale core outside the periphery of the retort are being characterized. The depth of the cores was approximately eighty feet, and samples taken were typically composites over one-foot depth intervals. Statistical analysis is being carried out to establish relationships which exist between the numerous variables determined at this laboratory and elsewhere. These variables include elemental and mineral analysis, as well as Fischer Assay oil and water content.

A method for the determination of sulfur in crude oil and petrolem products will be established, and thin specimens will be prepared. Fundamental x-ray scattering principles will be used to ascertain specimen mass. Detection limits of <0.01 percent sulfur should be achieved using five-minute counting periods.

X-ray fluorescence techniques applicable to multielement analysis of small quantities (<10 mg) of geochemical specimens and evaporated residues will be developed. Emphasis is being placed on establishing procedures for the preparation of deposits of uniform mass thickness. Several mathematical methods to compensate for matrix effects will be studied.

*This work was supported by the Director, Office of Energy Research, Basic Energy Sciences, Chemical Sciences Division of the U.S. Department of Energy under Contract No. DE-AC03-76SF00098.

REFERENCES

1. Giauque, R.D., Garrett, R.B., and Goda, L.Y. (1977), "Calibration of Energy Dispersive X-Ray Spectrometers for Analysis of Thin Environmental Samples" in X-Ray Fluorescence Analysis of Environmental Samples, T.G. Dzubay, Ed., Ann Arbor, Mich., Ann Arbor Science Publishers Inc., pp. 153-164.

Asymmetry of the Mitochondrial Membrane*

R. J. Mehlhorn and L. Packer

Mitochondria carry out aerobic metabolism in higher plants and animals by converting the energy contained in chemical bonds of low-molecular-weight substrates into transmembrane electrochemical gradients. These gradients are "coupled" to the synthesis of ATP, the fundamental unit of energy currency in cells. Peter Mitchell received the Nobel Prize in chemistry for his role in increasing our understanding of this "chemiosmotic" process. However, most of the molecular details of how electrochemical gradients are created and how energy is conserved in ATP synthesis remain to be elucidated.

This project seeks to define the primary energy-conserving events in time and space when substrates are added to mitochondria by monitoring electrochemical potentials with novel spin probe methods. These methods enable us to selectively probe the interior or exterior of mitochondria as well as surface and hydrophobic regions of the mitochrondrial membrane. Thus, we have the capacity to characterize the time-dependency of proton release and uptake of both membrane surfaces and the movement of charges across the membrane. A related application of site-specific spin probes is to observe one-electron redox reactions in terms of loss and recovery of the paramagnetic signal of the probes during electron transport activity in mitochondria and to correlate these redox reactions with the creation and collapse of electrochemical potentials.

ACCOMPLISHMENTS DURING FY 1981

Mitochondria were found to be unduly permeable to charged spin probes and other paramagnetic ions for routine studies. We therefore made preliminary studies with light-activated membrane systems which offered the opportunity to examine very rapid responses of spin probes to energy gradients.

Accurate Determinations of Electrical Gradients

A careful analysis was made of light-induced electrical transmembrane potentials in halobacterial envelope vesicles.[1] Previously, we had been puzzled because our analyses of spin-labeled phosphonium ion uptake invariably gave much smaller potentials than other techniques, including phosphonium electrode data. We have now shown that the discrepancy was due to erroneous analysis of the data obtained with these other methods. We confirmed that the depletion of the phosphonium spin label from the vesicle exterior was consistent with data obtained with our phosphonium electrode. Computer treatment of membrane-bound spin labels revealed that a significant increase in bound probes occurred upon illumination of the vesicles. This fact is not considered in analyzing electrode data and leads to substantial overestimates of electrical potentials.[1] Similar data misinterpretations may arise when radioactive phosphonium ions or fluorescent probes are used to estimate membrane potentials. The alternative for estimating membrane potentials, using curves derived from valinomycin-induced Nernst potentials, is also subject to artifacts because of experimental difficulties in creating the large chemical gradients required to extend calibration curves beyond 100 mV. Moreover, our experience indicates conventional protocols used to load vesicles with defined salt solutions fall far short of achieving complete loading. From these studies, we conclude that previous conclusions concerning the quantitative relationship between electrochemical potentials and ATP synthesis may have to be revised.

Use of Nitroxides for Radical Detection in Mitochondria

Although it had been shown previously that nitroxides are reduced by the mitochondrial electron transport chain, the electron spin resonance (ESR) signal of spin probes is quite stable in inner mitochondrial membranes when no substrates are present. However, when we illuminated such membrane preparations with visible light, we observed a loss of the ESR signal.[2] This spin loss occurred under conditions where visible light caused destruction of flavin-linked respiratory functions so it appeared possible that spin destruction was due to free-radicals and that these radicals were implicated in visible-light damage to the mitochondrial membrane. During the past year, we have characterized this phenomenon with the following results:

*This work was supported by the National Institutes of Health under Grant No. GM-24273 through the U.S. Department of Energy under Contract No. DE-AC03-76SF00098.

1. Free radicals are trapped by the nitroxides. A new technology has been evolved for discriminating between chemical reduction and free-radical capture by nitroxides. The method consists of comparing spin loss and reoxidation rates under carefully controlled conditions of oxygen tension during the ESR experiment.

2. Free radicals are generated by aqueous but not bound flavins. The flavins require a reductant or free-radical precursor which is released from the membranes as a function of time.

3. The initiation of light-mediated free radical reactions occurs in the aqueous phase, and some of these aqueous radicals subsequently react with the mitochondrial membrane to cause lipid peroxidation, a well-known membrane destruction process.

Spin-Trapping Studies of Microsomal Free Radicals

As part of our research to characterize free radical reactions with spin-trapping techniques, a study on hydrazine-derived radicals was performed.[3] It was shown that rat-liver microsomal preparations from phenobarbitol-treated animals reacted with ethylhydrazine and acetylhydrazine to form free-radical adducts with the trap α-phenyl-tert-butylnitrone. Curiously, no adducts could be demonstrated with another commonly used spin trap: 5,5-dimethylpyrroline-N-oxide. A similarly puzzling anomaly was seen in our study with illuminated mitochondrial membranes where free-radical trapping was seen with only one of these spin traps. We have, therefore, advocated the use of nitroxides as supplementary spin traps to help resolve ambiguities due to potential non-radical reactions of nitrones that may yield paramagnetic species.[2]

Spin-Labeling of Protein Carboxyl Groups

We have extended our studies of spin-labeled proteins by reacting carboxyl residues on bacteriorhodopsin with spin-labeled amines.[4] It was shown that the spin labels were bound to heterogeneous protein sites, as reflected in different mobility states of the probes and differential broadening of spectral features by paramagnetic quenching agents. Detachment of a hydrophilic segment of the protein by trypsin digestion was readily apparent in terms of signal changes in the ESR spectrum. Protein conformational changes resulting from denaturation with urea-SDS (sodium dodecyl sulfate) also gave rise to dramatic changes in ESR spectra. Studies are in progress to delineate the sideness of spin-label attachment and thus to map the topography of reactive carboxyl residues in the protein.

Surface Potential Changes Due to Oxidative Membrane Damage

The high sensitivity of our cationic amphiphilic spin probes to surface potential changes was exploited to detect new negative surface charges at mitochondrial membrane interfaces resulting from oxidative damage.[5] Damage was initiated by aerobic incubation, visible illumination, or respiration of exogenous substrates. Muscle mitochondria exhibited consistently greater charge changes than liver mitochondria, and vitamin E deficiency exacerbated these effects.

PLANNED ACTIVITIES FOR FY 1982

Improved mitochondrial preparations have become available and will be assayed with spin-probe techniques. A rapid mixing device is being constructed to extend measurements to the initial energization events and to overcome problems associated with excessive membrane permeability of some of the probes. Accurate electrical potentials will be determined in mitochondrial membranes for the first time by correcting for membrane binding artifacts.

REFERENCES

1. Mehlhorn, R.J., Candau, P., and Packer, L. (1982), "Measurements of Volumes and Electrochemical Gradients with Spin Probes in Membrane Vesicles," in Methods in Enzymology, S. Fleischer and L. Packer, Eds., Academic Press, New York (in press).

2. Mehlhorn, R.J., and Packer, L. (1982), "Nitroxide Destruction and Flavin-Sensitized Damage in Inner Mitchondrial Membranes," Can. J. Chem. (in press).

3. Augusto, O., Ortiz de Montellano, P.R. and Quintanilha, A. (1981), "Spin Trapping of Free Radicals Formed During Microsomal Metabolism of Ethylhydrazine and Acetylhydrazine," Biochem. Biophys. Res. Commun. 101, pp. 1324-1330.

4. Herz, J.M., Mehlhorn, R.J. and Packer, L. (1982), "EPR Studies of Carboxyl Groups in Spin-Labeled Bacteriorhodospin," Biophys. J. 37, p. 227a.

5. Quintanilha, A.T., et al. (1982), "Membrane Effects of Vitamin E Deficiency: Bioenergetic and Surface Charge Density Studies of Skeletal Muscle and Liver Mitochondria," in Vitamin E: Biochemical, Hematological and Clinical Effects, Ann. N.Y. Acad. Sci., B. Lubin and L. Machlin, Eds. (in press).

ENERGY ANALYSIS RESEARCH PROGRAM

INTRODUCTION

The objective of the LBL Energy Analysis Program is to assess a broad range of issues relating to energy demand, supply, prices, and policies. The Program also addresses a variety of more general resource and environmental issues such as water availability and quality and the environmental and human health effects of energy demand and supply. The main thrust of the program is to perform systems studies that include assessment of the technical, economic, social, and environmental impacts of alternative policies relating to energy and resources.

The approaches used by the Energy Analysis Program staff include a wide variety of disciplines and techniques--energy analysis of buildings, economics, computer simulations, architectural engineering, financial analysis, forecasting, operations research, and other--organized to solve problems. Most of these problems require the assembling of an interdisciplinary team consisting of LBL staff, faculty and students from the University of California at Berkeley or Davis, and consultants.

ISSUES IN ENERGY POLICY

In early 1980's, we are experiencing a radical change in the manner of government involvement in energy policy. Although the nature of the key energy policy problems have changed little in the past decade--potential oil disruptions, environmental issues of energy development, increasing energy prices, underinvestment in energy conservation, and the need to prepare for a transition to new sources of energy--the government has chosen to become less directly involved in seeking solutions to these problems. The prevailing philosophy in Washington is to achieve energy price deregulation to the greatest extent possible and let the market find solutions to energy problems.

There is, however, an opposing school of thought that maintains that many of the most important energy problems cannot be solved by the market alone. The key energy policy issues involve factors external to the market that are only partially amenable to market solutions.

The issue of energy policies to supplement the market or reduce market distortions is of particular interest to the Energy Analysis Program. The program is currently performing a comprehensive analysis of energy conservation in buildings. This analysis treats measures to achieve increased efficiency of energy use, estimates of energy savings from computer model simulations and from measured data, economics of conservation measures, forecasts of penetration of energy conservation, assessments of market barriers, impacts of conservation on electric utilities and other economic sectors, and policies to encourage investment of energy conservation measures in buildings. In the past, the Energy Analysis Program has addressed in a systematic way a similar set of issues dealing with understanding market behavior on energy supply. The Hawaii Integrated Energy Assessment from fiscal year 1980 is an example of one such study.

CURRENT RESEARCH ACTIVITIES

During FY 1981, the program addressed a series of energy supply issues, including environmental and institutional aspects of the coastal zone; water quality and efficiency of water use; and systems studies of energy development in the western United States, the California energy supply, and U.S. minerals requirements over the next several decades. On the demand side, the program was involved with a variety of studies of energy use in buildings, including technical studies of energy conservation in residential and commercial buildings, effects of occupant behavior of energy use in homes, hourly and peak impacts of energy conservation, analysis of historical indicators of residential energy use, energy demand forecasting, and the study of policies to promote energy conservation in buildings (described above). The program also included a study of energy conservation in Kenya. Several other international energy studies were begun during the year.

FUTURE DIRECTIONS

In the coming years, the program's existing research will be extended and research in several new areas will be initiated.

Significant improvements will be made in the energy-demand forecasting models, including the updating of demand and usage elasticities, development and testing of new algorithms to project market penetration and energy efficiencies of applicances and space conditioning equipment, inclusion of interactions among internal loads and equipment efficiencies, and inclusion of new end-use technologies. The hourly energy demand model will be validated for several electric utility service areas. Quantitative analysis of the performance of the market regarding investments in energy conservation will both improve energy demand forecasting tools and contribute to analyses of energy conservation policies. The energy and hourly

demand forecasting models will be combined with other analytic tools, especially financial analysis models, to produce a state-of-the-art package to assess conservation impacts on utility systems.

Research will continue on increasing our understanding of all factors affecting the energy use in building. This will include both computer calculations and measurements of energy use in occupied buildings.

The program will place special emphasis on its international energy demand studies. Research will be expanded to include European and selected less developed countries. We hope to begin an assessment of energy demand in the countries of the Pacific rim to complete our effort to analyze factors most likely to influence the patterns of world energy demand.

ENERGY SUPPLY STUDIES

Coastal Zone Assessment Program*

R. L. Ritschard

Many Federally supported coastal management programs are facing budget cuts or termination under initiatives from the new Administration. Programs such as the Coastal Zone Management Program (CZMP) and the Coastal Energy Impact Program (CEIP), concepts such as "national interest" and "Federal consistency," and many existing rules and regulations are being reevaluated. The substantive and procedural results of such reevaluation could directly and indirectly affect the process and pace of energy development in variable ways. This revised coastal management scene will cause readjustments within the Federal government and the states, generally resulting in program shifts from federal to state control. With many programs being transferred, increased, decreased, modified, or discontinued, the implications to environmental protection and energy development require attention. The basic intent of the FY 1981 activities was to identify and examine the new status of coastal management programs, rules, regulations, etc., that interact with energy programs and agency responsibilities, authorities, and procedures.

ACCOMPLISHMENTS DURING FY 1981

During FY 1981, in conjunction with the Brookhaven National Laboratory, the Energy Analysis Program at LBL continued the joint coastal assessment program. LBL's activities included an ecological assessment of fossil-fuel-based technologies and an environmental analysis of marine biomass (both reported elsewhere in this report) in addition to the accomplishments listed here.

The purpose of the FY 1981 study was to examine the coastal zone management programmatic changes that relate to energy at both Federal and state levels. It was anticipated that the differences in impact and response between states and regions would be identified as determined by the varying levels of coastal energy activity, their degree of participation in various programs, the state of development or implementation of various coastal plans, and the expected response to program changes.

Coastal Zone Management Program

The Coastal Zone Management Act of 1972 (CZMA) established a program of Federal grants to assist states in the development and implementation of programs aimed at more rational management of coastal resources through the preservation, protection, development, restoration, and enhancement of the Nation's coastal zone. In October 1980, Congress unanimously reauthorized the CZMA and rejected recommendations that Federal funding levels should be reduced during the next five years. As part of the 1980 reauthorization action, Congress acknowledged that the implementation phase is extremely critical in joint Federal-state efforts to deal with the intensity of both present and future development pressures and use conflicts confronting the Nation's coastlines.

As a result of the CZMA, effective state coastal management efforts are underway. Since 1972, all 35 eligible coastal states or territories have participated in the program. Twenty-five of these participants--representing 78 percent of the nation's coastline--have developed or are currently implementing coastal management programs, and another six are making reasonable progress toward program approval (Table 1). However, these states are not yet in a position to assume the full financial burden of coastal zone management. Of the 25 coastal states and territories with approved coastal management programs, 7 received approval in 1980, 6 in 1979, and 10 in 1978. In other words, half of the approved programs have been functioning for less than three years. Most of these programs have had little opportunity to become institutionized and still rely heavily on the Federal government's commitment to support their implementation efforts.

*This work was supported by the Assistant Secretary for Environment, Office of Environmental Assessments, Regional Impacts Division of the U.S. Department of Energy under Contract No. DE-AC03-76SF00098.

Table 1. Status of state coastal zone management programs.

State	Actual or Estimated Federal Approval Date By Fiscal Year (ends 9/30)	Comments and Status 1/30/81
Washington	1976	Approved
Oregon	1977	Approved
California	1978	Approved
Massachusetts	1978	Approved
Wisconsin	1978	Approved
Rhode Island	1978	Approved
Michigan	1978	Approved
North Carolina	1978	Approved
Puerto Rico	1978	Approved
Hawaii	1978	Approved
Maine	1978	Approved
Maryland	1978	Approved
New Jersey (Bay and Ocean Shore Segment)	1978	Approved
Virgin Islands	1979	Approved
Alaska	1979	Approved
Guam	1979	Approved
Delaware	1979	Approved
Alabama	1979	Approved
South Carolina	1979	Approved
Louisiana	1980	Approved
Mississippi	1980	Approved
Connecticut	1980	Approved
Pennsylvania	1980	Approved
New Jersey (Remaining Section)	1980	Approved
Northern Marianas	1980	Approved
American Samoa	1980	Approved
Florida	1981	DEIS in preparation
New Hampshire	1982	Legislation needed
Texas	1982	Public Hearing held in October on Public Hearing Draft
New York	1982	Legislation pending
Ohio	?	Legislation pending
Indiana	?	Legislation/Executive Order needed
Georgia	Probably Not	
Virginia	Probably Not	
Minnesota	Probably Not	
Illinois	Probably Not	

Source: Coastal States Organization, Coastal Management--A Sound Investment, April 1981.

From its inception in 1972, the Federal coastal zone management program has required participating coastal states and territories to give explicit recognition to the national interest in the formulation of state coastal management programs. In return, the coastal states and territories receive technical and substantial financial assistance to implement the programs. In addition, the law contains a unique provision requiring that federal activities and decisions that affect a state or territorial coastal zone will be consistent with the policies of the state or territorial coastal management program.

For the past seven years, the mutually beneficial partnership existing between the Federal government and the states and territories has worked quite well. For example, the following areas have been addressed:

1. One of the major goals of the CZMA is to eliminate unwarranted delays by Federal, state, and local governments in issuing environmentally related permits. The states have been encouraged to simplify and streamline their permitting processes and to coordinate their permitting efforts with Federal and local agencies that exercise concurrent permitting jurisdiction. The state coastal zone management programs also provide a mechanism for state assumption of coastal wetlands regulatory functions now administered by the U.S. Army Corps of Engineers and the Environmental Protection Agency under Section 404 of the Clean Water Act.

2. In conjunction with state port authorities and other Federal and state agencies, several state coastal management programs have undertaken extensive port planning and management efforts. California, South Carolina, Washington, Oregon, Hawaii, and the Virgin Islands have acted to prevent the exclusion of marine industrial uses by placing the highest priority on coastal-dependent uses.

3. State coastal management programs have protected natural resources including wetlands which provide habitat, nursery grounds, and food sources for most of the Nation's commercially and recreationally valuable fish and shellfish and breeding grounds for more than ten million waterfowl.

As part of the Administration's budget trimming efforts, the Office of Management and Budget (OMB) proposed that all Federal funding for the coastal zone management program be terminated at the end of FY 1981. The Congress, however, retained $33 million from other sources (specifically from the Coastal Energy Impacts Program that will be discussed below) to maintain the coastal management program through the current fiscal year (FY 1982). The future of continued funding for CZMA is unknown at this time.

Coastal Energy Impact Program (CEIP)

The 1976 amendments to the Coastal Zone Management Act state that "the national objective of attaining a greater degree of energy self-sufficiency would be advanced by providing Federal financial assistance to meet state and local needs resulting from new or expanded energy activity in or affecting the coastal zone." The CEIP, the central element for implementing this policy, is designed to help states minimize the social, economic, and environmental disruptions resulting from new or expanded coastal energy activity, especially oil and gas exploration and development on the Outer Continental Shelf (OCS). The program helps states plan for providing needed new public facilities and services while preventing or reducing "unavoidable" losses of environmental or recreational resources. CEIP is intended to balance the need for more energy resources in the national interest with the need to preserve our coastal areas for the myriad of other valuable functions they perform.

Money for the grants, loans, and guarantees comes from two inter-locking sources: the Coastal Energy Impact Fund and Formula grants. The Impact Fund is to be used only to plan and provide public facilities and services required as a result of all new coastal energy activity. Congress authorized appropriation of $800 million until October 1, 1986. Formula grants provide states with additional money (up to $50 million annually until September 30, 1984) to help mitigate the impacts of OCS activity; the total authorized was $1.2 billion. Grants may be used only after a state has

exhausted its Fund allotment and after offshore leasing begins. The exception is that Formula grants are the primary source of funds for environmental projects.

Support for the CEIP will change drastically in FY 1982. Congress decided in early June to support both the coastal zone management grants and the CEIP with the $40 million left in the CEIP loan fund. Most of the funds, $33 million, are allocated for state coastal management programs, while CEIP will receive only $7 million. In FY 1982, CEIP is scheduled to grant this money to participating states for the following specific activities: energy impact planning, OCS state participation, and mitigation of impacts from the transport and storage of coal at coastal sites. This will probably be the last year of the program.

Several important energy-related issues have been addressed by the CEIP over the past five years. Among these are the following:

- Investigation of the potential for and impacts of exporting coal from various coastal areas, including the Great Lakes region.
- Assessment of the Northern Tier Pipeline proposal to create a crude oil transshipment port in the state of Washington.
- Port and navigational hazards studies conducted for the Santa Barbara Channel and the Los Angeles/Long Beach harbors in California.
- Assistance to coastal states likely to be affected by OCS energy activities in carrying out their responsibilities under the OCS Lands Act.

Impacts of Decreased Federal Funding

Through CZMA program funds and CEIP funds, coastal states and territories have for the first time received Federal financial support to help plan for and address the social, economic, and environmental problems associated with energy-related activities occurring in or affecting the coastal zone. Coastal states and territories have used these funds for planning, mitigation of environmental effects of energy development, and public facilities and services required as a result of coastal energy activities.

Historically, there has been a disparity in the disposition of revenues between states that experience impacts from energy development activities on Federal lands within their borders and those states that experience similar impacts as a result of energy development on the OCS. In fact, the only Federal programs that provide financial assistance to coastal states for coastal dependent energy resources development are those created by the CZMA. If these programs are abolished by termination of Federal funding, the inequities of this situation will only increase. Furthermore, coastal states will be asked to assume this unexpected burden at the very time when the Administration has announced its intentions to intensify activities that will have impacts on coastal areas.

The Secretary of the Interior has recently announced that OCS oil and gas development will be expedited by an accelerated five-year leasing schedule. Since the coastal management program's inception in 1972, OCS oil and gas exploration, development, and production activities have for the most part been concentrated in areas with long histories of offshore energy development activities, primarily the western Gulf coast and offshore southern California. In the years ahead, however, the Department of the Interior plans to lease OCS lands in a number of "frontier areas" off northern California, Alaska, and the East Coast, where there has been little or no experience in offshore energy development. The Federal government is also encouraging other energy-related activities such as increased coal exports from coastal sites. The environmental, economic, and social impacts of these proposed expansions on local communities are significant and must be carefully assessed.

The Coastal Zone Management Act established a politically sensible and constructive approach for handling coastal problems by partnership of Federal, state, and local institutions. States, however, are not yet in a position to assume the full financial responsibility of coastal zone management. The coastal zone management program is consistent with the Administration's philosophy that state and local governments should assume a larger role in management and regulatory functions. Termination of this program will undoubtedly generate ill-will toward energy development activities in coastal states.

It is too early to predict whether or not the Administration's change in policy regarding coastal energy planning and mitigation will result in delays in energy development or in expedited activities. One can foresee, however, that many of the problems previously addressed by the coastal zone management program could become more critical and could result in further litigation.

PLANNED ACTIVITIES IN FY 1982

Several tasks planned for FY 1982 will continue and expand the coastal zone assessment program. These activities include:

- Identification, collation, verification, assembly, and reconciliation of existing data bases and coastal resource mapping efforts to enable construction of a composite data base of the natural environment.
- Compilation of a data base consisting of the location of known or suspected energy resources within the coastal zone and OCS as well as energy-related activities, facilities, etc.
- Identification of pertinent statutes, program activities, and policies that interact with coastal and offshore energy activities.

- Evaluation of viable alternatives to existing plans, policies, programs, statutes, and regulations of other agencies which appear to constrain energy production/development in the coastal zone.

Estuarine Impacts of Fossil-Fuel-Based Technologies: A Case Study*†

R. L. Ritschard, V. J. Berg, and M. A. Henriquez

Coastal regions, particularly estuaries and salt marshes, are rich in life forms. Of all ecological zones, estuaries have the greatest natural rate of food production. Man, at the same time, often burdens these productive regions with energy-related environment-disturbing activities, such as power plants and refineries with their accompanying terminals and storage tanks.

San Francisco Bay, largest estuary on the West Coast, is an example of a marine ecosystem which is impacted by numerous fossil-fuel-based energy activities. This is especially true in the upper reaches of the Bay, where more than 70 percent of the electrical generating capacity is located. Furthermore, most of the additional electricity generating facilities proposed for the area have recommended sites in the upper San Francisco Bay Area.

Man's past activities have already altered the Bay. Hydraulic mining of gold in the Sierras contributed large sediment loads. Water flow in the Delta has been controlled and reduced by storage reservoirs, irrigation withdrawals, and diversions to southern California. The marshes in the Delta have been diked for agriculture, and the periphery has been filled for urban development. Various exotic species, such as striped bass and certain ship-fouling organisms, have been introduced both accidentally and on purpose. A huge volume of municipal and industrial wastes is discharged daily into the Bay, wastes which are the main impact of energy-related facilities.

The purpose of this study is to investigate the potential cumulative ecological impacts on a specific estuarine system resulting from fossil-fuel-based technologies. The upper reaches of San Francisco Bay are used as a case study because the majority of such activities in California occur in this region. The specific study area used in this project is divided into six zones in the northern reach (see Fig. 1).

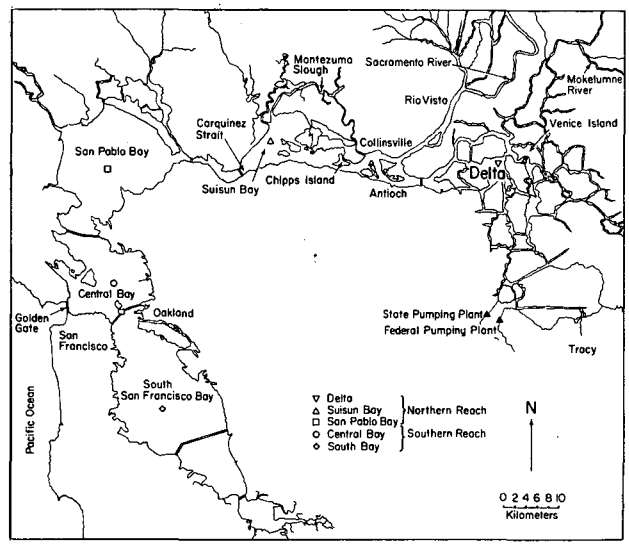

Figure 1. San Francisco Bay estuarine system. (XBL 8110-1382)

ACCOMPLISHMENTS DURING FY 1981

Data were collected on routine discharges from power plants and refineries and on oil spills from petroleum transporting, handling, or storage. For both plant discharges and oil spills, Zone 4 is a highly impacted region of the Bay. In fact, in 1978, 29 thousand gallons of petroleum from 34 spills (about 30 kg/day of oil and grease) and over 170 kg/day of copper were reported to have entered this zone. Because not all dischargers are required to monitor for all effluent constituents, it is difficult to obtain a complete picture of the total level of effluents reaching the Bay. In addition, it is best to interpret the values reported as low estimates of discharges into the Bay system because supporting data have not been included.

We conclude from the data available that energy-related discharges, as well as other industrial wastes, may not be the most significant contributors to pollutant loading of the Bay. Municipal outfalls, only briefly considered in this study, and Delta outflow seem more important to the well-being of the Bay ecosystem, at least in terms of the volume and mass loading of different effluents.

*This work was supported by the Assistant Secretary for Environment, Office of Environmental Assessment, Regional Impacts Division of the U.S. Department of Energy Under Contract No. DE-AC03-76SF00098.

†Condensed from R. Ritschard, V. Berg, and M. Henriquez, "Estuarine Impacts of Fossil Fuel-Based Technologies," Lawrence Berkeley Laboratory Report LBL-13145, September 1981.

A study based on field monitoring and computer modeling was conducted for the Association of Bay Area Governments (ABAG) as part of federally funded water quality planning.[1] Annual loads of biochemical oxygen demand (BOD), nutrients (total nitrogen and phosphorus), heavy metals, and total suspended solids (TSS) were estimated for San Francisco Bay for each source category: municipal, industrial, non-point, and Delta outflows.

The ABAG study reported that municipal wastewaters were the largest contributors of BOD (57 percent), nitrogen (58 percent), and phosphorus (79 percent).[1] Elevated BOD levels decrease dissolved oxygen, whose presence is essential for fish, shellfish, and other aquatic animals. Nitrogen and phosphorus are plant nutrients and are responsible for nuisance blooms of algae. Compliance with current water quality standards will also cause a decrease in certain pollutant loads from both municipal and industrial sources. These new treatment programs will decrease BOD loadings to the Bay but will not greatly affect the nitrogen or phosphorus inputs. However, the proposed Valley Drain, which would take agricultural waste water from the San Joaquin Valley and release it into Zone 4, could increase nitrogen concentrations significantly.

Delta outflow in responsible for much of the pollutant loading within San Francisco Bay. It contributes to the level of TSS (77 percent), heavy metals (56 percent), nitrogen (33 percent), phosphorus (17 percent), and BOD (26 percent).[2] Delta outflow also fluctuates in response to storms and to the level of diversions by the state and federal water projects. As a result of upstream development and diversions, Delta outflow for the next two decades is projected to average about 5.5 MAF during normal precipitation years.[3] This level is compared to 3.7 MAF during the 1977 drought and a typical present outflow of about 12 MAF per year.

There appears to be a well-established, direct relationship between the level of Delta outflow and the health of part of the Bay ecosystem. Suspended particulate materials carried by the Delta outflow are trapped in the null or entrapment zone of the northern reach, which is also the area where phytoplankton standing crops are the highest. Both the entrapment zone and the phytoplankton standing crop can be regulated, in turn, by manipulating the Delta outflow.[4] Zooplankton, especially Neomysis (mysid shrimp) and juvenile striped bass, are also concentrated in the entrapment zone.

This relationship can be further illustrated by examining low flow conditions. When the outflow is low, the null zone migrates from Suisun Bay to deep, narrow, upstream channels that do not support phytoplankton production. The standing crop in this area is therefore low. Under these conditions, the normal population of the mysid shrimp is reduced by about 75 percent and the young striped bass population by about 90 percent of normal. Therefore, the entrapment zone, the phytoplankton standing crop, and the population of zooplankton, shrimp, and juvenile striped bass are also regulated by controlling the Delta outflow.

If a water policy decision is made to maintain entrapment zones within Suisun Bay through July to protect the striped bass population, this same assemblage of organisms will be exposed for a longer period of time to effluents from the energy facilities (power plants and refineries) and to municipal outfalls in Zone 4. The consequences of this interaction are unknown at this time, but they will have to be considered in the future.

The major pollutants reported as discharges from energy-related facilities are oil and other petroleum products (oil/grease), total suspended solids (TSS), and copper. These pollutants also make up a significant portion of the municipal discharges and the load in the Delta outflow. In addition, we have shown that a considerable amount of oil and other hazardous substances are spilled in the Bay system each year.

Fuel and crude oil generally contain toxic materials that are harmful to estuarine life, even at very low concentrations. Their effect may also be accentuated by synergistic interactions. Oil damage in many regions can be persistent, sometimes lasting for years or decades, particularly if the oil becomes incorporated in bottom sediments. The impact of low-level, chronic oil discharges on organisms is still a debated scientific issue.

Total suspended solids, such as silt, clay and organic particles, can affect water transparency. This, in turn, may limit the amount of light available to aquatic producers, i.e., phytoplankton, and disrupt the base of the estuarine food chain. Furthermore, much of the heavy-metal load of any estuary has been found to be associated with suspended solids, as well as other toxicants. If the Delta outflow, the major contributor of TSS to the Bay, decreases over the next two decades because of additional Federal and state water diversions such as the Peripheral Canal, the level of TSS could also be expected to decline.

In sufficient concentrations, heavy metals such as copper can have damaging effects on aquatic organisms. These chemicals can also interact with other substances to create synergistic or antagonistic responses. A recent study of clams in the southern reach reported a fourfold variation in copper levels over time.[5] This observation was related to Delta outflow and local stream runoff. Because freshwater flushes high concentrations of metals out of organisms such as clams, the future levels of Delta outflow will be an important consideration. Striped bass in the bay have been reported to be heavily burdened with copper and zinc. This increased pollutant burden in the adult bass is believed to be at least partly responsible for the unhealthy state of the striped bass fishery.[6]

In the northern reach of San Francisco Bay, the impact of power plants and refineries is extremely site-dependent. These impacts include the routine introduction of pollutants into the aquatic environment, entrainment (passage of small organisms through the cooling water system), impingement (impaction of larger aquatic species on

water intake screens), and the possibility of thermal pollution. Entrainment and impingement may be very important at power plants using once-through cooling systems. However, in relation to other major activities in the Bay system such as the outflow of municipal discharges and Delta outflow, these effects may seem minimal. If we consider energy facilities in conjunction with other contributory factors, the health of the Bay may be at stake.

Pollution from fossil-fuel energy facilities must be considered in conjunction with pollution from other sources such as municipal waste discharge and Delta outflow. In addition, major activities of the Bay that must be included in a systemwide assessment are (1) the Peripheral Canal, which will divert large quantities of freshwater from the Bay; (2) the Valley Drain, which, if built, will become a significant contributor of algae-producing nitrogen to the study area; and (3) the proposed Baldwin Ship Channel, which could allow more salt water to intrude into important spawning and nursery areas.

As we have pointed out in this study, estuarine ecosystems are highly dynamic and, at times, unpredictable. Estuaries are also associated with marshes or wetlands, which serve as intermediate zones between the marine and terrestrial environments. Wetlands are highly productive, serve as a reservoir and buffer for nutrients, and are nursery areas for juveniles of many species.

Even though a technical evaluation of man's impact on estuaries is a complex and difficult task, it should be conducted in a more systematic and comprehensive fashion than in the past. This applies not only to studies of the San Francisco Bay system, but also to studies of estuaries located anywhere in the country or anywhere in the world, for that matter. Our modest effort here has attempted to develop this new paradigm. Studies in the future should monitor the health of the entire ecosystem, particularly species that man uses for food or that are considered as the most sensitive indicators of environmental health. These studies should consider all aspects of the environment--biological, chemical, and physical--and should address all sectors of the economy--municipal, industrial, and agricultural. Furthermore, we recommend that such an integrated ecological study include improved sampling techniques and an intercalibration of methods used by various researchers.

Data on pollutant loadings in the Bay are sparse. In addition, much of the existing data are of limited value because there is little or no mention of the sampling techniques or sample variability. Because natural variability caused by physical, chemical, or biological disturbances may be great enough to mask many effects of man's activities, we recommend that a more complete, better organized, and readily accessible data base on the pollutant loadings in the Bay be constructed. If all these recommendations are followed, a sound understanding can be developed of how the Bay ecosystem functions in relation to its multiple uses. An assessment of this nature can be a useful tool for decision-makers who are responsible for estuaries throughout the country.

PLANNED ACTIVITIES FOR FY 1982

Although this specific project was concluded in FY 1981, the information gathered and the methods developed will be used to support the Coastal Zone Assessment Program described previously in this Annual Report.

REFERENCES

1. Risebrough, R., et al. (1978), Toxicants in San Francisco Bay and Estuary, Association of Bay Area Governments, Berkeley.

2. Yucel, V., and Russell, P. (1980). Pollutant Loadings on the San Francisco Bay Estuary, Association of Bay Area Governments, Berkeley.

3. Kelley, D.W., and Tippets, W.E. (1977), Delta Outflow and San Francisco Bay, Delta Environmental Advisory Committee, State of California, Sacramento.

4. Arthur, J.F., and Ball, M.D. (1980), The Significance of the Entrapment Zone Location to the Phytoplankton Standing Crops in the San Francisco Bay Delta Estuary, U.S. Department of Interior, Water and Power Resources Division, Sacramento.

5. Luoma, S., and Cain, D. (1979), "Fluctuations of Copper, Zinc, and Silver in Tallenid Clams as Related to Freshwater Discharge--South San Francisco Bay," in San Francisco Bay: The Urbanized Estuary, T.J. Conomos, Ed., Pacific Division, AAAS, San Francisco, pp. 231-246.

6. Eldridge, M. (1981), National Marine Fisheries Service, Tiburon, Calif., Personal Communication.

Environmental Impacts of Marine Biomass*†

R. L. Ritschard, V. J. Berg, and S. Killeen

Lawrence Berkeley Laboratory (LBL), under the sponsorship of the Gas Research Institute (GRI), conducted a workshop on "Environmental Impacts of Marine Biomass." The Workshop, held in Napa, California, on April 7, 8, and 9, 1981, involved over 40 experts from a wide range of disciplines, including biological, chemical, and physical oceanography; ocean engineering; and several related marine areas.

The workshop had three objectives. First, the participants were asked to identify both positive and negative potential environmental issues of an open ocean biomass system that employs artificial upwelling. Second, each issue was evaluated by an extensive discussion to determine how critical the issue was to the success of the marine biomass program. Finally, the attendees submitted recommendations to GRI for research in the environmental aspects of the kelp farm system.

The format of the workshop provided a flexible structure emphasizing small working groups. The first day began with a presentation of the marine biomass program by the prime contractor, Re-Entry Systems Division of the General Electric Company. This presentation established boundary conditions for the subsequent working group sessions. The participants were divided into two working groups, biological and physical/chemical, that identified and evaluated the potential environmental issues in their areas of expertise. Interaction between the two groups was encouraged by periodic plenary sessions where each chairman and selected participants presented a summary of working group activities. These meetings provided an opportunity for further elaboration and refinement of the specific issues and subsequent research recommendations produced by each study group.

ACCOMPLISHMENTS DURING FY 1981

Marine Biomass Farm Concept

A marine biomass farm is one of the few biologically based systems that has the potential to contribute large quantities of synthetic gaseous fuels to the Nation's future energy supply because biomass grown in the open ocean would not be limited by space, plant nutrients, or water availability as it would be if grown on land. The basic concept of the marine biomass system is to culture and harvest seaweed plants on artificial structures submerged at the same depth as natural kelp beds. Marine kelp require light, carbon dioxide, water, and nutrients from the surface layers of the ocean. However, along the southern California coast, many of the areas capable of supporting marine algae may be nutrient-limited for most of the year because of a lack of upwelling. Therefore, fertilizing operations are clearly necessary to produce high yields of kelp on ocean farms. The selected fertilization process pumps nutrient-rich waters from depths of several hundred to a thousand feet.

Past and present work on this program has had the primary objective of determining the economic and technical feasibility of a system for producing methane from California giant kelp, Macrocystis pyrifera, grown on man-made structures in the open ocean. Macrocystis was selected as the biomass source because of its high growth rate; its size, structure, and growth patterns, which enable it to be mechanically harvested; and its year-round growth cycle.

A set of basic parameters for a hypothetical 1000-square-mile commercial-size farm was presented to the workshop attendees (Table 1). A farm of this size, which could theoretically contribute about 0.3 quads of substitute natural gas (SNG) to the Nation's current natural gas supply of 22 quads, could represent a commercial-scale operation. The specific configuration and other dimensions and properties of the farm should be viewed only as hypothetical values of the baseline system used by the participants in their environmental examination. Figure 1 depicts the elements of the hypothetical system. The actual dimensions and

Table 1. Basic parameters of a commercial kelp farm.

Site location	California coastal waters (about 20 miles offshore)
Biomass source	Macrocystis pyrifera
Biomass requirement	279 million kelp plants
Plant survival	20% plant loss per year due to environment and harvesting
Yield potential	50 DAF tons/acre-year (Range: 25-75 DAF tons/acre-year)
Nutrient requirement	3 microgram atoms Nitrogen/liter
Station-keeping method	Bottom moored
Upwelling system	Direct displacement wave pump
Upwelling requirement	2100 gallons/minute/acre
Upwelling depth	300-1500 feet
Construction material required	6690 kilotons concrete 760 kilotons steel 3970 kilotons synthetics

*This work was supported by Gas Research Institute through the U.S. Department of Energy under Contract No. DE-AC03-76SF00098.

†Condensed from R. Ritschard, V. Berg, and S. Killeen, "Proceedings of a Workshop on Environmental Impacts of Marine Biomass," Gas Research Institute Report (GRI 80/0076), September 1981.

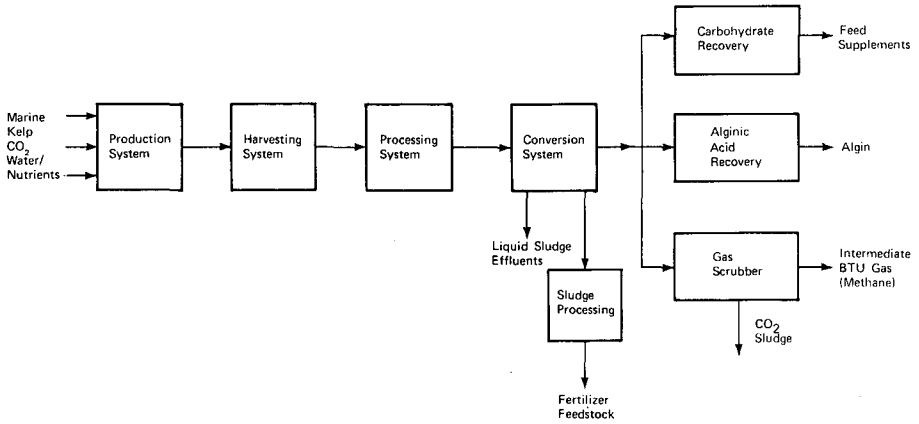

Figure 1. Complete marine biomass system. (XBL 781-13495)

parameters are dependent upon cost studies, yield analyses, and other technical research currently underway or planned.

The standing crop of the kelp farm discussed at the workshop would be harvested by special ships several times a year. These vessels would be patterned after the Kelco Company design used for commercial harvesting along the California coast for many years. Although some pre-processing, e.g., removal of water and grinding, could be accomplished on the harvesting ships prior to transporting the kelp to onshore processing plants, this pre-processing step was not included in the system used as a prototype. The only harvesting and transportation information available to the attendees was an estimate that a commercial size farm (1000 square miles) would require as many as fifty 10,000-dead-weight-ton ships making three roundtrips per day to the onshore dock facility and pipeline system.

The SNG processing and conversion plant was hypothetically sited one mile inland from the dock facility. It was assumed that the raw wet kelp would be shredded and subsequently transported by pipeline to the process site. The digester itself would require a unit capacity (inside volume) of about one million standard cubic feet, which is about 2.5 times the largest existing digester. The process would also include a carbon dioxide scrubbing unit, which releases pure carbon dioxide, and compressors for delivery of pipeline quality natural gas.

Since there are no full-scale marine farm systems in operation today, the parameters that were used at the workshop represent a compilation of data from bench-scale experiments and conceptual plans and data obtained on a biological test platform placed five miles off the southern California coast. To provide a data base on kelp yield, one of the key parameters affecting the initial capital requirements and unit gas costs, GRI and DOE have designed and constructed nearshore biological test farms. These experimental test facilities are used to conduct kelp yield experiments on adult kelp plants in a controlled fertilization environment.

Important environmental issues were identified and the research recommendations to address these issues were developed at the workshop using the design parameters described here. No attempt was made to predict the actual appearance of a marine biomass farm. Instead, the information was used to provide sample conditions within which a discussion of potential environmental concerns would be conducted.

Major Conclusions

During the three-day extensive discussions participants identified several issues that should be considered by the GRI environmental research program. The major research recommendations from both the biological and physical/chemical group are summarized in Table 2 (Biological) and Table 3 (Physical/Chemical). These issues and recommendations cover a wide spectrum of areas including biological, physical, and chemical oceanography as well as ocean engineering. Several issues critical to the development of the marine biomass concept as a whole emerged from the individual work group discussions. These overall concepts, which seemed to dominate the workshop, may serve as our main conclusions.

First, questions arose regarding kelp productivity in an open ocean system. Immediate efforts should be made to define more precisely the expected yield in offshore farms. This information is required for the projection and evaluation of several other potential impacts and also for determining the feasibility of the ocean farm concept from a biological standpoint. Because supplying the farm with proper nutrients in correct quantities is a major problem for cultivated kelp beds, the dynamics of upwelled water must be understood, especially their relation to nutrient availability and uptake and to kelp growth and stability. Workshop participants were concerned about the amount of upwelled water required to maintain desired productivity.

Second, participants were concerned about the stability and survivability of offshore kelp farms.

Table 2. Biological research recommendations.

Debris	Ranking
Define more precisely the kelp yield expected from offshore farming in order to evaluate potential environmental impacts of the loss and decomposition of kelp from a farm.	High
Assess the particulate organic matter (POM) flux from the kelp (due to kelp wrack, kelp fragments, fermentation residues disposal on the farm, fouling organisms) to the deep water column and sediments to determine impact on oceanic oxygen budgets.	High
Develop scenarios for disposal options or utilization of fermentation residues, including post-treatment processes, animal feed, fertilizer, ocean-farm disposal, and by-product utilization.	High
Assess the consequences of farm failure on the sea-floor and/or coastline.	Medium
Organisms	
Assess potential for entrainment of small organisms (small fish, crustaceans, and plankton) into a kelp farm's upwelling system.	Low
Assess potential of a kelp farm to restrict migratory patterns of larger marine organisms (such as whales and sharks).	Low
Communities	
Determine the relationship, positive or negative, of a large kelp farm to recreational and/or commercial fisheries.	Medium
Obtain a better understanding of the biological communities, both benthic and pelagic, expected to be associated with large offshore farms.	Medium
Biochemical/Biophysical	
Determine possible impacts of chemical treatments on the farm to control pests such as weed species, animal grazers, and fouling organisms.	Medium
Address possible changes, both positive and negative, to planktonic systems and detrital food wells downstream of the plume of upwelled water.	Medium
Investigate displacement of planktonic communities as a result of changes in light, nutrients, temperature, etc.	Medium
Consider ways by which polyculture (i.e., the intentional culture of organisms with kelp) could mitigate or modify issues such as particulate organic matter disposal, non-natural-chemical and waste additions, and organic exudates.	Low

Table 3. Physical/chemical research recommendations.

Oceanographic	Ranking
Develop a model to determine the fate and motion of upwelled water within the farm as a prerequisite to determining design issues such as pumping rates and siting criteria.	High
Analyze data on variable and medium scale currents to enable detailed farm structural design to be carried out.	Medium
Collect and analyze data on mixed layer depth distribution from the southern California Bright waters on a seasonal and locational basis. These upper waters make up the thermocline and this knowledge is crucial in estimating the amount of water to be pumped.	Medium
Determine the effects of a dampened wave field due to a large kelp farm, on local wave climate, shoreline formation and ultimately on inshore habitats. Obtain a better understanding of local climatic effects as a result of large scale upwelling.	Medium
Determine residence time of upwelled water.	Medium
Obtain a better understanding of the deep ocean circulation patterns which provide oxygen and nutrients to the kelp farm.	Low
Obtain a better understanding of local climatic effects as a result of large scale upwelling.	Low
Design	
Determine hydrodynamic loading on the kelp farm installations (kelp plants, mooring system, kelp attachment structure, and deep-water pipe and pumps) as a result of forces generated by ocean currents and large, long-period waves.	Medium
Assess survivability of the farm structure including fatigue, synthetics and flex joints.	Low
Study deepwater pumping in light of the efficiency and survivability of wave-powered pumps and other pumping alternatives.	Low
Investigate various farm configurations as methods to minimize current loads and maximize the utilization of wave energy.	Low
Operational	
Develop and apply practical site selection criteria that consider site features, farm characteristics, and site usage.	High
Examine the characteristics of the waste generated and develop disposal strategies or utilization options.	High
Investigate the environmental impact (air, water, land) of a continuous construction and maintenance period on the kelp farm.	Medium
Study legal issues associated with open ocean farms (international and U.S. policy).	
Determine the biotic and abiotic releases from the kelp farm.	Medium
Determine what other substances (gases, trace metals) may be released in upwelling the deep water.	Medium

Can kelp plants remain attached to a floating structure in the open ocean? If not, can the amount of drifting kelp that reaches the shore be restricted to socially acceptable levels? Kelp fragments and other organic particles are expected to sink from the farm and to affect oceanic oxygen budgets. The potential oxygen depletion in the water column and bottom sediments caused by enhanced sinking flux of organic particles is one of the most serious problems identified. Therefore, a detailed assessment of particulate organic matter flux from the kelp farm to deep water and sediments is needed.

Third, critical physical/chemical issues identified from an engineering and operational perspective included the integrity of the farm structure and its associated upwelling system with regard to ocean currents, waves, climate, and other hydrodynamic properties. To determine the feasibility of the offshore system, it was suggested that a critical test experiment of the farm structure, its associated wave-driven pumps, and mooring system be conducted.

Fourth, the residuals from the anaerobic digestion process seems to pose the greatest threat to the onshore environment. Several options were suggested for disposing of or utilizing these residues, including use as cattle feed and fertilizer or disposal at the farm site. Research into mitigation and monitoring of process residues could contribute to the ultimate success of the marine biomass program.

Finally, the overall theme of the suggested recommendations is that any energy system in the

open ocean must consider the existing natural biological, chemical, and physical oceanographic features. Therefore, a thorough review of engineering designs and process characteristics by experts from a wide range of marine sciences should be conducted early in the development process.

PLANNED ACTIVITIES FOR 1982

This project was completed in FY 1981 and will not continue in FY 1982.

Effectiveness and Implications of Technical Innovations to Reduce Water Use*

J. A. Sathaye, R. L. Ritschard, M. M. El-Gassier, and S. C. Rainey

Availability of adequate water to support municipal, industrial, agricultural, mineral, and steam generation activities has been a major concern, not only in the arid western United States, but also in the East. The 1981 drought in the eastern United States emphasizes this problem. Methods which may be used to mitigate anticipated water shortages include implementation of innovative water-saving techniques, further development of water supplies, and better management of ground-surface water systems. This study has focused on innovative techniques and their contribution to reducing water shortages.

There are three basic ways to reduce water usage: reuse, recycling, and conservation through process innovations. In this report, we provide national and regional perspectives of the problem of reducing water use. This is not a "national assessment" that would provide quantitative estimates of the conservation potential in each region and the impact on communities; rather, it is a perspective of the potential for reducing water usage.

The study concentrates on three areas of concern: agriculture, industry, and domestic consumption. For each area, we examine the application of water-saving innovations in a specific geographical region. We examine agricultural water use in the Northern Great Plains Region, industrial use in the Great Lakes Region, and domestic use in the Lower Colorado Region, as well as potential for savings in each area.

ACCOMPLISHMENTS DURING FY 1981

Background

Five major activities account for more than 99 percent of water use: agriculture, steam electricity generation, manufacturing (or industrial usage), municipal needs (both commercial and domestic), and mineral development. Agriculture uses by far the greatest amount of water, 47 percent of total water withdrawals (Table 1). The percentage used by agriculture is considerably larger in the West. For example, 85 percent of the withdrawals in California are used for agricultural irrigation. Nationally, steam electricity generation uses 26 percent and manufacturing, 15 percent of water withdrawals. Over 50 percent of water used for such generation is required by the Great Lakes and Ohio regions. Although steam generation accounts for 26 percent of withdrawals, its consumption is only one percent of the national total. Agricultural irrigation consumes the greatest amount, 81 percent of the total consumption; domestic, commercial, and manufacturing uses account for 13 percent.

Table 1. Fresh water withdrawal and consumption, 1975.

Type user	Total withdrawals bgd	%	Total consumption bgd	%	Consumption as percentage of withdrawals
Agriculture					
Irrigation	158.7	47	86.4	81	54
Livestock	1.9	1	1.9	2	100
Steam electric generation	88.9	26	1.4	1	2
Manufacturing	51.2	15	6.1	6	12
Domestic and commercial	28.8	9	7.4	7	26
Minerals	7.1	2	2.2	2	31
Other	1.9	1	1.2	1	63
Totals, Regions 1-21	338.5	100	106.6	100	32

Source: U.S. Water Resources Council, Second National Water Assessment, The Nation's Resources, 1975-2000, Vol. 2, December 1978, p. 57.

Agriculture

Water use in agriculture is a function of the irrigation system used, soil type, crop type, climate, and topography. A nationwide review of irrigation techniques suggests that the efficiencies of most irrigation systems can be measurably improved. This is especially true in the 17 western states where nearly 90 percent of all agricultural irrigation is located. It has been estimated that from 4 to 10 percent increases in off-farm[1] efficiencies and from 6 to 13 percent increases in on-farm[2] efficiencies are possible in the West, depending on the number and type of conservation measures adopted.

*This work was supported by the Assistant Secretary for Environment, Office of Environmental Assessments, Regional Impacts Division of the U.S. Department of Energy under Contract No. DE-AC03-76SF00098.

Optimum improvement of irrigation efficiency can be achieved by using

1. Physical systems that can deliver water with minimum losses and can apply water uniformly when needed and without waste,

2. Methods of determining the timing and optimum amounts of irrigation water to be applied, and

3. Technical and financial assistance programs.

Northern Great Plains Region. The Northern Great Plains Region was selected for more detailed analysis because it accounts for almost one-fourth of the total value of all irrigated crops in the United States and because irrigation is responsible for about 95 percent of the region's total water consumption. In addition, the extraction, processing, and use of energy resources in the Northern Great Plains Region will probably increase competition for water by agriculture and industry.

Our estimates indicate that, if various water conservation measures are implemented in the Northern Great Plains Region, off-farm efficiency could be increased by 14 percent and on-farm efficiency by 16 percent. Although the maximum potential reduction in water diverted for irrigation use could be as high as 27 percent, 15 percent is a more realistic estimate. Within this region, on-farm conservation measures have the greatest potential for water savings at least cost. Specific conservation measures include

1. Reducing seepage from ditch and conveyance systems;

2. Reducing on-farm irrigation return flows by use of tailwater recovery systems and land leveling; and

3. Reducing incidental water losses such as evaporation from canals and ditches, phreatophyte growth, and that portion of groundwater recharge that is not economically recoverable.

Controlling seepage from off-farm ditch and conveyance systems can also contribute significantly to water savings, but only at considerable expense.

Benefits from efficient water use and management include increased water supply for present users, especially during water-short years; increased water availability to meet increasing needs; improved water quality; and improved instream flows. Implementation of an irrigation water conservation program also can have major impacts upon the quality, quantity, and timing of the water supply available at diversion points within a hydrologic basin. Although water conservation and reuse will not increase the natural water supply of a hydrologic basin, these practices will generally provide increased beneficial use of the total water supply.

An effective national, regional, or local water conservation policy may include programs to subsidize capital-intensive conservations as well as incentives to reduce water consumption. This may also encourage irrigation districts and other water management agencies to institute water-pricing policies. Optimum methods for conserving water and the incentives to bring these methods into use can best be determined on a district-by-district basis. Determination of optimum conservation methods may also result in discovery of opportunities for districts, other political bodies, or individuals to exchange water or to establish water banking or other water reallocation schemes.

Industry

There are three methods used for industrial freshwater conservation: recycling, reuse, and process innovations. In recycling, water is circulated through a system as many times as process quality requirements and treatment costs permit. Recycling minimizes the water withdrawal rate of a plant. However, evaporation losses from cooling devices and from holding ponds will increase, resulting in a lower rate of water conservation.

In water reuse, a firm uses treated or untreated effluents released by another user. Compared to recycling, reuse has the advantage of adding to the diversity of water use within a community.

Process innovations are technological changes capable of reducing a manufacturer's dependence on water. Both withdrawal and consumption rates can be lowered by these process changes. The most promising innovations involve cooling systems. Development of dry cooling towers and hybrid cooling systems (wet and dry) will result in considerable water savings. However, the extent to which innovative technologies are used will be determined by time and location-dependent costs.

Recycling. At the present time, recycling is the dominant form of industrial freshwater conservation and will continue to be so in the immediate future; its use will increase over the next 25 years. The nation's total industrial withdrawals could diminish by about 62 percent of their 1975 level over the next 25 years. On the other hand, consumption will increase at an annual rate of 3.5 percent, and discharges will diminish. The anticipated rapid expansion of recycling use is not caused by water shortages as much as by industry's attempt to minimize the escalating costs of treating effluents to meet federal and state pollution control regulatory requirements. In areas where water shortages constrain water consumption, recycling may have a negative impact and even may be opposed.

Reuse. In the near future, reuse of industrial water will grow at a slower rate than recycling because the obstacles confronting reuse are greater than those facing recycling. An industrial firm will attempt to exhaust recycling opportunities within its own facilities before contracting for the effluents of another water user. However, water shortages provide more motivation for reuse than does pollution control. Consequently, as freshwater becomes more scarce, reuse will expand at an accelerated rate.

Water reuse will be hindered by downstream water rights. Discharges that may appear available for reuse in some instances are a source of supply for a downstream user, and any upstream reuse scheme could be considered a diversion of flow subject to court litigations. Most current water reuse projects are located in coastal states, along the oceans and the Great Lakes, at the very downstream end of use. In appropriative doctrine states, downstream senior water rights may be obstacles to upstream industrial use based on water reuse. In riparian doctrine states, where water availability is relatively less constrained, there is very little legal experience with water reuse.

Industrial water reuse will continue to be limited to using urban waste water. The dominant application will be for industrial cooling. Firms that have their own water supplies will not resort to reuse unless adequate economic incentives are created.

Considering only municipal effluents as the source of water, the potential for reuse is large, nationwide about 20,580 million gallons per day by the year 2000 compared to the present level of about 214 million gallons per day. Even if reuse is used only for cooling, the potential is still considerable: 14,526 million gallons per day by the year 2000.

Great Lakes Region. Although industrial withdrawals are projected to decrease in the Great Lakes Region, consumption of fresh water is expected to increase. Part of this growth in consumption will be caused by industrial expansion. The anticipated decline in withdrawals can be distributed to projected increases in the use of recycling.

Availability of adequate supplies of treated municipal effluents will limit industrial water reuse in many parts of this region. Self-supplied firms will be reluctant to change to reuse of renovated waste-water in place of fresh water supplies they already own. Because many of the community innovations will be made at the downstream end of water use, the resultant water savings are real because there are no downstream users in this region who might be deprived of the treated return flow.

Domestic

In the domestic sector, water is used both indoors and outdoors. Indoor water uses, such as for showers and dishwashing, is relatively constant throughout all regions of the country. However, outdoor water uses, such as for irrigation of lawns and landscaping, varies depending on the climatic region and on annual rainfall patterns.

From a national perspective, there is substantial potential, from 17 to 29 percent, for reducing domestic water use. Indoor water use is inelastic to price changes at current prices and can best be reduced by using conservation devices. Plumbing codes for new building construction have also been effective in reducing water use.

Exterior water use by the domestic sector can be influenced by pricing mechanisms. For example, converting user costs from flat rates to metering can reduce peak demands and average water usage.

Reuse of municipal waste water for irrigation is widespread and is the largest single use of these effluents. Power plant cooling and industrial cooling are two additional major uses for municipal waste water. Waste water reuse for domestic activities, however, has limited potential because of generally stricter water quality criteria. It is estimated that over 90 percent of municipal waste water is available for reuse.

Lower Colorado Region. In the Lower Colorado Region, domestic water withdrawal can be reduced from 25 to 36.5 percent. Housing stock, climate, conservation devices, pricing measures, and the level of implementation will determine how much conservation can be accomplished. Although it is not difficult to estimate the savings that can be achieved, the implementation plan and the subsequent availability of water to other users are questions which need to be examined far more carefully.

The example of Tucson suggests that conservation measures, especially pricing mechanisms, need to be analyzed carefully before implementation. New water sources for the Tucson area are acquired by buying prime agricultural land. Water-use conflicts between mining companies, urban residents, and agriculture are common. Energy development will add to this problem.

Although water reuse in the Tucson and Phoenix areas will solve part of the groundwater depletion problem, a long term strategy is needed to resolve both water use conflicts and groundwater depletion. The Arizona Groundwater Management Act, which emphasizes water conservation as the first alternative towards balancing supply and demand, is a major step toward eliminating groundwater depletion.

Other regions of the country can also benefit by implementing water conservation measures in the domestic sector. Although the amount of water saved may be small compared to agricultural water usage, the savings in distribution networks and treatment plants can be significant. It is possible that small local areas could implement a well-thought-out conservation plan, including pricing measures, as has been done by the Washington Suburban Sanitary Commission.

Implementing a statewide act, as has been done in Arizona, is much more difficult because this requires united and concerted political and legislative action both to initiate and carry out such a program. It is too soon to determine whether or not Arizona will be able to enforce the Act effectively. However, the Act does recognize, perhaps for the first time, that water is a finite resource that should be managed accordingly.

PLANNED ACTIVITIES IN FY 1982

This project was concluded during FY 1981 and will not be continued in FY 1982.

FOOTNOTES

1. Off-farm refers to systems conveying or storing water from its source or the point of diversion to the boundary of a farm.

2. On-farm refers to both conveyance and application and storage systems or methods used within farm boundaries.

Groundwater Impacts of Enhanced Oil Recovery*

J. A. Sathaye

Enhanced (tertiary) oil recovery (EOR) is a method which stimulates depleted oil reservoirs to yield additional crude oil. The method requires pumping steam, injecting chemicals or gases, or fire flooding the reservoirs to increase oil flow to the surface. Large quantities of brine are also produced with the oil. Federal and state regulations require safe disposal of brine by reinjecting it into the ground. During the reinjection process, brines can leak into surrounding freshwater aquifers. This study examined the potential for groundwater contamination from such leaks. Oil and chemicals which can contaminate groundwater aquifers were included in the analysis. The study also examined the water requirements for EOR techniques and evaluated the availability of water supplies.

ACCOMPLISHMENTS DURING FY 1981

This study was conducted over a period of two years. The findings of a workshop on environmental impacts of EOR techniques, reported in the 1981 Annual Report,[1] were published this year.[2] The groundwater impacts assessment was conducted mostly during FY 1981. The project is now complete.

Groundwater Availability

Numerous reports and studies have demonstrated that groundwater contamination is a widespread problem affecting every region of the country. Contamination may result from petroleum production, injection wells, surface impoundments, agriculture, landfills, leaks and spills, septic tanks, and mining activities. An EPA report[3] to Congress identified disposal sites as the most serious source of nationwide contamination. However, in many regions, petroleum activities are the primary cause of contamination. Often, industrial sources are located closer to population centers than petroleum-related sources and are therefore easier to detect.

*This work was supported by the Assistant Secretary for Environment, Office of Environmental Assessments, Technology Assessments Division of the U.S. Department of Energy under Contract No. DE-AC03-76SF00098.

The groundwater problems caused by petroleum development are not well documented. The extent of contamination has been quantified but is not generally available. Several different activities have caused contamination problems in the South Central and Southwest regions. In Texas alone, 23,000 cases of ground and surface water contamination have been reported. One of the major causes of contamination, the use of pits for brine disposal, is now banned in producing states. An EPA report[4] estimates that oil and gas and mining impoundments may have contaminated 0.1 percent of the Nation's useable aquifer area.

Brine is now disposed of by underground injection into deep saline formations and occasionally into lined pits. Underground injection will be regulated by the EPA's Underground Injection Control (UIC) Program. The Safe Drinking Water Act (1974) established the UIC program to prevent underground injection of wastes that endanger drinking water sources. States may assume primary enforcement responsibility for operating effective programs. We report on one such state, California, and its contamination data for brine injection wells later in this paper. An estimated 500,000 injection wells are in operation nationwide; 140,000 of these are Class II wells for disposal of fluids brought to the surface in connection with oil and gas production or to increase oil and gas recovery.

There are two major underground sources of groundwater contamination in oil fields: oil from oil wells and brine from injection or disposal wells. In tertiary recovery, the chemicals used for oil recovery are an additional hazard. Surface spills of these contaminants and leakages from storage tanks and ponds and from pipelines are the other major sources of contamination.

The main difference between oil and brine contamination is that brines are miscible with water, whereas oil is not. Brines will therefore mix with water and be carried away towards the user far more easily than will oil. Brine contamination and the release of inorganic and organic compounds and trace metals can be far more serious problems than oil contamination. In tertiary recovery, brines are injected under pressures ranging from 500-1500 psi. Injection pressures are at or slightly above

the natural formation pressure. Excessively high pressures are not used indiscriminately because a high pressure can cause fractures and fissures and can also cause brines to overwhelm semi-impermeable layers leading to freshwater aquifers.

Flow of brine into aquifers basically depends on the same variables that control oil flow. For surface spills, the adsorption coefficient, soil porosity, rate of brine leakage, and the distance to the aquifer play important roles in determining how fast brines will reach the aquifer. The extent to which brines will pollute an aquifer depends on the brine concentration and the initial aquifer concentration. In the case of direct releases from wells to aquifers, the pollutant concentration in the aquifers is a function of the distance travelled, the seepage velocity, aquifer porosity, the dispersion constants, and the pollutant decay rate.

Water Standards and Brine Characteristics

Elements in oil field waters commonly are present in the following concentration ranges.

Chemical Element	Concentration
Na, Cl	>1000 ppm
Ca, SO_4	Up to 1000 ppm
K, Sr	>100 ppm
Al, B, Ba, Fe, Li	1-100 ppm
Cr, Cu, Mn, Ni, Sn, Ti, Zr	ppb (most brines)
Be, Co, Ga, Ge, Pb, V, W, Zn	ppb (some brines)

No significant relationship exists between brines and the minerals in aquifer rocks.

The drinking water standards proposed by EPA specify the acceptable concentration for minerals in drinking water. These include barium and chloride that are found in oil-field brines. Total dissolved solids (TDS) are also present in large concentrations.

Brine concentrations of chloride exceed the drinking water standards by several orders of magnitude. Barium concentrations can also exceed concentrations specified in the standards by a factor of 10 or more. Chlorides and TDS are the two major pollutants from brine disposal that would be a cause for concern.

Incidents of Contamination

Recent data gathered by the California Division of Oil and Gas (CDOG)[5] (Fig. 1) suggest that incidents of groundwater contamination from oil

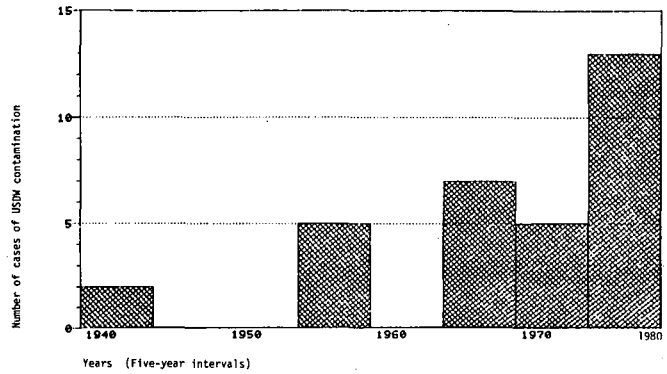

Figure 1. Underground source drinking water contamination (USDW) by date of occurrence.
(XBL 8111-1639)

drilling activity are increasing. In the last 40 years, CDOG records indicate that 32 cases of underground source drinking water (USDW) contamination have occurred as a result of Class II well operations. Discovery of these cases resulted mostly from CDOG surveillance work and from citizen and well operator complaints. In all but one case, the elapsed time from discovery to correction was less than one year.

Conversations with CDOG staff reveal several reasons why the increase in contamination cases may have occurred. Improved monitoring techniques, the age of the well, and the proximity of the water user to oil fields may explain the increase. These reasons have a direct bearing on EOR operations.

Oil field operators prefer to use old oil wells for reinjection of disposal fluids. The old well is usually cemented off below the brine injection zone, the casing is perforated at the injection formation, and the well is set up for brine reinjection. Although these old wells are inspected to ensure that the seal is tight and acceptable, they are more apt to have casings corroded by oil operations and are more likely to fail under corrosive brines injected at high pressures.

The second reason is already evident in several counties in Texas where multipurpose use of groundwater by municipal, agricultural, and oil producers is being litigated. Water users are closer to oil field operations and are likely to be affected by contamination before the pollutants can be diluted. However, the proximity of users helps institute corrective measures before the pollutant spreads.

Water Availability and Requirements

Water requirements vary by EOR techniques. Table 1 shows the water requirements for each technique. The quality of water required for oil recovery can vary among the techniques and even within a technique for specific processes. It should be noted that these water requirements are total volumes injected, not necessarily consumptive use.

Water used for injection in oil reservoirs must be compatible with the chemistry of the formation water, with the chemistry of injected fluids,

Table 1. Water requirements in bbl of water per bbl of oil produced.

Technique	Water requirement
Steam soak Steam drive	7
Improved waterflood	100
CO_2, N_2, HC, miscible	4-16 (generally lower values)
Caustic	10
Micellar polymer	10
In situ	<1-5.5

and with the formation itself. Waters are usually considered compatible if they can be mixed without producing chemical reactions among the different fluids. Precipitation of insoluble compounds is undesirable and may reduce the permeability in the formation. Some fluids may react with the formation clays, causing swelling and a reduction of permeability and production from a reservoir.

There are three main sources of water: (1) produced water, (2) surface water, and (3) groundwater. Water is produced with oil, generally in large quantities. Not uncommonly, 90 percent or more of the fluid in producing oil fields is water.

Large EOR production will occur in regions that currently face severe groundwater problems. However, this will not necessarily constrain the development of fields for EOR production. It will certainly create difficulties in acquiring water, it may delay projects, or it may force developers to use more produced water. Each development will require a unique set of decisions, partly institutional and partly economic. If water can be purchased at a relatively low price, the developer will probably do so as long as it is cheaper than treating produced water.

Kern County, California, is an interesting example with all the attendant problems. Groundwater overdraft is very large in the basin; all the water is already allocated. A new oil producer has the following choices, not necessarily in this order of priority: (1) use produced water directly, (2) use treated produced water, (3) contact the local water agency for additional water, (4) tap into groundwater reservoirs, (5) buy land in anticipation of expansion, or (6) buy water from other users. If freshwater is not readily available--and this may be the case in Kern County--producers will resort to the last two options. Many producers have already resorted to option (5). Both options (5) and (6) require additional initial capital to start a project. Small producers will be squeezed out if they cannot raise the required capital. Large producers, or those who already have access to water, will be less affected. In regions where water is in short supply, small EOR operators may be adversely affected and even forced out of the market.

In many situations, however, the rights to groundwater may not be clear. Multipurpose use of groundwater from the same reservoir for agriculture, industry, and oil production can create legal problems when the freshwater supply is shrinking. In Gaines County, Texas, for example, the rights to groundwater are being challenged legally. The outcome from such litigation may help clarify the rights to groundwater nationally. Similar problems may be expected in other areas as EOR production expands and conflicts with rights of other users to the same groundwater.

PLANNED ACTIVITIES IN FY 1982

This work was concluded in FY 1981 and will not continue in FY 1982.

REFERENCES

1. Energy and Environment Division (1981), Annual Report 1980, Lawrence Berkeley Laboratory Report LBL-11990, pp. 1-21.

2. Riedel, F., et al. (1981), "EOR Workshop Focuses on Environmental, Health, Safety Issues," Oil and Gas Journal 79, 40, pp. 157-164.

3. U.S. Environmental Protection Agency (Jan. 1977), The Report to Congress, Waste Disposal Practices and Their Effects on Groundwater, Section 9, Washington, D.C.

4. U.S. Environmental Protection Agency (June 1980), Planned Workshop to Develop Recommendations for a Groundwater Protection Strategy, Appendices, Washington, D.C.

5. Reid, R. (Feb. 1981), California Division of Oil and Gas, Sacramento, personal communication.

Growth and Energy Development in the Rural West*

R. G. Sextro and J. M. Bernier

The western inland states (Arizona, Colorado, Idaho, Montana, New Mexico, Nevada, Utah, and Wyoming) have experienced rapid population growth over the past decade. Energy and mineral resource development and an expanding economy have attracted increasing numbers of people to the region. Many of the more dramatic changes have occurred in the rural West where the traditional agricultural base has given way to growing towns and expanding resource development activities. Because the West has large, relatively untapped reserves of coal, oil shale, and natural gas, the development pressures may continue as the nation looks to increased domestic production of energy supplies.

This paper reviews the changes in rural employment and population growth over the past decade. We then discuss possible future energy activities and their implications for the rural areas of the western states.

ACCOMPLISHMENTS DURING FY 1981

General Population Trends

In the last ten years, overall population growth in the region has averaged 2.8 percent per year, compared with a 1 percent annual growth nationwide during the same period. This change actually accelerated during the course of the decade, from 2.7 percent per year from 1970 to 1975 to 3.7 percent per year from 1978 to 1980. State-by-state population trends[1] are shown in Figure 1.

The eight-state region grew 35 percent between 1970 and 1980. Approximately two-thirds of that growth was in urban areas, while one-third of the growth occurred in the rural areas. Although the metropolitan areas have had greater population growth in absolute numbers, the relative change in rural population in the last decade, 30 percent, is about the same as the change in metropolitan areas, 38 percent. By comparison, the overall population increase from 1960 to 1970 was 20 percent, with essentially all of this population change occurring in the metropolitan areas. The surge in rural population is consistent with the rapid acceleration in fossil fuel production during the 1970's.

Rural Population and Employment Changes

We have classified the rural areas into three groups corresponding to areas where the principal

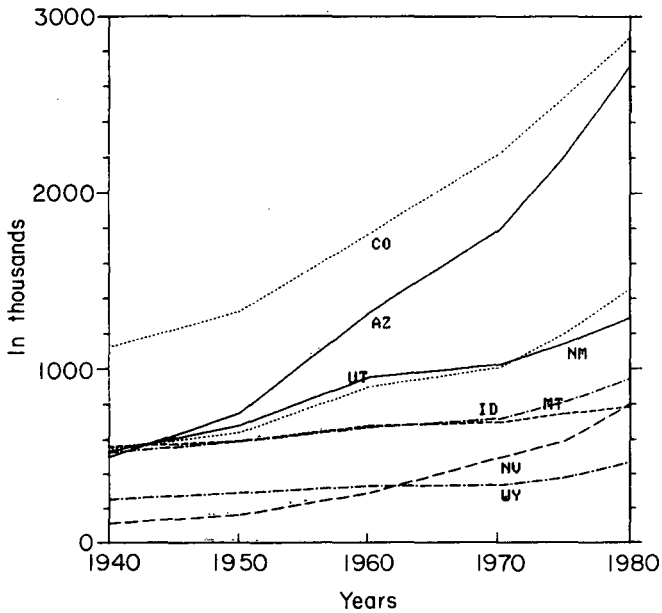

Figure 1. Population trends for the western states. (XBL 824-461)

activities are energy extraction, recreation, and/or agriculture. For some parts of the West, a growing retirement population also appears to be an important growth factor.[2] Much of the rural population growth in Arizona, for example, can be attributed to the development of retirement communities. This analysis focuses on the first three categories, with a detailed county-by-county analysis of the energy resource areas.

Energy resources. Rich in energy resources, the region currently produces 25 percent of the nation's coal, 10 percent of domestically produced oil, and 9 percent of natural gas. The fossil fuel production trends are shown in Table 1. As can be seen, coal production has shown the most dramatic change, growing from less than 20 million tons per year in the early 1960's to just over 160 million tons by 1980.

This rapid expansion of energy extraction activities in parts of the West is reflected in the population data shown in Table 2. In many of the energy resource counties, population declined or grew only slightly between 1960 and 1970. Between 1970 and 1980, as energy development occurred, the population increased rapidly, averaging over 50 percent in ten years. We have used the mining sector, which includes coal and uranium mining as well as oil and gas extraction, as our primary indicator for energy development. Significant employment in non-energy mineral mining occurs in only a few of the energy development counties, and we have eliminated these effects in the analysis of the changes in mining sector employment. As the data presented

*This work was supported by the Assistant Secretary for Environment, Office of Environmental Assessments, Regional Impacts Division of the U.S. Department of Energy under Contract No. DE-AC03-76SF00098.

Table 1. Fossil fuel production in the western states.

Annual Production	States: Arizona	Colorado	Montana	New Mexico	Utah	Wyoming	Total	Percent of total U.S. production
	Coal (millions of tons)							
1970	0.13	6.03	3.45	7.36	4.73	7.22	28.92	6
1975	6.97	8.22	22.05	8.79	6.96	23.80	76.81	13
1978	9.05	13.81	26.60	12.06	9.14	58.33	114.63	22
1980	11.80	19.50	32.92	16.50	16.23	88.92	161.82	24
Change, 1970-80 (%)	8800	225	850	125	240	1130	460	-
	Oil (millions of barrels)							
1970	-	25	38	128	23	160	374	11
1975	-	38	33	95	42	136	344	11
1978	-	37	30	83	30	137	317	10
Change, 1970-78 (%)	-	48	-21	-35	30	-14	-15	-
	Gas (billions of cubic feet)							
1970	-	106	-	1139	-	339	1548	7
1975	-	172	-	1217	-	316	1706	8
1978	-	184	-	1192	-	335	1711	9
Change, 1970-78 (%)	-	74	-	5	-	-1	8	-

Table 2. Changes in population and employment in energy resource counties.

State and County	Population in 1000s: 1960	1970	1980	% Change 1970-80	Employment: 1979 (1000s)	% Change 1970-79	% total employment change: Mining	Manufacturing	Retail	Services	Energy Resources
ARIZONA											
Navajo	38.0	47.8	67.7	42	9.3	91	22	20	32	9	coal
COLORADO											
Delta	15.6	15.3	21.2	38	3.0	68	17	-7	28	25	coal
Garfield	12.0	14.8	22.5	52	6.2	123	11	5	24	25	coal
Gunnison	5.4	7.6	10.7	41	3.8	196	10	6	31	28	coal, uranium
Mesa	50.7	54.4	81.5	50	25.9	123	10	11	22	23	coal, oil & gas, uranium
Moffat	7.1	6.3	13.1	107	3.2	133	26	7	38	2	coal, oil & gas
Rio Blanco	5.2	4.8	6.3	29	2.1	128	60	-1	18	1	coal, oil & gas
Routt	5.9	6.6	13.4	103	5.2	307	13	0	32	7	coal
MONTANA											
Big Horn	10.0	10.1	11.1	10	2.4	74	75	-32	0	44	coal
Rosebud	6.2	6.0	9.9	64	2.2	199	44	0	13	36	coal
NEW MEXICO											
McKinley	37.2	43.2	55.0	27	11.9	86	32	-3	33	27	coal, oil & gas, uranium
San Juan	53.3	52.5	80.8	54	20.7	103	4	-5	24	22	coal, oil & gas
Valencia	39.1	40.5	60.8	54	10.8	115	45	6	23	5	oil & gas
UTAH											
Carbon	21.1	15.6	22.2	42	5.3	10	43	5	21	12	coal
Duchesne	7.2	7.3	12.6	72	2.4	243	25	5	19	12	oil & gas
Emery	5.5	5.1	11.5	123	2.5	233	76	0	17	2	coal
Summit	5.7	5.9	10.2	74	3.2	262	8	3	40	28	oil & gas
Uintah	11.6	12.7	20.5	62	4.8	91	15	6	22	16	oil & gas
WYOMING											
Campbell	5.9	13.0	24.4	88	8.9	158	33	0	18	14	coal, oil & gas
Carbon	14.9	13.4	21.9	64	6.9	125	53	-7	14	21	coal, oil & gas, uranium
Converse	6.4	5.9	14.1	137	4.2	285	46	0	17	10	coal, oil & gas, uranium
Fremont	26.2	28.4	40.3	42	10.8	88	25	0	24	20	oil & gas, uranium
Lincoln	9.0	8.6	12.2	41	2.7	77	43	17	27	11	coal
Natrona	49.6	51.3	71.9	40	29.5	117	10	5	20	21	oil & gas, uranium
Platte	7.2	6.5	12.0	85	2.2	111	0	7	23	28	
Sheridan	19.0	17.8	25.0	40	6.8	97	7	1	20	20	coal
Sweetwater	17.9	18.4	41.7	127	12.4	170	38	2	23	14	coal, oil & gas, uranium
TOTAL	492.9	519.8	794.5	53	209.3	121	23	3	32	27	

in Table 2 indicate, with one exception, energy development is the only basic industry of any significance in these counties. Only Lincoln County, Wyoming, shows any sizeable growth in manufacturing sector employment. Thus, increased energy employment as a basic industry has been a significant factor in population growth in these areas. Secondary or induced employment, such as retail trade and services, also generally shows growth, reflecting increased demand in these sectors driven by growth in the primary employment sector.

Recreation. Outdoor recreation is also an important western resource and has contributed to population and employment growth in several rural areas. Population growth in these areas appears to be a function of the presence of outdoor recreation opportunities, such as skiing, and national parks or monuments, etc. We have examined a number of selected counties for changes in employment in service and retail sector establishments related to recreation such as hotels and eating and drinking establishments, and for the presence of significant employment in other recreation-related establishments. These data for selected recreational counties indicate that the service and retail sectors have changed significantly, while other major industrial categories such as mining or manufacturing are small and have changed very little.

Some counties have had both resource and recreation employment growth. Routt County, Colorado, is one such example. Coal mining and a mine-mouth electrical generating station are located on one side of the county, and the Steamboat Springs ski area is located on the opposite side.

Agriculture. Historically, agriculture has been a significant part of the western state economies. Almost every county has some agricultural activity. However, except for growth in farm employment in a few areas following World War II, farm employment has declined steadily since 1940 (Fig. 2). This overall trend is consistent throughout the western states, in urban and rural

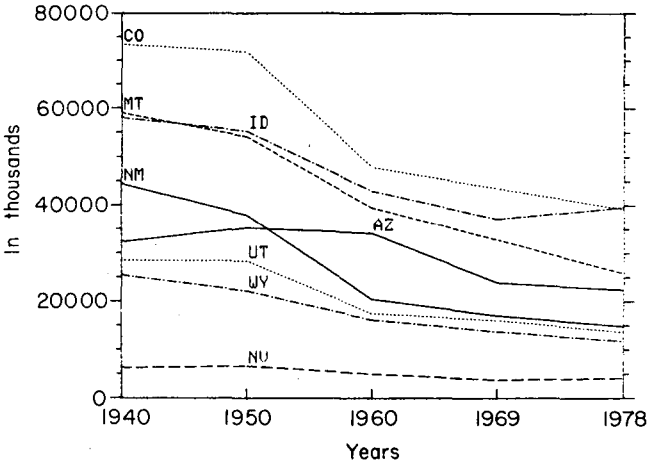

Figure 2. Agricultural employment trends for the western states. (XBL 824-464)

In part, these declining trends in farm employment reflect the migration from rural to urban areas as increased farm mechanization and larger farms displace employment and ownership. Around urban areas, the amount of land devoted to farming has also substantially decreased during this period because of expanding urban populations. There has also been a decline in farm employment throughout the rural areas, including counties where agriculture is a major economic activity as well as in those counties where energy development has occurred. In the case of the urban and energy development areas, the decline in agricultural jobs has been offset by expanding non-farm employment, and population has grown commensurately. On the other hand, areas that are predominately agricultural generally have experienced declining or, at best, stable population as farm employment decreased. In some cases, expanded retail and service sector jobs tempered the loss of farm employment.

Looking to the Future

Energy has been one of the key factors in changing the rural West, and it will have an important role in shaping the future. The projections of productive capacity for western coal (excluding production in North Dakota) for 1990 range between 420 million tons/year and about 650 million tons/year; production will approach one billion tons by the turn of the century.[3-5] While present production is 160 million tons/year, productive capacity is closer to 200 million tons. Thus, according to these estimates, coal production in the western states could double or triple over the present levels. Similarly, oil shale and deep natural gas, with substantial resource bases, have generated considerable interest in the western states.

The rural, resource-rich areas will continue to grow in population as additional energy development occurs. In some cases, new development will occur as existing resource production declines, thus substituting one employment sector with another. This appears to have happened, for example, in the uranium-producing regions of western Colorado, Wyoming, and New Mexico, where the uranium boom of the 1960's was replaced in the 1970's by coal mining and, in some cases, power-plant construction and operation. At the same time, the current trends in agricultural employment are expected to continue as the economy of the western states shifts to other sectors. This will mean that the existing differences in employment and population growth among various parts of the rural West will continue, and, as some counties expand economically, others will face economic stagnation.

PLANNED ACTIVITIES IN FY 1982

This work was completed in FY 1981 and will not continue in FY 1982.

REFERENCES

1. Population data were taken from: U.S. Bureau of the Census (1979), Statistical Abstract of the United States: 1979, Washington, D.C. and from the preliminary 1980 Census reports for each state: U.S. Bureau of the Census (1980 and 1981), 1980 Census of Population and Housing-Preliminary Reports, Series PHC80-P, Department of Commerce, Washington, D.C.

2. Freiwald, J.G., et al. (May 1980), Rural Migration in the Western States, Los Alamos National Laboratory Report LA-8284-MS.

3. ABT-West (Oct. 1980), Energy Activity in the West: Data Book, Denver, Colo.

4. Office of Coal Supply Development (1981), Western Coal Survey, U.S. Department of Energy, Washington, D.C.

5. Energy Information Administration (April 1981), Annual Report to Congress--1980, U.S. Department of Energy, DOE/EIA-0173(80)/3, Washington, D.C.

California Energy Systems Assessment Models*

J. A. Sathaye, H. Ruderman, P. T. Chan, and H. Schmidt

Early in 1980, the Assessments Division of the California Energy Commission (CEC) asked the LBL Energy Analysis Program to construct a set of models that could project the economic and environmental consequences of energy development in California. Because the California Air Resources Board (ARB) was interested in similar models, it became a joint sponsor. The models will be used by the CEC and ARB in assessing the impacts of various energy scenarios. Model development began in the first quarter of FY 1981 and continued through the fiscal year. The project will be completed early in 1982.

Construction of energy facilities requires steel, cement, generating equipment, manpower, etc., which are supplied by industries located within the state, elsewhere in the country, and in the rest of the world. The investment in energy facilities will stimulate employment and output in the industries supplying these materials and services. These industries will purchase goods and services from other supporting industries, setting up a chain effect that will filter through the entire economy of the state. To estimate direct and indirect economic impacts and environmental impacts of energy activities, the models simulate flow of fuels between various energy facilities and consumers and the structural interaction among economic sectors.

This project emphasizes development of a system of models and demonstrates their capability by comparing two scenarios formulated by CEC. The data used in making these comparisons are the best available to us and the CEC. No attempt was made to develop new data for this analysis.

*This work was supported by the California Energy Commission and the California Air Resources Board through the Department of Energy under Contract No. DE-AC03-76SF00098.

ACCOMPLISHMENTS DURING FY 1981

Overview of the Modeling System

Figure 1 is a schematic of the California Energy Planning Model. Energy scenarios specifying the primary energy from each type of fuel are the basic input for the chain of models: an Energy Planning Model (EPM) and a California Input-Output (I-O) Model. The scenarios specify the amount of energy supplied by oil, gas, coal, nuclear, solar, wind, ocean, and biomass facilities that is needed to fulfill the demand in the end-use sectors. Different end-use demands will affect the economy and the environment differently, depending on the investment in each end use.

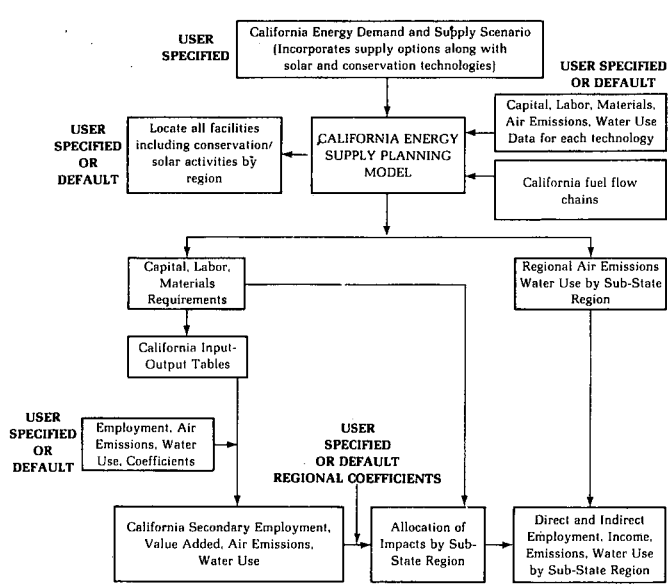

Figure 1. Analytical framework, California energy planning model. (XBL 823-268)

The California Energy Planning Model

The California EPM is patterned after a national model developed for the National Science Foundation by the Bechtel Corporation.[1] The EPM translates the scenarios into the number of energy facilities of each type that would have to be constructed to meet the specified energy demand. The energy supply facilities are coal mines, oil wells, power plants, solar and wind generators, etc.; the end uses are refrigeration, air conditioning, space heating, etc. The EPM contains algorithms for determining the number of transportation facilities required to move the coal, oil, gas, and other energy fuels, as determined by the origin of the projected energy resources and the demand at the destination.

All the energy facilities are sited by air basin. The user can site power plants in the appropriate basin if the location is available from utility plans. The model will select sites for end uses and for solar and biomass facilities if none are specified by the user.

The capital and labor to operate and construct each type of facility are subdivided into 140 categories of manpower, materials, and equipment. These data are used to calculate the direct capital costs and labor required to meet the prescribed energy supply. The 1978 EPM data were extended at LBL to include data on solar and other renewable facilities and residential end uses. Data on each type of facility have been included. In addition, data on airborne effluents from the operation of motor vehicles were developed using a transportation model.

The California Input-Output Model

The EPM estimates of capital expenditures on equipment, materials, and labor are treated as final demands in the I-O model. To match the I-O sectors, the equipment and material expenditures are disaggregated using fractional shares in the Gross Private Domestic Capital Formation vector and the manpower expenditures are disaggregated using the shares in the Personal Consumption Expenditures vector. The two vectors are combined into a single vector of final demands. The I-O model is then used to estimate the output of each industry required to meet these final demands over the next twenty years.

The California Input-Output Model was derived from the 496-sector national table for 1972 prepared by the Bureau of Economic Analysis.[2-4] The national table was projected to 1977 using data from the 1977 Economic Censuses, the National Income and Product Accounts, and numerous other sources. It was then converted into a California input-output table to reflect the state's economy during 1977. This conversion eliminates sectors of the national economy not in California, such as coal mining and tobacco. The technical coefficients which reflect the state of the technology do not change in such a conversion. To accurately reflect industrial energy consumption by fuel type in California, we modified the fuel-use coefficients in the I-O table.

The 1977 direct transactions coefficient were updated to 1985 and 1990 on the basis of projections made by the Bureau of Labor Statistics.[5,6] In arriving at the coefficients for 1985 and 1990, we assumed that the California coefficients would change at the same rate as the national. These energy coefficients were then adjusted to reflect the projected use of energy in California during those years. Employment and income coefficients were projected in a similar manner.

Using payroll data for 1977 from the County Business Patterns,[7] the output of each industry was disaggregated to air basins. Labor and income changes from energy plant construction can be estimated for each air basin by combining industrial output estimates with employment and income coefficients.

Vehicle Emissions Model

The vehicle emissions model enables users to estimate the annual tonnage of carbon monoxide, nitrogen oxides, and hydrocarbons emitted by highway transportation. The model can produce three sets of emissions for each of the years 1985, 1990, and 2000, depending on the data provided by the user. The first set of projections results from relatively few user-specified variables which are essentially identical to those produced by ARB's model and can be used as a reference. The second set results from user-provided values for the total number of vehicle miles traveled by each of six classes of vehicles for each air basin in 1985, 1990, and 2000. The third set is derived from user-provided values for the gallons of fuel used in the state during a given year.

In the first two sets, in addition to vehicle emissions, the model calculates total fuel used in each air basin in each future year. In the third set, where fuel use is given, the model calculates fleet average-vehicle efficiencies for each vehicle class and the sum of vehicle miles traveled for each air basin in each future year.

Factors such as vehicle use, number of vehicles, vehicle miles traveled, and fuel use can easily be changed, and the amount of atmospheric pollutants generated for each scenario thus can be quickly determined. To make updating the data as simple as possible, the data are input in the form provided by ARB and other state agencies.

PLANNED ACTIVITIES FOR FY 1982

Preliminary models completed during FY 1981 will be installed on the CEC computers. The models will be improved during the first quarter of FY 1982, and the two scenarios will be analyzed. We will compare the results with similar runs made at CEC to verify that the model has been transferred properly. Final models and user's manuals will be delivered early in the second quarter, completing work on the project.

REFERENCES

1. Bechtel Corporation (Aug. 1975), Energy Supply Planning Model, Vols. 1 and 2, San Francisco.

2. Ritz, Phillip M. (Feb. 1979), "The Input-Output Structure of the U.S. Economy, 1972," Survey of Current Business.

3. Ritz, Phillips M., Roberts, Eugene P., and Young, Paula C. (Apr. 1979), "Dollar-Value Tables for the 1972 Input-Output Study," Survey of Current Business.

4. Ritz, Phillip M. (July 1980), Definitions and Conventions of the 1972 Input-Output Study, Bureau of Economic Analysis Staff Paper BEA-SP 80-034.

5. Saunders, Norman C. (December 1978), "The U.S. Economy to 1990: Two Projections for Growth," Monthly Labor Review.

6. Andreassen, Arthur (Dec. 1978), "Changing Patterns of Demand: BLS Projections to 1990," Monthly Labor Review.

7. U.S. Department of Commerce, Bureau of the Census (Oct. 1979), County Business Patterns 1977, CBP-77-6, Washington, D.C.

Mineral Requirements for Energy Scenarios*

J. A. Sathaye and H. Ruderman

The next twenty to thirty years are expected to be a period of transition from an era dependent on conventional energy sources, such as oil and gas, to one more dependent on unconventional and virtually inexhaustible sources of energy. The viability of these alternative energy sources is contingent, in part, on the availability of certain materials and minerals. In June 1980, the Senate Committee on Energy and Natural Resources asked the General Accounting Office (GAO) to identify minerals critical to developing future energy technologies, their availability, and projected demand. GAO, in turn, asked LBL to develop a methodology to evaluate projected energy-related demand for nonfuel minerals. Work on the project began in November 1980 and was completed in March 1981. The results, conclusions, and recommendations of the study were transmitted to the Senate committee in June 1981.[1]

The analysis described in this report estimated and evaluated the materials and raw and processed minerals that would be demanded by energy development through the year 2000 under four national energy scenarios formulated by the Department of Energy (DOE). We examined the demand for minerals selected for their potential strategic importance in future energy development. Specific minerals which may be viewed as strategic and critical to U.S. energy development in light of their domestic and worldwide availability were identified. A more detailed discussion of the methods and results of this study may be found in another report.[2]

*This work was supported by the U.S. General Accounting Office through the Department of Energy under Contract No. DE-AC03-76SF00098.

ACCOMPLISHMENTS DURING FY 1981

Energy Scenarios

We investigated the minerals requirements for four DOE prepared scenarios of U.S. energy development to the year 2000. These national projections of energy supply and demand include a broad range of energy technologies from solar energy to nuclear power as supplements to oil, gas, and coal use. The Energy Information Administration (EIA) Annual Report to Congress[3] contains a series of scenarios based on different combinations of world oil prices and energy demand growths. The Office of Policy and Evaluation issued National Energy Plan II (NEP-2)[4] with two scenarios (NEP-2 High and NEP-2 Low) based on the EIA high and low oil-price cases. A set of scenarios emphasizing solar energy, developed by the Domestic Policy Review Committee (DPR),[5] served as the basis for the Technology Assessment of Solar Energy (TASE).[6] The TASE 14 and TASE 6 scenarios were also based on the NEP-2 High and Low cases, with the DPR projections of solar energy embedded in the TASE 14.

The NEP-2 High and Low scenarios differed in their assumptions about future world oil prices, while the two TASE scenarios differed in the amount of energy produced by solar and renewable facilities. All four show similar growth in primary energy use, reaching 123 to 129 quads (10^{15} Btu) in 2000. Primary energy use in the NEP scenarios increased from 74 quads in 1975 to 124 quads in 2000 in the high oil price cases, an annual rate of 2.1 percent, and from 74 quads to 129 quads in the low price case, an annual rate of 2.25 percent. In the TASE scenarios, primary energy supply grows from 73 quads in 1975 to 123 quads in 2000. Solar energy use in TASE 14 in 2000, excluding hydroelectric and geothermal generation, amounts to 13.8 quads as compared to 6.0 quads in the TASE 6 scenario. Figure 1 shows the projected energy use

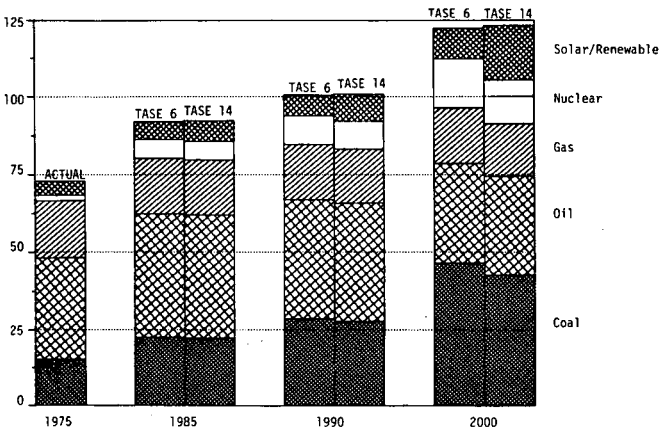

Figure 1. Primary energy supply 1975-2000, in quadrilion Btu's.

(XBL 8111-1582)

in the two TASE scenarios. By comparing the mineral requirements of the four scenarios, we could see the effects of different growth rates and technologies.

Methodology

Energy scenarios specifying the primary energy from each type of fuel serve as the basic input for the chain of models, an Energy Supply Planning Model (ESPM)[7] and a U.S. Input-Output (I-O) Model (Fig. 2). The ESPM translates the scenarios into the number of energy facilities of each type which would have to be constructed to meet the specified levels of energy supply. The 118 types of facilities in the model include stationary facilities such as coal mines, various types of power plants, oil wells, solar and wind generators, etc. The ESPM also contains algorithms for determining the number of transportation facilities required to move coal, oil, gas, and other energy fuels. The number of trains, pipelines, trucks, etc., are estimated on the basis of projected energy supply and demand by origin and destination for each federal region of the country.

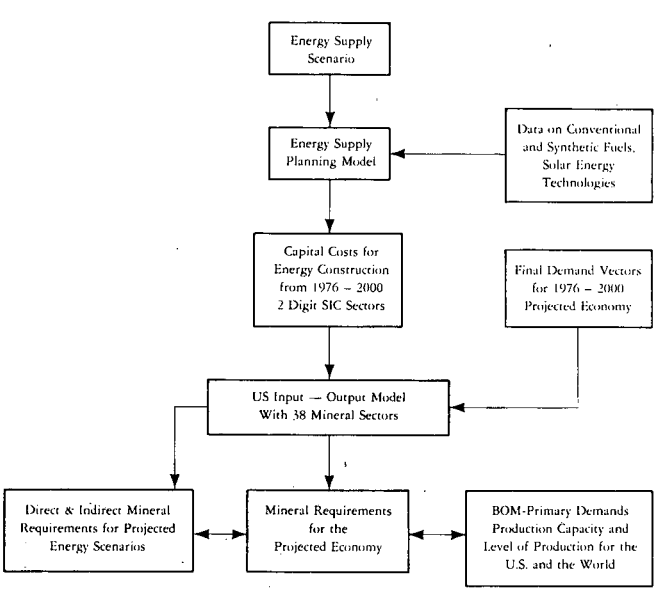

Figure 2. Minerals assessment methodology.

(XBL 8111-1583)

The capital and labor needed to construct and operate each type of facility are subdivided into 140 detailed categories. On the basis of these data, the direct capital costs and labor required to meet the prescribed energy supply scenario are computed. The 1978 ESPM data base was modified at LBL to include data on twenty additional solar and renewable technologies.

The capital costs include expenditures on manpower, equipment, and materials. Equipment and materials costs are presented by two-digit I-O sectors. These capital expenditures are treated as final demand vectors in the I-O table sectors. The equipment and materials expenditures are disaggregated using fractional shares in the Gross Private Domestic Capital Formation vector, and the manpower expenditures are disaggregated using the shares in the Personal Consumption Expenditures vector. The I-O model estimates the output of each industry required to meet these demands for the next twenty years.

The U.S. Input-Output Model was derived from the 496-sector national table for 1972 prepared by the Bureau of Economic Analysis.[8-10] The disaggregation of the minerals from 7 to 46 sectors was based on data from the Bureau of Mines and Bureau of Economic Analysis worksheets for 1972. This table was aggregated to 178 sectors, keeping the detail in the mineral producing and using sectors.

The dollar outputs of the minerals sectors of the input-output model were converted to physical quantities of minerals. These outputs are the direct and indirect demands for the minerals needed to construct the energy facilities called for in the scenario.

Results and Conclusions

Demand for 46 nonfuel minerals was projected in five-year intervals to the year 2000 for the four scenarios. Twenty of the mineral sectors were excluded from detailed analysis because (1) the United States is a net exporter of the mineral and has adequate reserves and resources; (2) there are readily available, geographically dispersed, and virtually inexhaustible world resources; (3) the sector included two or more minerals that could not be disaggregated; or (4) the sector was a service sector and thus not applicable to any one given mineral.

We compared our projections of domestic energy-related demand for the remaining 26 minerals to the Bureau of Mines' projections of total U.S. and world primary demands and to their projections of U.S. and world production capacities. The projected percentage of energy-related demand as a fraction of total demand and production capacity were calculated for both the alternative and conventional facilities under each scenario. A similar analysis was conducted, substituting a dif-

ferent technological design for the solar heating and cooling of building facilities.

Our analysis indicated that implementation of any of the national energy scenarios would require large increases in the supply and availability of certain nonfuel minerals. Energy-related demand for the 26 minerals is shown in Table 1. The four scenarios required an average of between 17 and 23 percent of total projected U.S. demand for these minerals to the year 2000. However, the percentage of each mineral varied sharply from a low of 3 percent for molybdenum to a high of 75 percent for tantalum. Requirements for minerals are highest in the high solar scenario, primarily due to the large component of solar and other renewable energy technologies.

Demand for the 26 nonfuel minerals by the conventional oil, gas, and coal technologies remained relatively constant among the four energy scenarios, averaging between 8 and 9 percent of total U.S. demand. However, demand by alternative solar, synfuels, and nuclear technologies varied from 8 to 15 percent, depending primarily on the amount of energy in the scenario provided by solar and other renewable technologies. Average energy-related demand for minerals was projected to be between 5 and 7 percent of the projected total world demand for the 26 minerals to the year 2000.

Table 1. Mineral requirements for the four scenarios (1976-2000).

Mineral	TASE 6	TASE 14	NEP-2 Low	NEP-2 High
Aluminum ores (10^3 st)	26,569	35,186	30,486	25,075
Antimony (10^3 st)	206	293	247	203
Asbestos (10^3 mt)	3,336	3,972	3,891	3,192
Barite (10^3 st)	6,434	8,520	8,299	6,951
Chromium (10^3 st)	9,859	13,043	12,153	10,016
Columbium (10^6 lb)	123	177	119	100
Copper (10^3 mt)	4,566	5,734	4,729	3,945
Feldspar (10^3 st)	2,776	4,274	4,073	3,210
Fluorspar (10^3 st)	6,657	7,900	7,317	6,258
Gold (10^3 oz)	25,521	39,018	24,789	20,623
Gypsum (10^6 st)	116	246	293	229
Iron (10^6 st)	425	472	441	384
Lead (10^3 mt)	3,010	5,223	2,954	2,491
Manganese (10^3 st)	26,388	30,010	27,610	23,913
Mercury (76lb flasks)	119,565	201,280	132,136	109,703
Molybdenum (10^3 lb)	104,510	119,140	109,331	94,417
Nickel (10^3 st)	1,606	2,139	1,597	1,362
Platinum group (10^3 oz)	3,385	5,173	3,262	2,720
Silver ore (10^6 oz)	594	906	579	479
Sulfur (10^3 mt)	7,924	10,973	9,915	8,144
Tantalum (19^3 lb)	49,283	70,625	48,040	40,518
Titanium (19^3 st)	1,990	2,971	2,439	1,982
Tungsten (10^3 lb)	76,577	87,709	76,892	64,885
Vanadium oxide (10^5 lb)	164	167	171	141
Zinc (10^3 mt)	3,056	4,785	3,143	2,641

Note:
st: short tons; lb: pounds; mt: metric tons; oz: troy ounces

While world supplies would appear adequate to meet U.S. energy-related demand, the uncertain availability of some minerals poses potential constraints to a smooth transition from oil and natural gas to alternative sources of energy. This uncertainty stems primarily from the possibility that there might be a serious disruption in supplies or a sharp increase in prices of certain minerals. Either could delay implementing a national energy program. In this sense, "strategic" refers to the relative availability of a mineral, while "critical" refers to its essentiality for energy-related uses.

Based on our analysis of energy-related demand and additional research at the General Accounting Office, we have identified nine minerals which may be "energy-critical" and "strategic": aluminum ores, chromium, cobalt, columbium (niobium), gold, manganese, nickel, platinum group metals, and tantalum. These minerals are characterized as coming from few and potentially unreliable foreign sources, having inadequate domestic mine capacity, being almost entirely imported, and being essential to energy development.

Alternate technology designs can help mitigate adverse supply disruptions or sharp price increases. For example, an alternate design for solar heating and cooling of buildings reduced the amount of chromium required for the solar group by over 50 percent. However, alternatives for a specific strategic and critical mineral may not always be available. Other possibilities for mitigating adverse impacts of a minerals shortage include reducing consumption through conservation, recycling, and drawing down industry and government stocks. Each mineral may have to be analyzed and evaluated on its own merits before comparative options can be completely assessed.

PLANNED ACTIVITIES IN FY 1982

This work was concluded in FY 1981 and will not continue in FY 1982.

REFERENCES

1. Peach, J. Dexter (June 25, 1981), Director of GAO, Letter to Senator Henry M. Jackson.

2. Sathaye, J., and Ruderman, H. (1981), Minerals Requirements for Energy Scenarios Lawrence Berkeley Laboratory Report LBL-12696.

3. U.S. Department of Energy, Energy Information Administration (1979), Annual Report to Congress, 1979, Vols. 1, 2, and 3, DOE/EIA-0173(79)/1,2,3, Washington, D.C.

4. U.S. Department of Energy, Office of Policy and Evaluation (Apr. 1979), National Energy Plan II, Washington, D.C.

5. U.S. Department of Energy (Oct. 1978), Domestic Policy Review of Solar Energy, TID-28835/1,2, Washington, D.C.

6. The Mitre Corporation (May 1981), Environmental and Socioeconomic Comparison of High and Low Solar Scenarios, MTR-80W215-01, McLean, Va.

7. Bechtel Corporation (Aug. 1975), Energy Supply Planning Model, Vols. 1 and 2, San Francisco.

8. Ritz, Phillip M. (Feb. 1979), "The Input-Output Structure of the U.S. Economy, 1972," Survey of Current Business.

9. Ritz, Phillip M., Roberts, Eugene P., and Young, Paula C. (Apr. 1979), "Dollar-Value Tables for the 1972 Input-Output Study," Survey of Current Business.

10. Ritz, Phillip M. (July 1980), Definitions and Conventions of the 1972 Input-Output Study, Bureau of Economic Analysis Staff Paper BEA-SP 80-034, Washington, D.C.

ENERGY DEMAND STUDIES

Residential End-Use Demand Modeling: Improvements to the ORNL Model*

J. E. McMahon

Estimates of future demand for energy are used by policy analysts, energy suppliers, utility companies, and some government agencies. Prior to 1973, very simple methods were adequate for forecasting demand growth in the United States. Two such models were (1) exponential growth at a constant rate, e.g., electricity demand increased seven percent per year, and (2) energy consumption proportional to the GNP. In the ensuing eight years, which encompassed rapidly rising oil prices, these models predicted energy demand substantially higher than actually occurred.

More refined models were developed to include the more complex relationships necessary to explain current demand. Specifically, conservation efforts and technological changes needed to be considered. The Oak Ridge National Laboratory (ORNL) developed a detailed end-use model[1] intended for use in analyzing alternative energy policies in the United States. Originally based largely on 1970 Census data, the model was subsequently updated to utilize 1977 input data. This important tool provides a framework within which further improvements are being made.

ACCOMPLISHMENTS DURING FY 1981

The ORNL model was altered to become the ORNL/LBL Residential Energy Demand Model during an analysis of U.S. Department of Energy proposed Consumer Product Efficiency Standards. Results of that analysis are described elsewhere.[2] Three major changes to the methodology were undertaken. First, the approach to changes in efficiency of new appliances was improved. The marketplace is changing for a variety of reasons, and newer appliances are generally more efficient than their predecessors. Second, methods of constructing new homes involve higher levels of insulation than in the past and should exhibit significant effects on energy consumed for space conditioning (heating and cooling). Third, the expected sales of appliances will depend not only on the number in stock but also on the age distribution of existing units. A vintaging approach, in which the age distribution is updated each year, provides a better guide for future replacement sales.

Before modification, the model accounted for changing efficiencies and housing characteristics in future years but from an incorrect starting point. For this reason, the first two changes were initiated. The third change, the vintaging approach, replaces the methodology for estimating the number of potential purchases of appliances to be installed in existing homes each year. All three modifications replace simpler assumptions with a more complex set, and all three impose additional data requirements on the model.

Efficiency of New Appliances

The ORNL model previously contained the assumption that, in the first year of a simulation (in this case, 1977), the efficiency of a new appliance was the same as the efficiency of the average unit already in use. With the passage of time and increases in energy costs, manufacturers are providing and consumers are purchasing appliances with higher efficiencies. The disparity between the efficiency of a new unit and the unit it replaces will be increasingly significant when

*This work was supported by the Assistant Secretary for Conservation and Renewable Energy, Office of Buildings and Community Development, Buildings Division of the U.S. Department of Energy under Contract No. DE-AC03-76SF00098.

estimating future energy consumption. Table 1 shows the efficiency improvements since 1972 and 1975.

The ORNL model was capable of projecting future equipment efficiencies from a base year starting point. The improvement to the model involved adding an input that specified the efficiency of new units relative to the average stock unit in the initial year. This removes the constraint that these efficiencies had to be the same. In addition, the set of design options available for purchase in future years was readjusted to begin with the base-year new unit rather than with the stock unit. The constraint that future appliances cannot be less efficient than a 1978 unit was retained.

Methods of Constructing New Houses

Just as new appliances are more efficient than those already in use, new houses are constructed in such a way as to reduce space conditioning energy requirements, compared to old houses. While measured data on the actual energy consumption of new houses are more difficult to obtain, the characteristics of new houses are available. Characteristics considered include amount of ceiling insulation, wall insulation, glazing level, floor area, floor insulation, and window area. Physical models of heat transfer in a house, such as the DOE-2.1 Building Energy Analysis Program, were used to determine the annual energy consumption for heating and for cooling, based on the characteristics of the house. The relative thermal integrity factor is defined as the ratio of annual heating requirements for a new house to the annual heating requirements for a stock house. The thermal integrity factor is accurate only for changes in housing construction. Correction for changes in the floor area of the house, efficiency of the heating system, and usage patterns are performed in addition to, and separate from, the thermal integrity factor.

Just as in the treatment of appliance efficiency, the new distinction made for thermal integrity is that the average new house has different characteristics and therefore different energy consumption than the average house already in existence. Similarly, the set of design options available in future years must begin with what is available in present-day new houses. The constraint that future new houses must be at least as efficient as 1978 new houses is retained.

Table 1. Efficiency improvements since 1972 in residential appliances.

	Shipments-weighted energy factors[a]			Percent change[b] in unit energy consumption since 1975	
	1975	1978	1980	1978	1980
Furnaces - Gas	63.24	63.55	63.3	-0.5	-0.1
- Oil	73.65	75.20	75.7	-2.1	-2.7
				Since 1972	
	1972	1978	1980	1978	1980
Room Air Conditioner	6.22	6.75	6.72	-7.9	-7.4
Central Air Conditioner	6.66	6.99	7.06	-4.7	-5.7
Water Heater - Electric	79.80	80.67	78.3	-1.1	+1.9
- Gas	47.35	48.17	47.9	-1.7	-1.1
Refrigerator/Freezer	4.16	5.09	5.51	-18.3	-24.5
Freezer	7.53	10.0	9.73	-24.7	-22.6
Range/Oven - Electric	42.8	53.6	43.25	-20.1	-1.0
- Gas	13.9	17.6	25.82	-21.0	-46.2
Dryer - Electric	2.61	2.59	2.88	+0.8	-9.4
- Gas	2.10	2.38	2.60	-11.8	-19.2

[a]1972, 1975, and 1978 values are from CS 179 surveys conducted by DOE (Ref. 3). 1980 values are from Engineering Analysis for CPES (Ref. 4).
[b][(SWEF (1975)/SWEF (X)) - 1]* 100, for year X.

Appliance Retirements

The model as originally written distinguished between purchase of appliances each year for new houses and purchase of appliances for installation in existing houses. Most of the latter are replacements of appliances that have reached the end of their useful service life. The original formulation uses an exponential retirement function equivalent to assuming that a constant percentage of the existing appliances retire each year. In a population that is growing at a significant rate, this assumption is poor because the most recently purchased appliance will not soon require replacement. The general solution to this problem involves keeping track of the vintage, or age distribution, of all appliances and retiring them only at appropriate intervals after the year of purchase. This vintaging approach requires a more complex computer model and a significant increase in computation time, but it provides a more accurate representation of the real turnover of appliances.

A derivation of retirement functions was found in the literature.[5] A retirement function is an expression of the percent of appliances that retire as a function of the number of years since they were originally purchased. A comparison of the retirement function and the exponential assumption that it replaced is given in Figure 1. While the

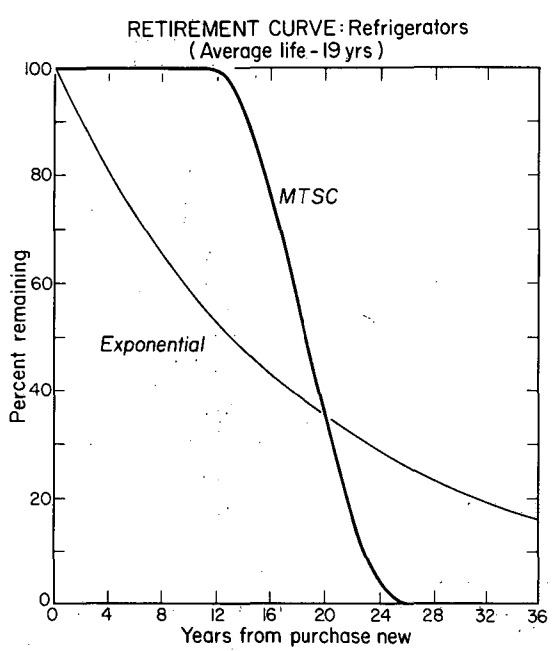

Figure 1. Percent survivors vs years since first purchase: refrigerators. (XBL 816-948)

old formula retired about 5.1 percent of the existing appliances each year regardless of their age, the new formulation retires no refrigerators until they are 12 years old. Presumably many refrigerators are sold as second-hand items, but continue to function under new ownership. Also, the old formula allowed a number of very old refrigerators to go on operating for 40 years, while the new approach effectively eliminates refrigerators older than 26 years.

The changes to the model required to consider a vintaging approach to appliances are general in nature and do not depend on the specific set of inputs selected. If other studies refine the retirement functions, only the input data to the model will need to be replaced, and the model itself will accommodate the new data without program modifications.

Future Directions

Modeling efforts have improved substantially in recent years. While forecasts of exactly what will come in the future are now--and will remain--impossible, model simulations can define the range of probable futures.

Considering the ORNL/LBL Residential Energy Demand Model as a framework, there are several areas in which changes need to be made (these proposed changes are discussed in more detail elsewhere[6]):

- Quantify and examine the uncertainty in the simulation
- Redefine the set of end uses to combine space heating and cooling
- Update historical econometric formations, especially the fuel split algorithm
- Consider the variety of decision segments involved in appliance purchase and use
- Broaden the applicability of the model to utility service areas.

PLANNED ACTIVITIES IN FY 1982

This work was concluded during FY 1981 and will not continue in FY 1982.

REFERENCES

1. Hirst, E., and Carney, J. (July 1978), The ORNL Engineering-Economic Model of Residential Energy Use, Oak Ridge National Laboratory Report ORNL/CON-24, Oak Ridge, Tenn.
2. McMahon, J., Levine, M., and Herring, H. (1982), "Analysis of Appliance Efficiency Standards," Energy and Environment Division Annual Report 1981, Lawrence Berkeley Laboratory Report LBL-13500.
3. U.S. Department of Energy, Conservation and Solar Energy, Office of Buildings and Community Systems (June 1980), Economic Analysis, Energy Efficiency Standards for Consumer Products, Washington, D.C.
4. U.S. Department of Energy, Conservation and Solar Energy, Office of Buildings and Community Systems (June 1980), Engineering Analysis, Energy Efficiency Standards for Consumer Products, Washington, D.C.
5. Fechtel, R.B., Novicky, E.R., and Wusterbarth, A.R. (Nov. 1980), Energy Capital in the U.S. Economy, MTSC, Inc., Bethesda, Md.
6. McMahon, J. (1981), "Residential End Use Demand Modeling: Improvements to the ORNL Model," in Beyond the Energy Crisis, Opportunity and Challenge, R. Fazzolare and C. Smith, eds., Pergamon Press, New York, pp. 297-304.

Analysis of Appliance Efficiency Standards*

J. E. McMahon, M. D. Levine, and H. J. Herring

The Energy Policy and Conservation Act, as amended by the National Energy Conservation Policy Act, requires that the Department of Energy prescribe energy efficiency standards for the following consumer products: refrigerators and refrigerator-freezers; freezers; clothes dryers; water heaters; room air conditioners; home heating equipment, not including furnaces; kitchen ranges and ovens; and central air conditioners. The law requires that standards be designed to achieve the maximum improvement in energy efficiency that is technologically feasible and economically justified.

The ORNL/LBL Residential Energy Demand Model[1] was developed as a tool for assessing the effects of proposed efficiency standards. Two important measures of those effects were:

- Energy savings to the Nation

*This work was supported by the Assistant Secretary for Conservation and Renewable Energy, Office of Buildings and Community Development, Buildings Division of the U.S. Department of Energy under Contract No. DE-AC03-76SF00098.

- Dollar savings to the consumer.

Much additional detail about projected energy demand (by end use, fuel type, home type, etc.) was provided by the model but will not be discussed here. Those details and other aspects of the standards, including their effects upon manufacturers, will be discussed in forthcoming publications of the Department of Energy.[2]

ACCOMPLISHMENTS DURING FY 1981

Synchronous with the improvements to the ORNL/LBL Residential Energy Demand Model, input data were updated to include recent survey data on the following:

- Efficiency of new appliances
- Current housing construction practice
- Appliance retirements as a function of age
- Saturation of appliances in new houses and in the existing housing stock.

In addition, the fuel price projection of the National Energy Policy Plan was utilized. The DOE Engineering Analysis provided estimates of the purchase cost of each appliance as a function of efficiency.

The methodology involved incorporating all available data into the Base-Case simulation. This simulation provided estimates of future energy consumption for each of the products, e.g., furnaces, water heaters, etc. Figure 1 illustrates the result. Then, a second simulation was performed using the same input data and model but assuming the efficiencies of regulated products to be at or above the proposed U.S. DOE Consumer Product Efficiency Standards. The differences between the first simulation, the Base Case, and the second, the Standards Case, are the expected effects of the Consumer Product Efficiency Standards (CPES).

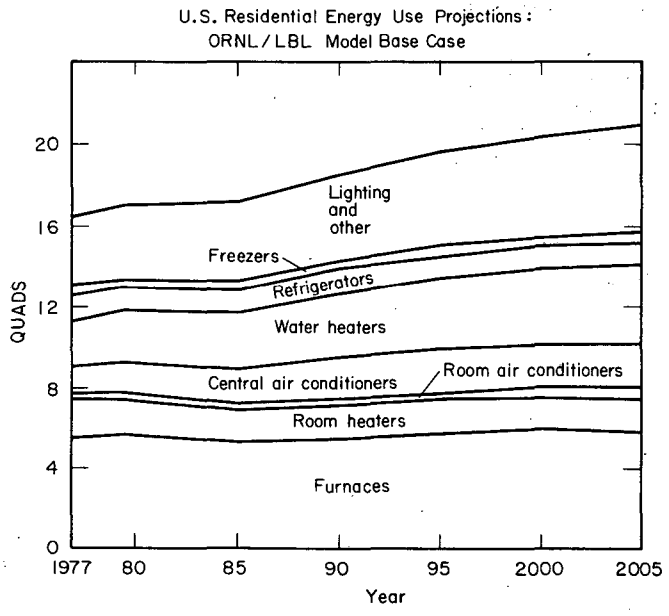

Figure 1. U.S. residential energy use projections, ORNL/LBL model case. (XBL 8112-1643)

Energy Savings to the Nation

The first effect studied is the amount of energy saved by the CPES for each product. Only small savings were found for ranges, ovens, and clothes dryers. The annual energy savings for the nation for other products are shown in Figure 2.

The aggregate energy savings include secondary effects in addition to the difference in efficiency. The Standards Case represents an alternative future in which the choice of appliance efficiency is restricted as a result of government policy. The ultimate result of such a policy is to alter the number of appliances purchased; the choice of fuel, e.g., electric or gas water heater; and the usage behavior of the consumer. These effects are included in the energy savings shown. In these simulations, the major effect of CPES was to decrease operating costs of appliances. This, in turn, caused no change or only a slight increase in appliance sales and in usage hours. Overall, utility of appliances was unchanged or increased.

The efficiencies of new central air conditioners for the two cases are shown in Figure 3. Note that the Base Case assumes a continuation of substantial efficiency improvements in the Base Case, even in the absence of standards. Energy savings are obtained by CPES, over and above the dramatic savings attributed to market forces.

Dollar Savings to the Consumer

The second major effect of CPES is to alter the cost to the consumer purchasing and operating an appliance. In the Standards Case, the mandated higher efficiency has a higher purchase cost but lower operating cost, compared to the Base Case. The proposed standard levels were chosen to reduce the life cycle cost of each product. That is, the

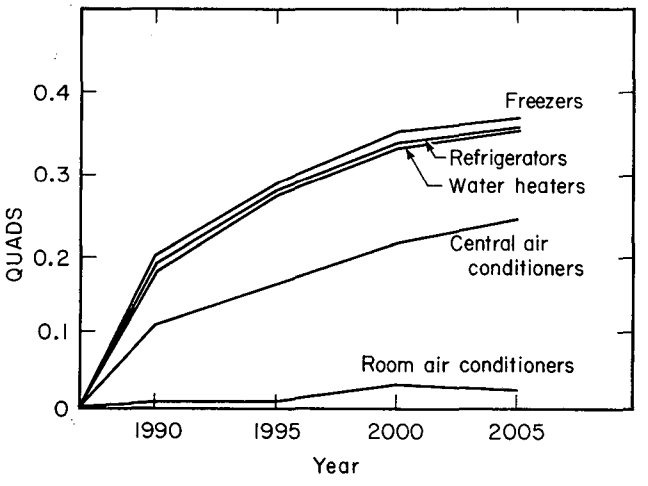

Figure 2. Annual energy savings of proposed DOE appliance standards relative to the ORNL/LBL model base case. (XBL 8112-1644)

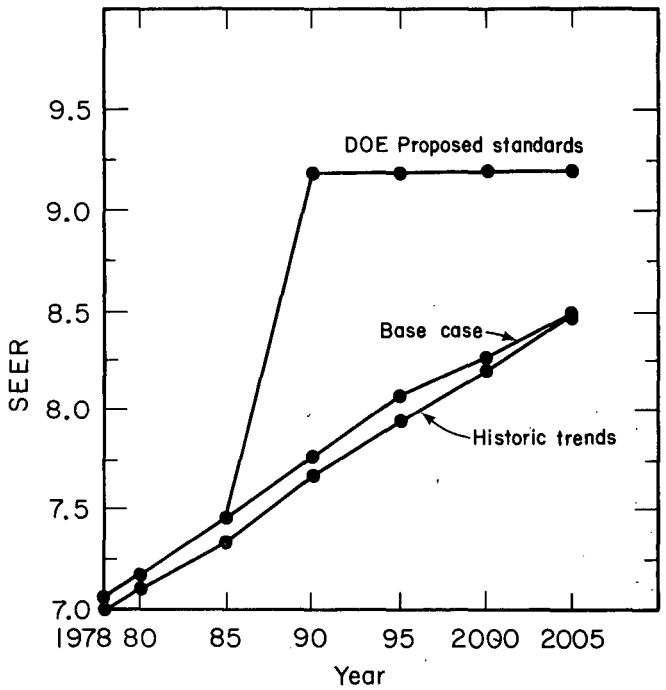

Figure 3. Central air conditioners, efficiency vs year. (XBL 8112-1645)

savings in operating costs, discounted and summed over the useful operating lifetime, exceed the increase in purchase cost for each individual appliance unit.

For all appliances purchased in the period 1987-2005, the total savings over their useful lifetimes would be over $5.5 billion, if the Consumer Product Efficiency Standards were enacted. This net savings is accrued from about $10 billion in reduced energy costs, less about $5 billion in increased equipment costs (these figures have been normalized to the sales of appliances in the Base Case).

PLANNED ACTIVITIES FOR FY 1982

Documentation of the input, assumptions, and model methodology will be completed.

REFERENCES

1. McMahon, J. (1981), "Residential End Use Demand Modeling: Improvements to the ORNL Model," Energy and Environment Division Annual Report 1980, Lawrence Berkeley Laboratory Report LBL-12860, 1981.

2. U.S. Department of Energy, Conservation and Solar Energy, Office of Buildings and Community Systems (Dec. 1981), Economic Analysis, Energy Efficiency Standards for Consumer Products, Washington, D.C.

Residential Hourly and Peak-Demand Model*†

G. Verzhbinsky and M. D. Levine

We have developed a model that simulates the hourly residential electricity demand for electric utility service areas. This model is integrated with the Oak Ridge National Laboratory (ORNL)/Lawrence Berkeley Laboratory (LBL) residential energy demand forecasting model. The most important new feature of the hourly demand model is that it is disaggregated to 12 end uses. This disaggregation, in addition to its extensive time of use and engineering/econometric data base, makes possible the evaluation of specific electric utility conservation programs and various energy conservation policies.

*This work was supported by the Assistant Secretary for Conservation and Renewable Energy, Office of Buildings and Community Development, Buildings Division of the U.S. Department of Energy under Contract No. DE-AC03-76SF00098.

†A more detailed description of this work is found in G. Verzhbinsky and M. Levine, "Residential Hourly and Peak Demand Model," Lawrence Berkeley Laboratory Report LBL-12856, 1981.

ACCOMPLISHMENTS DURING FY 1981

Electric utility systems design, capacity projections, financial impacts of alternative supply-and-demand management strategies, rate setting, and energy-conservation and load-management programs are all important facets of the electric utility industry. Each of these subject areas raises key issues confronting electric utilities today. Many of the issues relating to energy conservation and load management are assuming increasing importance to utilities in the current economic climate because of the difficulty in raising capital for new power plants.

In an effort to understand these issues and provide a quantitative evaluation of some of them, we have developed a computer model that forecasts hourly electricity demands for the residential sector. A key feature of this model is its disaggregation into each of the twelve major end uses. The model is based both on econometric and engineering/economic data, as well as measured data on time of use of energy demand by end use. The high degree of detail about hourly demand by end use, combined with economic information and a

specification of the average efficiency of each appliance type in and the thermal integrity of the house, make possible the evaluation of the potential impact of specific energy conservation and load management activities within an electric utility service area. The model has been applied to the evaluation of the likely impacts of the proposed Building Energy Performance Standards and the Consumer Products Efficiency programs of the U.S. Department of Energy.

The residential hourly demand model is currently integrated with the ORNL/LBL residential energy forecasting model.[1,2] In order to achieve this integration, selected changes were made in the ORNL/LBL model, especially in the characterization of their thermal integrity of new houses, and a utility specific data base was used as input to the ORNL/LBL model.[2,3] This approach of incorporating the hourly and average energy demand forecasting models takes advantage of the key features of the ORNL/LBL model: its treatment of socio-economic determinants of energy demand growth, its engineering/economic data, and its analysis of residential end-use efficiency choices. At the same time, including hourly demand data and appropriate algorithms substantially increases the analytical capabilities of the ORNL/LBL model.

We are currently testing the residential hourly load model. We anticipate completing a validation of the model results against one or two electric utility service areas, using historical data from the past five to ten years. After a full validation exercise is completed, probably requiring application to at least ten utilities, we intend to develop appropriate interfaces between the model and other utility planning tools: capacity expansion, dispatch, and financial models.

Overview of Residential Hourly Demand Model

This paper describes the structure, input data, operation, and results of the disaggregate residential hourly demand model developed by LBL with the assistance of Hittman Associates, Inc. (HAI).[4] The model does the following:

- Projects the hourly and peak electricity demand for the residential sector of an electric utility service area
- Estimates the impact of different energy conservation policies on the hourly demand curve (load shape, including peak demand in the residential sector)
- Estimates reductions in the fuels and capacity for electric generation, by fuel type, resulting from residential energy conservation programs.

The model considers 12 end uses divided into two groups: temperature sensitive (central space heating, room space heating, heat pumps, room air conditioning, and central air conditioning) and temperature insensitive (water heating, refrigerating, freezing, cooking, clothes drying, lighting, and miscellaneous). The model deals with three housing types: single family, multi-family, and mobile homes. Also, it disaggregates the total housing stock into three groups by age of the house (and hence, by average, its thermal integrity): houses built before 1974, those built from 1974 to the present, and homes built after the start of the U.S. Department of Energy Building Energy Performance Standards program, assumed to have its initial impact in 1982. The model can handle as many as five climate zones within a utility service area. It simulates hourly electricity demand for each year from 1977 to 2005 (8760 hours each year). The total hourly demand curve is transformed into the load-duration curve which presents the number of hours where load exceeds any fixed value.

The model is part of a larger modeling effort to assess conservation impacts on utilities (CIUS) with the following objectives:

- Computing hourly electricity demand profiles under a wide range of economic conditions
- Evaluating and projecting hourly load profiles by climate region within a service area, by building type (single family detached house, single family attached house, mobile home), and by building thermal integrity
- Evaluating the likely impacts of energy conservation programs on the hourly and peak demands of an electric utility
- Quantifying the costs and benefits of energy conservation programs to the consumer
- Evaluating the effect of utility conservation programs on the cost of delivered electricity and on the financial performance of electric utilities
- Estimating the degree to which energy conservation will reduce demands for oil and gas to generate peak and intermediate electricity
- Evaluating a range of potential load management strategies to reduce peak demand in the residential sector
- Providing a quantitative basis for comparing costs and effects of investments in energy conservation programs and in increased generating capacity (including expansion of transmission and distribution systems, if required) in specific electric utility service areas.

Input Data

The model is extremely data intensive. Estimates of time-of-use of each end use are the most important and most difficult data to obtain. For the five weather dependent end uses (central space heating, room space heating, heat pump, room air conditioning, and central air conditioning), time of use is a function of temperature and humidity, as well as time of day.

To keep track of the data, we have followed the NEPOOL model[5] procedure of defining time-of-use matrices. Initial matrices of relative fraction of capacity of individual appliances in use, as a

function of temperature and hour of day, are input into the model. Adjustments are applied for service area, climate zone, house type, house vintage, and day type (weekday or weekend). Specification of the hourly temperature profile permits selection of relative use values from the adjusted matrices. The final set of values is normalized to the annual demand obtained from the ORNL/LBL residential energy use demand model.

All calculations of hourly electricity demand for temperature-sensitive end uses are based on appliance-use matrices.[5] Each element of these matrices gives the fraction of the connected appliance that is operating at any specified temperature and time-of-day conditions. In other words, these matrices show the shape of hourly demand for any given hourly temperature curve.

Because space heater matrices have been derived for the temperature range from -22° to +62°F by steps of +3° (28 values), 28 x 24 matrices are used for a space heater. For space cooling (end uses 4,5), the temperature range is from 60° to 96°F; in this case we use 13 x 24 matrices. For heat pumps 41 x 24 matrices are used, corresponding to the temperature range from -22°F to +96°F. These matrices depend on house type, vintage of the house, and climatic zone. Usually, there is only one climate zone in the service area, and the model generates 9 matrices for each temperature sensitive appliance for each service area to account for 3 house types and 3 vintages.

For temperature-insensitive appliances, the corresponding appliance-use matrices do not depend on temperature conditions and house vintage but instead depend on housing type (single-family, multi-family, mobile homes), day type (weekday/weekend), season (winter/summer), and hour of the day. The load shapes for these appliances are considered to be the same for all service areas. These matrices are provided by California Energy Commission Study (1979).[6,7]

Illustrative Results

Figures 1 and 2 show the types of results that can be obtained from the model. Figure 1 illustrates the hourly demand for electricity by each of the major end uses in a winter-peaking electric utility during the peak day. Figure 2 provides the same information for a summer-peaking utility. From these hourly results, available from the model for each hour of the year, it is possible to derive a wide range of information useful for evaluating the impacts of energy conservation and load management on electric utilities.

PLANNED ACTIVITIES FOR FY 1982

While this attempt to build a highly disaggregated peak demand model has resulted in a new methodology being made available to the utility industry, there remain several major areas in which further research is desired.

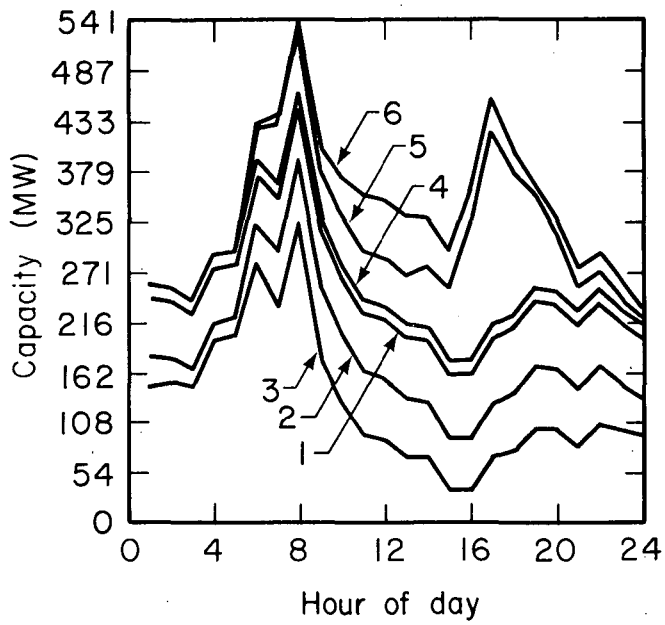

Figure 1. Peak day hourly residential electricity demand by end use for a winter-peaking utility. (XBL 824-865)

1. The electricity demand of commercial and industrial customers needs to be modeled in greater detail.

2. The model needs to be modified and extended so that the impact of some load management programs (such as time-of-day rate policy, customer energy storage, etc.) can be analyzed.

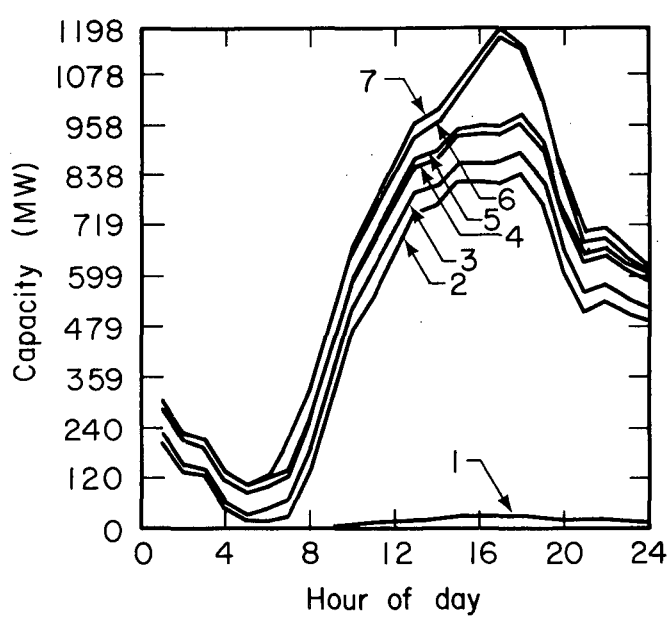

Figure 2. Peak day hourly residential electricity demand by end use for a summer-peaking utility. (XBL 824-863)

3. The model needs to be implemented and tested for more utility service areas.

4. It is desirable to make the model sensitive to the programs affecting utility financial performance, capacity expansion, and dispatch.

REFERENCES

1. Hirst, Eric, and Carney, Janet (1978), The ORNL Engineering-Economic Model of Residential Energy Use, Oak Ridge National Laboratory, Oak Ridge, Tenn.

2. McMahon, James E. (1981), The ORNL/LBL Residential Demand Model (In preparation).

3. Herring, Horace, and McMahon, James E. (1981), Applications of the ORNL/LBL Residential Energy Demand Model to Utility Service Areas.

4. Hittman Associates, Inc. (1980), An Analysis of Energy Efficiency Standards on Electric Utility Peak Loads, Task 5, Final Report, (HAI).

5. NEPOOL (1977), Model for Long Range Forecasting of Electric Energy Demand.

6. California Energy Commission (1979), Technical Amendations of the Residential Sales Forecasting Model: Electricity and Natural Gas, Sacramento.

7. California Energy Commission (1979), Technical Documentation of the Peak Load Forecasting Model, Sacramento.

Analysis of Energy Conservation Measures in Residential Buildings*

J. G. Ingersoll, J. Huang, J. J. Mass, and M. D. Levine

The objective of the residential energy analysis program is to research the technical aspects of efficient energy-use management in residential buildings. Using computer models to simulate the hour-by-hour performance of a building in any given climate, we can determine the impact of specific measures on energy requirements, including the building envelope, materials, design, equipment, and operation. These measures can then be evaluated as a means of improving the heating and cooling energy utilization in residential buildings.

ACCOMPLISHMENTS DURING FY 1981

The energy analysis of single-family residential buildings was completed during the year. Four prototype designs were produced: one-story, two-story, multi-level, and townhouse, and these designs were analyzed for 48 cities (Table 1). Three different foundation types were modeled: basement, slab on grade, and crawl space. Depending on the degree of usage of a foundation type in any given city, one, two, or even all three foundation types were analyzed for that city. The information on usage of foundation types, as well as all other building characteristics used in the design of the four prototype buildings, was obtained from relevant 1979 reports of the National Association of Homebuilders Research Corporation. For each prototype with a specific foundation type, between 15 and 20 different levels of envelope thermal integrity were analyzed in every city. These different levels of thermal integrity covered the whole spectrum of building thermal losses, from very loose to very tight. The envelope thermal integrity was a combination of: roof or ceiling insulation varying from R-0 to R-60 with intermediate levels of R-11, R-19, R-38, and R-49; wall

Table 1. Cities for the residential energy analysis.

1.	Albuquerque, NM	25.	Los Angeles, CA
2.	Atlanta, GA		
3.	Birmingham, AL	26.	Medford, OR
4.	Bismarck, ND	27.	Memphis, TN
5.	Boise, ID	28.	Miami, FL
		29.	Minneapolis, MN
6.	Boston, MA	30.	Nashville, TN
7.	Brownsville, TX		
8.	Buffalo, NY	31.	New Orleans, LA
9.	Burlington, VT	32.	New York, NY
10.	Charleston, SC	33.	Oaklahoma City, OK
		34.	Omaha, NB
11.	Cheyenne, WY	35.	Philadelphia, PA
12.	Chicago, IL		
13.	Cincinnati, OH	36.	Phoenix, AZ
14.	Denver, CO	37.	Pittsburgh, PA
15.	Detroit, MI	38.	Portland, ME
		39.	Portland, OR
16.	El Paso, TX	40.	Raleigh, NC
17.	Fort Worth, TX		
18.	Fresno, CA	41.	Richmond, VA
19.	Great Falls, MT	42.	Salt Lake City, UT
20.	Honolulu, HI	43.	San Diego, CA
		44.	San Francisco, CA
21.	Houston, TX	45.	Seattle, WA
22.	Jacksonville, FL		
23.	Kansas City, MO	46.	St. Louis, MO
24.	Lake Charles, LA	47.	Tulsa, OK
		48.	Washington, D.C.

*This work was supported by the Assistant Secretary for Conservation and Renewable Energy, Office of Buildings and Community Development, Buildings Division of the U.S. Department of Energy under Contract No. DE-AC03-76SF00098.

insulation including R-0, R-11, R-19, and R-27 levels; window glazing, either single, double, or triple; foundation insulation including R-5 and R-10 exterior perimeter insulation or no insulation (R-0) for all three foundations, varying in depth from two feet (slab on grade) to eight feet (basement), and R-0, R-11, and R-19 floor insulation for basements and crawl spaces. The average rate of infiltration for the five winter months (November-March) was 0.7 air changes/hour (ach) for the normal case and 0.4 ach for the tight case (both numbers include 0.1 ach due to the building operation, i.e., opening doors, windows, etc.). Equipment modeled included furnaces, air conditioners, and air-to-air heat pumps.

The DOE 2.1A computer program was used in all of the analyses to simulate the hourly performance of buildings. The standard output (public domain version) of the program was modified to extract a significant amount of information for each production run. This information is stored on tape for future use by homebuilders, architects, homeowners, and loan officers after an appropriate data base is developed early next year.

At the present time, a summary sheet of the energy consumption (heating and cooling) is given for any given building type with all the various insulation options available in each city (Table 2). To facilitate the analysis, we have also developed a graphics output that generates 14 two-dimensional bar graphs and 4 three-dimensional graphs per run. Samples of the graphics output are shown in Figures 1 and 2.

During the past year, a number of improvements and additions were made to our modeling capabilities. First, in DOE 2.1, we improved the modeling of the performance of air-to-air heat pumps and air conditioners by using what we believe to be more appropriate full-load and part-load curves for residential-size equipment. We also improved our capability of modeling heat losses through a foundation by using a two-dimensional, steady-state, heat-flow model instead of the one-dimensional model traditionally used. Hence, we can model full basements, partial basements (basement and crawl space or basement plus slab-on-grade), slab-on-grade, and ventilated as well as unventilated crawl spaces. We have added water-to-air heat pumps to the existing heating and cooling systems. Groundwater temperatures to 100 feet for 48 cities can be obtained from a specially created library outside of DOE 2.1. Depending on whether or not the groundwater temperature for any given location is below or about 60°F, the appropriate full load curve of a low temperature or a standard water-to-air heat pump is used. An add-on or hybrid heat pump (heat pump and furnace) heating system, with the heat pump operating as long as outdoor dry bulb temperature is above or equal to 40°F, can now be modeled. Furthermore, a whole-house fan, operating when outdoor dry bulb temperatures do not exceed 82°F, can also be modeled now as a separate cooling system and in addition to an air conditioner.

Another major analysis activity during the past year was development of a package of sensitivity analyses that permitted trade-offs to be made among a number of different conservation measures, as well as selected items of user behavior and amenity changes such as different window areas and different thermostat settings. The work in this area of sensitivity analysis was reported in an energy conservation rating system for Minnesota. The computer runs were also made for a rating system in a warm climate, Riverside, California, but no rating system was produced. The purpose of the rating system was to focus attention on the most important trade-offs among different conservation measures.

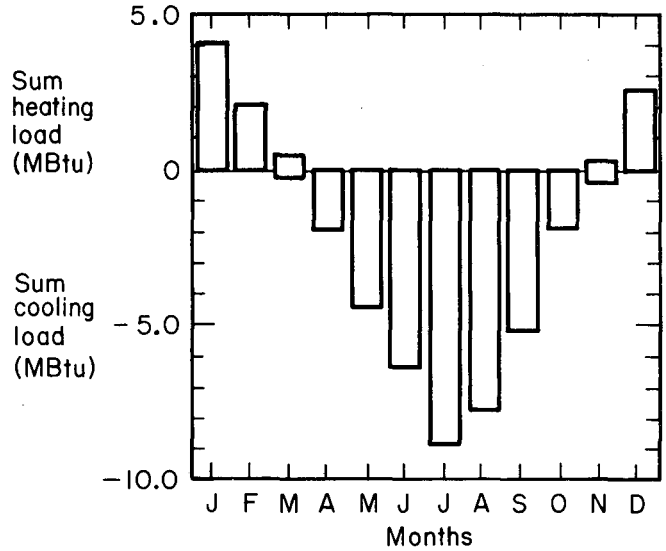

Month	Sum cooling load (MBTU)	Sum heating load (MBTU)
Jan.	0.000	4.065
Feb.	0.	2.094
Mar.	0.218	0.467
Apr.	1.897	0.000
May	4.381	0.
June	6.333	0.
July	8.819	0.
Aug.	7.695	0.
Sept.	5.116	0.
Oct.	1.859	0.000
Nov.	0.353	0.324
Dec.	0.000	2.588

Figure 1. Annual heating and cooling loads for one story, slab-on-grade house with R-30 ceiling insulation, R-19 wall insulation, R-5 perimeter slab insulation, 0.7 ach winter average infiltration and 2 glazings. (XBL 824-467)

Starting at the end of the past year and continuing into the next year, we are examining in great detail topics of special interest to energy-use management in residential buildings. A complete analysis of the management of heating energy requirements through temperature control has been completed. The effects of no temperature control, night set-back, and zonal control (day set-back) have been studied for various levels of building thermal-integrity and for the major climate zones in the country. Presently, we are examining the effects of microclimate modification (landscape) on

Table 2. Sample of summary output for one-story slab-on-grade house in Houston.

Code	Houston slab 1-story RC RW FLR IN GLS	Heating load, million Btu	Cooling load, million Btu	Heating energy, million Btu	Cooling, energy KWH	No. of hrs heated	No. of hrs cooled
A01	00-00-FM0-HI-1	36.393	58.794	51.991	7046.7	2170	3526
D01	19-11-FM0-HI-1	18.186	44.401	25.981	5566.2	1763	3836
E01	19-11-FM1-HI-1	14.701	40.174	21.002	5091.4	1542	3859
F02	19-11-FM1-HI-2	11.740	38.400	16.772	4898.1	1402	3928
G05	19-19-FM1-HI-2	10.522	37.629	15.032	4814.1	1345	3970
G01	30-11-FM1-HI-2	10.791	37.493	15.416	4797.4	1353	3960
H04	30-19-FM1-HI-2	9.578	36.734	13.683	4714.2	1291	3996
I07	30-19-FM1-HI-3	8.770	35.731	12.528	4600.6	1249	4009
I06	38-19-FM1-HI-2	9.234	36.387	13.191	4675.2	1270	4003
J06	38-19-FM1-HI-3	8.428	35.371	12.040	4559.9	1225	4010
K03	30-19-FM3-HI-3	8.284	35.080	11.834	4525.1	1191	3999
K01	38-19-FM3-HI-2	8.748	35.781	12.497	4605.4	1216	4002
L04	38-19-FM3-HI-3	7.949	34.781	11.356	4491.6	1175	4019
M03	38-27-FM3-HI-3	7.316	34.259	10.452	4432.0	1124	4018
H54	30-19-FM1-LO-2	6.338	33.644	9.055	4340.3	1053	4109
H04	30-19-FM1-HI-2-HP	9.552	36.735	3.612	4698.6	1273	3996

the heating and cooling loads of residential buildings. This work was prompted by another activity of the previous year involving the validation of the DOE 2.1 code. Simulation of the cooling energy requirements of measured data in Davis, California, during the summer of 1980 indicated that, for predicted and measured data to be compatible, landscape effects had to be properly taken into account. We have also attempted to validate DOE 2.1 by simulating the performance of 10 wood-frame, unoccupied houses built and monitored for one year (1977) by Owens-Corning. This work was concluded to the extent possible; a few critical data will not be released by Owens-Corning until early 1982. The results obtained thus far indicate a relatively good agreement between measured data and DOE 2.1 predicted values for the heating and cooling energy consumption of these buildings.

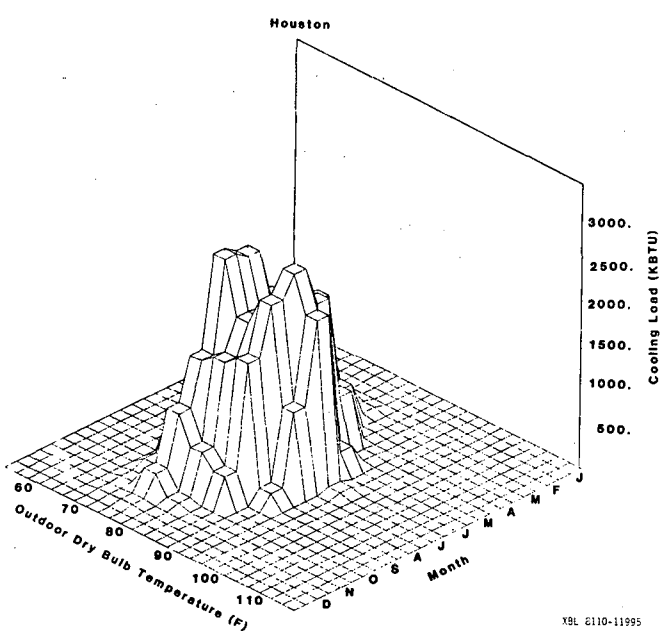

Figure 2. Annual cooling load binned by month and outdoor dry bulb temperature. (XBL 8110-11995)

Finally, effort was devoted to weather data related to the energy requirements of residential buildings. A program, CLIMA, under development for six months, will enable us to summarize weather data out of standard TRY or TMY tapes in a form that can be used for simplified energy calculations for buildings as well as other applications (design of equipment, etc.).

PLANNED ACTIVITIES FOR FY 1982

The analysis of residential buildings during FY 1982 will include completion of sensitivity studies involving building area, window area, window distribution, building construction materials, air infiltration, movable window insulation and shading, building internal loads, building shape, and equipment efficiency. In addition, the following tasks will be completed: weather program and attendant reports, the comparison and validation studies of DOE 2.1 with measured data, and development of a data base to facilitate access and dissemination of the DOE 2.1 results.

Assessment of Energy Conservation Rating Systems*

P. G. Cleary, J. G. Ingersoll, J. J. Mass, and M. D. Levine

There are at present a number of methods to estimate the average annual energy use of a residence. The simpler methods tend to be rather inaccurate, while the more accurate ones tend to be rather expensive. However, it is possible to process the results of computer-based calculations to construct a score card for energy-use estimation that is both accurate and simple and has wide-scale applicability. The processing method is a development of the effective degree-day method.

ACCOMPLISHMENTS DURING FY 1981

Energy Estimating Methods

Design Heat Loss and the Degree Day Method. It is not easy to estimate the annual heating load of a house because heat loss and gain are complex and dynamic. The traditional method used is the degree-day method, which assumes that solar heat and waste heat from appliances and occupants on the average will offset heat losses as long as the average outside temperature is greater than 65°F. The general equation for the method is

$$L = (H/t) \times DD \times 24$$

where

L = annual heating load, Btu per year
H = design heat loss, Btu per hour
t = design temperature difference, °F
DD = number of degree days, base 65°F

Note:
H/t includes infiltration losses; it is equivalent to UA, the overall heat transfer coefficient, Btu per hour per °F.

This method is admirably simple but not particularly accurate for today's houses. The number of degree days to base 65°F is not directly proportional to the heating load as calculated by hour-by-hour computer models. This is illustrated in Figure 1, which shows the results of calculations using the DOE-2 building energy-use model. It is clear that, although the load calculated by DOE-2 does vary almost linearly with design heat loss per °F, it does not pass through the origin as expected from the degree-day method. On the assumption that the hour-by-hour calculation is more accurate than the degree-day method, we explored simple methods to improve the agreement.

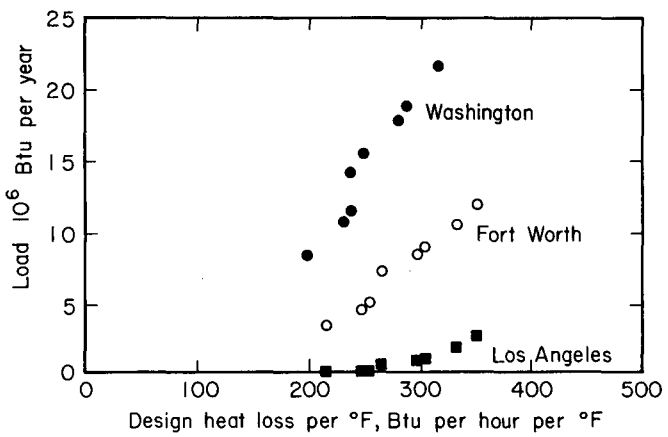

Figure 1. Variation of annual heating load with design heat loss per °F. Results of calculations with the DOE-2 building energy use model.
(XBL 824-462)

Interpolation Systems

Agreement can be improved by introducing an empirical constant to correct for the difference between degree days and heating load. However, a much greater improvement is possible by using the computer model to calculate the load of a base house and then using the degree-day model to extrapolate from the base house. The change in load is calculated as

$$L = (H/t) \times DD \times 24$$

A better fit may be achieved if a base other than 65° is used; by interpolating between two computed values of L an empirical value of DD can be found. The empirical DD is called the number of effective degree-days. Closer analysis reveals that it varies from component to component in a house. For example, in the Washington, D.C., house shown in Figure 1, the ceiling has approximately 5400 effective degree-days, while the walls have approximately 4200 effective degree-days. This suggests a final improvement: the load is best predicted by an equation of the form

$$L = Lbase + \frac{H_i}{t_i} \times D_i \times 24$$

where

Lbase = load of a base house, Btu per year

H_i = difference in design heat load of component i compared to the base house, Btu per hour

t_i = design temperature difference for component i, °F

*This work was supported by the Assistant Secretary for Conservation and Renewable Energy, Office of Buildings and Community Development, Buildings Division of the U.S. Department of Energy under Contract No. DE-AC03-76SF00098.

D_i = number of effective degree-days for component i.

This equation is an interpolation formula and can be expected to hold over small ranges where the contributions of all the components to the total load can be regarded as independent.

Extension of the Interpolation Formula

The linearity shown in Figure 1 suggests that the interpolation formula might hold over wide ranges of load. To test this hypothesis for commonly installed insulation values, the formula was rewritten:

$$L = L_{base} + f_1(R_{ceiling}) + f_2(R_{walls}) \ldots$$

Here, f_i is simply a table of difference in load from the base case caused by a change in component i. The functional form of f_i was not considered; it may be expected to be complex, because R_i is a proxy for the heat-transfer coefficient of the whole component. It is clear from comparing the two forms of the interpolation formula that, if the design heat loss per °F had been chosen as the variable, f_i would have been equal to 24 D_i times the difference in heat transfer coefficient. Table 1 shows a typical set of values of the interpolation function, f_i, for ceiling insulation for a 1540-square-foot light-construction ranch house in Minneapolis, Minnesota.

The house with R49 in the ceiling was chosen as the base house, and, therefore, the function is zero for this level of insulation. The numbers in Table 1 were obtained from five computer runs in which all house parameters except ceiling insulation level were kept constant at their base case values. The f_i for all other components can be found in the same way. The variables used need not be R-value: for windows, the parameters could be window area, window glazing, and window orientation; for night thermostat setback, the parameters could be simply yes or no for a well-defined setback.

To test the range over which the interpolation formula is accurate, a model house was set up for the DOE-2 computer program, and a number of calculations made for houses in Minneapolis, Minnesota, and Riverside, California, weather. A very wide range of component thermal resistances was used, although it was expected that the formula, with its implicit assumption that the heat loss through any component is independent of the total load, would only hold for a moderate range of loads. The interdependence can be considered as a variation in the number of effective degree-days. As the house becomes thermally tighter, more of its load is met by solar heat gain and by waste heat from appliances and occupants. The number of effective degree-days therefore decreases with the total house load, and f_i should become commensurately smaller. The results of the computer calculations for Minneapolis are shown in Table 2.

Table 1. Variation in annual heating load (10^6 Btu per year) caused by a change in ceiling insulation level in a Minneapolis house.

Insulation level	R19	R30	R38	R49	R60
Heating load change	8.1	3.3	1.5	0.0	-1.0
Cooling load change	0.7	0.3	0.1	0.0	-0.1

Range of Validity of the Interpolation Formula

If the interpolation formula were to apply accurately to all combinations of the variables given in Table 2, this table would be able to predict the energy consumption of over a quarter of a million different houses. For example, consider a Minneapolis house similar in construction to the base house but with R19 in the ceiling, R11 in the walls, no basement insulation, an infiltration rate of 0.67 air changes per hour, no night setback thermostat, with windows on the north-east and west sides totalling 15 percent of its floor area, with a south window of 2.5 percent of its floor area, all windows being single glazed. This house would, according to Table 2, have an annual heating load greater than the base house by

$$[8.1 + 9.7 + 16.6 + 9.6 + 2.3 + 31.7 + 4.6] \times 10^6 \text{ Btu per year}$$
$$= 82.6 \times 10^6 \text{ Btu per year more than the base house}$$
$$= 133.2 \times 10^6 \text{ Btu per year.}$$

Similarly, the cooling load would be 14.6×10^6 Btu per year. The table makes available sophistication of the hour-by-hour computer program in the format of a simple table. The possible advantages for energy auditors are obvious; a walkthrough audit

Table 2. Difference in annual heating loads for a Minneapolis house compared to the base house (annual heating load 50.6×10^6 Btu). Load differences are given in 10^6 Btu per year.

Ceiling insulation	R19	R30	R38	R49	R60	
Load difference	8.1	3.3	1.5	0.0	-1.0	
Wall insulation	R11	R19	R27			
Load difference	9.7	3.4	0.0			
Basement insulation	None	4' R5	4' R10	8' R5	8' R10	R19
Load difference	16.6	8.9	5.5	4.8	0.0	-1.6
Infiltration (ach)	0.67	0.50	0.33	0.17		
Load difference	9.6	0.0	-9.5	-18.6		
Setback thermostat	Yes	No				
Load difference	0.0	2.3				

Glazing as a Percentage of Floor Area

(a) North + East + West	Single	Double	Triple
2.5%	3.5	-0.3	-1.5
5%	9.1	1.5	-0.8
7.5%	14.8	3.5	0.0
10%	20.4	5.4	0.8
15%	31.7	9.3	3.7
(b) South glass	**Single**	**Double**	**Triple**
2.5%	4.6	1.0	0.0
5%	8.3	1.2	-0.8
7.5%	12.1	1.5	-1.6
10%	15.9	1.8	-2.3
15%	23.6	2.7	-3.3

Note:
Setback is from 70°F to 60°F from midnight to 6 a.m. R19 basement insulation is in floor.

could well produce the same results as a time-consuming individualized computerized audit, provided the interpolation formula holds. It is therefore important to examine its accuracy. One systematic way of doing this is to construct a series of houses, ranging from very loose to very tight, and to compare the load predicted by Table 2 with the value obtained by an individualized DOE-2 run. At the two locations mentioned earlier, Riverside, California, and Minneapolis, Minnesota, two series of model houses were set up, starting with a house with the most energy-consuming options listed in the tables. These houses were transformed, one component at a time, into the base houses, and then transformed, again one step at a time, into the tightest houses possible.

The values predicted by the interpolation formula are very close to those predicted by DOE-2 runs. For Riverside, the heating loads agree to within 15 percent except for the very tightest house. The cooling loads in Riverside agree to within 5 percent. For the Minneapolis house, the heating loads agree to within 5 percent, while the cooling loads agree to within 10 percent. It was not expected that the agreement would be this good, nor that it would hold over such a broad range of loads.

It should be noted that this conclusion applies only to those measures considered here: ceiling insulation; wall insulation; floor insulation; window size, glazing, and orientation; infiltration rate; and thermostat setback. There are a number of parameters which were not varied, including thermostat setting (except for night setback), cooling schedule, thermal mass, floor area, and shading. For example, exploratory DOE-2 runs for cooling loads in Davis, California, indicate a strong interaction between infiltration reduction and cooling schedule and systematically higher cooling loads per unit area for smaller houses.

Point Systems

For houses within the region where the total house load is well predicted, the interpolation formula may be used as the basis of a simple rating system. If the system is required to predict the heating and cooling loads, the figures in Table 2 can be used. If the system is required to produce an overall figure of merit for heating and cooling energy use, the values in the tables can be multiplied by appropriate conversion factors to account for heating and cooling system efficiency. For example, if the chosen figure of merit is the resource energy used per square foot of floor area per year, the conversion factors are

Heating factor =
$\text{Area}^{-1} \times \text{Efficiency}^{-1} \times \text{Resource factor}$

Cooling factor =
$\text{Area}^{-1} \times \text{COP}^{-1} \times \text{Resource factor}$

For the house in Minneapolis with gas heating efficiency of 70 percent, electric cooling (SEER 5.3), and an area of 1540 square feet, these factors are 0.93 and 1.23, respectively. The units are thousands of Btu of resource energy per square feet per year, with electricity counted at 11,600 Btu per kWh. For the sake of brevity, this unit is called one "point," and the method used to produce it a "point system." A table of points for the Minneapolis house is given in Table 3.

This table, with sub-tables to correct for different heating and cooling system efficiencies, may now be used to rate Minneapolis houses, with over 150,000 different combinations of components. The points for each component are simply added. For the vast majority of these houses, the rating provided by such a point system will be within 10 percent of the rating that would have been produced had an individualized DOE-2 run been made, providing that there are no gross differences between the base house and the rated house in parameters for which points are not awarded. For example, these parameters include size, shape, and window shading. The points system does not account for behavioral and other effects which tend to make actual energy use different from calculated energy use. It is no more or less than a simplified method of presenting processed results of computer calculations. There is no limitation on the computer models used to construct the point system. As long as the measures considered do not interact substantially over the range of houses to be considered, any model may be employed.

Conclusion

The point system presented can be used for ranch houses in Minneapolis. It would be extremely simple to develop a similar system for another house type in another weather zone, perhaps using another building energy model. The interpolation method on which the system is based was tested for a series of houses in Riverside, California, and Minneapolis, Minnesota, weather. The hypothesis of linear additivity of load contributions from all components of the house was found to hold over a

Table 3. A point system for Minneapolis single-family homes, gas or oil heated.

Ceiling insulation	R19	R30	R38	R49	R60	
	8.4	3.4	1.5	0.0	-1.1	
Wall insulation	R11	R19	R27			
	9.6	3.3	0.0			
Basement insulation	None	4' R5	4' R10	8' R5	8' R10	R19
	16.2	8.6	5.4	4.6	0.0	-0.9
Infiltration	Loose	Standard	Tight	Very Tight		
	9.1	0.0	-9.1	-17.7		
Setback thermostat	Yes	No				
	0.0	2.1				

Glazing as a Percentage of Floor Area

(a) North + East + West	Single	Double	Triple
2.5%	0.8	-3.0	-4.3
5%	7.7	0.2	-2.2
7.5%	14.9	3.6	0.0
10%	21.9	7.0	8.8
15%	36.2	14.1	6.8
(b) South glass	**Single**	**Double**	**Triple**
2.5%	4.6	1.1	0.0
5%	9.8	2.7	0.6
7.5%	15.3	4.7	1.3
10%	20.7	6.7	2.4
15%	32.2	11.2	4.8

Note:
R19 basement insulation is in floor. Thermostat setback is from 70°F to 60°F from midnight to 6 a.m.

rather wide range. It predicted heating and cooling loads within 15 percent of those predicted by individualized DOE-2 runs, except for some nonphysical negative heating loads. However, the difference in load caused by a change in one component is less well predicted. The predicted load changes from a thermostat setback in loose houses in both Riverside and Minneapolis were in error by almost a factor of five. The method could be improved, at the expense of added complexity, by the addition of cross terms to account for the interaction between components.

PLANNED ACTIVITIES IN FY 1982

This work was concluded in FY 1981 and will not continue in FY 1982.

Determinants of Residential Energy Use*

P. P. Craig, J. C. Cramer, T. M. Dietz, B. Hackett, D. J. Kowalczyk, M. D. Levine, and E. L. Vine

Lawrence Berkeley Laboratory, in conjunction with a number of other cosponsoring organizations,† is investigating residential energy consumption in the cities of Davis and Lodi, California. Data from this project are being used as input to the DOE-2.1 energy-use model to validate the model's energy-use estimates for residential buildings. The project data will allow validation checks for projections of hourly and weekly electricity use and for annual and monthly electricity and gas use. A second goal of this investigation is the construction of a multiple regression model that combines physical characteristics of a residence with appliance information, occupant behavioral information, occupant attitudes, demographics, and weather variables for explaining the variation in monthly energy use. A third and final goal of this project is the evaluation of utility-sponsored and locally run community electricity management programs in Davis and Lodi through the use of survey results and the analysis of actual billing data.

ACCOMPLISHMENTS DURING FY 1981

Data Collection

During the summer of 1980, 241 surveys were administered to a systematic random sample of Davis residents. To obtain hourly meter readings of electricity use, the sample had to be selected within a single electrical circuit served by the local utility company, Pacific Gas and Electric Company (PG&E). There are eleven circuits in Davis. Therefore, the sampling area was defined by the boundaries of a PG&E circuit that serves approximately 2,000 customers. This circuit was selected because more than 95 percent of the circuit's load was residential with only a small (540) commercial customers' contribution. PG&E recorded the electricity readings each half hour for the circuit. PG&E also provided monthly billing information for the entire survey sample under the condition that their customer's billing information remain confidential. Only adults over 18 years of age were interviewed. An 80 percent response rate was achieved in the Davis survey. The average length of the interview and the energy audit was approximately 75 minutes.

The questionnaire used in the survey consisted of two sections. The first section included information on the resident's life style, demographics, energy-use attitudes, energy knowledge, and appliance-use behavior. The second section gathered information on building characteristics such as type of wall construction; orientation; wall, window, floor, and ceiling areas; and appliances. The survey was administered by paid interviewers who received building audit training from a PG&E auditor.

Weather data for the project were provided by the University of California Davis Campus Climatic Station, which is partially funded by a Department of Energy grant to gather detailed solar radiation data. Hourly data for the following key weather variables were supplied by the station for this project: total radiation on a horizontal surface, direct normal radiation, dry bulb temperature, dew point temperature, pressure, wind speed, and wind direction.

Because one of the principal goals of this investigation is to validate the DOE-2.1 energy model, detailed information on internal house temperatures and infiltration rates was required. A subsample consisting of 50 households was randomly selected from the larger sample to participate in a phase of the project that gathered continuous data on internal house temperatures. Also, weekly electric meter readings for the subsample were recorded for an eight-to-ten week period from mid-August through early October.

*This work is supported in part by the Assistant Secretary for Conservation and Renewable Energy, Office of Buildings and Community Systems, Systems Analysis Division, U.S. Department of Energy under Contract No. DE-AC03-76SF00098.

†Kellogg Public Research Program, University of California, Davis; Pacific Gas and Electric Company, San Francisco, Calif; Center for Environmental and Energy Policy Research, University of California, Davis; and the California Energy Commission, Sacramento, Calif.

To characterize the infiltration rate of the houses, air pressurization measurements were taken with blower-door equipment made available by the LBL air-infiltration group. Air pressurization data were obtained for approximately 70 percent of the subsample.

During the summer of 1981, interviewing in Lodi was started; as of November 1, 1981, approximately 200 households had been interviewed. In contrast to the Davis survey, a reverse street directory was used for sampling, and a systematic random sample of the entire city was conducted. PG&E will again provide monthly billing information on gas use for the entire sample under the condition that their customer's billing information remain confidential. The City of Lodi will provide monthly billing information on electricity use for the entire sample under the same condition (Lodi purchases electricity wholesale from PG&E). Only adults over 18 years of age have been interviewed.

The questionnaire used in the Lodi survey is very similar to the one used in the Davis survey. The survey has been administered by paid interviewers who received building audit training from one of the members of the Davis Energy Group. Weather data for the project will be provided by the Stockton Weather Station, the nearest weather station. As in Davis, a subsample consisting of 49 households was randomly selected from the larger sample to participate in a phase of the project that gathered continuous data on internal house temperatures.

Analysis

The survey and billing information along with the more detailed engineering data on the subsample houses have been used for validating the DOE-2.1 model, for constructing a structural-behavioral regression model, and for evaluating peak-load management programs.

DOE-2.1 Validation. The U.S. Department of Energy's computer model (DOE-2.1) is currently being used by energy analysts for calculating energy use in residential and commercial buildings. To build confidence in the usefulness of this model, there is a need for comparing measured energy use with predicted energy use. The first part of the "validation process" was conducting sensitivity analyses on a "base case house." This house was constructed using the average values of key physical characteristics of single-family detached houses in the Davis sample. The "base case house" consisted of a one-story detached building with the following characteristics: wood frame construction with R-11 wall and R-19 ceiling insulation; slab-on-grade foundation with floor area 1975 square feet; window area 300 square feet with single glazing; glazing area shaded 50 percent and distributed equally on all four sides; wall area 1750 square feet; air conditioner with an EER of 7.1; summer thermostat setting 70°F operated between the hours 1200 and 2300; night venting (window opening) occurred down to 72°F outdoor temperature from 2300 to 0700 hours; natural-gas heating system; and house oriented north-south. Sensitivity analyses were conducted on the following parameters: summer thermostat setting, summer air conditioner operating schedule, infiltration level, wall and ceiling insulation level, house orientation, shading percentage and distribution, glazing area distribution, floor area, venting schedule, and foundation type. Many runs were conducted to determine the effect of the change in these parameters on the cooling load for three months in 1980 (July, August, and September).

In brief, the change in cooling load was linearly related to changes in all of the parameters examined. For example, it was discovered that a one-degree increase in the thermostat setting resulted in an increase of about 174 kWh in the cooling load. It was also found that varying the infiltration level from 0.45 air changes per hour to 0.64 air changes per hour had only a slight effect on the cooling load. It is important to note that air infiltration--the leakage of air through cracks, crevices, fan openings, and various other places in the building--may be a more important factor in the heating season. Similarly, the change in orientation of the house, change in wall and ceiling insulation levels, and change in insulation levels of the foundation produced comparatively small effects on the cooling load. The insulation effects are not very surprising because conductivity is not as important as direct light in the summer; in the winter, however, conductivity plays a more important role. In terms of their effect in the cooling load the most important parameters, were: thermostat setting, air conditioning schedule, floor and glazing areas, shading of glazing, and venting.

In the second part of the "validation process," the results of the DOE-2 sensitivity runs have been incorporated into a "point system," a series of equations containing key building parameters and coefficients derived from DOE-2 results. Preliminary analysis of a subset of 18 single-family detached homes has indicated that the Davis point system is a very good predictor of cooling loads in comparison with measured data provided by PG&E. For example, in difference-of-means tests, the point system was not significantly different at the 0.01 level than measured data provided by PG&E, the difference in means being 86 kilowatt hours over a three-month period. Future work will emphasize the refinement of the point system on larger samples and on different building types.

Regression Model. Previous research on energy consumption in the residential sector has emphasized structural features of residences, e.g., window area and floor area, for the modelling of energy use in the household. More recently, appliance-use behavior has been incorporated into these studies to improve the accuracy of these energy models. Except for a few studies, social and economic characteristics of occupants have not been included in the analysis of energy use in the residential sector. In this investigation, detailed information on physical characteristics of residences, social and economic characteristics of residents, and appliance-use behavior was collected to construct a regression model of residential energy consumption that combines these types of data for explaining the variation in monthly energy use.

The multiple regression model for predicting energy use in the residential sector is being developed in several phases. In the first phase, a model using structural and behavioral determinants was constructed and run on all the building types in our sample during the cooling season. This model is discussed in this report. Later analyses will construct a similar model for the heating season and for total energy use. In addition, other models will include demographic data as well as additional attitudinal and behavioral information, and these models will be tested during the cooling and heating seasons, as well as for the entire year. All of these models will be tested with the Lodi data in order to see how generalizable the results are.

Prior to constructing the structural-behavioral regression model, several parameters were selected from the survey and energy audit for statistical analyses: wall and ceiling insulation levels, floor and glazing areas, number of rooms, orientation of house, frequency of air conditioner use, venting, glazing shading areas, air conditioner settings and schedules, and a constructed conductivity measure. Bivariate correlation analysis was performed on single-family detached buildings with one of the correlates always being the amount of electricity consumed in July, August, and September (TELEC). The only variable that was statistically significant at the 0.05 level was floor area. Next, multiple regression analysis was conducted with the dependent variable being TELEC and with the above parameters as the selected independent variables. Stepwise regression was used, and many combinations of variables were tested to find the best equation. The models were run separately on single-family detached homes, all other households (e.g., apartments, duplexes, and single-family attached houses), to discover the independent variables which were statistically significant at the 0.05 level and to find out that model which explained the most variation in electricity use, i.e., high R^2. After testing for interaction effects and nonlinearity and examining the problem of multicollinearity, where independent variables are highly correlated with one another, a final structural-behavioral regression model was constructed:

Total Electricity (kWh) = -1093.29 + 229.53 (Frequency of Air Conditioner Use) + 0.65 (Appliance Saturation Index) + 0.80 (Floor Area) + 512.26 (Building Type)

The standardized form of this equation is

Total Electricity (kWh) = 0.40 (Frequency of Air Conditioner Use) + 0.54 (Appliance Saturation Index) + 0.62 (Floor Area) + 0.10 (Building Type)

where:

1. Frequency of Air Conditioner Use is coded from 0 (never) to 4 (always)
2. Appliance Saturation Index is composed of the following electrical appliances: water heater, clothes dryer, clothes washer, oven, refrigerator, freezer, dishwasher, and swimming pool filter/pump
3. Building Type is coded (1) single family detached and (0) for all other building types.

This model explains 73 percent of the variation in electricity use in the cooling season for all of the households in the Davis sample. In terms of the importance of the various parameters in the model, using the standardized coefficients as the basis of comparison, floor area is the most significant predictor followed by appliance saturation, frequency of air conditioner use, and building type.

Evaluation of Peak Load. During the summer of 1980, the City of Davis and PG&E implemented the first year of a two-year experimental peak-electricity load-management program named Prime Time. The program was based on the principle of implementing peak electricity-use reduction behaviors via goal-setting, community and individual financial incentives, and feedback. Similar programs were implemented in Chico and Merced in 1980 and in Lodi and Eureka in 1981. Unlike the Davis program, the Lodi program was scheduled to run for one year only.

In these programs, residents were asked to reduce their weekday use of electricity during a specified afternoon time period (in Davis, from noon to 6 P.M.). Throughout the program, literature drops, newspaper, radio, and television reports, and a wide variety of special community events organized by citizen activists and civic leaders brought the message of peak-load management to the public. The program's success is measured by reductions in peak demand in the experimental year compared to a control year. In Davis, each one-percent reduction in peak demand earned the city $10,000, up to a $100,000 limit, from PG&E.

Based on responses to questions in our survey, approximately one-half of the respondents reported that they were participating in the Prime Time program. Most of the other people stated that they either had not heard of the program (mostly people in apartments, where the program was not well publicized) or could not reduce afternoon electricity use because they already used so little. Many people responded to the program by reducing their total consumption of electricity rather than merely shifting consumption from afternoon to morning or evening. By comparing participants and non-participants, the average household saving of electricity due to the Prime Time program was estimated to be about seven to eight percent. Over one-half of this saving was accomplished by the reduced use of air-conditioning; the rest was due to a wide variety of conservation behaviors.

PLANNED ACTIVITIES IN FY 1982

For the Davis program, the point system will be refined for improving the validation process of the DOE-2.1 energy model, and regression models will be constructed for the heating season and for the entire year. It is also expected that an hourly electricity demand curve will be synthesized by DOE-2.1 and compared to actual circuit data on an hourly, daily, weekly, and monthly basis. For the Lodi program, all data collection activities will be completed, and data analysis will follow the procedure used in the Davis program.

Analysis of Energy Conservation Measures in Commercial Buildings*

I. Turiel, D. A. Boschen, M. D. Levine, J. R. Smith, and M. Zentner

An energy and life-cycle cost analysis was made of a six-story, 100,000-square-foot office building. The building energy analysis computer program, DOE-2.1, was used to obtain annual energy consumption by end use.[1] Annual energy used for the base-case building and for several energy-conserving designs, plus initial added cost of the energy-conserving measures, served as input to a life-cycle cost model (LCCM). The LCCM is used to assess the economic costs and benefits, with reference to a base-case building, to the commercial building owner who constructs a new building of varying initial cost and energy efficiency. The conservation measures that were evaluated include

1. Building orientation,
2. Added insulation,
3. Single and double glazing with varying solar transmission,
4. Use of daylighting, and
5. Use of night setback thermostats.

ACCOMPLISHMENTS DURING FY 1981

Many assumptions must be made concerning the base-case building's operating conditions and characteristics before its operation can be simulated with DOE-2.1. Our main source of information about appropriate assumptions is included in a report prepared for the Department of Energy (DOE).[2] It contains occupancy, lighting and hot-water use schedules, thermostat set points, etc., intended for use in obtaining the design energy consumption for various commercial building types.

Figure 1 shows the annual energy use profile for a six-story office building located in Denver, using a 1971 NOAA weather tape. This building is one of those studied during Phase II of the DOE Building Energy Performance Standards (BEPS) project.[3] The lighting load in the DOE-2.1 simulation is 2.6 W/ft^2, and the ratio of window to wall area is 25 percent. Cooling and space heating are provided by a zoned, water-to-air, unitary heat pump system with a circulating water loop. A 300-kW electric boiler provides heat generation to maintain the water temperature above 60°F. Also shown in Figure 1 is the peak demand for each month in kW. For this building type in Denver's climate zone, energy consumption and peak demand are greatest in the winter months. The total annual energy use is approximately 50,000 Btu/ft^2.

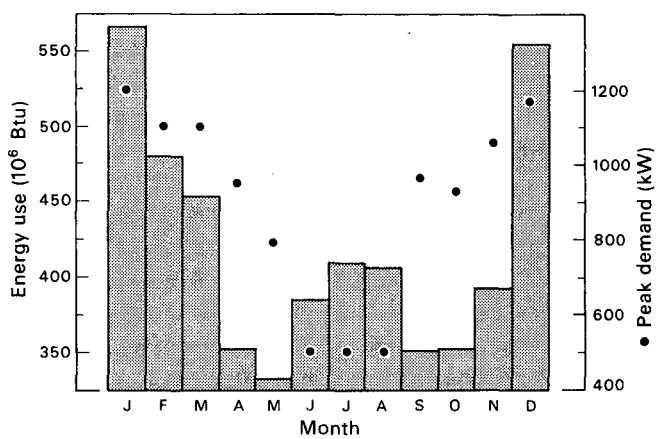

Figure 1. Total building site energy use and peak demand are shown for each month for a six-story office building in Denver, Colorado.

(XBL 815-879)

Energy Analysis of Redesigned Buildings

Glazing Choice and Use of Daylighting. Figure 2 shows the results of a parametric energy analysis of the office building located in Denver to determine the dependence of space conditioning energy use on the solar transmission of both single and double glazing. Changes in heating and cooling energy consumption tend to cancel each other when the transmission of the windows is varied. Figure 2 also shows that space conditioning energy use is approximately 25 percent lower for double pane as compared to single pane windows of the same solar transmittance.

*This work was supported by the Assistant Secretary for Conservation and Renewable Energy, Office of Buildings and Community Systems, Buildings Division of the U.S. Department of Energy under Contract No. DE-AC03-76SF00098.

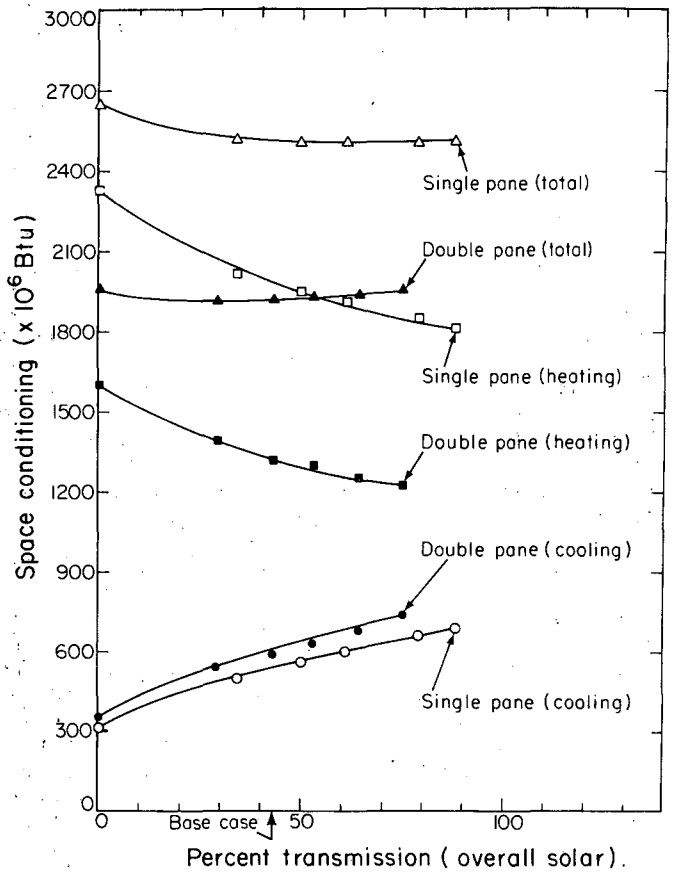

Figure 2. Space conditioning energy use is shown as a function of overall solar transmission for single and double pane windows. (XBL 813-578)

The weak dependence of the total space conditioning energy use on the solar transmittance of the glazing is a very important finding; it implies that in a climate zone similar to Denver's, the maximum benefit from the use of daylight to offset electric lighting consumption will occur when the glazing with the maximum visible light transmission is utilized. In the daylighting analysis, we assumed that lighting existed throughout the building perimeter at a level of 50 foot-candles and that the maximum lighting power reduction was 70 percent for the base-case building power use when the daylight availability reached 50 foot-candles. We also assumed that only diffuse sky light is used as a substitute for electrical lighting in order to minimize glare which would otherwise result from direct sunlight. The reduction in power use is achieved through a dimmable lighting-control system actuated by photoelectric sensors. The lighting schedules were modified in the perimeter zones, 40 percent of building floor space, for each orientation and for each of the four seasons of the year. Details of the method of analysis are discussed in a report prepared by LBL's Windows and Lighting Group.[4]

Table 1 shows energy consumption by end use for double pane windows with and without daylighting. It can be seen that daylight utilization allows a reduction in energy used for cooling, lighting, and fans. At the same time, it increases the energy required for space heating. The net result is a reduction in total building energy use; the maximum reduction is approximately 10 percent for double pane windows in the Denver climate zone.

A parametric energy analysis was also carried out for varying amounts of roof and wall insulation.[5] The maximum reduction in total energy use is quite small, between 2 and 3 percent for 12 inches of fiberglass insulation as compared to 3 inches of fiberglass insulation in both cases. The cost benefit analysis is discussed in a later section.

Other Energy Conserving Measures

Many other energy conserving measures were assessed in the six-story office building located in a Denver climate zone. A few are discussed below. The first measure, changes in orientation, produces less than a one percent change in total energy use. The original orientation of the building, with dimensions of 70 feet by 210 feet, is with the long axis oriented northeast to southwest at an angle of 60° east of north. The other two orientations that were simulated are a due north and a due east orientation for the long axis. All windows were set back one foot.

Table 1. Energy use as a function of glazing type and daylighting utilization in a six-story office building in Denver.

Site energy use, 10^6 Btu	Double-Pane					
	Base case bronzed glass	Base case daylighting	Clear glass, no daylighting	Clear glass, daylighting	Blue-green glass, no daylighting	Blue-green glass, daylighting
Space heating	1332	1423	1253	1357	1332	1445
Space cooling	586	509	685	586	586	498
HVAC auxiliary	50	48	55	53	50	48
Domestic hot water	409	409	409	409	409	409
Lights	2568	2167	2568	2095	2568	2108
Vertical transport	93	93	93	93	93	93
Total	5038	4649	5062	4594	5038	4601
% Hours, any zone Outside throttling range	7.9	8.1	8.9	8.6	7.9	8.1

Altering the thermostat setpoints produces a significant change in energy use. The base-case building utilized heating and cooling thermostat setpoints of 72°F and 77°F, respectively. Widening the deadband (temperature range where neither heating or cooling takes place) so that the setpoints are 69° and 81°F, respectively, results in a 6-percent decrease in total annual energy use. This is not a very large change in total annual energy use considering the large increase in deadband width from 3° to 10°F. The heating energy use, however, decreased by 23 percent and the cooling energy use by 7 percent. Because energy used for space heating is approximately one-fourth of the total energy use, a relatively large change in that end use resulted in only a 6-percent change in total energy use.

We have also studied the effect of varying the night setback temperature on total building energy use. The base-case building was modeled with a 60°F night setback temperature from 6:00 P.M. to 6:00 A.M. Monday through Friday and all day weekends and holidays. Reducing the night setback temperature to 55°F produces less than a one percent reduction in annual energy use. Removing the night setback entirely increases energy use by 8 percent.

A reduction of the electric lighting power density to 1.5 w/ft^2 from 2.6 w/ft^2 reduces annual energy use to 4100 x 10^6 Btu. Further investigation is necessary before we can determine if the comfort or productivity of building occupants would be affected by this energy-conserving measure.

Cost Benefit Analysis

Methodology. We applied the methodology of life-cycle cost analysis to the evaluation of the economic costs and benefits to the commercial building owner who constructs a new building with varying initial costs and energy efficiency. There are a number of economic parameters that may be evaluated to rank a series of potential capital investments: rate of return, net present benefit or life-cycle cost reduction, payback period, and benefit-to-cost ratio. All of these, except payback period, yield the same rank ordering when a list of potential investments of equal lifetime and cost is prioritized.

The life-cycle cost of owning and operating a building is equal to the purchase price plus the operating and maintenance costs over the lifetime of the building. In our analysis, we assumed that the purchase price is financed by a loan. The major inputs required for performance of a life-cycle cost analysis are initial cost, annual energy use, and an assortment of energy-cost and financial factors. Energy-cost factors include initial fuel costs, fuel-cost escalation rates, and peak-power charges. To rank a number of potential capital investments, energy-conserving measures or otherwise, a profit-making organization should consider the effects of taxes, depreciation, and the cost of capital. The LCCM developed at LBL takes account of these factors and computes all the economic parameters mentioned above. In developing this model we assumed that all expenses and revenues would not be known, and we therefore calculated differences in LCC between redesigned and base-case buildings. We assumed that unknown costs and revenues, such as insurance, property taxes, and rental income, remained constant as energy use varied.

It is important to consider the effect of taxes in the cost-benefit analysis because a reduction in energy use causes a decrease in expenses and corresponding increase in taxable income and, therefore, taxes. Hence, the benefit derived from an energy-conserving investment is lessened when it is appropriate to consider taxes. To compute taxes owed (one of the costs in total LCC), it is necessary to determine the annual cash flow before taxes. We make the conservative assumption, i.e., it lowers benefits, that revenues in the form of rental income are unchanged when the building is constructed in a more energy-efficient manner.

One of the objectives of the life-cycle costing process is the minimization of total cost or maximization of net benefit to the building owner. The net present benefit is essentially the difference between after-tax, energy-cost savings and initial investment, with proper discounting and energy-cost escalation. If the more efficient building design results in greater net benefit to the owner-builder over the lifetime of the building, the owner-builder benefits although a higher initial capital outlay may cause an adverse impact in the short run. This potential problem of higher first costs associated with greater net benefit of more energy-efficient buildings will be assessed in terms of a payback period, that is, the time required for the investor to recoup his or her additional investment in a more energy-efficient building.

Assumptions. The results of the economic analysis depend on estimates of several factors. These include discount rate, fuel-price escalation rate, initial fuel price, and additional cost of the conservation measure. Because there is almost always some uncertainty in projecting values of these parameters, a sensitivity study was performed. The Base-Case parameters are described below.

We chose an economic life time for the building and a loan amortization period of 25 years for our basic economic studies. The loan interest rate, discount rate, and fuel escalation rate were chosen to be 3, 3, and 2.5 percent real, respectively.[6] The initial electricity price, $0.023/kWh, and peak demand charge, $8.18/kw, were obtained from the Public Service Company of Colorado.

We assumed no change in maintenance costs and a 50 percent tax rate for all of our economic studies. Although we calculated all economic parameters for three depreciation methods (straight line, sum of years, double declining balance), we have only included results obtained from the first method because there was little difference in the final results among the three methods. However, the pattern of cash flow is altered by varying the method of depreciation. The cost of the various

conservation measures was obtained by telephone calls to equipment suppliers and from two other construction cost sources.[7,8]

Results. A cost-benefit analysis was made of varying amounts of roof and wall insulation, respectively. The added initial cost of the conservation measures includes only the added cost of insulation material and labor but not any other potential costs of additional framing. It appears to be cost-effective to use as much as 12 inches of roof insulation in the Denver climate zone. The payback period for 12 inches of insulation, relative to the base case of 3 inches, is 5.8 years. Many builders of commercial buildings may choose option 2, 6 inches of insulation, of this conservation measure because of its much shorter payback period (3.1 years). For energy-conserving measures in existing commercial buildings, the desired payback period is usually two to three years or less.[9] When wall insulation thickness is varied and roof insulation thickness remains constant at six inches, we find nine inches to be the greatest thickness of insulation that is cost effective. However, the payback period of seven years will probably discourage most builders from going beyond six inches of wall insulation (R-19). As stated earlier, the energy savings derived from increasing insulation are very small, and the cost of the conservation investment may be somewhat underestimated.

The cost-benefit analysis just described was also carried out for a building being designed by a non-profit-making organization such as a government agency. In this case, there are no tax considerations. As expected, the benefit-to-cost ratios of all measures increase by approximately a factor of two, and all the payback periods decrease by approximately a factor of two. Therefore, all conservation measures are more cost-effective when taxes are not one of the costs.

We have performed a cost-benefit analysis of different glazing types with and without daylighting. Figure 3 illustrates the relationship between the net present benefit, relative to the base case, derived from each conservation measure and the annual energy use. The maximum net present benefit occurs at a site energy use of approximately 47,000 Btu/ft^2 although there is less than a 10 percent difference in the net present benefit for double-pane glass with reflective coating (31 percent reflectance for overall solar spectrum) and blue-green tinted double-pane glass with daylighting. There is, however, a large increase in the discounted payback period from 1.7 to 5.5 years; this may discourage profit making organizations from making the added initial investment of approximately $27,000.

Sensitivity Studies. The sensitivity of the results described above to variations in a number of parameters was studied. The position of the maximum in net present benefit was unchanged by all of the following variations, made one at a time. We assessed variations in the fuel price escalation rate of zero to 5 percent real, discount rate of 1 to 6 percent, economic lifetime of 10 to 25 years, tax rate of 0 to 50 percent, depreciation period of

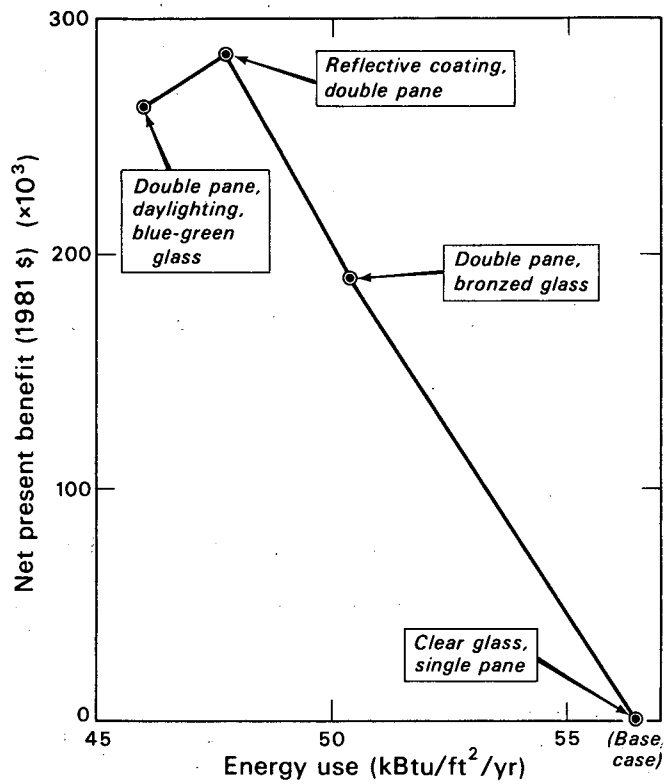

Figure 3. The relationship between net present benefit and energy use is shown for several measures in a six-story office building in Denver, Colorado. (XBL 815-877)

5 to 15 years, and initial cost of ±50 percent of original values. The marginal benefit to cost ratios are sensitive to values of the above parameters, particularly for daylighting relative to the reflective coating option.

PLANNED ACTIVITIES FOR FY 1982

We will study the sensitivity of office-building energy consumption by end use to variations in more than twenty design parameters in five climate zones. Simplified techniques for calculation of energy use will be developed. Lastly, we will compare DOE-2.1 energy-use predictions to actual energy use for one office building.

REFERENCES AND FOOTNOTE

1. Lokmnhekim, M., et al. (1979), DOE-2: A New State of the Art Computer Program for the Energy Utilization Analysis of Buildings, Lawrence Berkeley Laboratory Report LBL-8974, Berkeley, Calif.

2. Fleming, W.S., and Associates (1981), Draft Recommendations for the Standard Evaluation Technique (SET) of the Building Energy Performance Standards (BEPS), Landover, Md.

3. American Institute of Architects (1979), Life-Cycle Cost Study of Commercial Buildings, Final Report by American Institute of Architects (AIA) for Department of Energy, Washington, D.C.

4. Selkowitz, Steve (1980), Procedure to Estimate Savings with the Use of Day-Light in Buildings for BEPS Analysis, Lawrence Berkeley Laboratory Report (in draft form).

5. Turiel, I. (1981), Energy and Life-Cycle Cost Analysis of a Six-Story Office Building, Lawrence Berkeley Laboratory Report LBL-12387.

6. At a 10-percent annual inflation rate, these rates are 13, 13, and 12.5 percent, respectively.

7. Lee Saylor, Inc. (1981), Current Construction Costs 1981, Walnut Creek, Calif.

8. Winkelmann, F.C., and Lokmanhekim, M. (1981), Life-Cycle Cost and Energy-Use Analysis of Sun-Control and Daylighting Options in a High Rise Office Building, Lawrence Berkeley Laboratory Report LBL-12298, Berkeley, Calif.

9. Turiel, I., et al. (1981), Analysis of Energy Conservation Activities in the Commercial Sector, Lawrence Berkeley Laboratory Report (to be published).

Energy Conservation in Kenya: Progress, Potentials, Problems*†

L. J. Schipper, J. M. Hollander, M. V. Milukas, J. Alcamo, S. P. Meyers, and S. Noll

This study had four purposes: (1) to characterize the flows of commercial energy in the Kenyan economy, (2) to assess progress made to date in energy conservation in Kenya, (3) to determine the potential role for conservation in future Kenyan energy and economic development, and (4) to make recommendations for development of Kenyan conservation policies and international assistance programs. To accomplish these purposes, the study determined Kenyan oil and electricity use by sector and industry, quantified progress in conserving energy already made by individual firms, estimated the future potential for energy conservation in all sectors, and evaluated some of the major barriers to achieving this conservation potential.

Several methods were used to obtain and analyze data indicating energy flows and conservation in Kenya. The largest oil companies were asked to provide data on total sales of major products and sales to individual firms. At the same time, complete data from the Kenyan electric utility were analyzed to determine electric-power consumption. Personal interviews with personnel of nearly 50 firms produced additional information on energy consumption and its relation to output. With this consumption data, energy flows were quantified in seven sectors (residential, commercial, industrial, energy, construction, agriculture, and transportation) for many individual industries. By analyzing the changes in the energy/output ratios of large firms, progress in conservation was evaluated. Additional measures of output were taken from government statistics to illustrate the link between sector energy use and economic activity.

ACCOMPLISHMENTS IN FY 1981

Findings

Fuel and Electricity (Table 1). Total consumption of commercial energy forms in Kenya reached 80 PJ (10^{15} Joules) in 1979, equivalent to about 5 GJ (10^9 J) per person. Direct consumption of fuel accounts for 94 percent of the commercial energy used by Kenyan final consumers, with electricity accounting for 6 percent. The dominance of fuel in the overall Kenyan energy economy is due to the large relative size of the transportation sector in Kenya. As a result, the share of Kenyan electricity use is relatively small in comparison with most industrial countries or advanced developing countries such as Korea. In the commercial sector, however, consumption of electricity exceeds that of fuels.

Residences (Table 2). Households account for 21 percent of electricity consumption (about 1 percent of total energy) and 5 percent of commercial fuel consumption (about 5 percent of total energy). Electricity use is concentrated in the large cities, although found in no more than 7 percent of Kenyan homes overall, while fuels--kerosene and LPG--are most important in rural households. Commercial energy uses are overwhelmed by the use of charcoal, wood, and other non-commercial fuels not examined in this study. The number of customers using off-peak electricity to heat water is also growing at this rate. However, there has been little growth in electricity use per household for normal electric service, except among the lowest-income consumers. This suggests some restraint on increased use beyond basic services such as cook-

*This work was supported by the U.S. Department of Energy under contract No. DE-AC03-76SF00098, and by Resources for the Future, Inc., contractor for U.S. Agency for International Development, under Contract No. 4026-014.

†Condensed from L. Schipper, et al. (1981), Energy Conservation in Kenya Progress, Potentials, Problems, Lawrence Berkeley Laboratory Report LBL-12741, Berkeley, Calif.

Table 1. Commercial energy use in Kenya, 1979.

Sector	Fuel PJ	Fuel %	Electricity GWh	Electricity %	Total PJ	Total Primary PJ
Residential	3.48	77	286.8	23	4.51	5.20
%	4.6		21.4		5.6	
Commercial	0.92	41	363.1	59	2.22	3.09
%	1.2		27.1		2.8	
Industrial	15.73	88	598.8	12	17.89	19.33
%	20.8		44.7		22.3	
Energy	7.95	98	53.8	2	8.14	5.05
%	10.5		4.0		10.1	
Construction	0.8	97	7.5	3	0.83	0.85
%	1.1		0.6		1.0	
Agriculture	6.57	98	29.2	2	6.67	6.74
%	8.7		2.2		8.3	
Transport	39.84	100	0	0	39.84	39.84
%	52.7				49.7	
Road	(20.7)					
%	27.4					
Rail	(2.56)					
%	3.4					
Air	(15.0)					
%	19.8					
Marine	(1.6)					
%	2.1					
Other	0.33	-	?		0.33	0.33
Total	75.62	94	1339.2	6	80.43	80.43

NOTES: Percentages in rows give split between fuel and electricity within each sector. Percentages immediately below each sector's fuel or electricity consumption and the sector total show the sector percentage of the total national consumption of fuel and electricity, obtained by adding vertically. Total energy use includes consumption of oil for electric power production and oil refinery use, minus the value of thermal electricity produced by EAPL (960 TJ). Total Primary signifies energy consumption with electricity conversion losses (3218 TJ) removed from the energy sector and apportioned among the other sectors according to their end-use electricity consumption. Hydro is counted at 1 kWh = 3.6 MJ.

ing, refrigeration, and small appliances. Fuel use has outpaced electricity growth and has grown at nearly 8 percent per year until very recently when supply constraints slowed or stopped growth.

There is a significant potential for conservation of electricity by substitution of solar water heaters and replacement of inefficient appliances in upper income homes. We have insufficient data for evaluation of the conservation potential of fuel uses.

Industry (Table 3). Much of our analytical effort was devoted to the modern industrial (manufacturing) sector, which consumes 45 percent of all electricity and 21 percent of all fuel. Aside from the energy-intensive paper and cement industries, in which three firms consume nearly 10 percent of all electricity purchased in Kenya, electricity use is rather evenly spread throughout Kenyan industry, particularly in food and textiles, where the number of firms is large. The refining and basic metals industries account for about 7 percent of total electricity sales. These energy-intensive industries are important to the

Table 2. Residential energy use.

Year	Electricity[a] No. of Users[c]	Consumption Total GWh	Consumption Per Home kWh	Fuels[b] No. of Users	LPG Total TJ	Kerosene Total TJ
1972 Total	82025	160.0		-	253(208)	1615(2000)
Normal	39600	120.5	3042			
Small	41380	10.0	240			
Hot Water	~14000	35.0	~2500			
Staff, Bulk	1045	2.50	2380			
1977 Total	110456	242.8		-	384	2012
Normal	51115	172.4	3372			
Small	58120	17.2	297			
Hot Water	~20000[d]	50.0	~2500			
Staff, Bulk	1221	3.18	2606			
1978 Total	119417	264.7		-	-	-
Normal	55934	190.6	3408			
Small	62238	18.50	297			
Hot Water	21000	52.5	~2500			
Staff, Bulk	1245	3.11	2500			
1979[e] Total	127783	287		-	540	2939
Normal	77633	214.3	2760			
Small	48900	11.7	240			
Hot Water	21616	54.0	~2500			
Staff, Bulk[f]	1250	~6.8	?			

NOTES: (a) See App. 2, LBL-12741. (b) Data for 1977 and 1979 were obtained from each oil company. Data for 1972 in parentheses were extrapolated from 1972 Shell sales. Shell sales in 1977 and 1979, when extrapolated to the entire industry, were inconsistent with the actual industry-wide figures shown. Therefore we multiplied the 1972 Shell approximations by the average of the differences between these approximations and actual industry-wide data for 1977 and 1979. The results are shown outside of parentheses. (c) Total number excludes off-peak hot water consumers, who are already counted under normal service. "Normal" customers include households using more than 30 kWh/month, "small" use less than 30 kWh/month, "Hot Water" users are those using the off-peak tariff for hot water production. These definitions were slightly different before 1979. (d) Estimated from 1976 EAPL data. (e) 1979 figures are not strictly comparable with those for earlier years because they were taken from analysis of number of customers using less than 500 but more than 31 kWh/month, not tariff classifications. We assume all customers using >500 kWh/month are shops, probably leaving out some residential customers. (f) We have included about 1200 homes of EAPL employees, whose consumption is relatively high (2400 kWh/meter in 1972), in "staff" and included sales to employee housing maintained by other large firms for 1979 only.

Kenyan economy, generating substantial export earnings through sales of refined oil, paper, and cement. There is a considerable potential for reducing electricity and fuel use per unit of output in all Kenyan industries and in nearly every existing Kenyan factor. At 1980 oil prices, this potential is approximately 20-25 percent for fuel use and 15-20 percent for electricity use.

Table 3. Commercial energy use of manufacturing and commercial firms (units: TJ), 1979.

	Coal	Oil	Electricity	Total
Industrial	1310	15730.6	2155.7	17886.3
Food, kindred		3217	535.0	3752.0
Textiles		1354	290.4	1644.4
Paper		1684	85.5	1769.5
Rubber		281	56.6	337.6
Chemicals		837	70.4	907.4
Cement	1310	5570	446.3	6016.3
Clay & glass		794	37.4	831.4
Metals		330	202.2	532.2
Transport equip.		96	20.3	116.3
Sm. shops, misc.		1567.7	411.6	1979.3
Commercial		916.5	1307.3	2223.8
Schools & hospitals		276.0	126.1	402.1
Offices & other services		130.7	784.5	915.2
Hotels		509.8	157.8	667.6

NOTES: Source is Table A2.2, LBL-12741. Figures for "Hotels" derived by this survey, while remaining "Commercial" figures are from Shell.

Commercial Buildings (Table 3). Buildings use 27 percent of Kenyan electricity and about 1 percent of the fuel. These figures correspond to about 2 percent and 1 percent of total energy use, respectively. At least half of the fuel is used for heating water. At current energy prices, there is a significant conservation potential from the substitution of solar hot water heaters, particularly in hotels, hospitals, and schools, which dominate fuel use. Further potential for conservation of both fuels and electricity exists through improved ventilation and cooling practices in existing and new buildings, particularly in large office buildings.

Transportation (Table 1). The transportation sector consumes 53 percent of the fuel used in Kenya. Nearly half of this is used by automobiles and a smaller fraction by private use of autos. Even though the number of private automobiles will probably rise as incomes increase, there are recent signs of reduced driving per vehicle. Although the power of new autos imported is already decreasing, there is great potential for increased energy efficiency as the fleet turns over. Better maintenance of existing autos, trucks, and buses could also save significant quantities of energy.

International air travel consumes 18 percent of all oil in Kenya, second only to total land transportation. The importance of air transportation reflects the popularity of tourism in East Africa and the hub role of the Nairobi airport. The introduction of wide-bodied aircraft has reduced the ratio of energy inputs to growth in air traffic. This conservation, however, has been a mixed blessing for Kenya because sales of jet fuel to foreign carriers are an important source of hard currency. Because high fuel costs threaten tourism, tour and airline operators alike undoubtedly will seek opportunities to improve operating efficiency of passenger air traffic.

Energy (Table 1). The energy sector, including refining, thermal generation of electricity, and the oil pipeline, accounts for 11 percent of fuel use and 4.4 percent of electricity consumed in Kenya. Overall thermal-generation efficiency is low, and the recent sluggish world oil market has depressed operation of the refinery to well below its maximum capacity, thus reducing efficiency. Cogeneration of electric power is being practiced in some industries, but a significant potential for increase remains, especially in the food and sugar industries. The introduction of the oil pipeline has reduced by over tenfold the energy required to bring light oils from the Mombasa refinery to Nairobi. Finally, the transmission and unaccounted losses of the electric utility, which had reached over 10 percent generation in some years, have recently been reduced.

Solar Energy (Table 4). Although accounting now for only 0.01 percent of Kenya's total commercial energy supplies, use of solar water heating is expanding rapidly. This share could be increased more than fifty-fold over the next decade, according to our estimates of fuel and electricity requirements for water heating. The costs of this solarization would be competitive with costs of fuels or electricity, at present rates. Additionally, some remote users of electricity, such as lodges, may eventually be economically adaptable to the use of photovoltaic solar systems with storage, given the varying load and the high cost of running diesel generators at less than full load.

Table 4. Solar water heating, installed collector area in Kenya.

Year	Cumulative sq. meters	Additions sq. meters	Annual energy displaced, TJ	% Increase from previous year
1975	44.6	44.6	0.14	-
1976	199.6	155.08	0.61	336
1977	484.4	284.6	1.48	143
1978	1295.1	810.6	3.96	168
1979	1979.5	684.4	6.053	53
1980	2947	967.5	9.014	49

These data cover the three largest of the four firms selling solar water heaters. Displaced energy was estimated by apportioning delivered energy to the fuels that would otherwise have been used to heat water. In hotels and schools, water is heated primarily by fuel oil; in remote lodges and other structures, LPG or wood is used. For this calculation, we assumed that hot water in homes and all other buildings would otherwise have been produced by electricity. If the alternative assumption that fuel would have been used to produce hot water in homes had been made, the estimate of energy displaced would be roughly 50% greater because the efficiency of fuel used is lower than that of electricity at the point of application.

Potential for Energy Conservation

The most important conclusion reached in this study is that energy conservation, defined as reduced energy input for a given output, could slow the growth of energy use dramatically relative to economic growth in Kenya, especially if oil and electricity prices rise steadily over the coming decades. Even at today's oil prices, significant reductions in energy use are economically attractive. The net trade deficit in oil products has grown to 4 percent of GDP, making conservation an important method of saving foreign currency.

In the past, energy use grew about as fast as economic output in Kenya. Now, there is great potential for improvement in energy efficiency. In the near future, energy use in the production and services sectors could grow only 57-85 percent as fast as economic output if cost-effective conservation measures were taken. In transportation, efficiency can be enhanced by 20-25 percent through improved maintenance and operation of existing vehicles and by stock changeover to more efficient vehicles. In industry, a 20-25 percent improvement is also attainable by economically attractive process changes. Savings of up to 50 percent in energy consumption are available for residences and commercial buildings by installation of solar water heating systems. Conservation of hot water, especially in hotels, could also contribute significantly to energy saving.

Without attention to increasing energy-use efficiency and conservation, the Kenyan economy, as well as those of other developing countries, will

suffer increasingly from higher oil prices. With sufficient resolve, these countries can ease their oil import burdens significantly and foster a smooth transition to both higher priced conventional oil, gas, coal, or electricity and renewable energy sources.

In the future, the structure of the economy will affect profoundly the overall demand for energy. Kenyan energy planners need to have a fuller knowledge of the energy consequences of strategies that may favor heavy manufacturing vs light manufacturing and services, centralized vs decentralized production and services, and greater vs lesser dependence on transportation. The structure of the economy and the end uses of energy will also influence the appropriateness of renewable energy sources. The dominance of transportation in Kenya's energy-demand mix makes rapid substitution of biomass for a large share of the oil consumed today an expensive proposition because transportation fuels, unlike industrial or residential biomass, must be refined.

Barriers to Energy Conservation

Major barriers to more efficient energy use in Kenya will exist even after price controls on fuels have been removed. The most important barriers are the general lack of in-house expertise to install and maintain energy-saving devices, high tariffs on energy-saving equipment, and general problems with factory organization. Exceptions are some well-run local firms and multinational companies, which do have such expertise and are introducing wide-reaching conservation measures. While some industry and building managers and engineers fully understand the potential for conservation, most are so occupied with more immediate concerns that they have not taken the time to plan the best energy strategies for their firms or plants. In many cases, the difficulty firms encountered in assembling the data requested for this study suggests that they have not fully grasped the economics of their energy situation and the opportunities available for reducing costs through energy conservation. We found this to be the case in many medium-sized factories, hospitals, and hotels and even in some of the largest firms in Kenya.

Recommended Government Actions

The most important step towards promoting efficient use of energy in Kenya would be allowing fuel prices to reach world levels, but there are additional policy steps that could remove or reduce barriers to energy conservation. First, tariffs on imported conservation and solar water-heating equipment should be reduced or removed. Second, a careful and thorough system of energy-use reporting among large firms and energy suppliers would develop a much better sense of the economic aspects of energy use at management levels. This would also improve official efforts to monitor and deal with the energy situation, particularly in times of shortage. Third, government could encourage better utilization of present and future transportation equipment and systems, both by a program of improved maintenance and by careful study of the ways in which people and goods are moved in Kenya and how these patterns are affected by different development strategies. Fourth, government should regulate to some extent the designs of new large buildings and the importation or sales of equipment used in buildings, homes, and factories, to assure that the most energy-efficient designs and machines will be employed. Such regulations would have to be developed with full regard for the costs and benefits accruing both to the affected private firms and the Kenyan economy as a whole. The recent revision of auto tariffs that resulted in a more progressive tax on engine displacement represents a step in this direction. Finally, to maximize economic well-being and minimize the costs arising from the importation and use of scarce oil supplies, the Kenyan government should consider the energy implications of alternative development and investment strategies.

International and bilateral aid organizations, which have for the most part ignored energy use and conservation in their energy-related assistance, could do much to further the efficient use of energy in Kenya and in other developing countries. They should, for example, support and participate in demonstrations of energy audits and installation of energy-saving equipment. Demonstration metering of energy use in institutions, such as hotels or hospitals, would accelerate the acceptance of solar energy for both water heating and local electricity production. Equally useful would be assistance in developing expertise for establishing national energy-use accounts similar to those used in many OECD countries.

PLANNED ACTIVITIES FOR FY 1982

In FY 1982, we anticipate projects that will continue the analysis begun in Kenya. First, we will look carefully at energy use in the buildings sector in the members of the Association of South East Asian Nations. Second, we expect to compare studies similar to the present one from at least a dozen countries from among the Newly Industrializing Countries (NICS) and begin to draw conclusions about the general trend of energy use in middle-income countries. Finally, we expect to participate in detailed analysis of several countries that have not previously been examined.

Indicators of Residential Energy Use and Conservation*†

L. J. Schipper, S. P. Meyers, and A. N. Ketoff

For the last two years, we have been conducting a detailed international study of residential energy use in Canada, Denmark, France, West Germany, Italy, Japan, Sweden, the United States, and the United Kingdom (UK). Although this information is vital to understanding the progress and potential of conservation, much of it was unavailable through "official" government channels. The kind of information that the International Energy Agency (IEA) and other official agencies report is too aggregated and contains little on housing or appliance stock, climate, or other factors that must be included in any reasonable analysis of conservation. The IEA and other groups all are still too preoccupied with manipulating ratios of energy use to gross national product. Elsewhere, it has been shown that such a ratio tells us little about energy use efficiency or changes in efficiency.[1]

A further problem with the existing data is that they do not accurately portray energy use in the residential sector. Based on our extensive data base of national literature and studies, comparison of our own estimates of residential energy use for the countries in our study with those given by the IEA convinced us that the latter are severely flawed and probably unusable as representations of residential energy use.[2] Of course, the problem lies not with the IEA alone, but also with the responsible agencies in the member nations. Only recently have the OECD countries begun to earnestly analyze sector data. In fact, LBL research presentations in Italy, Canada, and Sweden for official bodies has resulted in further work in those countries.[3]

ACCOMPLISHMENTS IN FY 1981

Structure and Intensity: Indicators of Energy Use

Residential energy consumption is a function of the structure and intensity of energy use. Structural factors both define tasks for which energy is used and shape the way in which it is used. These factors include dwelling size, family size, climate, appliance ownership, etc., and often include measures of lifestyle (ownership of a freezer) or behavior (indoor temperature). Energy intensities tell us how much energy is used for a given task and are in part determined by the structural factors existing in a particular place. Energy per dwelling, energy per ton of industrial output, and energy per passenger mile are all intensities. Both structure and intensity are affected by economic factors, especially household incomes and energy prices.

To assess changes in energy use patterns, we believe it is important to connect energy intensities with the key structural factors that affect energy use. Thus, where reasonable and possible, we have combined energy intensities and structural factors to form what might be called "leading" energy indicators. An example is the indicator "Head/dw/DD," the average energy used for space heating per dwelling per degree-day. Comparing the intensity "heat/dw" between years within a country of among countries ignores the effect of climate. We can account for climate by dividing this intensity by an average number of degree-days, an approximate measure of the need for heating.

Measuring Conservation Progress

Macroscopic data, averages over an entire stock or some large subset of the stock, can show broad trends in energy use but are a useful source of conservation indicators only if properly disassembled. An examination of pre- and post-embargo residential energy consumption in the OECD countries reveals that the high growth rates of the 1960s have slowed considerably since 1973 (Table 1). By itself, however, this tells us little about conservation, since the difference could be due to changes in the structural components of energy demand and not necessarily to changes in energy utilization efficiency. Therefore, it is essential to look at the structural factors that affect residential energy consumption, not only the number of dwellings, but also the fraction of "single-family" dwellings, the penetration of central heating, the number of people per dwelling, dwelling size, and, of course, the relative saturation of appliances.

These structural parameters explain many of the changes in consumption over time or differences among countries. Dwellings have increased in size in most countries, but the number of persons per dwelling has generally decreased. As a result, the dwelling area per person increased 20-35 percent over the 1960-78 period in the countries studied. Thus, there is more space to be heated per person and more heat loss surface per person; on the other hand, there are fewer users of hot water. The expected decrease in hot-water use per dwelling has not occurred in most cases, however, as other structural changes, such as the increase in the saturation of hot-water-using appliances, have tended to override the decrease in users per dwelling. Much of the increase in dwelling area per

*This work was supported by the U.S. Agency for International Development and by the Assistant Secretary for Conservation and Renewable Energy, Office of Buildings and Community Development, Buildings Division of the U.S. Department of Energy under Contract No. DE-AC03-76SF00098.

†See "Indicators of Residential Energy Use and Efficiency" (L. Schipper, A. Ketoff, S. Meyers, LBL-11703, 1981) for a complete description of the LBL data base described herein.

Table 2. Indicators of end-use intensity.

Indicator	Canada	France	Germany	Italy	Japan	Sweden	UK	U.S.
Heat per degree-day (MJ/dw)								
1960-65	28.6	16.0	16.6	9.8	6.2	18.5	23.6	-
1970-73	31.5	30.6	22.8	27.1	12.1	20.3	19.9	-
1975-78	28.7	26.1	23.1	22.4	11.2	19.1	19.4	35.0
Cooking (GJ/dw)								
1960-65	6.8	4.5	4.5	3.4	4.7	3.2	7.8	-
1970-73	4.5	4.4	2.8	3.6	5.4	2.9	7.2	-
1975-78	3.2	7.8	2.3	4.6	5.1	2.7	8.3	-
Hot water (GJ/capita)								
1960-65	4.7	1.1	1.1	0.9	1.6	5.8	4.7	-
1970-75	7.6	3.0	3.2	1.2	2.6	9.4	5.9	-
1975-78	10.5	3.8	4.7	2.1	3.8	10.7	4.3	9.5
Appliance electricity (kWh/dw)								
1960-65	2225	535	375	255	640	1770	705	-
1970-73	3665	1115	950	1060	1345	2680	1315	-
1975-78	4320	1470	1225	1455	2055	2910	1975	5925

NOTES:

Source:
LBL data Base. US Data based on material from Oak Ridge National Laboratory.

Years Covered:
Canada: 1961, 1971, 1978; France: 1962, 1973, 1978; Germany: 1960, 1972, 1978; Italy: 1960, 1972, 1978; Japan: 1965, 1973, 1979; Sweden: 1963, 1972, 1978; UK: 1961, 1970, 1978.

To permit comparison, heat per degree-day uses normal climate for each country adjusted to an 18°C base. Hot water/capita refers to the total population and thus shows the effect of increasing saturation of hot water facilities. Appliance electricity does not include electricity used for space heat, hot water, or primary cooking devices.

Indicators for space heating and hot water adjust electricity to a fossil-fuel equivalent, using a hypothetical conversion efficiency of 65 percent in to avoid the structural bias that accompanies changes in the penetration of electricity.

even under tables. Although there are winter temperatures in northern Japan comparable to those of Northern Europe, most of Japan simply chooses not to heat in the Western sense.

Our data reveal the most striking differences in electric-specific appliance energy use. Although saturation data are not presented here, we can see the effects of the differing saturation levels in the indicator "appliance electricity per dwelling." It is also important to look carefully at the nature of the energy services offered by the electric appliances. For example, refrigerators, freezers, and most washers are much smaller in Europe and Japan than in the U.S. or Canada. Thus, measures of annual energy use may not reveal whether the device in question is more efficient, in the sense that it requires less energy per unit of service, in one country or the next. At the same time, the size of an appliance is not necessarily a measure of the amenity it delivers.

The Role of Prices and Incomes

In general, we can say that most other Western nations pay dearly for residential energy use, compared to the U.S. or Canada. At the same time there were notable exceptions, for example, electricity in Sweden and natural gas in the U.K. Not surprisingly, those countries with the lowest electricity prices tend to have the highest levels of appliance electricity use. It is interesting to note that there seems to be a threshold of consumption at about 4 kWh/dw/day; higher prices do not seem to cause electricity use to drop much below this level. Rising levels of disposable income fostered the rapid structural growth in energy services--more central heating, dwelling area, appliances--that took place in the 1960s and early 1970s.

Behavior and Energy Use

Behavior patterns, reflected as indoor temperature settings, bathing practices, hot water use, or cooking habits, explain in part the differences among countries and over time in energy demand for the various end-uses.[4] The evidence we have collected supports the theory that historical energy price levels affect energy-related behavior as well as efficiencies. Perhaps more important than price, per se, is the cost of providing energy services. As efficiency of utilization is improved, the cost of meeting a particular end-use becomes less than it otherwise would have been. Thus, some of the savings made by capital-investment efficiency improvements will doubtless be cashed in for greater amenity levels. If the marginal cost of heating, hot water, cooling, or refrigeration is considerably lower due to high efficiency devices, people are likely to demand a little more of the amenities for which these devices are used.

Conclusion

The data we have collected show that it is possible to construct a detailed portrait of historical and present residential energy use at the

Table 1. OECD residential end-use energy consumption, 1960-78.

	Canada	France	Germany	Italy	Japan	Sweden	UK	US
Growth rates (%/yr)								
Pre-1973 Embargo	3.3	5.1	4.1	6.6	5.4	1.9	0.5	2.2
Post-1973 Embargo	3.8	6.9	4.9	8.6	6.9	2.8	0.4	3.4
1978	2.3	0.6	2.1	2.1	2.7	0.4	0.5	0.4
Energy per dwelling (GJ)								
1960-65	164	42	62	24	21	98	88	141
1970-73	181	83	84	59	33	110	83	173
1978	170	80	87	63	36	102	81	149

person came about because families have become smaller and more affluent. The trend toward smaller families may continue, not without limit however, but this tends to mitigate the move toward larger dwellings.

Two structural factors contributed strongly to the rise in average energy consumption per dwelling observed in almost all of the countries over the 1960-73 period (Table 1): increasing penetration of central heating, from a low of 10-20 percent in most of Europe in 1960 to 50 percent or more in most countries by the oil embargo, and the rapid growth in saturation of major appliances. Typically, refrigerators increased their saturation by as much as four fold; dishwashers, clothes washers, freezers, and televisions increased by even greater amounts. Although cooking appliances were virtually saturated, there was a marked transition in all of Western Europe from cooking based upon solid fuels to gas or electricity. By the mid-1970s, however, the rapid increases in appliance saturations began to level off, as reflected in the slower growth, or decline, in energy-use per dwelling.

In Canada, France, Sweden, and the United Kingdom, end-use energy per dwelling decreased, and in the others, the increase was modest. Part of this decrease, however, is also due to a structural change: the continued penetration and substitution of electricity for other fuels. The large increase in the share of electrically heated dwellings in France and Sweden since 1972 might be counted as oil conservation, but reductions in energy use for heating in electrically heated dwellings, a change in intensity, have not been observed. Because electricity has practically no conversion losses inside the building, the same house will use less end-use energy if it is electrically rather than oil-heated. One must be careful not to confuse this substitution effect with a real change in intensity. In Sweden, some 25 percent of the reduction in space-heating energy consumption in oil-heated dwellings is due to the introduction of wood stoves and, to a lesser extent, electricity.

The increasing substitution of electricity for other fuels is evidenced by the primary energy use per dwelling shown in Table 2. Here, we use the same conversion factor to account for electrical losses for all countries. By so doing, comparisons among countries with differing electricity generating systems can be made, and changes in dwelling energy use are not confused with changes in the generation mix.

Because so many changing factors affect average energy use per dwelling, this average is not a very useful indicator of conservation. To accurately portray energy-use patterns, we have attempted to disaggregate residential energy consumption by the major end-uses: space heating, hot water, cooking, and electric-specific appliances. The latter refers to electricity other than that consumed by primary space heating devices, hot water devices, and kitchen ranges. This is usually done "from the bottom up"; that is, total consumption for each end-use is calculated from estimates of unit consumption and the number of energy-using devices. Although the data are sometimes weak, we feel that the time-series we have developed are reasonably accurate, particularly those for space heating, by far the most important end-use in terms of energy consumption. In Table 2 we present a summary of key end-use indicators.

Comparing Energy Use Indicators

The space heating indicator "Heat per dwelling per degree-day" reveals rather large differences in energy consumption between North America and Western Europe. But are these differences due more to efficiency (tighter houses), behavior, or structural factors such as dwelling size, central-heating penetration, or the fraction of single-family dwellings? The average size of a home in the U.S. (120 m^2) is 50 percent greater than similar averages in most of Western Europe. It also appears that internal temperatures in central European, and especially in English homes, are lower than those in North America, and Scandinavia, and central heating is still far from universal in most of those countries. Because of these features, the indicator for Sweden provides strong evidence for the greater thermal integrity of the Swedish housing stock. While it is true that Sweden has a higher proportion of multi-family dwellings (55 percent), this difference is not critical because heat losses per inhabitant or per square meter of dwelling are nearly equal in Sweden for single and multiple family dwellings, largely due to the fact that most multiples are unmetered.

The problems inherent in making international comparisons are illustrated by the case of Japan, where dwelling area per person is significantly less than in Europe or North America, and the presence of true central heating is rare. The most common forms of heating in Japan use small gas, oil, or electric stoves, called "Kotatsu," located in convenient places such as in sitting rooms or

national level. For the first time, the evolving patterns of residential energy use in major industrialized nations have been placed in a common framework. To understand the dynamics of energy use in the residential sector, it is necessary to break apart aggregate data and look at fuels and end-uses separately. The structural and economic factors that shape energy demand must also be part of the analysis of why residential energy use has changed with time and why it differs from one country to the next.

Preliminary analysis suggests that most of the differences in the amount of energy used to meet household tasks among countries can be attributed to structural and economic factors. Although structural and behavioral characteristics are shaped in part by relative incomes and energy prices, an analysis that looks only at economic variables will miss those elements that actually cause energy to be used in certain ways, e.g., the presence of central heating, the number of people per dwelling, etc. The data we have collected reflect the slowing of the structural trends that brought the rapid growth in residential energy demand in the 1960s and provide a basis for more informed prediction of future energy consumption. In general, it seems likely that the combined effect of higher energy prices and slower structural growth, visible in the post-1973 heating indicators, will bring a levelling or decline in aggregate residential energy demand in the OECD countries.

PLANNED ACTIVITIES IN FY 1982

In FY 1982, our work aims at concluding the econometric analysis of pooled, cross-sectional, consumption data, with W.C.C. Chern of the Lawrence Livermore National Laboratory. Using new data acquired recently, we will quantify the effects of the 1979-80 price increases and compare 1980 energy uses with those in 1972 to evaluate the magnitude of conservation. We will also investigate some of the lifestyle implications of our comparison and attempt to draw historical lessons of use to regional energy studies in the developed countries or energy planners in the newly industrializing countries. Finally, we will compare our observations with national goals and forecasts as expressed in official or recognized unofficial studies. These results will be used where possible to make a judgemental forecast of residential energy use in the year 2000.

REFERENCES

1. Schipper, L., and Lichtenberg, A. (1976), "Efficient Energy Use and Well-Being: the Swedish Example," Science, 194.
2. Schipper, L., Myers, S., and Ketoff, A. (1981), Progress in Residential Energy Conservation: A Multi-Country Perspective, Lawrence Berkeley Laboratory Report LBL-11701. (To be published in Proceedings of the IEA Conference "New Energy Conservation Technologies," Berlin, April 6-9, 1981). See also International Energy Agency (1980), Energy Balances of OECD Countries, 1974/1978, Paris.
3. Schipper, L., and Carlsson, L.G., Reconstruction and Analysis of Swedish Residential Energy Use Data 1960-1980, Lawrence Berkeley Laboratory Report LBL-11702 (forthcoming).
4. Schipper, L., and Ketoff, A. (1980), "International Residential Energy Use Data: Analysis of Historical and Present Day Structure and Dynamics," to be published in Energy, The International Journal, 1982.

APPENDIX

ENERGY & ENVIRONMENT DIVISION

PERSONNEL

Elton J. Cairns

Division Head

Donald F. Grether

Deputy Division Head

Roland J. Otto

Assistant Division Head

DIVISION OFFICE STAFF

Mark Alper
Charla Burgraff
Bron Hafner
Sandra Mocco
Sally Nasman
Maya Osowitt
Judith Pike
Janet Smith
Angela Smothers
Zenaida Yuson
Sharran Zeleke

CHEMICAL PROCESS RESEARCH AND DEVELOPMENT PROGRAM STAFF

Robert Antonopolis
Myra Baker
Harvey Blanch
Kathy Boyer
David Brink
Patricia Bronnenberg
Garth Burns
Elton Cairns*
Shin-Ger Chang
Gregg Cremer
Hubert Davis
Thomas Delfino
Robert Demyanovich
George Dove
Sabri Ergun
Mark Featherstone
Carlos Figueroa
Richard Fish
Alan Foss
Raymond Gansley
Edward Grens
Donald Hanson
Neil Hendy
Richard Hix
Cihan Karatas
Marc Katz
C. Judson King
Dieter Kloden
John Komlenic
Philip Lessner
Jeannette Lim
Nen-Hua Lin
David Littlejohn
Billy Long
Scott Lynn
John MacGlashan
Patricia MacKenzie
Frank McLarnon
Brian Maiorella
Anthony Mancuso
Manuel Martinez
Kenneth Miller
Donald Mohr
Curtis Munson
Thomas Murphy
Stuart Naftel
James Nichols
Steven Oblath
Stephan Orichowskyj
William Oswald
Michael Pedersen
Javier Perez
David Robinson
Steven Rosenberg
Larry Schaleger
Jeff Schonberg
Aldo Sciamanna
Linda Sindelar
Raja Tannous
Rodney Thompson
Anthony Tobias
Theodore Vermeulen
Bruce Vickroy
Dale Wiley
Charles Wilke
Harry Wong
Nasser Yaghoubzadeh
Suen-Man Yu
Rafael Zamora

*Program Leader

SOLAR ENERGY PROGRAM STAFF

Emmanual Altmayer
Claire Amkraut
Brandt Andersson
Harry Angerman
Richard Armer
Cynthia Ashley
Fred Bauman
Paul Berdahl
William Carroll
Eduardo Ceballos
Stephen Choi
Hannah Clark
Craig Conner
J. Pascal Coutier
M. Benay Curtis
Kim Dao
Marie Deiringer
Donald Elmer
David Evans
Ian Fry
Marc Fontoynont
Nina Friedman
Peter Fuller
Ashok Gadgil
Ronald Glas
Donald F. Grether
Lief Hansen
Michael Harms
Mary Hart
Albert Heitz
Jeffrey Herz
Victoria Horan
Patricia Hull
Arlon Hunt
Ronald Kammerud
Stephen Kanzler
Joshua Kay
Jeffrey Kessel
Mark Kruskopf
Eric Lam
Stella Lawrence
Janet Linse
Bart Lucarelli
Marlo Martin
Rolf Mehlhorn
Atila Mertol
Ashraf Mesbahi
Harvey Michaels
Mark Nansteel
Lester Packer
David Paydarfar
J. Wayne Place
Cindy Polansky
Alex Qunitanilha
John Randolph
Joseph Rasson
Fenwick Salter
Laurie Sampietro
Gail Schiller
Steven Schiller
Charlotte Standish
Jerry Stoker
Mehdi Tavana
John Thornton
Stephanie Tristram-Nagle
Michael A. Wahlig*
Mashuri Warren
Thomas Webster
Hayward Zwerling

ENERGY EFFICIENT BUILDINGS PROGRAM STAFF

ADMINISTRATION

Margaret Boyce
Michael Charney
Laurel Cook
Richard Crenshaw
Linda Davis
Theodore Edlin
Brigitte Fitzsimmons
Debbie Giallambardo
Mary Hart
Jeana McCreary
Moya Melody
Arthur Rosenfeld*
Lynne Sherman

ENERGY PERFORMANCE OF BUILDINGS

Jim Adams
David Anderson
Richard Beerman
Ake Blomsterberg
Richard Diamond
Darryl Dickerhoff
John Dickinson
Jim Dixon
Jean-Yves Garnier
David Grimsrud†
Michael Kennedy
David Krinkel
Mark Modera
Max Sherman
Brian Smith
Robert Sonderegger
Carol Stoker

BUILDING VENTILATION AND INDOOR AIR QUALITY

Richard Allen
Michael Apte
Keith Archer
James Berk
Rakefet Bitton
Mary Boegel
Pipon Boonchanta
Steve Brown
Lloyd Davis
Jim Dillworth
Suzanne Doyle
Badia El-Adawy
Arnold Falick
Leah Fanning
William Fisk
Kristin Geisling
John Girman
Craig Hollowell†
Linda Jenks
Irving Ko
Buck Koonce
Amey Lee
Vera Martin
Robert Miksch
Barbara Moed
Nancy Morrison
William Nazaroff
Anthony Nero
Francis Offermann
Maria Ossa
Kenneth Revzan
Alan Robb
Gary Roseme
John Rudy
Heidi Schmidt
Philip Strong
Miles Tashima
Greg Traynor
Isaac Turiel
Dora Wolosin
Rodger Young
Geordie Zapalac

---

*Program Leader

†Group Leader

BUILDING ENERGY ANALYSIS

Fred Buhl
Richard Curtis†
Kathy Ellington
Ender Erdem
Hideaki Hayashi
James Hirsch
Karen Olson
Tom Wagner
Frederick Winkelmann

ENERGY EFFICIENT WINDOWS AND LIGHTING

Pam Balch
Jo Dee Beck
Sam Berman†
Robert Clear
Bruce Dexter
Dennis DiBartolomeo
Jean Ferrari
Richard Johnson
Mahmut Karayel
Jeff Kessel
Joseph Klems
Doug Kosty
Carl Lampert
Clifford Lee
David MacGowan
Harry Miller
Eli Naor
Mojtaba Navvab
Eliyahu Ne'eman
Jeannie Nelson
Joyce Popendorf
Robert Richardson
Mike Rubin
Francis Rubenstein
Joel Ryan
Stephen Selkowitz
Sheelah Sigel
Paul Stuart
Rudy Verderber
Michael Wilde
Ruth Williams
Cecile Wolf

BUILDING ENERGY DATA COMPILATION, ANALYSIS, AND DEMONSTRATION

Jeff Harris
Alan Meier
Steve Meyers
Brian O'Regan
Arthur Rosenfeld†
Barbara Shohl
Jan Wright

ENVIRONMENTAL RESEARCH PROGRAM STAFF

ATMOSPHERIC AEROSOL RESEARCH

Tihomir Novakov*†
William Benner
Richard Brodzinsky
Shin-Ger Chang
Sidney Cohen
Ray Dod
Sergei Gomiscek§
Lara Gundel
Anthony Hansen
Evert Ljungstrom§
Samuel Markowitz
Michael McKinney
Steven Oblath
Hal Rosen
Richard Schmidt
Linda Wroth

APPLIED PHYSICS AND LASER SPECTROSCOPY RESEARCH

Nabil Amer†
Neil Bergstrom
Mark Cooper
Robert Gerlach
Warren Jackson
Ralph Johnson
Stanley Kohn
Marjorie Olmstead
Sidney Phillips
Douglas Wake
Zafer Yasa

OIL SHALE RESEARCH

Jess Albino
Glenn Boyce
Jeremy Cantor
Christian Daughton‡
Phyllis Fox†
Bob Giauque
Gloria Gill
Don Girvin
Dick Goodman‡
Bill Hall
Gloria Harris-Winston
Al Hodgson
David Jenkins‡
Bonnie Jones
Laura Joseph
Eric Ko
Bruce Koball
Greg Langlois
Linda Maio
Mohsen Mehran
Kumar Mehta‡
Carl Meyer
T.N. Narasimhan
Amos Newton
Peter Persoff
Martin Pollard
Joe Ratigan
Rick Sakaji
Bob Selleck‡
Irene Stachura
Jerry Thomas‡
Neil Thomsen
Hector Vallarreal
Skip Walker
Karen Yu

---

*Program Leader

†Group Leader

‡University of California, Berkeley

§Participating Guest

COMBUSTION RESEARCH

Abdel Abdel-Hafez[§]
Mary Jane Alpaugh[‡]
Diana Brehob
M. Quinn Brewster[‡]
Nancy Brown
Cam Carter
Minna Chan
Daih-Yeou Chen
Robert Cheng
Alexandre Chorin
Patrick Coico
Enrique Cuellar
John Daily
Fred Fisher[‡]
Ahmed Ghoniem
Gloria Gill
Cecile Grant
Ralph Greif
John Hart
Jean Hertzberg[‡]
David Hirvo
Kenneth Hom
Frank Hurlbut
Bruce Ingraham
Claire Johnson[‡]
Bill Kleiser[‡]
John LaFond
Terry Ling
Donald Lucas
John Metcalf
Kenneth Metchette
Michelle Milan[‡]
Mehdi Namazian[‡]
Izak Namer
Terry Ng
Antoni Oppenheim
Rebecca Palmer
Gary Parsons
Richard Peterson
William Pitz
Ola Rashed
Frank Robben
Robert Sawyer
Robert Schefer
Lily Shen[‡]
Pauline Sherman[§]
Gautam Shiralker
Horton Stewart[‡]
Lawrence Talbot
Cheng Tien
Lawrence Vaneveld
Steve Vosen
R. Brady Williamson
Joan Woodard[§]

LAKE ECOTOXICOLOGY

John Harte[†]
Don Levy
Gregory Lockett
Joan Oldfather
John Rees
Ellen Saegebarth
Richard Schneider
Kathy Tonnessen

TRACE ELEMENT ANALYSIS RESEARCH

Frank Asaro
Charles Case
Ray Clem
Robert Giauque
Ralph McLaughlin
Helen Michel
Anthony Nero
Mary Quinby-Hunt
Alexandre Quintanilha
Linda Sindelar

ENERGY ANALYSIS RESEARCH PROGRAM STAFF

Grace Afong
David Anderson
Betty Bratton
Peter Benenson
Jackie Bernier
Vincent Berg
Carl Blumstein
Richard Boschen
Peter Chan
Tim Chapman
Ray Coover
Karl Dake
Bill Dapkus
Peter Deibler
Tatyana Dinaburskaya
Mohamed El-Gasseir
Henry Estrada
Robert Feinbaum
Sandra French
Andre Ghirardi
Steve Gold
David Goldstein
Eric Gray
Kendall Haven
Mark Henriquez
Charles Henry
Horace Herring
Joe Huang
Kathleen Hudson
Dan Iacofano
John Ingersoll
Reid Judd
Ed Kahn
Andrea Ketoff
Sean Killeen
Dan Kowalcyzk
Mark Levine*
Jim McMahon
Carol Mancke
James Mass
Steven Meyers
Matt Milukas
Paul Podvin
Suzan Rainey
Lisa Rau
Ron Ritschard
Henry Ruderman
Jayant Sathaye
Susan Schaffer
Lee Schipper
Nancy Schorn
Rob Scott
Rich Sextro
Steve Shotland
William Siri
Renee Slonek
Barry Smiler
Jay Smith
Aram Sogomonian
Karen Tsao
Issac Turiel
Dorothy Turner
Tony Usibelli
Gleb Verzhbinsky
Ed Vine
Tom Wagner
Debbie Wilson
Winifred Yen
Carl York

---

*Program Leader

[†]Group Leader

[‡]University of California, Berkeley

[§]Participating Guest

This report was done with support from the Department of Energy. Any conclusions or opinions expressed in this report represent solely those of the author(s) and not necessarily those of The Regents of the University of California, the Lawrence Berkeley Laboratory or the Department of Energy.

Reference to a company or product name does not imply approval or recommendation of the product by the University of California or the U.S. Department of Energy to the exclusion of others that may be suitable.

TECHNICAL INFORMATION DEPARTMENT
LAWRENCE BERKELEY LABORATORY
UNIVERSITY OF CALIFORNIA
BERKELEY, CALIFORNIA 94720